
DISCORDANT BODIES OF POSTCUMULUS, ULTRAMAFIC ROCK IN THE UPPER CRITICAL ZONE OF THE BUSHVELD COMPLEX : IRON-RICH ULTRAMAFIC PEGMATITE BODIES AT AMANDELBULT AND THE DRIEKOP PLATINIFEROUS ULTRAMAFIC PIPE.

ROGER N. SCOON B.Sc (Hons.), M.Sc (Cardiff)

Thesis submitted in fulfilment of the requirements for the degree of :

DOCTOR OF PHILOSOPHY

in the Department of Geology, Rhodes University, P.O. Box 96, Grahamstown 6140, South Africa.

DECLARATION

This thesis is the original work of the author except where specific acknowledgement is made to the work of others.

Signed : ..... 30-APRIL-1985.

ABSTRACT

In the layered sequence of the Bushveld Complex a number of distinct, but possibly genetically related groups of transgressive, postcumulus, ultramafic and mafic rock are recognised. The main part of this thesis investigates a suite of postcumulus rocks for which the name iron-rich ultramafic pegmatite is proposed. The majority of iron-rich ultramafic pegmatite bodies examined are from the upper critical zone of the layered sequence at Rustenburg Platinum Mines Amandelbult Section, in the northern sector of the western Bushveld Complex. Field relationships imply that the iron-rich ultramafic pegmatites should be considered as an integral feature of the layered sequence, even though they transgress the cumulates. Consequently, this thesis also includes a study of the cumulate sequence at Amandelbult. A second group of postcumulus, ultramafic rocks which is investigated comprises platiniferous ultramafic pipes; the Driekop pipe has been selected as a case-study.

This thesis is presented in four sections, namely, an introduction and overview, and studies on the Driekop pipe, the cumulate sequence at Amandelbult and the iron-rich ultramafic pegmatite suite. A new classification scheme of discordant bodies of postcumulus, ultramafic rock in the Bushveld Complex is proposed (see also Viljoen & Scoon, in press). In the scheme presented here, two main varieties of postcumulus, ultramafic rock are recognised, namely, non-platiniferous magnesian dunites and iron-rich ultramafic pegmatites.

The platiniferous ultramafic (or hortonolite dunite) pipes, which include the famous mines of Driekop, Mooihoek and Onverwacht, appear to be restricted to a small area in the eastern Bushveld Complex. The Driekop pipe is primarily composed of a large, annular, sheath-like body of magnesian dunite which envelops an irregular and poorly-defined core of rather iron-rich dunite and wehrlite. The magnesian dunite is itself enclosed by a thin envelope of iron-rich olivine clinopyroxenite. Platinum-group elements were essentially restricted to the core, now mined out. Small, satellite bodies of magnesian dunite and iron-rich clinopyroxenite pegmatite occur within the cumulate wallrocks adjacent to the main pipe. The main pipe is aligned approximately at right angles to the undisturbed cumulate layering, although the cumulates adjacent to the pipe are downwarped and form a major fold structure. New structural evidence and geochemical data presented in this study suggest that the Driekop pipe should be considered as a composite feature, in which each mineralogical assemblage is treated as a separate entity. Formation of the main body of magnesian dunite is ascribed to remobilisation of early-formed dunite cumulates. It is difficult to sustain an unequivocally intrusive model with the new data; rather, they argue against a metasomatic model. The marginal envelope of iron-rich olivine clinopyroxenite is compared with iron-rich ultramafic pegmatite, which is not associated with magnesian dunite. It may have formed either by replacement of the cumulate hosts or by crystallization from an iron-rich, fractionated silicate liquid, derived from within the cumulate pile. Replacement of pre-existing magnesian dunite, by a similar liquid, resulted in formation of the platiniferous core assemblage. The platiniferous ultramafic pipes may thus be considered as unique combinations of two types of postcumulus, ultramafic rock, that is, non-platiniferous magnesian dunite and iron-rich ultramafic pegmatite.

The cumulate sequence in part of the upper critical zone at Amandelbult, between the UG-1 chromitite layer and the Bastard Reef, is described and defined within a new scheme of sub-division based on cyclic units (see also Scoon & de Klerk, in press). In this sequence cumulus olivine is unusually abundant, and the rocks include a series of olivine cumulates known as the pseudoreefs and the olivine-rich Merensky Reef. Many of these olivine cumulates, which occur at the base of cyclic units, host economic concentrations of base-metal sulphides and platinum-group elements. The distribution of Ni between olivine and silicate liquid is modelled in relationship to the formation of cyclic units. Compositional differences between olivine from different cyclic units indicate that new influxes of magma, each with its own chemical signature, entered the chamber at the base of the UG-2, Lower and Upper Pseudo, and Merensky cyclic units. Modelling of the distribution of Ni and Fe between olivine and molten sulphide has been completed. Co-existence of Ni-rich olivine and Ni-rich sulphide in the Merensky Reef suggests that segregation of an immiscible sulphide phase occurred concomitantly with the crystallization of olivine. The formation of these cyclic units is related to influxes of new magma. The new magma, which is postulated to be denser than the residual magma, enters the chamber as a flow along the crystal-liquid interface and initially forms a discrete layer at the base of the liquid column. Cyclic units consisting solely of ultramafic cumulates are related to fractional crystallization of this new magma as a separate entity. Cyclic units consisting of ultramafic cumulates which are sharply, and sometimes unconformably, overlain by felsic cumulates are attributed to mixing of new and residual magmas.

Iron-rich ultramafic pegmatite, which is abundantly distributed throughout much of the layered sequence, includes silicate-rich and Fe-Ti-(Cr) oxide-rich varieties. In the upper critical zone the silicate-rich, or typical, variety is composed essentially of iron-rich olivine (hortonolite) and clinopyroxene (augite), with subordinate Fe-Ti-(Cr) oxides (ilmenite and an unusual Fe-Ti-Cr spinel) and base-metal sulphides (essentially pyrrhotite) with accessory amphibole and mica. Other accessory phases include plagioclase and orthopyroxene; these, however, are interpreted as relict cumulus minerals and are not an integral feature of the pegmatites. Moreover, plagioclase is only rarely present in amounts of more than 5 modal percent, consequently these rocks are ultramafic in character. They are iron-rich rocks (with a low Mg/Fe ratio), are normally non-platiniferous, and typically exhibit the textural variability, especially in grain size, characteristic of pegmatites. Iron-rich ultramafic pegmatite occurs in veins, small, irregular, often pod-like or sheet-like bodies or large, pipe-like features with diameters in excess of 1 km. Field relationships do not favour an intrusive origin; however, whether they can be wholly attributed to replacement is equivocal. Locally, pegmatite bodies exhibit striking evidence of selective "replacement", and they clearly favour felsic cumulates at the expense of ultramafic cumulates.

Iron-rich ultramafic pegmatite is characterised by a unique mineral paragenesis and chemistry which is controlled by its height in the layered sequence. For example, in the upper critical zone at Amandelbult the composition of olivine in pegmatite varies between Fo_{49} and Fo_{41}. In comparison, the composition of cumulus olivine in the layered sequence at this position varies between Fo_{82} and Fo_{76}. In pegmatite at Amandelbult, Fe-Ti-(Cr) oxides rarely represent more than 20 modal percent, ilmenite may be of equal abundance to spinel, and the spinel typically contains over 5 wt.

percent Cr_2O_3 The sulphide assemblage is characterised by exceptionally high Fe/Ni and Fe/Cu ratios, the presence of troilite and cubanite, and a high Co content of the pentlandite. With increasing height in the layered sequence iron-rich ultramafic pegmatite becomes even more fractionated, as evidenced by a decrease in the Mg/Fe ratio of silicates (ferrohortonolite and ferroaugite occur), an increase in the modal percentage of Fe-Ti oxides, a decrease in the Cr content of the spinel, and the introduction of apatite as an accessory phase. Relict cumulus plagioclase is more calcic than primary, cumulus compositions and is usually partially saussuritised. Clearly, the pegmatitic liquids were undersaturated in, and in disequilibrium with, plagioclase.

Iron-rich ultramafic pegmatite exhibits, on a regional scale, a close spatial relationship with thick layers of cumulus anorthosites. Moreover, iron-rich ultramafic pegmatite bodies rarely occur above the highest Ti-magnetite layer in the upper zone. It is concluded that the putative pegmatitic liquid will only commence to form in the cumulate pile after mottled anorthosites occur, and they will cease to form after the residual liquid line of descent reaches an absolute enrichement in total iron. If a relatively sodic plagioclase were an integral component of the iron-rich ultramafic pegmatite suite, these rocks would, mineralogically and compositionally, be comparable with cumulates in the upper zone of the layered sequence (pegmatite from the upper critical zone would be comparable with cumulates in UZb). If this were the case then the formation of iron-rich ultramafic pegmatite could be attributed to intercumulus liquids, as described by Irvine's model of infiltration metasomatism (Irvine, 1980). However, the data in this study necessitate a hypothesis in which the putative pegmatitic liquids are plagioclase-undersaturated.

For this reason, a hypothesis is discussed in which the pegmatitic liquids are related to iron-rich, plagioclase-undersaturated, intercumulus and/or residual liquids derived during crystallization of thick layers of mottled anorthosite. Removal of these liquids, essentially by filter-pressing and annealing, and subsequent migration through the unconsolidated cumulate pile, results in the formation, essentially pene-contemporaneously with their host cumulates, of discordant pegmatite bodies. It has not been unequivocally established whether the pegmatites form by a process of magmatic replacement or by crystallization from a silicate liquid. However, these data do support an origin for the pegmatites from a silicate liquid which is at magmatic temperatures, and it is concluded that they are not the result of metasomatism related to aqueous fluid or vapour. Finally, formation of iron-rich ultramafic pegmatite may be considered as an ongoing, dynamic series of events that are an integral part of the crystallization of a cumulate pile.

ACKNOWLEDGEMENTS

I would like to express my sincere gratitude to the managements of the Johannesburg Consolidated Investment Co. Ltd., and Rustenburg Platinum Mines Ltd., for financial and logistical support, access to their properties and permission to use a large amount of unpublished information. I also received support from the South African C.S.I.R., without which financial problems would have been insuperable.

During the course of this Ph.D. project I have been fortunate enough to have had two supervisors who have literally provided every conceivable assistance and encouragement. During my field programme in the Bushveld the initial guidance of Dr. Morris Viljoen (who at that time was Divisional Consulting Geologist (Platinum) with JCI) proved invaluable. I would also like to thank Morris for unselfishly sharing with me his knowledge of the pegmatite bodies, for showing me many field locations and for his continued interest in my studies whilst I was at Rhodes University. I would like to express my sincere thanks to Prof. H.V.Eales who patiently guided me through 3 years of laboratory studies at Rhodes. "Prof" offered constant encouragement, constructive criticism, particularly in the way of new ideas, and patiently improved my presentation and corrected several rough drafts.

I am indebted to Dr. Ivan Reynolds who, besides sharing his knowledge of Fe-Ti oxides and base-metal sulphides, also participated in practically all aspects of my studies. He is also thanked for many fruitful discussions and for permission to use many unpublished ideas and data. I would also like to thank Dr. Goonie Marsh and Prof. Roger Jacob, both of whom assisted me in specific branches of my studies and, again, contributed by way of numerous discussions.

I particularly wish to thank my fellow research students, specifically Andrew Mitchell, Mike Botha, Moose Kruger and Dave Phillips. Both Andrew and Mike generously provided ideas and unpublished data, without which this thesis would have been poorer. They also provided advice with laboratory work. Billy de Klerk is thanked for his part in preparing our joint paper, many of the ideas of which are presented in this thesis.

I would like to thank the mines geological staff of RPM Amandelbult and Driekop Sections for their contribution, and particularly Mr. B. Sutherland, Consulting Engineer JCI, for his approval of my studies. In addition I would like to thank personally Bruce Walters, Kobus Theron and Piet Cilliers at Amandelbult, John Barry and Peter de Wet at Rustenburg and Chris Lee at James Park. Roger Mossom deserves special thanks for his unselfish assistance with my studies at Driekop. I would also like to thank Euan Kinloch, Wolf Peyerl and Lana Perreira at JCI laboratories for providing assistance with microprobe studies of sulphides and platinum-group minerals.

Prof. Bob Mason, now at Queens University, Kingston, Ontario is thanked for the part he played in providing me with the opportunity to embark upon this research project at its inception.

Finally, I would like to thank the late Mrs. Pat Shuttleworth for typing parts of the manuscript and Ms. Delores Jacobs for her constant encouragement and assistance with draughting many of the Figures.

CONTENTS

APPENDICES

LIST OF FIGURES

Parentheses denote whole-page Figures, in text after indicated page number.

LIST OF FIGURES (CONTINUED)

LIST OF FIGURES (CONTINUED)

LIST OF MAPS IN FOLDER

LIST OF TABLES

Parentheses denote whole-page(s) Tables, in text after indicated page number.

LIST OF TABLES (CONTINUED)

SECTION A : INTRODUCTION AND OVERVIEW

CHAPTER 1 INTRODUCTION

The Bushveld Complex underlies an area of approximately 65 000 km^2 and has been described by Willemse (1969a) as the "largest repository of magmatic ore deposits in the world". The ultramafic-mafic rocks in the layered sequence (or Rustenburg Layered Suite) of the complex host the world's predominant reserves of platinum, chromium and vanadium. Copper and nickel sulphides, together with the minor platinum-group elements (palladium, iridium, osmium, rhodium and ruthenium) and gold are produced as by-products from the platinum ores. The persistence and regularity of the layering is such that the layered sequence may be described using stratigraphic principles. The terminology of layered intrusions was originally formulated on the concept that the layering resulted from gravitational accumulation of minerals (Wager, Brown & Wadsworth, 1960). In modern usage this "cumulate" terminology is used without genetic implications (Irvine, 1982).

A distinctive feature of some large layered complexes is the presence of discordant bodies of ultramafic-mafic rock which transgress the layered cumulates. These rocks, which post-date the formation of the layering, are usually considered to have formed from postcumulus processes operating within the magma chamber. They may be described as postcumulus rocks.

In the layered sequence of the Bushveld Complex a number of distinct, but possibly genetically related groups of transgressive, postcumulus ultramafic and mafic rock are recognized (see Chapter 2). The main part of this thesis investigates a suite of postcumulus rocks for which the name iron-rich ultramafic pegmatite is proposed. These rocks, which are abundantly distributed through much of the layered sequence, include silicate-rich and Fe-Ti oxide-rich varieties. The former have been described as magnetite-bearing pegmatites (Cameron & Desborough, 1964) or ultramafic pegmatoids (Willemse, 1969a), and the latter are usually referred to as magnetite plugs (inter alia Willemse, 1969a,b). The silicate-rich varieties are composed essentially of iron-rich olivine (usually hortonolite) and clinopyroxene with subordinate ilmenite, Ti-magnetite and base-metal sulphide. They are iron-rich rocks (with high bulk $FeO + Fe_2O_3$ and a low Mg/Fe ratio), are normally non-platiniferous, and typically exhibit the textural variabilty, especially in grain size, characteristic of pegmatites. They occur in veins, small, irregular, often pod-like or sheet-like bodies

and large pipe-like features with diameters of over a kilometre.

The majority of iron-rich ultramafic pegmatite bodies examined in this study are from the upper critical zone of the layered sequence at Rustenberg Platinum Mines Amandelbult Section, in the northern sector of the western Bushveld Complex (fig. 1.1). Field relationships imply that the iron-rich ultramafic pegmatite suite should be considered as an integral feature of the layered sequence, even though they transgress the cumulates. Consequently, this thesis also includes a brief study of the cumulate sequence at Amandelbult.

A second group of postcumulus, ultramafic rocks which is investigated in this study is described as platiniferous ultramafic pipes. These bodies, which were first described by Wagner (1929) as hortonolite dunite pipes, include the famous orebodies of Driekop, Mooihoek and Onverwacht. The Driekop pipe has been selected as a case-study (fig. 1.1).

1.1 THE BUSHVELD COMPLEX - AN OVERVIEW

A detailed review of all the literature available on the Bushveld Complex would present a daunting task. The most comprehensive account of the complex is still that by Hall (1932). Detailed articles and reviews by Wager and Brown (1968), Willemse (1969), Hunter and Hamilton (1978), Von Gruenewaldt (1979) and Tankard et al.(1982) are recommended to the reader. Comprehensive bibliographies have been published by the Bushveld Research Institute, University of Pretoria.

The Bushveld Complex is dated at approximately 2000 Ma. An upper age limit for the earliest rocks in the Bushveld Complex, the Rooiberg Group felsites, is 2263 ± 85 Ma. The younger Bushveld granites are dated at 1920 ± 40 Ma (Nebo) and 1670 ± 70 Ma (Makhutso; Tankard et al., 1982). The layered sequence has been dated by strontium isotope techniques at 2095 ± 24 Ma (Hamilton, 1977). The layered sequence is intruded into sediments of the Transvaal Supergroup. The overall shape and extent of the layered sequence still not fully known, although the consensus of opinion is that it forms a number of separate intrusive bodies. Tankard et al. (1982) subdivide the complex into four lobes: western, eastern, southeastern and northern. In this study the western lobe is conveniently divided into the southern (or Rustenberg), northern (comprising R.P.M. Amandelbult and Union Sections) and far-western (area west of the Pilanesberg) sectors. The eastern lobe has been subdivided after the work of Cameron (see Cameron, 1982). The northern and southeastern lobes have not been investigated in this study. The layered sequence within the western and eastern lobes of the complex, although they

have many features in common, should be treated as quite separate intrusive bodies until evidence to the contrary is adduced. A generalised geologic map of the complex is presented in Figure 1.1.

The layered sequence of the Bushveld Complex is generally divided into five main units or zones: marginal, lower, critical, main and upper. This informal terminology, developed by Hall (1932) and subsequently modified by numerous workers is widely accepted and is preferred to the approach recommended by the South African Council for Stratigraphy, or SACS (1980). There is no common agreement as to the exact divisions between these zones, and these will only be discussed where relevant. A schematic stratigraphical column of the layered complex is presented in Figure 1.2.

The critical zone may be subdivided into a lower and upper unit and it is useful to refer to these as the lower critical and upper critical zones. The lower critical zone may be grouped with the lower zone as comprising a sequence of ultramafic (olivine-orthopyroxene-chromite) cumulates, which contain only intercumulus plagioclase. The base of the upper critical zone marks the introduction of plagioclase as a major cumulus phase in the layered complex, an important event in the evolution of the Bushveld magma chamber. The upper critical zone comprises a sequence of orthopyroxene-plagioclase cumulates and has many features in common with the main zone. Towards the top of the upper critical zone a minor reversal occurs and olivine and chromite are major cumulus phases in the sequence from the UG-1 chromitite layer to the Bastard Reef in the northern sector of the western Bushveld Complex. This limited stratigraphic interval comprises the major platiniferous cumulate orebodies, the UG-2 and Merensky Reefs, and, consequently, is well exposed in underground workings.

1.2 POSTCUMULUS PROCESSES AND SOME DEFINITIONS

A **cumulate** may be described as an igneous rock characterised by a **cumulus** framework of touching minerals that were evidently formed and concentrated primarily through fractional crystallization (Irvine, 1982). The fractionated crystals (which may result from crystal settling, bottom crystallization or other processes) are referred to as cumulus or primocryst grains. They are generally cemented together by a texturally later generation of **postcumulus material** that appears to have crystallized from **intercumulus liquid** in the interstices or pores of the cumulus framework (Irvine, 1982). The formation of the cumulus crystals is referred to as the primary or **cumulus crystallization stage**. Irvine refers to the processes involved in solidification of the intercumulus liquid as **postcumulus**

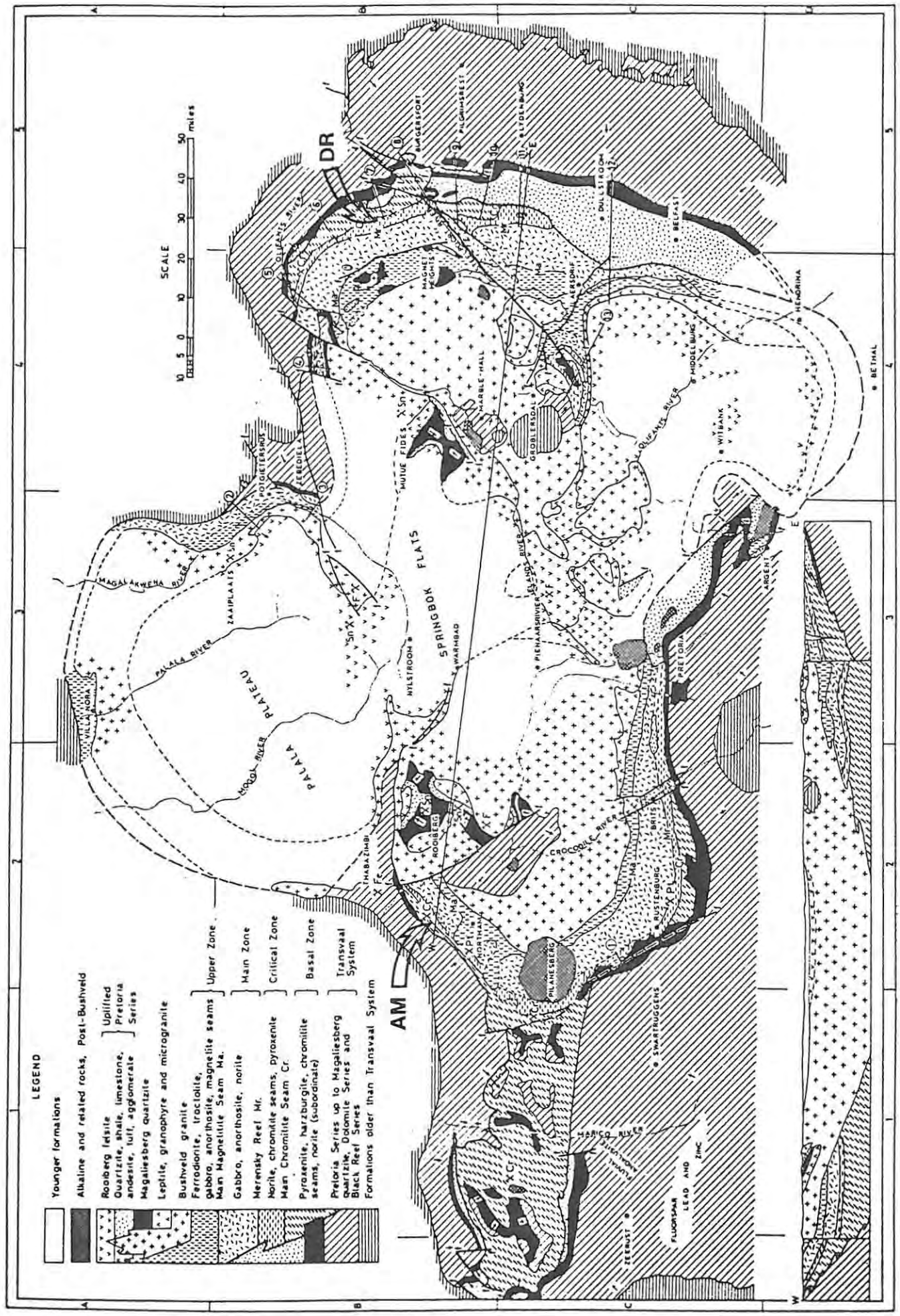

FIGURE 1.1 Geologic map of the Bushveld Complex (after Willemse, 1969a). Note location of two main study areas, Amandelbult (AM) and Driekop (DR).

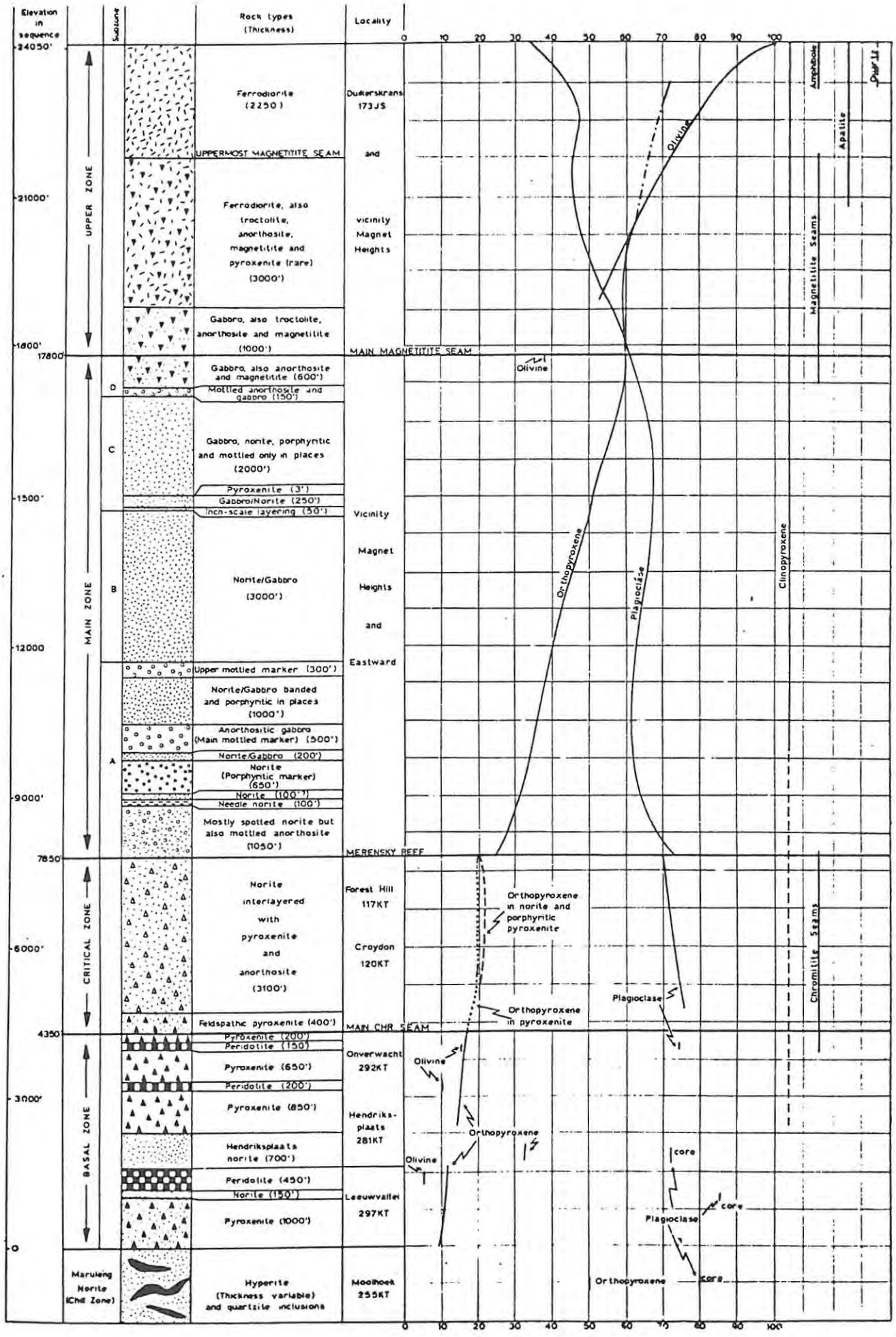

FIGURE 1.2 Schematic stratigraphic column of the layered sequence in the eastern limb of the Bushveld Complex (after Willemse, 1969a). Note that the basal zone is equivalent to the lower zone (see text).

processes. Jackson (1967) observes that postcumulus material in a cumulate may occur in three principal habits, as intercumulus-space filling, as overgrowths on cumulus minerals, and as reaction replacement of cumulus minerals. These features are related to intercumulus liquid which has been trapped within the cumulus framework, or has possibly migrated over short distances. A major problem in petrogenetic studies of cumulates is that their chemistry does not reflect the composition of the primary magma. The recognition of almost pure adcumulates and orthocumulates (which may comprise over 50 percent of trapped postcumulus material) is evidence that the movement of intercumulus liquid within a consolidating cunulate pile is an irregular process.

In this study it is useful to be able to reserve the term postcumulus for processes that operated after formation of a cumulate (i.e. after crystallization of both the cumulus and trapped intercumulus material). Thus non-cumulus material trapped within the cumulus framework is referred to as intercumulus material. Postcumulus processes then refer to events which result in the formation of minerals or rocks after the layered cumulates have developed. These may cover a considerable time span as obviously the formation of a large layered complex involves a dynamic series of on-going events. One of these is the large-scale movement of intercumulus liquid. This may result in the formation of postcumulus rocks by replacement of pre-existing cumulates. Alternatively, it is feasible to suggest that minerals may crystallize directly from this intercumulus, or postcumulus liquid. It may be surmised that postcumulus processes play an important role in a crystallizing cumulate pile.

1.3 MOTIVATION OF THIS STUDY

This study is the result of a joint research programme between Rhodes University and Johannesburg Consolidated Investment Company Limited (J.C.I.). Funding has been jointly supplied by J.C.I. and the South African C.S.I.R. In addition, full logistic support (transport, board and lodging, access to mines etc.) was supplied by Rustenburg Platinum Mines Limited (R.P.M.) during various field sessions, which totalled some 9 months. A preliminary programme was scheduled by Dr. M.J. Viljeon, Consulting Geologist (Platinum), J.C.I., in June 1981. This was directed primarily at investigating the transgressive bodies of iron-rich ultramafic pegmatite at R.P.M. Amandelbult Section. Because these bodies are unusually abundant at Amandelbult they have some detrimental effects on mining of the Merensky Reef, and large, pipe-like bodies may result in considerable loss of ore reserves.

Field work included mapping (mostly of mine workings), sample collection and logging and sampling borehole core. The results of a detailed ground-based geomagnetic survey over the Amandelbult area, completed by J.C.I. in 1978, were made available to the author. This was the main guide to these bodies on surface, as outcrop in the western Bushveld Complex is poor. This was then followed by petrological and geochemical studies at Rhodes University (1982-84).

1.4 THESIS LAYOUT

During the course of these studies the preliminary programme described above was broadened, consequently this thesis has been subdivided into four sections, as follows :-

SECTION A : OVERVIEW AND INTRODUCTION An overview and new classification of transgressive bodies of ultramafic-mafic rock in the layered sequence of the Bushveld Complex (Chapters 1, 2).

SECTION B : THE DRIEKOP PIPE The results of a comprehensive study of the Driekop platiniferous ultramafic pipe (Chapters 3,4).

SECTION C : THE CUMULATE SEQUENCE IN THE UPPER CRITICAL ZONE, AMANDELBULT Description of the cumulate sequence and cyclic units in the interval between the UG-1 chromitite layer and the Bastard Reef at Amandelbult, together with new mineralogical and whole-rock chemical data (Chapters 5,6).

SECTION D : IRON-RICH ULTRAMAFIC PEGMATITE This is the main part of this study, comprising sections on field relationships, petrography, mineralogy (of silicate, oxide and sulphide phases), whole-rock chemistry, formation, and summary/conclusions (Chapters 7 - 14).

CHAPTER 2

THE DISTRIBUTION AND MAIN GEOLOGICAL FEATURES OF DISCORDANT BODIES OF MAGNESIAN DUNITE AND IRON-RICH ULTRAMAFIC PEGMATITE

Discordant bodies of postcumulus, ultramafic rock in the layered sequence of the Bushveld Complex are categorised into a number of groups. Three of these, namely non-platiniferous magnesian dunites, the platiniferous ultramafic pipes, and the main suite of iron-rich ultramafic pegmatite, are then discussed in detail. This includes a comprehensive literature review. The distribution of some of these bodies is documented and the major occurrences are depicted on a series of regional maps. This chapter is partly based on a joint publication with Dr. M.J. Viljoen (Viljoen & Scoon, in press).

2.1 INTRODUCTION

Discordant bodies of postcumulus rock that transgress the layered cumulates are a characteristic feature of many large layered intrusions (see also Chapter 13). Within the Bushveld Complex a number of distinct, but possibly genetically related groups of transgressive, postcumulus ultramafic rock are recognized. Discordant bodies of ultramafic rock were first described from the Bushveld Complex by Wagner (1925, 1929).

Wagner recognized that "hortonolite dunite" may occur in two distinct associations. In the first of these it forms a core, which is invariably platiniferous, enclosed within a large, pipe-like body composed essentially of magnesian dunite. Similar composite pipes occur in which the platiniferous core is characterised by olivine more magnesian than hortonolite. For this reason, and because of their composite character, these discordant bodies of ultramafic rock are described as **platiniferous ultramafic pipes**. Although restricted to only four occurrences they include the famous mines of Driekop, Mooihoek and Onverwacht, which were once the major source of platinum in the Transvaal.

In the second association recognized by Wagner, hortonolite dunite is intimately associated with pegmatitic wehrlites and clinopyroxenites, in which Ti-magnetite and ilmenite are major constitutents. In this association, in which magnesian dunite does not occur, the hortonolite dunite is normally non-platiniferous. Wagner recognized over sixty separate occurrences of hortonolite dunite in the Bushveld Complex, of which the

majority were non-platiniferous. These are categorised in this study with the main suite of iron-rich ultramafic pegmatite.

It is suggested that these two classes of transgressive, ultramafic rock, namely platiniferous ultramafic pipes and iron-rich ultramafic pegmatite, should be considered as entirely separate phenomena until convincing evidence is presented to argue otherwise. It is important to emphasize that the dominant lithology in the platiniferous ultramafic pipes is magnesian dunite, which is usually more primitive than its host cumulates. In contrast, iron-rich ultramafic pegmatite is always more fractionated than its cumulate host.

Another important group of transgressive ultramafic rock is also described in this chapter. These rocks, for which the name non-platiniferous magnesian dunite is selected, are poorly understood and need to be studied further. Although by no means as abundant as iron-rich ultramafic pegmatite they appear to be widely distributed in the lower and lower critical zones of the Bushveld Complex.

With the recent expansion of mining activity, coupled with the results of detailed ground and helicopter-borne magnetic surveys, it has become evident that discordant bodies of iron-rich ultramafic pegmatite are widely distributed through parts of the Bushveld Complex. They are particularly abundant in the upper critical and main zones. In this chapter some new information from field and underground mapping, together with detailed magnetic data is collated with an overview of the available literature. The majority of occurrences described here have been re-examined by the author and categorised within the new nomenclature scheme.

Not all of the occurrences documented within the literature can be categorised within the classifications proposed in this study and it is likely that new subdivisions will be required as these enigmatic rocks become better known. In addition to the platiniferous ultramafic pipes, other commercially significant discordant pipe-like bodies in the Bushveld Complex include the nickel-rich Vlakfontein bodies and vanadium-rich magnetite plugs such as the Kennedy's Vale occurrence. None of these pipe-like orebodies is presently being mined and paradoxically many of the discordant bodies of ultramafic rock have a detrimental effect on modern mining activities. The iron-rich ultramafic pegmatite suite, except in specific situations, e.g., where they replace a cumulate orebody such as the Merensky Reef, is unlikely to contain exploitable reserves of precious or base-metals.

2.2 NOMENCLATURE

The name "iron-rich ultramafic pegmatite" has been selected to describe discordant bodies of postcumulus rock, composed essentially of iron-rich olivine (essentially hortonolite), clinopyroxene, ilmenite and Ti-magnetite, with accessory base-metal sulphide (predominantly pyrrhotite), which occur in the layered sequence of the Bushveld Complex. These rocks are always more fractionated than their host cumulates. Compositionally they are unusual and similar layered cumulates are not known in the Bushveld Complex. Further, as far as the author is aware, primary silicate liquids of a suitable composition have never been reported in the literature. Characteristic features include the iron-rich nature of the major silicates and the abundance of Fe-Ti oxides and iron-rich sulphides. Chromite is not normally observed although hybrid Cr-Ti-magnetite spinel may occur. The nature of the pyroxene (orthopyroxene occurs only as an accessory constituent) and the paucity of felsic phases are further distinguishing features. Included in the iron-rich ultramafic pegmatite suite are the magnetite-bearing pegmatites described by Cameron and Desborough (1964) and the diallagite and magnetite pegmatoids of Willemse (1969a). The name "pegmatoid" was introduced by Willemse, but as Irvine (1982) points out, this is really superfluous. It is suggested that pegmatoid, because it is so entrenched in Bushveld literature, should be restricted to use as a textural prefix for suitable cumulate rocks. This enables texturally pegmatitic cumulates (e.g., the Merensky Reef at Amandelbult) to be distinguished from postcumulus, transgressive, iron-rich ultramafic pegmatite.

The iron-rich ultramafic pegmatites are readily incorporated into Jahns (1955) definition of "pegmatite" as specifying "holocrystalline rocks that are at least in part very coarse-grained, whose major constitutents include minerals typically found in ordinary igneous rocks, and in which extreme textural variations especially in grain size are characteristic". Jahns' suggested that pegmatites could be further classified using accepted plutonic rock nomenclature without invoking any genetic constraints. Within the generic suite of iron-rich ultramafic pegmatite specific members such as dunite, wehrlite, Fe-Ti oxide-wehrlite etc., can be distinguished. It is important to realise that a distinction is made between a magnesian dunite, or dunite sensu stricto, and an iron-rich ultramafic pegmatite which itself may be dunitic. The iron-rich ultramafic pegmatite suite comprises a group of highly fractionated rocks which obey the genetic constraints implied by use of the name "pegmatite".

2.3 CLASSIFICATION

Various authors, including Wagner (1929), Söhnge (1963), and Willemse (1969a) have reviewed the different types of transgressive, postcumulus ultramafic rock that occur in the layered sequence of the Bushveld Complex. The following classification is proposed here :

GROUP 1 NON-PLATINIFEROUS MAGNESIAN DUNITE : this group is described here for completeness although they do not form a major part of this study.

GROUP 2 PLATINIFEROUS ULTRAMAFIC PIPES : these are composite bodies which may be interpreted as a combination of groups 1 and 3.

GROUP 3 IRON-RICH ULTRAMAFIC PEGMATITE : two subgroups are recognized -
- 3.1 silicate-rich (typical) variety in which Fe-Ti oxides are subordinate to olivine and clinopyroxene; and
- 3.2 Fe-Ti oxide pegmatite.

GROUP 4 Other bodies not described in this thesis include :
- 4.1 Vlakfontein nickel pipes
- 4.2 Orthopyroxenite pegmatite
- 4.3 Anorthositic pegmatite
- 4.4 Vermiculite pegmatite; and
- 4.5 Amphibolite or shonkinite bodies.

The Vlakfontein nickel pipes , which are restricted to a small area of the western Bushveld Complex, are composed essentially of orthopyroxenite and massive sulphide (Wagner, 1929; Schwellnus, 1935; Söhnge, 1963; Liebenberg, 1970; Vermaak, 1976a). Orthopyroxenite pegmatite, which may locally be feldspathic, occurs in the critical zone rocks exposed in some of the platinum mines of the western Bushveld Complex. A provisional examination suggests that these represent reconstituted cumulates and are unrelated to the iron-rich ultramafic pegmatite suite (see also Bristow & Wilson, 1983). Anorthositic bodies, composed almost essentially of calcium-rich plagioclase (which may suggest a relationship with the iron-rich ultramafic pegmatite suite) and pipe-like bodies of vermiculite occur in the upper zone of the eastern Bushveld Complex (Willemse, 1969a; Von Guenewaldt, 1973). In the eastern Bushveld Complex, on the farm Tweefontein, Ferguson and McCarthy (1970) describe an "ultramafic pegmatoid" which is composed of an assortment of

rounded inclusions, of which feldspathic amphibolite is the most abundant, in an ultramafic matrix. This body clearly displays an origin by violent emplacement and does not fall within the classification of iron-rich ultramafic pegmatite presented here. It may possibly be similar to pipe-like bodies of shonkinite, inferred to be of Pilanesberg age, described from the farm Grootkuil in the northern sector of the western Bushveld Complex (Ianello, 1967).

2.4 GROUP 1 : NON-PLATINIFEROUS MAGNESIAN DUNITE

This group of discordant ultramafic rocks, although entirely separate from the main class of iron-rich ultramafic pegmatite, is described here for completeness. They are composed essentially of magnesian dunite which is texturally and mineralogically comparable with typical cumulate dunites from the Bushveld Complex. Distinguishing features are the composition of the olivine (a magnesian variety) and the presence of accessory chromite. Schwellnus et al. (1962) describe a number of these bodies from the farms Clapham and Klipfontein in the northern sector of the eastern Bushveld Complex (fig. 2.1) where they occur as discordant, pipe-like features which clearly cut cumulate bronzitite and chromitite of the lower and lower critical zones. Olivine may occur in the cumulates adjacent to the transgressive dunite. Schwellnus et al. (1962) interpreted these bodies as intrusive, and concluded that they formed from a much earlier magmatic event than that which resulted in the iron-rich ultramafic pegmatites which are found in the same area, but much higher in the succession. Field relationships examined by the author support this hypothesis as the adjacent layered cumulates may be severely buckled and fractured. Similar dunitic bodies are described from the lower and lower critical zones of the western Bushveld Complex by Coertze (1962, 1974). They are particularly abundant in an area west of the Pilanesberg where they are apparently concentrated in an elongated belt adjacent to the Rustenburg Fault.

These discordant bodies of magnesian dunite are apparently restricted to the lower and lower critical zones of the Bushveld Complex. From a brief examination it is tentatively suggested that they are intrusive, not metasomatic features, resulting from remobilization and tectonism of pre-existing cumulate dunites. Similar transgressive bodies of magnesian dunite occur in the ultramafic series of the Stillwater Complex (see Chapter 13).

To the north of the Steelpoort valley in the eastern Bushveld Complex, on the farm Maandagshoek, a number of large, pipe-like, bodies transgress the critical zone cumulates (figs. 2.1, 3.1). These bodies, which have been

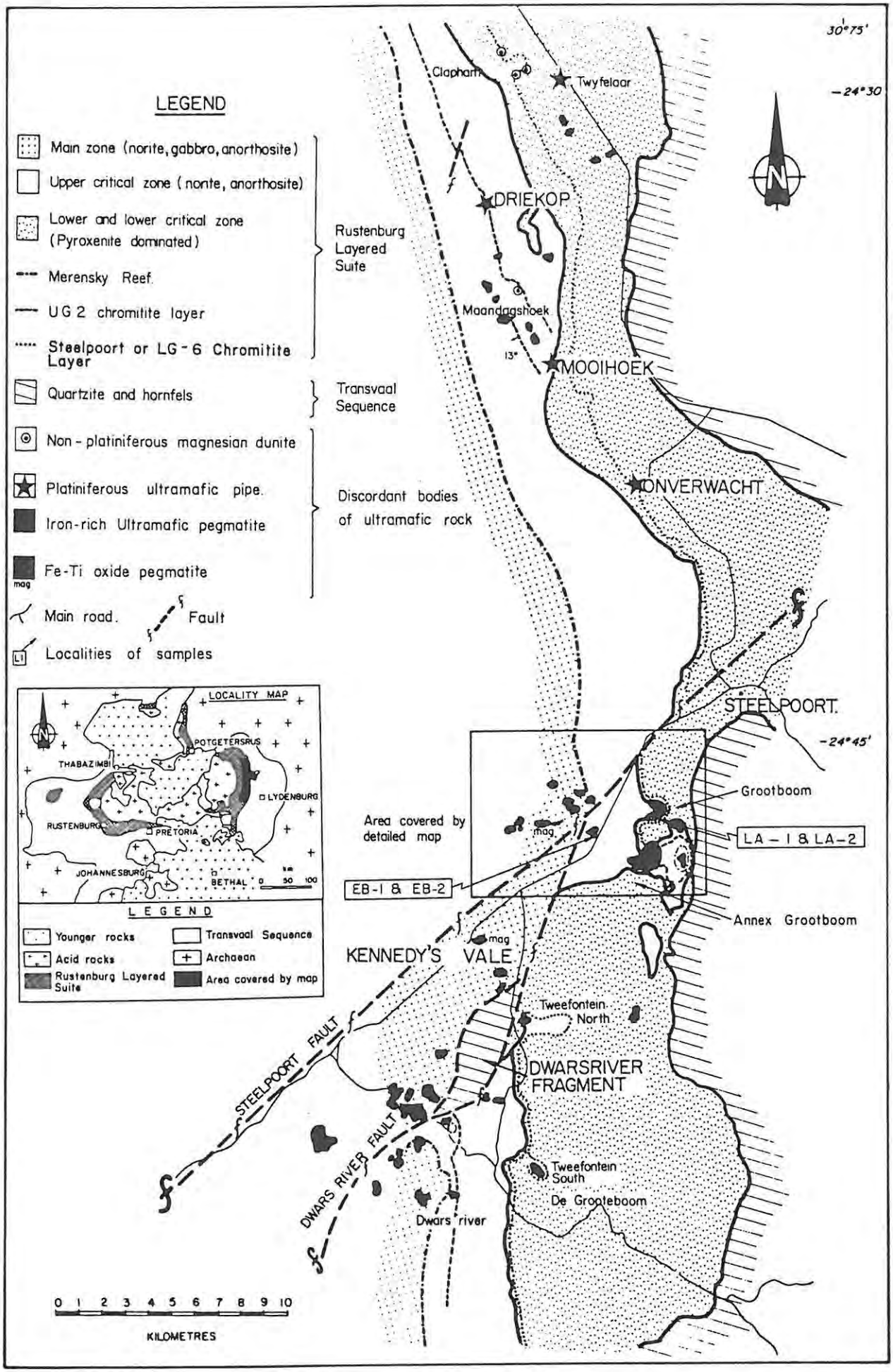

FIGURE 2.1 Geological setting of discordant bodies of ultramafic rock in the eastern Bushveld Complex.

described by Gain (1980), may have a core composed of olivine and orthopyroxene with accessory chromite, and a peripheral zone of wehrlite. Only three large bodies crop out, but Gain recognized a number of other occurrences from a detailed magnetic survey. He observed that these bodies are aligned along major NE-SW lineaments. Information from borehole cores showed that the cumulate sequence adjacent to some of these pipes is downwarped and attenuated, forming collapse structures similar to that around the Driekop platiniferous pipe (see Chapter 3). Both the olivine and orthopyroxene in these bodies are magnesian varieties which, together with the presence of chromite, suggests that they may be categorised as non-platiniferous magnesian dunite. They do not fall within my classification of iron-rich ultramafic pegmatite. The possibility that they may contain cores of platiniferous iron-rich dunite or wehrlite cannot be discarded.

2.5 GROUP 2 : THE PLATINIFEROUS ULTRAMAFIC PIPES

2.5.1 INTRODUCTION

The platiniferous ultramafic pipes comprise only four main occurrences. These include the once famous mines on the farms Driekop, Mooihoek and Onverwacht and a subeconomic body which occurs on the farm Twyfelaar. They appear to be unique to a 20 km linear belt within the eastern Bushveld Complex (figs. 2.1, 3.1). They are composite, pipe-like bodies which are aligned roughly at right angles to the cumulate layering. The pipes consist of large, downward tapering, annular bodies of magnesian dunite which enclose a core zone composed of coarse-grained or pegmatitic iron-rich dunite and wehrlite. An outer shell of pegmatitic iron-rich wehrlite or clinopyroxenite may occur (fig. 2.2). Platinum-group elements (PGE) and base-metal sulphides are essentially restricted to the core zone which represents only a small proportion of the overall pipe. Olivine from the platiniferous cores and pegmatitic outer shells is more iron-rich than that in the main body of magnesian dunite. The platiniferous ultramafic pipes cut both the lower and upper critical zone cumulates. A distinctive feature of the Driekop pipe is that the layered cumulates around the pipe are downwarped and form a major collapse structure (Mossom, 1977).

2.5.2 LITERATURE REVIEW

The most detailed description of these bodies is that by Wagner (1925, 1929) with subsequent contributions by Bateman (1951), Lombaard (1956),

Heckroodt (1959), Söhnge (1963), Cameron and Desborough (1964), McTaggart (1971), Tarkian and Stumpfl (1975), Cabri (1981), Peyerl (1982), Schiffries (1982) and Stumpfl and Rucklidge (1982).

PETROLOGY

Wagner (1929) classified dunitic platinum deposits in general into two groups : (1) Iron-rich dunites (Bushveld type) in which platinum-group elements (PGE) are associated with either hortonolite or hyalosiderite dunites or wehrlites; and (2) Iron-poor dunites (Uralian type) in which PGE are associated with chrysolite or forsterite dunite. In the Bushveld Complex economic concentrations of PGE are not known from cumulate dunites, and are apparently restricted to the discordant pipe-like bodies described here. In the pipes PGE are essentially restricted to the iron-rich rocks (dunites, wehrlites, or pegmatites) which occur as cores within a main body of magnesian dunite.

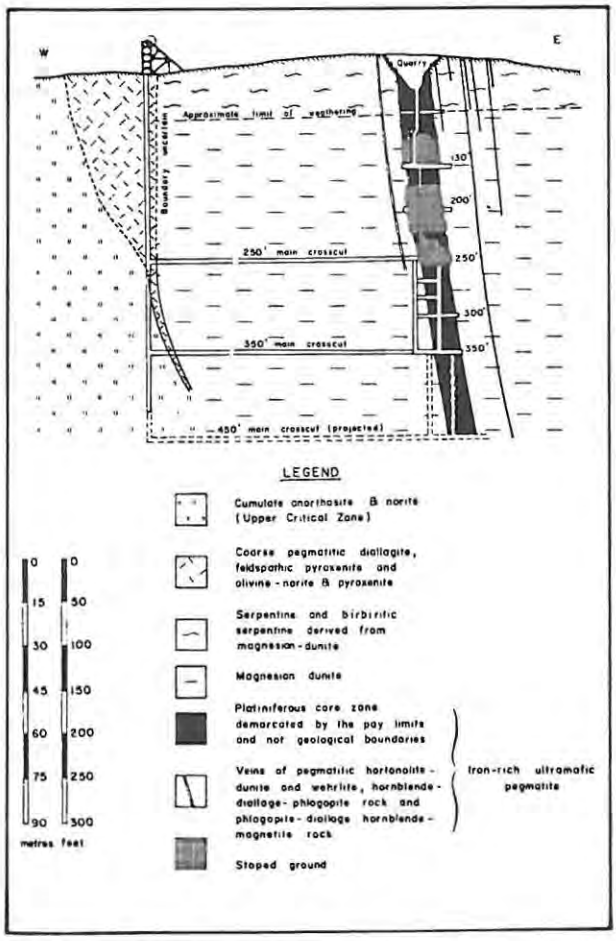

FIGURE 2.2 Schematic section through the Mooihoek pipe (after Wagner, 1929).

The platiniferous ultramafic pipes are composed of up to three, concentric, petrologically distinct units, as described above (see fig. 2.2). The main assemblage in each pipe is a magnesian dunite; this is essentially similar to cumulus magnesian dunites from the layered sequence. The core zone in each pipe is, however, different. The core of the Mooihoek pipe consists of platiniferous hortonolite dunite and wehrlite, with segregations of massive Ti-magnetite and ilmenite. Hornblende and phlogopite are also present in this core. At Driekop, hornblende, phlogopite and magnetite are found only as accessory constituents in the hyalosiderite dunite and wehrlite. The core of the Onverwacht pipe is composed of hyalosiderite dunite and wehrlite (Wagner, 1929; Lombaard, 1956; Cameron & Desborough, 1964).

The core of the Mooihoek pipe was apparently sharply defined (Wagner, 1929). In contrast the Driekop orebody (now mostly mined out) occurred as a poorly defined core in which platiniferous hyalosiderite dunite and wehrlite

were found as small, irregular bodies and lenses within the main body of magnesian dunite. A plan of the 160-foot level at the Driekop mine, (fig. 2.3B) shows fourteen discrete ore shoots within the core area, whereas a composite grade plan of the Mooihoek orebody, (fig. 2.3A) illustrates that this was a single unit, confined roughly within the contact between the iron-rich core and the magnesian dunite.

At both the Driekop and Mooihoek pipes, which are emplaced within plagioclase-rich cumulates of the upper critical zone, an outer shell of pegmatitic wehrlite and diallagite encloses the magnesian dunite. It is absent at the Onverwacht pipe which, unlike the other pipes, transgresses pyroxenites and chromitites of the lower critical zone.

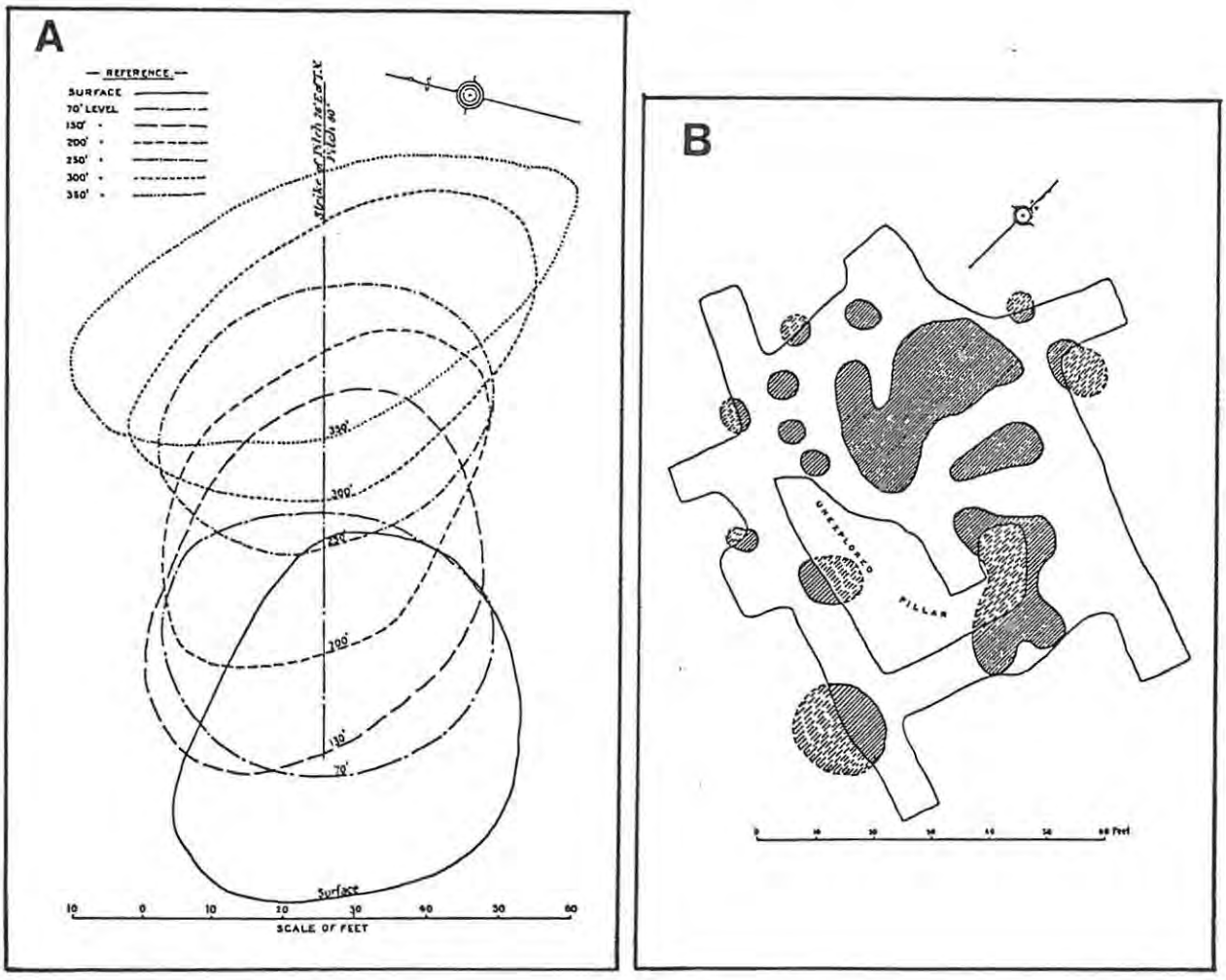

FIGURE 2.3

Pay zones in the Mooihoek and Driekop pipes (after Wagner, 1929). Composite plan of pay contours from surface to the 300 foot level illustrate that the orebody in the Mooihoek pipe (a) formed a continuous, cylindrical core, whereas a plan of the 160 foot level indicates that the orebody at Driekop (b) comprised a number of separate ore shoots within a central core-area.

Pegmatitic veins cut the magnesian dunite in all three pipes, usually adjacent to and parallel with the cores. At the Mooihoek pipe a conjugate set, which Wagner (1929) interpreted as occupying shrinkage cracks within the magnesian dunite, is composed of pegmatitic hortonolite, diallage, hornblende, phlogopite, magnetite and ilmenite. Only those veins that carried hortonolite were platiniferous. At the Dreikop mine platiniferous veins of hyalosiderite-diallage pegmatite were found in both the magnesian dunite and the adjacent cumulate wallrocks. A range of pyroxenitic pegmatite bodies occurs in the cumulate wallrocks adjacent to the Driekop pipe (Schiffries, 1982).

STRUCTURE

The platiniferous ultramafic pipes form strongly discordant features which clearly cut the layered cumulates. The Driekop and Mooihoek pipes are presently exposed in the upper critical zone, whereas the Onverwacht pipe is exposed in the lower critical zone. They form pipe-like bodies which are orientated roughly at right angles to the layering in the cumulate sequence. It may be inferred that they were emplaced when the layering was subhorizontal. The vertical extent of the pipes is not known. The orebodies at the Mooihoek and Onverwacht mines were reported as pinching out in depth. Wagner describes the core of the Onverwacht pipe as dividing into three small "roots" below the 350-foot level, of which two are represented by irregular, discontinuous bodies below the 450-foot level. The Driekop orebody, which was stoped down to a depth of approximately 180 m, showed no signs of pinching.

Wagner (1929) reported the presence of large, disorientated slabs of chromitite within the Onverwacht pipe, which he interpreted as xenoliths. He suggested that they occur at approximately the same elevation as would be expected if the adjacent LG-6 chromitite layer was undisturbed (fig. 2.4A). By contrast, Cameron and Desborough (1964) interpreted them as partially replaced relicts (fig. 2.4B).

Mossom (1977) and Schiffries (1982) report that the cumulate wallrocks adjacent to the Driekop pipe form a major downwarped structure.

PLATINUM-GROUP ELEMENT MINERALOGY

The PGE mineralogy of the pipes differs greatly from that of cumulate orebodies, such as the Merensky and UG-2 Reefs. For example, in the pipes there are no PGE-Bi-tellurides and PGE-sulphides are rare (Cabri, 1981). A definitive study of the platinum-group minerals (PGM) in the Driekop orebody by Tarkian and Stumpfl (1975) indicates that over 50 percent of these are Pt-

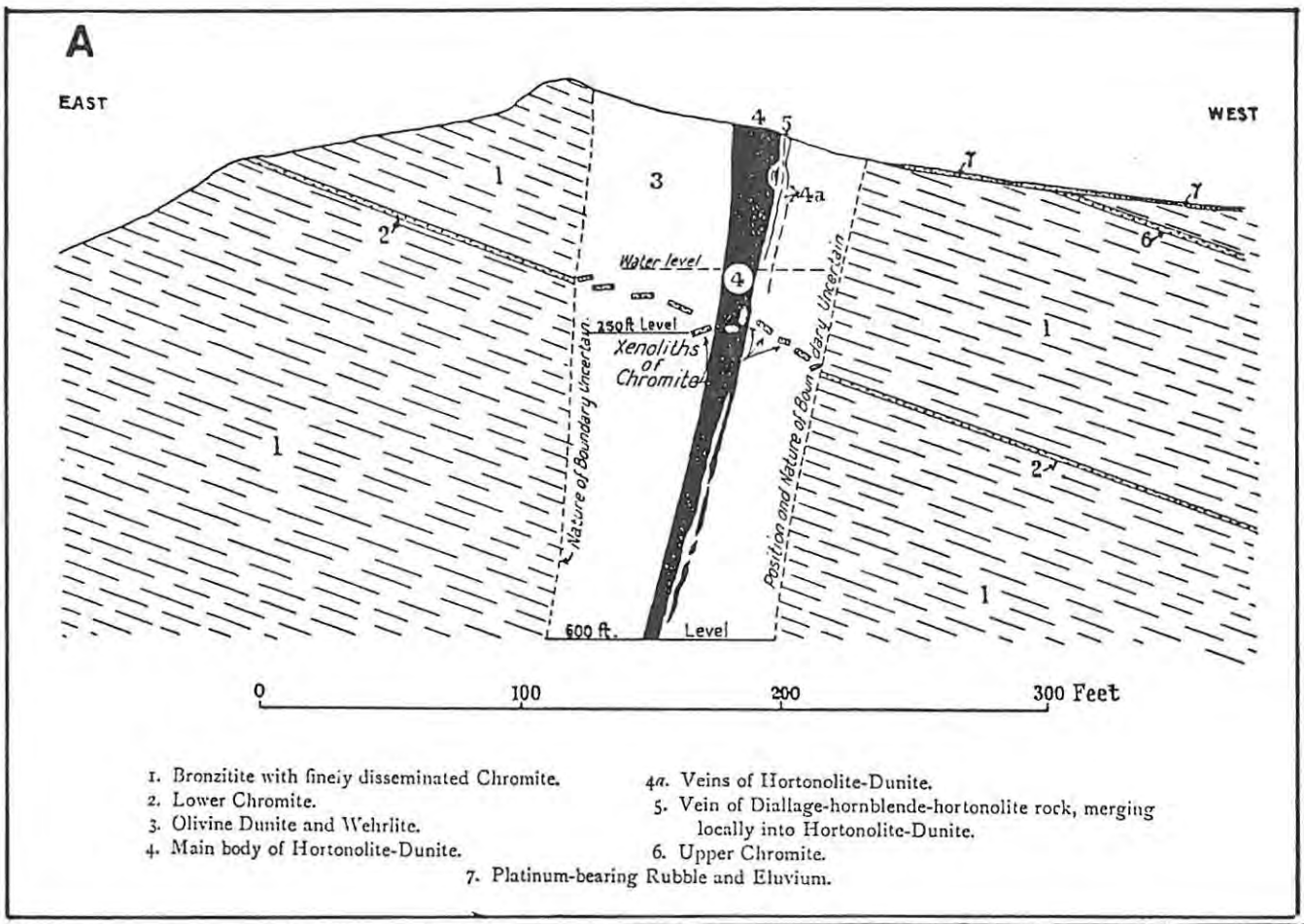

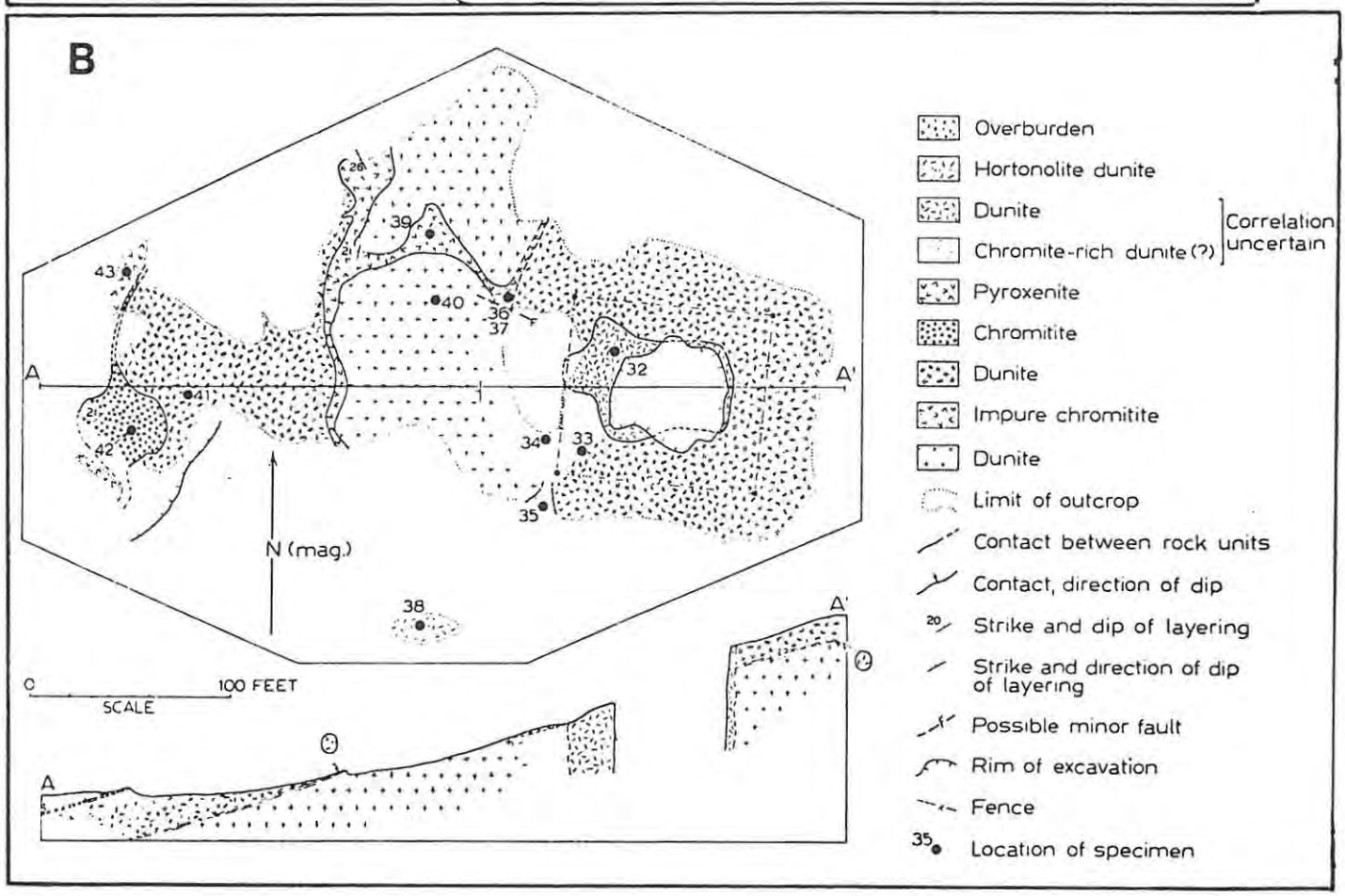

FIGURE 2.4 Structure of the Onverwacht pipe : (a) after Wagner (1929) and (b) after Cameron & Desborough (1964).

Fe alloys, with sperrylite ($PtAs_2$) and geversite ($PtSb_2$) accounting for 30 percent and hollingworthite (RhAsS) and irarsite (IrAsS) comprising 15 percent. They also describe several new PGM. Other ore minerals associated with these PGM are chalcopyrite, pyrrhotite, pentlandite, valleriite, native copper and gold. Cabri and Hall (1972) described two new minerals, mooihoekite ($Cu_9Fe_9S_{16}$) and haycockite ($Cu_4Fe_5S_8$) from Mooihoek. According to Peyerl (1982) the Driekop pipe has had a marked effect on the composition of the platinum-group phases in the adjacent UG-2 chromitite layer. Peyerl evaluated 1327 discrete precious-metal grains, which showed a progressive change from Pt-Fe alloys and PGE arsenides and antimonides adjacent to the pipe to a mineralogical assemblage similar to a "typical" Merensky/UG-2 Reef-type further away.

GENESIS

Wagner (1929) interpreted these pipes as intrusive features. He concluded that the platiniferous, iron-rich dunite, wehrlite and pegmatite in the cores of these pipes resulted from crystallization of a silicate melt that was introduced after intrusion and cooling of the magnesian dunite. He attributed the anomalous concentrations of PGE to a combination of primary magma content and to leaching from the layered cumulates that the pipes transgressed. By constrast, Cameron and Desborough (1964) suggest that the Onverwacht pipe resulted from in situ metasomatic replacement of the layered bronzitites. Field relationships (compare figs. 2.4A & B) are equivocal. The Driekop pipe has been investigated by several workers most of whom support an origin by in situ replacement. Schiffries (1982) attributes the formation of the dunite to reactions between low-temperature chloride solutions, that were channelled by a structural weakness in the axis of the pipe, and the noritic host rocks. The most important reactions were desilication of orthopyroxene to form olivine and dissolution of plagioclase. Cation exchange of Fe^{2+} for Mg^{2+} in the presence of chloride complexes resulted in the formation of an iron-rich olivine in the core of the pipe. Irvine (1982) describes the Onverwacht pipe as a "classic example of infiltration metasomatism" (see Chapter 13).

Although the replacement argument has been favoured by most recent authors this is by no means universally accepted. The recognition of a major collapse structure in the layered rocks adjacent to the Driekop pipe during recent mining activities presents a major problem to metasomatic models.

2.6 GROUP 3.1 : IRON-RICH ULTRAMAFIC PEGMATITE

2.6.1 REGIONAL DISTRIBUTION

Bodies of iron-rich ultramafic pegmatite are abundant in the upper critical and main zones, but are rare in the lower and lower critical zones. This stratigraphic control can be related to the presence of plagioclase as a major cumulus phase and the subsequent widespread formation of anorthositic layers in the cumulate pile. The distribution of these bodies, particularly the large pipe-like occurrences, is also controlled by structural features and they characteristically occur in disturbed areas marked by extensive faulting and post-Bushveld dykes. There appears to be a distinct relationship between the mineralogy of these bodies and their stratigraphic position. Pegmatites in the critical zone are essentially the silicate-rich variety and Fe-Ti oxide pegmatite is rarely observed below the main zone. In the upper zone Fe-Ti oxide pegmatite is the dominant variety. In the main zone and the lower parts of the upper zone composite silicate-rich and Fe-Ti oxide pegmatites are often observed. Both the silicate-rich and Fe-Ti oxide pegmatites exhibit cryptic mineralogical trends and it is evident that the iron-rich ultramafic pegmatites become increasingly fractionated with stratigraphic height. The major occurrences of silicate-rich pegmatite are documented below; the Fe-Ti oxide pegmatite bodies are described separately.

2.6.2 EASTERN BUSHVELD COMPLEX

Iron-rich ultramafic pegmatite bodies are particularly abundant in areas adjacent to the Steelpoort valley, but are apparently rare in the extreme northern and southern sectors of the eastern Bushveld Complex. In the vicinity of the Dwarsriver and Steelpoort faults a number of bodies occur on the farms De Goede Verwachting, Grootboom, Annex Grootboom, and along the Dwarsriver fragment. Another cluster occurs further south on the farms Tweefontein and De Grootboom (figs. 2.1, 2.5). North of the Steelpoort valley iron-rich ultramafic pegmatites are particularly abundant on the farms Klipfontein, Driekop and Goedverwacht (Schwellnus et al., 1962). Many of these bodies are well exposed and give rise to positive topographic features.

Wagner (1929) was the first to describe these iron-rich ultramafic pegmatite bodies, and he discusses occurrences from Dwarsriver and Grootboom. Field relationships enabled him to establish that the pegmatite

occurs preferentially in anorthositic cumulates, at the expense of more mafic cumulates, such as bronzitite and chromitite. This results in the formation of large, stratabound, sheet-like bodies which are vertically constrained over large areas. Cameron and Desborough (1964) investigated sheet-like bodies of iron-rich ultramafic pegmatite on the farms Grootboom, Annex Grootboom, Tweefontein, and De Grootboom. The pegmatites here cap large hills, selectively replacing a series of critical zone leuconorites over individual areas of 3.5 km^2 in the case of the largest body on Annex Grootboom. Here, two major chromitite layers (the X and Y layers - part of the MG series) can be traced around the hill and appear as relict cumulus layers within the pegmatite. Feldspathic pyroxenites adjacent to these chromitites are only partially replaced by pegmatite. These features are repeated at other exposures in this area and strongly suggest a replacement origin for these bodies (Wagner, 1929; Cameron & Desborough, 1964; see figs. 2.5, 2.6).

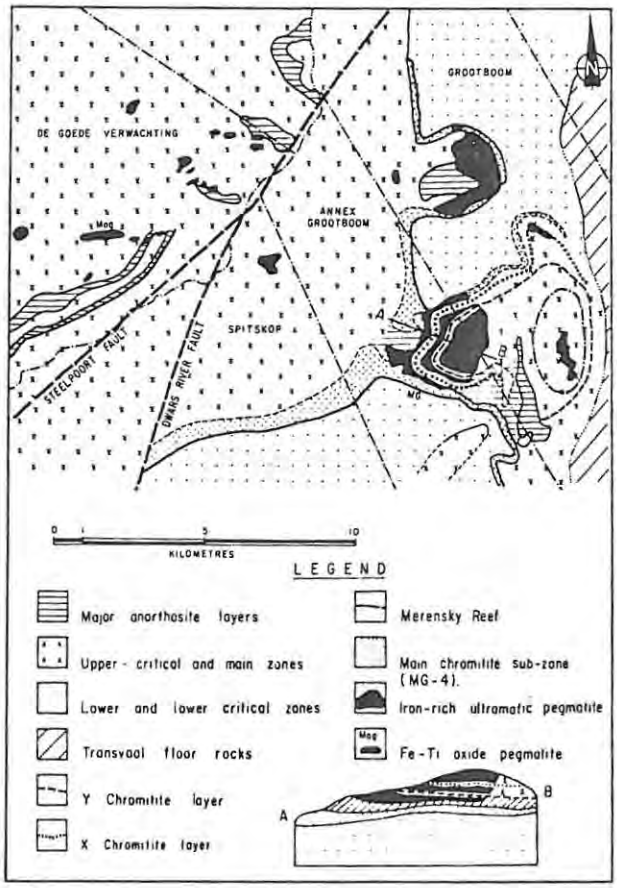

FIGURE 2.5 Iron-rich ultramafic pegmatite bodies in the Steelpoort and Dwars River area, eastern Bushveld Complex.

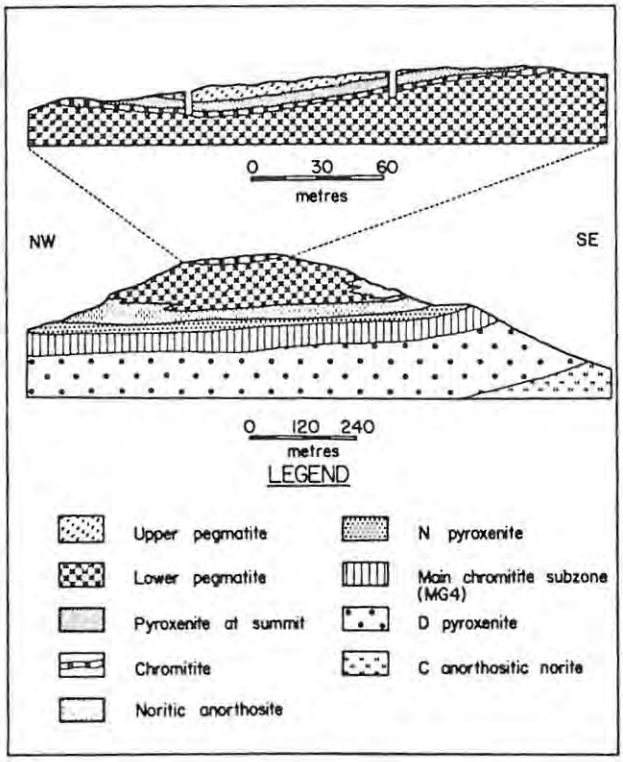

FIGURE 2.6 Cross-section of the iron-rich ultramafic pegmatite body on Tweefontein (after Cameron & Desborough, 1964).

2.6.3 SOUTHERN SECTOR OF THE WESTERN BUSHVELD COMPLEX

The map presented in Figure 2.7 has been compiled from the latest available mapping, Wagner's (1929) map and the results of an helicopter-borne magnetic survey over the lower part of the main zone between the Pilanesberg and the farm Rooikoppies, east of Rustenburg. A clustering of large bodies of iron-rich ultramafic pegmatite occurs in the vicinity of the UG-2 chromitite layer and the Merensky and Bastard Reefs. These include a number of large pipes on the farm Boschkoppie and the major pipe-like bodies of Townlands and Brakspruit. A number of smaller bodies also occur at this stratigraphic level between the latter two occurrences. The iron-rich ultramafic pegmatite bodies correlate with distinct magnetic anomalies, which are clearly discordant to the layered cumulates (the critical and main zone rocks are only very weakly magnetic). Typically they define ellipsoidal anomalies which are indicative of subvertical, fairly extensive pipe-like features. In this area of the Bushveld Complex the iron-rich ultramafic pegmatite bodies which occur at the boundary of the critical and main zones have negative , reversely polarised, magnetic anomalies. This is unusual as in the Amandelbult area in the northern sector of the western Bushveld Complex, at the same stratigraphic interval, they are normally polarised. This feature may indicate that the pegmatites in these two areas crystallized at different times.

For a distance of some 30 km between the farms Wildebeestfontein and Rooikoppies, in an area of minor structural disturbance, the lower part of the main zone is virtually devoid of iron-rich ultramafic pegmatite bodies. In this area three striking linear magnetic anomalies have been recognized (Viljoen & Burvenich, 1983; see fig 2.7). These give a much weaker anomaly than the iron-rich ultramafic pegmatites but are still very distinctive. Von Backström et al. (1960) related the presence of a number of "dunite" pipes that occur in the Rustenburg area to a linear magnetic anomaly situated just above the Merensky Reef. This is inferred to represent the linear anomaly between the Townlands and Brakspruit pipes which may be related to the giant mottled anorthosite layer at the top of the Bastard cyclic unit. Some 500 m above the Merensky Reef a second linear magnetic anomaly has been recognized on which is superimposed a number of discrete anomalies indicating the presence of abundant iron-rich ultramafic pegmatite. These bodies of pegmatite correlate with positive magnetic anomalies. This linear anomaly is related to an anorthositic assemblage (some 90 m thick) in the main zone. A third linear anomaly occurs 900 m above the Merensky Reef and is again related to an anorthosite layer. These well defined linear magnetic

FIGURE 2.7 Geological setting of discordant bodies of ultramafic rock in the southern sector of the western Bushveld Complex.

anomalies break down in structurally disturbed areas, which are characterized by faulting and post-Bushveld dykes. To the east and northwest of the relatively undisturbed area noted above, abundant scattered magnetic anomalies indicate the position of iron-rich ultramafic pegmatite bodies. Most of these bodies have a positive magnetic signature and are normally polarised.

A number of investigaters have referred to the occurrence of individual bodies of iron-rich ultramafic pegmatite in this area. Wagner (1929) described two such bodies from Doornspruit and Kookfontein in the Rustenburg area (fig. 2.7). These pegmatites occur within the Merensky cyclic unit and, although other, similar, pegmatites in the area were found to be non-platiniferous, these bodies were enriched in PGE. The platiniferous nature of these pegmatites, which elsewhere are usually depleted in PGE, is attributed to leaching from the cumulates (Wagner, 1929; see Chapter 11). Coertze (1974) describes a composite, pipe-like body from the farm De Kroon near Brits (fig. 2.7). This body has a core composed of magnesian dunite and harzburgite and should possibly be placed within my classification as a non-platiniferous magnesian dunite. From the Bafokeng area west of Rustenburg, Jones (1974, 1976) describes large pipe-like bodies of iron-rich ultramafic pegmatite, which may have diameters in excess of 300 m, as well as many small, irregular, often mushroom-shaped masses.

Underground development coupled with diamond drill holes allowed for a detailed examination of the Townlands pipe, situated 5 km to the north-northwest of Rustenburg (Viljoen et al., 1983). This is a large, composite, pipe-like body of iron-rich ultramafic pegmatite in a which a roughly defined core zone of hortonolite dunite pegmatite may be distinguished from wehrlite pegmatite. It crops out over the extrapolated position of the Merensky Reef and although poorly exposed gives rise to a distinctive red soil. The diameter of the pipe is estimated at 450 m. From a combined magnetic (both ground and airborne) and gravity survey, computer modelling infers that the Townlands pipe has a vertical extent of probably not more than 500 m and does not penetrate the floor of the layered sequence. A soil geochemical survey yielded a copper and nickel anomaly which correlates with both the gravity and magnetic anomalies. The layered cumulates adjacent to the Townlands pipe are downwarped and form a gentle collapse structure, a feature which has not been recognized from other occurrences of iron-rich ultramafic pegmatite. It may be compared with the structural disturbance associated with the Driekop platiniferous ultramafic pipe, although it is less severe. A borehole drilled into the core of the pipe, after passing through several hundred metres of continuous pegmatite, intersected the UG-2 chromitite

layer. This chromitite, together with a leader seam and adjacent cumulus orthopyroxenites are, superficially, unreplaced. Below these relict cumulate layers is typical pegmatite. Their presence suggests that the iron-rich ultramafic pegmatite formed by a process of in situ replacement.

2.6.4 NORTHERN SECTOR OF THE WESTERN BUSHVELD COMPLEX

In this area, iron-rich ultramafic pegmatite bodies have been described from R.P.M. Union and Amandelbult Sections, and the so called "Northern Gap" area between these two mines. They are particularly abundant in the upper critical and main zones adjacent to the gap area, a zone of structural disturbance where the earlier cumulates are displaced, or transgressed by upper zone rocks. In the Northern Gap Coertze and Schumann (1962) and Coertze (1974) describe a number of composite silicate-rich and Fe-Ti oxide pegmatite bodies. At Union Section a large pegmatite body apparently transgresses and terminates the upper critical zone cumulates on the farm Zwartklip. Bodies of iron-rich ultramafic pegmatite are exceptionally abundant at R.P.M. Amandelbult Section, where again they preferentially occur in the upper critical zone and lower part of the main zone. One large pegmatite body occurs at Amandelbult, the so-called Middellaagte pipe (de Bruyn, 1944). These will be discussed further in Chapter 7.

2.7 GROUP 3.2 : Fe-Ti OXIDE PEGMATITE

Disseminated Ti-magnetite and granular ilmenite occur as ubiquitous accessory constituents in typical silicate-rich ultramafic pegmatite. However, the proportion of Ti-magnetite and ilmenite may be such that these rocks are best described as Fe-Ti oxide pegmatite. Discordant bodies of Fe-Ti oxide pegmatite occur as pseudo-stratified sheets, irregular veins, and large pipe-like features. They may occur in association with silicate-rich pegmatite, in composite zoned bodies, or they may form practically pure Fe-Ti oxide bodies. It is emphasized that Fe-Ti oxide pegmatite forms a subgroup within my classification of iron-rich ultramafic pegmatite and it is inferred that there is a direct genetic relationship between the silicate- and oxide-rich varieties. Two types of Fe-Ti oxide pegmatite are recognized :

2.7.1 Cr-RICH Fe-Ti OXIDE PEGMATITE

In the critical zone sheet-like, pseudo-stratified layers composed of a magnetic spinel may occur. These were first described from the Amandelbult

area by Wasserstein (1936). The spinel in this variety of Fe-Ti oxide pegmatite is a hybrid, intermediate in composition between chromiferous spinel and Ti-magnetite. Hybrid Cr-rich Fe-Ti oxide pegmatites were first investigated thoroughly by Cameron and Desborough (1964) from the eastern limb of the Bushveld Complex. The sheet-like nature of these occurrences is a result of the resilient nature of the cumulus chromitites which form relict layers within, and at the margins, of the silicate-rich ultramafic pegmatite bodies (fig. 2.6). Chromite in these relict cumulates exhibits progressive replacement of Cr, Mg, and Al by Fe^{2+}, Fe^{3+}, and Ti (Cameron & Glover, 1973). A complete compositional range from chromiferous spinel to Ti-magnetite may be observed. Similar features have been observed in chromitite layers adjacent to bodies of iron-rich ultramafic pegmatite in the critical zone at Amandelbult. For example, the Merensky upper chromitite layer has been examined by Viljoen et al. (a, in press). The presence of a relict layer, or xenolith, of UG-2 chromitite in the Townlands pipe, near Rustenburg was referred to previously, as were the slab-like bodies of chromitite at Onverwacht. These exhibit similar compositional features to those identified by Cameron and Glover (Lombaard, 1956; Viljoen et al., 1983). In summary, discordant bodies of Cr-rich Fe-Ti oxide pegmatite are restricted to the critical zone. They are related to the formation of postcumulus iron-rich ultramafic pegmatite in the vicinity of cumulus chromitite layers (see Chapter 10).

2.7.2 NORMAL Fe-Ti OXIDE PEGMATITE

Discordant, typically pipe-like bodies composed almost entirely of Cr-poor Fe-Ti oxide pegmatite are abundant in the Bushveld Complex from the middle of the main zone up into the upper zone. Willemse (1969b) observed that pipe-like bodies of magnetite rarely occur above the highest cumulate Ti-magnetite layer. The Fe-Ti oxide in the discordant pegmatite bodies is comparable to cumulus Fe-Ti oxide in the Bushveld Complex, although minor compositional differences may occur (Coertze, 1966, 1974; Van Rensburg, 1965). Fe-Ti oxide from pegmatite bodies in the main zone, below the cumulus Ti-magnetite layers, is relatively rich in vanadium. The Kennedy's Vale body, in the eastern Bushveld Complex (fig. 2.1) has been exploited as a source of vanadium-rich magnetite. Van Rensburg (1965) described the Fe-Ti oxide pegmatite at Kennedy's Vale as forming a core within a much larger, pipe-like body of silicate-rich ultramafic pegmatite. However, Willemse (1969b) interpreted it as a fracture-filling rather than a pipe-like body. Immediately west of the junction between the Steelpoort and Dwarsriver

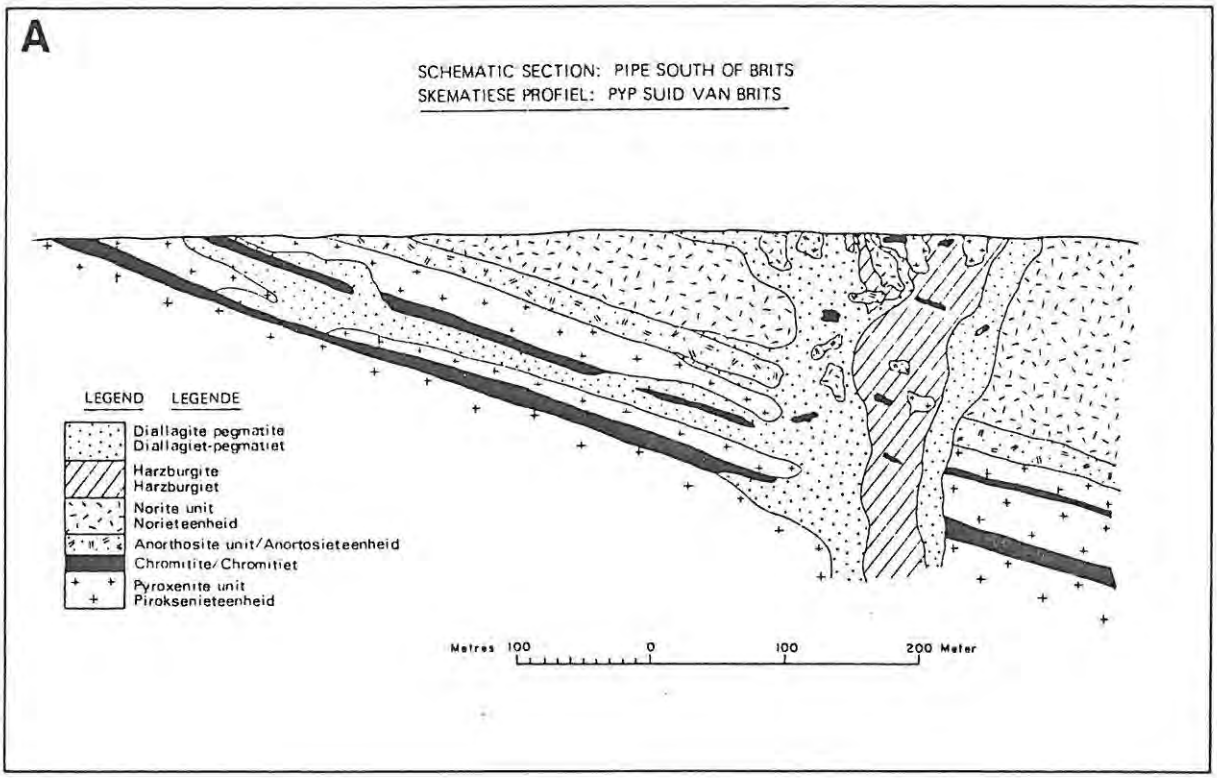

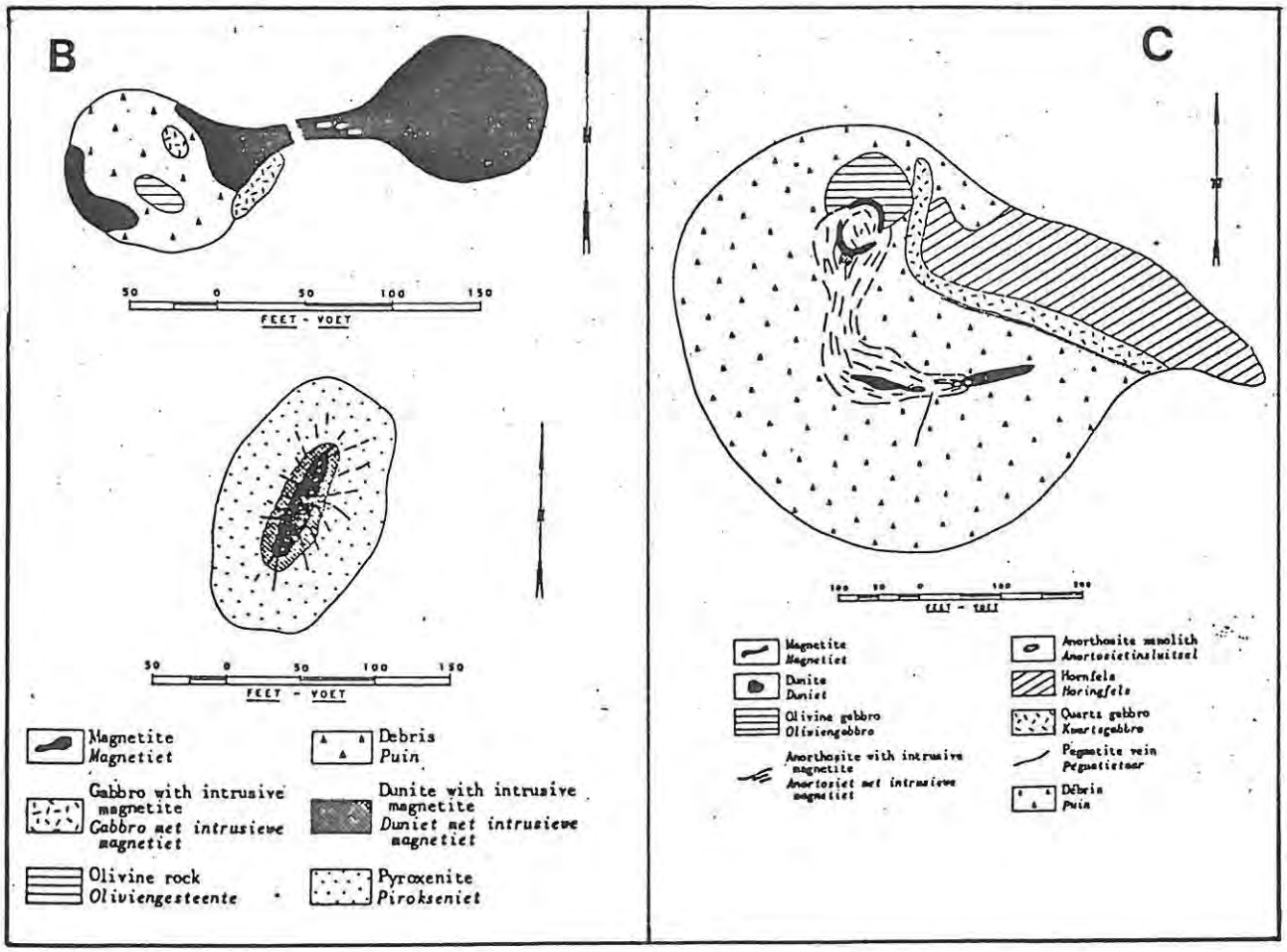

FIGURE 2.8 Some composite bodies of iron-rich ultramafic pegmatite. (a) Composite pipe, south of Brits (after Coertze, 1974). (b,c) Composite silicate-rich and Fe-Ti oxide pegmatite bodies, Goedverwacht (511KS) and Driekop (540KS), eastern Bushveld Complex (after Schwellnus et al., 1962).

faults is a prominent ridge composed essentially of Fe-Ti oxide pegmatite. Pipe-like bodies of Fe-Ti oxide pegmatite are particularly abundant in the lower part of the upper zone in the vicinity of the cumulus Ti-magnetite layers. In an 850 km^2 area of the eastern Bushveld Complex Von Gruenewaldt (1973) mapped over one hundred separate occurrences in the main and upper zones. Similar bodies were mapped in the northern sector of the eastern Bushveld Complex by Schwellnus et al. (1962) and Coertze (1966) and in the western limb of the complex by Coertze and Schumann (1962) and Coertze (1974).

In the eastern Bushveld Complex on the farms Goedverwacht and Driekop Schwellnus et al. (1962) describe a number of composite iron-rich ultramafic pegmatite bodies in which Fe-Ti oxide pegmatite occurs as a massive core within typical silicate-rich pegmatite. Veins and irregular layers of Fe-Ti oxide pegmatite cut both the peripheral silicate-rich pegmatite and the adjacent cumulates (fig. 2.8). The Fe-Ti oxide pegmatite clearly post-dates the silicate-rich pegmatite. Similar composite pegmatite bodies occur in the western Bushveld Complex (Coertze & Schumann, 1962; Coertze, 1974).

2.8 INTRODUCTION TO THE MINERALOGY AND GENESIS OF IRON-RICH ULTRAMAFIC PEGMATITE

Iron-rich ultramafic pegmatites are characterised by a rather simple mineralogy in which olivine, clinopyroxene, ilmenite, and Ti-magnetite are the major constituents. Within the generic group of iron-rich ultramafic pegmatite the dominant lithologies include hortonolite dunite, wehrlite and olivine clinopyroxenite with subordinate olivine websterite. If ilmenite and Ti-magnetite comprise over 10 normative or modal percent the prefix Fe-Ti oxide is applicable but if they predominate over silicate phases the description Fe-Ti oxide pegmatite is preferred (see Chapter 8). Locally plagioclase may be a significant component but it is usually restricted to the small, irregular bodies or the outer margins of large pipe- or sheet-like occurrences; the larger bodies are thus ultramafic in character.

2.8.1 SILICATES

The major silicate components are olivine, usually hortonolite, and clinopyroxene. Amphiboles and micas are common accessory constituents. Orthopyroxene and plagioclase are minor or accessory constituents; they are usually interpreted as relict cumulus minerals and are not directly related to the pegmatites. Cameron and Desborough (1964) investigated the mineralogy

of iron-rich ultramafic pegmatite in the eastern Bushveld Complex, which they interpreted as resulting from replacement of pre-existing cumulates. They observed that at the contacts with anorthositic cumulates clinopyroxene replaces plagioclase first and then orthopyroxene, whereas at the contacts with norites olivine replaces orthopyroxene before clinopyroxene is observed. Second-generation clinopyroxene may replace hortonolite in the main body of pegmatite. Local replacement of cumulus minerals (over contact zones of a few centimetres) may occur but there is no direct mineralogical evidence to suggest that wide-scale metasomatism of pre-existing cumulates is responsible for the formation of these postcumulus rocks. Mineralogical investigations have also been completed by de Bruyn (1944) and Jones (1974).

2.9.2 Fe-Ti OXIDES

Two groups of Fe-Ti oxide may be recognized in iron-rich ultramafic pegmatite : those that have developed at the expense of disseminated, cumulus chromite grains, or cumulus chromitite layers (resulting in hybrid Fe-Ti-Cr spinels), and those that have crystallized in the absence of cumulus chromite directly from the pegmatitic liquids (resulting in Cr-rich Ti-magnetite or Ti-magnetite and ilmenite). The majority belong to this latter category.

2.9.3 BASE METAL SULPHIDES

The principal sulphide is pyrrhotite (usually constituting over 95 modal percent of the bulk sulphide assemblage) with subordinate cubanite, pentlandite and chalcopyrite. Typically the sulphide mineralogy is rather simple and is characteristic of ultramafic-mafic magmatic ores. The bulk sulphide content is highly variable. De Bruyn (1944) investigated the sulphide mineralogy of the Middellaagte pipe. In the Townlands pipe Viljoen et al. (1983) have recognized an unusually diverse precious and base-metal mineralogy. The sulphide mineralogy of iron-rich ultramafic pegmatite has also been studied by Wagner (1929), Van Rensburg (1965), Liebenberg (1970) and Von Gruenewaldt (1979; see Chapter 11).

2.9.4 PLATINUM-GROUP ELEMENT MINERALOGY

Iron-rich ultramafic pegmatite is normally non-platiniferous, although no data in the ppb range are available. Wagner (1929), however, recorded traces of platinum in hortonolite dunite pegmatite which forms the core of a sheet-like body on the farm Dwarsriver in the eastern Bushveld Complex. In

specific circumstances these rocks contain economic or sub-economic levels of PGE. This may be attributed to leaching from the cumulates. At Amandelbult, for example, iron-rich ultramafic pegmatite which replaces the Merensky Reef (the so-called "replaced" Reef) may still contain economic concentrations of PGE. The replaced Reef has a unique, hybrid, precious metal mineralogy (see Chapter 11).

2.9.5 GENESIS

Although Wagner (1929) was convinced of the intrusive origin of the platiniferous ultramafic pipes, he ascribed the formation of sheet-like, pseudo-stratified bodies of iron-rich ultramafic pegmatite to a process of in situ magmatic replacement. A model involving metasomatism of pre-existing cumulates is presented by Cameron and Desborough (1964). Jones (1974) concluded that the metasomatising pegmatitic liquids resulted from migrating intercumulus liquids derived from within the crystallizing cumulate pile. This model is supported by most recent publications and the role of intercumulus liquids is consequently of direct importance (see Chapter 13). However, Willemse (1969a) observed that some of the discordant bodies of ultramafic rock in the layered sequence of the Bushveld Complex are clearly of an intrusive origin, such that in comparison with classic (granitic) pegmatites, both intrusive and replacement models may be applicable.

SECTION B : THE DRIEKOP PIPE

CHAPTER 3 DRIEKOP : FIELD RELATIONSHIPS AND PETROLOGY

The Driekop mine, which had not been operated since 1961, was recently reopened by J.C.I. as part of a feasibility study on the UG-2 chromitite layer. This included development of an exploration crosscut, driven from the old 3 level (97 m) shaft crosscut some 500 m into the cumulate wallrocks. Consequently, a complete radial section of the pipe is now exposed. Because surface exposure of the wallrocks is poor, geologists of J.C.I. were the first to recognize that the cumulates surrounding the Driekop pipe form a major collapse structure (Mossom, 1977). Much of the new structural and geochemical data presented in this thesis has been compiled from mapping and sampling of the section exposed in this new underground development. This section is divided into two chapters. The first of these, Chapter 3, discusses field relationships, structural setting and petrology and presents some new geochemical data. These results, together with some additional mineralogical data, are then collated and discussed in Chapter 4. Because the platiniferous ultramafic pipes are restricted to only four occurrences a realistic model should be applicable to all of these pipes. Consequently information relating to the Mooihoek and Onverwacht pipes is also discussed.

3.1 REGIONAL GEOLOGY

The platiniferous ultramafic pipes are restricted to a 20 km linear belt situated to the north of the Steelpoort Fault, in the eastern limb of the Bushveld Complex (fig. 3.1). Three of the pipes were mined for PGE earlier this century; these are situated on the farms Driekop (253KT), Mooihoek (255KT) and Onverwacht (292KT). A fourth pipe, on the farm Twyfelaar (119KT), was trial-mined but proved uneconomic. The Driekop pipe crops out over a low koppie (Willemskop) situated in the broad Moopetsi valley. The lower critical and main zone cumulates crop out in the mountains on the sides of the valley. The floor of this valley is covered by a layer of thick black "turf" which obscures the upper critical zone cumulates. The regional dip of the cumulates in this area is 10-12^{o} west or south-west. The Driekop pipe is exposed at roughly the same stratigraphic position as the UG-2 chromitite layer, assuming that the cumulate sequence is

undisturbed. A number of discordant bodies of non-platiniferous magnesian dunite also occur in this area, including those on the farms Clapham and Winnarshoek. In addition a number of dunitic pipes occur on the farm Maandagshoek (see section 2.4 and fig. 3.1).

The Onverwacht and Twyfelaar pipes cut bronzitites and chromitites of the lower and lower critical zones, whereas the Mooihoek and Driekop pipes cut essentially noritic cumulates of the upper critical zone. The Mooihoek

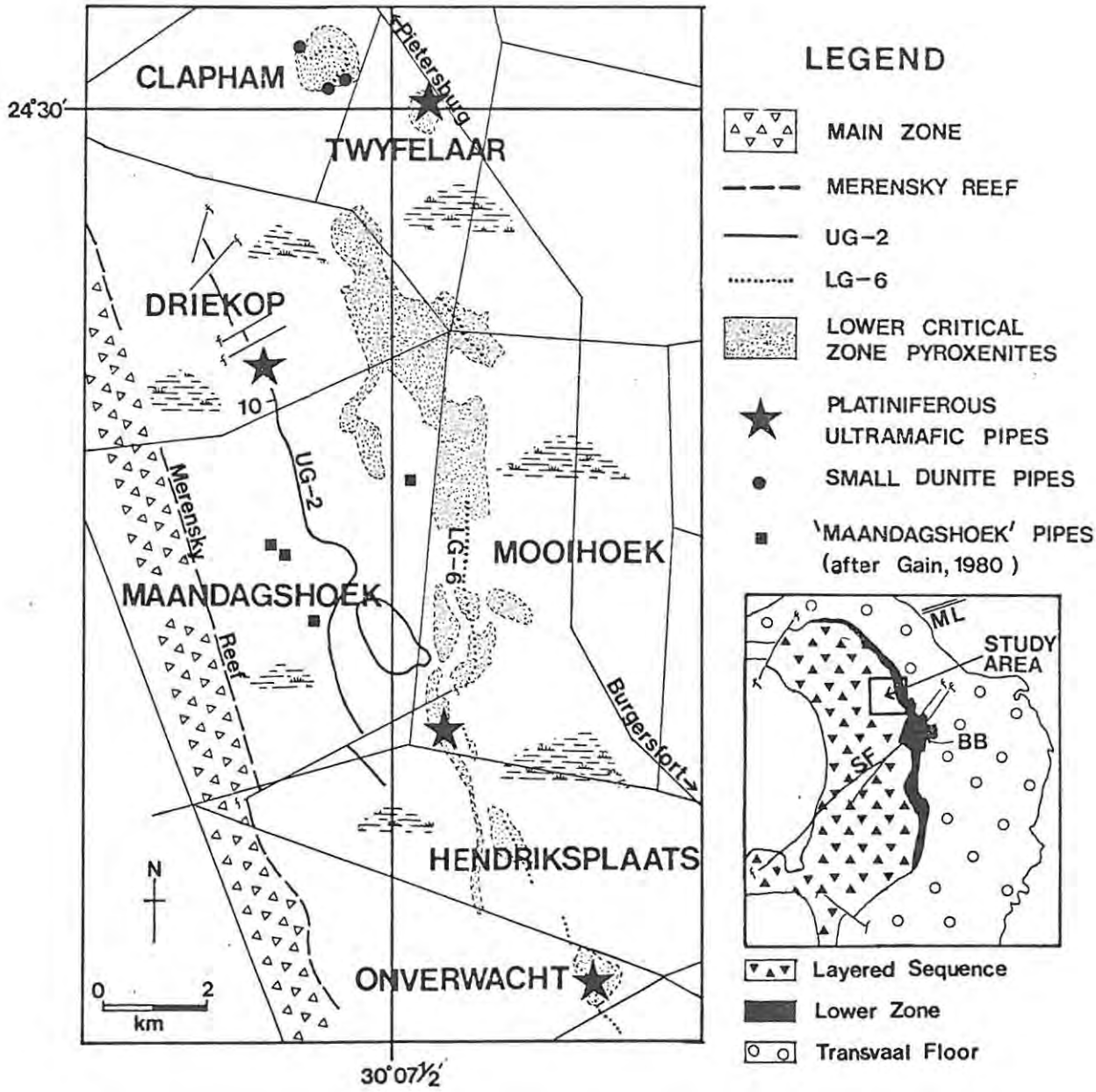

FIGURE 3.1 Geological setting of the platiniferous ultramafic pipes. Structural features shown in inset are ML - Murchison lineament; SF - Steelpoort fault; BB - Burgersfort "bulge".

pipe is poorly exposed and has not been studied in detail since the work of Wagner in the 1920's (Wagner, 1929; see section 2.5). There does not appear to be any sympathetic relationship between the petrology of the pipes and their statigraphic position. The Onverwacht pipe, the smallest of the four, is relatively well exposed and has been the subject of a number of publications.

3.2 FIELD RELATIONSHIPS AT THE ONVERWACHT PIPE

The surface features of this pipe have been described by Wagner (1929) and Cameron and Desborough (1964). Cross-sections presented by these authors differ considerably (fig. 2.4). Wagner interprets the Onverwacht pipe as an intrusive, clearly "pipe-like" feature that sharply cuts the layered cumulates, whereas Cameron and Desborough suggest that it forms a sheet-like feature on the down-dip side. The latter authors' observation that an orthopyroxenite cumulate overlies a chromitite layer that is exposed down slope on the western side of the pipe is correct (note that the regional dip is 10-12^{o} west). However, the impure chromitite which they located in the dunite itself may not be as distinctly layered as indicated on their section. Furthermore, underground exposures that would have been accessible to Wagner corroborate the pipe-like form at depth.

The presence of large, slab-like blocks of chromitite in the Onverwacht pipe (they occur in both the magnesian dunite and the platiniferous core - see fig. 2.4) was first reported by Wagner (1929). He observed that they occur at roughly the same stratigraphic position as the adjacent Steelpoort (or LG-6) chromitite layer, which crops out to the east of the pipe (such that if the layered sequence is undisturbed it must intersect the pipe at a shallow depth). As far as the author is aware this chromitite layer has not been actually observed intersecting the contact of the pipe, and, as the mine workings are now inaccessible, subsequent authors have to rely on Wagner's observations. He interpreted these blocks as xenoliths, a hypothesis which Lombaard (1956) supported.

Most recent authors, however, interpret them as partially replaced or relict rafts of the Steelpoort chromitite layer. They are usually cited as one of the strongest pieces of evidence in favour of a metasomatic origin (e.g., Cameron & Desborough, 1964). Chemical data have been used to support this interpretation but both these, and field relationships, are equivocal. The replacement hypothesis would seem to suggest that these chromitite slabs are structurally undisturbed, yet Wagner's section clearly shows them as irregular masses which dip in different directions. Furthermore, as outlined

above there is only circumstantial evidence to suggest that they are at the same position as the original layer. The layered sequence adjacent to the Onverwacht pipe appears to be undeformed, in contrast to the situation at Driekop, but the possibility that a major collapse structure occurs here cannot be ruled out. It is interesting to note that Kupferburger and Lombaard (1937) report that mining of the Steelpoort chromitite layer was stopped in the vicinity of the Onverwacht pipe because the seam was buckled and strongly disturbed.

The Onverwacht pipe is exposed at a much lower stratigraphic position than the other pipes - possibly quite close to the base of the pipe, as Wagner (1929) reports that the orebody was pinching out at a depth of 137 m. It is feasible to expect that different structural features would occur in the root zone and it may well be that the wallrocks to the Onverwacht pipe in fact do not form a collapse structure.

The contact between the magnesian dunite, which forms the main petrologic unit in the Onverwacht pipe, and the adjacent cumulate orthopyroxenite wallrocks, is irregular and gradational (Cameron & Desborough, 1964). In this contact zone olivine may replace cumulus orthopyroxene and Cameron and Desborough describe a net-textured assemblage consisting of olivine and chromite in which the former mineral pseudomorphs relict orthopyroxene grains. Similar net-textures are common in ultramafic cumulates in the layered sequence of the Bushveld Complex.

3.3 FIELD RELATIONSHIPS AT DRIEKOP

3.3.1 THE MAIN PIPE

The Driekop pipe is primarily composed of a large, annular, sheath-like body of magnesian dunite which envelopes an irregular and poorly-defined core of rather iron-rich dunite and wehrlite. The magnesian dunite is itself enclosed by a thin envelope of iron-rich olivine clinopyroxenite (this may be a wehrlite close to the contact with the magnesian dunite). The core, which occurs asymmetrically within the magnesian dunite and represents less than one volume percent of the entire pipe, constituted the platiniferous orebody. It has been stoped out to a depth of 165 m. Small, satellite bodies of pipe-related ultramafic and mafic rock are emplaced within the cumulate wallrocks adjacent to the pipe; these are of considerable genetic significance. The Driekop pipe is inclined at roughly 78-80^{o} north-east, and has a surface diameter of between 250 and 300 m, athough it tapers with depth (figs. 3.2, 3.3). The reader is also referred

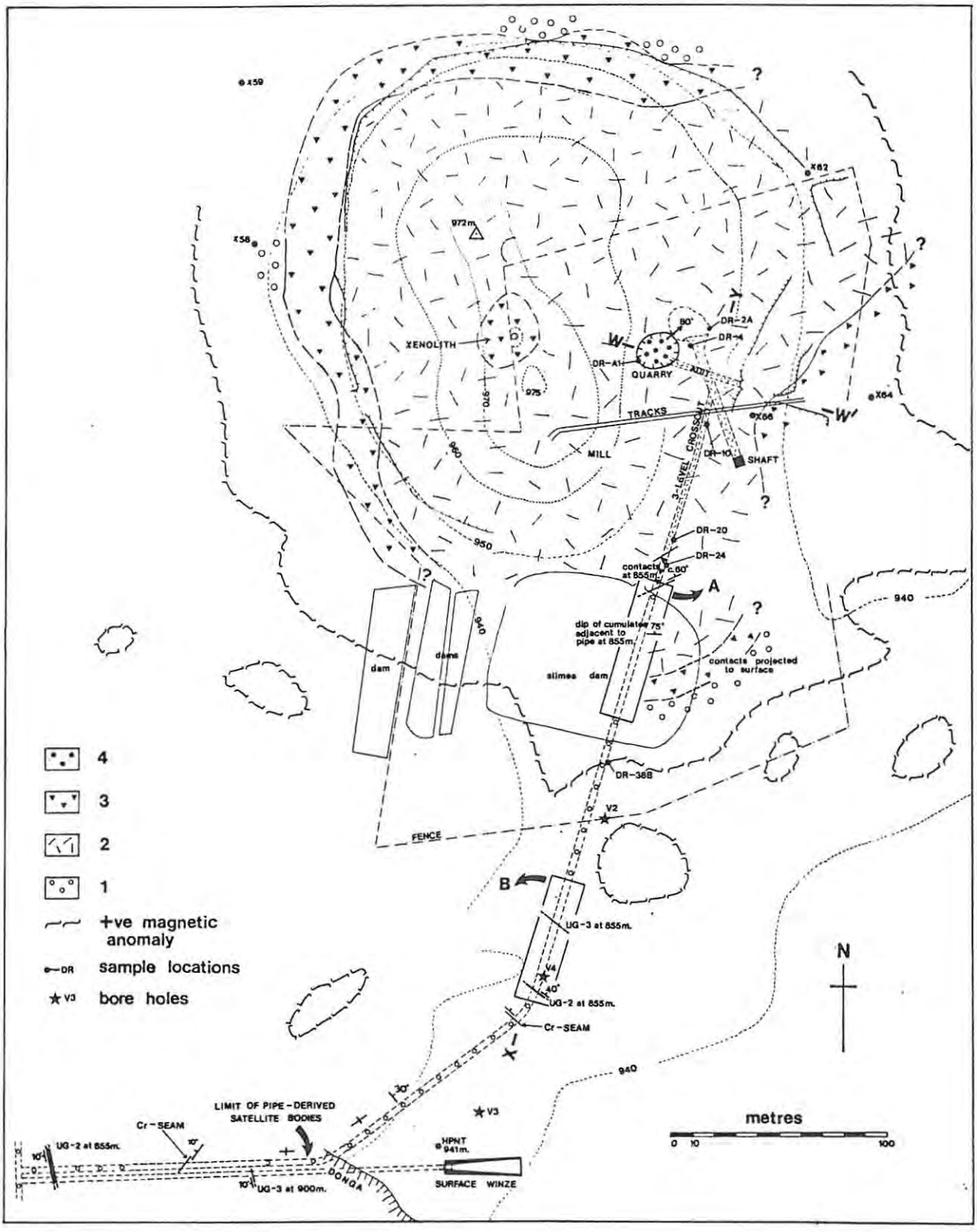

FIGURE 3.2 Composite geologic plan of the Driekop pipe.

Elevation of surface mapping shown by contours (in metres; X58 etc. are survey beacons), underground mapping at an elevation of 855 m. W-W' is Wagner's section; X-Y refers to the section in Figure 3.3. "A" and "B" refer to the detailed maps presented in Figure 3.4. Note strike and dip of the layered cumulates intersected in the underground development.

EXPLANATION OF LEGEND : 1 - Upper critical zone cumulates

2 - Magnesian dunite (main pipe)

3 - Iron-rich olivine clinopyroxenite (marginal envelope)

4 - Platiniferous, iron-rich dunite/wehrlite (core)

to the detailed maps presented in the folder in the end cover. These include a composite surface and underground plan (Map 1), at a scale of 1:1000 (this has been reduced to form fig. 3.2), and a plan of the 3-level crosscut at a scale of 1:200 (Map 2). These maps, on which all relevant sample locations are plotted, are the results of the authors own mapping.

The platiniferous core of the Driekop pipe occurs as an irregular, poorly defined unit, unlike the sharply defined cores of the Mooihoek and Onverwacht pipes (see Chapter 2). It is composed of a number of small, irregular bodies of platiniferous, iron-rich dunite and wehrlite which are

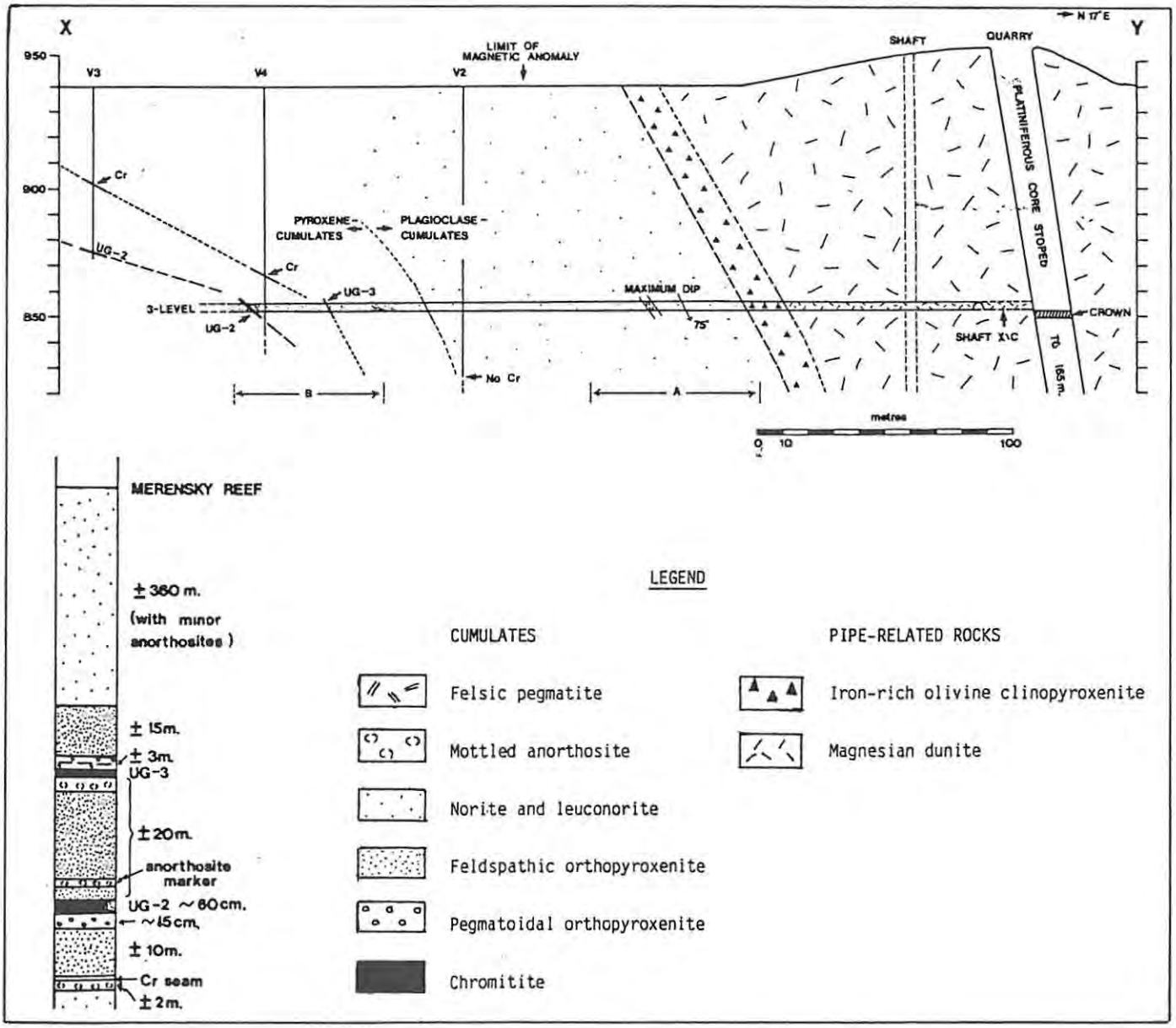

FIGURE 3.3 Cross-section of part of the Driekop pipe. For location of points X-Y see Figure 3.2. Labels "A" and "B" refer to detailed sections presented in Figure 3.4. Borehole data and details of cumulate sequence from Mossom (1977).

concentrated to form a pipe-shaped "core-area" within the main pipe. Careful sampling was necessary to delineate the orebody (Wagner, 1929). For example, in a grade plan of the 160-foot level 14 discrete ore shoots are located within the core-area (fig. 2.3). The individual bodies of platiniferous, iron-rich dunite and wehrlite are between a few centimetres and a metre in diameter.

Although the platinum mineralization at Driekop did not form a sharply-defined core, the contention of Stumpfl and Rucklidge (1982) that the mineralized zone is not delineated by a distinct rock type is incorrect. The platiniferous, iron-rich dunite and wehrlite are dark-coloured, coarse-grained rocks readily distinguished from the non-platiniferous magnesian dunite (typically medium-grained and yellow-green in colour). Although much of the orebody has been stoped remnants can be observed both on surface and underground. It consists of irregular veins and wedge-shaped lenses which radiate out from the central core-area. The magnesian dunite adjacent to this core-area was also locally platiniferous, but the mineralization is clearly related to the iron-rich rocks (Wagner, 1929). Some of the larger veins outside the main-core area were also mined, and small veins and lensoid bodies of iron-rich dunite and wehrlite are found over almost the entire outcrop of the magnesian dunite. The contacts between small bodies of iron-rich dunite or wehrlite and magnesian dunite are sharp, if irregular.

The envelope of iron-rich olivine clinopyroxenite which encloses the magnesian dunite is exposed on surface, at the base of the koppie on the northern and western sides, and underground. The contact with the cumulate wallrocks is poorly exposed and the overall dimensions of the pipe on surface can only roughly be estimated; this contact is sharp, but extremely irregular (fig. 3.5B). The contact between this assemblage and the magnesian dunite, which is exposed underground, also appears sharp in the field. Veins of iron-rich wehrlite and olivine clinopyroxenite cut the magnesian dunite (fig. 3.5A). Boulders of wehrlite and leuconorite found at the top of the koppie, described as picrite by Heckroodt (1959), probably represent a large xenolith (Map 1).

Field relationships indicate that the iron-rich assemblages, which form the platiniferous core and the outer envelope of olivine clinopyroxenite, postdate the formation of the magnesian dunite. It is thus necessary to consider the pipe as a composite feature which consists of three main petrologic assemblages or units.

3.3.2 DEFORMATION OF THE WALLROCKS

The Driekop pipe is emplaced within, or replaces, cumulates of the upper critical zone, which at the present erosional level consist essentially of leuconorites between the UG-2 chromitite layer and the Merensky Reef. The stratigraphic column for the Driekop-Maandagshoek area, which has been compiled after Mossom (1977) is presented in Figure 3.3. The attitude of the wallrocks adjacent to the Driekop pipe has been severely disturbed resulting in the formation of a major collapse structure. The sequence exposed in the 3-level crosscut is on the regional down-dip side of the pipe (note that the regional dip is 10-12 ^{o} west or southwest) but the dips in this section are reversed (figs. 3.2, 3.3 and Maps 1, 2). In the section exposed in the 3-level crosscut the layered sequence adjacent to the pipe is inclined subvertically and dips at roughly 85^{o} to the north-northeast. The dip becomes progressively less with distance from the pipe and eventually flattens out. Banding in a 25 m thick layer immediately adjacent to the pipe is subhorizontal, and may represent a large xenolith (fig. 3.4A). This downwarping of the layering is accompanied by a swing in strike of roughly 90 ^{o}. A contour plan based on the UG-2 chromitite layer, a useful marker horizon, illustrates the extent of this disturbance (Schiffries, 1982).

This structural disturbance can be described as a major downwarping of the layered sequence. It forms a structurally disturbed zone around the main pipe with a radial extent of some 500 m on the down-dip side. The continuity of the layering in this zone indicates that the deformation, which is presumably related to the Driekop pipe, occurred after the cumulate layering was well defined.

The layered sequence exposed in the 3-level crosscut adjacent to the pipe consists of a thick unit of leuconorites with minor anorthosite layers. This sequence is essentially unaltered, but contains satellite bodies related to the pipe. On a small scale, cross bedding and slump structures occur. The latter is interpreted as resulting from plastic attenuation during the downwarping event. They are particularly common where thin bands of anorthosite intercalate with leuconorite. Faults and joints are rare and the strike and dip changes are continuous, rather than abrupt, with no major breaks (fig. 3.4A).

At a lateral distance of approximately 150 m from the pipe in the 3-level crosscut these felsic cumulates are sharply underlain by a 40 m-thick unit of ultramafic cumulates. These consist essentially of orthopyroxenites but also include the UG-2 and UG-3 chromitite layers (fig. 3.4B). At this

point the dip has flattened out slightly, such that the UG-2 chromitite layer dips at 40^{o} to the north-east. The cumulate sequence below this intersection of the UG-2 chromitite layer forms the core to the asymmetric anticline referred to above. On the limb of this anticline which is furthest from the pipe the UG-2 chromitite layer is again intersected, but here it dips at between 10^{o} and 12^{o} to the west. From here a surface winze intersects a normal cumulate sequence, which includes the UG-3 chromitite layer (fig. 3.2).

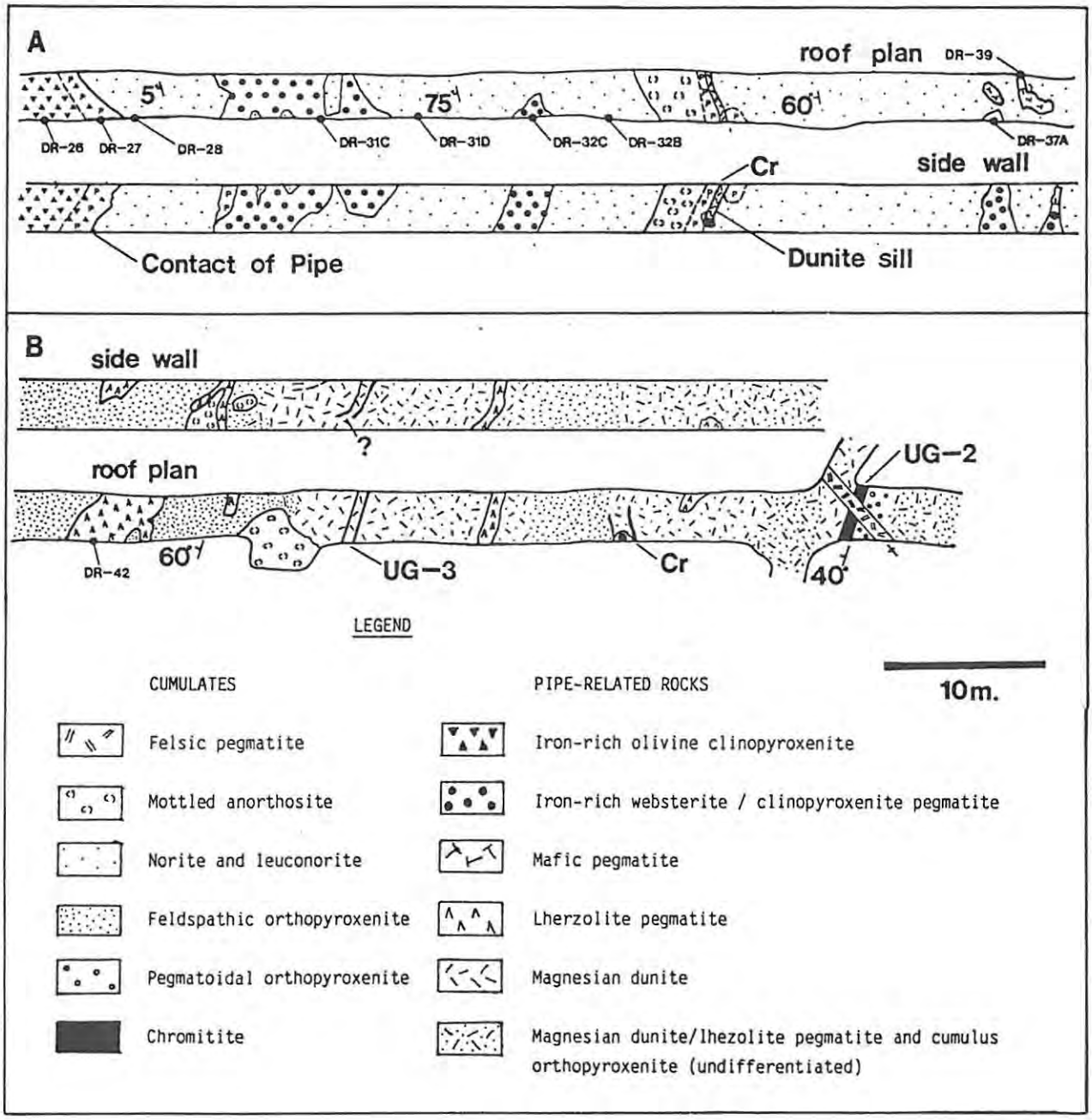

FIGURE 3.4 Detailed plans (roof level) and sections (side walls) of part of the 3-level crosscut, Driekop. See Figures 3.2 and 3.3 for location. Original mapping on 1:200 scale mine plans.

The sequence of ultramafic cumulates exposed in the 3-level crosscut closest to the pipe (which dip at 40^{o} towards the pipe) differs from that observed in "normal" intersections (borehole core from other areas in the eastern limb of the Bushveld Complex, provided by J.C.I., were examined). In this section individual cumulates are mineralogically atypical, specific cumulate layers are not recognised (or are absent) and they are intimately associated with a range of pipe-related satellite bodies (fig. 3.4B). Furthermore, faults and fractures are common. The UG-3 chromitite layer consists of several very thin layers, less than 2 cm thick, that are discontinuous, faulted and cut by small, satellite bodies of magnesian dunite. The UG-3A chromitite and the distinctive mottled anorthosite, which elsewhere underlies the UG-3 chromitite layer, are absent. Anorthosite is, however, found as irregular wedges and lensoid bodies squeezed into the orthopyroxenite above the UG-3 chromitite layer. In comparison, the UG-2 chromitite layer, which is approximately 1 m thick, is relatively undisturbed, although it also is faulted and cut by pegmatite veins. The footwall and hangingwall to the UG-2 are locally composed of magnesian dunite (which is evidently related to the pipe) with only minor relict orthopyroxenite (the normal cumulate footwall and hanging-wall).

These features suggest that the orthopyroxenite and chromitite cumulates in this sequence have been subjected to extensional deformation and have suffered brittle failure. It is suggested that the orthopyroxenite and chromitite cumulates behaved in a brittle manner in comparison with the felsic cumulates.

3.4 PETROLOGIC UNITS IN THE DRIEKOP PIPE

3.4.1 MAGNESIAN DUNITE

PETROGRAPHY

This is the principal unit in all of the platiniferous ultramafic pipes. It is a fine-to-medium grained rock, yellow-green in colour, with no apparent mineral foliation or layering. Olivine accounts for between 98 and 99 modal percent; the remainder is essentially chromiferous spinel. Clinopyroxene and secondary serpentine minerals occur as rare accessory constituents. Fine-grained ($<$ 1 mm), interlocking, subhedral grains of olivine may exhibit a foam-like or polygonal texture, or the olivine may occur as large ($>$ 5 mm), anhedral grains which embay each other (fig. 3.6A, B). This texture, which may be described as hypautomorphic granular or polygonal granular (depending on which form of olivine predominates),

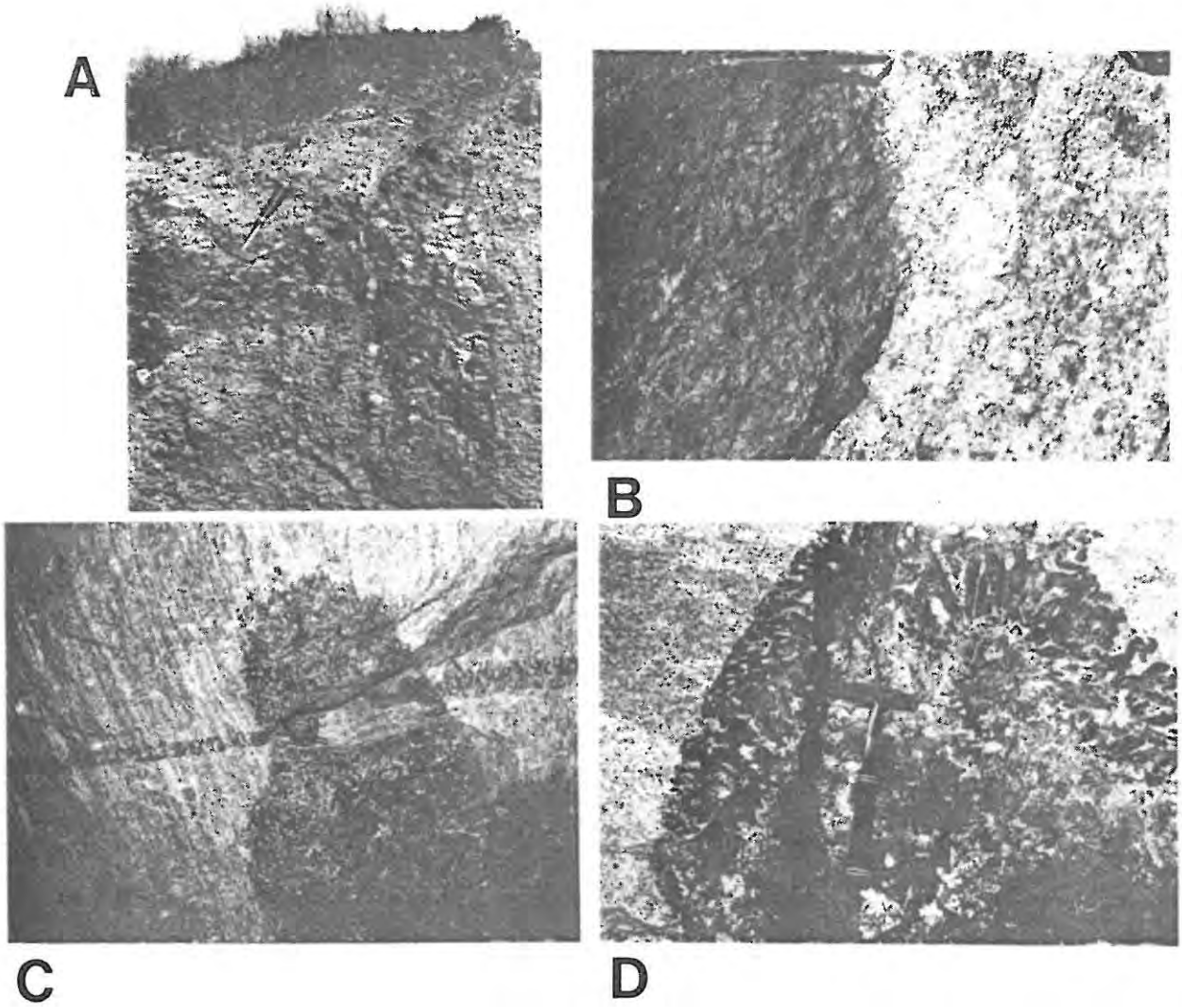

FIGURE 3.5 SOME FIELD RELATIONSHIPS AT DRIEKOP

A. Dark-coloured veins of olivine clinopyroxenite cutting the magnesian dunite near the margin of the main pipe. The soil covering the dunite is a distinctive red colour and is much thinner than the black "turf" covering the typical upper critical zone cumulates.

B. Sharp contact between the mariginal assemblage of olivine clinopyroxenite (dark) and the cumulate wallrocks (leuconorites).

C. Tip of a small, satellite body of websterite pegmatite, adjacent to the main pipe, exposed on the sidewall of the 3-level crosscut. Note sharp lateral contacts and irregular, diffuse upper contact (evidence of local replacement). Wallrocks are leuconorites between the UG-3 chromitite layer and the Merensky Reef - note steep dip of layering.

D. Satellite body of mafic pegmatite, adjacent to the main pipe exposed on the sidewall of the 3-level crosscut. Note radial orientation of coarse, tabular, clinopyroxene grains (dark) in a matrix of plagioclase (light). Wallrocks are leuconorites between the UG-3 chromitite layer and the Merensky Reef.

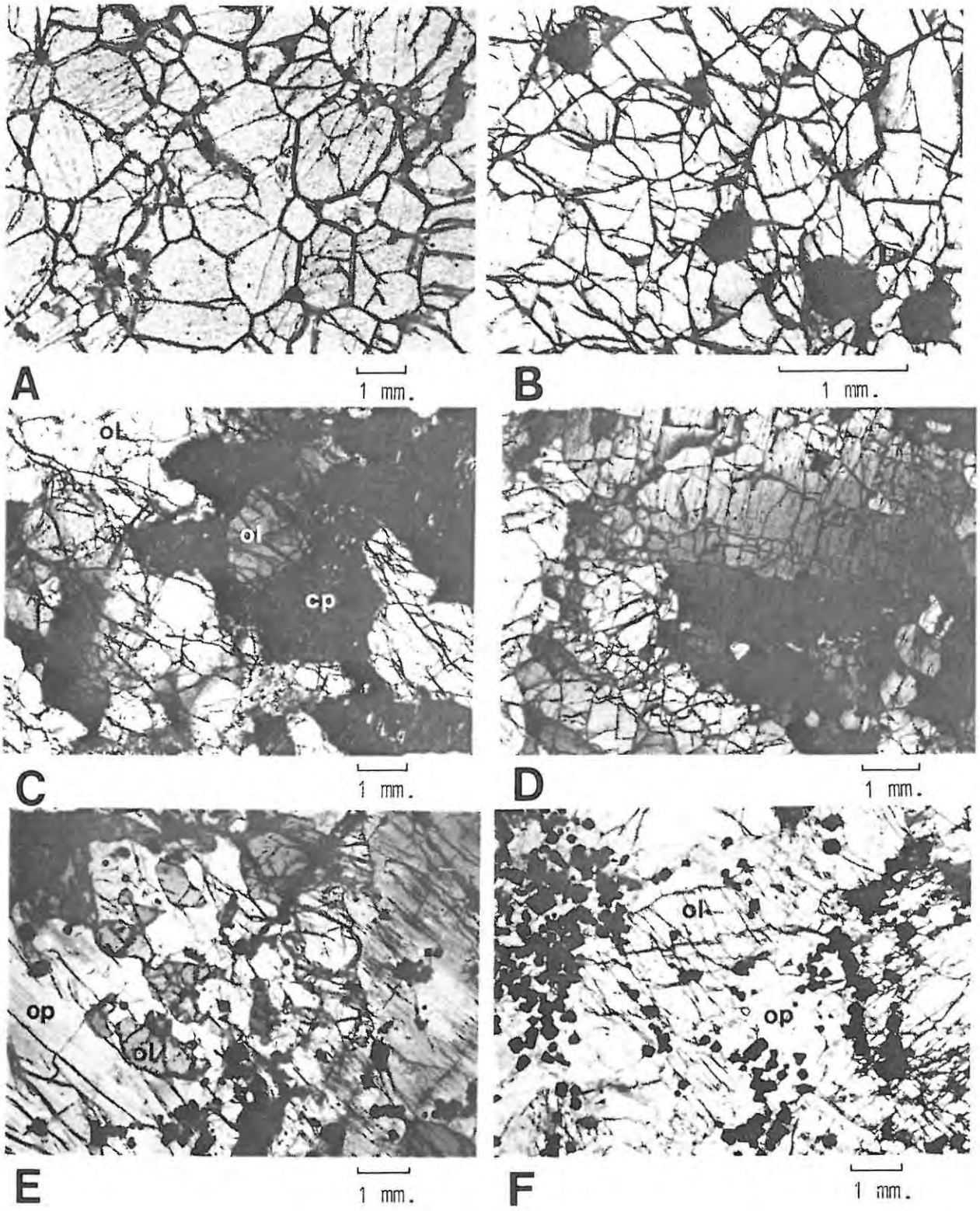

FIGURE 3.6 PHOTOMICROGRAPHS OF SAMPLES FROM DRIEKOP

a. Fine-grained olivine exhibiting a well developed foam-like texture. Magnesian dunite, main pipe (sample DR-1). b. Disseminated chromiferous spinels interstitial to, and enclosed by, olivine. Magnesian dunite, main pipe (sample DR-1). c. Iron-rich clinopyroxene resorbing magnesian olivine. Wehrlite, contact assemblage between magnesian dunite and marginal envelope of olivine clinopyroxenite, main pipe (sample DR-22). d. Hypautomorphic granular texture in coarse-grained clinopyroxenite pegmatite. Satellite body (sample DR-38C). e. Magnesian olivine resorbing large, cumulus orthopyroxene grain. Lherzolite pegmatite, adjacent to altered UG-3 chromitite layer (sample DR-46). f. Magnesian olivine resorbing cumulus orthopyroxene grain and enclosing cumulus chromite grains. Partially replaced UG-3 chromitite layer (sample DR-45).

("a", "b" and "f" in plane polarised transmitted light; "c", "d" and "e" in transmitted light with crossed polarisers; ol - olivine; op - orthopyroxene; cp - clinopyroxene)

probably results from incomplete (secondary ?) enlargement and subsequent annealing (see also Chapter 8). The large anhedral grains usually display undulatory extinction, whereas the small, polygonal grains extinguish normally. Olivine from all of these pipes, irrespective of its composition or which petrologic unit it occurs in, often displays a fine-grained, dendritic intergrowth, described by many authors, including Wagner (1929), Hatch, Wells and Wells (1974, p. 427) and Schiffries (1982). Putnis (1973) describes similar dendrites or platelets in olivines from the Rhum Complex which are composed of clinopyroxene and magnetite. He interprets them as resulting from high-temperature oxidation of the host olivine. They have not been documented in cumulus olivine from the Bushveld Complex, but are also present in olivine from the iron-rich ultramafic pegmatite suite.

Chromiferous spinel occurs in a range of habits in the magnesian dunite, but textural evidence generally suggests that it is an early-formed mineral. For example, large grains (typically with diameters >3 mm) are usually euhedral and appear to inhibit subsolidus grain boundary migration of olivine. Furthermore, small grains (often with diameters <0.1 mm) may occur in intragranular sites within olivine (fig. 3.6A,B). Large grains which occur in intergranular sites may be extremely anhedral and may contain numerous silicate inclusions. In reflected light these are observed to be optically heterogeneous (Stumpfl & Rucklidge, 1982). These heterogeneous spinels are unusual and warrant a separate discussion (see Chapter 4). The modal proportion of chromite is typical of cumulus magnesian dunites in the layered sequence of the Bushveld Complex.

Base-metal sulphide is rare in this assemblage and PGM are not normally observed. Pentlandite may occur, however, as tiny grains in serpentinite veinlets, but pyrrhotite is even less abundant. This assemblage contains only trace amounts of trapped interstitial material and in comparison with cumulus magnesian dunites from the Bushveld Complex exhibits a greater degree of annealing.

The main body of magnesian dunite at Driekop was sampled at 5 m intervals (spaced at 10 m intervals for analytical purposes; see Appendix 3) along an underground traverse (Map 2 in folder).

MINERAL CHEMISTRY

OLIVINE from this assemblage is the variety chrysolite. Stumpfl and Rucklidge (1982) quote an average value of Fo_{80} (no analyses given) and Schiffries (1982) suggests that the composition varies between Fo_{82} and Fo_{78} (he presents two analyses, $Fo_{79.6}$ and $Fo_{78.9}$).

In this study, the results of electron microprobe analyses indicate that the average composition is $Fo_{83.6}$ (13 analyses on samples DR-1,4,10,12; standard deviation (d) = .2774; Table 4.1). As these dunites are essentially monomineralic, whole-rock analyses may also be used to calculate the composition of olivine. From these data an average composition of Fo_{83} is estimated (10 analyses, see Table 3.1 and Appendix 5). This results in a slightly more iron-rich composition, possibly because three of the samples are relatively strongly serpentinised (these have low Mg/Fe ratios and low Ni contents). The distribution of nickel in olivine is discussed in Chapter 4. Other minor elements analysed for are Mn and Ca. There does not appear to be any horizontal zonation in the olivine composition in the magnesian dunite unit, other than contact features (see section 3.4.5), but the possibility of vertical zonation has not been investigated. Furthermore, there is no correlation between composition and textural habit of the olivine, and significant compositional zonation within individual grains has not been observed.

The composition of olivine from the magnesian dunite unit at Onverwacht has been investigated by Cameron and Desborough (1964). They found a compositional zonation with the most magnesian values towards the periphery of the pipe. Olivine from close to the core of the pipe is in the compositional range Fo_{84-80} and that from the margin is Fo_{92-88}. The composition of olivine from the magnesian dunite unit at Mooihoek has not been determined by the author but the data of Wagner (1929) suggest that it is comparable with that at the other pipes (Table 3.1). Olivine from the Twyfelaar pipe has a similar composition (sample TW-1, Table 4.1).

OPAQUE MINERALS : The chemistry of spinels and base-metal sulphides from the magnesian dunite assemblage is discussed in Chapters 4 and 11, respectively.

WHOLE-ROCK CHEMISTRY

Three, typical whole-rock analyses of magnesian dunite from the inner, central and outer parts of the main pipe at Driekop and an average analysis (of 10 samples) are presented in Table 3.1 (for complete analyses see Appendix 5). Analyses of magnesian dunite from Onverwacht and a cumulus dunite from the lower zone of the layered sequence (from the farm Jagdlust 418KS, in the eastern limb of the Complex) are also presented. Analyses of magnesian dunite from Driekop are comparable with the analyses presented by Wagner (1929), the only previous whole-rock data published on these rocks. From the results of this study it is concluded that the main body of

TABLE 3.1 WHOLE-ROCK ANALYSES OF MAGNESIAN DUNITES

	DR-4	DR-10	DR-20	A		ON-12	DUN-1	WAG-1	WAG-2
wt.%				x	d				
SiO_2	37.97	38.41	37.85	38.67	.251	35.63	38.79	36.55	38.4
TiO_2	.02	.03	.02	.02	.005	.05	.03	.10	n.d.
Al_2O_3	.19	.22	.08	.17	.073	.67	.74	1.70	)
Fe_2O_3	.08	.08	.08	.08	.004	.08	.06	1.80	)5.9
FeO	15.39	15.07	15.28	16.03	.909	16.57	11.82	16.85	16.5
MnO	.25	.24	.18	.23	.025	.29	.17	.15	n.d.
MgO	42.33	44.09	44.45	43.84	.996	37.82	43.13	37.95	38.0
CaO	.41	.20	.11	.28	.168	.50	.39	1.00	n.d.
Na_2O	.01	.01	.01	.01	.007	n.d.	n.d.	Tr	-
K_2O	n.d.	n.d.	n.d.	n.d.	-	n.d.	n.d.	Tr	-
P_2O_5	n.d.	n.d.	n.d.	n.d.	-	.02	n.d.	Tr	-
Cr_2O_3	.43	.43	.44	.42	.134	1.35	.97	.40	.5
NiO	.23	.23	.24	.25	.027	.18	.24	Tr	n.d.
L.O.I.	2.95	1.59	1.28	-	-	7.65	4.89	2.60	n.d.
TOTAL	100.26	100.60	100.02	100.00	-	100.81	101.23	99.95	99.3
ppm									
Co	188	190	196	195	11.4	183	154	-	-
Cu	11	12	9	17	13.2	14	12	-	-
Zn	85	81	90	87	6.3	95	68	-	-
V	63	40	54	52	11.7	162	38	-	-
Sc	7	5	5	6	1.1	9	7	-	-
Y	n.d.	n.d.	6.8	-	-	n.d.	n.d.		
Mg-No	.83	.84	.83	.83	-	.80	.87	-	-
Olivine	83.5	83.5	-	83.6	-	-	87.1	-	-

n.d.: not detected; Tr : trace; - not determined; Olivine composition (mol.% Fo) determined by microprobe. For analyses by author Fe_2O_3 / FeO = 0.005

DR-4,-10 & -20 : The inner,central and outer parts,respectively,of the main Driekop pipe (97m level).
A : Average of 10 samples from the main Driekop pipe (97m level; x: mean; d: standard deviation).
ON-12 : Magnesian dunite from near the core of the main Onverwacht pipe (surface).
DUN-1 : Cumulate dunite, lower zone of the layered sequence, Jagdlust, Eastern Bushveld Complex.
WAG-1 : Magnesian dunite, 200-foot level Mooihoek (Wagner 1929,includes .4% S, .25% CO_2, .4% H_2O^-).
WAG-2 : Magnesian dunite, 65-foot level Onverwacht, at contact with platiniferous core (Wagner 1929).

magnesian dunite at Driekop does not exhibit any lateral zonation or fractionation trends.

In this assemblage the minor and trace elements Ni, Co, Zn, and Mn may be attributed to olivine, and Cr, Al_2O_3 and Fe_2O_3 are attributed to chromite. The trace elements Sc and V are probably present in both olivine and chromite. Locally clinopyroxene may account for some of the CaO. The extremely low Cu values are indicative of the paucity of sulphides. The trace elements Nb, Zr, Sr, Rb and Ba are not detectable by XRF spectrometry in these samples. Yttrium was detected in one sample (DR-20 close to the "contact zone", see section 3.4.5). The minor and trace element chemistry is comparable with cumulus dunites from the layered sequence of the Bushveld Complex (e.g., sample DUN-1, Table 3.1; see also Cameron, 1978; Botha, in prep.) and with magnesian dunites worldwide (see Wyllie, 1967).

3.4.2 PLATINIFEROUS, IRON-RICH DUNITE AND WEHRLITE FROM THE CORE

PETROGRAPHY

The dark-coloured, platiniferous rock found in the core of the Driekop pipe varies from a dunite to a wehrlite. It consists of dark-green olivine (iron-rich chrysolite) and greenish-grey clinopyroxene, the latter often

occurring as large, euhedral grains with dimensions over 15 mm. The purely dunitic variety is coarse-grained, but texturally otherwise similar to the magnesian dunite. Chromiferous spinel is absent in this assemblage. Magnetite (a Ti-poor variety - probably secondary) is occasionally observed, athough Wagner (1929) reports that it may occur in large grains. Amphibole and mica have been observed by the author only as secondary phases associated with either altered olivine or clinopyroxene. Sulphides in the core of the Driekop pipe, although widely distributed, represent less than 0.1 modal percent.

The platiniferous core of the Mooihoek pipe is quite different. It is composed of a dark-coloured olivine (hortonolite) with varying amounts of lustrous black clinopyroxene, hornblende, mica and coarse segregations of coarse-grained Fe-Ti oxides. Ti-magnetite, ilmenite, amphibole and mica are all primary constituents in this assemblage. It is clearly more highly fractionated than the platiniferous assemblage in the Driekop pipe and is also much coarser-grained. It may be described as a platiniferous, iron-rich ultramafic pegmatite and may provide a genetic link between these pipes and the essentially non-platiniferous, iron-rich ultramafic pegmatite suite.

MINERAL CHEMISTRY

OLIVINE : Electron microprobe analyses completed in this study indicate that the average composition of olivine in the platiniferous core of the Driekop pipe is $Fo_{72.7}$ (samples DR-A1/A2, Table 4.1). These data are corroborated by 3 whole-rock analyses (analysis "AA", Table 3.2) and by the data of Wagner (1929) and Schiffries (1982). The contention of Stumpfl and Rucklidge (1982) that the composition of olivine throughout the Driekop pipe is Fo_{80} is thus incorrect. The author's analyses of olivine from the cores of the Mooihoek and Onverwacht pipes are in agreement with published data. Olivine in the core of the Onverwacht pipe is hyalosiderite (Fo_{65-64}; sample ON-2) and in the core of the Mooihoek pipe it is hortonolite (Fo_{44-43}; sample MO-4; Table 4.1).

PYROXENE : the average X_{Mg} ($Mg/(Mg+Fe^{2+})$) of clinopyroxene and orthopyroxene (exsolution lamellae) in platiniferous wehrlite from the Mooihoek pipe is .688 and .577, respectively (sample MO-3, Table 4.2). Olivine in this sample has a composition of $Fo_{52.6}$ (Table 4.1). Pyroxene from the cores of the Driekop and Onverwacht pipes has not been analysed.

OPAQUE MINERALS : The chemistry of Fe-Ti oxides and base-metal sulphides in these assemblages is discussed in Chapters 4 and 11, respectively.

TABLE 3.2 WHOLE-ROCK ANALYSES OF THE PLATINIFEROUS CORE ASSEMBLAGES

	DR-A1	AA		ON-2	MO-4	MO-3	WAG-3	WAG-4	WAG-5	WAG-6
wt. %		x	d							
SiO_2	35.19	37.94	.179	36.27	33.22	45.87	37.92	38.60	34.25	36.72
TiO_2	.02	.02	.006	.03	.16	.47	-	-	.05	Tr
Al_2O_3	n.d.	n.d.	-	n.d.	n.d.	1.80	-	-	1.45	1.63
Fe_2O_3	.11	.12	.006	.15	.22	1.97	-	-	2.90	n.d.
FeO	22.18	23.23	.477	30.27	43.91	17.29	25.96	23.61	35.55	38.04
MnO	.28	.32	.015	.48	.65	.35	-	-	.40	1.05
MgO	35.33	37.76	.611	30.73	18.60	18.19	34.47	32.51	22.00	22.18
CaO	.30	.31	.021	.59	.67	12.83	n.d.	3.44	2.35	.50
Na_2O	n.d.	n.d.	-	.02	.03	.17	-	-	.20	.32
K_2O	n.d.	n.d.	-	n.d.	n.d.	.02	-	-	n.d.	n.d.
P_2O_5	n.d.	n.d.	-	n.d.	n.d.	.02	-	-	.05	Tr
Cr_2O_3	.03	.05	.038	.02	.01	.29	-	-	.10	n.d.
NiO	.23	.25	.030	.18	.06	.07	-	-	Tr	Tr
L.O.I.	5.41	-	-	.78	.87	1.52	-	-	.55	-
TOTAL	99.08	100.00	-	99.52	98.52	100.64	98.35	98.16	99.85	100.49
ppm										
Cr	184	-	-	115	41	2004	-	-	-	-
Ni	1816	-	-	1424	445	517	-	-	-	-
Co	247	248	5.0	296	308	154	-	-	-	-
Cu	44	54	47	23	51	54	-	-	-	-
Zn	106	105	6.6	159	166	103	-	-	-	-
V	47	46	6.0	57	52	574	-	-	-	-
Sc	7	8	1.7	12	18	69	-	-	-	-
Nb	n.d.	n.d.	-	n.d.	n.d.	n.d.	-	-	-	-
Zr	n.d.	n.d.	-	n.d.	2.8	15.8	-	-	-	-
Y	2.9	2.7	.4	3.5	2.9	16.6	-	-	-	-
Sr	n.d.	n.d.	-	n.d.	n.d.	16	-	-	-	-
Rb	n.d.	n.d.	-	n.d.	n.d.	n.d.	-	-	-	-
Mg-No	.74	.74	-	.64	.43	.65	-	-	-	-
Olivine	73.1	72.7	-	64.1	43.1	52.6	-	-	-	-

n.d.: not detected; Tr: trace; - : not determined; olivine composition (mol.% Fo) determined by microprobe. For authors samples Fe_2O_3 / FeO = 0.005 except sample MO-3 in which Fe_2O_3 was estimated by using the technique of Irvine & Barragar (1971).
DR-Al : Iron-rich (chrysolite) dunite, Driekop (adit).
AA : Average of 3 samples of the iron-rich (chrysolite) dunite from Driekop (surface,adit &3 level).
ON-2 : Iron-rich (hyalosiderite) dunite, Onverwacht (surface).
MO-4 : Iron-rich (hortonolite) dunite, Mooihoek (mine dumps).
MO-4 : Iron-rich (hyalosiderite) wehrlite, Mooihoek (mine dumps).
WAG-3 & 4 (Driekop), WAG-5 (Onverwacht) and WAG-6 (Mooihoek) from Wagner (1929).

WHOLE-ROCK CHEMISTRY

Whole rock analyses of dunitic samples from the platiniferous cores of these pipes are presented in Table 3.2. Sample DR-A1 is from the adit level at Driekop, and analysis "AA" is an average of 3 samples from the core of the Driekop pipe (samples DR-A1,A2,A3 - see Appendix 5). Sample ON-2 is from outcrop at the Onverwacht pipe. Samples MO-3 and MO-4 are from the mine dumps at Mooihoek, but as they contain PGM it may be assumed that they are from the core of the pipe (they are not representative, however, due to the pegmatitic nature of this assemblage). Analyses WAG-3 to WAG-6 are from Wagner (1929). Most of the samples of the platiniferous core assemblages are of essentially monomineralic dunites from the marginal parts of these core units, as representative traverses are not available.

The extreme paucity of Cr_2O_3 and Al_2O_3 in these iron-rich dunites may be attributed to the absence of chromite. Other chemical differences between these and the magnesian dunites may be related to the more fayalitic nature of the olivine, including an increase in Mn, Co, and Zn, and possibly Sc (see also Chapter 9). The distribution of Ni, however, is less readily explained (see Chapter 4). These iron-rich dunites are also characterised by

the presence of low levels of Y, although other incompatible elements (Nb, Zr, and Rb) were not detected. The V content remains constant, although this may partly be a function of the absence of chromite. Sample MO-3 is an iron-rich wehrlite; the presence of clinopyroxene results in an increase in the trace elements Sc, V and Sr. It is also associated with an increase in the incompatible elements, a feature which may possibly be related to the presence of mica and amphibole. All of these samples are slightly richer in Cu than the magnesian dunites, a reflection of the presence of small quantities of base-metal sulphide. It may be concluded that, unlike magnesian dunites in the pipes (which may be compared with dunite sensu stricto), the iron-rich dunites are unusual rocks.

3.4.3 MARGINAL ENVELOPE OF IRON-RICH OLIVINE CLINOPYROXENITE

PETROGRAPHY

The marginal envelope to the Driekop pipe is a coarse-grained olivine clinopyroxenite, a dark-coloured rock in which large, tabular crystals of clinopyroxene (up to 50 mm in length) are prominent. Close to the contact with the magnesian dunite the olivine clinopyroxenite is gradational into a hybrid assemblage that may be referred to as a wehrlite (section 3.4.5).

Petrographically this assemblage exhibits a close resemblance to iron-rich ultramafic pegmatite (see Chapter 8). Clinopyroxene may occur in a variety of habits including large, euhedral to subhedral grains and medium-sized, subhedral to anhedral grains, which exhibit extensive mutual interference. These grains may contain exsolved lamellae of orthopyroxene and orientated intergrowths of an opaque phase (probably ilmenite). They usually demonstrate distinctive polysynthetic twinning and partial amphibolisation. The exsolution and twinning result in microtextures that are not observed in cumulus clinopyroxenes from the critical or main zones of the Bushveld Complex (see Chapter 8 for further details). Olivine in this assemblage occurs as large, anhedral grains and small, polygonal grains. The latter form aggregates which exhibit a foam-like texture that may be attributed to annealing. Olivine is distinctly interstitial to the clinopyroxene and may be observed to have partially replaced clinopyroxene, often as small, lath-like grains orientated along cleavage traces but also as pervasive aggregates along the margins of grains (similar features are described in Chapter 8).

Minor phases in this assemblage include plagioclase and orthopyroxene. Spinels and base-metal sulphides are not normally observed in this assemblage. Plagioclase occurs as either unusually large, anhedral grains or as small, sliver-like grains that are interstitial to both clinopyroxene and

olivine. These usually exhibit very coarse and poorly-formed albite twinning, the lamellae of which wedge-out in an irregular fashion, undulatory extinction and are often partially altered to saussurite. Furthermore, large aggregates often consist of small, polygonal grains, probably a result of secondary recrystallization. Both clinopyroxene and olivine exhibit disequilibrium textures with plagioclase and may locally replace it (see also Chapter 8). Orthopyroxene occurs as small, anhedral grains that are either interstitial to, or enclosed by clinopyroxene or olivine. These features suggest that both plagioclase and orthopyroxene may be relict minerals after partial replacement of the adjacent cumulates. The coarse grain size and microtextures exhibited by plagioclase suggest that it has recrystallized during this replacement process. Significantly, large aggregates of saussuritised plagioclase are particulary abundant immediately adjacent to the contact with the cumulate wallrocks.

At Mooihoek, the magnesian dunite is encased within an outer shell composed of coarse-grained olivine clinopyroxenite, feldspathic pyroxenite and olivine gabbro. Hortonolite, hornblende and phlogopite, which also occur in the core of this particular pipe, are observed in these marginal rocks (Wagner, 1929). These latter minerals do not occur in the marginal assemblage at Driekop (other than possibly as secondary or very minor accessory constituents) and it may be inferred that the rocks in the cores and marginal assemblages of the pipes are related. This assemblage is absent at Onverwacht.

MINERAL CHEMISTRY

OLIVINE : Electron microprobe data indicate that the average composition of olivine in olivine clinopyroxenite at Driekop is $Fo_{65.1}$ (samples DR-25,27, Table 4.1).

PYROXENE : The X_{Mg} of clinopyroxene and orthopyroxene (exsolution lamellae) from this assemblage at Driekop is .776 and .700, respectively (samples DR-25,27, Table 4.2). As far as the author is aware there are no published data on the chemistry of olivines and pyroxenes from this assemblage.

PLAGIOCLASE : Schiffries (1982) reports very calcic plagiolase from the margin of the Driekop pipe, with compositions varying from An_{100} to An_{75}. Plagioclase has not been analysed in the current study.

WHOLE-ROCK CHEMISTRY

Two whole-rock analyses of olivine clinopyroxenites from Driekop are presented in Table 3.3 (samples DR-26,27). Because the olivine / pyroxene

TABLE 3.3 WHOLE-ROCK ANALYSES OF THE MARGINAL/SATELLITE ASSEMBLAGES AND CUMULATES AT DRIEKOP

	DR-26	DR-27	DR-31	DR-32	DR-38	DR-39	DR-42	DR-29	DR-30
wt.%									
SiO_2	47.77	49.55	51.06	51.79	50.05	47.30	43.25	51.13	50.83
TiO_2	.17	.20	.22	.25	.35	.75	.06	.09	.10
Al_2O_3	5.25	3.85	3.22	3.27	3.25	10.90	6.43	18.70	19.52
Fe_2O_3	1.67	1.70	1.72	1.75	1.85	2.25	.06	.60	.60
FeO	12.38	10.85	10.65	9.83	8.63	6.31	12.53	5.99	5.99
MnO	.21	.25	.33	.31	.29	.18	.20	.16	.20
MgO	19.08	17.92	18.62	17.73	16.21	8.79	28.98	10.30	9.99
CaO	12.54	14.71	12.02	13.76	17.65	13.94	7.43	10.67	11.05
Na_2O	.09	.27	.23	.25	.24	.57	n.d.	1.58	1.53
K_2O	.01	.01	.07	.01	n.d.	1.05	n.d.	.07	.07
P_2O_5	n.d.	.01	.01	n.d.	.01	4.39	n.d.	n.d.	n.d.
Cr_2O_3	.09	.11	.07	.07	.11	.06	.19	.08	.07
NiO	.07	.06	.05	.05	.04	.02	-	.03	.03
L.O.I.	.95	1.29	1.26	1.48	.92	4.66	1.15	1.25	.91
TOTAL	100.28	100.78	99.54	100.54	99.60	101.17	100.28	100.67	100.89
ppm									
Cr	590	769	470	449	756	396	1316	525	471
Ni	536	440	413	498	340	158	-	195	202
Co	130	112	103	95	92	45	149	51	52
Cu	25	30	18	164	16	21	8	19	19
Zn	75	78	73	68	49	32	72	43	49
V	323	415	393	425	497	182	89	116	114
Sc	57	68	68	70	91	34	18	20	20
Nb	n.d.	n.d.	n.d.	n.d.	n.d.	16.3	n.d.	n.d.	n.d.
Zr	4.9	6.0	6.4	9.4	9.2	26.1	n.d.	2.5	n.d.
Y	6.7	8.8	8.4	11.4	13.1	27.5	n.d.	2.8	3.5
Sr	78	58	35	35	34	216	84	244	261
Rb	n.d.	n.d.	n.d.	n.d.	n.d.	52	n.d.	n.d.	n.d.
Mg-No	.73	.75	.76	.76	.77	.71	.80	.75	.75
Olivine	65.5	64.8	-	62.8	-	-	78.9	-	-

n.d.: not detected; - : not determined; Olivine composition (mol.% Fo) deteremined by microprobe. Fe_2O_3 determined using the technique of Irvine & Barragar (1971) except for samples DR-42,-29 & -30 where an Fe_2O_3 / FeO ratio of 0.005, 0.1 & 0.1, respectively, was used. All samples are from the 97m level at Driekop.

DR-26 : Iron-rich olivine clinopyroxenite, marginal envelope of main pipe.
DR-27 : Iron-rich olivine clinopyroxenite, marginal envelope of main pipe.
DR-31/32 : Iron-rich websterite pegmatites, satellite bodies.
DR-38 : Iron-rich clinopyroxenite pegmatite, satellite body.
DR-39 : Mafic pegmatite, satellite body.
DR-42 : Lherzolite, satellite body, associated with the UG-3 chromitite layer.
DR-29/30 : Leuconorite cumulates, 0.5m and 5m from edge of pipe.

ratio of this assemblage is rather variable an average composition is not presented. These rocks may be distinguished from the magnesian dunite by a comparatively low Mg-number - it varies between 75 and 73, depending on the bulk mineralogy (as compared with values of 84 to 82 for the magnesian dunite; note that the presence of clinopyroxene results in a Mg-number which is higher than the forsterite component of the olivine). Compared with the magnesian dunite these rocks are richer in bulk SiO_2, CaO, Al_2O_3, TiO_2 and Na_2O and depleted in bulk FeO and MgO, features attributable to both modal and mineral compositional differences. The trace elements Ni, Co and Zn are present in olivine, and to a lesser extent in clinopyroxene, and Cr, V and Sc, together with TiO_2 , are present mostly in clinopyroxene. Sr is present mostly in plagioclase with minor quantities in clinopyroxene.

3.4.4 VEINS

Two groups of veins cut the main body of magnesian dunite at Driekop,

those that are related to the platiniferous core and those that are related to the marginal envelope of iron-rich olivine clinopyroxenite. Veins which may be related to the platiniferous core at Driekop were referred to briefly in section 3.3.1. They occur as both parallel-walled veins and irregular bodies which radiate out from the central core-area. These veins may be be observed over almost the entire outcrop of the dunite, where they are emphasized by numerous small prospecting pits and the presence of secondary magnesite veins. Whether all of these veins, which occur for distances of over 200 m from the central core-area, radiate from the core has not been established. They are, however, concentrated preferentially adjacent to the main core-area where they occur primarily as a radial set. Some veins also occur here as a concentric group. Wagner (1929) reported that most of these veins at Driekop were platiniferous. Some of them formed important ore-shoots outside of the main core-area. They consist of varying proportions of iron-rich olivine and clinopyroxene with accessory plagioclase, amphibole, mica and magnetite.

Wagner (1929) also reported the presence of veins, which are related to the platiniferous cores, in the Mooihoek and Onverwacht pipes. Again, they occur in concentric and radial zones, concentrated close to the central cores. These two sets of veins, which cut each other approximately at right angles, are aligned parallel to the circumference and dip of the overall pipe. Consequently, Wagner (1929) interpreted them as occupying shrinkage cracks in the magnesian dunite. Veins in the Onverwacht pipe, which may be platiniferous, are more fractionated than the main core assemblage. They consist of coarse-grained iron-rich dunite and pegmatitic clinopyroxene - hornblende - phlogopite - Ti-magnetite - ilmenite varieties (Wagner, 1929). Veins at Mooihoek are pegmatitic and may exhibit considerable mineralogical variation. Hortonolite occurs in the narrower veins but may be absent in the thicker veins. These latter consist of clinopyroxene, phlogopite, hornblende, Ti-magnetite and ilmenite and are very coarse-grained (with grain sizes of up to 15 cm). The hortonolite-bearing veins contain minor PGE, but the more fractionated veins are barren (Wagner, 1929).

The second group of veins found at Driekop comprise very coarse-grained wehrlite, olivine clinopyroxenite and clinopyroxenite varieties. They appear to be restricted to the margin of the pipe. They can be observed in the adit (on which Wagner based his cross section) and at the base of the koppie on the western and southern sides. They occur as parallel-walled veins, usually 0.5 to 1 m in thickness and as wedge-shaped bodies which may be traced into the marginal envelope of iron-rich olivine clinopyroxenite (fig. 3.5A). They do not normally contain base-metal sulphide, or PGM.

3.4.5 CONTACT ZONES

MAGNESIAN DUNITE / PLATINIFEROUS, IRON-RICH DUNITE CORE

In the field (see section 3.3.1) and in thin section this contact is sharp and no gradational compositional trends have been recorded. A distinctive feature is the abrupt disappearance of primary spinel.

MAGNESIAN DUNITE / MARGINAL ENVELOPE OF IRON-RICH OLIVINE CLINOPYROXENITE

This contact is sharp and regular in the field, although the magnesian dunite adjacent to it is serpentinised and veined by secondary magnesite. In thin section, however, this contact is clearly gradational. For distances of 1 to 2 cm from the actual contact clusters of olivine and clinopyroxene grains, related to the iron-rich olivine clinopyroxenite assemblage, project into the magnesian dunite. This hybrid assemblage may be described as a wehrlite. Large, anhedral grains of clinopyroxene poikilitically enclose and partially resorb the magnesian olivine (fig. 3.6C; note that clinopyroxene is earlier than the iron-rich olivine in the olivine clinopyroxenite). Two generations of olivine may be observed in this assemblege. Small, relict grains (presumably related to the primary magnesian dunite) are enclosed by large, anhedral grains (derived from the olivine clinopyroxenite). This second generation olivine is later than the clinopyroxene. Spinel is usually absent in this assemblage, and for a lateral distance of several metres from the contact the magnesian dunite is depleted in spinel. Furthermore, spinel which does occur is invariably the polyphase variety (see Chapter 4).

Olivine in this contact assemblage has an average composition of $Fo_{73.6}$ (sample DR-22, Table 4.1); the two generations of olivine do not exhibit any compositional differences. The measured composition is part-way between olivine from the magnesian dunite ($Fo_{83.6}$) and the iron-rich olivine clinopyroxenite ($Fo_{65.1}$). The average X_{Mg} of clinopyroxene in this contact assemblage is .828 (sample DR-22, Table 4.1). These two minerals are probably in equilibrium (see Chapter 9). The paucity of chromite in this contact zone is supported by one whole-rock analysis (sample DR-22, Appendix 5).

Field relationships indicate that the marginal envelope of iron-rich olivine clinopyroxenite formed after the main body of magnesian dunite. Petrographic studies and chemical data imply that these two assemblages are in disequilibruim. The hybrid contact assemblage described above may be attributed to replacement (or metasomatism) of pre-existing magnesian dunite in response to disequilibrium with an iron-rich liquid, that resulted in

formation of the olivine clinopyroxenite assemblage. Disequilibrium resulted in exchange of Mg by Fe^{2+} to produce a hybrid olivine that is compositionally midway between the original magnesian olivine and that in eqiulibrium with the iron-rich liquid. The Ni content of this "metasomatic" olivine may support this argument (see Chapter 4). The hybrid clinopyroxene probably resulted by resorption of magnesian olivine. Chromiferous spinel in the magnesian dunite was evidently unstable in the presence of this iron-rich liquid and was resorbed. This is an unusual feature as chromite is normally a very stable mineral.

3.5 SATELLITE BODIES OF ULTRAMAFIC-MAFIC ROCK ADJACENT TO THE DRIEKOP PIPE

3.5.1 CLASSIFICATION AND DISTRIBUTION

Satellite bodies which may be directly related to the Driekop pipe may be subdivided into three main types : (1) magnesian dunite with subordinate lherzolite; (2) iron-rich clinopyroxenite and websterite pegmatite; and (3) mafic pegmatite. In addition, pegmatite veins composed of plagioclase, orthopyroxene, amphibole and mica occur, and a pegmatitic texture may occasionally be observed in the cumulates. These latter two features are attributed either to exomorphic processes related to the pipe, or to normal deuteric postcumulus processes operating within the cumulate pile. The distribution of some of the satellite bodies of ultramafic and mafic rock located in the 3-level crosscut can be seen in Figure 3.4 (see also Map 2). Bodies of iron-rich clinopyroxenite pegmatite have been located on surface for distances of over 1.5 km from the pipe, but are clearly most abundant in proximity to the main pipe. Bodies of magnesian dunite and lherzolite appear to be restricted to the structurally disturbed envelope.

3.5.2 SATELLITE BODIES OF MAGNESIAN DUNITE AND LHERZOLITE

FIELD RELATIONSHIPS

These satellite bodies, which have only been observed in the 3-level crosscut at Driekop, are essentially confined within pyroxenitic cumulates associated with the UG-chromitite layers (see section 3.3.2 and fig. 3.4B). Well-defined bodies of magnesian dunite may be mapped here, but often the distinction between a transgressive body of dunite and an orthopyroxenite cumulate is difficult to establish. A marginal zone may occur, in which cumulus orthopyroxene is replaced by magnesian olivine (fig. 3.6E,F). Olivine may also occur in partially replaced cumulates, and Schiffries

(1982) refers to the olivine-rich matrix to both the UG-2 and UG-3 chromitite layers in this section. The larger satellite bodies of magnesian dunite transgress the cumulate layering which is structurally disrupted (see section 3.3.2). They may themselves be cut and replaced by later bodies of iron-rich pyroxenite pegmatite. Veins composed of noritic or gabbroic material (probably remobilised cumulates) cut and displace (usually by high angle normal faults with throws of less than 1 m) the layered sequence here. They clearly postdate the formation of the pipe-related satellite bodies.

A satellite body of magnesian dunite has also been observed at Driekop which is emplaced in felsic cumulates, approximately 40 m from the contact of the pipe (fig. 3.4A). This is a sill-like body, approximately 0.5 m thick, which is inclined at 63^{o}. It occurs along the lower contact of a thick layer of mottled anorthosite. The upper contact is knife-sharp and is marked by a thin selvage of chromitite, a few grains thick. A 2 m thick layer of massive plagioclase occurs in the hangingwall of this body, above which is normal mottled anorthosite. Cumulus plagioclase in the hangingwall has recrystallized and is partially replaced by clinozoisite. The lower contact of this body is irregular, diffuse and gradational into unaltered leuconorite. Coarse-grained clinopyroxene crystals occur at the base of the sill, which terminates abruptly within the exposure observed. This body appears to exhibit an intrusive relationship to the cumulates. The thin chromitite layer on the upper contact is presumably derived from the dunite, as the cumulate wallrocks are essentially devoid of chromite.

PETROGRAPHY AND MINERAL CHEMISTRY

OLIVINE : Olivine in the small, sill-like body of magnesian dunite has an average composition of $Fo_{84.7}$ (sample DR-111, Table 4.1), and is comparable to that from the main body of magnesian dunite (although it is more nickel rich - see Chapter 4). The average composition of olivine from satellite bodies of magnesian dunite and lherzolite that are intimately associated with pyroxenite-chromitite cumulates (including the UG-2 and UG-3 chromitite layers) is $Fo_{79.0}$ (samples DR-42,46, Table 4.1).

PYROXENE : The average X_{Mg} of clinopyroxene and orthopyroxene from lherzolite pegmatite bodies at Driekop is .887 and .829, respectively (sample DR-46, Table 4.2). In comparison, the X_{Mg} of cumulus clinopyroxene and orthopyroxene from unaltered orthopyroxenites (associated with the UG-2 chromitite layer, 0.5 km from the pipe) is .861 and .811, respectively (sample DR-52, Table 4.2). The pegmatite-hosted pyroxenes are thus slightly more magnesian.

CHROMITE : Chromite grains from orthopyroxenite cumulates adjacent to

the UG-2 chromitite layer and from the magnesian dunite and lherzolite bodies have been analysed and are discussed in Chapter 4.

WHOLE-ROCK CHEMISTRY

One analysis of a lherzolite pegmatite is presented in Table 3.3 (sample DR-42). It is a hybrid rock, the chemistry of which reflects elements of both a cumulus orthopyroxenite and the magnesian dunite. Further investigations of these satellite bodies are required before any detailed genetic conclusions can be established.

3.5.3 IRON-RICH CLINOPYROXENITE AND WEBSTERITE PEGMATITE

FIELD RELATIONSHIPS

Satellite bodies of iron-rich clinopyroxenite and websterite pegmatite are particularly abundant close to the main pipe, where dozens of individual occurrences have been mapped (fig. 3.4A, Map 2). They usually occur as irregular bodies that are discordant to the cumulate layering, and have maximum lateral dimensions of between 10 and 15 m, but may have dimensions of less than 1 m. The smaller occurrences occur as pod-shaped bodies, dykes and small, spheroidal masses, whereas the larger bodies tend to form sill- or sheet-like bodies which are locally concordant. The lateral contacts between these bodies and their cumulate hosts are usually sharp, but irregular. Typically the pegmatite body transgresses the layering with no structural disturbance being evident (fig. 3.5C). The upper, or lower contacts of these bodies may, however, be diffuse. This is indicative of a replacement front. These features suggest that these bodies formed after the layering was downwarped. Furthermore, the field relationships indicate that they probably formed by in situ, passive replacement (see also Schiffries, 1982). Similar field relationships are exhibited by iron-rich ultramafic pegmatite bodies (see Chapter 7).

PETROGRAPHY

Satellite bodies close to the pipe are composed of websterite or clinopyroxenite pegmatite, in which olivine and plagioclase are accessory phases. Mineralogically they are similar to the marginal envelope of iron-rich olivine clinopyroxenite. With increasing distance from the pipe clinopyroxenite pegmatite becomes the dominant variety. This increase in modal clinopyroxene is sympathetically associated with an increase in grain size. Clinopyroxenite pegmatites exhibit a hypautomorphic granular texture in which individual, subhedral or anhedral grains, often with dimensions

over 100 mm, exhibit extensive mutual interference (fig. 3.6D). Microtextures are similar to those documented in Chapter 8. Discrete grains of orthopyroxene occur in this variety of pegmatite, but olivine is fairly rare; it may, however, be observed as tiny, lath-like grains that replace clinopyroxene along cleavage traces. The websterite pegmatites are composed of clinopyroxene with up to 40 modal percent orthopyroxene. Again, olivine is a rare accessory pkase. Chromite is only rarely observed in these rocks; it is probably a relict cumulus mineral. Primary Ti-magnetite, ilmenite and base-metal sulphides are not normally observed.

A thin outer selvage of orthopyroxene, plagioclase and mica is present in some of these bodies. It is attributed to partial metasomatism of the cumulate host. Composite magnesian dunite-lherzolite and iron-rich clinopyroxenite-websterite pegmatite bodies have also been observed. These exhibit a complex mineralogy and have not been studied in detail. Field relationships, however, suggest that the iron-rich assemblages formed after the magnesian dunite-lherzolite, as may be expected by comparison with the main pipe.

MINERAL CHEMISTRY

OLIVINE : The average composition of olivine in this assemblage is $Fo_{62.8}$ (2 analyses only; sample DR-32, Table 4.1).

PYROXENE : The X_{Mg} of clinopyroxene and orthopyroxene from websterite pegmatite is .761 and .723, respectively (sample DR-32) and that from clinopyroxenite pegmatite is .755 and .671, respectively (sample DR-38, Table 4.2). Both olivine and pyroxene are thus compositionally comparable to samples from the marginal envelope of iron-rich olivine clinopyroxenite. These data also indicate that the pegmatites become slightly more fractionated with distance from the pipe, as is also evidenced by the eventual predominance of clinopyroxene, initially over olivine and then over orthopyroxene.

WHOLE-ROCK CHEMISTRY

Selected whole-rock analyses of iron-rich websterite pegmatite (samples DR-31,32) and clinopyroxenite pegmatite (sample DR-38) are presented in Table 3.3 (for complete analyses see Appendix 5). These rocks are mineralogically and chemically similar to the iron-rich olivine clinopyroxenite assemblage from the main pipe (samples DR-25,27, Table 3.3), if allowance is made for modal variation. The slightly higher Mg-number of these samples (average =.77-.76) is a reflection of the higher modal proportion of clinopyroxene. The minor and trace element chemistry of these

rocks is comparable to that described for the iron-rich olivine clinopyroxenite. It is noticeable that clinopyroxenite pegmatite, which is less primitive (as evidenced by X_{Mg} of pyroxene grains) than websterite pegmatite, is richer in the incompatible elements.

3.5.4 MAFIC PEGMATITE

Mafic pegmatites in the structurally disturbed zone adjacent to the Driekop pipe form small, exceptionally irregular, often spheroidal bodies in which the pegmatite and cumulate host merge into each another. They are considerably less abundant than the other satellite bodies, and are usually associated with larger bodies of clinopyroxenite or websterite pegmatite. Mafic pegmatites often exhibit a radial arrangement of large, euhedral clinopyroxene crystals set in a matrix of plagioclase. Locally this may define a pseudo-graphic texture (fig. 3.5D). The plagioclase in between the clinopyroxene crystals is in optical continuity over large areas and is invariably saussuritised. It has probably been derived from the cumulates as a result of local recrystallization. Large crystals of amphibole and biotite are common in these pegmatites and apatite and quartz may also be observed.

The mineral chemistry of this assemblage has not been investigated. One whole-rock analysis is presented in Table 3.3 (sample DR-39). Compared with iron-rich clinopyroxenite pegmatite it is richer in plagioclase, as indicated by the higher Al_2O_3 and Sr contents, and is poorer in ferromagnesian silicates. The proportion of incompatible elements (Ti, K, P, Nb, Zr, Y and Rb) is much greater, partly due to the presence of apatite.

3.6 PETROLOGY OF THE CUMULATE WALLROCKS

Two whole-rock analyses of samples of leuconorite immediately adjacent to the Driekop pipe are presented in Table 3.3 (samples DR-29,30; see also Appendix 5). Mineralogically and chemically they are unaltered and indistinguishable from typical cumulates from the upper critical zone of the layered sequence. Pipe-related olivine and clinopyroxene have not been located in these felsic cumulates. Microprobe analyses of cumulus orthopyroxene (X_{Mg} =.768) and intercumulus clinopyroxene (X_{Mg} = .837) are presented in Table 4.2 (samples DR-28,29,30; note that the sequence of cumulates exposed in the 3-level crosscut at Driekop represents an inclined section of part of the layered sequence and because of fractionation effects, the composition of cumulus minerals varies.). These cumulus and intercumulus pyroxenes are more magnesian than pyroxenes from the marginal

envelope of iron-rich olivine clinopyroxenite at Driekop. Field relationships suggest that some assimilation or replacement of the adjacent cumulates has occurred at the edge of the pipe, and resorption of cumulus plagioclase is particularly evident. The data of Schiffries (1982) indicate that plagioclase associated with the iron-rich olivine clinopyroxenite is unusually calcic; similar features are observed in plagioclase that has been partially resorbed by iron-rich ultramafic pegmatite at Amandelbult (see Chapter 8).

The ultramafic cumulates (orthopyroxenites and chromitites), which were intersected in the 3 level crosscut, have been referred to in sections 3.3.2 and 3.5.2. Here, replacement of cumulus orthopyroxene by pipe-related, magnesian olivine is evident, resulting in the formation of hybrid rocks. Similar features were documented by Cameron and Desborough (1964) in the pyroxenite wallrocks to the Onverwacht pipe. The author concurs with the conclusions of Cameron and Desborough that metasomatic replacement of cumulus orthopyroxene by olivine occurs at the contact between orthopyroxenite cumulates and discordant bodies of magnesian dunite. However, there is no evidence to extrapolate this process to the main pipe at Driekop; metasomatic replacement of the felsic cumulates (which host the Driekop pipe at the present exposure level), by magnesium-rich fluids has not been observed.

CHAPTER 4 DRIEKOP : MINERALOGY AND GENESIS

This chapter presents some additional mineralogical studies on olivine, pyroxenes, Fe-Ti-Cr oxides and the ore minerals. Data for the different petrologic assemblages, which were presented in the previous chapter, are modelled in relationship to the whole pipe. Finally, the genesis of the platiniferous ultramafic pipes is discussed.

4.1 OLIVINE

4.1.1 COMPOSITIONAL VARIATION

The composition of olivine is fundamental to the recognition and interpretation of petrologic assemblages in the Driekop pipe. Averages of electron microprobe analyses of olivines from each assemblage are presented in Table 4.1 (some of these data have been corroborated by whole-rock analyses - see previous chapter). These data may be summarised as follows :-

(1) Magnesian dunite, main pipe, Driekop : $Fo_{83.6}$
(2) Platiniferous core, main pipe, Driekop : $Fo_{72.7}$
(3) Olivine clinopyroxenite, main pipe, Driekop : $Fo_{65.1}$
(4) Contact zone, magnesian dunite - olivine clinopyroxenite, main pipe, Driekop : $Fo_{73.6}$
(5) Magnesian dunite, sill-like satellite body, Driekop : $Fo_{84.7}$
(6) Websterite pegmatite, satellite body, Driekop : $Fo_{62.8}$
(7) Hybrid, magnesian dunite - orthopyroxenite cumulates, satellite bodies, Driekop : composition variable; approximately Fo_{79}

In addition, the composition of olivine from the platiniferous cores of the Onverwacht and Mooihoek pipes has been determined as Fo_{65-64} and Fo_{44-43}, respectively. Thus olivine from the platiniferous cores of these pipes defines a compositional range from $Fo_{72.7}$ (iron-rich chrysolite) to Fo_{44-43} (hortonolite). It is also possible that olivine in the core of each pipe may exhibit some compositional variation, but as only restricted samples are now available this has not been investigated further.

4.1.2 MODELLING OF NiO-MgO RELATIONSHIPS IN OLIVINE

DISCUSSION

Data from electron microprobe analyses of olivines completed in this study are plotted on a binary graph of wt. percent NiO versus wt. percent

TABLE 4.1 ELECTRON MICROPROBE ANALYSES OF OLIVINE FROM THE PLATINIFEROUS ULTRAMAFIC PIPES

	DR-A1, A2		DR-1/4/10/12		DR-22		DR-25/27		DR-32		DR-42/46		DR-111	
wt.%	x	d	x	d	x	d	x	d	x	d	x	d	x	d
SiO_2	37.96	.4645	39.52	.5138	38.11	.2316	38.15	.2481	36.87	.3960	39.19	.2657	39.96	.1253
FeO	24.74	.5837	15.58	.2436	24.31	.1682	30.53	.3139	32.33	.2404	19.57	.2134	14.48	.1060
MnO	.34	.0263	.22	.0227	.30	.0171	.43	.0239	.47	.0141	.26	.0095	.20	.0058
MgO	37.05	.2751	44.47	.4669	38.00	.0963	31.96	.4208	30.57	.6081	41.27	.2355	44.84	.2468
CaO	.08	.0243	.07	.0330	.03	.0141	.04	.0275	.03	.0283	.03	-	.01	.0153
NiO	.26	.0239	.28	.0136	.27	.0171	.20	.0130	.20	.0071	.31	.0252	.34	-
TOTAL	100.43	-	100.14	-	101.02	-	101.31		100.47	-	100.63	-	99.83	-
cations														
Si	.9963		.9953		.9919		1.0171		1.0038		1.0000		1.0033	
Fe^{2+}	.5430		.3281		.5292		.6807		.7361		.4176		.3041	
Mn	.0076		.0047		.0066		.0097		.0108		.0056		.0043	
Mg	1.4492		1.6691		1.4740		1.2699		1.2403		1.5695		1.6779	
Ca	.0022		.0019		.0084		.0011		.0009		.0008		.0003	
Ni	.0055		.0057		.0057		.0043		.0044		.0064		.0069	
TOTAL	3.0038		3.0047		3.0081		2.9829		2.9963		3.0000		2.9967	
n	8		11		4		4		2		7		4	
Fo	72.7	.3741	83.6	.2774	73.6	.1258	65.1	.5135	62.8	.6435	79.0	.2231	84.7	.1680

	ON-2		MO-4		MO-3		TW-1		DUN-1	
wt.%	x	d	x	d	x	d	x	d	x	d
SiO_2	37.68	.1344	35.23	.5026	36.11	.0493	41.02	1.4213	40.16	.6650
FeO	31.33	.2915	45.75	.1702	39.21	.1901	15.15	.0071	12.38	.1399
MnO	.41	.0217	.66	.0476	.51	.0231	.21	.0141	.18	.0303
MgO	31.34	.2013	19.48	.3048	24.43	.2065	44.48	.6293	46.74	.3803
CaO	.04	.0150	.04	.0305	.04	.0115	-	-	-	-
NiO	.21	.0164	.09	.0141	.13	.0153	.26	.0283	.30	.0164
TOTAL	101.01	-	101.25	-	100.45	-	101.12	-	99.76	-
cations										
Si	1.0127		1.0180		1.0175		1.0167		.9995	
Fe^{2+}	.7042		1.1056		.9235		.3140		.2577	
Mn	.0093		.0162		.0121		.0044		.0038	
Mg	1.2553		.8389		1.0253		1.6430		1.7336	
Ca	.0012		.0012		.0012		-		-	
Ni	.0046		.0021		.0030		.0052		.0060	
TOTAL	2.9873		2.9820		2.9826		2.9833		3.0005	
n	5		5		3		2		5	
Fo	64.1	.3358	43.1	.4383	52.6	.3259	83.95	.1838	87.1	.1346

- : not determined; x: mean; d: standard deviation; n: number of samples; Fo : mol.% forsterite.

DR1/2 : Iron-rich chrysolite, platiniferous core, Driekop.
DR1/4/10/12 : Chrysolite, magnesian dunite, main pipe, Driekop.
DR-22 : Iron-rich chrysolite, "contact zone", main pipe, Driekop.
DR-25/27 : Hyalosiderite, olivine clinopyroxenite, main pipe, Driekop.
DR-32 : Hyalosiderite, satellite body of clinopyroxenite, Driekop.
DR-42/46 : Chrysolite, satellite body of lherzolite, Driekop.
DR-111 : Chrysolite, satellite body of magnesian dunite, Driekop.
ON-2 : Hyalosiderite, platiniferous core, Onverwacht.
MO-4 : Hortonolite, platiniferous dunite, Mooihoek.
MO-3 : Hyalosiderite, platiniferous wehrlite, Mooihoek.
TW-1 : Chrysolite, Twyfelaar.
DUN-1 : Cumulus olivine, lower zone.

MgO (fig. 4.1). These data fall into two groups. The first includes olivine ($Fo_{83.6}$) from the magnesian dunite in the main pipe at Driekop, and may also include olivine ($Fo_{84.7}$) from the sill-like body of magnesian dunite. The NiO content, or NiO/MgO ratio of these magnesian olivines is comparable with cumulus olivines from the lower and critical zones of the Bushveld Complex (Cameron, 1980; Botha, in prep.; see also Chapter 9). Scatter in individual samples may be explained by analytical error, particularly in the NiO content, or by minor fractionation (see below).

The second group incorporates all iron-rich olivines (i.e. more fayalitic than Fo_{75}) from the platiniferous pipes. This group includes olivine from the platiniferous cores of Driekop, Onverwacht and Mooihoek, as well as olivine from the iron-rich olivine clinopyroxenite, websterite and clinopyroxenite pegmatite assemblage at Driekop. In comparison with iron-rich cumulus olivine from the upper zone of the Bushveld Complex (see Chapter 9) and with published analyses of iron-rich olivines (Deer et al., 1982), it may be concluded that iron-rich olivine in the platiniferous ultramafic

pipes has an unusually high NiO/MgO ratio. In Figure 4.1 it can be seen that the iron-rich olivines plot on a straight line for which a linear regression may be calculated (based on 35 analyses of 9 separate samples; see Appendix 7 for complete analyses), thus :

wt.% NiO = (wt.% MgO * .0096) - 0.1 (correlation coefficient = .988)

Olivine from the sill-like body of magnesian dunite at Driekop also plots on this line, if it is extrapolated to more primitive compositions. This olivine contains 44.84 wt. percent MgO and .34 wt. percent NiO (sample DR-111, Table 3.5); a theoretical NiO content of .33 wt. percent may be calculated with the above formulae.

THEORETICAL FRACTIONATION MODEL

If olivine from this sill-like body is taken as a starting composition (being the most primitive of the samples analysed in this study) theoretical fractionation curves can be generated to predict the NiO and MgO contents of more iron-rich olivines that would be derived by progressive crystallization of an initial liquid that is in equilibrium with this olivine. This technique uses the formulae of Hart and Davis (1978) to calculate the

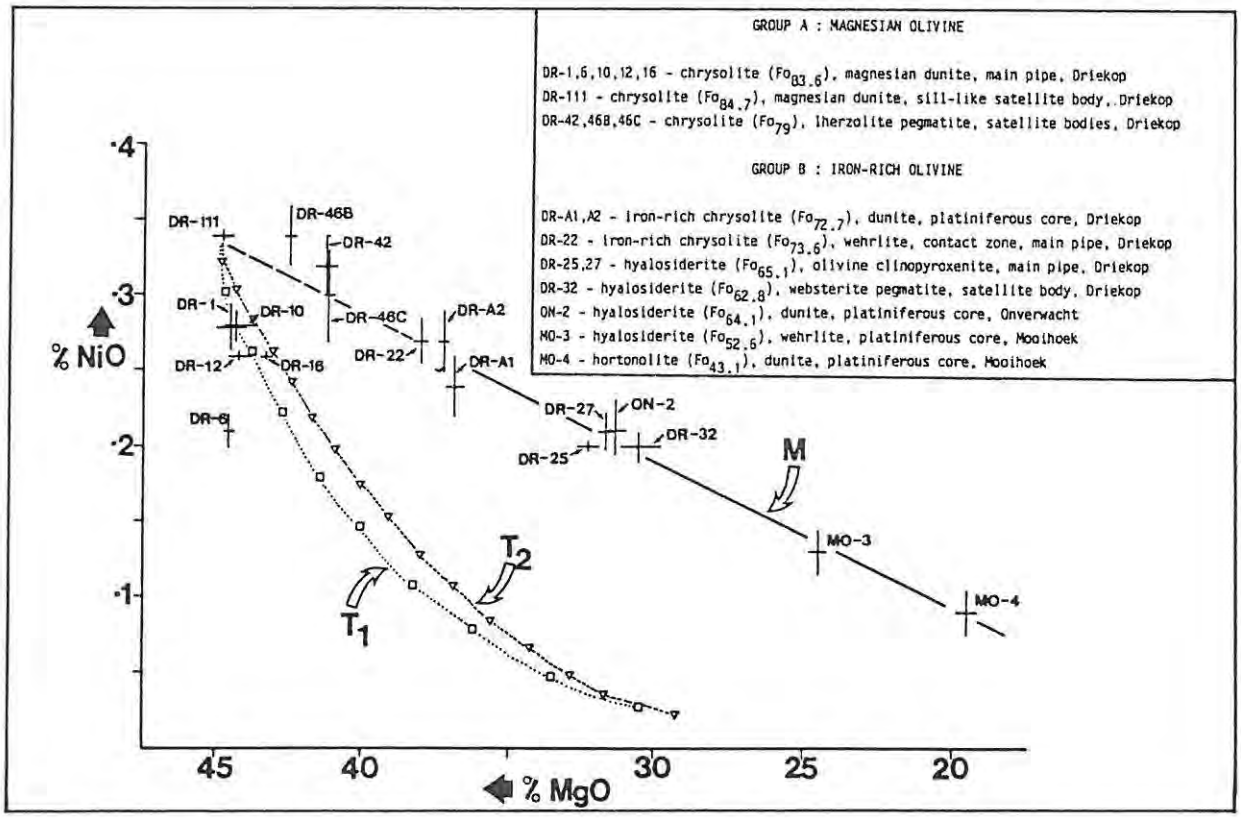

FIGURE 4.1 Plot of wt. % NiO vs. wt. % MgO in olivine

Data for each sample plotted as a cross in which the error bars are equal to 2 standard deviations (from electron microprobe data presented in Table 4.1). The iron-rich olivines plot on a straight line ("M"); this may be extrapolated to include magnesian olivines from the lherzolite pegmatite bodies and sample DR-111. Olivine from the magnesian dunites may plot on a fractionation path. The composition of olivine calculated for two theoretical fractionation paths is plotted, T_1 (assuming initial liquid contains 20.0 wt. % MgO) and T_2 (assuming initial liquid contains 39.7 wt. % MgO), both of which are initially in equilibruim with olivine in sample DR-111. Each point on these fractionation lines (open squares or triangles) represents 5 % crystallized.

distribution of Ni between silicate liquid and olivine, and the formulae of Roeder (1974) to calculate the distribution of Mg and Fe^{2+} between silicate liquid and olivine (for explanation see Chapter 9). The theoretical fractionation curves plotted on Figure 4.1 indicate that the magnesian olivines plot on a possible fractionation path. However, the iron-rich olivines do not lie on a fractionation path, an argument that is corroborated by actual measured fractionation paths for cumulus olivines in the Bushveld Complex (see Chapter 9). It is important to note that the starting composition and the initial MgO content of the liquid do not significantly affect the trend of this fractionation path. The iron-rich olivines do not then appear to have resulted from in situ fractionation of a silicate liquid that is initially in equilibrium with magnesian olivines in these pipes. Furthermore, it is evident that the iron-rich olivines themselves do not lie on a separate fractionation path. Compositional variation within the iron-rich olivine group may be explained by a mixing model between two liquids or by a metasomatic model. The former model would requre an implausibly stringent sequence of events, and thus the latter model is preferred.

METASOMATIC MODEL

This is based on the recognition of metasomatism in the contact zone between the magnesian dunite and the marginal unit of iron-rich olivine clinopyroxenite (see section 3.4.5), and the NiO-MgO relationships of "metasomatic" olivines from the contact zones of pegmatite bodies at Amandelbult (see Chapter 9). In the contact zone at Driekop disequilibrium between olivine in the magnesian dunite ($Fo_{83.6}$, 0.28 wt. percent NiO) and an iron-rich liquid has resulted in formation of "metasomatic" olivine with a composition of $Fo_{73.6}$ and 0.27 wt. percent NiO. Olivine in the platiniferous core of the Driekop pipe has a similar composition, and it is thus plausible that it also has resulted from metasomatism of magnesian olivine. Metasomatic fayalitic olivines may thus have similar Ni contents to primary, more magnesian olivine. This feature is also exhibited by metasomatic olivines at Amandelbult. Furthermore, Irvine (1980) describes "metasomatic" olivine from the Muskox Intrusion which is characterised by a high Ni/(Ni+Mg+Fe) ratio.

It is concluded that at least some, if not all, of the iron-rich olivines in these pipes are of metasomatic origin. Iron-rich olivine in the cores of the pipes has probably resulted from metasomatism of pre-existing magnesian olivine, in response to iron-rich liquids that have reacted with the magnesian dunite after it was crystalline. The marginal envelope of iron-rich olivine clinopyroxenite and satellite bodies of

websterite and clinopyroxenite pegmatite do not all replace magnesian dunite, and consequently olivine in this assemblage has not resulted from metasomatism of magnesian olivine. It may be compared with olivine from iron-rich ultramafic pegmatite at Amandelbult, and may be directly representative of the composition of the iron-rich liquid from which it formed, either as a result of crystallization or by metasomatism of pre-existing cumulates.

These data indicate that the iron-rich liquid responsible for the formation of the iron-rich assemblages in the pipes was not neccessarily unusually rich in Ni. It must also be realised that this modelling provides no insight into the origin of magnesian olivine in the pipes.

4.2 PYROXENES

4.2.1 COMPOSITIONAL VARIATION

Selected electron microprobe analyses of orthopyroxene-clinopyroxene pairs are presented in Table 4.2 (see also Appendix 8). These data are plotted on a triangular diagram of Wo-En-Fs in Figure 4.2. X_{Mg} of cumulus orthopyroxene from the cumulates exposed in the 3-level crosscut adjacent to

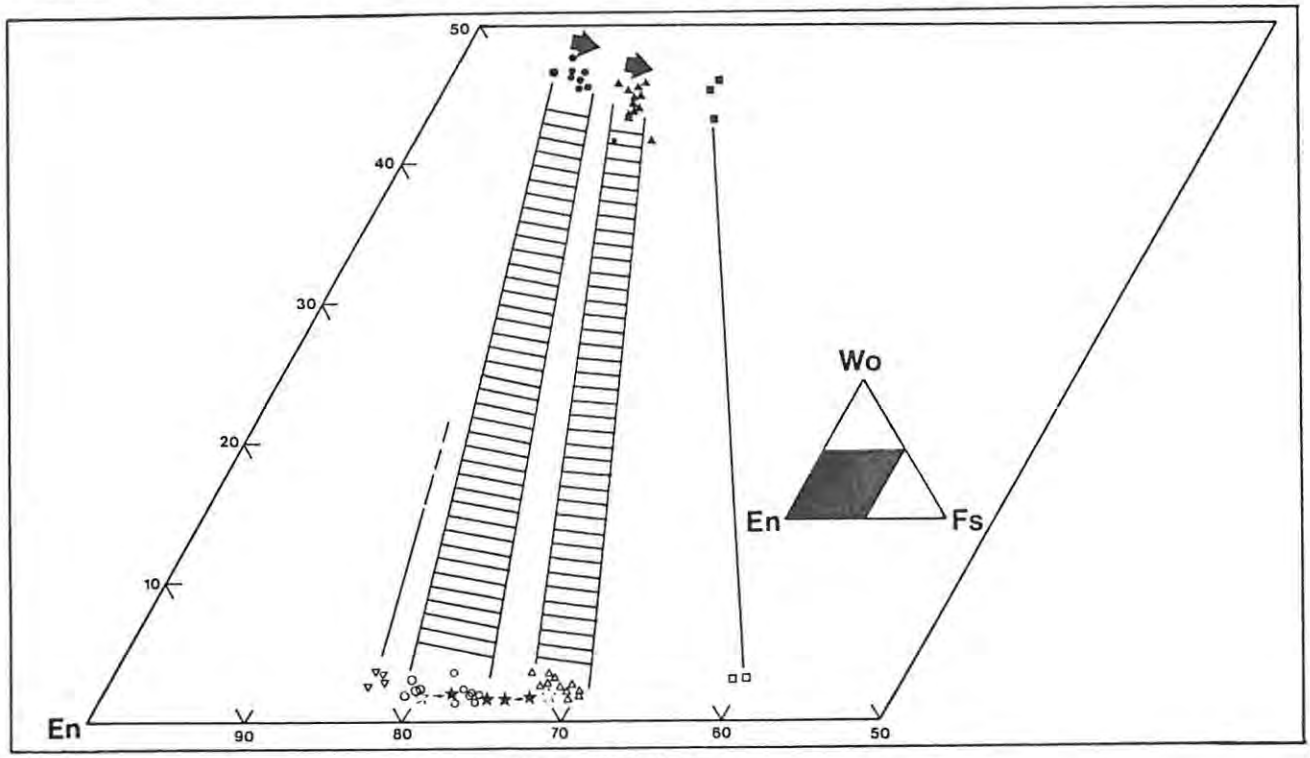

FIGURE 4.2 Part of the pyroxene triangular diagram of En-Wo-Fs.
The following sample groups are recognized (each symbol represents one electron microprobe analysis) :
○ ● GROUP A - Upper critical zone cumulates adjacent to the Driekop pipe (between the UG-2 and the Merensky Reef)
△ ▲ GROUP B - Iron-rich, pipe-related rocks at Driekop (main pipe and satellite bodies of pyroxenite pegmatite)
□ ■ GROUP C - Mooihoek pipe (probably from the core)
▽ - GROUP D - Magnesian, pipe-related rocks at Driekop (satellite bodies of lherzolite pegmatite)
(Clinopyroxenes represented by solid symbols, orthopyroxenes by open symbols. Shaded areas represent tie-lines for the two main population groups, A and B, and the arrows indicate fractionation in these two groups).
★ Orthopyroxene from pegmatite contact zone (2 cm. in width)
☆ End-member compositions (averages; cumulus, X_{Mg} = .80, pegmatite, X_{Mg} = .71)

TABLE 4.2 ELECTRON MICROPROBE ANALYSES OF PYROXENES FROM DRIEKOP AND MOOIHOEK

	DR-22		DR-25/27			DR-32				DR-38			
	CLINOPYROXENE		CLINOPYROXENE		ORTHOPYROXENE			CLINOPYROXENE		ORTHOPYROXENE		CLINOPYROXENE		ORTHOPYROXENE	
wt.%	x	d	x	d	x	d		x	d	x	d	x	d	x	d
SiO_2	53.13	.3547	53.18	.2377	54.08	.1982		52.38	.1229	53.72	.2798	52.82	.3800	53.31	.2687 2
TiO_2	.31	.0058	.28	.0168	.14	.0194		.31	.0577	.16	.0050	.28	.1190	.16	.0495 2
Al_2O_3	2.20	.2458	1.85	.0624	1.27	.1554		2.04	.0881	1.18	.0835	1.86	.0635	1.23	.0849 2
FeO	5.95	.1097	7.92	.7456	18.54	.4022		8.51	.5495	17.05	.4862	8.64	1.2636	20.28	1.5556 2
MnO	.25	-	.23	.0214	.36	.0841		.23	.0346	.35	.0299	.27	.0655	.36	.0707 2
MgO	16.07	.3931	15.36	.3259	24.33	.1776		15.23	.2954	25.00	.2956	14.93	.5883	23.18	.9051 2
CaO	21.52	.1153	21.17	.9970	1.06	.2396		20.71	.7441	1.74	.2434	21.01	1.7672	1.31	.6293 2
Na_2O	.25	.0462	.19	.0465	n.d.	-		.51	.3523	n.d.	-	.21	.0100	n.d.	-
Cr_2O_3	.65	.2303	.14	.0267	.08	.0103		.35	-	.21	.0129	.15	.0096	.10	.0071 2
NiO	.04	-	.02	.0107	.03	.0207		.04	.0100	.06	.0206	.07	.0252	.08	.0100 2
TOTAL	100.37	-	100.34	-	99.89	-		100.31	-	99.47	-	100.24	-	100.01	-
cations/ 6 oxygens															
Si	1.9455		1.9598		1.9793			1.9519		1.9685		1.9562		1.9692	
Ti	.0085		.0078		.0039			.0085		.0044		.0078		.0044	
Al	.0950		.0804		.0548			.0881		.0510		.0812		.0536	
Fe^{2+}	.1822		.2441		.5675			.2607		.5225		.2676		.6265	
Mn	.0078		.0072		.0112			.0071		.0109		.0085		.0113	
Mg	.8770		.8436		1.3271			.8315		1.3652		.8241		1.2761	
Ca	.8443		.8359		.0416			.8130		.0683		.8338		.0518	
Na	.0177		.0136		-			.0362		-		.0151		-	
Cr	.0188		.0041		.0023			.0101		.0061		.0044		.0029	
Ni	.0012		.0006		.0009			.0012		.0018		.0021		.0024	
TOTAL	3.9980		3.9970		3.9884			4.0085		3.9986		4.0007		3.9982	
n	3		7		6			3		4		4		2	
Wo	44.36		43.46		2.15			42.67		3.49		43.30		2.65	
En	46.07		43.85		68.54			43.64		69.80		42.80		65.29	
Fs	9.57		12.69		29.31			13.69		26.71		13.90		32.06	
X_{Mg}	.828	.0062	.776	.0149	.700	.0053		.761	.0096	.723	.0081	.755	.0203	.671	.0255
Al/Cr	5.4		20.2		23.7			8.7		8.4		18.5		18.3	

	DR-28/29/30		DR-52		DR/28/29/30		DR-52	MO-4				DR-46		
	ORTHOPYROXENE		ORTHOPYROXENE		CLINOPYROXENE		CLINOPYROXENE*	ORTHOPYROXENE*		CLINOPYROXENE		CLINOPYROXENE	ORTHOPYROXENE	
wt.%	x	d	x	d	x	d		x	d	x	d			
SiO_2	55.61	.4440	55.43	.1909 2	54.50	.7839	53.22	52.55	.2456	52.23	.8524	53.39	56.68	.2475
TiO_2	.15	.0219	.13	.0071 2	.23	.0130	.30	.16	.0071	.50	.0889	.26	.13	-
Al_2O_3	.92	.1452	1.52	.0212 2	1.20	.3648	2.49	1.16	.0141	2.34	.2201	1.79	1.47	.1131
FeO	14.63	.3223	11.82	.6152 2	5.47	.4126	4.49	25.09	.3253	10.56	.3798	3.59	10.70	.1202
MnO	.31	.0215	.23	- 2	.16	.0277	.13	.50	.0212	.27	.0321	.24	.31	.1061
MgO	27.13	.5907	28.49	.1414 2	15.74	.2824	15.60	19.22	.2970	13.06	.2548	15.78	29.19	.3111
CaO	1.20	.2714	2.13	.9334 2	22.37	.5803	22.21	.87	.0100	20.70	.5205	22.98	1.59	.4808
Na_2O	n.d.	-	n.d.	-	.17	.0251	.49	n.d.	-	.24	.1266	.34	n.d.	-
Cr_2O_3	.17	.0121	.49	.0212 2	.29	.0173	.93	.09	.0283	.18	.0115	.75	.43	.0990
NiO	.07	.0147	.10	- 2	.05	.0371	.04	.03	.0071	.02	.0110	-	.05	.0283
TOTAL	100.19	-	100.34	-	100.18	-	99.90	99.67	-	100.10	-	99.12	99.95	
cations/ 6 oxygens														
Si	1.9914		1.9653		1.9920		1.9490	1.9892		1.9523		1.9665	1.9754	
Ti	.0040		.0035		.0063		.0083	.0046		.0141		.0072	.0035	
Al	.0388		.0635		.0517		.1075	.0518		.1031		.0777	.0615	
Fe^{2+}	.4382		.3505		.1672		.1375	.7943		.3301		.1106	.3175	
Mn	.0094		.0069		.0050		.0040	.0160		.0085		.0075	.0093	
Mg	1.4479		1.5054		.8574		.8514	1.0843		.7275		.8662	1.5434	
Ca	.0460		.0809		.8761		.8715	.0353		.8291		.9069	.0604	
Na	-		-		.0120		.0348	-		.0174		.0243	-	
Cr	.0048		.0137		.0084		.0275	.0027		.0053		.0218	.0121	
Ni	.0020		.0029		.0015		.0012	.0009		.006		-	.0014	
TOTAL	3.9827		3.9926		3.9776		3.9927	3.9790		3.9881		3.9887	3.9844	
n	7		2		5		1	2		3		1	2	
Wo	2.38		4.18		46.09		46.84	1.84		43.94		48.15	3.15	
En	74.94		77.72		45.11		45.76	56.65		38.56		45.98	80.33	
Fs	22.68		11.69		8.80		7.39	41.50		17.50		5.87	16.52	
X_{Mg}	.768	.0050	.811	.0071	.837	.0113	.861	.577	.0071	.688	.0066	.887	.829	.0007
Al/Cr	8.1		4.6		6.2		3.9	19.2		19.4		3.6	5.1	

n.d.: not detected; - not determined; x: mean; d: standard deviation; n: number of samples; * : exsolution lamellae

DR-22 : "Contact zone", main pipe, Driekop.
DR-25/27 : Olivine clinopyroxenite, main pipe, Driekop.
DR-32 : Websterite pegmatite, satellite body, Driekop.
DR-38 : Clinopyroxenite pegmatite, satellite body, Driekop.
DR-28/29/30 : Leuconorite cumulate, adjacent to Driekop pipe.
DR-52 : Orthopyroxenite cumulate, adjacent to unaltered UG-2 chromitite, Driekop.
MO-4 : Platiniferous core of the Mooihoek pipe.
DR-46 : Lherzolite, satellite body, Driekop.

the Driekop pipe varies from .811 to .768 (field "A", fig. 4.2). This compositional range may be explained by fractionation trends within a number of cyclic units. Pyroxenes from the iron-rich olivine clinopyroxenite, websterite and clinopyroxenite pegmatite assemblage are more iron-rich than these cumulus samples (field "B", fig. 4.2). These samples become slightly less primitive with distance from the pipe (see section 3.5.3). Pyroxene

from the Mooihoek pipe (sample MO-3 - see section 3.4.2) is considerably more iron-rich (field "C", fig. 4.2). Pyroxenes from satellite bodies of lherzolite at Driekop are more primitive than the cumulus samples; they plot in field "D" on Figure 4.2.

These data corroborate the trend of olivines in these rocks. The magnesian dunite - lherzolite assemblage is more primitive than the cumulates which host the Driekop pipe (at the present level of exposure), whereas the iron-rich assemblages (which include the platiniferous core, the marginal envelope of olivine clinopyroxenite and the satellite bodies of websterite and clinopyroxenite pegmatite) are more evolved than their cumulate wallrocks. Pyroxene from the margins of satellite bodies of iron-rich websterite or clinopyroxenite pegmatite may have a hybrid composition. The compositions of these samples plot between that of cumulus (magnesian) pyroxene and pegmatite (iron-rich) pyroxene (fig. 4.2). These hybrid pyroxenes probably formed due to metasomatism of cumulus pyroxene by iron-rich liquids.

4.2.2 MINOR ELEMENTS IN PYROXENES

The levels in pyroxene of the minor elements Al, Cr and Ti have been widely studied (see also Chapter 9). In the Bushveld Complex the ratio of cations Al to cations Cr is a sensitive indicator which increases with fractionation. Values of this ratio for cumulus orthopyroxenes (4-8) and intercumulus clinopyroxenes (4-6) from cumulates in the upper critical zone at Driekop fit the trends obtained for pyroxenes in the lower critical (low ratios) and main zones (high ratios) obtained by Botha (in prep.) and Mitchell (in prep.). Zonation in large pyroxene grains is a problem, consequently the analyses presented in Table 4.2 and Figure 4.3 are all based on the cores of grains.

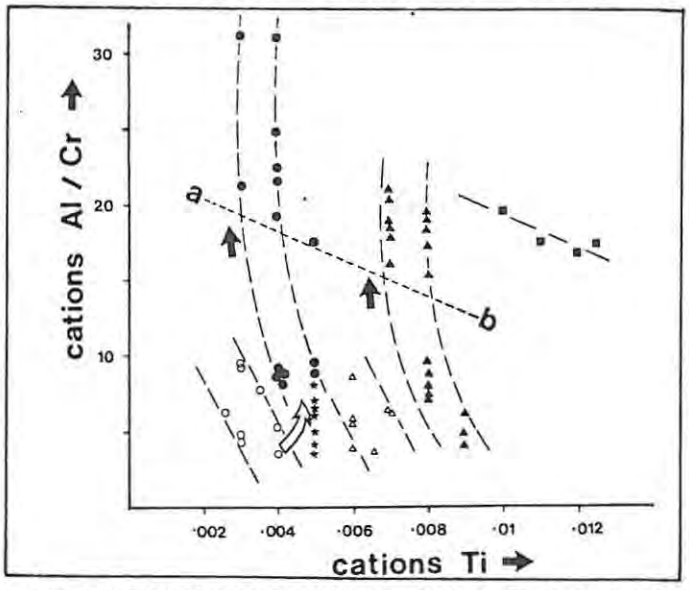

FIGURE 4.3 Plot of cations Al/Cr vs. cations Ti in pyroxene

The following sample groups are recognized (each symbol represents one electron microprobe analysis; all from Driekop, unless otherwise stated) :

- O Cumulus orthopyroxene
- △ Intercumulus clinopyroxene
- ● Pipe-hosted orthopyroxene
- ▲ Pipe-hosted clinopyroxene
- ★ Orthopyroxene, contact zone
- ■ Clinopyroxene, Mooihoek

Arrows indicate direction of fractionation. Below the line a - b chromite is associated with the host rock.

Pyroxenes from the iron-rich, pegmatitic assemblages at Driekop have much higher Al/Cr ratios (greater than 17) than the cumulus samples. This is an indication of

their fractionated nature. The Al/Cr ratio of pyroxene from the satellite bodies of lherzolite is similar to that found in the cumulus samples.

If the Al/Cr ratio is plotted against cations Ti, pyroxene from the lherzolites can be distinguished from the cumulus samples (fig. 4.3). The iron-rich pyroxenes, which might be expected to be richer in Ti, contain similar Ti contents to the cumulus pyroxenes. It is, however, interesting to observe that clinopyroxene from the Mooihoek pipe, which is associated with granular ilmenite, is much richer in Ti. Chromite is not found in the samples plotted above the line a - b in Figure 4.3; pyroxene in these samples contains only very low levels of Cr.

4.2.3 GEOTHERMOMETRY

Using the Wells (1977) geothermometer, equilibration temperatures of 920^0C for pyroxene from the marginal envelope of iron-rich olivine clinopyroxenite unit and 970^0C for cumulus pyroxene from the adjacent wallrocks are indicated. Clinoyroxene in the iron-rich assemblages in these pipes usually contains exsolved orthopyroxene, a further indication that they formed at magmatic temperatures.

4.3 Fe-Ti-Cr OXIDES

Fe-Ti-Cr oxides in the platiniferous ultramafic pipes may be subdivided into three groups : (1) disseminated chromiferous spinels that are an intimate component of the magnesian dunites; (2) disseminated grains and coarse segregations of Fe-Ti-Cr spinel and ilmenite in the platiniferous core of the Mooihoek pipe; and (3) slab-or raft-like masses of "chromitite" that have been extraneously introduced. This latter group is variously interpreted as xenoliths or metasomatic relicts (see p.27). They do not occur at Driekop and are not discussed further here. In addition, secondary magnetite (essentially pure Fe_3O_4), probably a result of serpentinisation, is found in many of the olivine-rich assemblages in these pipes, and orientated intergrowths of an opaque phase occur in many of the olivine grains (see p.34).

4.3.1 DISSEMINATED CHROMIFEROUS SPINELS

DISTRIBUTION

From the petrologic descriptions presented in Chapter 3, the distribution of chromiferous spinels at Driekop may be summarised as follows :-

(1) they are an ubiquitous accessory constituent in magnesian dunite, both from the main pipe and satellite bodies; (2) they are absent from all of the iron-rich assemblages associated with the Driekop pipe, including the platiniferous core; (3) cumulus chromite is only a rare accessory constituent of the felsic cumulates that host the pipe at the present level of exposure; and (4) metasomatism in response to iron-rich fluids may result in resorption and eventual dissolution of primary chromite grains in magnesian dunite. This results in iron-rich assemblages that are chromite-free.

MINERALOGY

Stumpfl and Rucklidge (1982) recognized three types of disseminated spinel in the platiniferous ultramafic pipes (note that they do not describe the particular petrologic assemblage in which they occur). These are (1) monophase chromites; (2) polyphase spinels; and (3) magnetite. The latter may occur as part of the polyphase grains, but is much more widespread as secondary grains which are related to serpentinisation of olivine (these are not discused further). The distinction between monophase and polyphase chromites is based on optical (reflected light) and electron microprobe data.

(1) MONOPHASE (HOMOGENEOUS) CHROMITES

DESCRIPTION : Monophase, optically homogeneous chromites occur in magnesian dunites in intergranular and intragranular sites within olivine (figs.3.6,4.4A). Chromites in intragranular sites are invariably very small, euhedral or rounded grains, whereas those in intergranular sites vary from tiny grains with diameters of less than 0.1 mm to large, anhedral grains with maximum dimensions of over 5 mm. Texturally, these chromites are comparable with cumulus chromites in dunite or harzburgite cumulates from the Bushveld Complex.

CHEMISTRY : Electron microprobe analyses of monophase chromites from Driekop, Mooihoek and Onverwacht are presented in Table 4.3. These comprise samples from the magnesian dunite unit in the main pipe at Driekop (samples DR-1,2,16,17,20), the sill-like satellite body of magnesian dunite at Driekop (sample DR-111), satellite bodies of lherzolite at Driekop (sample DR-43B,46B) and the magnesian dunite unit in the Mooihoek and Onverwacht pipes (samples MO-14 and ON-12, respectively). They include analyses of intergranular and intragranular grains, the composition of which may differ due to subsolidus effects.

All of the optically homogeneous grains analysed in this study were found to be essentially compositionally homogeneous, but some compositional

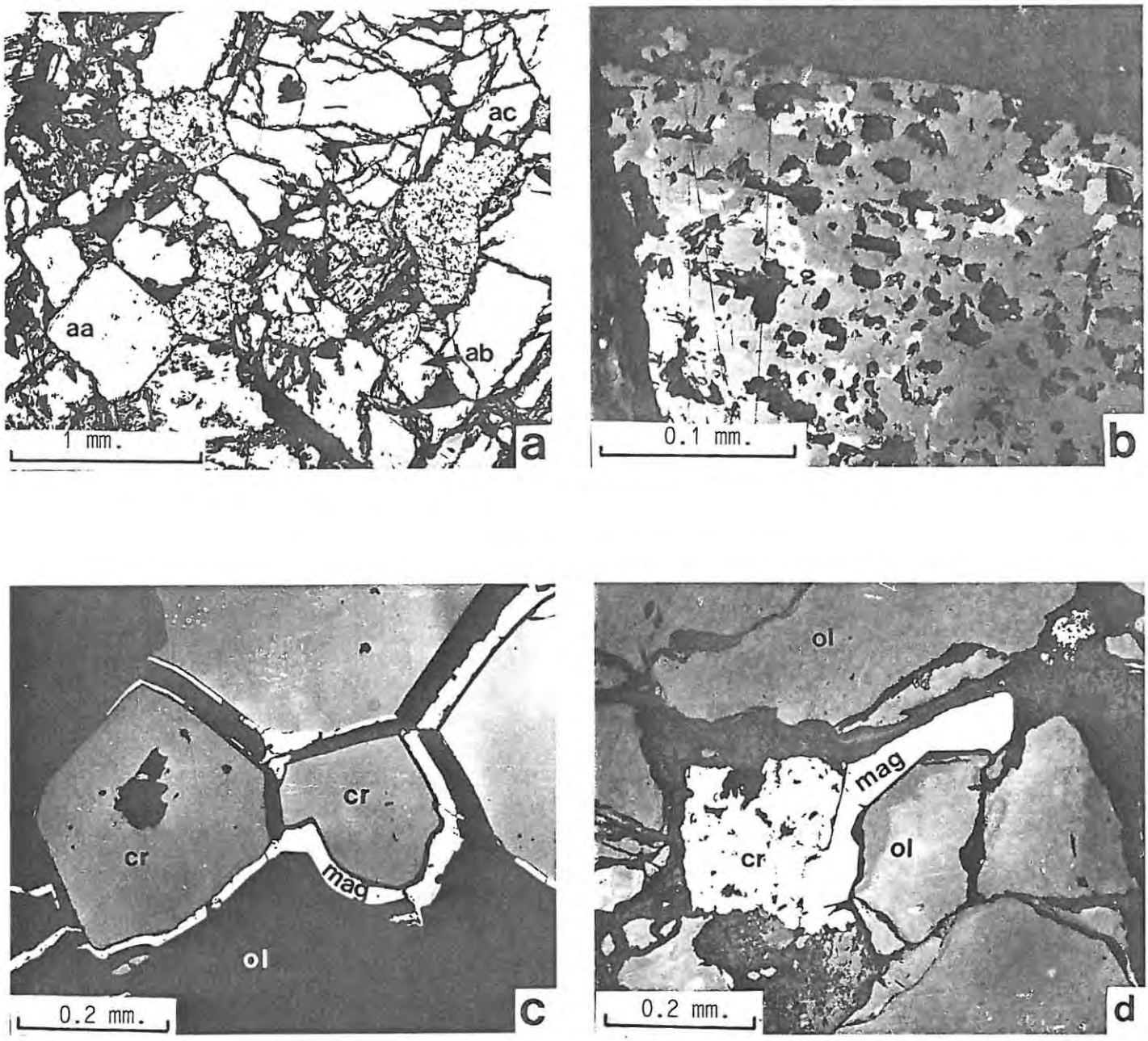

FIGURE 4.4 CHROMIFEROUS SPINELS IN MAGNESIAN DUNITE FROM THE MAIN PIPE, DRIEKOP

a. Medium-sized chromiferous spinel grains (light grey) in intergranular sites between olivine grains (medium grey) : "aa" is a monophase chromite grain (note euhedral form, paucity of inclusions), "ac" is a polyphase, chromiferous spinel grain (note anhedral form, abundance of silicate inclusions), and grain "ab" is exhibiting signs of partial alteration. Sample DR-17 (for analyses of grain "aa" see Table 4.3).

b. Part of a single, polyphase, chromiferous spinel grain exhibiting at least two optically resolvable phases (light grey and medium grey) and abundant silicate inclusions (very dark grey to black). Whole is enclosed by olivine (black). Note extremely ragged margin. Sample DR-17, grain "b".

c. Rims of pure magnetite on monophase chromite grains, all enclosed by olivine. Surface sample.

d. Composite grain of polyphase, chromiferous spinel and pure magnetite. Latter exhibits typical anhedral form and is interstitial to olivine, whereas former was probably originally euhedral. Sample DR-1.

(All in reflected light with partially crossed or uncrossed polarisers; cr - chromiferous spinel; mag - magnetite; ol - olivine)

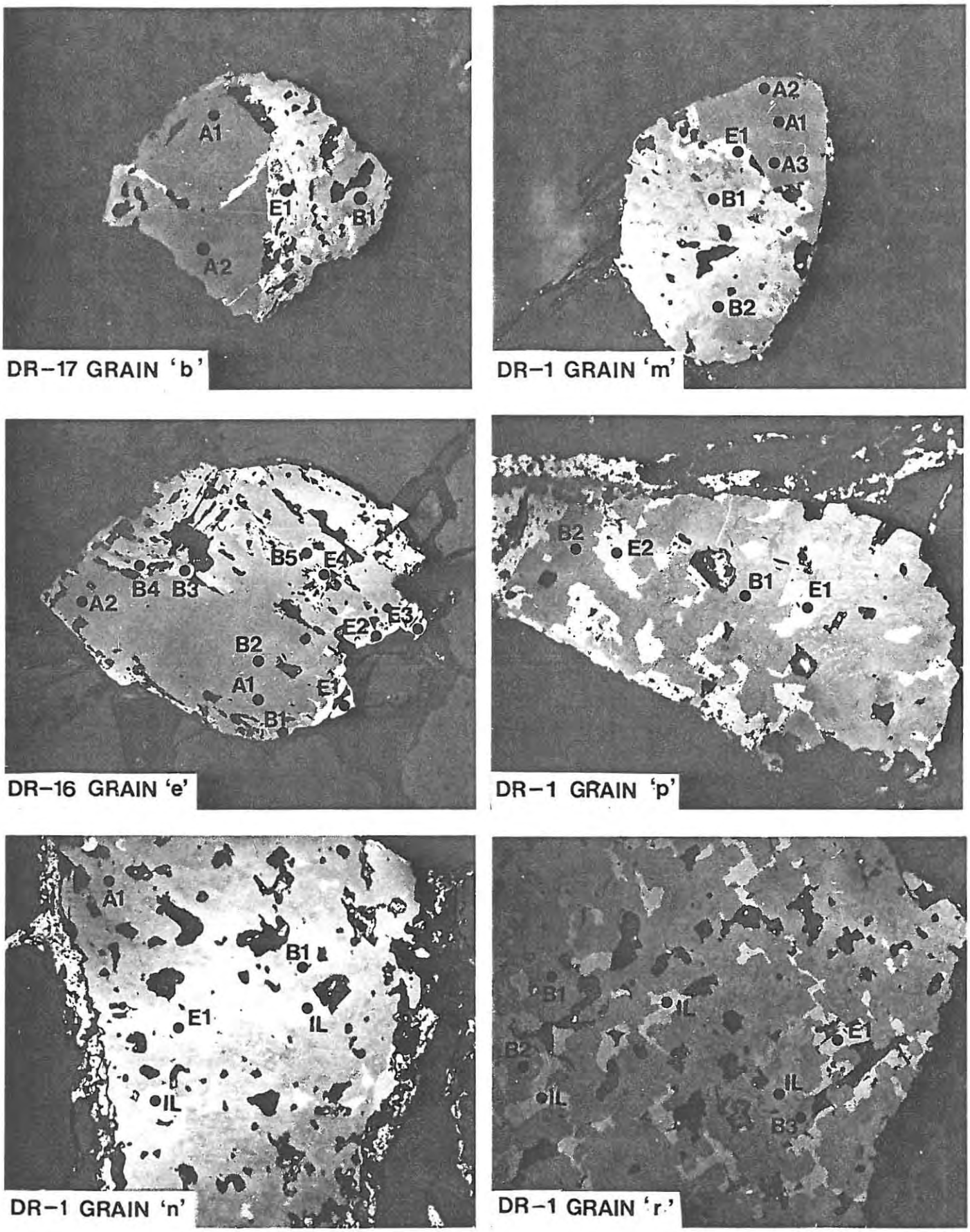

FIGURE 4.5 POLYPHASE, CHROMIFEROUS SPINELS IN MAGNESIAN DUNITE FROM THE MAIN PIPE, DRIEKOP

For explanation of phases A, B, E - see text; A1, A2, B1, E1 etc. (e.g., in sample DR-17 grain "b") represent electron microprobe analyses presented in Tables 4.4, 4.5; chromium ilmenites are labelled "IL" - for analyses see Table 4.5.

(All in reflected light with partially crossed or uncrossed polarisers).

TABLE 4.3 ELECTRON MICROPROBE ANALYSES OF MONOPHASE (HOMOGENEOUS ?) CHROMIUM - SPINELS

	DR-1		DR-1		DR-16		DR-22		DR-1		DR-1		DR-1		DR-2		DR-16		DR-16		DR-16	
	wt.%	cations																				
TiO_2	.58	.1209	.56	.1165	1.32	.2635	1.65	.3240	1.47	.2921	1.34	.2749	1.35	.2712	1.10	.2170	1.17	.2267	1.17	.2272	1.23	.2405
FeO	-	.1209	-	.1165	-	.2635	-	.3240	-	.2921	-	.2749	-	.2712	-	.2170	-	.2267	-	.2272	-	.2405
Cr_2O_3	47.77	10.4748	47.14	10.3104	41.97	8.8086	38.09	7.9887	42.69	8.9194	40.23	8.6794	42.86	9.0536	43.34	8.9891	40.76	8.3032	41.23	8.4203	40.24	8.2729
Al_2O_3	10.47	3.4218	9.97	3.2501	16.13	5.0458	21.29	6.5520	16.45	5.1227	12.06	3.8701	15.98	5.0312	18.63	5.7593	21.17	6.4278	20.91	6.3650	20.78	6.3675
Fe_2O_3	8.91	1.8613	10.59	2.2063	8.10	1.6184	4.12	.8109	6.90	1.3735	14.08	2.8924	6.82	1.3726	4.14	.8174	4.20	.8154	3.91	.7600	4.48	.8784
FeO	25.86	5.8782	24.19	5.4806	26.30	5.5773	25.98	5.3517	25.89	5.4307	21.76	4.6921	25.09	5.3363	25.06	5.2818	24.48	5.0493	24.96	5.1651	25.29	5.3245
MgO	4.78	1.9761	5.78	2.3834	5.77	2.2832	6.53	2.5421	6.17	2.4305	7.78	3.1645	6.37	2.5369	6.61	2.5848	7.37	2.8306	7.05	2.7146	6.59	2.5543
MnO	.62	.1456	.58	.1359	.62	.1394	.48	.1061	.62	.1387	.62	.1433	.56	.1267	.60	.1333	.55	.1200	.55	.1203	.55	.1211
TOTAL	99.00		98.82		100.22		98.75		100.20		97.88		99.04		99.48		99.71		99.78		99.46	
R1	.240		.287		.224		.131		.201		.381		.204		.134		.139		.128		.141	
R2	.236		.282		.216		.125		.193		.368		.196		.129		.133		.123		.136	
R3	.118		.139		.104		.052		.089		.187		.088		.052		.052		.048		.056	
R4	.251		.303		.290		.322		.309		.402		.322		.328		.359		.344		.324	
R5	.247		.298		.281		.309		.298		.389		.311		.319		.349		.334		.314	
HABIT	Intragranular encl. in oliv.		Intragranular encl. in oliv.		Intragranular encl. in oliv.		Intragranular encl. in oliv.		Intergranular small		Intergranular small		Intergranular medium		Intergranular medium		Intergranular medium		Intergranular medium		Intergranular medium	

	DR-16		DR-16		DR-17		DR-17		DR-17		DR-20		DR-20		DR-20		DR-20		DR-111		DR-111	
	wt.%	cations																				
TiO_2	1.10	.2176	1.24	.2472	1.38	.2759	1.40	.2821	1.35	.2720	1.35	.2651	1.54	.3010	1.40	.2759	1.50	.2902	.94	.1784	1.00	.1906
FeO	-	.2176	-	.2472	-	.2759	-	.2721	-	.2720	-	.2651	-	.3010	-	.2759	-	.2902	-	.1784	-	.1906
Cr_2O_3	39.42	8.2074	40.36	8.4598	42.53	8.9394	42.46	8.9962	41.78	8.8523	37.59	7.7609	38.36	7.8830	36.91	7.6497	36.84	7.4951	40.69	8.1221	40.57	8.1312
Al_2O_3	20.32	6.2994	20.25	6.3265	16.32	5.1128	16.02	5.0590	15.36	4.8507	22.78	7.0100	22.18	6.7936	23.06	7.1234	23.48	7.1200	22.30	6.6346	22.04	6.5840
Fe_2O_3	5.34	1.0578	3.60	.1792	6.97	1.3958	6.84	1.3803	8.69	1.7527	3.55	.6987	3.68	.7211	3.42	.6748	4.14	8.0420	4.86	.8863	4.73	.9034
FeO	25.92	5.4853	26.52	5.6340	26.25	5.3607	26.22	5.5943	24.63	5.2501	26.53	5.5288	26.85	5.5359	27.58	5.7706	25.70	5.2410	22.62	4.5980	22.46	4.5727
MgO	6.10	2.3921	5.68	2.2447	5.82	2.3064	5.67	2.2649	6.56	2.6205	6.06	2.5288	6.07	2.3518	5.41	2.2239	6.92	2.6543	8.75	3.2929	8.78	3.3177
MnO	.55	.1275	.54	.1212	.59	.1328	.62	.1407	.57	.1293	.49	.1083	.51	.1122	.52	.1154	.48	.1046	.51	.1090	.51	.1095
TOTAL	98.79		98.20		99.86		99.23		98.95		98.36		99.19		98.30		99.07		100.47		100.10	
R1	.161		.113		.200		.197		.250		.112		.115		.104		.133		.161		.164	
R2	.156		.108		.192		.190		.240		.107		.109		.100		.126		.156		.159	
R3	.067		.046		.090		.089		.113		.045		.046		.043		.052		.056		.057	
R4	.303		.284		.293		.288		.332		.299		.298		.268		.336		.417		.420	
R5	.295		.276		.283		.278		.321		.289		.287		.259		.324		.408		.410	
HABIT*	Intergranular medium		Intergranular medium				Intergranular medium						Intergranular medium								Intergranular medium	

RATIOS : R1 = Fe^{3+} / Fe^{3+} + Fe^{2+} (octahedral); R2 = Fe^{3+} / Fe^{3+} + Fe^{2+} (total); R3 = Fe^{3+} / Fe^{3+} + Al + Cr; R4 = Mg / Mg + Fe^{2+} (octahedral); R5 = Mg / Mg + Fe^{2+}(total).

* For description see text. (small : less than 1 mm in diameter; medium : 1 - 3 mm in diameter. Note that monophase large grains are rare.

TABLE 4.3 (CONTINUED)

	DR-111				DR-46B										DR-2					
	wt.%	cations																		
TiO_2	.78	.1506	1.00	.1965	1.02	.1952	1.07	.2063	1.02	.1947	1.20	.2347	1.16	.2239	1.22	.2429	1.18	.2345	1.26	.2521
FeO	–	.1506	–	.1965	–	.1952	–	.2063	–	.1947	–	.2347	–	.2239	–	.2429	–	.2345	–	.2521
Cr_2O_3	39.96	8.1151	40.68	8.4046	42.04	8.4610	40.14	8.1383	41.06	8.3559	40.06	8.2405	39.31	7.9771	42.98	9.0000	42.84	8.9513	43.34	9.1171
Al_2O_3	22.08	6.6834	20.60	6.3436	19.54	5.8615	20.04	6.0559	19.72	5.9815	19.14	5.8683	21.40	6.4726	18.24	5.6928	18.39	5.7272	17.73	5.5691
Fe_2O_3	4.65	.9000	4.36	.8586	6.71	1.2868	7.21	1.3929	6.54	1.2767	7.26	1.4215	5.70	1.1023	4.12	.8211	4.28	.8523	4.09	.8194
FeO	22.10	4.5967	24.56	5.1709	23.57	4.8235	27.54	4.6285	22.93	4.7387	24.66	5.1324	22.83	4.6774	26.71	5.6738	26.13	5.5414	26.41	5.6261
MgO	8.61	3.2966	6.99	2.7228	8.07	3.0622	8.53	3.2606	8.21	3.1500	7.11	2.7574	8.40	3.2138	5.54	2.1871	5.90	2.3242	5.65	2.2408
MnO	.49	.1066	.48	.1062	.53	.1142	.51	.1107	.51	.1111	.50	.1101	.50	.1087	.62	.1390	.60	.1347	.59	.1329
TOTAL	98.67		98.67		101.49		100.05		99.99		99.93		99.31		99.43		99.32		99.08	
R1	.163		.142		.210		.231		.211		.216		.190		.126		.133		.127	
R2	.159		.137		.204		.223		.204		.209		.183		.121		.128		.122	
R3	.057		.055		.082		.089		.081		.091		.070		.052		.054		.052	
R4	.417		.344		.388		.413		.399		.349		.407		.278		.295		.284	
R5	.409		.336		.378		.402		.389		.339		.396		.269		.286		.275	
HABIT*	Intergranular				Intergranular										Intragranular					

	DR-43B						MO-14								ON-12			
	wt.%	cations																
TiO_2	1.71	.3391	1.95	.3888	1.95	.3859	2.38	.4910	2.37	.4945	2.36	.4890	2.45	.4999	1.08	.2096	.97	.1913
FeO	–	.3391	–	.3888	–	.3859	–	.4910	–	.4945	–	.4890	–	.4999	–	.2096	–	.1913
Cr_2O_3	37.17	7.7505	38.20	8.0081	38.66	8.0443	42.69	9.2591	42.05	9.2252	43.50	9.4770	42.88	9.1993	43.07	8.7913	41.52	8.6131
Al_2O_3	17.60	5.4699	16.78	5.2430	17.21	5.3374	13.26	4.2866	13.08	4.2770	12.69	4.1207	13.76	4.3999	19.43	5.9113	19.40	5.9982
Fe_2O_3	10.58	2.1011	9.87	1.9711	9.32	1.8463	7.13	1.4722	7.22	1.5085	6.86	1.4241	6.86	1.4070	4.51	.8779	5.09	1.0057
FeO	28.28	5.8991	27.90	5.7980	28.04	5.7859	28.29	5.9999	28.65	6.1561	27.74	5.9036	28.23	5.9079	26.15	5.4372	25.65	5.4384
MgO	5.02	1.9735	5.27	2.0829	5.32	2.0870	4.55	1.8606	4.10	1.6958	4.78	1.9634	4.82	1.9496	6.33	2.4360	6.22	2.4327
MnO	.57	.1273	.53	.1190	.57	.1270	.60	.1394	.63	.1480	.57	.1330	.60	.1425	.58	.1268	.58	.1289
TOTAL	100.94		100.50		100.07		98.90		98.11		98.50		99.62		101.16		99.44	
R1	.262		.253		.241		.197		.196		.194		.191		.139		.156	
R2	.251		.241		.230		.184		.184		.182		.179		.134		.151	
R3	.137		.129		.121		.098		.100		.094		.093		.056		.064	
R4	.250		.264		.265		.238		.215		.249		.248		.309		.309	
R5	.240		.251		.252		.222		.203		.234		.233		.301		.301	
HABIT*	Intergraular medium		Intergranular large		Intergranular medium		Intergranular medium								Intergranular medium			

RATIOS : R1 = Fe^{3+} / Fe^{3+} + Fe^{2+} (octahedral); R2 = Fe^{3+} / Fe^{3+} + Fe^{2+} (total); R3 = Fe^{3+} / Fe^{3+} + Al + Cr; R4 = Mg / Mg + Fe^{2+} (octahedral); R5 = Mg / Mg + Fe^{2+}(total)

* For description see text (small : less than 1 mm in diameter; medium 1 – 3 mm in diameter. Note that monophase large grains are rare.

variation between grains is evident. Polyphase, complex chromites are not found in the sill-like body of magnesian dunite at Driekop, consequently the chemistry of monophase chromites (which contain between 39.9 and 40.7 wt. percent Cr_2O_3) may be indicative of primary compositions (sample DR-111, Table 4.3). In fact, the composition of cumulus chromites from magnesian dunites is comparable with these samples (sample DUN-1, Table 4.6).

GEOTHERMOMETRY : In slowly cooled rocks subsolidus spinel-silicate re-equilibration may modify primary liquidus compositions. Wilson (1982) suggests that spinel geothermometry can only be applied to thick seams, which have been unable to equilibrate with silicates. In this study only disseminated chromite was available, such that the results indicate minimum (blocking) temperatures at which subsolidus re-equilibration was terminated. The olivine-spinel geothermometer used is that of Roeder et al. (1979). The following temperatures have been obtained for chromites from magnesian dunites at Driekop : 700°C (intragranular chromite, satellite body), 580°C (intragranular chromite, main body) and 545°C (intergranular chromite, main body).

(2) POLYPHASE, COMPLEX CHROMIFEROUS SPINELS

DISTRIBUTION : In magnesian dunite in the main pipe at Driekop, optically and compositionally polyphase, complex chromiferous spinels are common. Similar spinels have not been reported from cumulates in the Bushveld Complex. They are also absent from the satellite bodies of magnesian dunite and lherzolite at Driekop. This is an important observation and it may be concluded that these complex spinels have formed in response to processes that only affected the main pipe. Data presented elsewhere in this study indicate that the magnesian dunite in the main pipe and satellite bodies is similar, consequently it is inferred that the complex spinels are the result of processes that occurred after the magnesian dunite was crystalline. Furthermore, the complex spinels are preferentially concentrated towards the margins (i.e. adjacent to the platiniferous core and the outer contact with the marginal envelope of iron-rich olivine clinopyroxenite) of the main pipe. For example, complex spinels are abundant in samples DR-1,2 and DR-20,22 and relatively rare in samples DR-6 to DR-14 (see Map 2).

DESCRIPTION : Complex spinels are characterised by a wholly anhedral form, the presence of abundant, and often quite large, silicate inclusions, and the presence of more than one optically distinct phase (figs. 4.4B,4.5). They

often form quite large grains, commonly with maximum dimensions in excess of 3 mm. They always occur in intergranular sites.

Stumpfl and Rucklidge (1982) recognised up to four optically distinct phases in these complex spinels. In this study three optically distinct phases are normally observed, but up to six phases may be recognised in specific samples (this includes one phase which is a Cr-rich ilmenite - see below). These optically distinct phases are recognised by differences in reflectivity. The lowest reflectance phase is probably equivalent to optically homogeneous chromite and that with the highest reflectivity is an iron-rich phase (fig. 4.5). The optical difference between these two extremes is marked, and it is significant that the phase with the highest reflectivity occurs as a separate entity, whereas only very subtle differences occur in the lower reflectivity range, which may include up to four separate phases. These separate phases do not occur as concentrically disposed zones but as irregular and complicated intergrowths, in which the lower reflectivity phases are located towards the central parts of grains and the higher reflectivity phases occur towards the margins. This may result in the preservation of relict primary chromite islands in the central parts of grains (but still in a highly irregular manner) with iron-rich spinel found as irregular, and isolated bodies at the margins of grains. Well developed rims do not occur. The exception to this is the presence of rims of essentially pure Fe_3O_4 on otherwise optically homogeneous chromites from surface samples (fig. 4.4C). This is probably related to serpentinisation.

Spinels at Driekop may be only partly polyphase, with half or more of the grain remaining as optically homogeneous chromite (fig. 4.5A, B). At the other extreme polyphase spinels, with complicated spinel intergrowths, may contain over 50 modal percent of silicate inclusions (fig. 4.4). These usually occur as anhedral, often shard-like features with maximum dimensions in excess of 0.1 mm. They are quite distinct from the small, often rounded silicate inclusions observed in cumulus chromites in the Bushveld Complex. For further details see Stumpfl and Rucklidge (1982).

CHEMISTRY : The results of electron microprobe analyses of polyphase, complex chromites are presented in Tables 4.4 and 4.5. All these samples are from the magnesian dunite unit in the main pipe at Driekop (see Map 2 for sample locations). Three optically distinct phases, which may be readily recognised; are labelled A, B and E, where the relative reflectivity (R) of these phases is $R_A < R_B < R_E$ (phases C and D were originally recognised but R_C and R_D are very close to R_B). These analyses are subdivided into two groups, Cr-rich spinels (phases A and B, Table 4.4) and Fe-rich spinels

TABLE 4.4 ELECTRON MICROPROBE ANALYSES OF POLYPHASE CHROMITE - SPINELS

	DR-1 GRAIN "a"						DR-1 GRAIN "b"										DR-1 GRAIN "n"				DR-1 GRAIN "r"	
	wt.%	cations																				
TiO_2	.67	.1386	.60	.1253	.70	.1448	1.16	.2326	1.17	.2378	1.18	.2379	.65	.1386	.80	.1644	.59	.1272	.65	.1395	.62	.1319
FeO	-	.1386	-	.1253	-	.1448	-	.2326	-	.2378	-	.2379	-	.1386	-	.1644	-	.1272	-	.1395	-	.1319
Cr_2O_3	46.44	10.1056	48.32	10.6101	47.16	10.2626	42.05	8.8672	41.43	8.8537	41.22	8.7391	47.72	10.7022	34.41	7.4361	46.06	10.4408	48.23	10.8868	44.89	10.0465
Al_2O_3	12.65	4.1028	10.93	3.5772	12.37	4.0122	15.96	5.0163	15.67	4.9912	15.29	4.8316	8.72	2.9148	11.04	3.5560	10.80	3.6489	9.89	3.3274	10.86	3.6226
Fe_2O_3	7.31	1.5141	7.47	1.5619	6.98	1.4353	8.22	1.6510	8.25	1.6793	9.67	1.9532	9.86	2.1055	22.74	4.6788	7.67	1.6558	7.01	1.5065	9.70	2.0668
FeO	27.52	6.1962	28.43	6.4791	28.88	6.5039	26.11	5.5931	25.97	5.6328	24.90	5.3483	29.12	6.7704	23.96	6.3128	27.05	6.3596	27.99	6.5455	26.22	6.0773
MgO	4.05	1.6616	3.31	1.3703	3.30	1.3539	5.73	2.2781	5.54	2.2321	6.31	2.8222	2.55	1.0782	6.26	2.5505	3.52	1.5043	3.07	1.3065	4.21	1.7764
MnO	.61	.1422	.64	.1505	.61	.1422	.57	.1287	.59	.1350	.57	.1294	.63	.1513	.59	.1365	.56	.1359	.62	.1499	.61	.1462
TOTAL	99.25		99.70		99.95		99.81		98.62		99.15		99.25		99.80		96.25		97.46		97.12	
R1	.196		.194		.180		.227		.229		.267		.237		.468		.206		.187		.253	
R2	.192		.191		.177		.220		.222		.259		.233		.460		.203		.183		.249	
R3	.096		.099		.091		.106		.108		.125		.133		.298		.105		.095		.131	
R4	.211		.174		.172		.289		.283		.320		.137		.324		.191		.166		.226	
R5	.207		.171		.169		.281		.275		.311		.134		.317		.188		.163		.222	
ANALYSIS	A1		A2		A3		A1		A2		A3		A4		B1		A1		A2		B1	

	DR-1 GRAIN "p"				DR-1 GRAIN "q"				DR-16 GRAIN "b"								DR-16 GRAIN "e"					
	wt.%	cations																				
TiO_2	.61	.1291	.41	.0880	.34	.0734	3.58	.7709	1.23	.2380	.73	.1475	1.20	.2369	1.23	.2427	1.00	.2004	1.38	.2736	1.21	.2532
FeO	-	.1291	-	.0880	-	.0734	-	.7709	-	.2380	-	.1475	-	.2369	-	.2427	-	.2004	-	.2736	-	.2532
Cr_2O_3	47.55	10.5805	47.72	10.7698	35.66	8.1038	43.86	9.9297	40.98	8.3379	43.33	9.2056	40.30	8.3675	39.36	8.1672	39.81	8.3897	41.29	8.6075	39.03	8.7340
Al_2O_3	9.16	3.0379	8.70	2.9265	7.53	2.5505	8.54	2.8817	21.16	6.4169	15.99	5.0633	20.19	6.2482	19.81	6.1267	17.69	5.5566	19.34	6.0092	11.33	3.7031
Fe_2O_3	10.02	2.1232	9.90	2.1275	24.03	5.1985	7.64	1.6466	3.97	.7690	7.10	1.4359	4.60	.9102	6.17	1.2204	8.23	1.6526	4.21	.8359	14.65	3.0580
FeO	26.15	6.0278	28.09	6.6197	29.02	6.9032	30.83	6.6129	24.14	4.9587	26.57	5.8235	26.20	5.5183	25.80	5.4221	25.43	5.4698	27.05	5.6930	26.85	5.9769
MgO	4.36	1.8291	2.92	1.2424	2.31	.9897	2.92	1.2463	7.61	2.9192	5.07	2.0308	6.01	2.3526	1.26	2.4490	6.01	2.3879	6.54	2.1774	4.49	1.8563
MnO	.60	.1430	.57	.1378	.44	.1071	.58	.1406	.56	.1220	.64	.1456	.58	.1290	.58	.1289	.63	.1422	.58	.1295	.71	.1667
TOTAL	98.46		98.32		99.33		97.95		99.65		99.43		99.09		99.22		98.81		99.40		99.07	
R1	.260		.243		.429		.199		.134		.197		.141		.183		.232		.128		.338	
R2	.256		.240		.426		.182		.128		.193		.136		.177		.225		.122		.329	
R3	.134		.134		.327		.113		.049		.091		.058		.078		.105		.054		.197	
R4	.232		.158		.125		.158		.370		.258		.298		.311		.303		.276		.236	
R5	.229		.156		.124		.144		.359		.253		.290		.301		.296		.267		.229	
ANALYSIS	A1		A2		B1		B2		A1		A2		A1		A2		B1		B2		B3	

RATIOS : R1 = Fe^{3+} / Fe^{3+} + Fe^{2+} (octahedral); R2 = Fe^{3+} / Fe^{3+} + Fe^{2+} (total); R3 = Fe^{3+} / Fe^{3+} + Al + Cr; R4 = Mg / Mg + Fe^{2+} (octahedral); R5 = Mg / Mg + Fe^{2+}(total).

TABLE 4.4 (CONTINUED)

	DR-22 GRAIN "e"				DR-17 GRAIN "d"				DR-17 GRAIN "a"							
	wt.%	cations														
TiO_2	1.02	.2104	2.97	.6421	1.26	.2515	.65	.1376	1.20	.2371	1.04	.2088	1.18	.2365	1.18	.2349	.52	.1132
FeO	-	.2104	-	.6421	-	.2515	-	.1376	-	.2371	-	.2088	-	.2365	-	.2349	-	.1132
Cr_2O_3	40.25	8.7305	35.74	8.1237	43.04	9.0321	48.65	10.8323	43.46	9.0310	43.49	9.1829	42.36	8.9268	42.15	8.8219	45.43	10.3973
Al_2O_3	16.85	5.4475	10.04	3.4014	16.46	5.1484	10.00	3.3187	16.76	5.1910	15.93	5.0134	16.68	5.2329	17.13	5.3438	8.21	2.8005
Fe_2O_3	6.78	1.4010	14.74	3.1905	6.59	1.3164	7.42	1.5736	6.59	1.3035	6.89	1.3857	6.78	1.3608	6.84	1.3643	11.82	2.5756
FeO	29.18	6.4853	31.09	6.8351	25.65	5.4442	28.52	6.5814	24.90	5.2381	25.67	5.5257	25.49	5.4465	26.19	5.5648	2.71	6.4473
MgO	3.38	1.3822	2.40	1.0285	6.13	2.4253	3.01	1.2635	6.72	2.6328	5.88	2.3408	6.08	2.4157	5.83	2.3005	3.28	1.4153
MnO	.57	1.3240	.56	.1363	.58	.1303	.65	.1550	.58	.1291	.59	.1334	.61	.1377	.60	.1345	.56	.1373
TOTAL	98.03		97.56		99.72		98.91		100.22		99.50		99.18		99.93		96.92	
R1	.177		.318		.194		.192		.199		.200		.199		.196		.285	
R2	.173		.299		.187		.189		.192		.194		.193		.190		.281	
R3	.089		.216		.084		.100		.083		.088		.087		.087		.163	
R4	.175		.130		.308		.161		.334		.297		.307		.292		.180	
R5	.171		.120		.298		.158		.324		.289		.298		.284		.177	
ANALYSIS	A1		B1		A1		A2		A1		A2		A3		A4		B1	

	DR-17 GRAIN "b"						DR-11 GRAIN "a"					
	wt.%	cations										
TiO_2	1.16	.2358	1.11	.2237	.68	.1449	1.15	.2452	.72	.1549	1.28	.2588
FeO	-	.2358	-	.2237	-	.1449	-	.2452	-	.1549	-	.2588
Cr_2O_3	39.91	8.5301	40.26	8.5321	42.51	9.5258	47.08	10.5567	47.21	10.6810	42.71	9.0814
Al_2O_3	16.52	5.2627	17.00	5.3698	10.27	3.4301	9.86	3.2953	9.70	3.2709	15.90	5.0390
Fe_2O_3	8.53	1.7355	8.18	1.6504	12.91	2.7541	7.76	1.6573	8.07	1.7380	6.72	1.3616
FeO	25.78	5.5932	25.74	5.5480	24.43	5.6457	28.47	6.5079	27.45	6.4159	25.84	5.5542
MgO	5.66	2.2808	5.79	2.3134	5.26	2.2222	3.20	1.3528	3.35	1.4289	5.76	2.3091
MnO	.55	.1259	.61	.1384	.55	.1320	.58	.1398	.64	.1551	.60	.1366
TOTAL	98.11		98.69		96.91		98.10		97.14		98.82	
R1	.236		.229		.327		.202		.213		.196	
R2	.229		.222		.322		.197		.209		.189	
R3	.111		.106		.175		.106		.110		.087	
R4	.289		.294		.282		.172		.182		.293	
R5	.288		.286		.277		.166		.178		.284	
ANALYSIS	A1		A2		A3		A1		A2		B1	

RATIOS

R1 = Fe^{3+} / Fe^{3+} + Fe^{2+} (octahedral)
R2 = Fe^{3+} / Fe^{3+} + Fe^{2+} (total)
R3 = Fe^{3+} / Fe^{3+} + Al + Mg
R4 = Mg / Mg + Fe^{2+} (octahedral)
R5 = Mg / Mg + Fe^{2+} (total)

(phase E, Table 4.5). Samples were selected for analysis after examination by reflected light microscopy. Individual grains were then photographed so that the different phases could be located with the electron microprobe. This was important as it avoided the problem of an analysis across the contact of two phases. Each grain was then labelled alphabetically (lower case), and analyses of different phases on various grains were recorded (e.g., analyses A1, A2 (phase A), B1, B2 (phase B), E1 (phase E) all of grain "m", sample DR-1 - see fig. 4.5B and Tables 4.4, 4.5).

These results are treated as preliminary data; more detailed studies are required before these complicated minerals may be fully understood. The composition of phase A in the polyphase spinels may be compared with the composition of monophase chromites. If chromites from the sill-like body of magnesian dunite are accepted as primary compositions, then it is interesting to observe that phase A in the polyphase spinels may be actually richer in Cr_2O_3, but much poorer in Al_2O_3. Phase B in the polyphase chromites is relatively depleted in Cr_2O_3 and Al_2O_3 and enriched in FeO and Fe_2O_3. Phase E may be described as an Fe-Cr spinel; it usually contains less than 30 wt. percent Cr_2O_3 and is compositionally part-way between chromite and

TABLE 4.5 ELECTRON MICROPROBE ANALYSES OF IRON-RICH POLYPHASE CHROMIUM – SPINELS AND CHROMIUM – RICH ILMENITES

	DR-1 GRAIN "a"				DR-1 GRAIN "m"		DR-1 GRAIN "n"		DR-1 GRAIN "p"				DR-1 GRAIN "g"				DR-16 GRAIN "e"					
	wt.%	cations																				
TiO_2	.13	.0282	.13	.02800	.48	.1043	.44	.0952	.09	.0203	.19	.0432	.23	.0495	.08	.0181	.17	.0380	.27	.0608	.18	.0394
FeO	–	.0282	–	.02800	–	.1043	–	.0952	–	.0203	–	.0432	–	.0495	–	.0181	–	.0380	–	.0608	–	.0394
Cr_2O_3	16.39	3.7434	21.59	4.9061	30.31	6.9252	30.08	6.8688	8.68	2.0667	20.46	4.8913	17.96	4.0704	10.15	2.4225	7.13	1.6792	6.80	1.6099	9.72	2.2395
Al_2O_3	2.99	1.0178	3.52	1.1922	5.44	1.8525	6.43	2.1821	1.01	.3584	3.70	1.3184	2.98	1.0066	1.50	.5336	2.83	.9934	.98	.3458	3.76	1.2912
Fe_2O_3	51.43	11.1821	45.52	9.8454	32.25	7.0134	31.27	6.7784	59.72	13.5340	42.64	9.7037	50.17	10.8237	57.25	13.0074	59.11	13.2511	61.78	13.9226	56.50	12.3903
FeO	30.10	7.2448	30.95	7.4136	29.77	7.0904	29.57	7.0274	30.30	7.6116	28.71	7.2186	31.73	7.5572	30.79	7.7572	28.71	7.1166	23.01	5.7027	27.56	6.6796
MgO	1.64	.7062	1.17	.5012	1.85	.7969	2.01	.8628	.78	.3501	1.58	.7121	.90	3.8450	.46	.2070	1.91	.8481	5.05	2.2541	2.96	1.2858
MnO	.20	.0489	.35	.0852	.46	.1125	.45	.1097	.15	.0382	.27	.0691	.24	.0582	.14	.0357	.14	.0353	.17	.0431	.14	.0345
TOTAL	102.89		103.24		100.56		100.26		100.73		97.56		104.21		100.38		100.01		98.07		100.83	
R1	.606		.570		.497		.490		.640		.573		.588		.626		.650		.709		.649	
R2	.605		.569		.493		.487		.639		.571		.587		.625		.649		.707		.648	
R3	.701		.617		.444		.428		.848		.609		.680		.814		.832		.876		.778	
R4	.088		.063		.101		.109		.043		.089		.048		.025		.106		.283		.161	
R5	.088		.063		.099		.108		.043		.089		.048		.025		.105		.281		.160	
ANALYSIS	E1		E2		E1		E1		E1		E2		E1		E2		E1		E2		E3	

	DR-A2				DR-2A				DR-1 GRAIN "n"						DR-1 GRAIN "r"				DR-11A			
	wt.%	cations																				
TiO_2	.14	.0331	.01	.0023	.08	.0185	.08	.0184	44.97	.8269	42.28	.7753	27.17	.5011	48.23	.9064	51.07	.9664	51.28	.9705		
FeO	–	.0331	–	.0023	–	.0185	–	.0184	–	–	–	–	–	–	–	–	–	–	–	–		
Cr_2O_3	.04	.0098	.08	.0200	–	–	.03	.0073	7.51	.1452	10.42	.2008	21.69	.4205	4.07	.0804	.11	.0022	.37	.0736		
Al_2O_3	.06	.0220	.10	.0373	.13	.0471	.09	.0324	1.47	.0424	2.20	.0632	4.15	.1200	.84	.0247	.13	.0039	.19	.0564		
Fe_2O_3	68.06	15.9028	68.34	15.9378	68.76	15.9159	69.20	15.9235	8.62	.1586	10.10	.1854	24.77	.4572	4.36	.0820	3.23	.0612	2.43	.0460		
FeO	29.73	7.6867	30.48	7.8976	30.42	7.8062	29.34	7.4813	35.37	.7232	33.02	.6733	16.93	.3473	38.75	.8098	39.93	.8403	40.58	.8541		
MgO	.66	.3054	.20	.0943	.40	.1834	1.11	.5058	2.33	.0849	2.34	.0850	3.71	.1356	2.14	.0797	2.68	.1005	2.53	.0949		
MnO	.03	.0079	.03	.0080	.04	.0104	.05	.0129	.91	.0188	.82	.0850	.88	.0183	.80	.0169	1.20	.0256	1.01	.0215		
TOTAL	98.71		99.26		99.83		99.90		101.17	2.0000	101.18	2.0000	99.30	2.0000	99.19	2.0000	98.35	2.0000	98.39	2.0000		
R1	.674		.668		.671		.680		mol. % ilmenite													
R2	.673		.668		.670		.680															
R3	.998		.996		.997		.998		90.71		88.63		64.60		95.43		96.72		97.53			
R4	.038		.011		.229		.063															
R5	.038		.011		.229		.063															
ANALYSIS	Magnetite		Magnetite		Magnetite		Magnetite		Cr-ILMENITE		Cr-ILMENITE		?		Cr-ILMENITE		ILMENITE		ILMENITE			

RATIOS : R1 = Fe^{3+} / Fe^{3+} + Fe^{2+} (octahedral); R2 = Fe^{3+} / Fe^{3+} + Fe^{2+} (total); R3 = Fe^{3+} / Fe^{3+} + Al + Cr; R4 = Mg / Mg + Fe^{2+} (octahedral); R5 = Mg / Mg + Fe^{2+}(total).

Note that here "magnetite" refers to Ti- and Cr- poor ("secondary") magnetite.

magnetite. It usually contains only low levels of MgO and Al_2O_3. The TiO_2 content is also low, such that this spinel cannot be compared directly with the Fe-Ti-Cr spinels in iron-rich ultramafic pegmatite (see Chapter 10). An unusual Cr-rich ilmenite has been located in two polyphase spinel grains (grains "n" and "r", sample DR-1; fig. 4.5E,F). Analyses of these are presented in Table 4.5. Analyses of (typical) ilmenite, from an iron-rich vein in the Driekop pipe (sample DR-11A) and secondary magnetite (essentially pure Fe_3O_4) from the platiniferous core (samples DR-A2, A3) are also presented in Table 4.5.

DISCUSSION : Stumpfl and Rucklidge (1982) suggest that the formation of these spinels is related to complex, polyphase processes linked to low temperature iron-rich fluids. The data presented in this study also favour a metasomatic model, athough it is likely that metasomatism was related to an iron-rich silicate liquid at magmatic temperatures. It is suggested that the formation of these complex spinels is directly related to the formation of the iron-rich assemblages in the pipes (see below). Significant support for this interpretation lies in the observation that grains wholly encapsulated in olivine are always homogeneous; only those of interstitial habit are of the complex variety. Furthermore, the complex chromites are concentrated at the margins of the magnesian dunite unit and Cr-spinel is entirely absent from the iron-rich assemblages themselves.

(3) CUMULUS CHROMITES

Electron microprobe analyses of cumulus chromites are presented for comparative purposes in Table 4.6. These include samples from the orthopyroxenite that overlies the UG-2 chromitite (approximately 1.5 km. from the Driekop pipe; sample DR-52) and samples of cumulus magnesian dunites from the lower zone in the eastern Bushveld Complex (samples DUN-1, DUN-3).

TABLE 4.6 ELECTRON MICROPROBE ANALYSES OF CUMULUS CHROMITES

	DUN-3					
	wt.%	cations				
TiO_2	1.35	.2748	1.47	.2997	2.11	.4331
FeO	-	.2748	-	.2997	-	.4331
Cr_2O_3	39.87	8.5326	39.23	8.4089	39.03	8.4237
Al_2O_3	13.50	4.3062	13.98	4.4663	12.29	3.9535
Fe_2O_3	12.82	2.6115	12.37	2.5252	13.41	2.7563
FeO	24.53	5.2788	25.35	5.4483	25.82	5.4628
MgO	6.42	2.5904	5.99	2.4207	5.90	2.4008
MnO	.57	.1306	.57	.1308	.59	.1364
TOTAL	99.06		98.97		99.16	
R1	.330		.316		.335	
R2	.319		.305		.318	
R3	.169		.163		.182	
R4	.329		.307		.305	
R5	.318		.296		.289	
Description	Intergranular chromites from lower zone cumulate dunite, Jagdlust section					

TABLE 4.6 ELECTRON MICROPROBE ANALYSES OF CUMULUS CHROMITES FROM DRIEKOP (CONTINUED)

	DR-52										DUN-1					
	wt.%	cations														
TiO_2	1.07	.2076	.98	.1905	1.06	.2069	.84	.1673	1.21	.2426	.65	.1276	.66	.1301	.62	.1220
FeO	-	.2076	-	.1905	-	.2069	-	.1673	-	.2426	-	.1276	-	.1301	-	.1220
Cr_2O_3	42.53	8.6786	42.20	8.6281	42.77	8.7778	40.76	8.5356	40.76	8.5927	39.89	8.2365	42.16	8.7424	42.51	8.7998
Al_2O_3	17.89	5.4412	17.90	5.4549	17.21	5.2645	17.11	5.3405	16.34	5.1342	18.21	5.6042	17.43	5.3871	17.75	5.4765
Fe_2O_3	7.54	1.4646	7.89	1.5357	7.90	1.5437	8.97	1.7891	8.90	1.7877	9.68	1.9639	8.15	1.6100	7.50	1.4794
FeO	20.09	4.1296	19.95	4.1259	20.84	4.3191	25.10	5.3931	23.97	5.1031	21.74	4.6211	22.76	4.8641	23.04	4.9236
MgO	9.81	3.7742	9.80	3.7777	9.24	3.5733	6.29	2.4834	7.01	2.7862	8.35	3.2506	7.72	3.0182	7.57	2.9544
MnO	.44	.0961	.44	.0963	.48	.1055	.55	.1233	.49	.1106	.58	.1283	.53	.1177	.55	.1219
TOTAL	99.37		99.17		99.51		99.62		98.67		99.11		99.42		99.35	
R1	.261		.271		.263		.249		.259		.291		.248		.231	
R2	.262		.262		.254		.243		.250		.286		.243		.226	
R3	.093		.098		.099		.114		.115		.120		.102		.093	
R4	.477		.477		.452		.315		.353		.412		.382		.375	
R5	.465		.466		.441		.308		.342		.406		.376		.369	
Description	Hosted within the UG-2 layer				Intergranular, within bronzitites below the UG-2 layer						Intergranular chromites from lower zone cumulate dunites, Jagdlust section					

TABLE 4.7A ELECTRON MICROPROBE ANALYSES OF Cr-MAGNETITES

	MO-11	MO-11	MO-11	MO-11	MP-2	MP-2
wt.%						
TiO_2	11.49	9.84	11.76	10.36	15.29	16.25
Cr_2O_3	3.47	3.70	3.25	3.60	.49	.46
Al_2O_3	16.18	4.57	4.62	3.33	3.72	3.73
Fe_2O_3	27.58	40.76	38.03	41.67	35.30	33.80
FeO	40.05	38.99	40.76	39.94	43.60	44.37
MgO	3.18	.93	1.07	.65	1.27	1.42
MnO	.39	.35	.37	.32	.36	.37
TOTAL	102.34	99.15	99.87	99.88	100.03	100.40
cations						
Ti	2.3100	2.2011	2.6049	2.3207	3.3861	3.5786
Fe^{2+}	2.3100	2.2011	2.6049	2.3207	3.3861	3.5786
Cr	.7334	.8701	.7568	.8478	.1140	.1065
Al	5.0973	1.6019	1.6036	1.1688	1.2909	1.2871
Fe^{3+}	5.5489	9.1255	8.4295	9.3418	7.8227	7.4489
Fe^{2+}	6.6445	7.4995	7.4379	7.6306	7.3527	7.2884
Mg	1.2672	.4123	.4698	.2886	.5574	.6198
Mn	.0883	.0881	.0923	.0807	.0897	.0917

Samples from mine dumps, Mooihoek.

TABLE 4.7B ILMENITES

	MO-11	MO-11	MP-2	MP-2
wt.%				
TiO_2	50.53	50.27	52.51	52.66
Al_2O_3	.37	.77	.20	.20
FeO	41.93	41.21	41.92	41.62
Fe_2O_3	5.08	5.82	3.00	3.29
MnO	.53	.64	.55	.51
MgO	1.67	1.88	2.66	2.93
Cr_2O_3	.30	.27	.01	n.d.
TOTAL	100.41	100.85	100.85	101.21
cations				
Ti	.9441	.9322	.9693	.9669
Al	.0108	.0224	.0058	.0057
Fe2+	.8711	.8498	.8606	.8498
Fe^3	.0950	.1079	.0554	.0605
Mn	.0112	.0134	.0114	.0105
Mg	.0618	.0691	.0973	.1066
Cr	.0059	.0053	.0002	-
mol.%	ilmenite			
	95.02	94.28	97.06	96.77

Samples from mine dumps, Mooihoek.

4.3.2 Fe-Ti-Cr SPINEL AND ILMENITE

In the platiniferous core of the Mooihoek pipe coarse-grained Fe-Ti-Cr spinel (that superficially resembles Ti-magnetite) and granular ilmenite are an intimate component of an assemblage which may be referred to as an iron-rich ultramafic pegmatite (see p.37). According to Wagner (1929) similar phases, although in smaller quantities, occurred in the core of the Driekop pipe. The author has observed these phases in iron-rich dunite and wehrlite veins, evidently genetically related to the platiniferous core, but not in the actual core of the Driekop pipe. The results of electron microprobe

analyses of massive segregations of magnetite and ilmenite from Mooihoek are presented in Table 4.7 (samples MO-11 and MP-2 from the mine dumps). This spinel typically contains between 3 and 4 wt. percent Cr_2O_3 and between 9 and 16 wt. percent TiO_2. It may be compared with magmatic Ti-magnetite in which the Cr content is unusually high (Cr is probably displacing Fe^{3+}). The microtextures and composition of this spinel are directly comparable with Fe-Ti-Cr spinels in iron-rich ultramafic pegmatite (see Chapter 10).

Using the magnetite-ilmenite geothermometer of Spencer and Lindsley (1981) an equilibration temperature of 655°C at $\log_{10} fO_2$ of - 19.3 is obtained for Fe-Ti oxides from the core of the Mooihoek pipe. The range of exsolution textures present in these oxides is also suggestive of crystallization at magmatic temperatures.

4.4 ORE MINERALS

4.4.1 BASE-METAL SULPHIDES : A SYNTHESIS

(1) Co-poor pentlandite occurs as a rare constituent in serpentinite veinlets in the magnesian dunite, but other sulphides are not normally observed.
(2) In these pipes, base-metal sulphides are essentially restricted to the platiniferous cores.
(3) Pyrrhotite (usually the hexagonal variety, although troilite also occurs) is the dominant sulphide in the platiniferous core.
(4) Pentlandite, a subordinate phase in the platiniferous core is a Co-rich variety, similar to that found in iron-rich ultramafic pegmatite.
(5) For further details see Chapters 2 (literature review) and 11 (tabulation of new data).

4.4.2 PLATINUM GROUP ELEMENTS : A SYNTHESIS

(1) PGE in the pipes are essentially restricted to a specific, iron-rich assemblage that occurs as a central core and as veins that cut the main body of magnesium dunite. The magnesian dunite adjacent to the platiniferous core may contain sporadic PGE, but is usually depleted in PGE.
(2) Wagner (1929), however, reports that at Mooihoek economic concentrations of PGE occurred outside of the core in the main body of magnesian dunite. They were usually associated with schlieren of chromite. A comparison may be drawn with the forsterite dunite deposits of the Urals where PGE occur in the dunite and are preferentially associated with chromite (Razin, 1976). It is known that dunites generally contain higher than average concentrations of

PGE (Naldrett & Cabri, 1976; Crocket, 1979; Cabri, 1981). Few data are available on the dunitic cumulates in the Bushveld Complex, although Hulbert and Von Gruenewaldt (1982) have worked on the lower zone in the Potgietersrus limb.

(3) The iron-rich ultramafic pegmatite suite in the Bushveld Complex is usually non-platiniferous, except where replacement of platinum- rich cumulates, such as the Merensky Reef, is evident. Accordingly, it is considered unlikely that an iron-rich liquid derived from the cumulate pile would be enriched in PGE.

(4) For these reasons the magnesian dunite is considered to be the primary source of the PGE in the platiniferous ultramafic pipes.

(5) The PGE mineralogy of these pipes has been reviewed in Chapter 2. A comparison may be drawn with the PGE mineralogy of "replaced" Merensky Reef at Amandelbult (see Chapter 11).

(6) Peyerl (1982) has documented the PGE mineralogy of the UG-2 chromitite layer adjacent to the Driekop pipe. He found that it is atypical of the normal chromitite layer and attributes the formation of different PGM to the pipe. These PGM are also characterised by different inter-element ratios (e.g., the percentage of Ru is unusually high). It is suggested that metasomatic liquids emanated from the pipe to produce the observed changes. The mineralogy of the host chromite is apparently unaffected. It may be deduced that these liquids were hot enough to raise the PGM above their solidus temperatures and to transport new PGE in solution.

4.5 WHOLE-ROCK CHEMISTRY

Mineralogical differences between the major petrologic assemblages in the platiniferous ultramafic pipes discussed in Chapter 3 are apparent from CIPW norms (see Appendix 6). These modal features, together with some differences in the major element chemistry are evident on a triangular "AFM" diagram (in wt. percent) of ($Na_2O + K_2O$) - FeO - MgO (fig. 4.6C). In this diagram, samples of iron-rich dunite from the platiniferous cores of the various pipes and samples of magnesian dunite from Driekop plot on a straight line (trend A'-A'). This trend is directly related to a decrease in the whole-rock Mg-number of these samples. Samples of the iron-rich olivine clinopyroxenite, websterite and clinopyroxenite pegmatite assemblage at Driekop define a separate trend (field "B"). Samples of leuconorite cumulates from the wallrocks to the Driekop pipe also plot in a separate field ("C").

These different assemblages also plot in quite separate fields in a

binary graph of wt. percent CaO versus wt. percent MgO (fig. 4.6B). In this diagram the trend C'-C' represents part of a plagioclase-orthopyroxene mixing line for the relevent cumulus composition, and the trend B'-B' is a mixing line between iron-rich olivine (essentially Fo_{65-62}) and clinopyroxene of a suitable composition. The slight curvature evident in trend B'-B' may be a feature of the small degree of fractionation in this assemblage.

Similar trends are also seen on a binary graph of ppm Co versus wt. percent MgO (fig. 4.6A). In this diagram trend A'-A' is related to increases in the Co content of olivine which is becoming increasingly more fayalitic. Trend B'-B' is again a mixing line between iron-rich olivine and clinopyroxene and trend C'-C' is a mixing line between cumulus plagioclase and cumulus orthopyroxene of a fixed composition.

In these rocks both Sc and V partition preferentially into clinopyroxene, to a lesser degree into orthopyroxene and olivine, and are practically absent in plagioclase (fig. 4.7C). The magnesian and iron-rich dunites define a straight line relationship (A'-A'), which indicates that the iron-rich dunites are slightly richer in Sc, but the V content does not exhibit any variation. Samples of iron-rich olivine clinopyroxenite, websterite and clinopyroxenite pegmatite also define a straight line

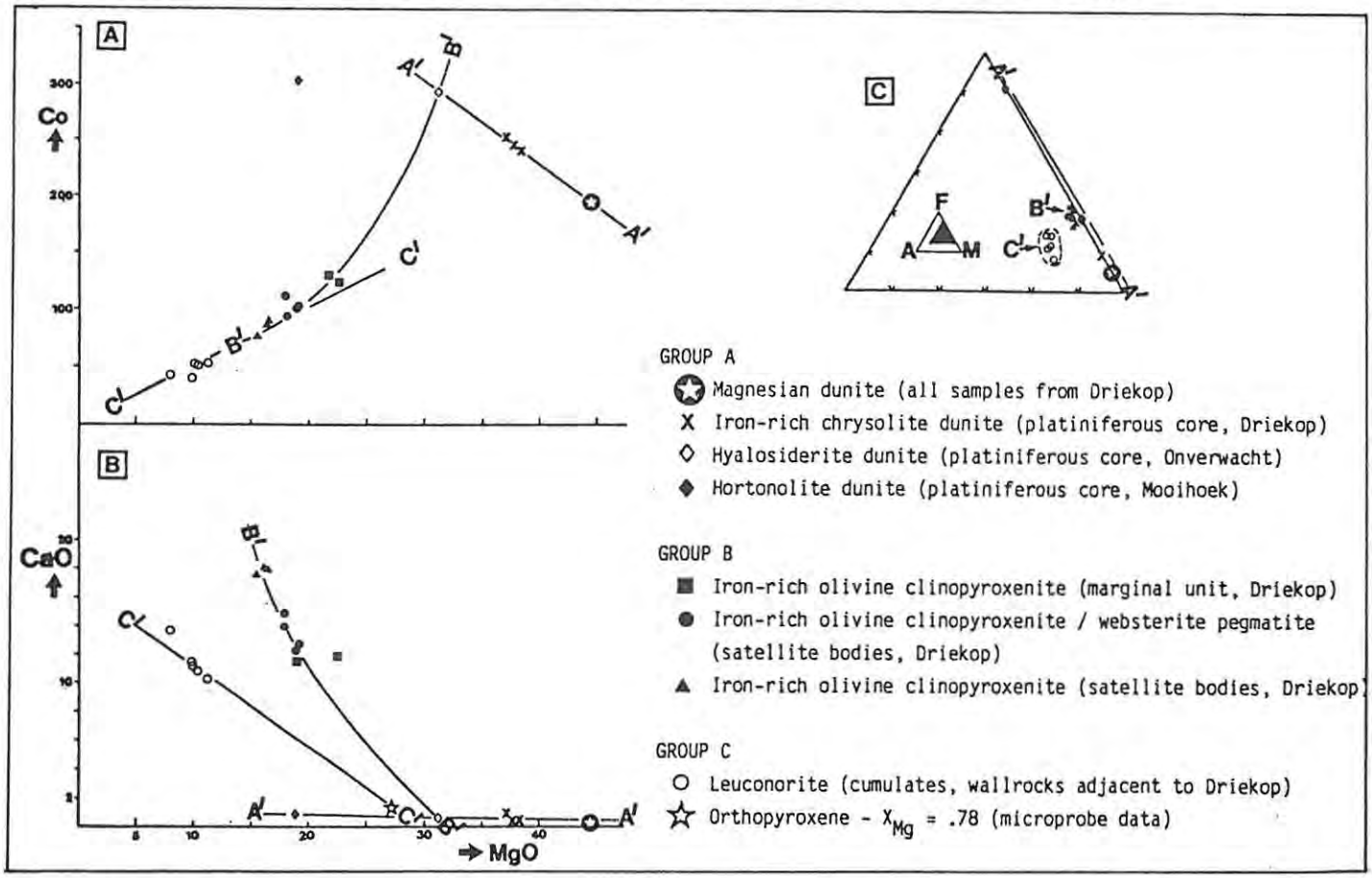

FIGURE 4.6 Whole-rock data plotted on variation diagrams : (A) ppm Co vs. wt. % MgO; (B) wt. % CaO vs. MgO; and (C) an AFM diagram (wt. % (Na_2O+K_2O) - FeO - MgO).

The following trends may be recognized. A' - iron-enrichement trend in dunites (samples from group A); B' - mixing line between olivine ($\sim Fo_{65}$) and clinopyroxene (samples from group B, plus hyalsoiderite dunite); C' - mixing line between orthopyroxene ($\sim X_{Mg}$ = .78) and plagioclase (samples from group C).

relationship, which includes samples of leuconorite cumulates (trend B'-B'). This represents two mixing lines, plagioclase-orthopyroxene (for the cumulates) and iron-rich olivine- clinopyroxene (for the pipe-related rocks). This indicates that clinopyroxene is much richer in Sc and V than orthopyroxene (see also Chapter 12).

In Figure 4.7A, B the incompatible elements, Zr and Y are plotted against Sc. These elements are below the lower limit of determination in the magnesian dunites and in some of the iron-rich dunites. Samples of iron-rich olivine clinopyroxenite, websterite and clinopyroxenite pegmatite define a straight line B'-B' in Figure 4.7B, which indicates that Y is preferentially concentrated in the clinopyroxene-rich rocks. Thus the satellite bodies of clinopyroxenite pegmatite, which are also distinguished by containing the most iron-rich clinopyroxene, are richer in incompatible elements.

A binary graph of wt. percent Cr_2O_3 versus wt. percent NiO is presented in Figure 4.7D. It illustrates quantitively the modal variations in chromite discussed previously; note that magnesian dunite from Driekop contains on average roughly 1 modal percent chromite (corresponding to approximately 0.42 wt. percent Cr_2O_3), whereas the iron-rich dunites contain less than .05 wt.

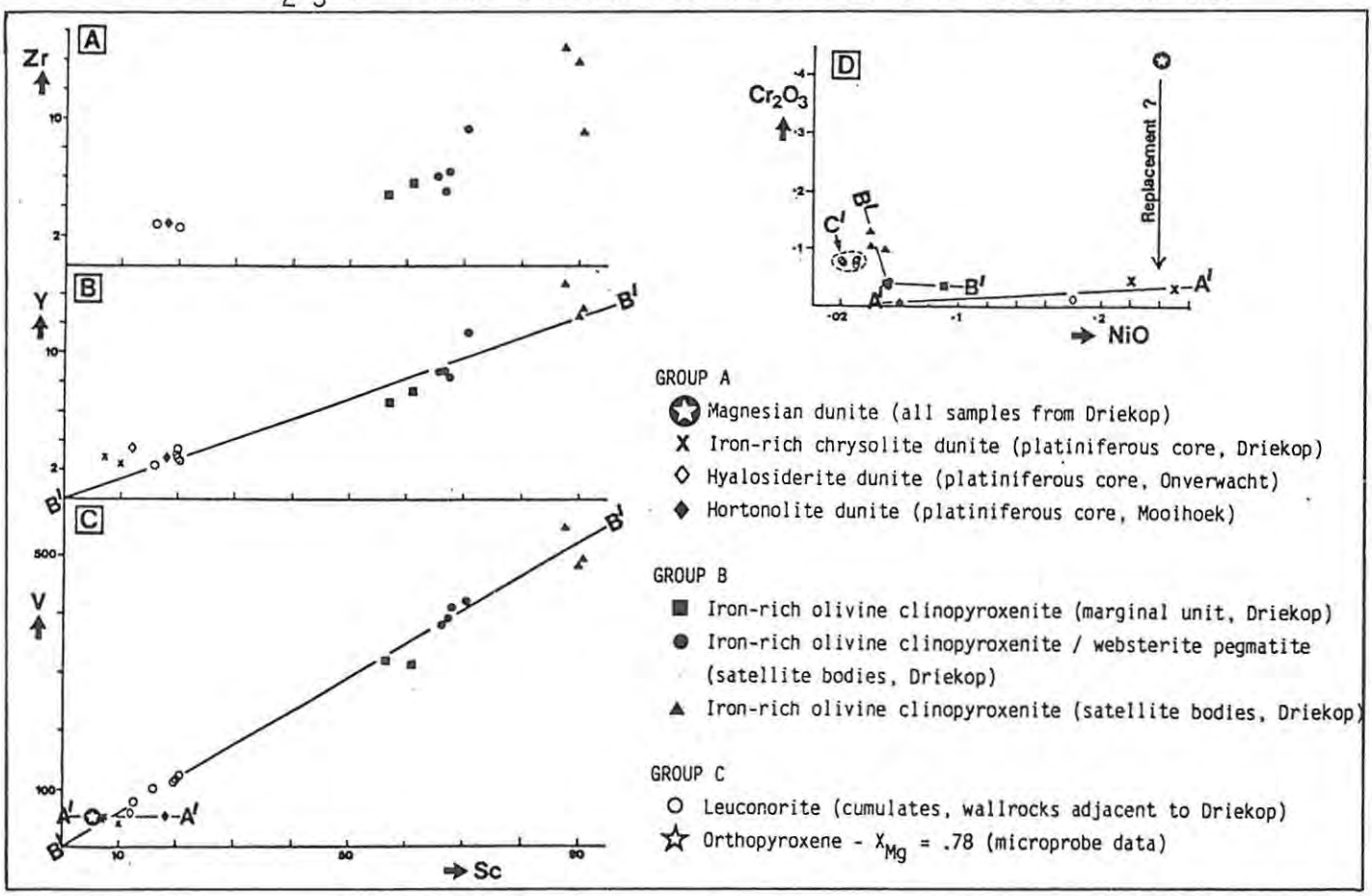

FIGURE 4.7 Whole-rock data plotted on variation diagrams : (A) ppm Zr vs. ppm Sc; (B) ppm Y vs. ppm Sc; (C) ppm V vs. ppm Sc; and (D) wt. % Cr_2O_3 vs. wt. % NiO.

The following trends may be recognized. A' - iron-enrichement trend in dunites (samples from group A) - the magnesian dunites do not lie on this trend in "D", it is postulated that the iron-rich dunites are a result of replacement of the magnesian dunites; B' - straight line representing a modal increase in clinopyroxene (samples from group B) - the rocks from the margin of the Driekop pipe do not lie on this trend - they also are interpreted as resulting from replacement of the pre-existing magnesian dunite; C' - samples from group C.

percent Cr_2O_3. However, iron-rich dunite in the core of the Driekop pipe contains roughly the same proportion of NiO as the magnesian dunite. These features cannot be reconciled with a fractionation model for these assemblages. Assuming the metasomatic model is correct then it may be concluded that the formation of iron-rich olivine does not, initially, affect the NiO content of the olivine but does result in resorption (and dissolution and removal ?) of Cr-spinel. Samples of iron-rich olivine clinopyroxenite, websterite and clinopyroxenite pegmatite, that do not replace magnesian dunite, plot in a separate field in this diagram (trend B'-B'). Thus they do not represent either fractionation or metasomatic replacement of the magnesian dunite.

4.6 EVOLUTION OF THE PLATINIFEROUS ULTRAMAFIC PIPES

Hypotheses which invoke replacement of pre-existing cumulates in a layered intrusion usually attribute the replacement process to either silicate liquids or hydrothermal fluids which stream up through the cumulate pile (see sections 13.1 and 13.4). Cameron and Desborough (1964) suggest that the Onverwacht pipe has resulted from metasomatism of the pre-existing cumulates, which at the present level of exposure consist of orthopyroxenites and chromitites. Irvine (1982) cites the Onverwacht pipe as a classic example of "infiltration metasomatism", although he may well be referring just to the platiniferous core and not to the whole pipe. Schiffries (1982), however, suggests that the Driekop pipe has formed by replacement of pre-existing cumulates by chloride-rich hydrothermal brines. This model is less attractive than Cameron and Desborough's because it involves replacement of cumulates in which plagioclase is the major constituent. Secondly, the data presented in this study indicate that all of the petrologic assemblages present in these composite pipes formed at magmatic temperatures, and unless convincing evidence can be produced to the contrary a low temperature origin is untenable. Thirdly, Schiffries' hypothesis is based on the incorrect assumption that the composition of olivine in the magnesian dunite at Driekop is Fo_{79} (which is equivalent to the En component of cumulus orthopyroxene in the wallrocks at the present level of exposure), whereas data presented here suggest an average composition of $Fo_{83.6}$. Thus where a metasomatic model is referred to in this study it is assumed to be at magmatic temperatures.

Finally, it must be stressed that all the data presented in this study, including field relationships, indicate that these pipes are of a composite nature and each mineralogical assemblage must be considered as a separate entity.

4.6.1 THE MAGNESIAN DUNITE ASSEMBLAGE

PETROGENESIS : Three principal hypotheses can be postulated : (1) intrusion of a dunitic melt; (2) intrusion of remobilised magnesian dunite cumulates in the form of a crystal-rich mush; and (3) metasomatism of pre-existing cumulates. Evidence for dunitic melts has come under attack in recent years such that the first hypothesis is discarded.

Criticisms against a metasomatic model may be listed as follows :

(1) It is difficult to justify the very primitive metasomatizing liquids or fluids required to convert cumulus orthopyroxene (En_{81-77}, at Driekop) to olivine with a composition of $Fo_{83.6}$. It may be predicted that intercumulus liquid derived during cumulate formation would be more fractionated than the primary magma. The composition of this assemblage matches the most primitive cumulates in the Bushveld Complex, such that even if the postulated intercumulus liquids were derived at depth this problem is still not solved. Further, it is unlikely that a hydrothermal fluid would be rich in MgO.

(2) The primitive nature of the magnesian dunite is further emphasized by the Ni content of the magnesian olivine. If the magnesian olivine in these pipes has formed by metasomatism of cumulus orthopyroxene from the adjacent wallrocks, then it must have involved liquids that were rich in Ni.

(3) The presence of chromite as an ubiquitous accessory phase in the magnesian dunite has been completely ignored by some of the proponents of a metasomatic origin for the Driekop pipe (see Schiffries, 1982). Cumulus chromite is essentially absent from the silicate cumulates that the Driekop pipe is purported to replace, at the present level of exposure.

None of the metasomatic models have explained these features; surely it is unlikely to expect an intercumulus liquid to have a high Mg/Fe ratio and to be rich in Ni and Cr, elements which are rapidly depleted from a magma undergoing fractional crystallization ? (see also Chapter 13). Furthermore, the formation of metasomatic chromite is considered to be unlikely according to our present knowledge.

Consequently, the second model is favoured by the present author, although no clear-cut evidence has been established. The author has been particularly influenced by the fact that the magnesian dunite in the pipes is mineralogically and chemically similar to cumulus dunites in the Bushveld Complex. The pipe-hosted dunites are purer "adcumulates" than cumulus dunites, presumably because trapped intercumulus liquid has been expelled during intrusion. Furthermore, the major collapse structure in the cumulate wallrocks at Driekop is difficult to reconcile with a replacement origin and is more tenable with an intrusive origin.

EMPLACEMENT

These pipes have some features in common with the zoned Alaskan complexes (Noble & Taylor, 1960; Wyllie, 1967) and it is interesting to observe that Irvine (1980) also remarks on the adcumulate texture of dunite in the Alaskan bodies. Irvine interprets the Alaskan dunites as early olivine cumulates which have been tectonically forced upwards into overlying pyroxene cumulates. It is suggested that the magnesian dunite unit in the Driekop pipe has resulted from remobilisation of cumulus dunite lower in the layered sequence of the Bushveld Complex. Subsequent upward movement may be described in terms of a crystal-rich diapir.

Diapiric intrusion of a crystal-rich dunitic mush, which has only a small proportion of trapped intercumulus fluid, can readily be explained by the strong tendency which crystalline olivine exhibits to flow (see, for example, Rayleigh, 1968). Plastic deformation and flow of olivine-rich rocks is an important concept in plate tectonic models. Remobilisation and subsequent intrusion of a cumulus dunite may occur in response to tectonics extraneous to the Bushveld magma chamber. Features in this area of the Bushveld Complex which may reflect major tectonic activity include the Steelpoort fault, the unusually thick accumulation of lower zone cumulates in the Burgersfort "bulge" area and the presence of ultramafic sills in the adjacent floor rocks. Gain (1980) discusses the N40^{o}E alignment of transgressive ultramafic bodies on Maandagshoek. This is subparallel to the Murchison lineament, a major structural control which continued throughout deposition of the Transvaal Supergroup (Hunter & Hamilton, 1978), and is presumed to have been active during intrusion of the Bushveld Complex (fig. 3.1). Whether any of these features may be related to intrusion of the platiniferous pipes is a matter of conjecture.

The paradox of a major collapse structure in the wallrocks of an intrusive body has been described and modelled by Bridgwater et al. (1974). Their model relates the downwarping and lack of upward drag to viscosity differences and the associated pressure gradient between a fluid diapir and a large, rigid plate. Structures in the wallrocks at Driekop imply that they were still very hot during intrusion of the diapiric pipe-like body and additional heat gained from the dunite would cause a decrease in their viscosity, resulting in plastic slumping. The regular increase in dip observed in the layered cumulate wallrocks at Driekop is consistent with the ideal pressure profile model of Bridgwater et al. An important concept in this model is that deformation phenomena are related to injection of a less viscous material through a viscous plate, and are not density controlled. The relationship between viscosity and heat transfer led Grout (1945) to

suggest that rocks overlying a diapir may become so reduced in viscosity that they move aside and down the sides of the diapir, permitting the rise of a large intrusive body by volume adjustments in a mobile zone (see also Marsh, 1982).

4.6.2 THE IRON-RICH OLIVINE CLINOPYROXENITE-WEBSTERITE-CLINOPYROXENITE PEGMATITE ASSEMBLAGE

Data presented in this study indicate that the marginal envelope of iron-rich olivine clinopyroxenite in the Driekop pipe and the adjacent satellite bodies of websterite and clinopyroxenite pegmatite are related by a common parentage. Formation of this assemblage may be explained by five possible hypotheses : (1) in situ fractionation of the magnesian dunite (this was rejected in the previous text); (2) a metasomatic contact feature, resulting from interaction between the magnesian dunite and the cumulate wallrocks (this model, which was suggested by Wagner (1929), was also rejected in the previous text); (3) intrusion of a second, entirely different magma; or (4) metasomatism of pre-existing cumulates in response to injection of a second, entirely separate, iron-rich liquid; (5) Irvine (1980) interprets hornblende-anorthite pegmatites in the Duke Island Complex, Alaska as resulting from intercumulus liquids which have been removed from the dunite during intrusion. This model cannot be applied to Driekop.

Data in this study favour the third or fourth alternatives. This iron-rich liquid may be of a similar nature and origin to that responsible for iron-rich ultramafic pegmatite. It is an intercumulus, or postcumulus liquid derived from within the crystallizing cumulate pile, and subsequently injected around the margin of the pipe, after emplacement of the main body of magnesian dunite. It is postulated that the structural downwarping associated with the magnesian dunite unit would provide a favourable site into which dense, iron-rich postcumulus liquids would readily migrate. Probably the bulk of the satellite bodies of iron-rich websterite and clinopyroxenite pegmatite adjacent to the Driekop pipe, and the marginal envelope of olivine clinopyroxenite, formed by replacement of the cumulates. However, crystallization directly from the liquid cannot be excluded.

4.6.3 THE PLATINIFEROUS, IRON-RICH CORE ASSEMBLAGES

Mineralogical and compositional similarity between the platiniferous core unit and a metasomatic assemblage at the contact of the magnesian dunite and iron-rich olivine clinopyroxenite implies that the core of the

Driekop pipe is of a metasomatic origin. It is related to the same iron-rich liquids that are responsible for the formation of the iron-rich olivine clinopyroxenite, websterite and clinopyroxenite pegmatite assemblage. The formation of irregular pod-like bodies and veins throughout the pipe must be taken into account, but why these liquids should be preferentially concentrated into a single, core-like feature is difficult to explain. The iron-rich assemblages that do not replace magnesian dunite are not platiniferous, thus it is concluded that the magnesian dunite is the source of the PGM. This has been concentrated into economic orebodies during the metasomatic process.

The polyphase chromites in the magnesian dunite at Driekop are attributed to disequilibrium between primary chromite and this iron-rich silicate liquid which was possibly injected along serpentinisation cracks after the dunite cooled. Cr-spinel is absent in the iron-rich core of the Driekop pipe; it has presumably been dissolved and removed during the metasomatic event. This reworking of the PGM in the magnesian dunite is feasible, when it is appreciated that the alteration of the chromite points to pervasion by late-stage liquids.

The core of the Mooihoek pipe forms a well-defined unit and consists of a pegmatitic, highly fractionated assemblage in which Fe-Ti-Cr oxide, ilmenite, amphibole and mica are abundant. This unit may in part have crystallized from a silicate liquid, and it may provide a link between the platiniferous ultramafic pipes and the (non-platiniferous) iron-rich ultramafic pegmatite suite.

4.7 SUMMARY

(1) Field relationships of the Driekop platiniferous ultramafic pipe are documented.

(2) Detailed whole-rock and mineral chemical data for the major petrologic units in the pipe are documented.

(3) The evolution of the pipe is discussed in terms of a model which supports a separate origin for the two main petrologic assemblages in the pipe. These data do not favour a single metasomatic event.

(4) The magnesian dunite unit (which is the main component of the pipe and also occurs in satellite bodies) is interpreted as a remobilised cumulate.

(5) Metasomatic replacement of the orthopyroxenite cumulates by this magnesian dunite may have occurred, but there is no evidence to support metasomatism of felsic cumulates.

(6) The iron-rich olivine clinopyroxenite, websterite and clinopyroxenite

pegmatite assemblages are interpreted as resulting from a later, and quite separate event. This is compared with the iron-rich ultramafic pegmatite suite, and may be related to metasomatism of pre-existing cumulates in response to iron-rich liquids.

(7) Injection of these iron-rich liquids through the already crystalline magnesian dunite resulted in metasomatism of the dunite to form the platiniferous, iron-rich core assemblages. This process was also responsible for the formation of polyphase, complex Cr-spinels and locally the complete dissolution of these spinels. The resulting, iron-rich metasomatic olivine is characterised by unusually high NiO / MgO ratios.

(8) The source of the PGE is possibly related to the magnesian dunite, as iron-rich assemblages that do not replace dunite are non-platiniferous.

(9) The platiniferous ultramafic pipes may thus be considered as unique combinations of two groups of transgressive, ultramafic rock. The fact that they are restricted to only four known occurrences in a specific area of the Bushveld complex may lend support to their hybrid parentage.

SECTION C : THE CUMULATE SEQUENCE IN THE UPPER CRITICAL ZONE, AMANDELBULT

CHAPTER 5 DESCRIPTION AND PRESENTATION OF NEW DATA

The regional geology of the Amandelbult area is described, with particular reference to part of the upper critical zone of the layered sequence, from the UG-1 chromitite layer to the Bastard Reef. Some new mineralogical and whole-rock chemical data are presented in the last section of this chapter. This part of my studies has been achieved with considerable assistance from the resident geological staff at R.P.M. Amandelbult, particularly J.C. Theron and B.M. Walters.

5.1 REGIONAL GEOLOGY

Amandelbult section of R.P.M. is situated in the northern sector of the western Bushveld Complex. The lower, critical, and main zones of the layered sequence occur as a discrete segment which is overlain by upper zone cumulates. The upper zone rocks conformably overlie the earlier cumulates to the southeast but transgress and truncate them to the southwest. This transgression of upper zone cumulates is known as the "Northern Gap". It separates the lower, critical and main zone rocks in this area from those at the adjacent R.P.M. Union Section. At the north-eastern extremity of Amandelbult, which coincides roughly with the Crocodile River, the layered sequence is transgressed by later Bushveld granites. The average dip of the upper critical zone cumulates in this area is 20^{o} to the south-east. At the south-western extremity of the area the strike of the cumulates swings northwards in an arc, such that they eventually dip at $40\text{-}50^{o}$ to the north-west. This structural feature is related to the Northern Gap, where magnetic data illustrate the transgressive nature of the upper zone cumulates (Viljoen et al.,a, in press; fig. 5.1). The critical zone is exposed along strike for 22 km in the Amandelbult area and, although outcrop is poor, recent mining operations provide detailed exposure of this sequence.

STRUCTURE

In the Amandelbult area a number of post-Bushveld structural features occur (Viljoen et al.,a,in press). The most important of these are major

NW-SE trending faults. In the central or Middellaagte sector of the mine a major NW-SE graben structure occurs with downthrows of up to 600 m over a 2.5 km strike length. To the northeast of the Middellaagte graben three generations of faulting are recognized. The oldest of these are commonly flat-lying reverse faults with fault planes dipping at between 15 degrees and 30 degrees. The majority of faults are normal and steeper, however, with dips varying between 70 degrees and vertical. The youngest faults have only been exposed at a few localities underground and are essentially strike faults. The latter have only small displacements but the two older generations have throws of up to 50 m and present a problem to mining. In the southwestern sector of the mine area, the major fault direction is northwest-southeast which is at right angles to the strike of the layering and parallel to the faults defining the Middellaagte graben. To the northeast of the Middellaagte graben, the direction of faulting changes to north-south and northeast-southwest. The northwest-southeast direction corresponds to a lineament observed on satellite imagery of the adjacent Transvaal Supergroup sediments, which lie to the northwest of the layered complex (Viljoen et al.,a, in press).

Four major and a number of minor dykes occur in the central and southwestern sectors of the mine leasehold. The positions of the four major dykes are delineated by airborne and ground magnetics and underground exposures. They all strike northwest-southeast and their thickness varies from a few centimetres up to 50 m. The dykes are usually dolerites and appear to represent a single emplacement episode. They have a negative magnetic signature and may be related to the Pilanesberg swarm (Viljoen et al.,a, in press). Carbonate-rich dykes, which contain inclusions and have a brecciated appearance, are often observed in the northeastern sector of the mine. They have kimberlitic affinities and may be related to Pilanesberg alkaline activity and/or the pipes of pyroxenite shonkinite described from the farm Grootkuil 376 KQ (Iannello, 1967; Viljoen et al.,a, in press).

SURFACE FEATURES

The Amandelbult lease area measures 20 X 4 km and is situated in the Thabazimbi district of the northwest Transvaal. It occupies the following farms or portions thereof : Elandsfontein 386 KQ, Schilpadnest 385 KQ, Zwartkop 369 KQ, Middellaagte 382 KQ, Elandskuil 378 KQ, and Haakdoorndrift 374 KQ (Viljoen et al.,a, in press; fig 5.2). Much of the geology of this area is relatively unknown due to poor outcrop. A thick layer of black "turf", a soil ubiquitous over mafic cumulates in the western Bushveld

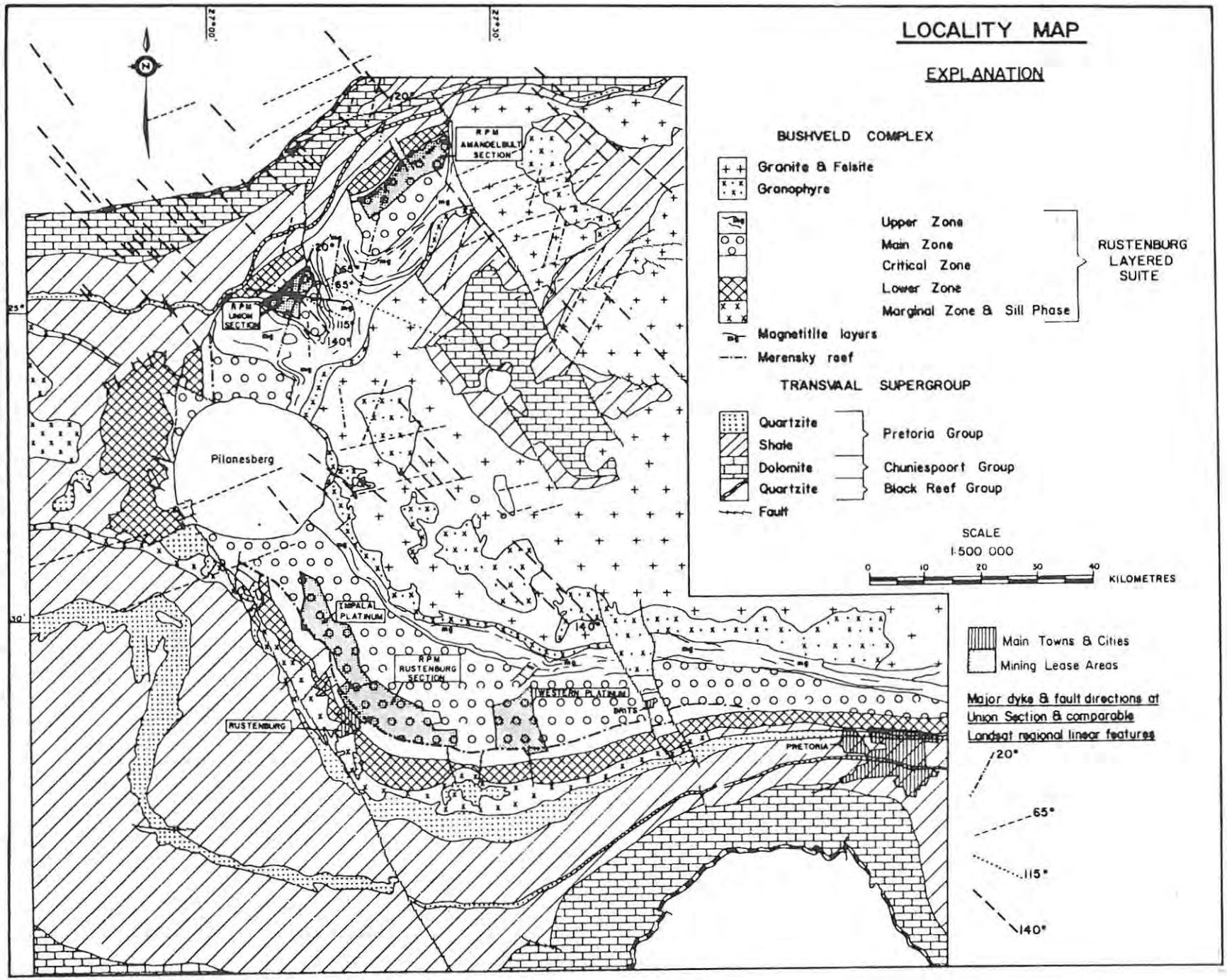

FIGURE 5.1 Locality map showing the major platinum mines in the western Bushveld Complex (from de Klerk, 1982).

Complex, is present and the topography is flat and featureless. This is particularly true of the area underlain by the upper critical and lower main zone rocks. To the north of the mine leasehold, where an inselberg (Mooskop) is a local feature, lower critical zone pyroxenites and chromitites crop out, often as low, laterally extensive ridges. To the south of the mine leasehold a range of conical hills rising 150 m above the plain is correlated with the "pyramid gabbros", which are well known from other areas of the complex. In the lower main zone a number of marker horizons, including the giant mottled anorthosite and leopard marker crop out. The edge of the Bushveld Complex is marked by a range of hills, the Witfonteinrand, comprising resistant quartzites of the Transvaal Supergroup (Viljoen et al.,a, in press).

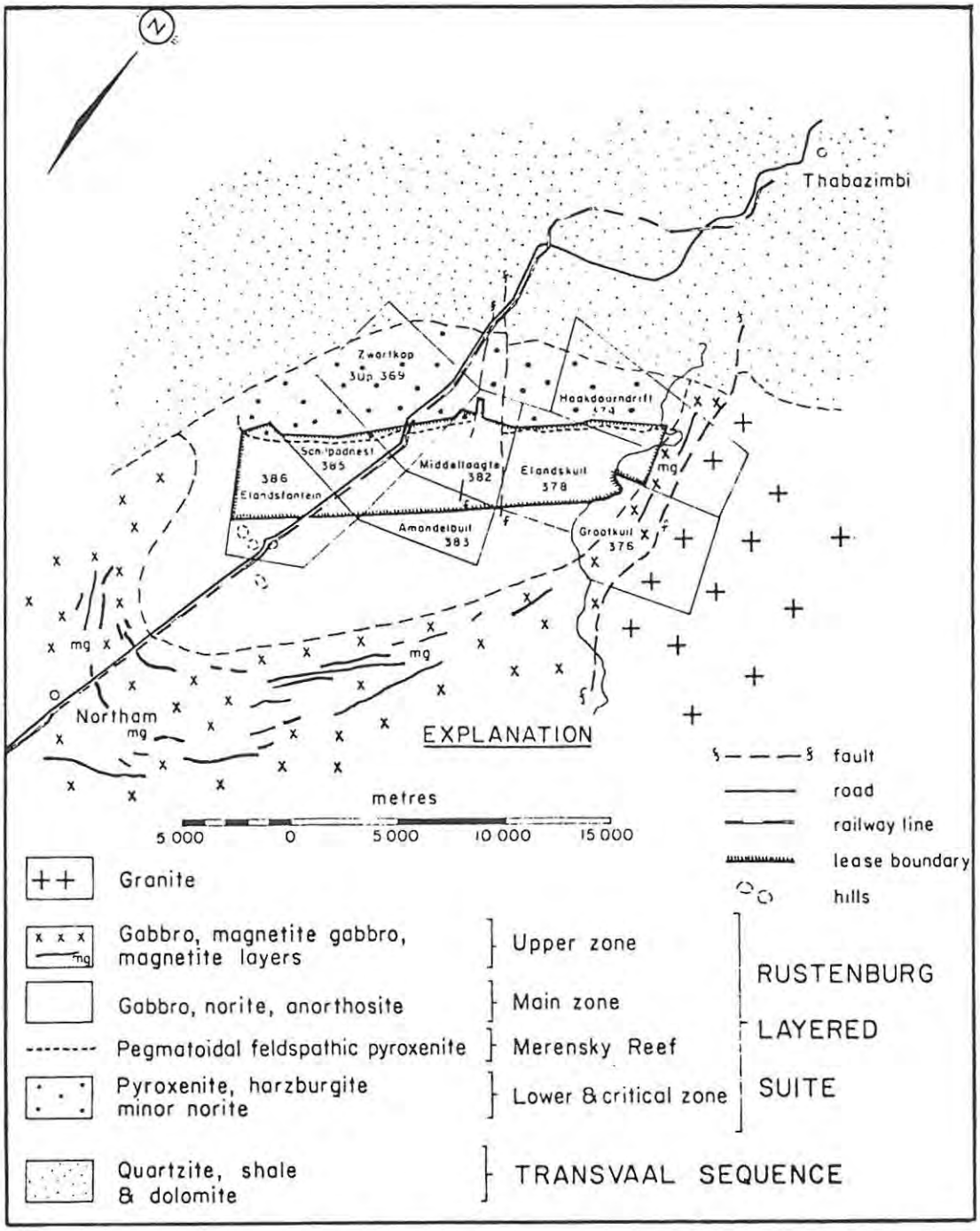

FIGURE 5.2 Main geological features of R.P.M. Amandelbult Section (from Viljoen et al. a, in press).

MINING OPERATIONS

After discovery of the Merensky Reef in the Lydenburg and Rustenburg sectors of the Bushveld Complex, the Reef was rapidly located in the northern sector of the western Bushveld Complex. In the Elandsfontein-Elandskuil sector (now part of the Amandelbult mine) Wagner (1929) reported that the Reef was delineated over a strike length of 16.5 km, although the only section of commercial interest in the 1920's and 30's was restricted to the farm Schilpadnest. Two boreholes here averaged 7.3 and 11.4 dwt/ton (probably total PGE + Au) over 30 inches in the Merensky pyroxenite. The Merensky Reef itself assayed at 42.5 dwt/tons over 18 inches. The Merensky upper chromitite layer assayed at from 15-59 dwt/tons over 0.5-3.5 inches, whereas the lower chromitite layer was relatively poor in PGE (Wagner, 1929). R.P.M. Amandelbult Section commenced mining in 1974 and by 1982 these operations extended over a strike length of 12 km. Amandelbult is essentially a platinum mine with minor PGE's, Au, Ni and Cu as by-products. At present the only orebody mined is the Merensky Reef.

5.2 THE LAYERED SEQUENCE BETWEEN THE UG-1 AND BASTARD REEF

The cumulates comprising the layered sequence of the Bushveld Complex define a generalised stratigraphic sequence which was reviewed briefly in Chapter 1. In the Amandelbult area iron-rich ultramafic pegmatite has been located from just above the LG-6 chromitite layer (in the lower critical zone) to magnetite seam number 6 (in the upper zone). Unfortunately, little detailed mapping has been possible in this area of the Bushveld Complex, outside of the stratigraphic interval between the UG-1 and the Bastard Reef. In this area this sequence has been discussed by Hall (1932), Wasserstein (1936), Coertze (1974) and Viljoen et al. (a, in press). The following section draws heavily on this latter publication. This discussion is compiled on a basis that adopts the concept of cyclic units, such that some differences with the terminology of Viljoen et al. are suggested. The sequence discussed here is based on that in the western section of Amandelbult (see fig. 5.3).

5.2.1 THE UG-1 CYCLIC UNIT

The base of this unit is marked by the UG-1 layer which is usually a single chromitite layer up to 1.5 m thick. In some cases, several layers or stringers of chromitite are "detached" from the bottom of the main layer.

These appear to diverge into the footwall mottled anorthosite, only to converge again to join the main layer. The lenses of anorthosite so formed, are usually speckled with numerous chromite grains. Below the UG-1 there is invariably a layer of mottled anorthosite up to 3 m wide, which contains elongated blebs and stringers of chromitite. These occur below the detached, diverging and converging chromitite layers described above. The intimate association of chromitite and anorthosite is a characteristic of the UG-1 chromitite layer throughout the Bushveld Complex. A layer of poilitic feldspathic orthopyroxenite, approximately 15-20 m thick overlies the UG-1 and is, in turn, overlain by the UG-2 chromitite layer.

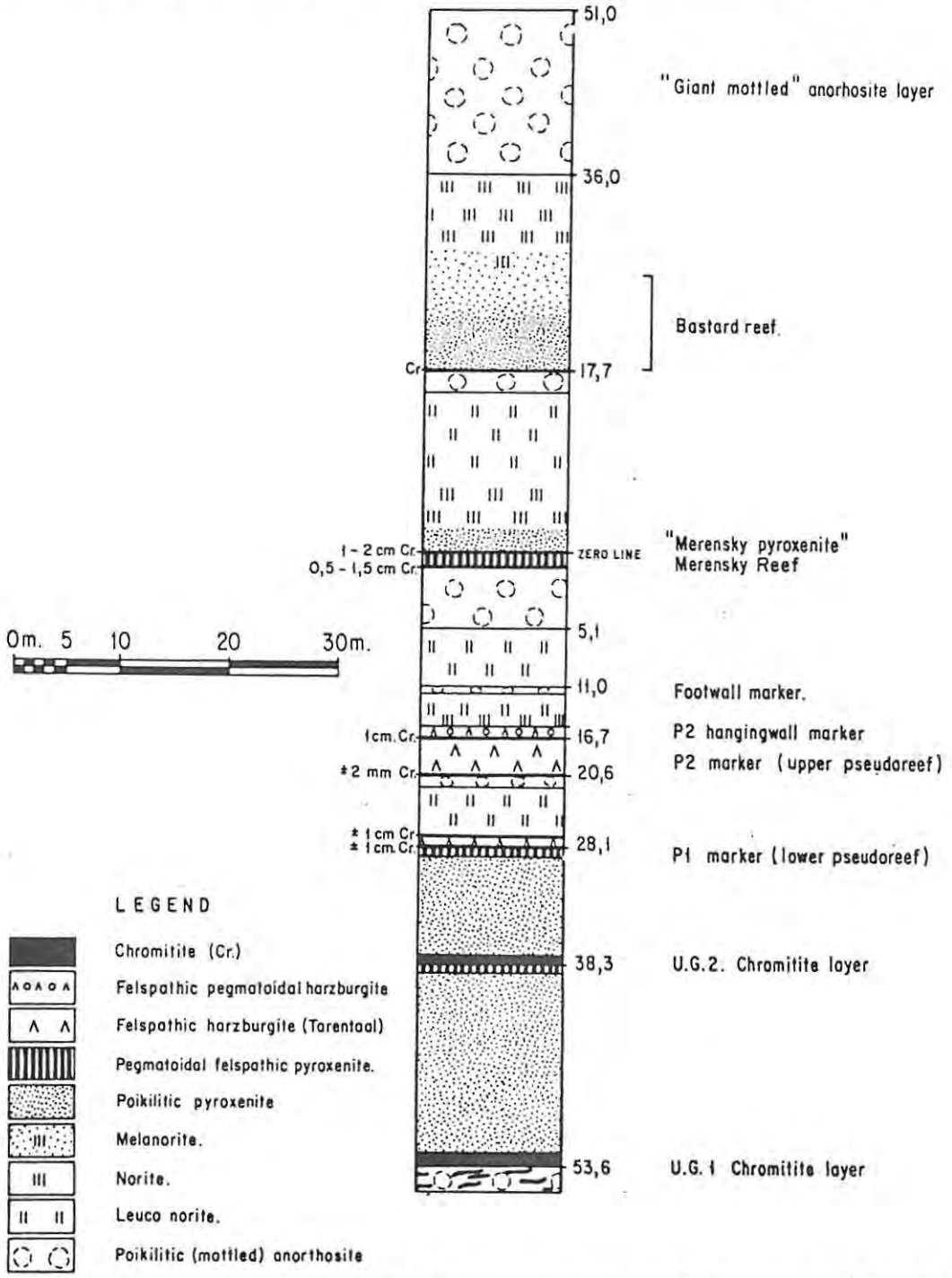

FIGURE 5.3 Schematic geological column of part of the upper critical zone in the western section of Amandelbult (from Viljoen et al. a, in press). Nomenclature of the marker horizons is that in use by geologists of R.P.M. - for nomenclature preferred by the author and subdivision of the cyclic units see Figure 6.1, and for details of the Pseudo macro unit see Figure 6.3.

5.2.2 THE UG-2 CYCLIC UNIT

The average thickness of the UG-2 chromitite layer, or stack of layers, is approximately 1-1.2 m. Typically the UG-2 is divided into a main layer (60-80 cm thick) and two or three "leader" layers, averaging 11 cm in thickness, which occur above the main layer. The chromitite is interlayered with a poikilitic feldspathic orthopyroxenite which normally contains lenses and stringers of chromitite. The chromitite layers themselves contain occasional spheroids of pyroxenite. The immediate footwall of the UG-2 is usually a pegmatoidal feldspathic orthopyroxenite (similar to the Merensky Reef in appearance), which varies in thickness from 0-70 cm. It is interesting to note that there is no apparent fractionation in the wide zone of orthopyroxenite below and above the UG-2 as is evidenced by the lack of mineralogical and textural variation. It is feasible to commence the UG-2 cyclic unit at either the chromitite layer itself or the underlying pegmatoidal layer. The UG-2 is overlain by roughly 10 m of poikilitic feldspathic orthopyroxenite. The chromitite of the UG-2 and its leader layers are economically important as they host significant PGE. The pegmatoidal pyroxenite contains some base-metal sulphides, but the precious metal content is generally low.

5.2.3 THE PSEUDO MACRO UNIT

The interval between the UG-2 and Footwall cyclic units at Amandelbult is referred to as the Pseudo macro unit. It shows considerable lateral variation and may comprise up to four separate cyclic units. In the western section of the mine (where most of this study is based) up to four separate harzburgitic layers may occur. These are described by Viljoen et al. (a) as a lower pseudoreef (colloquially known as the P1 marker), an upper pseudoreef (or P2 marker) which may comprise two separate layers and a harzburgite layer which occurs above the P2 at the base of the Footwall cyclic unit. These are redefined as follows (see figs.5.3, 6.1).

THE LOWER PSEUDO CYCLIC UNIT

This consists solely of a layer of pegmatoidal feldspathic orthopyroxenite (0.5 - 1.5 m thick), known as the lower pseudoreef. It comprises the lower part of the P1 marker of Viljoen et al. (a). The lower contact, with the UG-2 cyclic unit, is gradational over a few centimetres. This layer is interpreted as a separate cyclic unit. It resembles the Merensky Reef and contains subeconomic PGE mineralization.

THE UPPER PSEUDO CYCLIC UNIT A

Immediately overlying the lower pseudoreef is a thin (1 cm thick) chromitite layer above which is an irregular layer of feldspathic harzburgite (average thickness 0 - 50 cm), referred to here as the upper pseudoreef A (fig. 6.1). This in turn has a thin upper chromitite. Above this discontinous layer of harzburgite is a fine-grained mottled anorthosite, which in turn grades up into leuconorite and spotted anorthosite. The top of this cyclic unit is terminated by a layer of mottled anorthosite. These rocks form the Upper Pseudo cyclic unit A. In the definition of Viljoen et al. (a) the harzburgite in this cyclic unit is incorporated with the previous unit and forms the lower pseudoreef or P1 marker (fig. 5.3).

THE UPPER PSEUDO CYCLIC UNIT(S) B AND C

The Upper Pseudo cyclic unit A is sharply overlain by a harzburgite layer which is referred to here as the upper pseudoreef B. This is overlain by felsic cumulates, which in turn are overlain by a third harzburgite layer referred to here as the upper pseudoreef C (fig. 6.1). The Upper Pseudo cyclic unit B comprises the upper pseudoreef B and the overlying felsic cumulates, and the Upper Pseudo cyclic unit C consists solely of the upper pseudoreef C. In the definition of Viljoen et al.(a) the upper pseudoreef or P2 marker consists of both of these harzburgite layers (fig. 5.3). The layer of felsic cumulates between these two harzburgite layers is colloquially known as the P2 middling.

In the western part of the mine the upper pseudoreef B is approximately 3 m thick and usually has a thin chromitite layer at its base. The upper contact of the harzburgite is sharp, but undulatory ("rolling" in local terminology) with an average wavelength of 10 cm and a maximum wave amplitude of 6 - 7 cm (average 3 - 4 cm; see fig. 7.8A).

The P2 middling is a composite layer of felsic cumulates, 1 - 1.2 m thick. The composition of this layer changes along strike. In the western section of the mine it consists of a basal layer of mottled anorthosite (or leucotroctolite - see section 5.4), roughly 20 cm thick, which is sharply overlain by a layer of leuconorite. This is transitional up into a spotted anorthosite. A thin layer of pure anorthosite occurs at the lower and upper contacts. This separates the felsic cumulates from the adjacent harzburgite layers, the contacts of which are strongly dimpled (fig. 7.8A). A thin chromitite stringer occurs at both of these contacts.

The upper pseudoreef C is approximately 1 m thick and has a thin basal chromitite stringer (1 mm thick). The P2 middling and the upper harzburgite

layer wedge out eastwards and only one harzburgite layer persists. Whether this represents only unit B or units B and C combined is not known, as the entire Pseudo macro unit thins along strike to the east (fig. 6.1).

5.2.4 THE FOOTWALL CYCLIC UNIT

The Pseudo macro unit is overlain by the Footwall cyclic unit, so-called because it forms the footwall to the Merensky Reef. It commences with a chromitite layer (10 mm thick) overlain by a layer of coarse-grained or pegmatoidal feldspathic harzburgite (10 - 15 mm thick). This harzburgite layer is transitional upwards into feldspathic-olivine orthopyroxenite and melanorite, which form a layer approximately 2 m thick.

Approximately 70 cm above the top contact of the upper pseudoreef C is a thin, but remarkably persistent, layer of mottled anorthosite (10 - 15 mm thick). It is overlain by melanorite and has a footwall of orthopyroxenite. This thin anorthosite, known as the P2 hangingwall marker, is very consistent and is always present where the hanging wall of the P2 has not been disrupted by the formation of potholes.

The melanorite above the P2 hangingwall marker is gradational up into norite and leuconorite. Within the leuconorite is a well defined layer of mottled anorthosite, roughly 40 - 50 cm thick, known as the footwall marker. It occurs approximately 8 m above the upper pseudoreef C and 10-11 m below the Merensky Reef. The contacts of the footwall marker are usually gradational, consisting of approximately 10 cm of interlayered leuconorite and anorthosite. The leuconorite above the footwall marker extends vertically for 3-5 m. It is sharply overlain by a layer of mottled anorthosite (5 - 6 m thick), known as the Merensky footwall anorthosite.

5.2.5 THE MERENSKY CYCLIC UNIT

The Merensky Reef occurs at the base of the Merensky cyclic unit. The Reef is sandwiched between two thin chromitite layers, the Merensky lower and upper chromitites. The contact between the lower chromitite and the underlying mottled anorthosite is undulating and sharp, whereas the contact with the Reef is gradational. The lower chromitite is loosely packed and often consists of anhedral grains (a distinctive feature). The Merensky Reef at Amandelbult is typically about 1 m thick, although it may locally be absent (e.g., where the section is "potholed" and in the eastern section of the mine; see fig. 6.1). It consists of a pegmatoidal, (exceptionally coarse-grained) feldspathic-olivine orthopyroxenite or felds-

pathic orthopyroxenite. The Reef is sharply overlain by the upper chromitite layer. This forms a prominent layer usually 15 - 20 mm thick, consisting of euhedral, well packed chromite grains.

The Merensky upper chromitite layer is overlain by a poikilitic feldspathic orthopyroxenite, known as the Merensky (hanging-wall) pyroxenite. It is gradational upwards into melanorite and leuconorite. The top of the Merensky cyclic unit is marked by a layer of mottled anorthosite (2 - 3 m thick) that forms one of the most consistent horizons in the upper critical zone. The distance from the top of the Merensky pegmatoid to the top of the anorthosite is approximately 14 m at Amandelbult.

Vermaak and Hendriks (1976) defined the Merensky Reef as "comprising a mineralised pegmatitic, feldspathic pyroxenite,bounded at the top and bottom by thin chromitite stringers". Because economic sulphide mineralisation is not restricted to the pegmatoidal part of the Reef, Von Gruenewaldt (1979) prefers to define the Merensky Reef as "the basal, pyroxenitic portion of the Merensky cyclic unit; this includes the porphyritic pyroxenite, the pegmatitic pyroxenite and any chromitite stringers that may be developed". The definition of Vermaak and Hendriks is preferred in this study.

5.2.6 THE BASTARD CYCLIC UNIT

The Bastard cyclic unit is similar to the Merensky cyclic unit but is much thicker (approximately 32 m at Amandelbult; fig. 5.3). No pegmatoidal pyroxenite is associated with this cyclic unit and a chromitite layer is not always present at the base. The base of the unit is marked by a poikilitic feldspathic orthopyroxenite, similar to the Merensky hanging-wall pyroxenite. This is abruptly terminated by a layer of much finer-grained orthopyroxenite, which grades upwards into norite and leuconorite. The contact between the two textural types of pyroxenite is sharp although it is not marked by a chromitite. The layer of poikilitic pyroxenite at the base of this cycle is referred to as the Bastard reef. Minor amounts of base-metal sulphides may occur in the Bastard reef, usually concentrated near the base of the poikilitic pyroxenite and also immediately below the contact with the overlying fine-grained pyroxenite. The Bastard cyclic unit and the critical zone are terminated by a 15 m thick layer of mottled anorthosite, colloquially known as the "giant mottled".

5.3 LATERAL VARIATION AT AMANDELBULT

The following has been precised from Viljeon et al. (a, in press). "A number of regional stratigraphic variations are evident along the strike length of Amandelbult Section. Some of the major variations across approximately 20 km of strike are depicted in Figure 6.1. One of the most striking regional variations is the change of character of the Upper Pseudo cyclic units B and C from southwest to northeast. As noted earlier, a thin, composite feldspathic unit (the P2 middling) is developed within the Upper Pseudo cyclic unit B in the southwestern part of the mine. It is best developed on Elansdsfontein and the western part of Schilpadnest. The feldspathic layer changes into anorthosite on the central portion of Schilpadsnest and dies out completely eastwards.

Within the northeastern portion of the area the succession referred to here as the Pseudo Macro unit becomes somewhat problematic. In this area a noritic sequence occurs below the footwall marker and grades down into pyroxenitic norite as the lower pseudoreef is approached. The pyroxenitic norite contains "harzburgite schlieren" or irregular stringers of olivine norite and feldspathic olivine pyroxenite, which are usually grouped into one of two layers of "harzburgite" which have gradational contacts. In some localities the lowermost harzburgite layer overlies a mottled anorthosite; the sequence then bears some resemblance to the "normal" upper pseudoreef (fig. 6.1).

In the eastern part of the mine a thin chromitite layer (roughly 10 mm thick) has been intersected approximately 17-19 m below the Merensky Reef, which is where the upper pseudoreef would have been expected. The footwall of this chromitite layer is either anorthosite or mottled anorthosite varying in width from 5 mm to about 100 mm while the hangingwall is a norite. This chromitite layer is aptly known as the "lone chrome seam" (fig. 6.1).

Another striking feature is a pronounced apparent arching and thinning of the footwall rocks in the central section of the mine. In this region, the distance between the Merensky Reef and the lower pseudoreef is considerably reduced, from 25 m compared to 37 m in the thickest succession. The effect of the apparent arching appears to die out as the Merensky Reef is approached. It must, of course, be borne in mind that the arching is only a visual effect created by the fact that the bottom of the Merensky Reef was taken as the datum line.

Towards the north-eastern boundary of the property, there is a slight but clear thinning of the hangingwall sequence of the Reef, while the

thickness of the footwall rocks increases. Towards the south-west the whole succession thins and this might be related to a sudden swing in strike towards the footwall i.e. to the northwest. This thinning of the succession may be related to an upwarping of the Transvaal floor rocks prior to deposition of the Bushveld rocks in the northern gap area (Viljoen & Feuchtwanger, 1977). The strata in this area are highly disturbed with undulations, faulting and numerous pegmatite and magnetite veins. Generally, there is a high degree of serpentinisation of both the olivines and pyroxenes. In some cases, there is virtually complete alteration of the Merensky Reef in this specific area.

Apart from the upper pseudoreef changing character towards the north-east, another peculiar feature encountered in boreholes on the farm Haakdoorndrift, is the apparent duplication of the Merensky Reef i.e. two pegmatoidal layers exist. The lower pseudoreef also disappears in this succession and is replaced by large bodies of mottled anorthosite and norite. The UG-2 chromitite layer, however, remains the same and maintains the same position at approximately 64 m below the Merensky Reef".

5.4 PETROGRAPHY AND CHEMISTRY

Detailed petrographic and chemical studies of specific cumulates from the upper critical zone at Amandelbult have been completed. Schematic maps and sketch sections of the sample sites are included in Appendices 1 and 2. Sample locations are indicated on a stratigraphic section compiled by the author for the 30W - 25W area in the western section of Amandelbult (fig. 5.5). Unless specifically indicated these samples are typical of the cumulate sequence in this area and have not undergone postcumulus effects related to the iron-rich ultramafic pegmatite suite. Pothole sequences have also been avoided. These studies are restricted to the interval beteween the lower pseudoreef and the Merensky hanging-wall pyroxenite.

5.4.1 PETROGRAPHY

HARZBURGITE

In all of the "harzburgite" cumulates in the upper critical zone at Amandelbult intercumulus plagioclase represents over 10 modal percent, such that in accordance with other Bushveld workers the prefix "feldspathic" is used. If the olivine to orthopyroxene ratio is less than 60:40 these rocks may be described as feldspathic-olivine orthopyroxenites rather than feldspathic harzburgites. The prefix "pegmatoidal" is applicable to the

exceptionally coarse-grained varieties (such as the Merensky Reef).

Jackson (1961), who worked on the ultramafic succession in the Stillwater Complex, makes an important distinction between granular and poikilitic harzburgites. This classification is based on the textural relationships between olivine and orthopyroxene and ignores the presence of minor intercumulus phases. In a poikilitic harzburgite olivine and chromite are the only cumulus (or primocryst) phases; orthopyroxene occurs as oikocrysts or by reaction replacement of cumulus olivine. Granular harzburgite contains cumulus olivine, chromite and orthopyroxene; it is texturally comparable with orthopyroxenite, differing only by the relative percentage of olivine and orthopyroxene. Chromite may also be less abundant in granular harzburgite. The distinction between granular and poikilitic harzburgites has important genetic implications.

The upper pseudoreef layers B and C at Amandelbult are coarse-to medium-grained feldspathic harzburgites. They have a distinctive spotted appearance (which resembles the markings on a guineafowl) and are comparable with the "tarentaal" at Union Section. The upper pseudoreef layer A is coarser-grained, but otherwise similar. All the harzburgites in the Pseudo macro unit at Amandelbult may be described as poikilitic varieties, using the scheme of Jackson (1961). The olivine-bearing cumulate at the base of the Footwall cyclic unit is similar, athough it may have a pegmatoidal texture; it is transitional up into granular olivine orthopyroxenite.

The tarentaal is typically composed of cumulus olivine (60-70 modal per cent) and chromite (0.5-1.5 modal percent) with intercumulus orthopyroxene (10-25 modal percent) and plagioclase (10-15 modal percent). Accessory phases include biotite (fairly common), amphibole and clinopyroxene. Much of the olivine is serpentinised and secondary magnetite is abundant. Olivine occurs as large (5-10 mm) anhedral grains and as small (usually less than 1 mm) euhedral to subhedral grains. The small grains are enclosed in plagioclase. The large grains embay each other and define a xenomorphic texture. This texture may be attributed to in-situ (secondary ?) enlargement, a process arrested by the crystallization of plagioclase (Jackson, 1961). Orthopyroxene occurs as large oikocrysts (up to 30 mm) which enclose olivine and as small, euhedral to subhedral grains enclosed in plagioclase. Olivine enclosed within the orthopyroxene oikocrysts is severely corroded and may occur as relicts. Reaction replacement of olivine is inferred. This process results in a xenomorphic texture. Orthopyroxene evidently nucleated after crystallization of olivine, as an intercumulus phase, and developed as large anhedral oikocrysts which reacted with the early-formed olivine. The onset of plagioclase crystallization in the

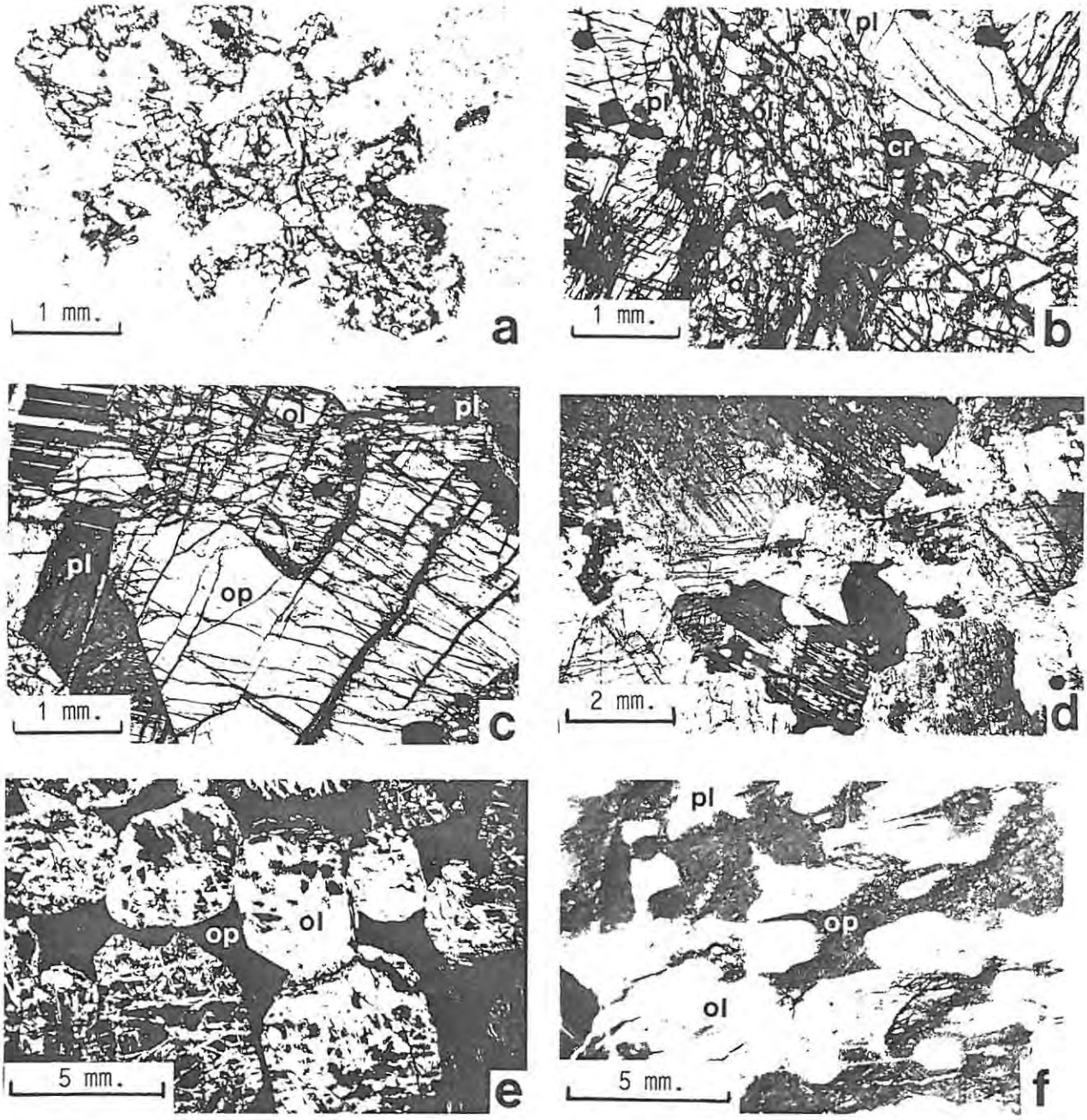

FIGURE 5.4 PHOTOMICROGRAPHS OF OLIVINE-BEARING CUMULATES

a. Olivine mottle (oikocryst) interstitial to, and enclosing, cumulus plagioclase. Plagioclase grains not enclosed by olivine consist of polygonal grains and are well annealed. Leucotroctolite, P2 middling (sample A-7). b. Sharp contacts between subhedral grains of cumulus olivine and orthopyroxene and anhedral grains of intercumulus plagioclase. Where plagioclase is absent reaction replacement of olivine by orthopyroxene results in a xenomorphic texture. Chromite occurs along the margins of olivine grains and in intragranular sites in orthopyroxene and plagioclase. Granular feldspathic olivine orthopyroxenite, UG-2 hangingwall (sample U-31). c. Subhedral orthopyroxene grain moulded around euhedral olivine, both enclosed by intercumulus plagioclase. Latter has arrested reaction between olivine and orthopyroxene (as sample in "b"). d. Orthopyroxene exhibiting a xenomorphic texture (as sample "b"; "b", "c" and "d" are all from the same thin section). e. Cumulus olivine (note serpentinisation) in a matrix of intercumulus orthopyroxene. Poikilitic feldspathic harzburgite, upper pseudoreef (sample U-26). f. Typical texture of the tarentaal - cumulus olivine poikilitically enclosed by large, optically continuous grains of orthopyroxene, with minor intercumulus plagioclase. Olivine adjacent to plagioclase is subhedral; that adjacent to orthopyroxene is anhedral, due to reaction replacement (sample A-8).

("a" in plane polarised transmitted light, "b", "c", "d" and "e" with crossed polarisers, and "f" in reflected light; ol - olivine; op - orthopyroxene; pl - plagioclase; cr - chromite)

remaining intercumulus sites resulted in the trapping of small euhedral orthopyroxene grains. Growth of the large orthopyroxene oikocrysts occurred concurrently with the crystallization of plagioclase and essentially after enlargement of the cumulus olivines (fig. 5.4E, F).

THE MERENSKY REEF

The Merensky Reef at Amandelbult comprises a pegmatoidal feldspathic orthopyroxenite in which olivine occurs locally as an accessory constitutent (Viljoen et al.,a, in press). The base of the Reef may be olivine-rich (compare analyses A-2 to A-5, Table 6.2) and it is then described as a pegmatoidal feldspathic olivine orthopyroxenite or feldspathic harzburgite.

Both olivine and orthopyroxene are cumulus phases in the Merensky Reef; it is thus a granular olivine orthopyroxenite or harzburgite, even though plagioclase demonstrates a poikilitic relationship to both olivine and orthopyroxene. Olivine and orthopyroxene occur as large, euhedral grains, or chadacrysts, (grains with diameters of over 10 cm are common), which are enclosed by exceptionally anhedral oikocrysts of plagioclase. Occasionally, aggregates of orthopyroxene display a xenomorphic, or mosaic texture. Reaction replacement of olivine by orthopyroxene has not been observed. Chromite occurs in both intra- and intergranular sites. Clinopyroxene (often as large oikocrysts which enclose the early-formed minerals, including plagioclase), mica and ampibole are common accessory phases. Rare accessory phases include zircon and quartz. Graphite may locally be an important constituent (see Kennedy, 1983). The distribution of base-metal sulphides and PGM is discussed in Chapter 6. The pegmatoidal texture exhibited by the Merensky Reef at Amandelbult does not permit the determination of meaningful modal analyses, but the CIPW norm provides a useful mineralogical guide (see Table 6.2 and Appendix 6).

The Merensky Reef is characterised by its pegmatoidal nature, the presence of olivine, the unusual concentrations of incompatible and volatile elements, as indicated by the abundance of accessory phases such as mica and amphibole and exotic phases which include zircon and graphite, and the concentration of precious and base-metals.

The Merensky Reef and the upper chromitite layer are overlain by a medium-grained, poikilitic orthopyroxenite (the Merensky hangingwall pyroxenite). It consists typically of 80-85 modal percent cumulus orthopyroxenite and 15-20 modal percent intercumulus plagioclase. Chromite is a ubiquitous accessory constituent and base-metal sulphides occur in the lower part. Olivine has not been observed, or reported in the literature, from this unit. Further distinguishing factors, compared to the Merensky

Reef, are the non-pegmatoidal texture and the paucity of exotic accessory phases.

ORTHOPYROXENE-PLAGIOCLASE CUMULATES

These two minerals are the dominant constituents of the upper critical zone. Plagioclase usually represents from 15 to 95 modal percent, and few cumulates in this sequence occur outside of this range. However, using the cumulus terminology, orthopyroxenites (or bronzitites) are defined as consisting of cumulus orthopyroxene (usually 80-90 modal percent) and intercumulus plagioclase (usually 10-20 modal percent). If both orthopyroxene and plagioclase are cumulus phases the description melanorite (over 70 modal percent orthopyroxene), norite (30-70 modal percent orthopyroxene), leuconorite (10-30 modal percent orthopyroxene) or spotted anorthosite (less than 10 modal percent orthopyroxene) is applicable. The petrography of orthopyroxene - plagioclase cumulates in the upper critical zone has been discussed by a number of authors (inter alia Wager & Brown, 1967; Van Zyl, 1970; Cameron, 1982; de Klerk, 1982; Kruger, 1984).

ANORTHOSITES

Spotted anorthosite, in which both orthopyroxene and plagioclase are cumulus phases, may be considered as the felsic end-member resulting from cotectic crystallization of orthopyroxene and plagioclase. A second variety of anorthosite is recognized in the layered sequence of the Bushveld Complex; this is traditionally referred to as mottled anorthosite (see Wager & Brown, 1967). In a mottled anorthosite plagioclase (which usually, but not always represents over 90 modal percent) is the only demonstrably cumulus phase. Orthopyroxene and clinopyroxene, or rarely olivine, occur interstitially and form coarse mottles. These ferro-magnesian minerals, although they occur intersitially are not neccessarily intercumulus phases as temperature considerations suggest that it is unlikely that they have crystallized after plagioclase from an intercumulus liquid. The formation of mottled anorthosites and their role within cyclic units is not fully understood (see Chapter 6).

In the sequence studied here mottled anorthosites occur at the top of most of the cyclic units. They are also observed directly overlying harzburgitic cumulates and occur as thin, well-defined layers within norites or leuconorites (fig. 5.3). A mottled anorthosite, or leucotroctolite, has been recognized in the P2 middling in which the "mottles" consist of olivine (fig. 5.4A). Pyroxene has not been observed in this rock. Olivine occurs as rather poorly defined mottles and forms small, optically continuous,

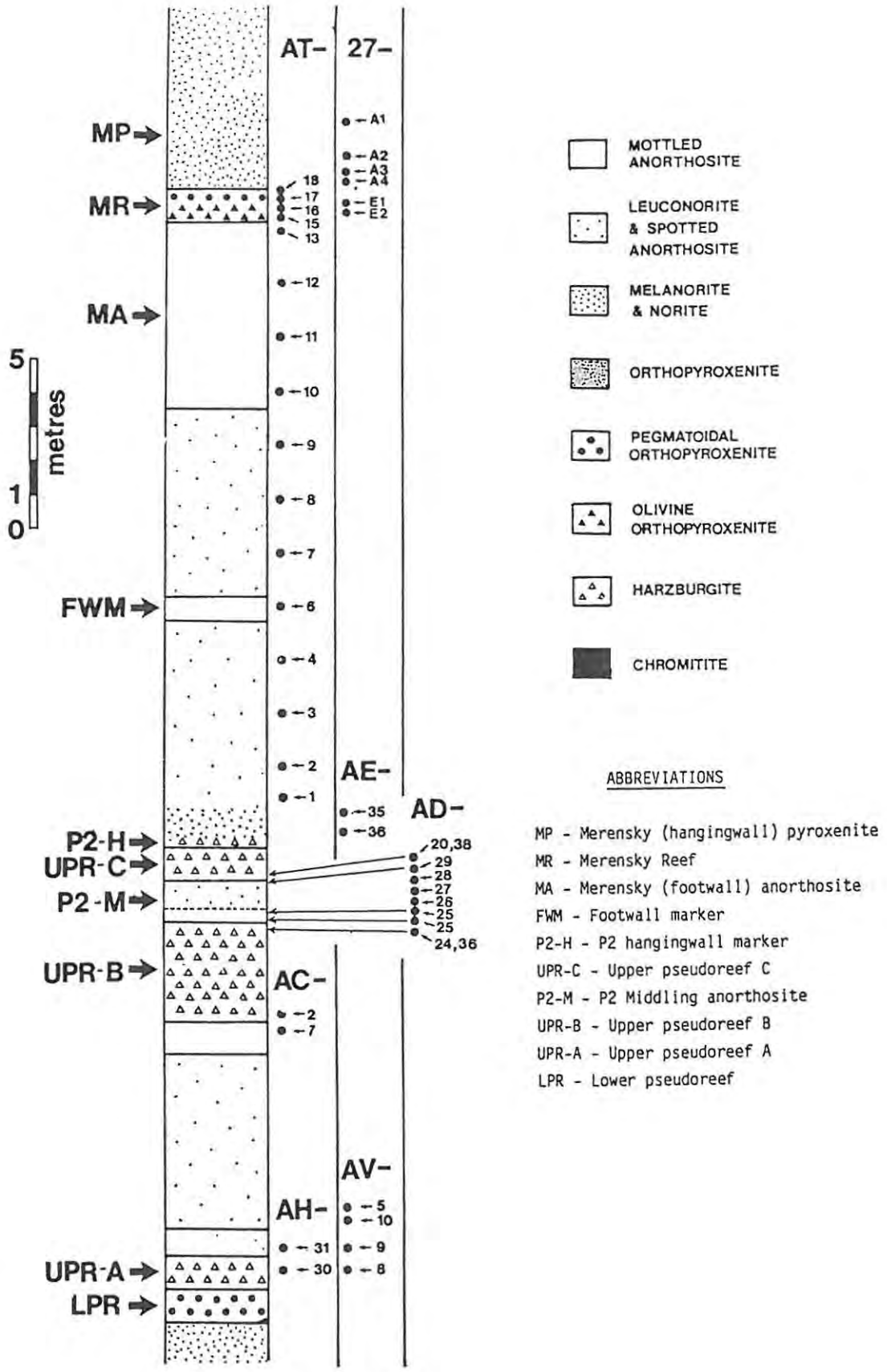

FIGURE 5.4 Location of whole-rock samples of cumulates analysed in this study.

For specific sample locations and details of geographic location of various sample groups see Appendices 1 and 4. For details of cyclic units see Figures 6.1 and 6.3. Specific samples which are discussed in detail in Chapter 6 have been re-labelled (for ease of reference). These, are as follows (see also Figure 6.3) :

A-1 (27-A1); A-2 (AT-18); A-3 (AT-17); A-4 (AT-16); A-5 (AT-15); A-6 (AD-25B); A-7 (AD-36); A-8 (AD-24); A-9 (AV-8); A-10 (AH-30).

oikocryts which enclose euhedral grains of plagioclase. Adjacent to the mottles, medium-grained, typically well-annealed, plagioclase is observed. The CIPW norm simulates the mineralogy of this unusual cumulate (analysis A-7, Table 6.2).

In this succession a third type of anorthosite may be recognized : this consists of pure plagioclase. It occurs as poorly defined layers at contacts between harzburgitic and felsic (usually spotted or mottled anorthosite) cumulates (e.g., in the P2 middling - see fig.7.8A). It forms a monomineralic assemblage and is typically well-annealed.

5.4.2 CHEMISTRY

Whole-rock analyses of a suite of samples from this sequence have been completed. Sample positions are indicated on Figure 5.5 - these samples provide a detailed sequence through the Pseudo, Footwall and part of the Merensky cyclic units at Amandelbult. These data are presented in Appendix 5. Electron microprobe analyses of cumulate-hosted olivine, pyroxene, chromite, plagioclase and base-metal sulphide have also been completed on some of these samples. These results are discussed in conjunction with the mineralogy of iron-rich ultramafic pegmatite and data are presented with the relevant text, or in Appendices 7 to 11. In addition, selected results are modelled in relationship to the formation of these cumulates (Chapter 6).

CHAPTER 6 THE RELATIONSHIP BETWEEN OLIVINE CUMULATES, MINERALIZATION AND CYCLIC UNITS IN THE UPPER CRITICAL ZONE

Data from an electron microprobe study of cumulus olivine in the upper critical zone at R.P.M Amandelbult and Union Sections are discussed in conjunction with some whole-rock analyses. The major platiniferous layers, the UG-2 and Merensky Reefs, occur within this stratigraphic interval and accordingly these data may be significant in relation to the base-metal sulphide and platinum-group element mineralization. Samples from Amandelbult were analysed by the author (see Chapter 6), and samples from Union Section were provided by W.J. de Klerk (see de Klerk, 1982 ; Scoon & de Klerk, in press).

6.1 INTRODUCTION

The appearance of plagioclase as a major cumulus phase is a significant event in the evolution of the layered sequence of the Bushveld Complex. Below this level, in the lower and lower critical zones, magnesian olivine, orthopyroxene, and chromite are the dominant cumulus minerals, whereas in the upper critical and main zones pyroxene and plagioclase are the principal phases. In the central sector of the eastern Bushveld Complex, Cameron (1982) calculates that the F-M units of the upper critical zone below the UG-1 chromitite layer consist of 47.1 modal percent orthopyroxene and 45.1 modal percent plagioclase. Cumulus olivine is rarely observed in the upper critical zone below the UG-1 chromitite layer, but it may represent a significant component of the upper critical zone above this position. In the northern sector of the western Bushveld Complex, at R.P.M. Amandelbult and Union Sections, cumulus olivine is unusually abundant in the upper critical zone between the UG-2 chromitite layer and the Merensky pyroxenite. It occurs as a major component of ultramafic layers (harzburgites and olivine orthopyroxenites) in cyclic units, which include the UG-2 chromitite layer, the pseudoreefs, and the Merensky Reef. The reappearance of magnesian olivine as a cumulus phase, after the crystallization of a thick sequence of orthopyroxene-plagioclase cumulates must surely indicate that the chamber was replenished with new influxes of magma.

The regional geology and stratigraphic sequence at Amandelbult were discussed in the previous chapter (see fig. 5.1). For details of the upper critical zone sequence at Union Section the reader is referred to de Klerk (1982).

6.2 CYCLIC UNITS

A cyclic unit may be descibed as a sequence of, usually sharply defined, petrologic layers in which the cumulus mineral sequence can be identified as the fractional crystallization order of the magma (Jackson, 1961, 1970; Irvine, 1982). Cryptic mineralogical variation often, but not always, occurs within a cyclic unit. Cyclic units are almost invariably truncated, and Irvine (1982) observes that "almost by definition cyclic units are inherently incomplete". Cyclic units may develop due to processes operating wholly within a magma chamber, e.g., due to classic cumulus processes as described by Wager et al. (1960), or due to bottom crystallization as envisaged by McBirney and Noyes (1979)), or they may be related to replenishment of the chamber by influxes of fresh magma (inter alia Brown, 1956; Irvine & Smith, 1967; Irvine, 1982).

A minimum of seven cyclic units is recognized in the mine workings in the upper critical zone above the UG-1 chromitite layer at Amandelbult and Union Sections. These comprise the UG-1, UG-2, Lower Pseudo, Upper Pseudo, Footwall, Merensky and Bastard units (fig. 6.1). The UG-1, UG-2, Merensky and Bastard cyclic units are well known and may be correlated throughout the western sector of the Bushveld Complex (Feringa, 1959; Wager & Brown, 1968; Van Zyl, 1970; Vermaak, 1976b). Vermaak describes the Merensky and Bastard as the two most complete cyclic units within the layered sequence of the Bushveld Complex. The Footwall and Pseudo cyclic units, which are difficult to correlate with their equivalents in the Rustenburg area, show considerable lateral variation. At Amandelbult the interval between the UG-2 and Footwall cyclic units (described as the Pseudo macro unit in this study) is unusually complicated and and may comprise up to four cyclic units (Lower Pseudo and Upper Pseudo, A, B, and C; see figs. 6.1, 6.3).

All the cyclic units described here, with the exception of the Lower Pseudo unit, commence with a basal chromitite layer. Thin chromitites, some of which may be reaction chromites (see Lee et al., 1983) also occur within the lower parts of cyclic units and do not perforce imply commencement of a new cycle. In the upper critical zone the sequence of crystallization of cumulus phases, from the base of a cyclic unit upwards, is as follows: chromite - olivine - orthopyroxene - plagioclase. In a reasonably complete cyclic unit the following sequence of rock types may be observed with increasing height : chromitite, harzburgite, olivine-orthopyroxenite, orthopyroxenite, melanorite, norite, leuconorite, and anorthosite. It is significant that in these cyclic units melanorite and norite are rare; orthopyroxenite may be transitional up into leuconorite over a few metres.

The Footwall, Merensky, and Bastard cyclic units are all terminated by anorthosite, whereas some of the other cyclic units were beheaded before plagioclase accumulated. It is possible that in some of these cyclic units olivine was a cumulus phase before chromite (e.g., as in the Stillwater Complex; see Jackson, 1970), such that, for example, the UG-2 cyclic unit would commence at the base of the pegmatoidal layer below the chromitite layer.

The formation of mottled anorthosites and their role within cyclic units is not fully understood (see Chapter 5). For example, Vermaak (1976b) and Eales (in press) have speculated that plagioclase may float above a new, denser input of magma such that a mottled anorthosite may consist of plagioclase originating from more than one cyclic unit. It is thus inappropriate to establish new cyclic units above the position of each mottled anorthosite, although it is significant that many of the cyclic units at this stratigraphic level are in fact terminated by anorthosites.

6.3 CORRELATION BETWEEN R.P.M. AMANDELBULT AND UNION SECTIONS

The UG-1, UG-2, Merensky and Bastard cyclic units are laterally persistant and may be correlated throughout the western Bushveld Complex. Local petrologic variation occurs in specific layers but generally these units are similar at Amandelbult and Union Sections. The sequence at Union Section is relatively rich in olivine, which is a significant component of the Merensky Reef and the pyroxenitic layer above the UG-2 chromitite layer. The Merensky Reef at Union Section has been described by Van Zyl (1970), de Klerk (1982) and Viljoen et al. (b, in press). It comprises a feldspathic harzburgite or olivine orthopyroxenite. However, major differences between Amandelbult and Union Section do occur in the Pseudo and Footwall cyclic units (fig. 6.1).

At Union Section the pseudoreef is divided into two units which are separated by a chromitite layer that is 1 cm thick. The Lower Pseudo cyclic unit consists solely of the lower pseudoreef, a pegmatoidal, feldspathic, olivine orthopyroxenite. The Upper Pseudo cyclic unit consists of a basal chromitite layer and the upper pseudoreef. The latter is a coarse- to medium-grained feldspathic harzburgite, colloquially known as the "tarentaal". The Lower Pseudo cyclic unit is correlated with the lower pseudoreef at Amandelbult, although olivine is absent in this unit at Amandelbult (see p.79). The tarentaal at Union Section is correlated with the harzburgite layers A, B and C in the Upper Pseudo cyclic unit at Amandelbult (see p.80). The felsic cumulates in the Pseudo macro unit at

Amandelbult are not present at Union Section, where the Upper Pseudo cyclic unit consists of only two layers, a chromitite and harzburgite.

The Upper Pseudo cyclic unit at Union Section is overlain by a chromitite layer, 1 cm thick, and a layer of pegmatoidal feldspathic harzburgite (the "Pseudo Marker"), 20 cm thick, which mark the base of the Footwall cyclic unit. The pegmatoidal harzburgite is transitional up into medium-grained harzburgite and melanorite. This in turn is transitional up into a sequence of leuconorites and spotted anorthosites. It is terminated by a well defined layer of mottled anorthosite (the footwall to the Merensky Reef). Within the melanorite, 0.5 m above the basal chromitite, is a persistent layer, 1 to 2 cm thick, of anorthosite (the "Pothole Marker"). It may be correlated with the P2 hangingwall marker at Amandelbult (see p.81).

Lateral variation within discrete layers and composite cyclic units is particularly prevalent at Amandelbult (see p.83). At Union Section the thickness of certain layers changes along strike, but major stratigraphic variation does not occur. Thinning of layers along strike and the pinching out of specific layers are obviously of direct genetic relevance. For example, Vermaak (1976b) discusses lateral variation within cyclic units below the Merensky Reef in the western Bushveld Complex and he suggests that the Merensky lower chromitite unconformably overlies the footwall mottled anorthosite. Kruger and Marsh (1982, 1983), who present convincing evidence that the chamber has been replenished by a major new influx of magma at this position, suggest that this unconformity is related to resorption of the cumulate pile, immediately below the crystal-liquid interface. At Amandelbult lateral variation along strike is related almost exclusively to the ultramafic layers at the base of cyclic units. This is particularly applicable to the thin harzburgitic layers within the Pseudo macro unit, whereas, in contrast, delicately layered felsic marker horizons are laterally persistent.

Another feature of many of the ultramafic layers is that they display dimpled contacts. At Amandelbult the footwall contact of the Merensky Reef is dimpled as are the lower and upper contacts of most of the harzburgite layers within the Pseudo macro unit (fig. 7.8A). Dimpled contacts suggest that some resorption of the cumulate pile has occurred. Most of these dimpled contacts occur where ultramafic and anorthositic layers are in contact. Resorption of an anorthositic cumulate in response to a new input of fresh, relatively hot magma is acceptable, but dimpled upper contacts of ultramafic layers are less readily explained.

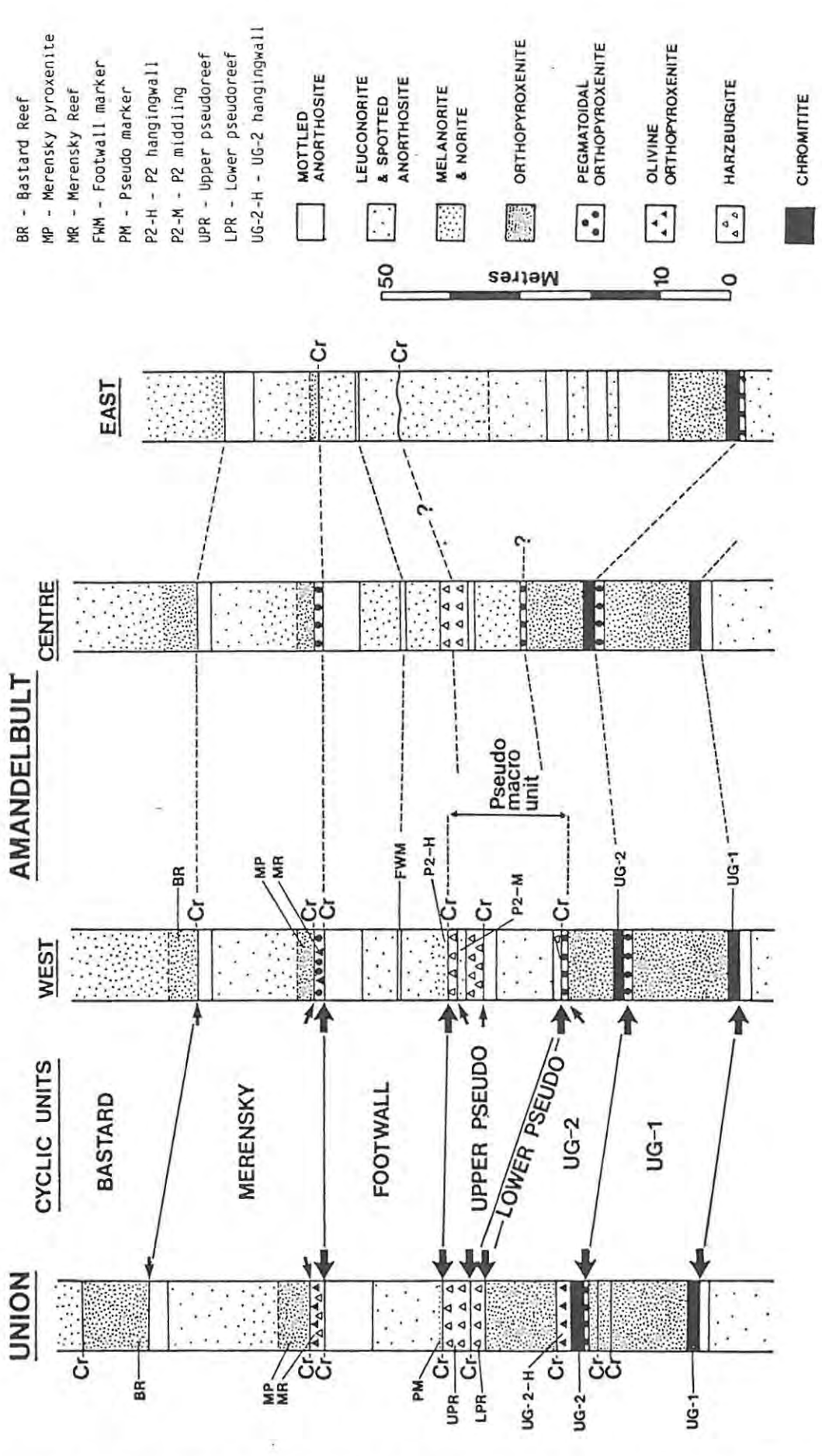

FIGURE 6.1 Geologic columns of part of the upper critical zone illustrating the lateral variation at Amandelbult and correlation between R.P.M. Amandelbult and Union Sections (partly after de Klerk, 1982 and Viljoen et al. a, in press; section for Amandelbult west compiled by the author, specifically for 5 level / 27W section). Arrows (large = probable; small = possible) indicate the positions at which influxes of new magma into the chamber are postulated to have occurred. Thin chromitite layers and stringers are labelled "Cr".
For details of the Pseudo macro unit at Amandelbult see Figure 6.3.

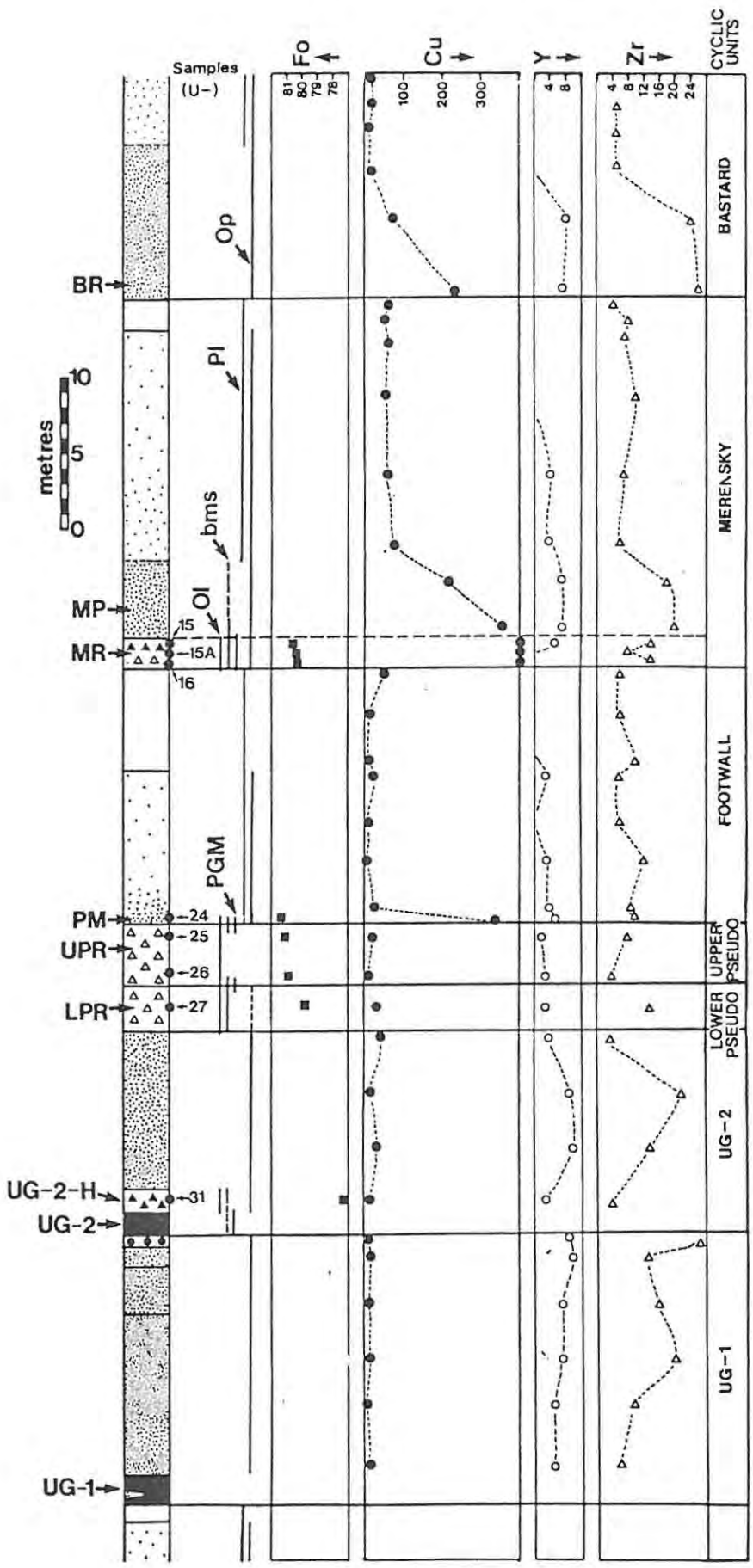

FIGURE 6.2 Study section at Union Section.

For explanation of lithologies and marker layers see Figure 6.1. Sample positions are labelled U-15, U-31 etc.. Solid vertical lines indicate the distribution of cumulus olivine (Ol), base-metal sulphide (bms), platinum-group minerals (PGM), cumulus plagioclase (Pl), and cumulus orthopyroxene (Op). Composition of olivine (mol.% Fo) is based on microprobe data, and the distribution of Cu, Y, and Zr is based on whole-rock data (in ppm).

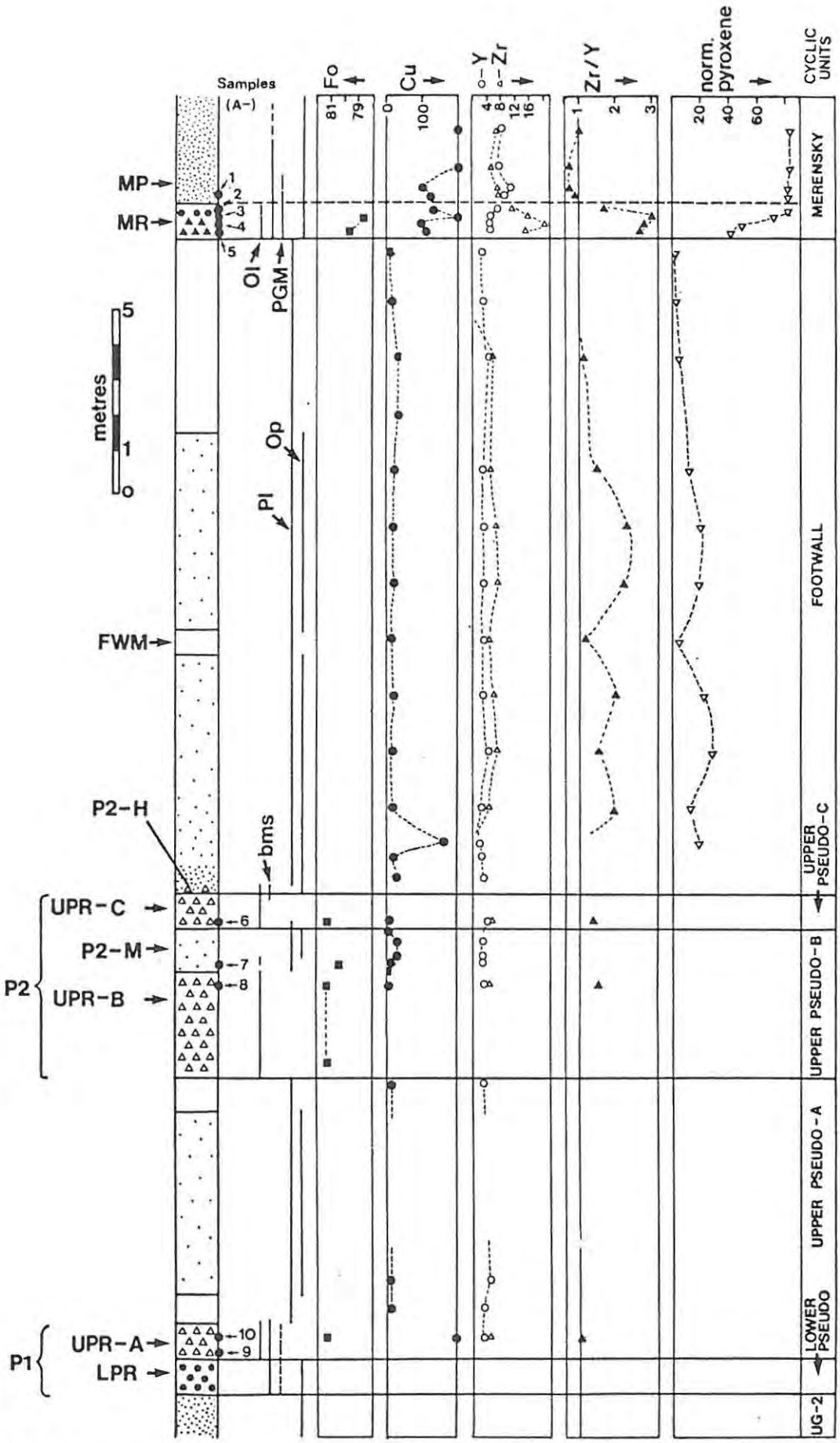

FIGURE 6.3 Study section at Amandelbult.

For explanation of lithologies and marker layers outside of the Pseudo macro unit see Figure 6.1. The Pseudo macro unit consists of four cyclic units, the Lower Pseudo and the Upper Pseudo A, B and C. These include the following marker layers : the lower pseudoreef (LPR), the upper pseudoreefs A, B and C (UPR-A/B/C), the P2 middling (P2-M) and the P2 hangingwall (P2-H). Sample positions are labelled A-1 through A-10. Solid vertical lines indicate the distribution of cumulus olivine (Ol), base-metal sulphide (bms), platinum-group minerals (PGM), cumulus plagioclase (Pl), and cumulus orthopyroxene (Op). Composition of olivine (mol.% Fo) is based on microprobe data, and the distribution of Cu, Y, and Zr is based on whole-rock data (in ppm). Normative pyroxene (orthopyroxene plus clinopyroxene) is calculated from the CIPW norm.

TABLE 6.1 ELECTRON MICROPROBE ANALYSES OF CUMULUS OLIVINES IN THE UPPER CRITICAL ZONE

	U-15	U-15A	U-16	U-24	U-25/26	U-27	U-31	A-3	A-5	A-7/8	A-9/10	A-6
wt.%												
SiO_2	39.56	39.25	39.58	38.86	39.56	39.13	38.75	38.80	39.10	39.28	39.35	38.75
FeO	17.85	18.91	18.31	17.03	18.08	18.82	21.04	19.69	18.93	17.50	17.25	18.14
MnO	.22	-	.24	.23	.22	.23	.26	.25	.22	.23	.23	.24
MgO	42.17	41.88	41.36	43.13	42.83	41.22	39.76	40.45	41.34	42.44	42.33	41.96
CaO	.03	-	.03	.01	.02	.02	.03	.02	.01	.02	.02	.10
NiO	.44	.42	.37	.40	.32	.38	.36	.42	.41	.37	.34	.31
TOTAL	100.27	100.46	99.89	99.66	101.03	99.80	100.20	99.63	100.01	99.84	99.52	99.50
cations												
Si	1.0049	.9996	1.0107	.9915	.9981	1.0036	1.0007	1.0018	1.0015	1.0009	1.0045	.9951
Fe^{2+}	.3792	.4028	.3910	.3634	.3815	.4037	.4544	.4252	.4055	.3730	.3683	.3896
Mn	.0047	-	.0052	.0050	.0047	.0050	.0057	.0055	.0048	.0050	.0050	.0052
Mg	1.5964	1.5895	1.5740	1.6401	1.6105	1.5756	1.5302	1.5565	1.5780	1.6118	1.6103	1.6059
Ca	.0008	-	.0008	.0003	.0005	.0005	.0008	.0006	.0003	.0006	.0005	.0028
Ni	.0090	.0086	.0076	.0082	.0065	.0079	.0075	.0088	.0085	.0078	.0070	.0064
TOTAL	2.9950	3.0005	2.9893	3.0085	3.0018	2.9963	2.9993	2.9984	2.9986	2.9991	2.9956	3.0050
mol.% Fo	80.81	79.78	80.10	81.86	80.85	79.60	77.10	78.54	79.56	81.21	81.39	80.48
n	5	3	6	4	11	7	9	12	10	11	7	4
Fo x	80.61	79.65	80.17	81.76	81.02	79.61	77.33	78.68	79.66	81.31	81.37	80.51
d	.2473	.1665	.1670	.0821	.2473	.1778	.1576	.2232	.1612	.2621	.1746	.0222
NiO x	.43	.42	.38	.39	.33	.40	.37	.42	.425	.36	.35	.31
d	.0158	-	.0245	.0082	.0009	.0160	.0107	.0173	.0127	.0143	.0198	.0050

x - mean; d - standard deviation; n - number of samples.
Merensky Reef : U-15, U-15A, U-16, A-3, A-5 ; Pseudo marker - U-24; Pseudo reefs : U-25/26, A-7/8, A-9/10; P2 Middling : A-6; UG-2 Hangingwall : U-27. For sample positions see Figures 6.1 (U - Union Section) and 6.2 (A - Amandelbult).

6.4 OLIVINE CHEMISTRY

Representative electron microprobe analyses of olivines from the cumulates described in the previous section are presented in Table 6.1 (see also Appendix 7). Averages of the various sample groups are also included. These data are plotted on diagrams of stratigraphic height versus mol. percent Fo (figs. 6.2, 6.3) and wt. percent NiO versus mol. percent Fo (fig. 6.4). All these analyses are of the cores of grains, although no chemical zonation was detected. From Figure 6.4C it can be seen that these data define four separate populations. These, with increasing stratigraphic height, are : the immediate UG-2 hangingwall (sample U-31), the lower pseudoreef (sample U-27), the upper pseudoreefs (samples U-25,26 and A-6,8,9,10) and the Merensky Reef (samples U-15,15A,16 and A-3,5). Data for the pseudo marker (sample U-24) may possibly be correlated with that for the upper pseudoreefs, as may olivine from the mottled anorthosite in the P2 middling (sample A-7). Olivine from the base and top of the Merensky Reef exhibit a slightly different chemistry, but the scatter within these data may reflect the exceptionally pegmatoidal nature of this cumulate.

Theoretical fractionation curves have been generated to predict the NiO and MgO contents of more iron-rich olivines that would be derived by progressive crystallization of an initial liquid in equilibrium with the

most magnesian olivine in this study (see p.52, also Chapter 9 for full explanation; theoretical fractionation path plotted in Figure 9.5 using sample A-7/8 as an initial olivine composition). This makes a number of large assumptions, but the crux of this argument is that olivine in the harzburgitic layers within the upper pseudoreefs may have been derived by fractionation of a common parent magma, whereas olivine in the other population groups is related to chemically distinct magma batches. Fractionation of one magma within a closed chamber cannot account for the compositional differences observed between olivines from the UG-2, Pseudo and Merensky cyclic units. This argument is valid even if the D_{Ni} predicted by the Hart and Davis (1978) formula is subject to major inaccuracies. It is inferred that new influxes of relatively primitive magma, each of which has its own chemical signature, occurred at the base of the UG-2, Lower Pseudo, Upper Pseudo, and Merensky cyclic units. Data for the Upper Pseudo and Footwall cyclic units is equivocal, but field relationships suggest that separate magma inputs, probably from a common magma batch, were responsible for each of the harzburgitic layers in these units.

From these data the NiO/FeO ratio of olivine in the Merensky Reef at Union Section is determined as .0223 (NiO : x = .3748, d = .0307; FeO : x = 18.2846, d = .3748; and n = 14) and at Amandelbult it is determined as .0221 (NiO : x = .4245, d = .0150; FeO : x = 19.2345, d = .5022; and n = 24). Note that these are averages (x = mean; d = standard deviation; n = number of samples) and do not reflect the data spread which is evident from Figure 6.4. An average value for the NiO/FeO ratio of olivine in the Merensky Reef in the northern sector of the western Bushveld Complex of 0.0222 is proposed.

6.5 WHOLE-ROCK CHEMISTRY OF THE OLIVINE-BEARING CUMULATES

Whole-rock analyses of olivine-bearing cumulates from Amandelbult and Union Section are presented in Table 6.2. A triangular plot of normative olivine - plagioclase-orthopyroxene illustrates the mineralogical variations discussed previously (fig. 6.5A). Scatter in the samples of the Merensky Reef is a result of sampling difficulties presented by the pegmatoidal texture. The variation in the Mg/Fe ratio of olivines from the different cyclic units is confirmed by plotting whole rock data on a triangular diagram of $(CaO + Na_2O + K_2O)$ - FeO - MgO (fig. 6.5B). In Figure 6.5C additional data for orthopyroxene-plagioclase cumulates from the Footwall cyclic unit at Amandelbult and the Merensky cyclic unit at Union Section are plotted. These two population groups define separate linear relationships.

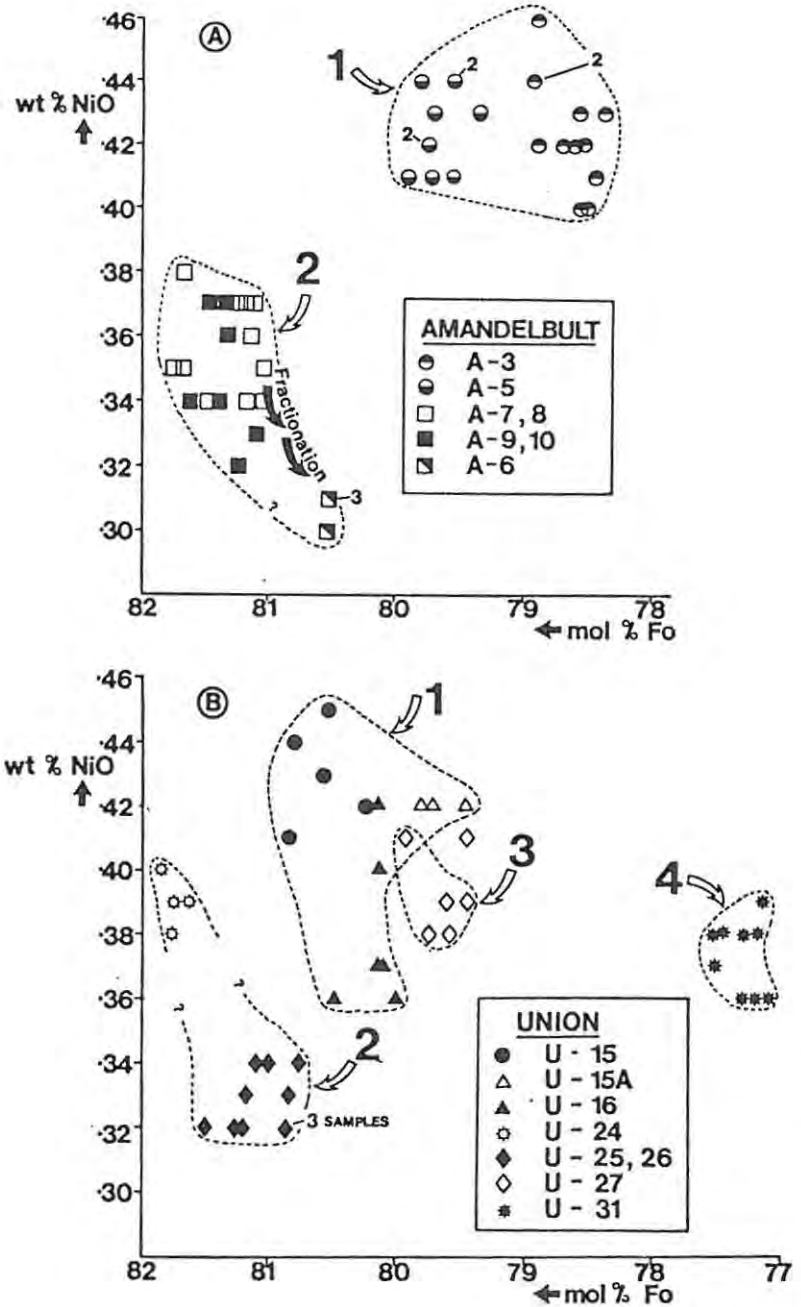

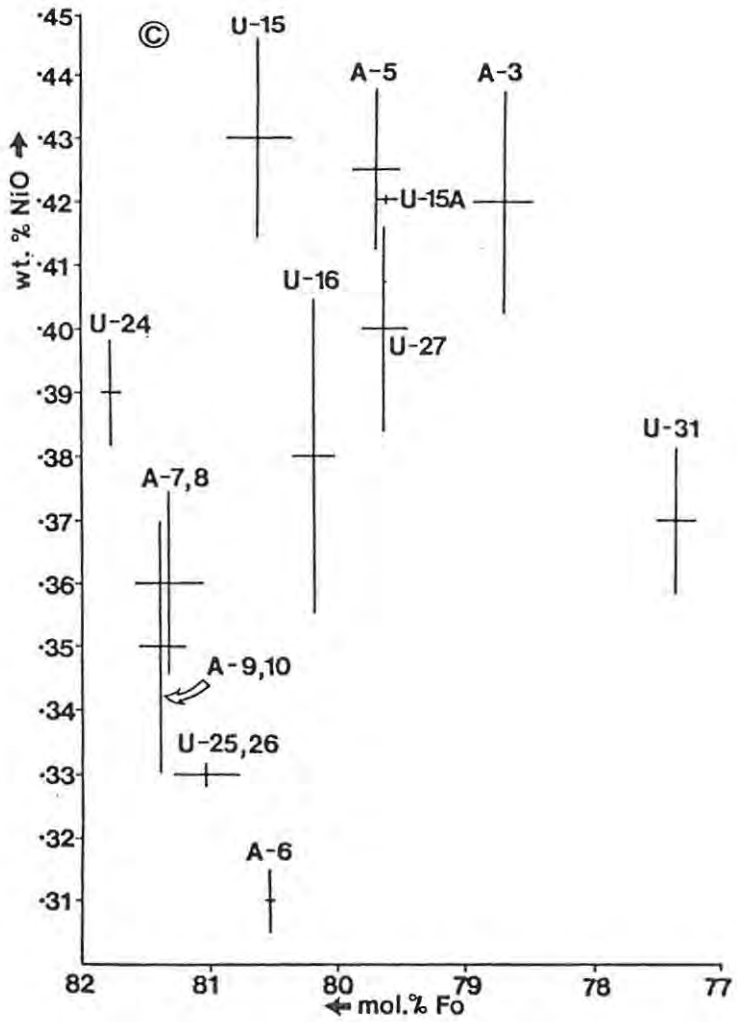

FIGURE 6.4 Plot of wt. % NiO vs. mol. % Fo in olivine.

(A) : samples from Amandelbult; (B) : samples from Union Section; and (C) average data for both mines. For sample positions see Figures 6.2 and 6.3. In plots A and B each symbol represents one analysis by electron microprobe. In plot C averages are depicted as crosses in which the error bars represent plus or minus one standard deviation (d) from the mean (x) - for complete analyses see Table 6.1.

The following sample groups are recognised :

GROUP 1 - The Merensky Reef (both mines; samples U-15, U-15A, U-16, A-3, A-5).

GROUP 2 - The upper pseudoreefs (both mines; samples U-25, U-26, A-7, A-8, A-9, A-10). This group may include samples from the Pseudo Marker (U-24) and the P2 middling anorthosite (A-6).

GROUP 3 - The lower pseudoreef at Union Section (sample U-27).

GROUP 4 - The UG-2 hangingwall at Union Section (sample U-31).

TABLE 6.2 WHOLE-ROCK ANALYSES OF OLIVINE BEARING CUMULATES IN THE UPPER CRITICAL ZONE

	U-15	U-15A	U-16	U-24	U-25	U-27	U-31	A-1	A-2	A-3	A-4	A-5	A-6	A-7	A-8	A-9	A-10
wt.%																	
SiO_2	44.10	40.50	42.10	50.20	40.70	45.00	46.10	53.00	52.66	50.83	50.88	46.67	45.22	38.46	39.25	39.93	37.94
TiO_2	.14	.15	.15	.18	.09	.14	.13	.24	.36	.17	.17	.15	.06	.11	.19	.10	.16
Al_2O_3	6.62	4.56	4.10	5.16	4.00	6.50	4.90	5.31	4.67	5.57	11.65	9.11	26.11	3.21	4.31	3.86	5.67
Fe_2O_3	1.12	1.49	1.30	.97	1.10	1.10	1.20	1.05	1.11	1.07	.86	1.02	.31	1.18	1.16	1.31	1.22
FeO	11.15	14.94	13.04	9.74	10.98	10.98	11.97	10.55	11.05	10.70	8.59	10.23	3.10	11.77	11.59	13.12	12.18
MnO	.20	.19	.19	.22	.23	.17	.24	.29	.22	.18	.13	.20	.03	.15	.15	.18	.19
MgO	25.40	27.60	28.10	26.00	32.20	27.50	28.70	23.12	24.23	24.02	19.21	22.90	7.31	31.03	31.05	30.01	28.91
CaO	3.66	2.28	2.62	3.67	2.23	3.70	3.40	4.89	3.65	3.61	5.38	4.28	12.63	2.87	2.39	2.24	2.35
Na_2O	.60	.40	.40	.50	.40	.60	.60	.43	.43	.50	.91	.58	1.78	.11	.13	.13	.26
K_2O	.09	.11	.09	.04	.07	.11	.05	.03	.19	.15	.78	.64	.23	.06	.06	.03	.03
P_2O_5	n.d.	n.d.	n.d.	n.d.	.01	.02	.01	.01	.02	.01	.02	.01	.01	n.d.	n.d.	n.d.	n.d.
Cr_2O_3	.58	.51	.51	.59	.16	.42	.53	.52	.60	.57	.18	.36	.12	.18	.17	.18	1.99
NiO	.32	.39	.60	.25	.26	.20	.18	.11	.12	.36	.15	.20	.05	.26	.25	.33	.36
L.O.I	5.77	6.40	7.02	2.80	7.10	4.95	2.50	1.06	1.41	2.04	1.20	4.22	3.31	10.91	10.45	8.57	8.36
TOTAL	99.75	99.52	100.22	100.32	99.53	101.39	100.51	100.61	100.72	99.78	100.11	100.57	100.27	100.30	101.15	99.99	99.62
ppm																	
Cu	400	600	1100	400	19	37	10	216	130	820	99	111	15	8	10	386	504
Co	143	201	182	118	145	93	142	101	105	130	100	125	42	146	152	166	169
V	74	58	68	106	39	56	86	168	133	108	44	53	12	51	41	41	45
Sc	–	–	–	–	–	–	–	36	25	20	4	9	4	10	8	11	9
Sr	80	72	58	70	58	88	73	63	49	65	145	109	412	54	60	53	61
Rb	4	3	4	n.d.	3	3	n.d.	n.d.	6	5	28	29	4	n.d.	3	n.d.	n.d.
Zr	14	8	14	10	8	14	4	8	11	16	85	15	n.d	6	5	4	3
Y	5	n.d.	n.d.	5	2	3	3	9	7	6	5	6	3	5	4	4	n.d.
CIPW wt.% norm																	
Ol	37.3	56.1	49.7	15.2	63.1	41.5	41.0	–	3.6	9.7	10.7	27.9	16.8	65.5	62.3	56.9	58.5
Op	35.2	24.2	29.9	60.3	19.2	31.9	34.8	70.7	72.5	65.8	48.6	39.4	.9	16.7	21.1	26.7	19.7
Cp	2.6	.9	3.3	5.3	1.8	2.9	5.1	9.4	6.2	4.5	.9	.6	–	5.5	.8	1.1	–
Pl	22.1	15.4	14.0	16.6	13.8	21.2	16.2	16.6	15.2	18.2	38.2	30.3	81.6	10.5	13.8	12.2	15.4
Mg-No.	.80	.77	.79	.83	.84	.82	.81	.80	.80	.80	.80	.80	.81	.82	.83	.80	.81

For sample positions see Figures 6.1 (U – Union Section) and 6.2 (A – Amandelbult); Mg-No = at.% Mg/(Mg+Fe); n.d.–not detected;
CIPW NORMS : Ol – olivine; Op – orthopyroxene; Cp – clinopyroxene; Pl – plagioclase.
Merensky Reef : U-15, U-15A, U-16, A-2, A-3, A-4, A-5 ; Pseudo marker : U-24 ; Pseudo reefs : U-25, U-27, A-7, A-8, A-9, A-10 ; P2 Middling : A-6 ; Merensky Pyroxenite : A-1 ; UG-2 Hangingwall : U-31.

The distribution of Co, V, and Sc in these rocks is illustrated in Figure 6.6. Data for these plots include samples from most of the cyclic units in this study. The distribution of these trace elements is modally controlled, consequently plagioclase-orthopyroxene (pl-op) and plagioclase-olivine (pl-ol) mixing lines are evident. Scatter from these lines is related to modal variation caused by either plagioclase-orthopyroxene-olivine rocks or accessory phases, including chromite (cr) and base-metal sulphide (bms). It may be deduced from this diagram that, in comparison with orthopyroxene, olivine has a higher distribution coefficient (D) for Co and a lower D for V and Sc (see Chapter 12 for further details). Because these D's are all fairly low the concentration of the trace elements Co, V, and Sc in olivine and orthopyroxene cumulates cannot be used to distinguish between the different cyclic units in this study section (in comparison olivine has a much higher D for Ni). It may be concluded that these elements are not sensitive enough indicators of the subtle compositional differences envisaged in the primary magmas. The presence of chromite and clinopyroxene negates use of whole-rock data to examine the concentration of Cr in orthopyroxene.

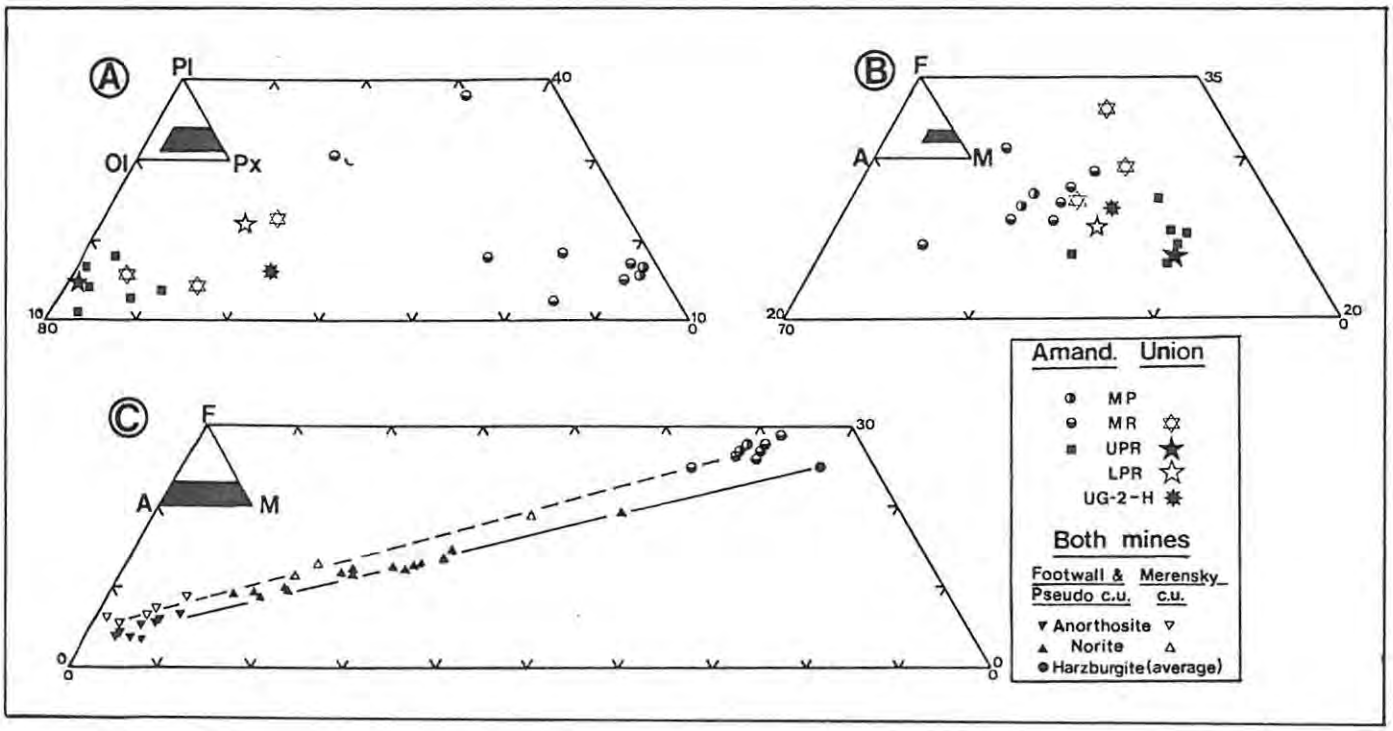

FIGURE 6.5 (A) : part of a triangular graph of normative olivine (Ol), plagioclase (Pl) and pyroxene (Px). Each symbol is based on the CIPW norm calculated from one whole-rock analysis.

(B) and (C) : Part of an AFM diagram (wt. % ($CaO+Na_2O+K_2O$) - FeO - MgO). Each symbol represents one whole-rock analysis. Data for the olivine-bearing cumulates (MR - Merensky Reef; UPR - upper pseudoreefs; LPR - lower pseudoreef; PM - pseudo marker; UG-2-H - UG-2 hangingwall), together with samples of the Merensky pyroxenite (MP) are plotted in B. On plot C it can be seen that samples (various lithologies) from the Merensky and the Footwall / Pseudo cyclic units define separate trends.

The chemistry of orthopyroxenes in the equivalent stratigraphic interval at Rustenburg has been examined by Kruger and Marsh (1983). Their data indicate that considerable fractionation occurs in the Merensky and Bastard cyclic units, but they record a reversal in the Footwall unit. It is suggested that this indicates that their Footwall unit comprises more than one cyclic unit and the apparent reversal may be related to replenishment of the chamber. Naldrett et al. (1983) report that the X_{Mg} of orthopyroxene in the Merensky pyroxenite may be lower than orthopyroxene from the Merensky Reef. Electron microprobe analyses of orthopyroxene from the Merensky Reef (X_{Mg} = .802; 0.12% NiO) and Merensky pyroxenite (X_{Mg} = .794; 0.10% NiO) at Amandelbult corroborate this (see Appendix 8 for analyses).

Strontium partitions almost exclusively in these rocks into plagioclase (very minor quantities occur in orthopyroxene and practically none in olivine - see fig. 6.7) and appears to be very sensitive to primary magma composition (see also Eales et al., 1983; Kruger & Marsh, 1983; Naldrett et al., 1983). A plot of Sr versus wt. percent Al_2O_3 can be used to assess the composition of plagioclase in different cyclic units. Kruger and Marsh (1983) obtained values of 480, 430, and 400 ppm Sr for plagioclase in the Footwall, Merensky, and Bastard cyclic units at Rustenburg. A similar value may be calculated with these data (although with a range of $\pm$ 20 ppm) for the Footwall and Merensky cyclic units (fig. 6.7B). These data

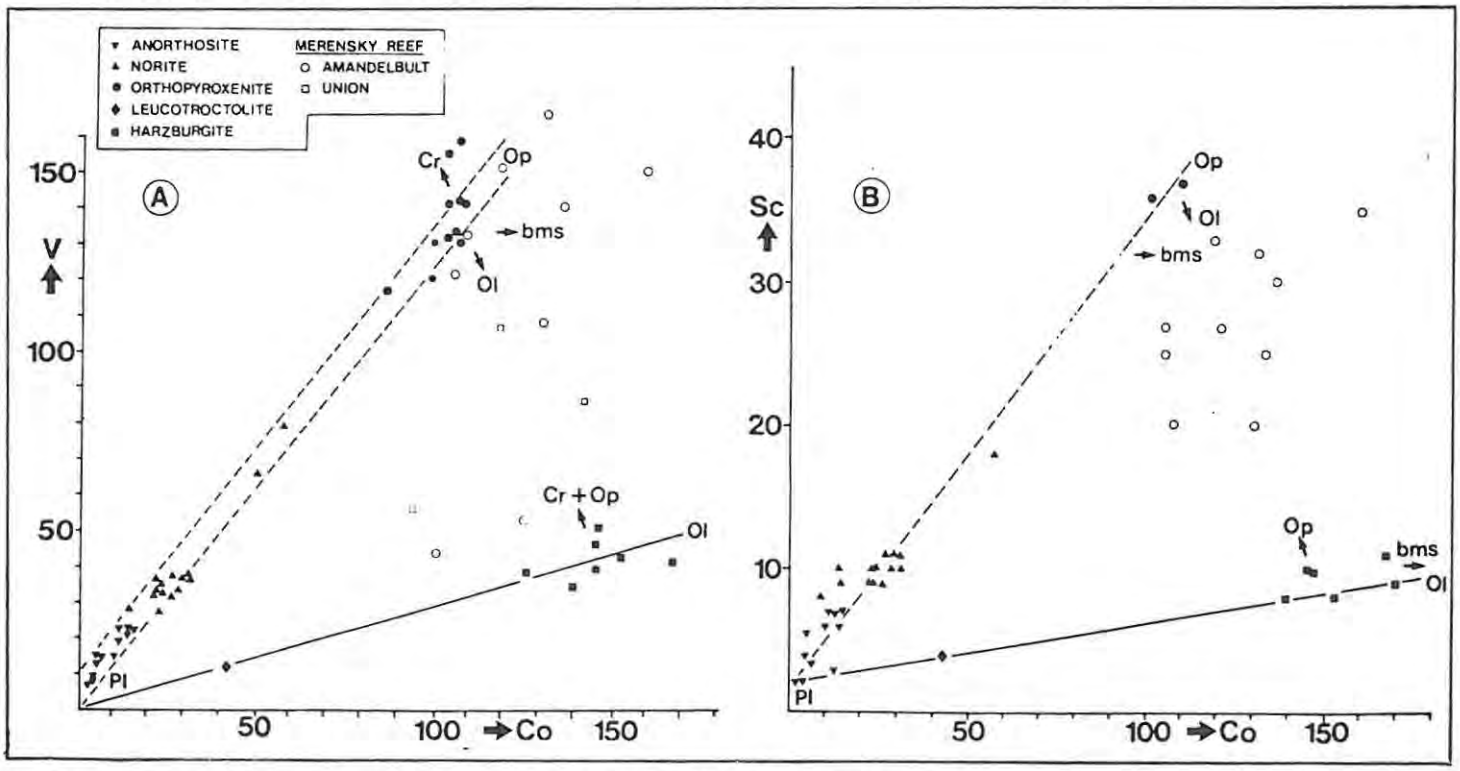

FIGURE 6.6 Whole-rock data on plots of ppm V vs. ppm Co (A) and ppm Sc vs. Co (B).

Each data point represents one whole-rock analysis. Straight lines are defined by plagioclase (Pl) - orthopyroxene (Op) and plagioclase (Pl) - olivine (Ol) mixing lines. Scatter from these lines is caused by chromite (Cr), olivine (Ol), orthopyroxene (Op) and base-metal sulphide (bms).

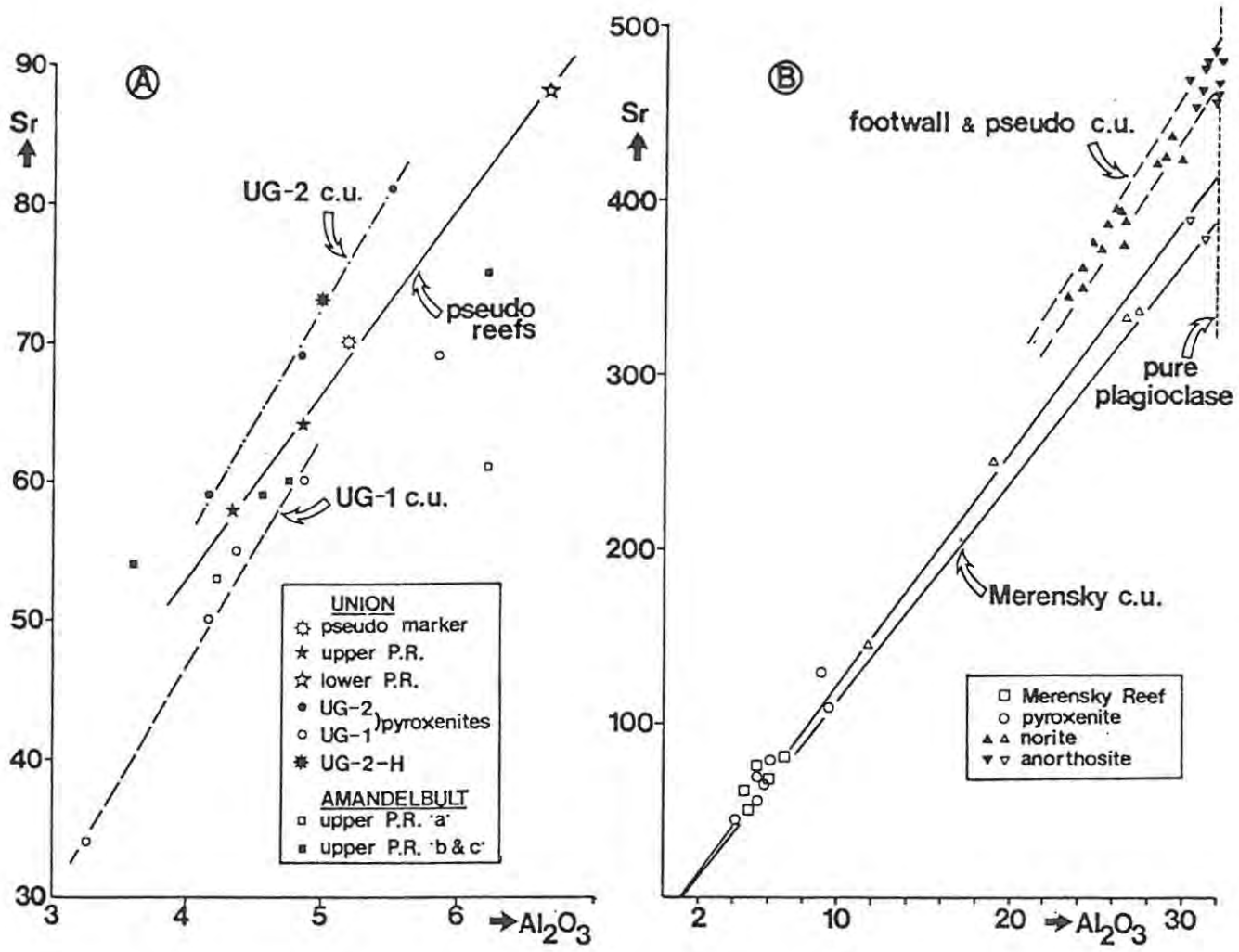

FIGURE 6.7 Whole-rock data on plots of ppm Sr vs. wt. % Al_2O_3.

(A) : Intercumulus plagioclase in "ultramafic" cumulates, including the pseudo marker, the upper and lower pseudoreefs (PR), and orthopyroxenites from the UG-1 and UG-2 cyclic units.

(B) : Total plagioclase (cumulus plus intercumulus) in cumulates from the Footwall/Pseudo cyclic units (solid symbols) and the Merensky cyclic unit (open symbols). The Al_2O_3 component of plagioclase represents an average of electron microprobe analyses.

The straight lines in plot B represent plagioclase - orthopyroxene mixing lines which may be extrapolated to intersect the Al_2O_3 axis at between 1.0 and 1.5 wt. %, corresponding to the composition of orthopyroxene. Some of the straight lines in plot A regress through zero indicating that olivine contains practically no Sr. The slope of these lines indicates that intercumulus plagioclase in the ultramafic cumulates is richer in Sr than total plagioclase in the mafic and felsic cumulates.

are subject to errors due to zonation and chemical differences between cumulus and intercumulus grains (features recognized by Kruger & Marsh). Cumulus plagioclase is absent in some of the other cyclic units and it is evident from Figure 6.7A that intercumulus plagioclase is relatively enriched in Sr for a given An component. Eales et al. (1983) calculate values of 664 ppm and 688 ppm for intercumulus plagioclase in feldspathic orthopyroxenites in the lower critical zone. It can be argued that plagioclase in most of these cyclic units is characterised by a distinctive Sr value.

Naldrett et al. (1983) suggest that incompatible elements, such as Nb, Zr, Y, and Rb, may be used as indicators of trapped intercumulus material. In the succession studied here inter-incompatible element ratios are fairly constant, athough ultramafic layers at the base of cyclic units may be rich in bulk values of these elements (figs. 6.2, 6.3). Pegmatoidal layers such as the Merensky Reef are unusually rich in these elements, a feature also recognized by Naldrett et al. (1983). This may partly be a function of porosity control, but the author attributes a proportion of these incompatible (and volatile) components to infiltration metasomatism, as described by Irvine (1980).

6.6 DISTRIBUTION OF Ni, Cu AND Co

In the rocks in this study Cu behaves as an almost perfect chalcophile element - its distribution is directly related to the presence of base-metal sulphide and it is incompatible with respect to the other cumulus phases (fig. 6.8A). The low levels of Cu found in anorthosites, which may be slightly enriched compared to sulphide-poor pyroxenites or harzburgites, is attributed to microscopic specks of sulphide. In contrast, the distribution of Ni and Co is influenced by both ferromagnesian silicates and sulphides. The strong octahedral site preference energy of Ni is well known such that the sulphide control envisaged by Lee (1983) in the Merensky cyclic unit, which is clearly exceptionally sulphide-rich, is not generally applicable. Both Ni and Co partition strongly into olivine, and to a lesser extent into orthopyroxene. Naldrett et al. (1983) suggest that orthopyroxene in the Merensky cyclic unit contains about 700 ppm Ni, such that levels in excess of this value (allowing for modal variation) are attributable to sulphide. If this "excess" Ni is plotted against Cu the Ni/Cu ratio of the sulphide may be obtained. Sulphide control becomes evident when harzburgites contain over 1800 ppm Ni and orthopyroxenites over 700-800 ppm Ni (fig. 6.8A; note

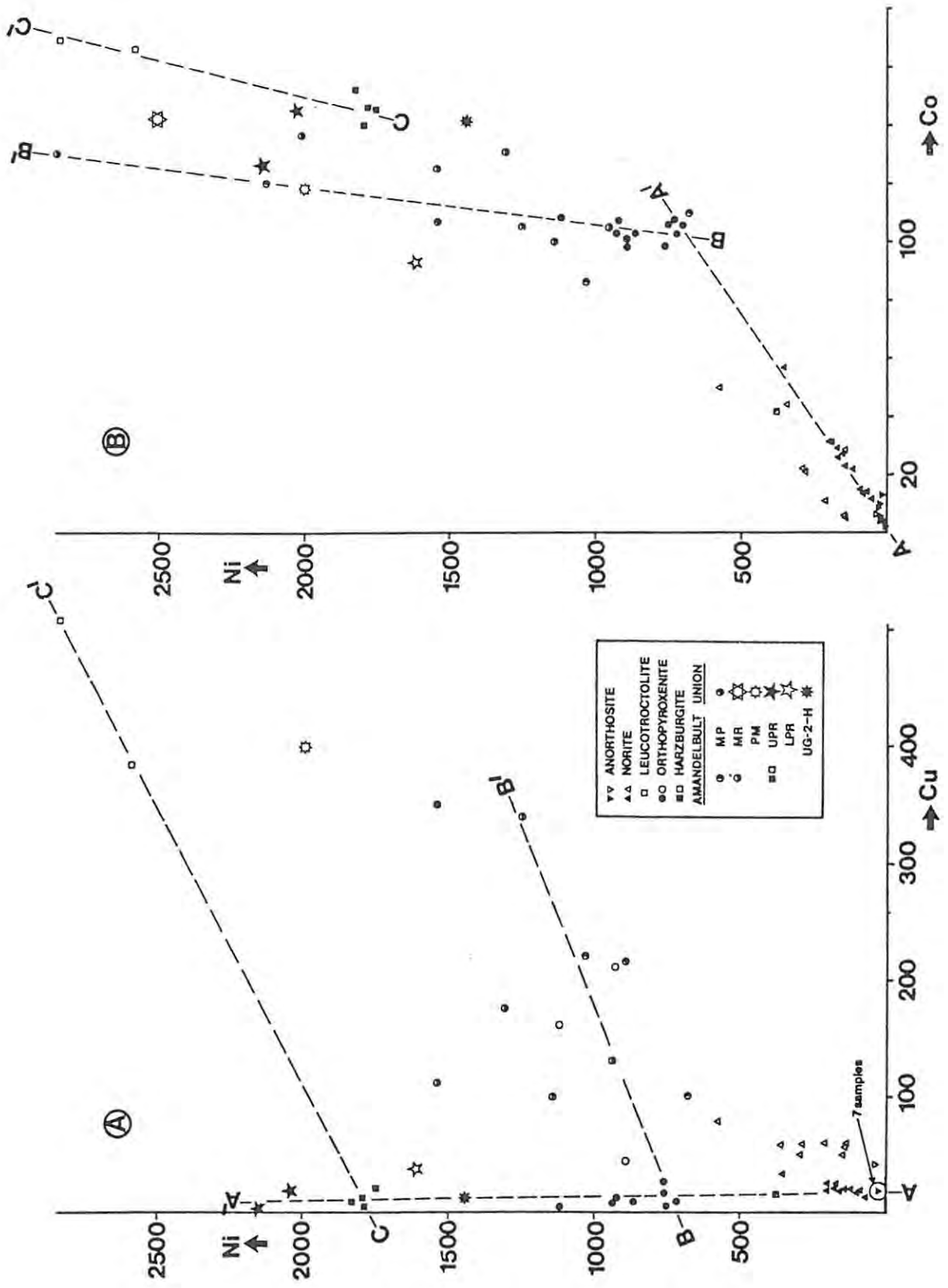

FIGURE 6.8 Whole-rock data on plots of ppm Ni vs. ppm Cu (A) and ppm Ni vs. ppm Co (B).

Solid symbols represent sulphide-poor samples and open symbols are sulphide-rich samples. Samples of specific marker layers include the Merensky pyroxenite (MP), the Merensky Reef (MR), the pseudo marker (PM), the upper pseudoreefs (UPR), the lower pseudoreefs (LPR) and the UG-2 hangingwall (UG-2-H).

In plot A sulphide-poor samples regress to a line (A-A'), roughly parallel to the Ni-axis, irrespective of silicate mineralogy. Dilution by sulphide results in sample scatter, athough poorly-defined mixing lines for sulphide-rich pyroxenites (B-B') and sulphide-rich harzburgites (C-C') may be established. In plot B sulphide-poor samples of plagioclase-orthopyroxene cumulates define a mixing line (A-A'). Scatter off this line is caused by sulphide (B-B') and olivine (C-C').

that these samples contain rougly 15 modal percent plagioclase). Data for sulphide-rich samples are limited but the Ni/Cu ratio is estimated at from unity to 2. Naldrett et al. (1983) obtained values of 2.3 : 1 for the Merensky Reef and 1.2 : 1 for the remainder of the Merensky cyclic unit.

In sulphide-poor plagioclase-orthopyroxene cumulates the Ni/Co ratio is estimated at 6. In sulphide-rich plagioclase-orthopyroxene samples and sulphide-rich and sulphide-poor harzburgites this ratio increases to a maximum of approximately 40 (fig. 6.8B). It is suggested that $D^{oliv-liq}_{Ni/Co}$ and $D^{sulf-liq}_{Ni/Co}$ are similar, as the sulphides are evidently Co-poor. The samples here show only limited fractionation and these data are not adequate to recognize trends within different cyclic units.

6.7 BASE-METAL SULPHIDE MINERALIZATION

From Figures 6.2 and 6.3 it can be seen that anomalous concentrations of Cu, and hence base-metal sulphide, occur typically within ultramafic cumulates at, or towards the base of cyclic units. They occur preferentially in pegmatoidal layers. Anomalous concentrations of base-metal sulphides occur in the UG-2 chromitite layer, in the Merensky Reef and in the lower part of the Merensky pyroxenite. At Union Section sulphides also occur for a few centimeters either side of the chromitite layer which separates the two pseudoreefs. The lower pseudoreef and the upper pseudoreef unit A (which exhibit a pegmatoidal and coarse-grained texture, respectively) contain base-metal sulphides, whereas the upper pseudoreef units B and C (the medium-grained tarentaal) are relatively poor in sulphide. Anomalous concentrations of sulphide also occur in the harzburgitic layers at the base of the Footwall units at both mines.

Base-metal sulphides in the Merensky Reef, in order of decreasing abundance, include pyrrhotite, pentlandite, chalcopyrite and pyrite. The low sulphide content (0.5 - 2.0 wt. percent) and the high Ni/Fe and Cu/Fe sulphide ratios are unusual for magmatic ores (Cousins,1969). Vermaak and Hendriks (1976) quote an average sulphide value of 2.75 wt. percent for the Merensky Reef at Rustenburg, which is composed of pyrrhotite (39.64 percent), pentlandite (22.18 percent), chalcopyrite (16.36 percent), and pyrite (21.82 percent). From the data of Brynard et al.(1976) the following normative sulphide contents can be calculated : pyrrhotite (50.19 percent), pentlandite (34.30 percent), chalcopyrite (10.57 percent), and pyrite (4.93 percent). Detailed studies of the sulphide mineralogy of the Merensky Reef have also been completed by Liebenberg (1970), Van Zyl (1970) and Von Gruenewaldt (1979).

TABLE 6.3 ELECTRON MICROPROBE ANALYSES OF BASE-METAL SULPHIDES IN THE MERENSKY REEF

	1		2		3		4	5		6	7	8
wt.%	x	d	x	d	x	d		x	d			
S	36.50	.185	38.96	.035	37.9	.690	39.44	33.59	.314	31.85	35.21	33.1
Fe	64.18	.393	62.45	.339	59.9	.54	60.53	34.48	.847	32.95	31.08	30.5
Co	n.d.	-	n.d.	-	.1	-	n.d.	.28	.180	.90	-	-
Ni	n.d.	-	n.d.	-	.2	-	n.d.	30.78	1.162	33.55	-	-
Cu	-	-	-	-	n.d.	-	-	-	-	-	33.34	33.7
TOTAL	100.68		101.41		98.1		99.57	99.13		99.25	99.75	97.3
at.%												
S	49.78	-	52.08	-	52.37	-	53.16	47.75	-	45.81	50.35	49.0
Fe	50.22	-	47.92	-	47.45	-	46.83	28.14	-	27.16	25.31	25.9
Co	-	-	-	-	.06	-	-	.22	-	.69	-	-
Ni	-	-	-	-	.12	-	-	23.89	-	26.34	-	-
Cu	-	-	-	-	-	-	-	-	-	-	24.14	25.1
n	3		2		3		1	9		2	7	1
M:S	1.009		.920		.909		.881	8.75		9.40	-	-
Ni/Ni+Co	-		-		-		-	.99		.97	-	-

x-mean; d-standard deviation; n-number of samples; M:S ratio=(Fe+Co+Ni)/S (assumes S=8 for pentlandite)
1-troilite ; 2,3-hexagonal pyrrhotite; 4-monoclinic pyrrhotite; 5,6-pentlandite; 7,8-chalcopyrite.
Analyses 3,6, & 8 from Vermaak and Hendriks (1976).

Electron microprobe analyses of base-metal sulphides in the Merensky Reef at Amandelbult are presented in Table 6.3 (for complete analyses see Appendix 11). Pyrrhotite is typically an intergrowth of the hexagonal and monoclinic varieties, although occasionally an intergrowth of troilite and hexagonal pyrrhotite may be observed. Pentlandite is an extremely cobalt-poor variety and is further distinguished by a low Ni/Fe ratio. The association of hexagonal-monoclinic pyrrhotite and cobalt-poor pentlandite is typical according to Harris and Nickel (1972), although the low Ni/Fe ratio of pentlandite from the Merensky Reef may be unusual (see also Chapter 11). Chalcopyrite is the dominant copper mineral and cubanite is only rarely observed. Mackinawite is a common exsolution feature in pentlandite. Microscope studies indicate that the base-metal sulphide mineralogy of the Merensky Reef at Amandelbult conforms with the modal data of Brynard et al. (1976).

The Ni/Fe sulphide ratio of the Merensky Reef is estimated at 0.15 (using the data of Vermaak & Hendriks) and 0.22 (using the data of Brynard et al.), from the microprobe data in Table 6.3 (it was assumed that all the Ni is in pentlandite).

6.8 DISTRIBUTION OF THE PLATINUM-GROUP ELEMENTS

The major platiniferous orebodies in the Bushveld Complex, the UG-2 and Merensky Reefs, occur within this stratigraphic interval (inter alia Cousins, 1969; Vermaak & Hendriks, 1976; Brynard et al., 1976; Von Gruenewaldt, 1979; Kinloch, 1982). The maximum concentrations of PGE in the Merensky Reef at Amandelbult and Union Sections occur in the Merensky chromitite layers (particularly in the upper layer), to a lesser extent in the pegmatoid itself, and for a few centimetres in the Merensky hangingwall pyroxenite (in contrast, the maximum concentrations of sulphide Cu and Ni occur in the lower part of the Merensky pyroxenite, with lesser amounts in the pegmatoid and very sparse amounts in the chromitite layers). The footwall contact is sharp. The relative distribution of PGE, Cu, and Ni in the Merensky Reef is illustrated clearly by the data of Lee (1983). The UG-2 chromitite layer hosts economic levels of PGE, but again contains only very low concentrations of base-metal sulphide.

Subeconomic concentrations of PGE occur within some of the other ultramafic layers between the UG-2 and Merensky Reefs. At Union Section significant concentrations of PGE and base-metal sulphides occur for roughly 20 cm above and below the chromitite layer which divides the upper and lower pseudoreefs, and within and for 20 cm above, the chromitite layer at the base of the Footwall cyclic unit. At Amandelbult the pegmatoidal orthopyroxenite which constitutes the lower pseudoreef contains notable PGE and base-metal sulphides; this layer may be considered as a subeconomic equivalent to the Merensky Reef. The coarse-grained harzburgite in the Upper Pseudo cyclic unit A at Amandelbult also contains PGE and base-metal sulphide. No data are available on the chromitite layer between these two units. In contrast, the tarentaal at Amandelbult is depleted in base-metal sulphide and contains no significant PGE.

In summary, economic and subeconomic concentrations of PGE in this stratigraphic interval are restricted to ultramafic cumulates at the base of cyclic units. The bulk of the PGE are associated with chromitite layers with lesser amounts in silicate-rich, usually pegmatoidal, cumulates. In contrast, base-metal sulphides are concentrated within silicate-rich ultramafic, (usually pegmatoidal) cumulates. Further, the PGE are essentially in PGM, which occur as discrete phases and do not show any marked preference for base-metal sulphides (Vermaak & Hendriks, 1976; Von Gruenewaldt, 1979; Kinloch, 1982). This results in a wide range of PGE/bulk sulphide ratios. It may also be deduced that this would require a large range in the value of D_{Pt}, D_{Pd} etc. The models of Campbell et al. (1983) and

Campbell and Barnes (1984) require exceptionally high D's for the PGE, and it is suggested that the sulphide-control they envisage on the distribution of the PGE in the Bushveld Complex is a major flaw in their argument. The role of chromite as a collector for PGE is well established (although this process is not understood) e.g., the "xenoliths" of chromitite in the Onverwacht pipe and the chromite schlieren in the Mooihoek dunite (cf. pp. 27, 64; after Wagner, 1929) and the dunitic ores of the Urals (Razin, 1976), as well as the cumulate-hosted chromitite concentrations referred to above. The association of PGE with ultramafic rocks is well known and has been reviewed by Naldrett and Cabri (1976) and Crocket (1979).

6.9 DISTRIBUTION OF Ni AND Fe BETWEEN OLIVINE AND SULPHIDE

Thompson et al. (1984) investigated the distribution of Ni and Fe between olivine and molten sulphide, expressed by the distribution coefficient K_D, where :-

$$K_D = (X_{NiS}/X_{FeS})^{sulp} * (X_{FeO}/X_{NiO})^{oliv}$$

and X_{NiS} etc. are mole fractions. For natural assemblages Thompson et al. quote an average value for K_D of 9.8. This is consistent with the findings of Duke and Naldrett (1978), Naldrett (1979) and Boctor (1982), but does not support the high values (greater than 40) obtained experimentally by Fleet et al. (1977, 1981) and Fleet and MacRae (1983). This is clearly a controversial subject and the reader is referred to the discussions by Fleet (1979) and Naldrett (1979, 1981).

In this study the average NiO/FeO ratio of olivine in the Merensky Reef is determined at 0.0222 (section 6.4), and the NiS/FeS ratio of the Merensky Reef is estimated at between 0.15 and 0.22 (section 6.7). K_D for the Merensky Reef is thus estimated at between 6.5 and 10. This is consistent with data for the H.P. Reef in the Stillwater Complex and the average findings of Thompson et al. (1984). It is concluded that the Merensky and H.P. Reefs are characterised by coexisting Ni-rich sulphides and Ni-rich olivines in equilibrium.

This value of K_D does not necessarily reflect liquidus compositions, as it is known that the distribution of Ni and Fe can be seriously affected by subsolidus reequilibration between olivine and Mss, or monosulphide solid solution (Naldrett & Clarke, 1972). In massive sulphide ores it may be predicted that subsolidus reequilibration will modify liquidus compositions, such that the magmatic immiscibility models of Naldrett and others

(inter alia Naldrett, 1981) cannot be tested. However, in unaltered, disseminated sulphide ores it is unlikely that silicate compositions will have been affected by subsolidus reequilibration with sulphides. Furthermore, if the sulphides occur dominantly within interstitial sites, or enclosed by intercumulus phases, such as plagioclase, it may be predicted that sulphide compositions will not have suffered subsolidus effects with olivine. The author concludes that in the Merensky Reef the value of K_D is a measure of the distribution of Ni and Fe between primary olivine (liquidus composition ?) and molten sulphide.

Magmatic immiscibility models which explain the origin of nickel sulphide ores associated with ultramafic-mafic rocks have been reviewed by Naldrett (1981). They are subject to several criticisms, two of which are investigated here. Coexisting olivines are often enriched in Ni, not depleted as might be expected, and, secondly, magmatic ores show a wide range in Ni/Fe (and Ni/Cu) sulphide ratios. Both these features may be explained by considering the stage at which S-saturation occurs within an ultramafic melt which may crystallize olivine (inter alia Rajamani & Naldrett, 1978; Duke & Naldrett, 1978; Duke, 1979; Campbell et al., 1983).

Three possibilities are evident. Firstly, if an immiscible molten sulphide phase segregates after crystallization of olivine it is reasonable to expect that the resulting Mss will be depleted in Ni, and that the Ni content of the olivine will probably be "normal" (i.e. unaffected by the presence of sulphide). Secondly, if S-saturation is reached before crystallization of olivine then it may be inferred that the Mss will be Ni-rich and the olivine will be depleted in Ni.

In the third alternative S-Saturation may be concomitant with crystallization of olivine. In this situation, assuming equilibrium conditions, the distribution of Ni and Fe between olivine and molten sulphide is controlled by the value of K_D. If K_D is fixed, or varies within narrow limits (as suggested by the investigations of Thompson et al., 1984), then the Ni/Fe ratio of coexisting olivine and Mss will show a positive linear relationship. Thus, if the sulphides have a high Ni/Fe ratio then it is predicted that coexisting olivine will also exhibit a high Ni/Fe ratio. As argued above, in unaltered disseminated ores it is reasonable to calculate a value for K_D from subsolidus compositions. It may be concluded that if Ni-rich sulphides and Ni-rich olivine coexist segregation of an immiscible sulphide phase was concomitant with crystallization of olivine.

The causes of S-saturation are only poorly known. Magma mixing, decrease in temperature, fractional crystallization, changes in fO_2 and fS_2, and magma composition (particularly in FeO content) are some of the proposed

mechanisms (Haughton et al., 1974; Shima & Naldrett, 1975). Naldrett (1981) observes that in large magma chambers fO_2, fS_2 and a_{FeO} are buffered such that the relative proportions of Fe, S, and O within the molten sulphide phase are tightly controlled, athough this is not true of the minor components, Ni, Cu, Co and PGE. Segregation of an immiscible sulphide phase early in the crystallization history of a cooling magma is not a new concept and a comparison with peridotite/komatiite - hosted sulphide ores may be applicable. In a review article Naldrett (1981) observes that most authorities agree that peridotite/komatiite-hosted sulphides reached equilibrium with their host magma well before they reached their present position, probably before eruption.

6.10 NEW MAGMA INPUTS

It is concluded from the data and arguments propounded above that new influxes of magma entered the main chamber at the base of the UG-2, Lower Pseudo, Upper Pseudo, and Merensky cyclic units. A new magma input is also postulated to have occurred at the base of the UG-1 cyclic unit. Each of these magma inputs is broadly comparable, but they are recognized by subtle compositional differences. They may be categorised as discrete magma batches. In contrast, up to four separate influxes of the same magma batch are inferred to have occurred in the Upper Pseudo and Footwall cyclic units at Amandelbult (see figs. 6.2, 6.3). It is suggested that each of these new magmas was picritic or olivine tholeiitic in composition; it is not necessary to postulate that they have ultramafic affinities.

In the previous section it was deduced that segregation of an immiscible sulphide phase was concomitant with the crystallization of olivine. Olivine is clearly an early cumulus mineral in the cyclic units studied here, and may locally predate the formation of chromite. It is possible that some of this olivine entered the chamber as xenocrysts, although it is difficult to establish any evidence for this. It has been proposed by Lesher et al. (1981) that in komatiitic sulphide deposits olivine phenocrysts may assist with upward transportation of the dense sulphide droplets; a similar mechanism may be applicable to the sequence studied here. Crystallization of olivine and concomitant S-saturation may have occurred prior to irruption (during ascent from the mantle, in a low-level holding chamber or within feeder channels) or immediately after the new magma entered the main chamber. It is suggested that these events occurred before this new magma mixed with the residual magma in the chamber (see below). This model accounts for the close spatial association of ultramafic cumulates and base-metal sulphides in

the upper critical zone at Amandelbult and Union Sections.

This model requires that the new influxes of magma were denser than the residual magma in the chamber and entered the chamber quiescently as a flow along the crystal-liquid interface. The residual magma in the upper critical zone of the Bushveld chamber was largely tholeiitic with orthopyroxene and plagioclase as the main liquidus phases. Crystallization of large amounts of plagioclase from a tholeiitic magma results in an increase in the density of the residual magma (Campbell et al., 1983; Sparks & Huppert, 1984). Eventually a "crossover point" occurs at which time the residual magma is denser than a new (more primitive) magma. The model of Campbell et al. requires that this crossover point has been reached at the level of the Merensky Reef. The author believes that their argument is equivocal and that the data in this study are best explained if a new influx of magma, entering the chamber in the upper critical zone, would still be denser than the residual magma at this level.

Campbell et al.(1983) suggest that in the upper critical zone iron-rich residual liquids produced by fractional crystallization remain in the resident magma in the chamber, resulting in a further increase in density. A distinctive feature of the upper critical and main zones (e.g., where plagioclase is a major cumulus phase) is the presence of discordant bodies of iron-rich ultramafic pegmatite. These may represent trapped intercumulus liquid (see Chapter 13). If this interpretation is correct then they would have a major effect in modifying the density calculations of Campbell et al. (1983).

6.11 FORMATION OF CYCLIC UNITS IN THE UPPER CRITICAL ZONE

Having made this assumption concerning the relative densities of the new and residual magmas, the following model is presented to explain the formation of cyclic units in the upper critical zone at Amandelbult and Union Sections. It draws heavily on the models of Huppert and Sparks (1980) and Sparks and Huppert (1984). A similar model has been developed by Smewing (1981), who studied the Oman ophiolite complex. Density and thermal differences between the new (relatively dense and hot) magma and the residual magma result in the formation of a stratified layer at the base of the chamber. It is assumed that the new influx of magma enters the chamber as a flow along the crystal-liquid interface, and does not jet as suggested by Campbell et al. (1983). This new influx of magma sharply truncates the previous cyclic unit and may result in some resorption, as the new crystal-liquid interface is not likely to be in equilibrium. The new cyclic unit may

then develop as follows.

As the new magma begins to cool, fractional crystallization, probably dominantly bottom crystallization as described by McBirney & Noyes (1979), but possibly with some cumulus mineral formation with settling over a few metres or tens of metres, results in the formation of an ultramafic cumulate at the base of the new cyclic unit. Settling of olivine xenocrysts, if present, and of suspended droplets of sulphide, over a vertical extent of a few or possibly tens of metres, will occur at this early stage. Recent consensus of opinion suggests that chromitite layers form as a result of magma mixing (inter alia Irvine & Sharpe, 1983; Eales & Reynolds, 1983; Hatton & Von Gruenewaldt, 1983), and thus are likely to occur at the base of new cyclic units. If the new pulse of magma remains as a discrete layer at the base of the chamber for a reasonable time span, fractional crystallization will result in a cyclic unit in which ultramafic cumulates are gradational up into felsic cumulates (e.g., the Merensky and Bastard cyclic units). It is predicted that cryptic mineralogical variation, relating to fractional crystallization, will occur in these well-formed cyclic units. Convection may occur within the new pulse of magma, which forms a discrete layer at the base of the chamber, but at this point in time the new and residual magmas do not mix.

As cooling and fractional crystallization proceed this density stratification must break down and mixing of the the new and residual magmas will occur (which is why complete cyclic units are not usually observed). If mixing of the new and residual magmas occurs relatively soon after the new influx, whilst an ultramafic cumulate is still forming, the liquidus relationships may show a marked change. This may be particularly apparent if the volume of new magma compared to the residual magma is low. In this situation, if mixing is efficient, the liquidus relationships may suddenly revert back to those prevalent in the residual magma before the new influx. This process may account for hybrid cyclic units in which harzburgitic layers are sharply overlain by leuconorites or anorthosites (e.g., the Upper Pseudo cyclic units A and B at Amandelbult). This may result in the formation of disequilibrium contact zones within a cyclic unit (e.g., at the top of harzburgite layers). It is tentatively suggested that the formation of certain mottled anorthosites may be related to this process, either as a result of incomplete mixing or by uplift from an earlier cycle (see Eales, in press).

If a new influx of magma occurs whilst the previous influx still forms a discrete layer at the base of the chamber, the developing cyclic unit will be beheaded before mixing can occur. If this happens before plagioclase has

become a cumulus phase a series of ultramafic cumulates, each a result of separate influxes, may result (e.g., the UG-1, UG-2 and Lower Pseudo cyclic units at both mines, the Upper Pseudo cyclic unit at Union Section and the Upper Pseudo unit C at Amandelbult). These cyclic units thus result solely from the new influx, unlike the hybrid units described above.

From strontium isotope studies Kruger and Marsh (1982) concluded that a major new influx of magma occurred at the base of the Merensky cyclic unit. In comparison some of the new influxes that are postulated to have occurred between the UG-1 and the Merensky Reef by the present author, were probably volumetrically much smaller. Kruger and Marsh attribute the scattered isotope signature within the Merensky cyclic unit to contamination by upward-streaming intercumulus liquid. It is possible that two separate influxes occurred at the base of the Merensky Reef, the first of these forming the lower chromitite and the pegmatoid. This was then beheaded by a second influx which formed the upper chromitite and the remainder of the cyclic unit. The recognition of two separate magma inputs accounts for the presence of the two chromitite layers and the mineralogical and compositional differences between the pegmatoid and the hangingwall pyroxenite.

The model discussed above accounts for some of the field relationships and lithological variations observed in the cyclic units at the top of the upper critical zone in the northern sector of the western Bushveld Complex. In particular the thinning and eventual wedging out of ultramafic layers along strike is best explained by replenishment of the chamber with new influxes of magma entering the chamber as a flow rather than as a jet or plume. These lateral stratigraphic features may be directly related to distance from a feeder site.

6.12 RELATIONSHIP TO BASE-METAL SULPHIDE AND PGE MINERALIZATION

The decoupling of Ni-Cu sulphide and PGE mineralization in the upper critical zone was described earlier. It is suggested that base-metal sulphides and PGE mineralization may have a cumulus and intercumulus component (see also Lee, 1983). The bulk of the base-metal sulphide mineralization is probably cumulus as it is intimately related to its host cumulate (see also Naldrett et al., 1983). It is difficult to reconcile this with the gravity settling model proposed by Campbell et al. (1983). Furthermore, the bulk of the sulphide and PGE mineralization occur as very small grains and it is difficult to envisage settling of such small droplets through a thick column of liquid, particularly if the liquid was stratified. It is also unlikely that a gravity settling process would be efficient enough

to produce the observed distribution trends. The bulk of the sulphide is thus considered to be an intimate component of the new influxes of (picritic ?) magma. The R-factor (bulk silicate/sulphide liquid ratio of Campbell & Naldrett, 1979) is not considered to be a problem for the base-metal sulphides. The bulk sulphide content is low and equilibration with the silicate magma prior to irruption or in response to convection currents within the stratified magma at the base of the chamber are alternative hypotheses.

Intercumulus sulphide is related to the upward movement of intercumulus liquid (and infiltration metasomatism as described by Irvine, 1980). The bulk of the PGE mineralization is also postulated to be intercumulus. The concentration of minor sulphide and important PGE mineralization in chromitite layers is difficult to explain by any other mechanism. Distribution patterns indicate upward-movement, not gravitational settling (inter alia Cousins, 1964; Vermaak & Hendriks, 1976; Brynard et al., 1976; Lee, 1983). The bulk of the PGE mineralization is best explained by a process of infiltration metasomatism (see also Vermaak, 1976). One of the main attractions of the model of Campbell et al. is that it explains the relative position of platiniferous layers in layered complexes, whereas the infiltration metasomatism model does not.

6.13 SUMMARY

(1) Evidence is presented for separate influxes of magma into the chamber at the base of some of the cyclic units in the upper critical zone in terms of new electron microprobe data and whole-rock analyses.
(2) The distribution of base-metal sulphide and PGE mineralization is re-examined, and it is concluded that they do not exhibit direct correlation.
(3) The sulphides are in equilibrium with olivine, consequently segregation of an immiscible sulphide liquid from the silicate magma occurred concomitantly with crystallization of olivine. This accounts for the close spatial relationship between sulphides and ultramafic cumulates at the base of cyclic units in this part of the layered complex.
(4) Decoupling of sulphide and PGE mineralization must therefore point to later introduction of PGE into their present position, possibly by upward movement of intercumulus liquid.
(5) The formation of pegmatoidal cumulates has not been investigated.

SECTION D : THE IRON-RICH ULTRAMAFIC PEGMATITE SUITE

CHAPTER 7 DISTRIBUTION AND FIELD RELATIONSHIPS

The distribution and main geological characteristics of iron-rich ultramafic pegmatite were discussed, in conjunction with a literature review, in Chapter 2. This section presents a range of new data for the iron-rich ultramafic pegmatite suite. It is divided into six chapters, distribution and field relationships, petrography, mineralogy of the silicate, oxide and base-metal sulphide (and PGE) phases and whole-rock chemistry. Discordant bodies of iron-rich ultramafic pegmatite are particularly abundant in the upper critical and lower main zones of the layered sequence at R.P.M. Amandelbult Section. Consequently, this area has been selected as the main study section.

In this chapter the distribution and field relationships of iron-rich ultramafic pegmatite bodies at Amandelbult are described. These may be divided into two groups, namely typical, small, often irregular bodies and a large, pipe-like body, the so-called Middellaagte pipe. Cr-rich Fe-Ti oxide pegmatites have also been located at Amandelbult; these are described in Chapter 10. The field relationships of iron-rich ultramafic pegmatite bodies at other localities in the Bushveld Complex which have been investigated in this study are also described in this chapter.

7.1 DISTRIBUTION

7.1 INTRODUCTION

The poor outcrop and lack of detailed geological mapping in the Amandelbult area was referred to previously (pp. 74-77). Prior to commencement of recent mining operations (in the mid 1970's) the large pipe-like body of pegmatite which crops out on the farm Middellaagte had been recognized (de Bruyn, 1944), but the distribution of the small, irregular bodies of pegmatite at Amandelbult only became apparent as mining operations progressed. It was soon evident that these pegmatite bodies were unusually abundant in the Amandelbult area. Moreover, a number of pegmatite bodies were found to replace the Merensky Reef, hampering mining operations.

In 1977 J.C.I. completed a detailed ground geomagnetic survey over most of the Amandelbult leasehold (for location maps see figs. 5.1, 5.2). This

survey was directed primarily at locating the strongly magnetic iron-rich ultramafic pegmatite bodies. It covered most of the strike length of the mine and extended laterally some 2 km in the hangingwall of the Merensky Reef. Because of the extremely limited outcrop these data are the main guide to the surface distribution of the pegmatite bodies.

7.1.2 GEOMAGNETIC DATA

The ground-based geomagnetic survey completed by J.C.I. was based on a grid with interline and station spacings of 20 m. Because the cumulate rocks in this area of the Bushveld Complex were known to be essentially non-magnetic it was anticipated that pegmatite bodies with diameters greater than 20 m would be located (Heidstra, 1978). These bodies were found to be highly magnetic and gave well-defined, near equidimensional, positive anomalies. Heidstra located a number of other features which gave magnetic signatures. These included post-Bushveld dykes which have a negative magnetic signature (see also p. 75), red-soil outwash from the adjacent Transvaal Supergroup and a number of weak linear anomalies evidently related to the main zone cumulates (see also pp. 18-19).

Detailed isomagnetic contour maps of this survey were produced on a scale of 1:5 000. Heidstra (1978) interpreted the presence of a number of iron-rich ultramafic pegmatite bodies from this survey, the distribution of which is summarised in Figure 7.1. From these data, which were made available to the author, overlays at a scale of 1:10 000 were produced for aerial photographs. All areas in which magnetic anomalies were indicated were then examined in the field. The results of this fieldwork are discussed below*.

Heidstra (1978) correlated the magnetic signature of the iron-rich ultramafic pegmatite bodies with moderately to steeply dipping, plug- or pipe- like bodies with a large vertical extent. Viljoen and Scoon (in press) observed that many of the small, satellite bodies adjacent to the Middellaagte pipe have an asymmetric magnetic signature which suggests that they plunge steeply to the northwest, that is approximately normal to the cumulate layering. It may be inferred that they were emplaced at an early stage when the Bushveld layering was horizontal.

Iron-rich ultramafic pegmatite bodies at Amandelbult occur in three main clusters (figs. 7.1, 7.2). These, from west to east, occur in the western

---

* The reader is also referred to detailed maps in field reports, completed by the author in December 1981 (filed in the Geology Dept., Rhodes University)

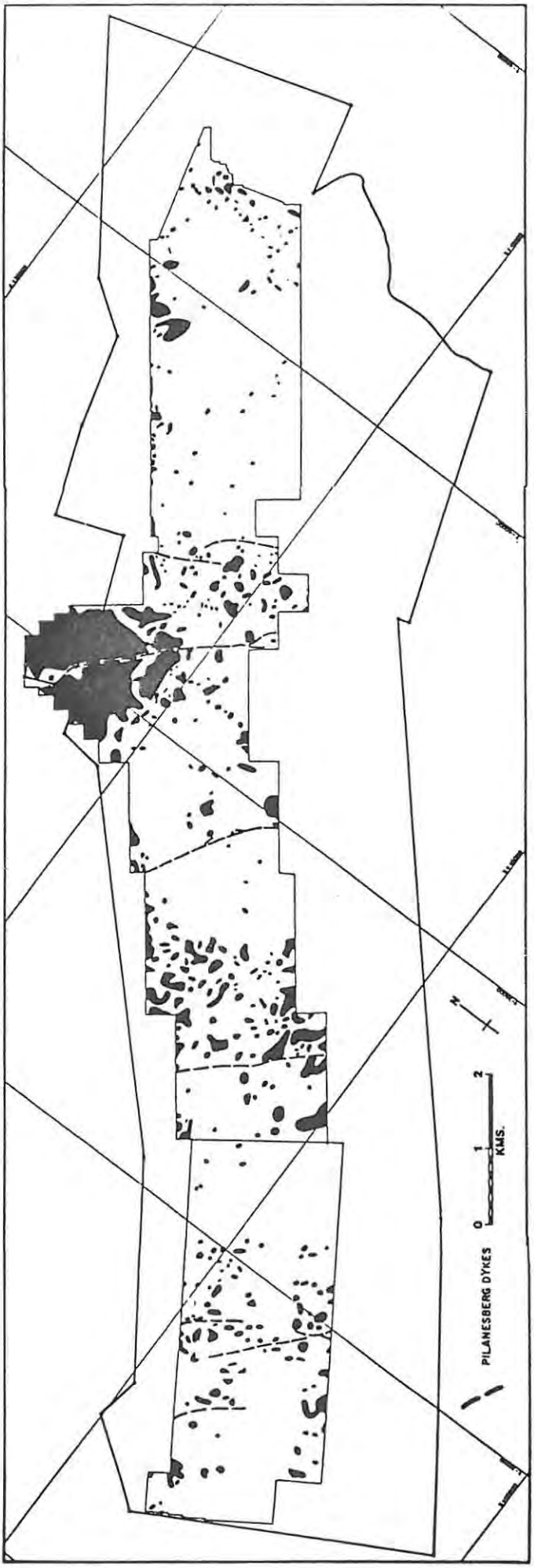

Figure 7.1 Principal magnetic anomalies at R.P.M. Amandelbult - these are probably all associated with subout-cropping iron-rich ultramafic pegmatite bodies. Results of a detailed ground magnetics survey (from Heidstra, 1978).

sector of the mine (specifically in the area of the mine delineated by the mine sections 30W to 20W), the central sector of the mine (in an area delineated by the mine sections 6W to 7E), and in the Middellaagte area. Only minor pegmatite bodies exist in the area to the east of Middellaagte. This distribution pattern has been supported by underground exposures in mine development. Heidstra (1978) concluded that some 20 percent of the survey area at Amandelbult (which included the large Middellaagte body) was underlain by over 400 separate pegmatite bodies. Viljoen and Scoon (in press) observe that a definite clustering of these bodies occurs in zones of structural weakness which are also exploited by post-Bushveld dykes. Underground mapping of mine development indicates that Heidstra's (1978) predictions were inaccurate. Iron-rich ultramafic pegmatite bodies are much less abundant and probably represent less than 5 percent of the layered sequence in the Amandelbult area.

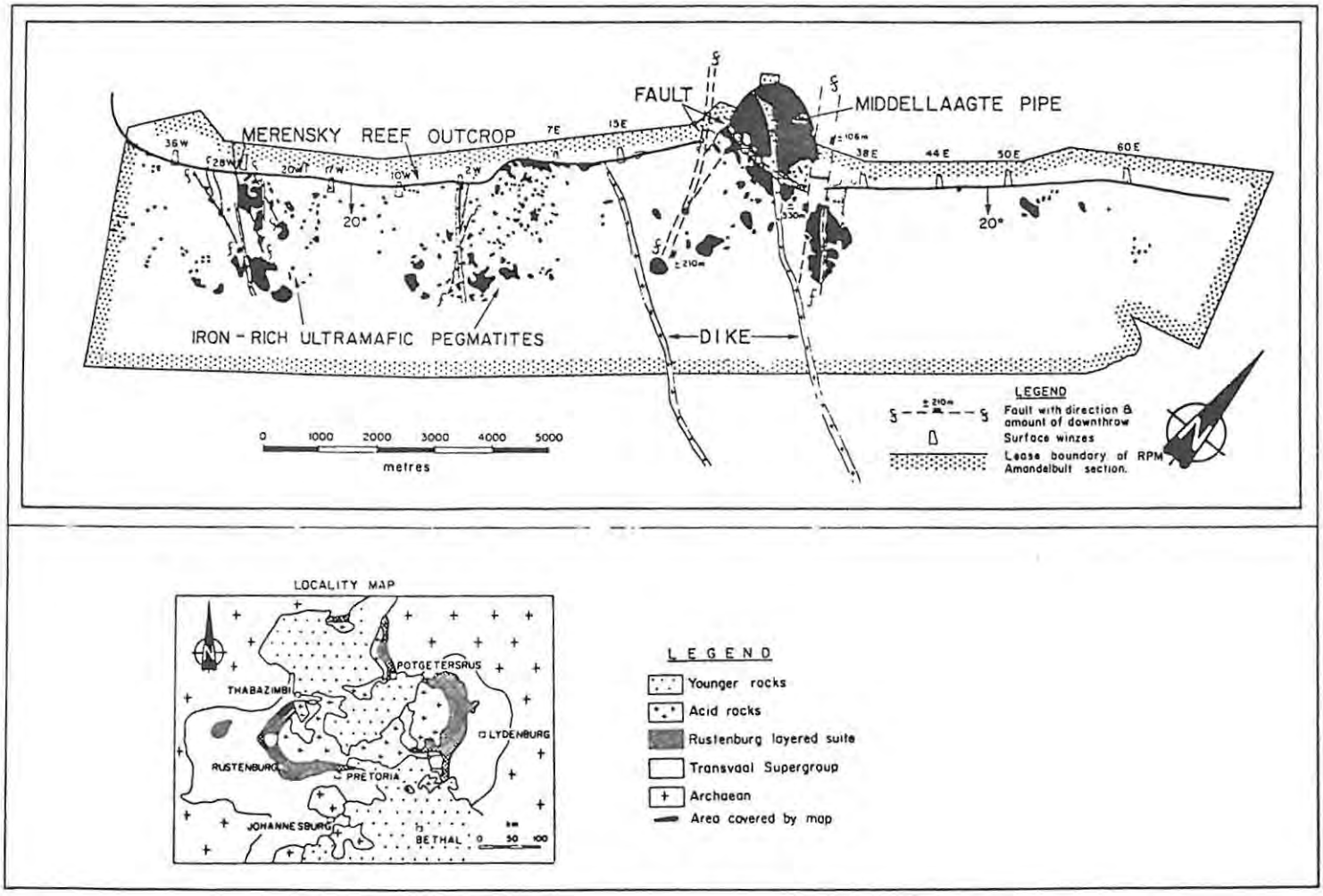

Figure 7.2 Distribution of the major centres of iron-rich ultramafic pegmatite at R.P.M. Amandelbult. Largely based on results of ground magnetics survey. Note relationship between clusters of pegmatite bodies and post-Bushveld structural features, namely faults and dykes.

7.1.3 SURFACE MAPPING

Surface mapping was restricted to following up geomagnetic anomalies and locating pegmatite bodies which were known to crop out. From mapping of underground development, which is essentially restricted to the interval between the UG-1 and Bastard cyclic units (see Chapter 5), it is known that many of the pegmatites form sheet-like bodies which are locally stratabound. The geomagnetic survey only covered an area in the hangingwall of the Merensky Reef, consequently surface data are lacking on most of the exposures which have been mapped underground. In the area which is covered by the geomagnetic survey outcrop is very sparse such that surface mapping is usually restricted to recording float, soil type, vegetation and topographic features. Many of these observations can be used as an indirect aid to locating suboutcropping bodies of iron-rich ultramafic pegmatite (see below). These features were used to imply that suboutcropping pegmatite bodies exist in most of the areas delineated by the geomagnetic anomalies. However, the resistant nature of the pegmatite in comparison with deep weathering of ultramafic and mafic cumulates results in features which a ground magnetic survey, susceptible to near-surface magnetic float, will exaggerate. For these reasons it is important to stress that geomagnetic data, although an invaluable exploration tool, should be treated with some reservation.

A few pegmatite bodies have been located at Amandelbult which occur outside the area covered by the geomagnetic survey. A large, zoned, probably pipe-like body occurs at the western extremity of the farm Elandsfontein. This body comprises a 100-150 m diameter core composed of Fe-Ti-oxide pegmatite with an outer shell of poorly-exposed silicate-rich pegmatite. It is emplaced in main zone cumulates just above the porphyritic "Tiger" marker. Two composite pegmatite bodies have been located to the north of the mine leasehold in which sheet-like masses of Cr-rich Fe-Ti oxide pegmatite are associated wtih typical silicate-rich pegmatite (see Chapter 11).

7.1.4 BOREHOLE DATA

The distribution of iron-rich ultramafic pegmatite at Amandelbult in boreholes (from logs and the core of recently drilled holes) has been assessed and compares favourably with the geomagnetic data. A number of boreholes have been collared above suboutcropping pegmatite bodies. It is deduced that the 32 000 gamma contour, or greater, reflects the presence of a

suboutcropping, probably well formed, pegmatite body, whereas below the 31 500 gamma contour only very irregular, sporadic segregations of pegmatite exist (see fig. 7.5).

The percentage of pegmatite intesected in all boreholes at Amandelbult (ignoring core-loss and deflections) has been estimated. These data are subjective as, obviously, most of the boreholes intersect the sequence in the hangingwall of the Merensky Reef with only a small proportion continuing below the UG-2 chromitite layer. These boreholes may be subdivided into two groups. The first group is referred to by farm-locations (e.g., Elandsfontein (EL), Middellaagte (ML) etc.); these often intersect a considerable thickness of main zone cumulates. The second group are based on mine sections (labelled numerically west and east from a central reference section, e.g., 42W, 7E etc. - see fig. 7.2); these are usually collared only a short distance above the Merensky Reef.

From boreholes on Schilpadnest (SKN series only) and Elandsfontein (EL series only) it is estimated that 8.6 and 8.4 percent, respectively, of the layered sequence consists of iron-rich ultramafic pegmatite bodies. From these data it has also been calculated that 6 and 15 percent, respectively, of the Merensky Reef intersections are replaced by pegmatite (see section 7.4). Based on the second group of boreholes it is estimated that 1.8 percent of the succession consists of pegmatite in the western sector of the mine (as delineated by the sections 43W to 18W) and of 87 Merensky Reef intersections 4 are replaced by pegmatite (equivalent to 5 percent). In the eastern sector of the mine, using both groups of boreholes east of EK-1, it is estimated that 1.9 percent of the succession consists of pegmatite and 8 percent of the Merensky Reef intersections are replaced by pegmatite.

7.1.5 UNDERGROUND EXPOSURES

Most of the pegmatite bodies presently exposed in underground development at Amandelbult occur in the western sector of the mine, specifically in the area delineated by sections 30W to 25W (see Map 6). Bodies of iron-rich ultramafic pegmatite have also been mapped and sampled from underground exposures in the 44 to 43W, 4E to 7E and 44E areas of the mine. No obvious petrologic changes have been observed along strike, although considerable lateral variation is apparent in the layered sequence (see p. 83). These exposures are discussed further in section 7.3).

7.2 FIELD RELATIONSHIPS - THE MIDDELLAAGTE PIPE

The presence of minor quantities of nickeliferous sulphide in the large, pipe-like body of iron-rich ultramafic pegmatite on the farm Middellaagte at Amandelbult has resulted in some speculative economic interest and de Bruyn (1944) implied a comparison with the nickel-bearing Vlakfontein bodies. Recent interest in the Middellaagte pipe is related to mining activities at Amandelbult, which have been directed primarily at delineating the cumulate succession in the structurally disturbed area adjacent to the pipe. The pipe itself results in a considerable loss of ore reserves of the Merensky Reef.

7.2.1 STRUCTURAL SETTING

The Middellaagte pipe is situated wholly within a major northwest trending graben structure which is aligned parallel to the dominant structural lineament in this area of the Bushveld Complex (figs. 5.1, 7.2). This lineament may well have been active during deposition of the Traansvaal Supergroup, prior to formation of the Bushveld Complex. The Middellaagte graben structure is extrapolated to correlate with the Brits graben in the southern sector of the western lobe of the Bushveld Complex (see fig. 1.1). Preliminary results of an airborne geomagnetic survey completed by J.C.I. seem to corroborate this. The graben-edge faults can be traced to the northwest into the adjacent Transvaal floor rocks. At Thabazimbi this fault trend has swung round until it is aligned approximately north-south. Major east-west faults also occur in the Transvaal rocks at Thabazimbi.

The Middellaagte graben forms a block, approximately 2 km wide, with a maximum downthrow (on the eastern side) of some 600 m. The cumulate sequence in this block is poorly known, and the Merensky Reef is not mined here. The map of Coertze (1962) which shows the layered cumulates delineated within the downfaulted block is incorrect, as the inferred position of the upper critical zone cumulates in the graben is almost completely occupied by the discordant pegmatite body (fig. 7.2). The structural interpretation presented in Maps 3 and 4 (in folder) has been compiled by the author and does not neccessarily agree with the mine plans. The contour plan in Map 4 is based on the UG-2 chromitite layer; this was selected as a marker horizon in preference to the Merensky Reef to avoid the problems of pothole structures.

On the down-dip side of the pipe the Merensky Reef was intersected at a depth of 478 m in borehole ML 22 (see Maps 4 an 5). Borehole ML29 was then positioned to intersect the postulated Merensky Reef to the north of the pipe, assuming an average dip of 21^{o}. This assumption was found to be

incorrect; borehole ML29 in fact intersected a sequence of feldspathic pyroxenites with minor chromitite layers, which probably occur between the MG- and UG- chromitite layers. This structural interpretation was based entirely on faulting and assumed a constant dip of 20^{o}. This is now considered to be incorrect and the most likely explanation is that the layered sequence adjacent to the pipe is downwarped, e.g., in a manner similar to that at the Townlands pipe (see section 7.5). The data available so far, however, are not sufficient to allow a more detailed interpretation.

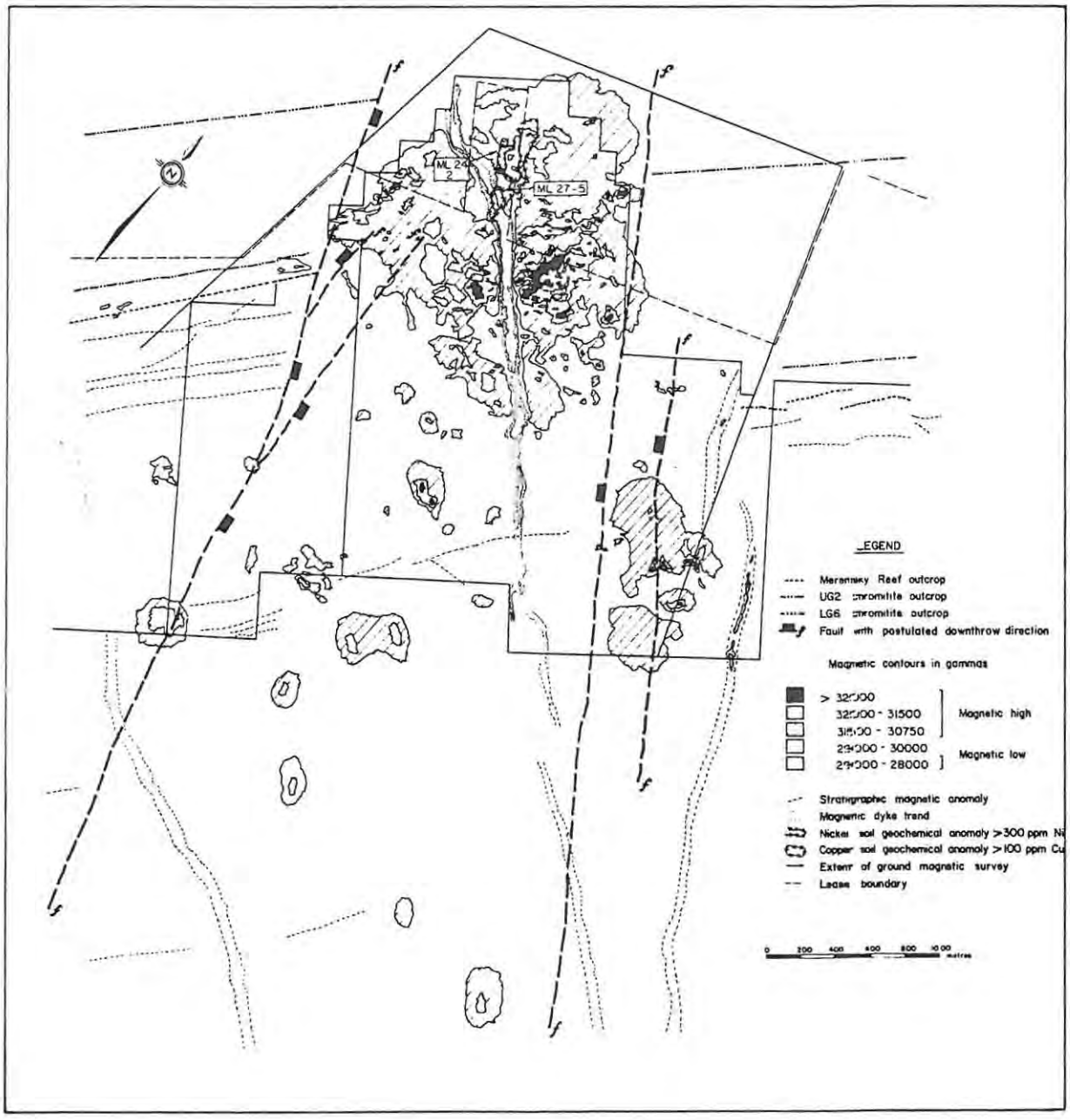

Figure 7.3 Summary map of the surface features of the Middellaagte pipe, R.P.M. Amandelbult.

7.2.2 STRUCTURE OF THE PIPE

INDIRECT TECHNIQUES

The detailed ground geomagnetic survey at Amandelbult discussed above was extended to include the area covered by the Middellaagte pipe (fig. 7.1 and Map 3). The inferred suboutcrop of the pipe corresponds with a major positive magnetic anomaly, which defines an area of some 1.7 x 1.4 km, with maximum values of over 32 000 gamma (the background count is roughly 30 000 gamma). This anomaly forms a composite feature in which magnetic "cores" and "windows" can be observed. The magnetic cores may form poorly-defined ring structures within the composite anomaly. One of these magnetic cores has been drilled (borehole ML 27) and it clearly relates to maximum concentrations of Fe-Ti oxides. A borehole (ML 22) has also been drilled into one of the magnetic windows. In this hole a fairly normal cumulate succession was located with only sporadic, irregular bodies of pegmatite. The composite magnetic anomaly associated with this large body of pegmatite is inferred to relate to a large pipe-like feature with considerable vertical extent (fig. 7.3).

A Ni and Cu soil geochemical survey has been completed by J.C.I in the Middellaagte area (Map 3). A linear Ni anomaly was located over the suboutcrop of the Merensky Reef to the west of the graben structure, but no linear trends were located within the downfaulted block. A strong Cu and moderate Ni anomaly occurs over part of the suboutcrop of the pipe. This area has recently been quarried on a small scale (for roadstone) and the suboutcropping pegmatite may be observed. The Ni and Cu soil anomaly does not correlate with maximum magnetic anomalies but defines a specific, rather small, portion of the evidently composite pipe. Three boreholes (ML24, ML25 and ML26) have been drilled here. Compared to samples from other areas of the pipe the pegmatite in this area is enriched in base-metal sulphides.

SURFACE MAPPING

The area underlain by the pipe is flat and low-lying with a seasonal water-course which flows northwards into the Bierspruit. Vegetation is restricted to grass, low thorn scrub and sparse trees, a distinctive feature, readily recognizable on 1:10 000 aerial photographs. Outcrop is very poor, and borehole data indicate that the depth of weathering varies from 20 to 30

m. The centre of the postulated suboutcrop of the pipe is delineated by a distinctive red soil (Map 3). This soil, which contrasts strongly with the black turf which overlies the critical and main zone cumulates, is characteristic of most of the iron-rich ultramafic pegmatite bodies in the Bushveld Complex. Detailed colour or infrared aerial photographs could well prove useful in this respect. The red soil contains small magnetic grains and pegmatite float. Again, this contrasts with the ubiquitous black turf in which float is rarely observed. At Middellaagte the area covered by this red soil forms an elongated ovoid within a much larger area of brown soil. The brown soil, within which discrete pockets of red soil occur, contains only sparse pegmatite float and is only very weakly magnetic. It is transitional between the red soil, which is related to suboutcropping pegmatite, and the ubiquitous black turf. It probably represents a peripheral area of the pipe in which irregular offshoots of pegmatite, intimately associated with the normal cumulates, occur . The limit of this (brown and red) soil anomaly corresponds roughly with the 30 750 gamma contour of the magnetic anomaly (Map 3).

BOREHOLE DATA

The structural features discussed above were based to a large extent on drilling information. Boreholes drilled recently (numbers ML22 to 29) have been logged and sampled by the author, but core from the earlier holes is no longer available. Cross-sections of the pipe, based on this information, are presented in Map 5. The following conclusions can be drawn regarding the structure of the Middellaagte pipe-like body of iron-rich ultramafic pegmatite :-

(1) It forms a large pipe-like feature in which a central core (or cores) of sub-vertically orientated pegmatite occur(s).
(2) It is strongly discordant and transgresses and truncates the cumulates of the upper critical zone and lower part of the main zone.
(3) It is a composite body in which the pegmatite exhibits different mineralogical features.
(4) The irregular nature of the pipe-like body is enhanced by the preferential development of the pegmatite within certain cumulate horizons. The overall discordant nature is evident, but locally the pegmatite forms stratabound, sheet-like bodies.
(5) Relict layers of unreplaced or partially replaced cumulates are enclosed within the pipe.

7.3 FIELD RELATIONSHIPS - SMALL, IRREGULAR BODIES OF PEGMATITE AT AMANDELBULT

7.3.1 EXTERNAL FORM

The majority of iron-rich ultramafic pegmatite bodies examined at Amandelbult occur as irregular, sheet-like bodies which are constrained within specific cumulate layers. Small, pipe-like, vertically extensive bodies are comparatively rare. The sheet-like bodies form laterally extensive bodies with strike lengths of over 300 m, often with thicknesses of only a few metres. Their down-dip extension is difficult to assess, but they are probably vertically extensive. Irregular, branching bodies radiate from these sheet-like bodies to form exceptionally irregular bodies, varying from sill-like to dyke-like and including wedge-shaped and spheroidal forms. The latter may vary from a few centimetres in size to several metres. These, apparently haphazard, irregular bodies are often interconnected with the larger sheet-like masses by a network of veinlets (possibly only a few millimetres in diameter), veins and feeder channels.

In summary, iron-rich ultramafic pegmatite at Amandelbult may occur as vertically extensive, irregular, pipe-like bodies with diameters of over 1.5 km, as thin, laterally extensive, stratabound, sheet-like bodies or as irregular sills, dykes, wedge-shaped and spheroidal bodies with dimensions of less than one metre.

It is suggested that the small, irregular bodies are related to the larger occurrences by a network of feeder channels. Field relationships do not enable one to establish whether the pipe-like bodies may be interpreted as feeders from which the smaller occurrences have developed, or alternatively whether the small occurrences channelled the pegmatitic liquids into the larger bodies, which thus acted as the loci of accumulation. This has important petrogenetic implications and it is unfortunate that the field relationships are equivocal (see Chapter 13).

7.3.2 RELATIONSHIPS WITH THE WALL ROCKS

The cumulate wallrocks adjacent to large, pipe-like bodies, such as Townlands, and possibly Middellaagte, may form collapse structures (in which the layering is increasingly downwarped as the pipe is approached) similar to that at the Driekop pipe (see pp. 19 and 31). In contrast, the cumulates which host small, irregular pegmatite bodies at Amandelbult are invariably structurally undisturbed, even though these bodies are preferentially concentrated in areas of structural weakness. This is particularly evident

where a pegmatite body selectively replaces a specific cumulate layers, which may be only a few centimetres thick. In this situation *del*icate layering in the adjacent cumulates is unaffected. It is evident from these features that the cumulate layering was well defined prior to formation of iron-rich ultramafic pegmatite, consequently their formation may be related to postcumulus processes. The influence of layering in the cumulate sequence is particularly evident where pegmatite occurs in contact with either chromitite layers or ultramafic cumulates (such as the pseudoreefs). In these situations an apparently sharp contact separates the cumulus and postcumulus rocks. Locally, relict segments of the cumulate which is replaced occur within the pegmatite body, such that the primary layering is preserved.

7.3.3 SELECTIVE "REPLACEMENT" AND DEFINITION OF REPLACEMENT

The preferential replacement of specific cumulate layers by iron-rich ultramafic pegmatite has long been known. Field relationships enabled Wagner (1929) to establish that pegmatite develops preferentially at the expense of the most felsic rocks (i.e. anorthosites and norites). He observed that mafic cumulates such as chromitites and pyroxenites may be unaffected, resulting in large sheet-like bodies. This feature led Wagner to interpret these bodies as replacement features, a conclusion which Cameron and Desborough (1964) supported (see pp. 16-17 and p.24). This constraint is particularly evident at Amandelbult (fig. 7.4). Typically, ultramafic cumulates (i.e. the pseudoreefs, the Merensky hangingwall pyroxenite and chromitite layers) are "unreplaced", whereas the intervening felsic cumulates may be completely "replaced".

"Replaced" is used here to designate a physical feature and does not implicitly infer an origin by in situ replacement or metasomatism.

The refractory nature of the cumulates with respect to replacement by iron-rich ultramafic pegmatite may be expressed sequentially thus :-
chromitites harzburgites pyroxenites norites anorthosites, such that anorthosites readily act as traps for the pegmatitic liquids whereas chromitites behave as relatively impervious barriers.

7.3.4 SMALL, PIPE-LIKE BODIES

A small, pipe-like body of iron-rich ultramafic pegmatite on the farm Elandskuil (at 57E section) has been examined in detail (fig. 7.5). This body is associated with a well-defined magnetic anomaly within an elliptical area. This anomaly corresponds to an area some 50 x 25 m in size in which a

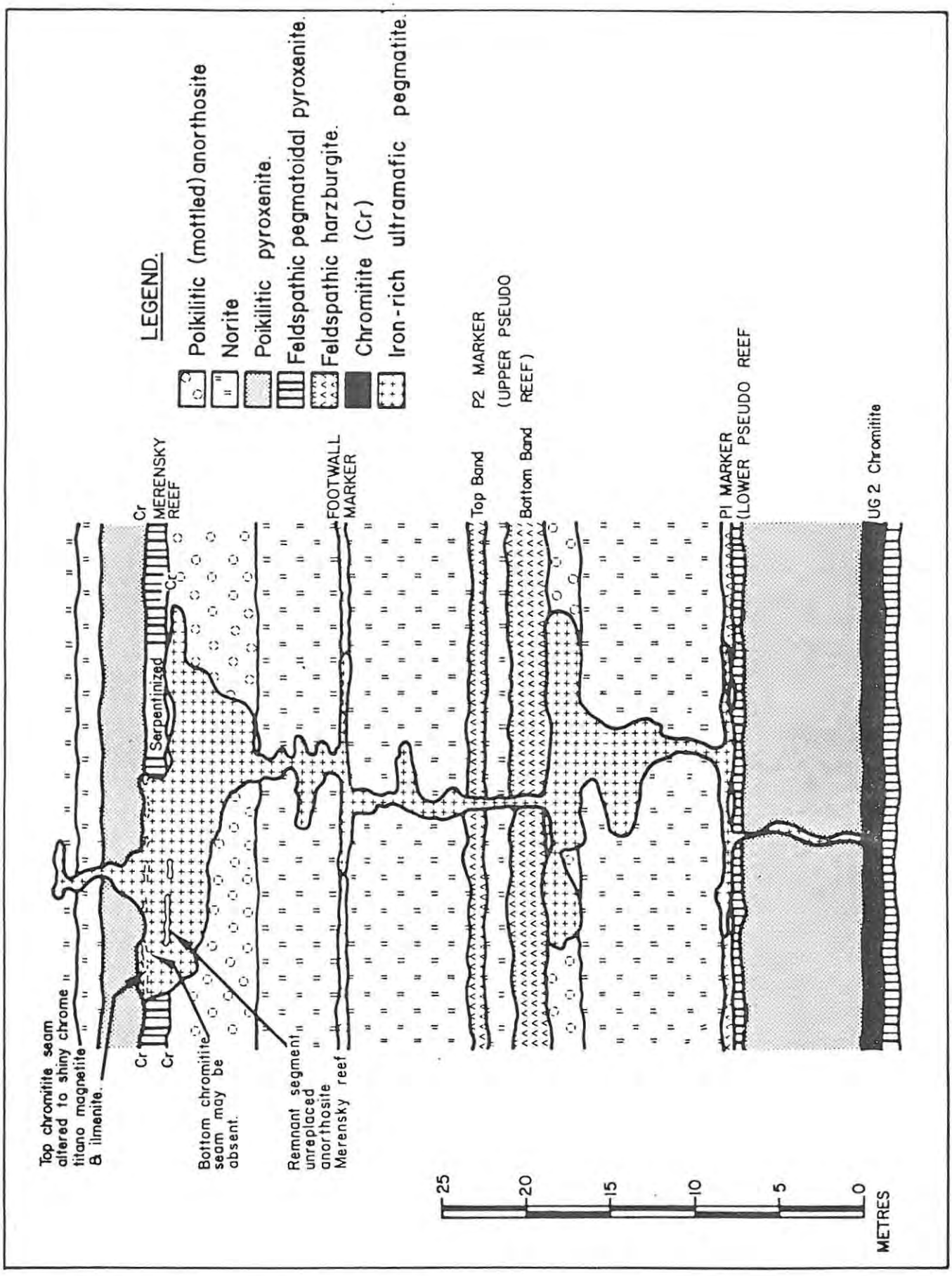

Figure 7.4 Schematic strike section illustrating the vertical distribution of iron-rich ultramafic pegmatite in some of the upper critical zone rocks at R.P.M. Amandelbult (western section of the mine). The selective nature of the pegmatite is particularly evident in the vicinity of the pseudoreefs and the Merensky Reef. Terminology of the pseudoreefs is that used by the mine geologists - plan drawn by M.J. Viljoen (see Viljoen & Scoon, in press).

magnetic "core" (corresponding to the 32 000 gamma contour) some 15 m in diameter is located. Red soil and pegmatite float correlate with this magnetic core. A borehole (number 57E/3), collared approximately in the centre of the area delineated by the magnetic anomaly, intersected a continuous sequence of pegmatite (with minor post-Bushveld dyke material) to a vertical depth of 137 m. Below this position the upper pseudoreef was located. A second borehole (number 57E/2), drilled into the anomaly at a position corresponding to the 31 500 gamma contour, intersected a typical cumulate succession with only very minor pegmatite. Boreholes drilled on the adjacent 56E and 58E section lines also intersected minor pegmatite, in an otherwise typical cumulate sequence. The vertical extent of a small pipe-like feature such as this is not known, but is probably dependent on stratigraphic position, as ultramafic layers such as the pseudoreefs clearly behave as impervious barriers even to these pipe-like bodies. It may be inferred that pipe-like bodies located in the main zone (where ultramafic cumulates are essentially absent) are probably vertically more extensive than those in the upper critical zone.

7.3.5 STRATABOUND, SHEET-LIKE BODIES

The 30W - 25W area of Amandelbult on the farms Schilpadnest and Elandsfontein forms one of the areas of major magnetic disturbance described previously (fig. 7.2). This occurs as a large, composite, magnetic anomaly in which a number of "cores" may be located (fig. 7.6). This contrasts with the well-defined, elliptical and concentric disposition of isomagnetic contours which, it was demonstrated above, correlate with single pipe-like features. Outcrop within this area is limited and only minor red soil could be located as much of the area is covered by mine infrastructure. It corresponds to one of the most structurally disturbed areas at Amandelbult and is characterised by the presence of major faults and post-Bushveld dykes. The cross-section presented in Figure 7.6 is based on borehole logs and surface and underground mapping (see also fig. 7.7). The sheet-like nature of the pegmatite is evident, although the major magnetic anomaly to the south of the cross-section probably corresponds to a pipe-like feature. It is evident here the pegmatite in the main zone forms relatively thick, sheet-like bodies compared to those in the upper critical zone.

Numerous pegmatite bodies have been exposed in the underground development in this area of the mine. A composite plan, compiled from 1:1000 scale mine plans (with additional geological data by the author) in which geological information is plotted on the main levels (as developed up

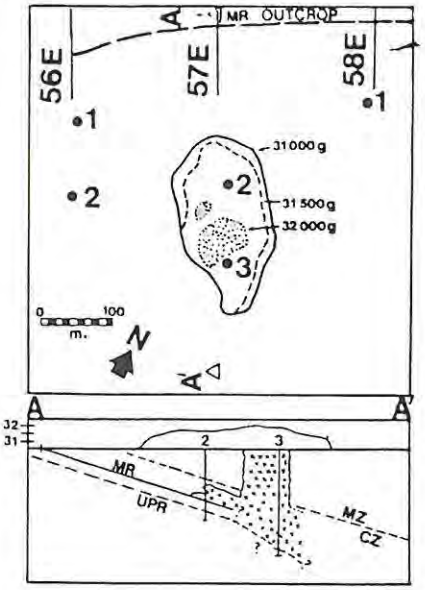

Figure 7.5 Schematic plan (surface) and dip section illustrating the relationship between a well-defined elliptical magnetic anomaly and a pipe-like pegmatite body - in the eastern section of R.P.M. Amandelbult, specifically at 57E section (see fig. 7.2).
ABBREVIATIONS : MR - Merensky Reef; UPR - Upper Pseudoreef B,C (or P2); CZ - critical zone; MZ - main zone; iron-rich ultramafic pegmatite is depicted by crosses and red soil anomaly is depicted by dots. Magnetic contours in gammas (g). Boreholes labelled 56E / nos. 1,2, 57E / nos. 2,3 etc.

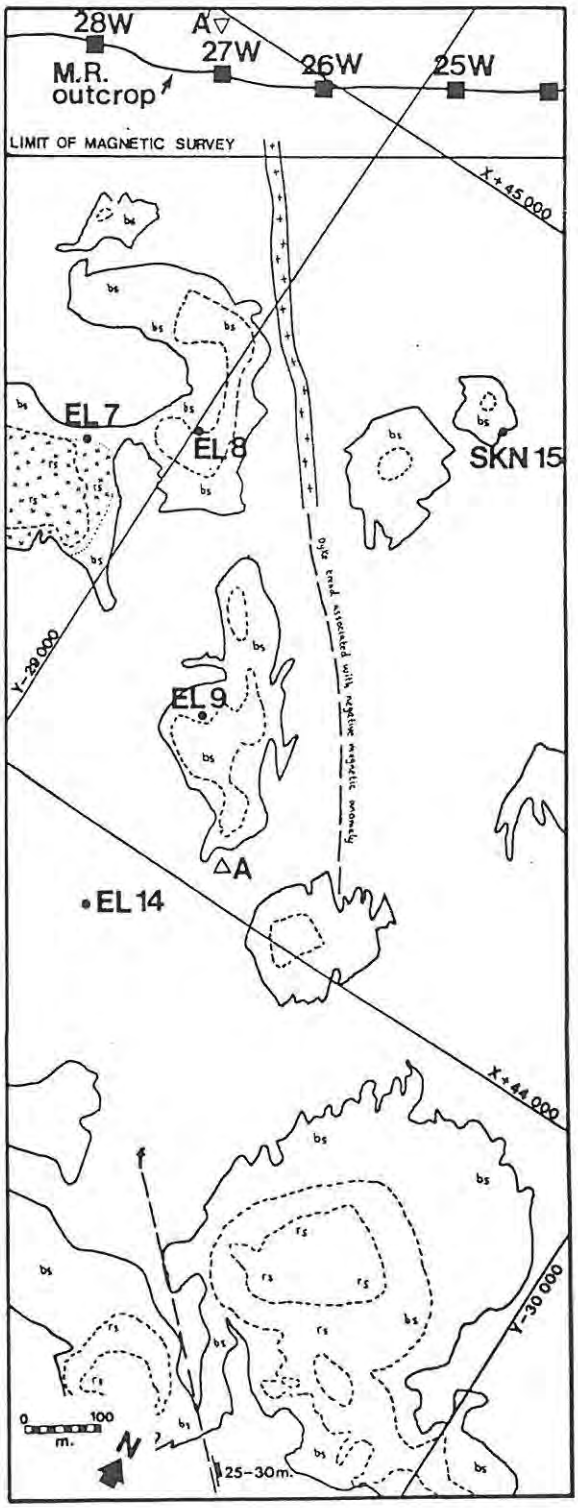

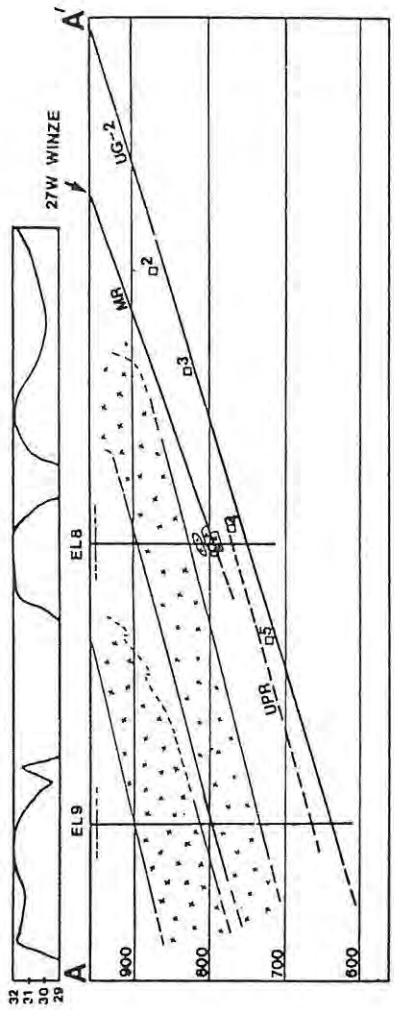

Figure 7.6 Schematic plan (surface) and dip section illustrating the relationship between a cluster of poorly-defined magnetic anomalies and sheet-like pegmatite bodies - in the western section of R.P.M. Amandelbult, specifically 28W - 25W sections (see fig. 7.2 and Map 6).
ABBREVIATIONS : MR - Merensky Reef; UPR - Upper Pseudoreef B,C (or P2); CZ - critical zone; MZ - main zone; iron-rich ultramafic pegmatite is depicted by crosses; red soil anomaly is labelled "rs" and brown soil "bs"; soil not labelled is the typical black turf. Magnetic contours in gammas (g). Boreholes labelled EL (on the farm Elandsfontein) and SKN (on the farm Skilpadnest).

to July 1982) is presented as Map 6. Cumulate markers, such as the upper contact of the upper pseudoreef unit A (or the P1), the the upper pseudoreef B and C (or the P2) and the base of the Merensky Reef, are also included. A laterally extensive, sheet-like pegmatite body, situated between the lower pseudoreef and the Merensky Reef, occurs in this area. On 4-level it is exposed along strike for over 300 m, although its maximum thickness is only between 5 and 6 m. On 3-level this body has pinched out and forms a series of irregular, discontinuous, dyke- and wedge-shaped bodies. At the eastern limit of this body a major wedge-shaped mass cuts up into 2-level, where it transects the upper pseudoreef and has replaced the Merensky footwall anorthosite and the Merensky Reef (not shown in Map 6). The down-dip extent of this body is difficult to assess as the cumulate sequence between the two pseudoreefs is only poorly exposed below 4-level.

A number of specific localities in this area have been examined and sampled in detail (see Appendix 1). Two of these are illustrated in Figure 7.7 (case-studies (2) and (3)). Case-study (2) is based on a well exposed section through the sheet-like body described above, in 5 level 27W crosscut. The sheet-like, yet transgressive form of this body, the upper contact of which is clearly constrained by the Merensky Reef and/or the Merensky pyroxenite, is illustrated in Figure 7.7. This body selectively replaces felsic cumulates in the Footwall cyclic unit.

Even more selective replacement is illustrated by case-study (3); here the felsic cumulates comprising the P2 middling anorthosite are replaced, whereas the adjacent harzburgitic layers are apparently unaffected (see figs. 7.7, 7.8C and Appendix 1). A well defined layer of mottled anorthosite (or leucotroctolite - see p. 87) occurs towards the base of the P2 middling anorthosite (fig. 7.8A); this may occur as a relict, unreplaced layer as the cumulates above and below are more readily replaced (fig. 7.8C,D).

The refractory nature of harzburgitic cumulates is also illustrated at a number of other localities. Pegmatite may occur in the immediate footwall of the upper pseudoreef unit B. The contact between the pegmatite and the harzburgite is sharp, whereas the lateral contact of the pegmatite body against an anorthosite is irregular (see case-study (4), Appendix 1). A fault truncates both the cumulate sequence and the pegmatite body at this particular exposure.

Pegmatite bodies also occur in the immediate hangingwall of harzburgitic layers, such as the upper pseudoreef unit A. Again, the contact between the pegmatite and harzburgite is sharp and is stratigraphically constrained (see case-study (5), Appendix 1). At this same stratigraphic position, but at a different locality (3 level, 7E section) a number of irregular, discontinuous

Figure 7.7

GEOLOGICAL PL

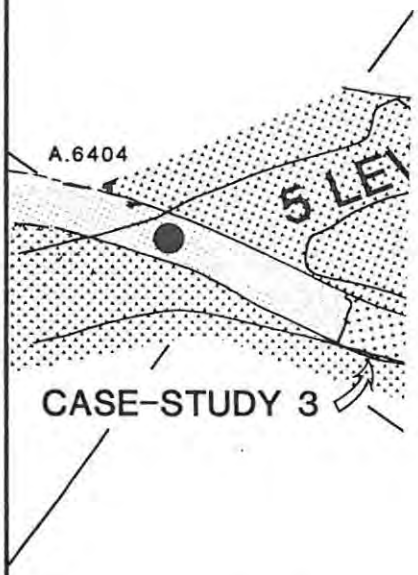

1 : 200

0 5 10 15

metres

LEGEN

- Iron-rich Ultra
- Partially repla
- Merensky Ree
- Felsic Cumula
- Upper Pseudc
- Cr — Merensky Up Layer
- Survey Pegs
- A.7115

Based on 1:200 mine plan of 5 reef raise. Geology and draug

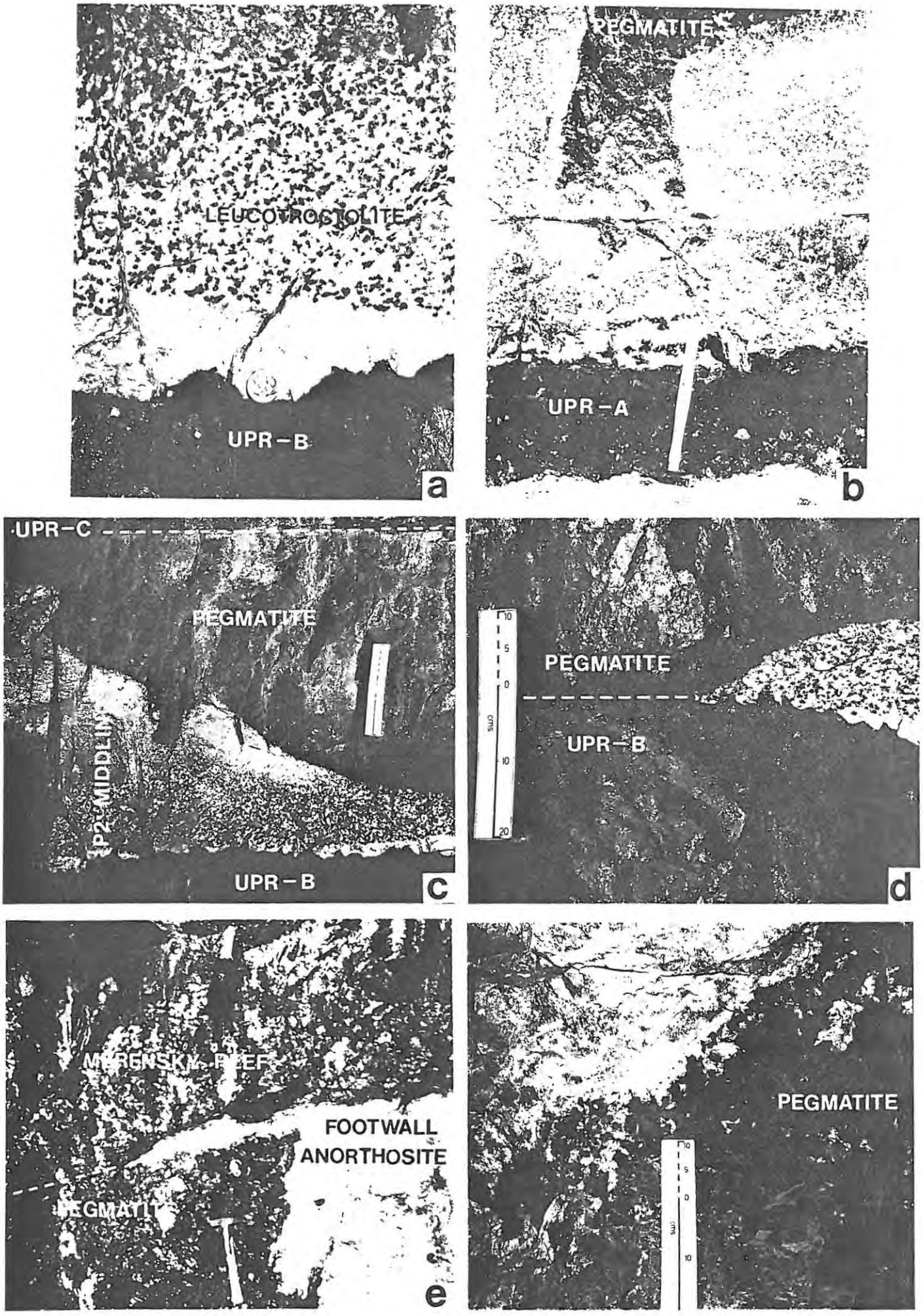

FIGURE 7.8 FIELD RELATIONSHIPS EXHIBITED BY IRON-RICH ULTRAMAFIC PEGMATITE BODIES AT AMANDELBULT

bodies of pegmatite are exposed along a strike section of several hundred metres. They occur as dyke-like or wedge-shaped masses which project down from the roof of the development drive. They may be abruptly truncated within the mottled anorthosites or they may project onto the upper contact of the harzburgite (fig. 7.8B; see case-study (6), Appendix 1). Downward migration of the pegmatitic liquids is suggested. Again, a harzburgite layer acted as an impervious barrier, whilst the anorthosite trapped or reacted with the pegmatitic liquids.

7.4 THE "REPLACED" MERENSKY REEF

The Merensky Reef at Amandelbult is commonly replaced by iron-rich ultramafic pegmatite, resulting in the so-called "replaced Reef". In contrast, the Merensky hangingwall pyroxenite is only rarely replaced. This has considerable significance, as the hangingwall contact of an iron-rich ultramafic pegmatite body which occupies space normally characterised by the Merensky Reef, is almost always (at Amandelbult) stratigraphically constrained. Replaced Reef is thus overlain by the Merensky upper chromitite layer (which is typically partially replaced to a hybrid Cr-rich Fe-Ti oxide layer - see Chapter 10) and the Merensky hangingwall pyroxenite (which is not normally replaced). In contrast, the Merensky lower chromitite layer and the Merensky footwall anorthosite are normally replaced in conjunction with the Reef (fig. 7.9). In this situation the lower chromitite may be absent (and

---

CAPTION FOR FIGURE 7.8

a. The base of the P2 middling, illustrating the dimpled upper contact of the upper pseudoreef B (or lower band of the P2 marker), the layer of plagioclase and the well-defined layer of mottled anorthosite / leucotroctolite (the dark mottles are olivine - see also fig. 5.5A). Locality is 5 level / 27W haulage, south sidewall.

b. Tip of an irregular, dyke-like body of iron-rich ultramafic pegmatite replacing leuconorites above the upper pseudoreef A (or P1 marker). Note diffuse, irregular lower contact of pegmatite body (indicative of replacement). Field relationships at this locality infer that the pegmatitic liquids moved downwards (see also case-study (6), Appendix 1). Locality is 3 level / 7E haulage, south sidewall.

c, d. Selective replacement of the P2 middling. The leuconorite / spotted anorthosite at the top of this felsic layer is replaced in preference to the leucotroctolite layer at the base (compare with "a"); both are replaced in preference to the adjacent harzburgite layers, comprising the upper pseudoreefs B and C. The contact between the pegmatite and the harzburgite is difficult to see (as both rock types are black); however, in the field it is sharp and conforms to the primary layering (see also case-study (3), Appendix 1). Locality is 5 level / 27W crosscut, west sidewall.

e. Selective replacement of the Merensky footwall anorthosite. In this exposure the Merensky Reef is not replaced, and the lensoid bodies of relict anorthosite occur below the lower chromitite layer (see also fig. 7.9). Locality 5 level / 27W raise, east sidewall.

f. Irregular and diffuse contact of an iron-rich ultramafic pegmatite body that has replaced leuconorites in the Pseudo macro unit. Locality 3 level / 7E haulage, south sidewall.

has presumably been completely resorbed), or is observed as either partially resorbed relict rafts (which are in situ) or as (displaced) xenoliths. These latter always occur above their original position, indicating that some upward transportation has occurred. Relict pod-shaped bodies of anorthosite may be observed immediately below relict rafts of the lower chromitite. These probably reflect the refractory nature of the chromitite, such that the pegmatitic liquids have been channelled away from these sites into places where they can readily pass through the lower chromitite. In contrast, the upper chromitite layer and the hangingwall pyroxenite provide an effective barrier to the upward migrating pegmatitic liquids. The reason why the Merensky Reef is replaced in preference to the hangingwall pyroxenite may possibly be explained by the pegmatoidal texture of the former.

Because the upper chromitite and the hangingwall pyroxenite are not replaced the replaced Reef can usually be delineated. Stoping can then proceed as normal (if the grade is adequate) by assuming a typical Reef thickness (as if both the footwall anorthosite and the Reef are completely replaced the footwall contact is difficult to recognize). In normal Merensky Reef the hangingwall cut is usually made 10 to 20 cm above the upper chromitite to include the base-metal sulphides concentrated at the base of the hangingwall pyroxenite. In replaced Reef it has been found that the PGE are concentrated in the upper chromitite layer, and possibly at the base of the hangingwall pyroxenite, such that the overall grade may be approximately the same (see Chapter 11).

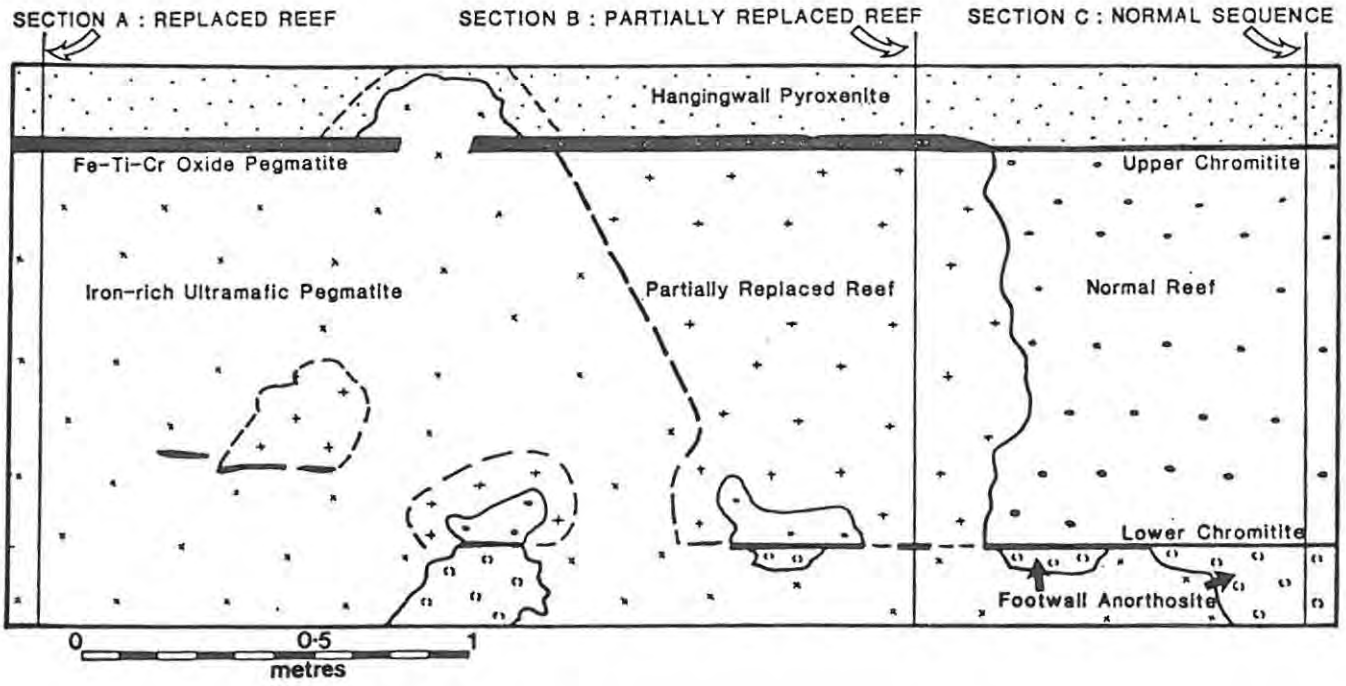

Figure 7.9 Schematic strike section illustrating the relationship between the Merensky Reef and iron-rich ultramafic pegmatite (see also fig. 7.8E).

7.5 IRON-RICH ULTRAMAFIC BODIES AT OTHER LOCALITIES IN THE BUSHVELD COMPLEX

The distribution of iron-rich ultramafic pegmatite bodies in the layered sequence of the Bushveld Complex was discussed in Chapter 2 (pp. 16-20). Some of these have been investigated and sampled during the course of this study (for details of sampling see Appendix 2).

PEGMATITE IN THE MAIN ZONE AT AMANDELBULT AND UNION SECTIONS

Borehole ML22, which was drilled in the graben block adjacent to the Middellaagte pipe intersected a number of small pegmatite bodies in the lower part of the main zone. These probably represent minor offshoots from the Middellaagte pipe. Three separate bodies were examined, body A approximately 300 m above the Merensky Reef, body B approximately 255 m above the Merensky Reef and body C which replaces part of the Bastard cyclic unit.

At Union Section a number of iron-rich ultramafic and mafic pegmatites have been investigated from the main zone in borehole SK-2 by Mitchell (in prep.). These form small, probably pod-like masses, and provide a sequence of samples through a large part of the main zone.

IRON-RICH ULTRAMAFIC PEGMATITE BODIES FROM THE RUSTENBURG AREA

Large, pipe-like bodies of iron-rich ultramafic pegmatite are particularly abundant in the Rustenburg or southern sector of the western Bushveld Complex (see pp. 18-20 and fig. 2.7). The salient features of the TOWNLANDS PIPE were described previously (p.19). The following points are of interest:

(1) Computer modelling of a combined ground magnetics and gravity survey indicate that the Townlands body forms a subvertical, pipe-like feature with a vertical extent estimated at 500 m (Viljoen et al., 1983).

(2) The pipe is emplaced within a zone of structural weakness, marked by NW trending faults and post-Bushveld dykes.

(3) The layered cumulates adjacent to the pipe are structurally disturbed, and form a downwarped structure ; the dip of the cumulates changes from 10^{o} to the northwest to approximately 20^{o} to the southeast. This is the only iron-rich ultramafic pegmatite body at which this structural downwarping has been indisputably proved.

(4) A borehole drilled into the approximate core of the pipe (TLP-1) to a depth of 269.6 m intersected the UG-2 chromitite layer at a depth of 262.7 - 263 m. This is the only recognizable cumulate horizon within the body, although partially replaced (cumulate) feldspathic pyroxenite occurs above the chromitite. Cryptic mineralogical and chemical changes may occur within

the chromitite (Viljoen et al., 1983). Viljoen et al. report that the UG-2 was intersected in the pipe roughly 20 m above its inferred position, which they attribute to doming within the pipe. This is considered to be unlikely by the author and, as the UG-2 occurs above its inferred position (this is exaggerated by the downwarping) it is possible to interpret this chromitite body as either a displaced, partially metasomatised raft, or as a xenolith.

The **BRAKSPRUIT PIPE**, situated at the eastern limit of R.P.M. Rustenburg Section, also cuts upper critical and lower main zone cumulates (fig. 2.7). This occurrence also correlates with a large magnetic anomaly but, unlike the Townlands pipe, it has not been investigated in detail. A number of Fe-Ti oxide pegmatite "cores" have been located within the main body. The western edge of the pipe is exposed in underground development at the Brakspruit shaft. This pipe forms a strongly discordant feature, the contacts of which are sharp and regular. Layering within the wallrocks is undisturbed, but plagioclase in adjacent anorthosites and norites is saussuritised.

Small, typically irregular bodies of iron-rich ultramafic pegmatite are abundant in the vicinity of the Brakspruit pipe. From a cursory examination it is concluded that they are comparable with the pegmatites at Amandelbult. It is also of interest that replaced Merensky Reef is common in this area of the Rustenburg mine. In 16 level haulage (west) a dyke-like body of pegmatite, 1 to 2 m in width, can be observed cutting the Boulder Bed marker. In 17 level haulage (west) an irregular, dyke-like body of pegmatite occurs in which small, core-like pods of very dark coloured pegmatite (composed essentially of olivine and clinopyroxene) are enclosed by an outer shell of pegmatite in which coarse-grained plagioclase is evident. In an exposure of replaced Reef, cross-cutting bodies of pegmatite can readily be observed, unlike the stratabound bodies typical of Amandelbult. The Merensky hangingwall pyroxenite may be replaced in preference to both the Reef and the footwall anorthosite at Brakspruit.

The **BOSCHKOPPIE PIPES** form a composite series of iron-rich ultramafic pegmatite bodies which occur to the west of Rustenburg (fig. 2.7). They crop out over an area of several square kilometres. Preliminary studies indicate that this occurrence can be classified within my definition of iron-rich ultramafic pegmatite, but the size and structural complexity of this occurrence warrant a detailed study.

CHAPTER 8 MINERALOGY AND PETROGRAPHY OF SILICATE-RICH PEGMATITE

The basis of selecting the name "iron-rich ultramafic pegmatite" was discussed in Chapter 2 (p. 8). Two subgroups of iron-rich ultramafic pegmatite are recognized - silicate-rich pegmatite and Fe-Ti-(Cr) oxide pegmatite. This chapter describes the mineralogy and petrography of silicate-rich (typical) pegmatite, in which Fe-Ti oxides are subordinate to the silicate constituents. This is essentially a descriptive study; the chemistry of the principal pegmatite minerals is discussed in Chapters 9-11. Specific lithologies within the generic group "iron-rich ultramafic pegmatite" can be distinguished, and may be described using accepted plutonic nomenclature; a classification scheme based on the CIPW norm is presented in the final section of this chapter. A separate section in this chapter describes the mineralogy and petrography of contact assemblages observed at Amandelbult.

8.1 INTRODUCTION

An introduction to the mineralogy of these rocks was presented in Chapter 2 (pp. 22-24). To recap, they are characterised by a rather simple mineralogy in which iron-rich olivine and clinopyroxene with subordinate Fe-Ti-(Cr) oxides are the major constituents and base-metal sulphides are common accessory constituents. Most pegmatite varieties at Amandelbult comprise olivine clinopyroxenites and wehrlites; pure clinopyroxenite and dunite varieties are less common. The proportion of Fe-Ti-(Cr) oxide is usually between 10 and 20 modal percent (see section 8.5).

This superficially simple mineralogy is a characteristic that may not readily be reconciled with the name "pegmatite". Comparison with "simple" granitic pegmatites, in which quartz, feldspar and mica are the dominant constituents may, however, be applicable. Individual bodies of iron-rich ultramafic pegmatite are usually characterised by a large variation in the modal proportion of the three main constituents, namely olivine, clinopyroxene and Fe-Ti oxide. Modal variation is complicated by the presence of mineralogical zonation within individual bodies and is accompanied by extreme textural variations, particularly in grain size. These features are commonly exhibited by granitic or felsic pegmatites (for example, coarse-grained "simple" quartz-feldspar pegmatite is often associated with exceptionally fine-grained aplite). According to the definition proposed by Jahns these are characteristic features of pegmatites

(see p. 8).

An origin by in situ magmatic or metasomatic replacement is preferred for iron-rich ultramafic pegmatite in the Bushveld Complex by most previous workers (see p. 24). From field relationships it is evident that some replacement of the cumulate hosts has occurred (e.g., contact features). This presents a problem with distinguishing between iron-rich ultramafic pegmatite sensu stricto and hybrid pegmatite-cumulate rocks that represent partial replacement of pre-existing cumulates. In the latter, both pegmatite (or postcumulus) and cumulate-derived (cumulus and intercumulus) minerals may be recognized. Consequently, the mineralogy of pegmatite from contact zones is described separately.

8.2 IRON-RICH ULTRAMAFIC PEGMATITE sensu stricto

In hand-specimen iron-rich ultramafic pegmatite is readily recognized by its dark colour, coarse granular texture and exceptionally high specific gravity (usually in excess of 4). The dark colour of these rocks is particularly evident where they cut felsic cumulates (fig. 7.8). In fresh samples olivine and clinopyroxene are observed as dark-coloured minerals (an indication of their iron-rich composition). Olivine is usually a dark grey or dull black colour, whereas clinopyroxene is much darker and has a submetallic lustre. In coarse-grained pegmatite clinopyroxene is observed as large, tabular crystals, typically with lengths of 1 to 3 cm, but crystals in excess of 10 cm are not uncommon. Olivine is usually observed as anhedral, sometimes poikilitic grains, which are interstitial to the clinopyroxene; it may form a very fine-grained ("aplitic") matrix. Ilmenite may be observed as subhedral crystals with a silver-grey colour and a characteristic metallic lustre. They typically occur as small (1 to 5 mm) grains, or in large, aggregates intergrown with a dark-coloured (purplish-grey or black) spinel. Large, composite aggregates of Fe-Ti-(Cr) oxides often have dimensions in excess of 20 cm.

Disseminated sulphides are a common accessory constituent of most pegmatite assemblages examined in this study. Amphibole and mica are minor accessory constituents. In large clinopyroxene crystals amphibole may be observed as irregular bleb-like bodies along cleavage planes. Orthopyroxene and plagioclase occur as a minor constituent of some pegmatite varieties. Plagioclase is usually observed as large, anhedral grains or composite aggregates, often with dimensions in excess of 2 cm. A characteristic feature of plagioclase in these rocks is its distinctive green colour; it may also be unusually soft. These features are attributed to saussuritisation.

It will be demonstrated later that plagioclase and orthopyroxene are not pegmatitic minerals as such but are relict cumulus minerals.

In cut borehole core (which takes a partial polish) the mineralogy of these rocks may be more readily studied. Clinopyroxene is observed here as large, tabular crystals and medium- to fine-grained xenomorphic aggregates, which are medium grey in colour and have the distinctive schiller texture, characteristic of the variety diallage. Olivine is observed as a greenish-grey phase, which is usually anhedral and is cut by innumerable hairline cracks. Extreme variation in grain size may be evident even in a 15 cm length of core.

8.2.1 MICROSTRUCTURES AND MICROTEXTURES OF THE SILICATE MINERALS

These may be subdivided into three main groups, principal phases (clinopyroxene and olivine), accessory phases (Fe-Ti-(Cr) oxides, amphiboles, micas and base-metal sulphides) and relict cumulus minerals (plagioclase and orthopyroxene).

PRINCIPAL PHASES - (1) CLINOPYROXENE

In pegmatites in the upper critical zone clinopyroxene is the variety augite; it may be gradational into ferroaugite in pegmatites in the main zone (see Chapter 9). It occurs in three main habits, as large, subhedral grains, as medium-sized, anhedral grains (that exhibit extensive mutual interference) and as medium to small, polygonal grains (figs. 8.1A,B and 8.2A,B). Clinopyroxene grains in these rocks are usually colourless in thin section, but may be slightly pleochroic in shades of brown, and often exhibit a well developed parting parallel to (100), a characteristic of the variety diallage. Zoning is occasionally observed in large, subhedral grains. It is absent in the medium or small grains.

Exsolution lamellae of Ca-poor pyroxene in clinopyroxene may comprise orthopyroxene, inverted pigeonite or uninverted pigeonite. In cumulus clinopyroxene from the Bushveld Complex Wager and Brown (1968) recognized both orthopyroxene and inverted pigeonite lamellae in augite from the main zone, and uninverted pigeonite lamellae in ferroaugite from the upper zone. Extremely iron-rich ferroaugites show complex exsolution products which are not discussed here. Orthopyroxene lamellae are usually exsolved parallel to (100), whereas pigeonite is exsolved parallel to the (001) plane in an augite host. However, Robinson et al. (1971) found a relationship between lamellar orientation and the stage at which lamellar nucleation occurred. They

suggest that the lamellar angles may be used to elucidate pressure-temperature regimes. In this study, however, it is assumed that exsolution lamellae are orientated roughly along major crystallographic axes.

Clinopyroxene from iron-rich ultramafic pegmatite at Amandelbult exhibits three forms of exsolved lamellae of Ca-poor pyroxene. Only two of these are common. The first of these, which is also typical of cumulus clinopyroxene in the main zone of the Bushveld Complex (Wager & Brown, 1968; Buchanan, 1979) are observed as very fine, closely-spaced, elongated lamellae orientated parallel to (100). They probably form parallel-sided continuous sheets. A second set of lamellae, usually finer than the first, parallel to (001), may also occur. If both sets of these lamellae are well formed a characteristic trellis-like texture is observed. Both sets of lamellae are optically similar and are probably orthopyroxene. In the very large, subhedral grains this exsolution texture is unusually well-developed, as compared to the equivalent texture found in cumulus clinopyroxenes. Occasionally, small bleb-like bodies of orthopyroxene may be associated with this sheet- or trellis-like exsolution (fig. 8.1C,D).

The second type of exsolution consists of exceptionally fine-grained, also closely-spaced, elongate lamellae of Ca-poor pyroxene (possibly orthopyroxene) that are orientated parallel to (100) only. Lamellae at right angles to these have not been observed. They are often associated with exsolved lamellae of an opaque Fe-Ti oxide. This exsolution feature is much finer-grained than those resulting in the trellis-like structure. These two varieties appear to be mutually exclusive.

The third type of exsolution is only occasionally observed in pegmatite at Amandelbult, but is ubiquitous in clinopyroxene from the satellite bodies at Driekop (see p. 39). Here, the Ca-poor pyroxene (also probably orthopyroxene) forms coarse, plate-like bodies orientated parallel to (100) and (001) that may themselves contain an exsolved phase (possibly augite). Sections which are cut at low angles to either the (100) or (001) plane illustrate a chequerboard-like extinction.

Orientated intergrowths of an opaque Fe-Ti oxide are extremely common; they may be interpreted as exsolution lamellae or as a replacement phenomenon related to deuteric events (see below). They occur in two main forms, as tiny, rod- or plate-like lamellae (up to 3 sets) and as small granular bodies (fig. 8.1A,E). These latter often occur in close proximity to the lamellae and may form a ring-like feature in large clinopyroxene grains (fig. 8.1A). Most of these lamellae are too thin to analyse on the electron microprobe, but from optical studies under reflected light it is evident that the coarser lamellae are mostly ilmenite.

Two types of twinning are present, simple and polysynthetic. Simple twins, with (100) as the twin plane, are occasionally observed in large, subhedral grains (fig. 8.2A), whereas polysynthetic twins, with either (100) or possibly (001) as the twin plane, are a ubiquitous feature of polygonal clinopyroxene grains. These latter may be observed as very thin, parallel stripe-like or broad lath-like features which resemble albite twinning in plagioclase (figs. 8.2B, 8.6C). If a grain exhibits both well developed exsolution lamellae (of Ca-poor pyroxene or Fe-Ti oxide) and polysynthetic twinning a herringbone structure may be observed (fig. 8.1F).

Partial amphibolisation is an ubiquitous feature of many of the pegmatitic clinopyroxenes. Brown amphibole, a member of the hornblende group, occurs as irregular blebs and laths, usually along cleavage traces. Textural evidence suggests that this is a replacement feature of both large, subhedral and anhedral grains. Most of the small, polygonal grains that demonstrate well formed polysynthetic twinning are comparatively free of amphibole (compare figs. 8.1B, 8.2A with 8.2B)

(2) OLIVINE

Olivine, which in iron-rich ultramafic pegmatite from the upper critical zone is the variety hortonolite (see Chapter 9), usually occurs in anhedral grains, although polygonal grains exhibiting a foam-like texture may also occur. These occur in a range of grain sizes varying from tiny polygonal grains to coarse, granular aggregates (figs. 8.2C-F and 8.3). The large, anhedral grains commonly demonstrate undulatory extinction; this is a common feature of cumulus olivines in layered intrusions. Large, anhedral grains often contain minute, orientated intergrowths of an opaque phase (see p. 34). Olivine in these rocks is almost always fresh and unaltered, although in contact zones or adjacent to relict plagioclase grains it may be altered to a red-brown serpentine. Secondary, pale-green amphiboles and magnesite have occasionally been observed replacing olivine. The fresh nature of the pegmatitic olivine may be contrasted with cumulus olivine in the upper critical zone which is usually serpentinised.

ACCESSORY PHASES - (1) Fe-Ti-(Cr) OXIDES

Fe-Ti-(Cr) oxides are a ubiquitous accessory constituent of iron-rich ultramafic pegmatite at Amandelbult. Microstructures exhibited by these phases, which comprise ilmenite and Fe-Ti-(Cr) spinel, are described in Chapter 10; this section describes the textural relationships between oxides and silicates. Individual grains of ilmenite may show good crystal form, and

textural evidence suggests that they may have crystallized in available sites, interstitially to clinopyroxene, but possibly concomitantly with olivine. By contrast, composite spinel grains occur interstitially to both olivine and clinopyroxene (figs. 8.3 and 8.4). Composite oxide aggregates may form extensive poikilitic grains which enclose a number of clinopyroxene grains, and less commonly olivine grains. Oxide grains or composite aggregates may be moulded around clinopyroxene which retains its primary habit (fig. 8.4F), or they may exhibit scalloped (replacement ?) contacts (fig. 8.4D,E). Replacement of both olivine and clinopyroxene by spinel is evident. Arrested stages of this replacement process result in the preservation of discrete oxide grains and tongue-like bodies that penetrate the silicate grains (fig. 8.4C).

They may also form complex silicate-oxide symplectites, although these are not common in pegmatite samples from the upper critical zone. Olivine-oxide symplectites are the most abundant, although pyroxene-oxide and plagioclase-oxide symplectites have also been observed. In olivine symplectites, orthopyroxene (hypersthene) is commonly developed as a contact feature between the oxide and host olivine (fig. 8.4A,B,C). Symplectites observed in these rocks almost always occur adjacent to discrete oxide grains.

(2) AMPHIBOLES AND MICAS

Amphibole, usually a member of the hornblende group (see Chapter 9), is found in iron-rich ultramafic pegmatite in three main habits. These are as follows : (1) irregular lath-like grains which replace clinopyroxene grains, in a process that may be described as amphibolisation; (2) coronas; and (3) discrete grains. Amphibole coronas occur around silicate and oxide grains where the latter have partially replaced the former (fig. 8.4B,E). Coronas are most common adjacent to irregular oxide layers. Amphibole is only rarely observed to have replaced olivine. Discrete grains of amphibole are usually restricted to either clinopyroxene-rich pegmatite or to contact zones. Mica, essentially biotite (see Chapter 9), is usually only observed as discrete grains or as intergrowths associated with amphibole. Both amphibole and mica are only minor accessory constituents and usually represent less than 1 modal percent.

(3) BASE-METAL SULPHIDES

The mineralogy of base-metal sulphides is discussed in Chapter 11. They are clearly interstitial to the principal silicate phases, but do not exhibit any replacement textures.

RELICT CUMULUS MINERALS - (1) PLAGIOCLASE

In iron-rich ultramafic pegmatite in the upper critical zone, plagioclase occurs as a very minor accessory constituent, and from evidence presented elsewhere (field relationships, mineral chemistry) it is interpreted as a relict cumulus mineral. It is usually observed as small, anhedral, often sliver-like grains which occur interstitially to the pegmatite minerals, or as large, composite aggregates. The latter often have dimensions of over 5 cm and average sizes of between 1 and 3 cm are typical. They may consist of either very large, anhedral grains or fine-grained mosaics. Both show strong strain extinction. The fine-grained mosaics are not twinned, but the large, anhedral grains exhibit coarse albite twinning, with curved and bent twin lamellae which normally wedge out towards grain boundaries (fig. 8.6F). By contrast, cumulus plagioclase in the upper critical zone is usually observed as small, tabular laths with well developed, regular twinning (fig. 8.6A). Consequently, relict grains in pegmatite may readily be distinguished. These textures indicate that plagioclase in the pegmatites has completely recrystallized, either due to strain annealing or as a result of dissolution (see also Spry, 1969, pp.82 and 85).

Relict plagioclase in pegmatite is usually partially replaced by a fine-grained to cryptocrystalline intergrowth, referred to as saussurite (fig. 8.6E). It consists of clinozoisite, epidote and sericite. Saussuritised plagioclase is also characteristic of contact zones. The large, anhedral plagioclase relicts may be almost completely replaced by an intergrowth of saussurite suggesting that alteration occurred after recrystallization. Small, mosaic-like aggregates are rarely saussuritised (fig. 8.6F).

Pegmatitic clinopyroxene, olivine and Fe-Ti oxides may all be observed to have partially replaced relict plagioclase aggregates (fig. 8.6). These may exhibit scalloped replacement fronts (fig. 8.6C). In this situation brown amphibole and mica are often found, either as coronas between the pegmatitic minerals and the plagioclase, or as discrete grains (fig. 8.4E). Olivine in the vicinity of relict plagioclase, where a replacement relationship may be demonstrated, is often altered to a reddish-brown serpentine.

(2) ORTHOPYROXENE

Orthopyroxene is not normally observed here as a pegmatitic mineral, other than as exsolution bodies in clinopyroxene. It occurs as a relict cumulus mineral, that is usually partially replaced by clinopyroxene or olivine.

8.2.3 TEXTURAL FEATURES OF THE PRINCIPAL PEGMATITE ASSEMBLAGES

It is useful to summarise the textural features of iron-rich ultramafic pegmatite in terms of the following mineral assemblages, even though they are mutually gradational : clinopyroxene-rich pegmatite, olivine-rich pegmatite and clinopyroxene-olivine pegmatite. Fe-Ti-(Cr) oxide pegmatite is discussed in Chapter 10.

(1) CLINOPYROXENE-RICH PEGMATITE

Iron-rich ultramafic pegmatite in which clinopyroxene represents over 80 modal percent is common at Amandelbult. In this assemblage clinopyroxene may occur in three habits. In the first of these clinopyroxene occurs as large, subhedral grains that may have maximum dimensions of over 50 mm. These have not suffered extensive post-crystallization modification. They are best preserved in clinopyroxene-olivine pegmatite, where olivine has crystallized interstitially. This variety of clinopyroxene is usually amphibolised and may exhibit poorly developed polysynthetic or simple twinning. Exsolution lamellae of Ca-poor pyroxene and orientated intergrowths of Fe-Ti oxide may also occur (figs. 8.1A and 8.2A). Secondly, clinopyroxene occurs as medium to coarse, anhedral grains that exhibit extensive mutual interference. Exsolution lamellae of Ca-poor pyroxene and orientated intergrowths of Fe-Ti oxide are common. They are commonly moderately amphibolised and may exhibit polysynthetic twinning (fig. 8.1B). Thirdly, clinopyroxene occurs as small- to medium-sized, polygonal grains which exhibit sharp, regular contacts. Polysynthetic twinning (usually as broad, regular laths) is ubiquitous to this variety. They are usually fresh, with only minor amphibole, and only occasionally exhibit exsolution lamellae and orientated intergrowths (fig. 8.2B).

The first variety of clinopyroxene is interpreted as representing primary grains that formed during conditions that promoted the development of large, euhedral crystals. They are gradational into the second habit as a result of continued nucleation, such that individual grain growth was arrested by mutual interference. This results in a xenomophic texture. The third variety of clinopyroxene is interpreted as an annealing feature (see below).

(2) OLIVINE-RICH PEGMATITE

Olivine-rich pegmatite is not as common as clinopyroxene-rich pegmatite at Amandelbult, although it is the dominant assemblage in the Townlands pipe. Typically, both habits of olivine, large anhedral grains and small, polygonal

grains (see above), may be observed in one thin section. Similar textures occur in olivine-rich cumulates in the upper critical zone at Amandelbult and in the magnesian dunite at Driekop (see pp. 33-34 and 84-86). It may be described as a xenomorphic or polygonal granular texture, depending on which habit predominates. The fine-grained olivine is interpreted as an annealing feature.

(3) CLINOPYROXENE-OLIVINE PEGMATITE

Divergence from monomineralic to more complex assemblages influences the textural habit of olivine and clinopyroxene, and in particular inhibits development of mutual interference textures. Clinopyroxene-olivine (wehrlite or olivine clinopyroxenite) pegmatite is characterised by seriate variation in grain size. Olivine-clinopyroxene pegmatite in which olivine is distinctly subordinate to clinopyroxene exhibits a hypautomorphic texture. Olivine is observed as anhedral, often elongate grains which are interstitial to large, subhedral clinopyroxene grains (fig. 8.3A). The latter may demonstrate extensive mutual interference and polygonisation. Olivine grains are often moulded around clinopyroxene grains. Sharp contacts may be preserved and the latter retains its primary form - olivine is clearly later than clinopyroxene in this assemblage (fig. 8.2A). If olivine is of equal abundance to clinopyroxene this texture becomes xenomorphic granular. Again, olivine occurs as elongate, anhedral grains, but here they form coarse aggregates which may partially, or completely enclose aggregates of clinopyroxene (fig. 8.3B). Contacts between olivine-rich and clinopyroxene-rich aggregates may be either sharp (specifically where polygonal grains are in contact) or gradational. In this assemblage these two minerals demonstrate a disequilibrium relationship - olivine is evidently later than, and may replace clinopyroxene (see also Cameron & Desborough, 1964).

The first stage in this replacement process results in the presence of small, anhedral grains of olivine (often with maximum dimensions of less than 1 mm) orientated along cleavage traces in clinopyroxene. Secondly, olivine occurs as anhedral grains which cut across both cleavage traces and exsolution lamellae. Eventually this may result in the formation of coarse, tongue-like masses, often of optically continous grains, that penetrate the large clinopyroxene grains. The contact between these olivine tongues and the primary clinopyroxene grains usually exhibits a scalloped, very irregular "replacement front" (fig. 8.2D). It is deduced that replacement is originally controlled by crystallographic features (e.g., grain margins, cleavage traces), but soon becomes of a pervasive nature. These tongue-like features are usually observed connecting with the large, anhedral aggregates of

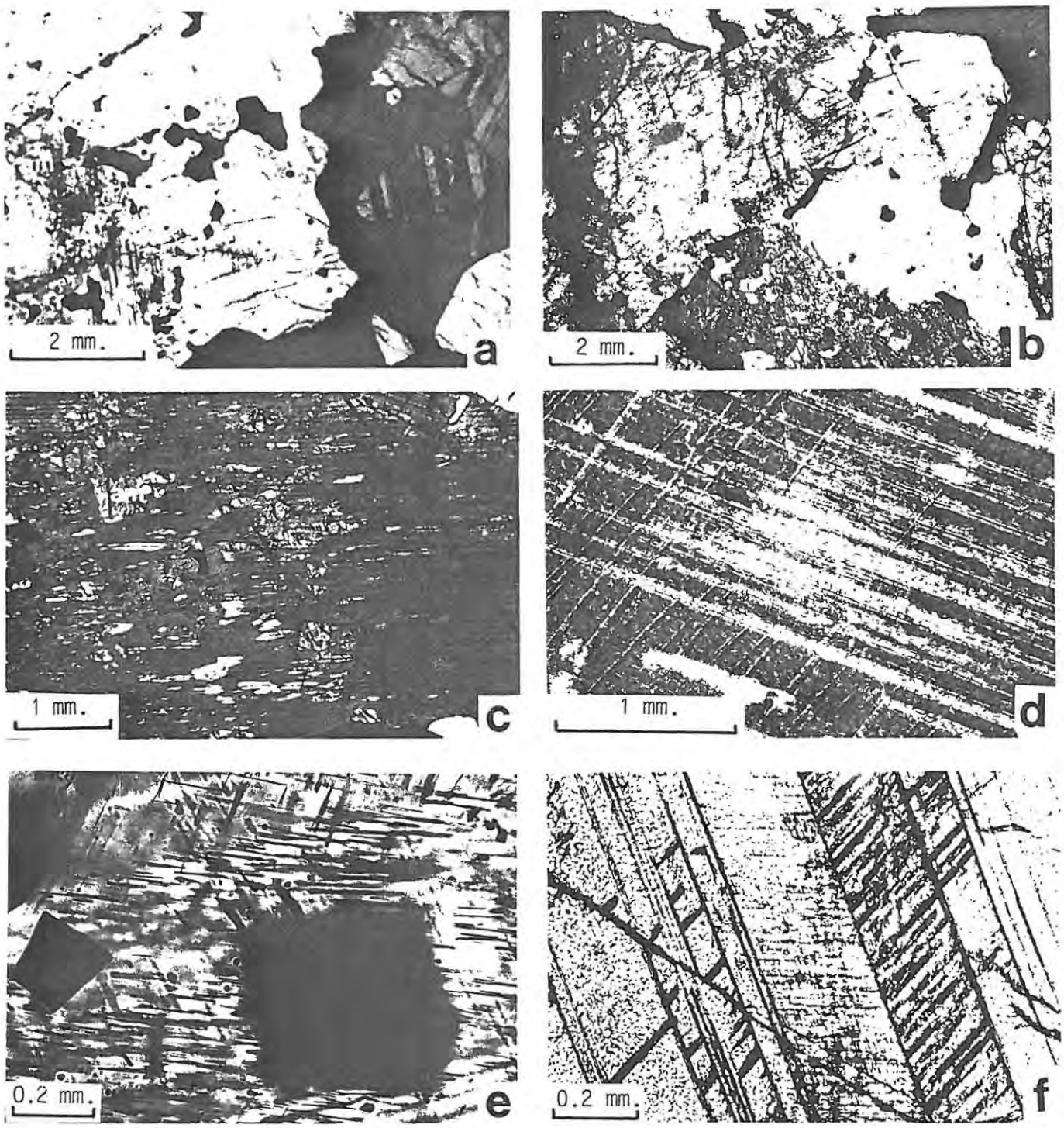

FIGURE 8.1 MICROSTRUCTURES EXHIBITED BY PEGMATITIC CLINOPYROXENES

a. The large, subhedral, grain on the left side exhibits lamellar intergrowths and irregular grains of Fe-Ti oxides and some amphibolisation (particularly in the core), whereas the medium to small, polygonal grains on the right side (which are partially enclosed by Fe-Ti oxides) are characterised by polysynthetic twinning and lack of exsolution or alteration. Whole has an hypautomorphic granular texture - a reasonable proportion of primary, subhedral grains remain (sample AE-20). b. Medium-sized, characteristically anhedral grains, exhibiting extensive mutual interference and amphibolisation. Whole has a xenomorphic granular texture, typical of mononmineralic pegmatite (sample AE-10) c. Part of a large, subhedral clinopyroxene grain with exsolved, parallel-sided sheets and bleb-like bodies of orthopyroxene and exhibiting minor amphibolisation (sample AE-10). d. Two sets of Ca-poor pyroxene lamellae in part of a large, subhedral clinopyroxene host (sample AE-10). e. Cubic grains and 3 sets of lamellae of an opaque Fe-Ti oxide in a medium-sized, anhedral clinopyroxene grain. Poor focus is an indication of the plate-like nature of these phases (sample AD-32). f. Herringbone texture in medium-sized clinopyroxene grain resulting from combined polysynthetic twinning and opaque Fe-Ti oxide lamellae (the twinning strikes up and down and the lamellae form a zig-zag feature from left to right (sample AE-12).

("a", "b", "c", and "d" in transmitted light with crossed polarisers, and "e" and "f" in plane polarised transmitted light; am - amphibole)

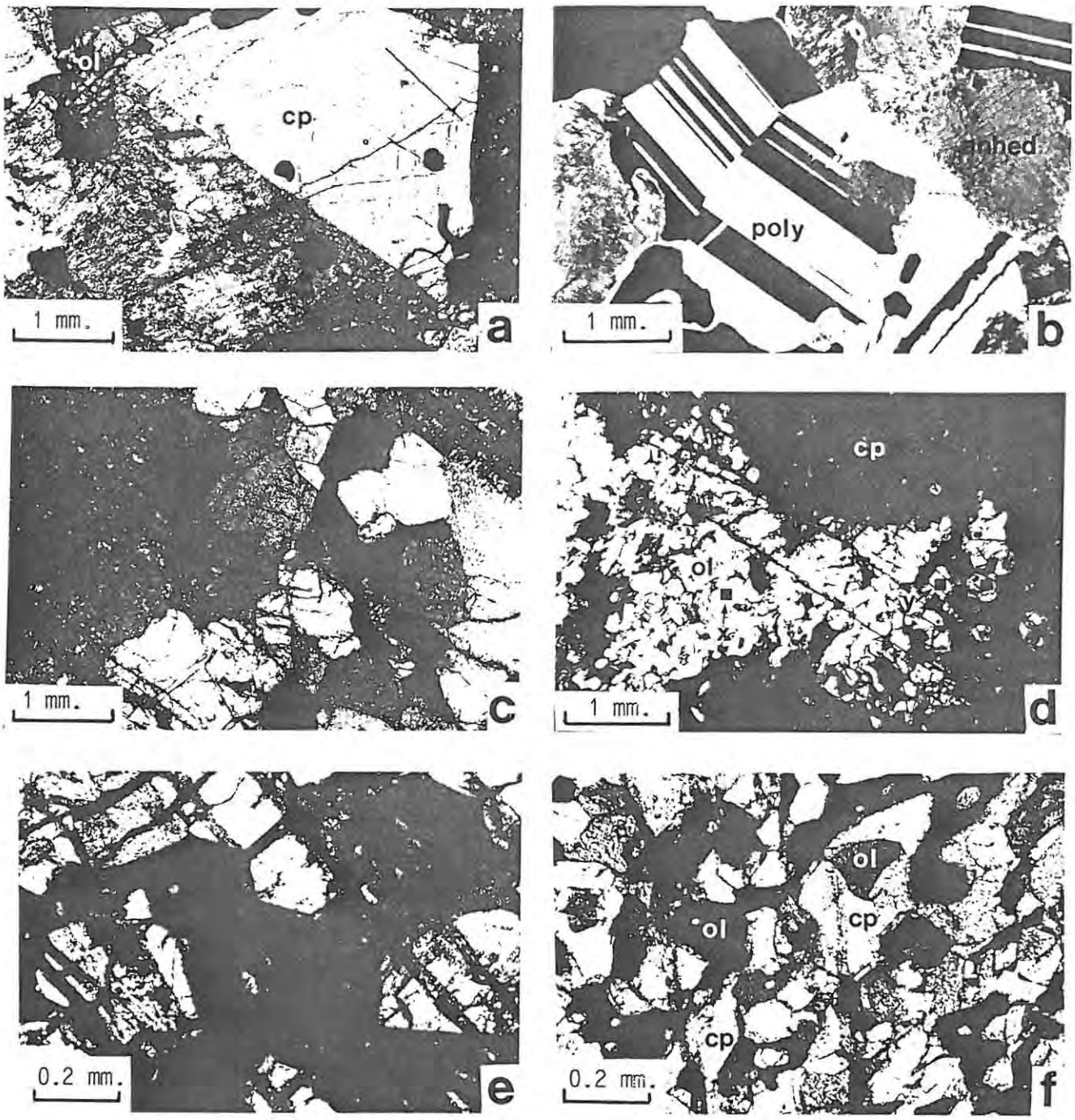

FIGURE 8.2 MICROSTRUCTURES EXHIBITED BY PEGMATITIC CLINOPYROXENE AND OLIVINE

a. Cross-section of a large, subhedral clinopyroxene grain, exhibiting partial amphibolisation and a simple twin, around which is moulded a small, anhedral olivine grain (sample AE-10). b. Medium- to fine-grained clinopyroxene illustrating typical anhedral ("anhed") and polygonal ("poly") forms. The former exhibit mutual interference, usually contain exsolution lamellae and are invariably amphibolised, whereas the polygonal grains are fresh, unaltered and exhibit a characteristic polsynthetic twinning (seen here as a broad, lath-like feature, resembling albite twinning in plagioclase) (sample AE-20). c. Fine-grained olivine exhibiting a foam-like texture; note also part of large, anhedral olivine grain on left side (sample AD-10). d. Tongue-like aggregate of olivine (white) penetrating and replacing part of a large, subhedral clinopyroxene grain (in extinction) (sample AF-A4). e. Very fine-grained olivine exhibiting a chain-like texture. Note that each chain extinguishes sympathetically (from position "x" in "d"). f. Extremely fine-grained olivine observed as anhedral, sometimes skeletal grains (with high relief; many of the olivine grains here are in extinction) in a matrix comprising part of a large clinopyroxene grain (low relief, white or dimpled grey colour) (from position "y" in "d").

("a", "b", "c" and "d" in transmitted light with crossed polarisers, and "e" and "f" in plane polarised transmitted light; ol - olivine; cp - clinopyroxene)

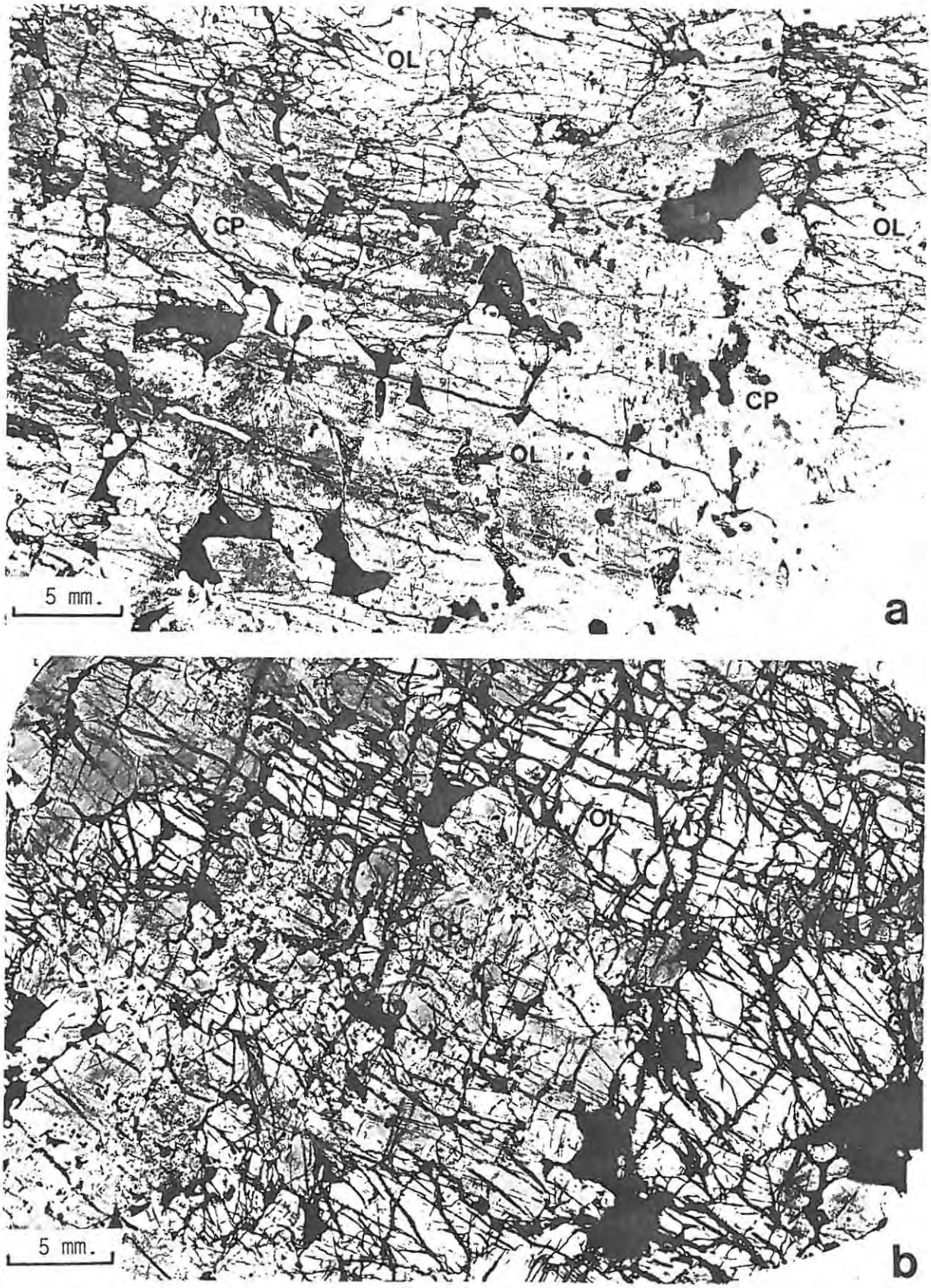

FIGURE 8.3 MACROTEXTURES OF CLINOPYROXENE- AND OLIVINE- RICH PEGMATITE ASSEMBLAGES

a. Clinopyroxene-rich pegmatite. Clinopyroxene occurs as large- to medium-sized, subhedral or anhedral grains that demonstrate mutual interference and some polygonisation (see also fig. 8.1A,B) and olivine and Fe-Ti oxides occur interstitially. The whole demonstrates an hypautomorphic to xenomorphic granular texture (sample AE-20).
b. Olivine-rich pegmatite. Note coarse-grained, anhedral aggregates of olivine that partially enclose and replace clinopyroxene; the latter are usually anhedral. Compare grain size of interstitial Fe-Ti oxides to those in "A" (sample AE-12).

(Both in plane polarised transmitted light; ol - olivine; cp - clinopyroxene; Fe-Ti oxides are black).

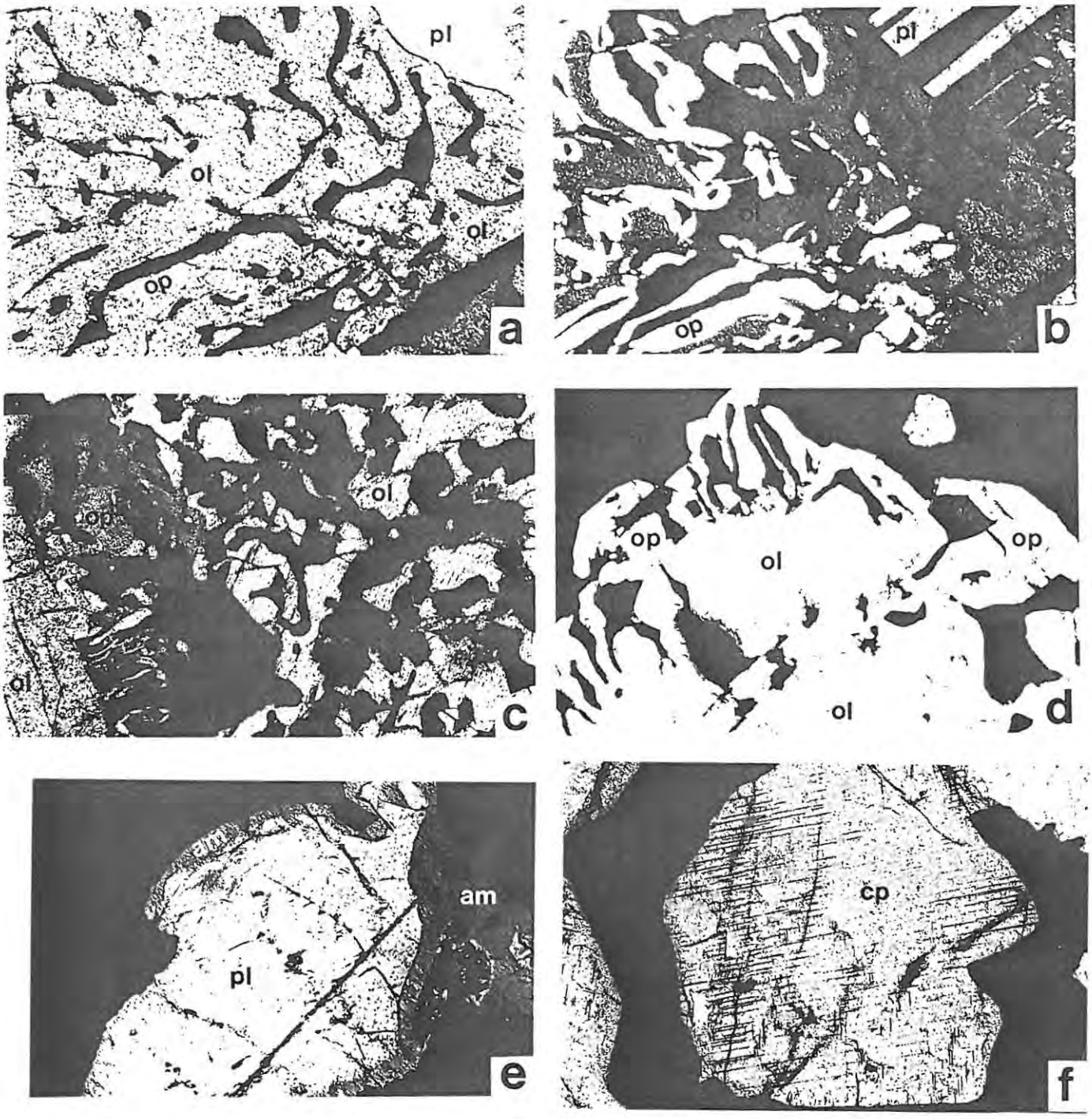

FIGURE 8.4 TEXTURAL RELATIONSHIPS BETWEEN OXIDES AND SILICATES

a,b. Poorly developed olivine-magnetite symplectite - note orthopyroxene coronas around vermicular magnetite bodies. From a hybrid contact assemblage (sample ML22-A10). c. Bleb-like bodies of magnetite replacing olivine, plus olivine-magnetite-orthopyroxene symplectite near margin of fresh olivine grain at lower left (as sample "a"). d. Vermicular bodies of Fe-Ti-Cr oxide aligned at right angles to an Fe-Ti-Cr oxide layer. Oxide is replacing pegmatitic olivine - note orthopyroxene corona (sample AH-21). e. Fe-Ti-Cr oxide replacing relict, recrystallized plagioclase - note amphibole corona (sample AE-15). f. Subhedral grain of clinopyroxene enclosed and partially replaced by interstitial ilmenite. Note ilmenite lamellae in clinopyroxene; here they are probably a replacement feature (as sample "a").

(All in plane polarised transmitted light, except "b" which is with crossed polarisers; ol - olivine; op - orthopyroxene; am - amphibole; pl - plagioclase; oxides are black)

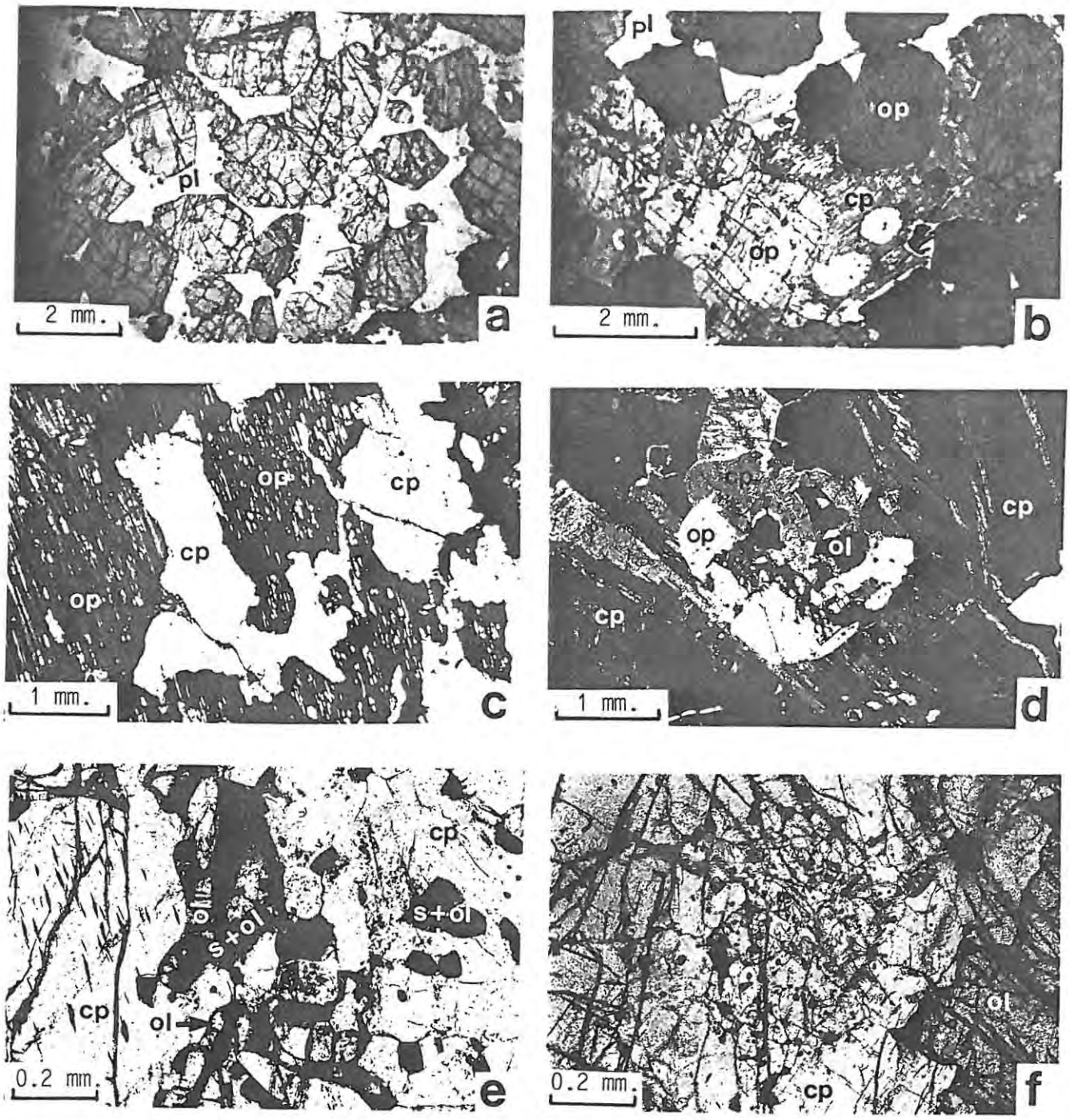

FIGURE 8.5 REPLACEMENT OF CUMULUS MINERALS - (1)

a. Orthopyroxenite (cumulus orthopyroxene and intercumulus plagioclase) exhibiting an automorphic granular texture. Merensky pyroxenite (sample AF-A1). b. Initial stage in the replacement of the Merensky pyroxenite - the large pegmatitic clinopyroxene grains have replaced the intercumulus plagioclase and poikilitically enclose the cumulus orthopyroxene grains (which are superficially unaffected) (sample AF-A2). c. Initial stage in the replacement of chadacrysts of orthopyroxene in the Merensky Reef, in this example, by pegmatitic clinopyroxene (which is all in optical continuity) (sample AF-A4). d. Relict, cumulus orthopyroxene grain which has been partially replaced by very fine-grained, pegmatitic olivine and clinopyroxene; whole is enclosed by a large, subhedral clinopyroxene grain (note twinning), resulting in an enclave-like feature (sample AE-32). e,f. Pegmatitic olivine and spinel observed as very fine, disseminated grains in a large, pegmatitic clinopyroxene grain. This texture is probably a pseudomorph after cumulus orthopyroxene, and is thus a more advanced stage of the replacement process observed in "d"; e.g., the orthopyroxene has been completely replaced (sample AE-32).

("a", "e" and "f" in plane polarised transmitted light, and "b", "c" and "d" with crossed polarisers; pl - cumulus plagioclase; op - cumulus orthopyroxene; ol - pegmatitic olivine; cp - pegmatitic clinopyroxene; s - pegmatitic spinel)

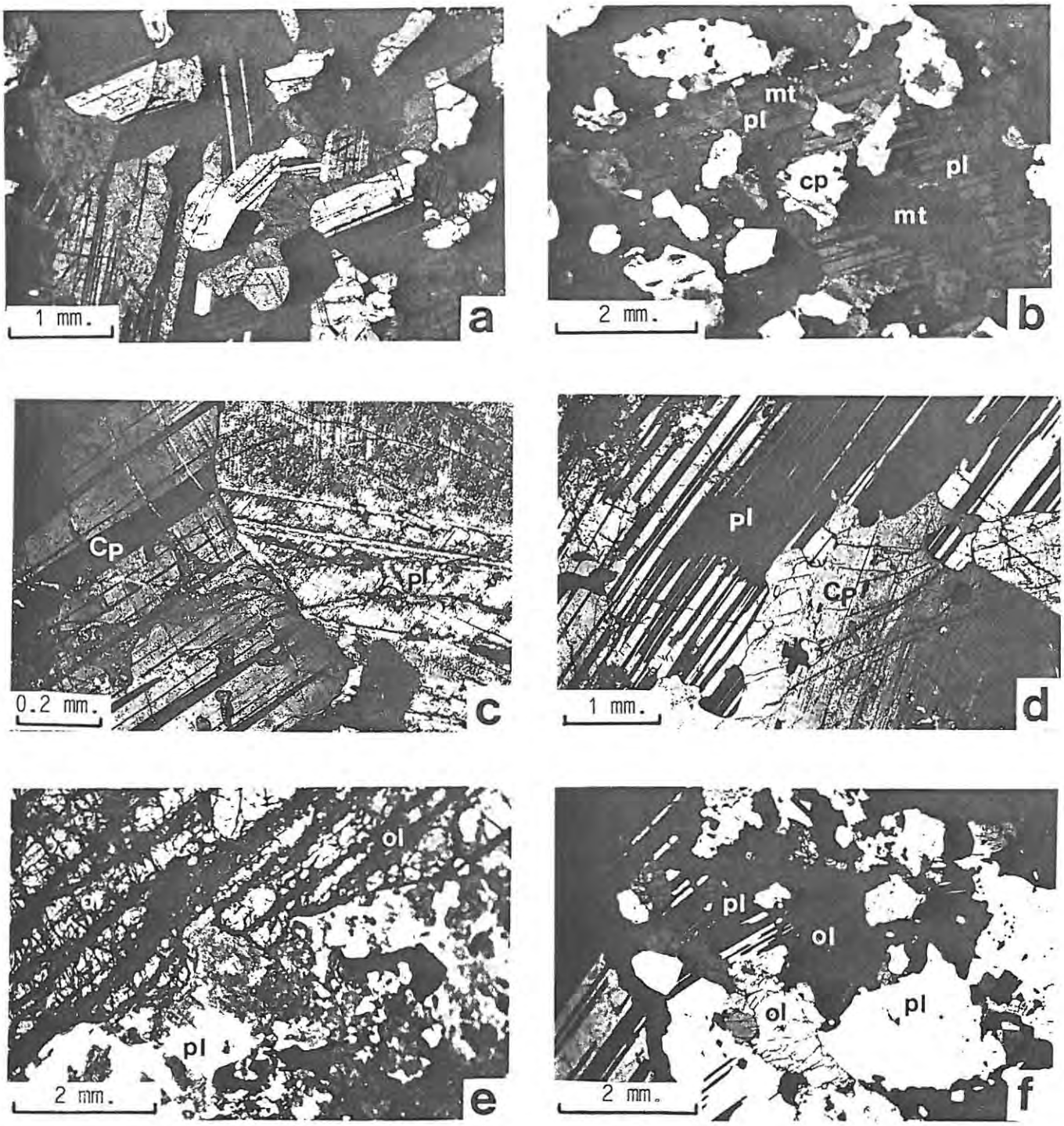

FIGURE 8.6 REPLACEMENT OF CUMULUS MINERALS - (2)

a. Plagioclase adcumulate exhibiting characteristic well-annealed texture (sample AB-3). b. Coarse, recrystallized grain of plagioclase poikilitically enclosing pegmatitic minerals (Ti-magnetite and clinopyroxene - note simple twin) in a contact assemblage adjacent to a pegmatite body in the main zone. Compare texture and grainsize of plagioclase with that in "a" (sample ML22-A18). c,d. Pegmatitic clinopyroxene that has partially replaced relict cumulus plagioclase; note sharp, regular contact in "c" and sharp, scalloped contact in "d". Note also coarse grainsize of plagioclase (it has evidently recrystallized - compare with that in "a") and twinning in clinopyroxene. Plagioclase in "c" is partially saussuritised (samples AE-32 and ML22-A10). e,f. Pegmatitic olivine that has partially replaced relict cumulus plagioclase; note saussurite in plagioclase in "e" and mosaic-like intergrowth of plagioclase grains in "f" that are not saussuritised or twinned, but exhibit strain extinction (samples AD-10 and AE-25).

(All in transmitted light with crossed polarisers, except "e" which is in plane polarised transmitted light; ol - olivine; cp - clinopyroxene; mt - magnetite; pl - plagioclase)

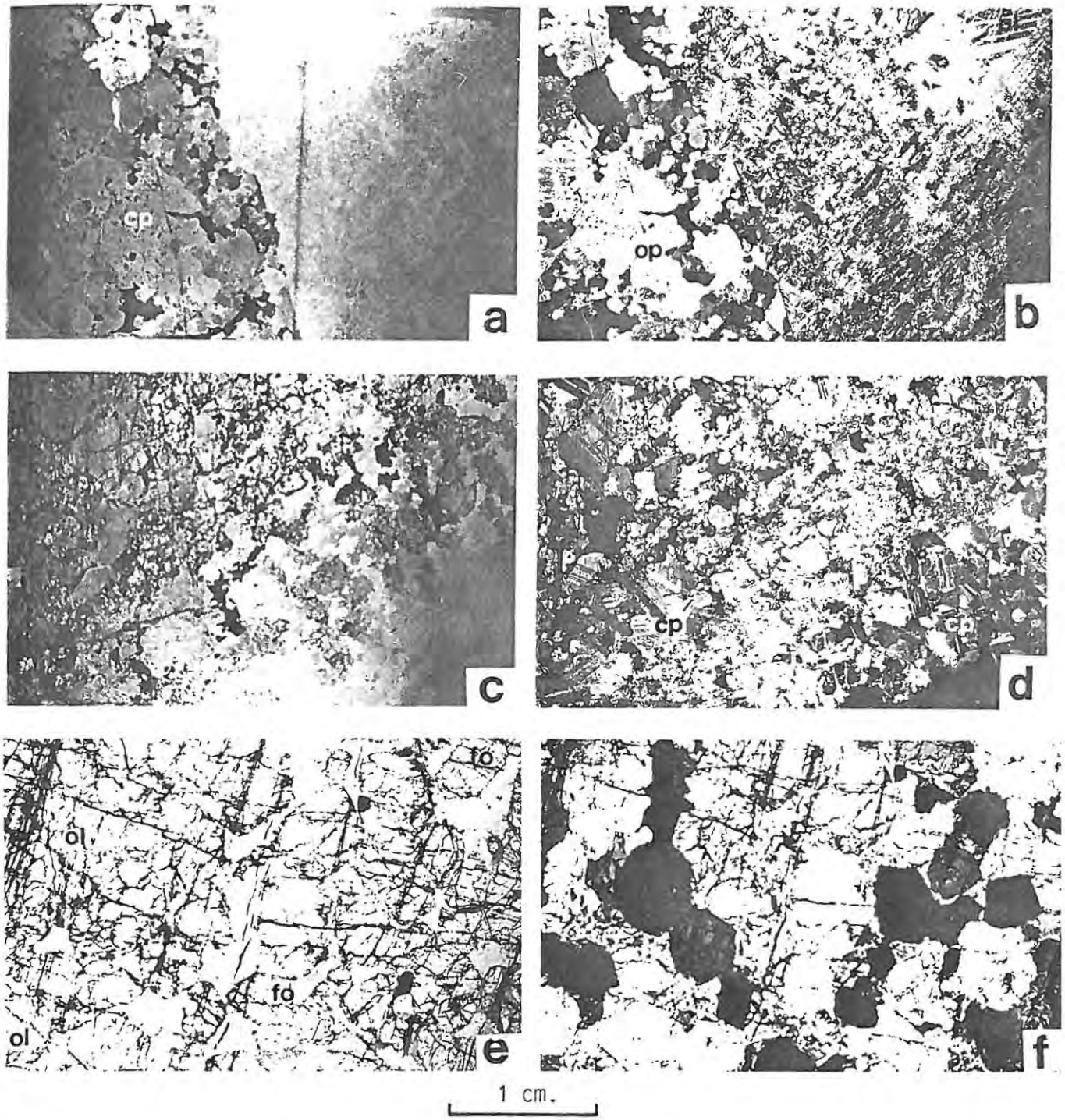

FIGURE 8.7 CONTACT RELATIONSHIPS

a,b. Sharp, regular contact between pegmatite (left) and anorthosite (right). Pegmatite comprises fine-grained clinopyroxene and Fe-Ti oxide, and coarse-grained, relict plagioclase and orthopyroxene that have recrystallized to form anomalously large grains. Plagioclase in the anorthosite is saussuritised and has also recrystallized; relict grains exhibiting some twinning are visible in the top right of "b" (sample AC-6). c,d. Irregular, diffuse contact beween pegmatite (left) and norite (right). Pegmatite comprises medium-grained, often polygonal clinopyroxene (note distinctive twinning) and anhedral grains of olivine and Fe-Ti oxide. Norite consists of saussuritised and recrystallized plagioclase (individual grains not visible) and pegmatitic clinopyroxene grains that pseudomorph cumulus orthopyroxene grains (sample AE-33). e,f. Metasomatic contact between pegmatite (right) and feldspathic harzburgite (left). Latter consists of cumulus, euhedral olivine and intercumulus plagioclase and orthopyroxene (see also fig. 5.5). In the metasomatic contact assemblage the intercumulus minerals have been replaced by pegmatitic clinopyroxene and olivine, but cumulus olivine (which is anomalously iron-rich) may still be recognized (sample AC-A; see fig. 9.4).

("a", "c" and "e" in plane polarised transmitted light, and "b", "d" and "f" with crossed polarisers; pl - cumulus plagioclase; op - cumulus orthopyroxene; fo - cumulus olivine; ol - pegmatitic olivine; cp - pegmatitic clinopyroxene)

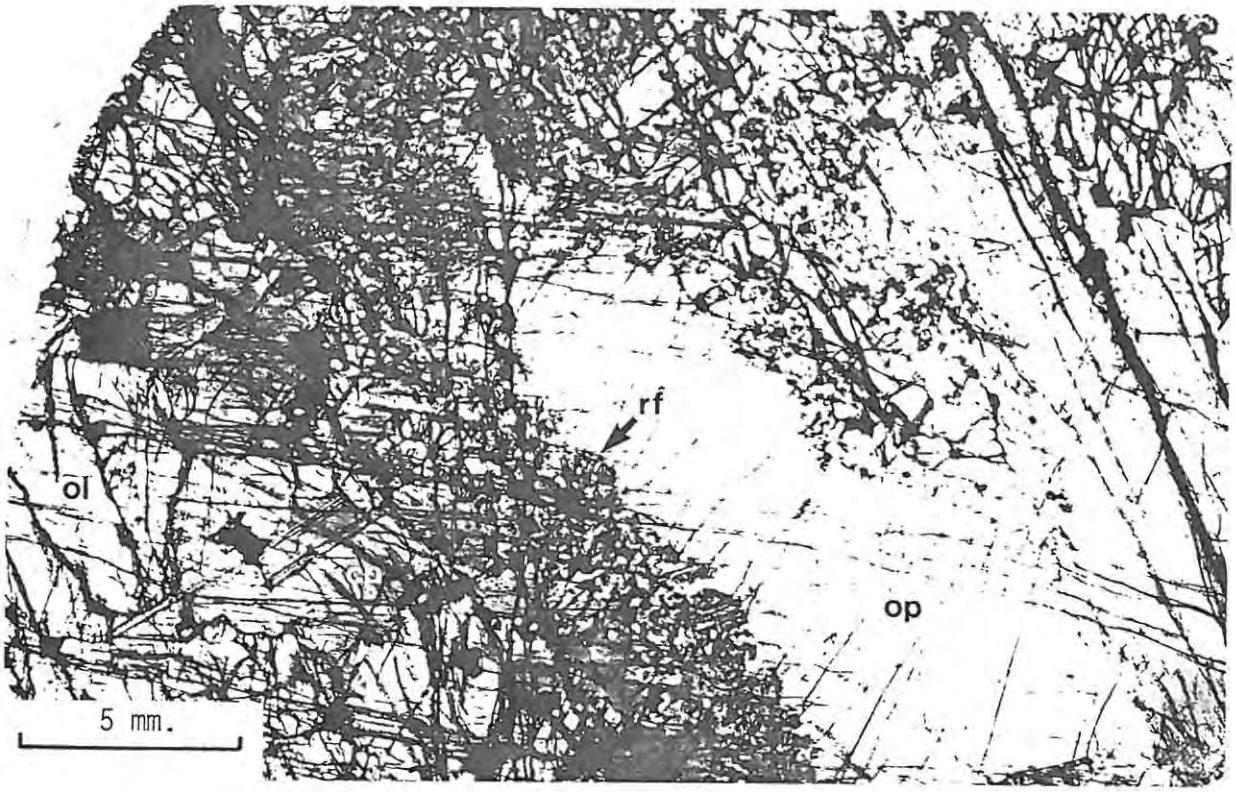

FIGURE 8.8 THE PARTIALLY REPLACED MERENSKY REEF

This hybrid assemblage consists of relict cumulus orthopyroxene (part of a single large chadacryst) and pegmatitic clinopyroxene, olivine and spinel. Intercumulus plagioclase has been completely replaced by the pegmatitic minerals, resulting in typical, coarse-grained clinopyroxene -olivine - Fe-Ti-Cr oxide pegmatite with a xenomorphic granular texture. Between the relict orthopyroxene chadacrysts is a zone of fine-grained olivine-clinopyroxene pegmatite which has partially replaced the former along the margins and cleavage traces. Note the irregular and scalloped replacement front (sample 27-D1).

(In transmitted light with crossed polarisers; op - cumulus orthopyroxene; ol- pegmatitic olivine; cp - pegmatitic clinopyroxene; rf - replacement front)

olivine that occur interstitially to the clinopyroxene, as described above. This suggests that it is likely that at least some of the olivine has crystallized in intersitial sites and has not all resulted from replacement of pre-existing clinopyroxene.

An intermediate, or possibly separate, stage in the replacement process is observed in which olivine occurs as very fine, almost skeletal grains (with dimensions of less than 0.1 mm) within the host clinopyroxene (fig. 8.2F). These skeletal grains may abutt onto the tongue-like olivine masses via a gradual increase in the proportion and size of the individual olivine grains. Further away from the replacement front olivine replacing the clinopyroxene may occur as small, polygonal grains. Occasionally these display a chain-like texture in which individual grains are optically continuous (fig. 8.2E). A final stage of replacement is reached where large, anhedral olivine grains poikilitically enclose a number of small clinopyroxenes. It is suggested that some of these large olivine grains may have resulted from annealing of the small, mosaic-like aggregates. Eventually, an almost monomineralic olivine pegmatite may result.

A feature of some of these bodies is the presence of small, enclave-like features, consisting of very fine-grained olivine and Ti-magnetite, that are completely enclosed by large clinopyroxene grains. Often, relict orthopyroxene grains can be observed, which suggests that they represent partially replaced cumulus orthopyroxene grains (fig. 8.5D,E). If this replacement process is further advanced, then fine-grained olivine and Ti-magnetite are observed as clusters of disseminated grains in a clinopyroxene host (fig. 8.5F).

8.3 DISCUSSION

8.3.1 MINERAL PARAGENESIS

Petrographic studies indicate that the pegmatitic minerals fit the following paragenetic sequence :

clinopyroxene → olivine → ilmenite → spinel → (sulphide,amphibole,mica)

Each of these minerals demonstrates disequilibrium textures, and may replace those earlier in the sequence. Thus olivine may replace clinopyroxene and Fe-Ti oxides may replace both olivine and clinopyroxene. Clinopyroxene is particularly susceptible to replacement by amphibole, but amphibole is usually observed only as coronas around olivine and Fe-Ti oxides. This para-

genesis conforms with field relationships, including mineralogical zonation within individual bodies. Clinopyroxene-rich pegmatite is often found at the margins of bodies, whereas Fe-Ti oxide-rich, olivine-clinopyroxene pegmatite occurs as central core-like features. Furthermore, large pipe-like bodies are often composed of olivine-rich pegmatite with high concentrations of Fe-Ti oxides. This zonation is also shown by pegmatite bodies in the main zone where massive cores composed almost entirely of Fe-Ti oxide are common, particularly in large, pipe-like bodies. Textural studies indicate that clinopyroxene, olivine and Fe-Ti oxides may have crystallized directly from a magmatic liquid. The characteristic xenomorphic texture is attributed to random nucleation and differential grain growth.

8.3.2 PRIMARY REPLACEMENT : MAGMATIC PROCESSES (?)

Textural relationships in ultramafic rocks indicate that reaction relations exist between many ferromagnesian minerals. Jackson (1961) refers to this phenomenon as reaction replacement; it may be considered to be the reverse of incongruent melting. Reaction replacement of magnesian olivine by orthopyroxene and clinopyroxene has been described by Jackson (1961). According to Bowen's reaction series iron-rich olivine will crystallize after clinopyroxene, consequently it may be postulated that reaction replacement of clinopyroxene by iron-rich olivine could occur.

The influence of iron on the relations between olivine, Ca-poor pyroxene, and silica minerals may be investigated in the system MgO-FeO-SiO_2 (Bowen & Schairer, 1935; see also Morse, 1980, pp. 325-344). Depending on starting compositions it is possible to follow the crystallization path Mg-olivine - Ca-poor pyroxene - Fe-olivine, such that at some value of iron enrichment Fe-olivine is in equilibrium with silica. The point at which the reaction relationship between Ca-poor pyroxene and melt breaks down is dependent on many factors and a definite composition cannot be fixed. Reaction between iron-rich olivine and Ca-rich pyroxene may be simulated in the system CaO-MgO-FeO-SiO_2 (Yoder, 1979, pp. 141-144). This system, although considerably more complicated than the CaO-free system, also implies that with suitably iron-rich compositions the reaction relationship gives way to equilibrium crystallization. Consequently, Ca-rich pyroxene and olivine may coprecipitate. Evidence for this is found in the upper zones of the Skaergaard and Bushveld layered series, where cumulus iron-rich olivines exhibit equilibrium textures with clinopyroxene (inter alia Wager & Brown, 1968).

Analogy with layered rocks thus suggests that the disequilibrium

textures between clinopyroxene and olivine in iron-rich ultramafic pegmatite cannot be attributed to reaction replacement. Furthermore, these minerals may be in chemical disequilibrium (clinopyroxene exhibits an unusually high Mg/Fe ratio as compared to olivine; see Chapter 9). However, it is possible that the physico-chemical conditions of the pegmatitic liquid resulted in a reaction relationship between Ca-rich pyroxene and Fe-rich olivine existing at more iron-rich compositions than in the layered rocks. In fact Kushiro (1969) found that in simple silicate systems the addition of H_2O causes the diopside-forsterite cotectic to shift toward the olivine composition. Whether this is applicable to more iron-rich compositions is not known. Irvine (1980, p. 377) suggests that the loss of H_2O from an intercumulus liquid that previously had been in equilibrium with both clinopyroxene and olivine might have induced the reaction whereby pyroxene is resorbed and olivine precipitated in its place (Irvine applies this to the formation of transgressive bodies in Duke Island; see Chapter 13). Alternatively, it is possible to interpret disequilibrium between clinopyroxene and olivine in iron-rich ultramafic pegmatite in terms of magmatic replacement in an open system (see also Chapter 13).

Symplectites in iron-rich ultramafic pegmatite are also interpreted as replacement features. They only occur where silicates (usually either olivine or plagioclase) are in juxtaposition with large ilmenite and Ti-magnetite crystals. Secondly, they are usually found as bulbous bodies associated with "secondary" minerals, such as hypersthene or amphibole. A reaction may be written, for Fo_{50} olivine thus :

$$3Fe_2SiO_4 + 3Mg_2SiO_4 + O_2 \rightarrow 2Fe_3O_4 + 6MgSiO_3 \quad \text{(Zeck } \underline{\text{et al.}}\text{, 1982)}$$

Zeck et al. (1982) also attribute olivine - Fe-Ti oxide symplectites to magmatic replacement, and they found that secondary orthopyroxene produced during this reaction is more magnesian than the primary olivine. Symplectites and scalloped replacement fronts occur both above and below Fe-Ti-Cr oxide pegmatite layers (see also Chapter 10). These features suggest that these oxide layers also develop partly by replacement at the expense of adjacent silicates. Orthopyroxene and amphibole coronas are also present.

8.3.3 LATE-STAGE REPLACEMENT : DEUTERIC PROCESSES (?)

REVIEW

Deuteric processes may be defined as those which arise from residual solutions which are inherently derived from within a crystallizing magmatic

assemblage. They are distinguished from extraneously introduced fluids, which result in metasomatic changes. Not infrequently it is impossible to distinguish between metasomatic and deuteric phenomena (Hatch et al., 1975 p. 178). Deuteric processes occur when a rock is nearly solid and to a large extent result in veining and replacement of earlier minerals. In granitic magma systems deuteric processes may be used to incorporate all late-stage crystallization events, including pegmatitic stages.

DISCUSSION

In the rocks in this study deuteric processes are regarded as those which occur after a combination of crystallization and magmatic replacement has resulted in formation of the main pegmatitic minerals, as described above. This may be confusing as the iron-rich ultramafic pegmatites themselves may be related to deuteric processes operating within the cumulate pile. This argument, however, has major genetic implications and is developed further in Chapter 13. The present section interprets events related to late-stage processes operating within the iron-rich ultramafic pegmatite system. These are related to late-stage fluids which remain after the principal pegmatite minerals have formed.

Deuteric processes result in incipient amphibolisation of early formed clinopyroxene, possibly resulting in the formation of large amphibole grains. These themselves may be partially replaced by biotite. This process of amphibolisation may be associated with the formation of orientated intergrowths of Fe-Ti oxide in clinopyroxene. Serpentinisation of olivine may also be described as a deuteric process, as is saussuritisation of plagioclase, although in many cases it is a primary feature of wallrock alteration attributable to the main pegmatitic liquids. These deuteric processes result from interaction between the main pegmatite minerals and late-stage fluids.

8.3.4 DEFORMATION AND ANNEALING PROCESSES

REVIEW

Annealing is the process by which residual stresses within minerals and polycrystalline aggregates are reduced and eventually eliminated (Stanton, 1972). Stanton considers annealing as a process which operates totally within solids, at temperatures high enough to permit atomic mobility but below the solidus. Annealing is closely related to, and may be considered the antithesis of deformation. In slowly cooled igneous rocks some degree of self-imposed deformation is inevitable, in response to factors such as

overburden pressure, removal of interstitial liquid etc. If cooling were sufficiently slow annealing might be expected to totally eliminate these effects. However, in practice one would expect to find textures that reflect a combination of primary crystallization and post-crystallization deformation and annealing. These latter two processes would also be expected to operate concurrently with processes such as subsolidus reequilibration, exsolution and deuteric events.

Annealing may commence in silicate-oxide rocks at temperatures below the solidus of one phase (e.g., a cumulus mineral), but above that of others. This is particularly evident in layered cumulates, where many workers, including Reynolds (in press), envisage an early annealing process which results in the removal of intercumulus liquid. Reynolds describes textures, which he interprets as resulting from annealing, in cumulus Ti-magnetite layers in the Bushveld Complex. Three stages are recognized : initial neck growth, an intermediate stage (in which intergranular pores remain interconnected, but are volumetrically reduced due to liquid expulsion as the cumulus magnetite grains enlarge) and a final stage. This results in a dense, polycrystalline aggregate that is characterised by a foam-like texture (which demonstrates equilibrium grain boundary relationships). Similar textures are found in polycrystalline aggregates of Fe-Ti-(Cr) oxide in the pegmatites (see Chapter 10). This early annealing process is an attractive model for explaining the formation of adcumulates (such as Ti-magnetite layers) in layered intrusions. It explains two main features (1) the lack of intercumulus material i.e. it offers a mechanism for the removal of intercumulus liquid; and (2) the coarse grain size and polygonal textures present in many adcumulates.

In an entirely solid polycrystalline aggregate, annealing may be considered as a three stage process : recovery, subgrain growth and recrystallization (Stanton, 1972, p. 285). In a slowly cooling rock recrystallization is probably the most important annealing event. This may be considered in the light of five processes : nucleation, primary recrystallization, normal (or gradual) grain growth, secondary recrystallization and differential recrystallization. Grain growth and secondary recrystallization are analogous to the early annealing processes which occur in the presence of interstitial liquid. They result in a coarsening of grain size and may produce a coarse foam-like texture. A polycrystalline aggregate will result in a disequigranular texture (Stanton, 1972, p. 299).

By contrast, primary recrystallization results in a decrease in grain size (Stanton, 1972, p. 292). It results from the development of appropriate nuclei within a strained grain, which is then replaced by a number of strain-

free grains. This process of primary recrystallization ends with the complete impingement of grains. They may then grow at each others expense, if the annealing process continues. Primary recrystallization results in a fine-grained foam-like texture. This explains why foam-like textures that are both coarser and finer than the primary grains may occur. Finally, annealing may produce new textures, such as twinning and extinction features, which are similar to, and easily confused with, deformation textures.

DISCUSSION

Many of the textures observed in iron-rich ultramafic pegmatite may be interpreted as annealing features. In clinopyroxene-rich pegmatite mutual interference of individual grains is interpreted as a primary igneous texture, but the polygonal grains (which characteristically exhibit polysynthetic twinning and do not usually contain exsolution lamellae or secondary amphibole) are attributed to annealing. This results in the formation of a polygonal granular texture which is finer-grained than the primary xenomorphic texture. Whether the twinning is a feature of deformation prior to recrystallization or is a result of annealing is uncertain. They do not show features of annealing twins as described by Stanton (1972), but the larger grains which have not recrystallized do not exhibit the regular, lath-like twinning. This recrystallization process may be responsible for the following features : (1) formation of small, polygonal grains; (2) "removal" of exsolved lamellae of Ca-poor pyroxene, of Fe-Ti oxide platelets and of secondary amphibole; and (3) formation of polysynthetic twinning.

In olivine-rich pegmatite very fine-grained olivine may also be attributed to annealing (primary recrystallization). This results in well-developed foam-like textures, unlike the polygonal aggregates resulting from recrystallization of clinopyroxene. This different behaviour during annealing is probably a function of anisotropy. Similar textures occur in dunite cumulates and it may be deduced that olivine is much more susceptible to annealing than pyroxene.

Primary recrystallization implies that the original grains were subject to deformation strain. Certainly olivine grains are traversed by numerous microcracks and they show undulatory extinction (features which are absent in the foam textured grains), but it is difficult to establish clear proof of deformation. Foam-like aggregates of olivine are often found either entirely within or at the margins of clinoyroxene grains and adjacent to replacement fronts. This suggests that olivine that has partially replaced clinopyroxene is more susceptible to strain annealing. It may be postulated that massive, or pervasive replacment results in the development of strained crystals,

presumably due to controls on crystal growth.

Fe-Ti-(Cr) oxides, which are much more readily annealed than olivine, demonstrate a similar range of annealing textures to those found in cumulus magnetite layers, as discussed in Chapter 10.

8.4 IRON-RICH ULTRAMAFIC PEGMATITE FROM CONTACT ZONES

8.4.1 REVIEW

Two main types of contact relationship may be recognized at the margins of iron-rich ultramafic pegmatite bodies. Contacts may be either sharply discordant and cut across the cumulate layering or they may be locally concordant and constrained by the cumulate layering (see Chapter 7). Sharply discordant contacts may be found at the margins of large, pipe-like bodies (e.g., the Brakspruit and Townlands pipes) and at the lateral margins of small, irregular bodies. At Amandelbult discordant contacts have been observed where pegmatite bodies cut anorthositic and noritic cumulates. Discordant contacts may also be recognized in partially replaced Merensky Reef. Pegmatite bodies have not been observed actually cutting harzburgitic cumulates, although borehole data provide evidence that this may happen. Pegmatite bodies commonly exhibit concordant contacts with ultramafic cumulates, such as chromitites, harzburgites and orthopyroxenites. Furthermore, pegmatite bodies exhibit different contact features within different cumulates; these are all described separately. Contact relationships with chromitite layers are a special case; these are described in Chapter 10.

Cameron and Desborough (1964) have examined contact zones between sheet-like pegmatite bodies and orthopyroxene-plagioclase cumulates in the eastern Bushveld Complex. They show a definite paragenetic sequence of replacement and exhibit different features depending on whether they replace anorthositic or pyroxenitic cumulates. In leuconorites the first stage of replacement is marked by the formation of clinopyroxene, largely at the expense of cumulus orthopyroxene, but also at the expense of plagioclase. At this stage clinopyroxene occurs partly as rims on orthopyroxene, partly as tiny laths and irregular patches within orthopyroxene grains (these are all in optical continuity) and as near-pseudormorphs. In the second stage reported by Cameron and Desborough cumulus orthopyroxene is absent and pegmatitic olivine is now observed, usually as small grains along the contact between clinopyroxene crystals. Plagioclase is still a major constituent of this contact assemblage. In more advanced stages olivine forms large,

ramifying crystals which poikilitically enclose corroded relict plagioclase and clinopyroxene. This may result in the formation of dunitic pegmatite. In wehrlite pegmatite, olivine is followed by second generation clinopyroxene. This develops at the expense of earlier clinopyroxene and olivine (Cameron & Desborough, 1964). Arrested stages in this process result in the preservation of large, poikilitic clinopyroxene crystals which enclose first generation clinopyroxene, olivine and relict cumulus plagioclase. The final stages of silicate formation are marked by the presence of rims of hornblende on the earlier silicates and local replacement of hornblende by biotite (Cameron & Desborough, 1964). This may be summarised thus :-

clinopyroxene (1) - olivine - clinopyroxene (2) - amphibole - mica

In melanorite or feldspathic orthopyroxenite the first stage of replacement is marked by the abrupt appearance of olivine (Cameron & Desborough, 1964). It forms at the expense of cumulus orthopyroxene, which disappears within 1 to 2 mm from the contact. Simultaneously, cumulus chromite is replaced or altered to an Fe-Ti-Cr spinel (see Chapter 10). Clinopyroxene then appears at the outer edge of this subzone. Plagioclase is then gradually replaced, resulting in typical olivine-clinopyroxene-magnetite pegmatite (Cameron & Desborough, 1964).

8.4.2 CONTACT FEATURES AT AMANDELBULT

Many of the features described by Cameron and Desborough (1964) are also observed in contact zones at Amandelbult; these are discussed for each main type of cumulate.

(1) ANORTHOSITE

Discordant contacts between pegmatite bodies and mottled or spotted anorthosite cumulates are common at Amandelbult. These are either sharp and regular (fig. 8.7A,B), or irregular and diffuse, forming a hybrid contact zone a few millimetres thick. The immediate wallrock is often a pale green colour and may be unusually soft, thus forming an alteration halo several centimetres thick. Adjacent to large, pipe-like bodies this may be over 5 m wide (e.g., the Brakspruit pipe; see sample RB-7). In thin section the anorthosite in these alteration haloes can be seen to consist of severely saussuritised and recrystallized plagioclase grains. These exhibit similar textures to relict plagioclase grains within pegmatite bodies and are more

calcic than the original cumulus composition (see Chapter 9). Pyroxene may be absent, and pegmatite minerals as such do not usually occur. A mosaic of fine-grained clinopyroxene grains, often with planar edges, occurs in the pegmatite at the contact. Fe-Ti oxide is also prevalent close to the contact, but olivine may be absent (fig. 8.7A,B). Large, relict aggregates of plagioclase are common in the pegmatite for distances of up to 1 m from the contact.

(2) NORITE

Contacts with norite (including leuconorite and melanorite) cumulates are invariably discordant. They are usually irregular and diffuse, being gradational over widths of between 1 and 2 cm. Within this hybrid contact zone cumulus orthopyroxene may be replaced, often pseudomorphically, whereas plagioclase is unreplaced (fig. 8.7C,D). This feature accounts for the irregular form of the contact, but contradicts the preferential replacement of felsic cumulates by pegmatite.

Cumulus orthopyroxene in this contact zone is replaced by both pegmatitic clinopyroxene and olivine; textures observed here are comparable to those described by Cameron and Desborough (1964). In addition, tongue-like aggregates of clinopyroxene and olivine, often observed as very fine-grained mosaics, may have partially replaced plagioclase grains adjacent to pseudomorphs of cumulus orthopyroxene. This is evidently a second stage in the replacement process. Plagioclase grains in this zone may be unusually large and exhibit strained twin lamellae and undulatory extinction; they have recrystallized and may be partially saussuritised. Large grains of plagioclase, that poikilitically enclose olivine and clinopyroxene are clear evidence of recrystallization. Amphibole and mica are commonly observed in these contact zones and clinopyroxene is often amphibolised. Pegmatitic olivine may also be altered, or serpentinised, an unusual feature in the main pegmatite bodies. Pegmatite adjacent to this contact assemblage may contain relict orthopyroxene grains, but these, evidently, are readily replaced. Relict fragments and large recrystallized aggregates of plagioclase, however, occur in the pegmatite for some distance from the contact. The contact itself may be marked by saussuritised aggregates of plagioclase.

(3) THE MERENSKY REEF

At Amandelbult the Merensky Reef, which comprises a pegmatoidal feldspathic orthopyroxenite (in which olivine may be an accessory phase), is readily replaced by iron-rich ultramafic pegmatite. The contact between replaced and normal Reef is transitional, consequently an irregular contact

zone, with lateral dimensions of several metres, is present (see pp. 121-122). This may be referred to as partially replaced Reef.

Plagioclase is usually absent in partially replaced Reef, thus it is ultramafic in character and may be difficult to recognize from typical iron-rich ultramafic pegmatite. However, it is distinguished by the presence of extremely large chadacrysts of (cumulus) orthopyroxene, which typically occur in a matrix of finer-grained, pegmatitic olivine and clinopyroxene (fig. 8.8). Accessory Fe-Ti-(Cr) oxides, base-metal sulphides and rare, sliver-like grains of relict plagioclase also occur in this matrix. The orthopyroxene grains are either fresh, with unmodified contacts, or partially replaced. Both olivine and clinopyroxene may be observed to have replaced orthopyroxene, in a similar manner to that described before (fig. 8.5 C-F).

In Merensky Reef which contains cumulus olivine, plagioclase is again replaced first. Electron microprobe data indicate that both olivine and orthopyroxene in partially replaced Reef may be slightly iron-rich in comparison with normal cumulus compositions (see Chapter 9). Eventually, cumulus olivine is pseudomorphed by pegmatitic olivine, usually resulting in a fine-grained mosaic.

Hybrid contact zones in replaced Merensky Reef thus exhibit major differences to those described above. In the Merensky Reef plagioclase is replaced (by olivine and clinopyroxene) in preference to both orthopyroxene and olivine, whereas the reverse is true in felsic cumulates.

(4) THE MERENSKY PYROXENITE

The Merensky hangingwall pyroxenite, a medium-grained, poikilitic feldspathic orthopyroxenite, is only occasionally replaced, and, again, gradational contacts are in evidence. This results in a hybrid assemblage in which unusually coarse, composite blebs of sulphide (these exhibit both cumulus and pegmatitic characteristics; see Chapter 11) and coarse aggregates of recrystallized plagioclase are prominent. In other respects this hybrid assemblage is mineralogically similar to partially replaced Reef, thus pegmatitic olivine and clinopyroxene, with rare grains of relict plagioclase form a matrix to unreplaced or partially replaced cumulus orthopyroxene grains. Further from the pegmatite body a contact assemblage is observed in which small, anhedral grains of clinopyroxene, that mantle unreplaced orthopyroxene grains, are the only contact phenomenon (fig. 8.5 A,B).

(5) FELDSPATHIC HARZBURGITE

These are not usually replaced and consequently often present concordant contacts against pegmatite bodies. However, detailed examination reveals

that a gradational contact assemblage, often only a few millimetres thick is usually present. Furthermore, even if a chromitite layer delineates these contacts the underlying feldspathic harzburgite (e.g., the pseudoreefs at Amandelbult) may be partially replaced. In this situation grains of pegmatitic olivine and clinopyroxene project down into the harzburgite preferentially replacing intercumulus plagioclase. Oikocrysts of orthopyroxene may also be replaced, often pseudomorphically. At this stage cumulus olivine (a magnesian variety that is invariably serpentinised) may be partially replaced by pegmatitic olivine and clinopyroxene. Cumulus olivine may be distinguished from pegmatitic olivine in thin section as the latter has higher relief, is fresh, may contain orientated intergrowths of an opaque phase and typically shows strong undulatory extinction. Further into the harzburgite cumulus olivine remains, superficially, unreplaced, with fine-grained aggregates of pegmatitic olivine and clinopyroxene in intercumulus sites (fig. 8.7 E,F).

Electron microprobe data indicate that cumulus olivine in this contact assemblage, even though it may appear unaltered, becomes progressively more iron-rich towards the pegmatite body (see Chapter 9). This is convincing evidence of contact metasomatism, over a distance of a few centimeters.

(6) CHROMITITES

Field relationships suggest that chromitite layers, which present concordant contacts against pegmatite bodies, act as fairly impervious barriers to the pegmatitic liquids. Compositional changes within these chromitite layers are discussed in Chapter 10. Immediately above or below chromitite or hybrid oxide layers, essentially unreplaced cumulates are usually found. These exhibit only minor development of pegmatite minerals, usually at the expense of intercumulus plagioclase, and amphibole and mica are unusually abundant. Examination of one particular assemblage, in which harzburgite is overlain by pegmatite which passes laterally into anorthosite indicates that chromitite layers act as channels for the pegmatitic liquid. This conclusion is also evidenced by the alteration and saussuritisation of the anorthosite immediately above the chromitite layer for a lateral distance of several metres from the contact with the pegmatite body (fig. 10.2).

(7) CONTACT FEATURES OF SMALL PEGMATITE BODIES IN THE MAIN ZONE

Pegmatite bodies examined from the lower part of the main zone at Amandelbult all occur within noritic cumulates. Pegmatite at this height in the cumulate pile is richer in Fe-Ti oxides as compared with that from the upper critical zone. Contact assemblages are invariably gradational, usually

over distances of between 0.5 and 2 m; sharp contacts have not been observed. In contact assemblages here cumulus orthopyroxene is readily replaced by both clinopyroxene and olivine. Plagioclase, however, is less susceptible to replacement and often occurs as large, poikilitic grains which enclose pegmatitic minerals (including Fe-Ti oxides) and relict orthopyroxene, in which circumstance it has clearly recrystallized (fig. 8.6B). Ti-magnetite and ilmenite are usually observed in these contact assemblages as discrete, euhedral to subhedral grains. In comparison, disseminated grains of cumulus Fe-Ti oxide in the upper zone of the layered sequence usually occur as anhedral grains which are interstitial to silicates. Fe-Ti oxide symplectites are also common in these contact assemblages. Fe-Ti oxides are not normally observed in contact assemblages in the upper critical zone.

(8) SUBTLE TEXTURAL FEATURES

The previous sections describe mineralogical and textural variations in contact zones in which pegmatite-derived minerals are evident, suggesting that addition of new material has occurred. These contact zones are readily recognized as they comprise mineralogical assemblages in which cumulus, intercumulus and pegmatite (or postcumulus) minerals occur, and they may be associated with cryptic compositional variation. Adjacent to these contact zones are essentially normal cumulates which may exhibit subtle textural features that are also related to the proximity of pegmatite bodies. Two main subtle textural variations are recognized; these have only been recognised in the hangingwall of pegmatite bodies.

Firstly, plagioclase may have recrystallized to form unusually large grains, which often poikilitically enclose other cumulus minerals. A second recrystallization stage then results in formation of a characteritisic mortar texture in the plagioclase. Large grains, which have not undergone secondary recrystallization, often exhibit curved and deformed twin lamellae and strain deformation. The twinning is usually coarse albite twinning, and the twin lamellae often taper towards the grain margins. In this situa tion primary recrystallization results in a coarsening of the grainsize, and secondary recrystallization is responsible for the fine, mortar-texture, whereas in the pegmatitic minerals an initial recrystallization stage was postulated to form the fine-grained foam-like textures. The latter is attributed to annealing during cooling of an essentially crystalline material, whereas plagioclase in these rocks is subjected to addition of heat from an extraneous source, e.g. a pegmatite body. Conversion of the normal cumulus grains into much larger, poikilitic grains in contact zones may be attributed to dissolution and subsequent recrystallization, but here there is no evidence of the addition

of material, hence an annealing process is called upon. Subsequent to "formation" of these large grains similar annealing events to those that affect the pegmatitic minerals during cooling may then occur. Thus it is possible that a third recrystallization stage could result in annealing of the fine, mortar-textured grains to totally eliminate stress in these grains.

Secondly, cumulus orthopyroxene in pyroxenitic cumulates may exhibit unusual annealing features, that may be compared with annealing processes in cumulus Ti-magnetite layers as described by Reynolds (in press; see section 8.3.4). Annealing in these rocks is attributed to excess heat (and possibly some movement of aqueous fluid) related to an adjacent pegmatite body. It results in grain growth, probably by necking and subsequent migration of grain boundaries, and expulsion of intercumulus material, essentially plagioclase. This results in an unusually coarse-grained orthopyroxenite, in which the proportion of intercumulus material is very low. Large aggregates of orthopyroxene may exhibit triple junctions and 120^{o} dihedral angles. Intercumulus plagioclase may also have recrystallized, as described above.

8.5 MINERALOGICAL CLASSIFICATION

8.5.1 CLASSIFICATION

Iron-rich ultramafic pegmatite is characterised by a rather simple mineralogy which readily lends itself to a mineralogical classification, using accepted plutonic rock nomenclature. A classification is proposed here which is based on the weight percent CIPW norm (see Appendix 5). This has been selected in preference to a modal scheme, because sampling difficulties due to coarse grain size and modal variations are more easily overcome by preparing representative samples for chemical analysis, than by petrographic techniques.

Normative olivine, clinopyroxene and Fe-Ti oxide usually constitute over 90 percent of the weight percent CIPW norm. Normative orthopyroxene is also included in this scheme. Plagioclase in these rocks is interpreted as a relict cumulus mineral; it is not a pegmatite mineral as such, but as it usually represents less than 10 modal percent, these rocks are ultramafic in character. The norm calculation used in this study does not include sulphide (sulphur was not analysed for). The Fe-Ti oxides are calculted as normative magnetite and ilmenite. It is important to realise that some inaccuracies are inherent in this system as the CIPW norm is very sensitive to the Fe_2O_3/FeO ratio, the selection of which is rather arbitrary (see Appendix 5).

Triangular diagrams of normative olivine-clinopyroxene-orthopyroxene and olivine-Fe-Ti oxide-total pyroxene are presented in Figure 8.9. Fields defining the relevant plutonic rock nomenclature are superimposed. The scheme used here is modified slightly from that of Streckeisen (1976). The distinction between olivine-clinopyroxene rocks and those with significant orthopyroxene is drawn at 10 normative percent, not 5 modal percent (note that much of the orthopyroxene in these rocks is present as exsolution lamellae in clinopyroxene). If Fe-Ti oxides comprise more than 10 normative percent the prefix Fe-Ti oxide (or magnetite-ilmenite) is applied. If Fe-Ti oxides are dominant over silicates the description Fe-Ti oxide pegmatite is preferred (see also Chapter 2).

To illustrate this classification 13 samples from various localities in the Bushveld Complex have been selected. Major- element data and the CIPW norms for these samples are presented in Table 8.1. Using this classification scheme it can be seen that sample 5, for example, is a dunite pegmatite and samples 13 and 10 are wehrlite and olivine clinopyroxenite pegmatites, respectively. These samples contain accessory Fe-Ti oxides only. Sample 12 may be described as an Fe-Ti oxide-olivine clinopyroxenite (it contains significant Fe-Ti oxide, but olivine is of greater abundance).

This classification does not take into allowance the composition of the silicate phases. This may be obtained from whole rock data or mineralogical analysis. For example, the 13 samples presented in Figure 8.9. are also plotted on a triangular "AFM" diagram of wt. percent ($CaO+Na_2O+K_2O$ - FeO - MgO; fig. 12.3; see Chapter 12 for explanation). If mineralogical composition is brought into this classification scheme sample 5, for example, may be more fully described as an hortonolite dunite pegmatite (it consists of olivine in the compositional range Fo_{50-30}). This is of considerable importance as it must be emphasized that an iron-rich ultramafic pegmatite that may petrographically be described as a dunite is, obviously, quite distinct from a magnesian dunite, or dunite sensu stricto.

8.5.2 MINERALOGICAL VARIABILITY IN PEGMATITE AT AMANDELBULT

GENERAL FEATURES

All pegmatite samples from Amandelbult, including those from the Middellaagte pipe, are plotted on triangular diagrams of normative olivine-orthopyroxene-clinopyroxene (fig. 8.10), olivine-Fe-Ti oxide-total pyroxene (fig. 8.11), olivine-plagioclase-total pyroxene (fig. 8.12) and (olivine + clinopyroxene) - (plagioclase + orthopyroxene) -Fe-Ti oxide (fig. 8.13). Other combinations of these five main normative components were plotted but

TABLE 8.1 SELECTED WHOLE-ROCK ANALYSES OF IRON-RICH ULTRAMAFIC PEGMATITES

	1	2	3	4	5	6	7	8	9	10	11	12	13
wt%													
SiO_2	30.50	31.25	40.65	42.77	34.43	32.35	35.07	42.36	32.30	41.46	39.08	41.78	36.57
TiO_2	2.93	8.01	2.90	3.70	.36	1.80	6.09	3.43	6.18	2.32	5.08	2.85	1.64
Al_2O_3	.58	2.25	1.70	2.22	.08	.97	2.22	1.40	.52	1.58	1.50	1.71	.72
Fe_2O_3*	4.43	9.51	4.40	5.20	1.86	3.30	7.59	4.93	7.68	3.82	6.58	4.35	3.07
FeO	39.83	25.77	23.02	17.86	38.16	43.61	25.67	20.75	32.05	23.70	20.03	21.11	32.60
MnO	.54	.40	.42	.35	.53	.67	.45	.43	.60	.44	.36	.27	.44
MgO	20.03	9.81	12.89	11.03	21.17	12.24	13.61	10.90	15.33	13.62	12.86	13.35	17.11
CaO	.80	11.51	12.90	15.84	1.92	3.15	7.65	14.17	4.81	12.18	12.75	13.56	6.10
Na_2O	.01	.09	.12	.12	.03	.08	.11	.08	.10	.29	.12	.14	.12
K_2O	Tr	Tr	Tr	Tr	Tr	Tr	.02	.01	Tr	.05	Tr	Tr	Tr
P_2O_5	.01	.03	.04	.04	.30	.03	.03	.03	.04	.15	.01	.02	.02
Cr_2O_3	.43	1.42	.10	.16	.01	.01	.05	.09	.05	.11	.17	.19	.06
NiO	.04	.03	.02	.02	.12	.05	.02	.02	.04	.04	.04	.03	.05
L.O.I	.44	.84	1.03	1.20	.71	1.33	.76	.77	-.09	1.03	.90	.90	1.53
TOTAL	100.57	100.92	100.19	100.51	99.68	99.59	99.34	99.37	99.61	100.79	99.48	100.26	100.03
wt% C.I.P.W. Norm**													
Ap	.02	.07	.09	.09	.71	.07	.07	.09	.09	.36	.02	.05	.05
Cm	.63	2.09	.15	.24	.01	.01	.07	.13	.07	.17	.26	.29	.08
Il	5.66	15.63	5.64	7.18	.69	3.52	11.89	6.70	11.95	4.48	9.93	5.54	3.21
Mt	6.45	13.98	6.44	7.60	2.73	4.87	11.16	7.25	11.18	5.55	9.70	6.37	4.52
Or	-	-	-	-	-	-	.12	.06	-	.30	-	-	-
Ab	-	-	1.10	1.10	.25	.68	.93	.68	.85	2.45	1.02	1.18	1.02
An	1.54	5.82	4.11	5.53	.08	2.34	5.61	3.49	.97	2.89	3.61	4.07	1.48
Di (En	-	9.85	11.94	16.21	1.37	1.67	6.90	13.44	4.40	11.15	14.01	13.44	5.29
Di (Fs	-	10.38	12.86	13.55	1.80	4.14	6.44	14.42	5.00	12.29	10,34	12.53	6.88
Di (Wo	-	19.40	25.15	30.68	3.17	5.57	13.65	28.24	9.49	23.72	25.31	26.59	12.17
Hy (En	-	-	2.47	5.36	.45	.35	8.32	7.55	4.77	2.48	5.58	3.52	1.00
Hy (Fs	-	-	2.66	4.48	.59	.87	7.76	8.10	5.42	2.73	4.12	3.28	1.30
Ol (Fo	35.10	10.85	12.63	4.31	36.13	20.34	13.47	4.62	20.45	14.32	9.11	11.61	25.96
Ol (Fa	50.58	12.60	14.99	3.97	52.20	55.69	13.85	5.46	25.60	17.39	7.41	11.93	37.20
Ne	.05	.41	-	-	-	-	-	-	-	-	-	-	-
Cs	.73	1.68	-	-	-	-	-	-	-	-	-	-	-
			-										
TOTAL	100.76	102.76	100.23	100.30	100.18	100.12	100.24	100.23	100.24	100.28	100.42	100.40	100.16
Mg-No	.47	.40	.50	.52	.50	.33	.49	.48	.46	.51	.53	.53	.48
mol% Fo	50	45	47	-	46	32	-	34	43	-	42	42	43

* Calculated using the technique of Irvine and Baragar (1971); ** Using the algorithm of Kelsey(1961); Mg-No = atomic% Mg/(Mg+Fe) mol% Fo from electron microprobe analyses. Samples from outcrop except nos.5,6,9,&10 (drill-core) and 7,11,12,&13 (mine workings). 1,2: LA-1 &-2,Grootboom-Annex Grootboom; 3,4: EB-1 &-2,Spitskop; 5,6: TLP-1A &-2,Townlands pipe; 7: RB-5,Brakspruit Pipe; 8: BK-2,Boschkoppie; 9,10: ML27-5 & ML24-12,Middellaagte Pipe; 11,12,13: Small,irregular bodies at Amandelbult.

did not exhibit any relevant trends.

Practically all of the pegmatites at Amandelbult may be classified as wehrlites or olivine clinopyroxenites. Dunites and olivine-poor clinopyroxenites are rare. Orthopyroxene is a significant component of a reasonable proportion of pegmatites, which may then be described as lherzolites or olivine websterites (fig. 8.10). However, it is possible that the CIPW norm exaggerates the proportion of orthopyroxene, as petrographic studies indicate that it is less abundant than this. The majority of these pegmatites contain significant Fe-Ti oxides, the proportion of which is usually between 5 and 20 normative percent. Olivine-rich pegmatite appears to contain less Fe-Ti oxide than pyroxene-rich pegmatite, but there is no clear-cut trend (fig. 8.11).

Most pegmatites contain less than 10 normative percent plagioclase (fig. 8.12). Pegmatite with more than 10 normative percent plagioclase may be considered as a hybrid rock, or partially replaced cumulate. This diagram shows that pegmatite rich in pyroxene, and thus poor in olivine tends to be richer in plagioclase. Typically, olivine-rich pegmatite contains less than 5 percent plagioclase, whereas clinopyroxene-rich pegmatite contains between 7 and 10 percent plagioclase. Pegmatites that contain more than 10 normative percent plagioclase should really be referred to as mafic, not ultramafic.

In Figure 8.13 two trends may be recognized. Firstly, scatter towards the (plagioclase + orthopyroxene) apex is demonstrated by hybrid samples in which a considerable proportion of relict cumulus minerals occur. These samples do not exhibit any corresponding increase in Fe-Ti oxides. Secondly, in pegmatite sensu stricto an increase in Fe-Ti oxides is accompanied by an increase in plagioclase and orthopyroxene. This is also evident from textural studies and whole-rock chemical data.

MINERALOGICAL ZONATION IN SMALL PEGMATITE BODIES

Within small pegmatite bodies an increase in the proportion of plagioclase and orthopyroxene usually occurs towards the margins. This is a contact feature and is not related to pegmatite zonation as such. Secondly, small pegmatite bodies in the lower main zone usually have a poorly-defined core of Fe-Ti oxide and, of course, large, composite pipe-like bodies in the main and upper zones consist of cores of Fe-Ti oxide pegmatite with an outer shell of silicate-rich pegmatite. No obvious mineralogical zonation is evident in small pegmatite bodies in the upper critical zone at Amandelbult. However, one sheet-like body has been examined in detail (see case study (2), Appendix 1).

From a sequence of samples through this body three principal mineralog-

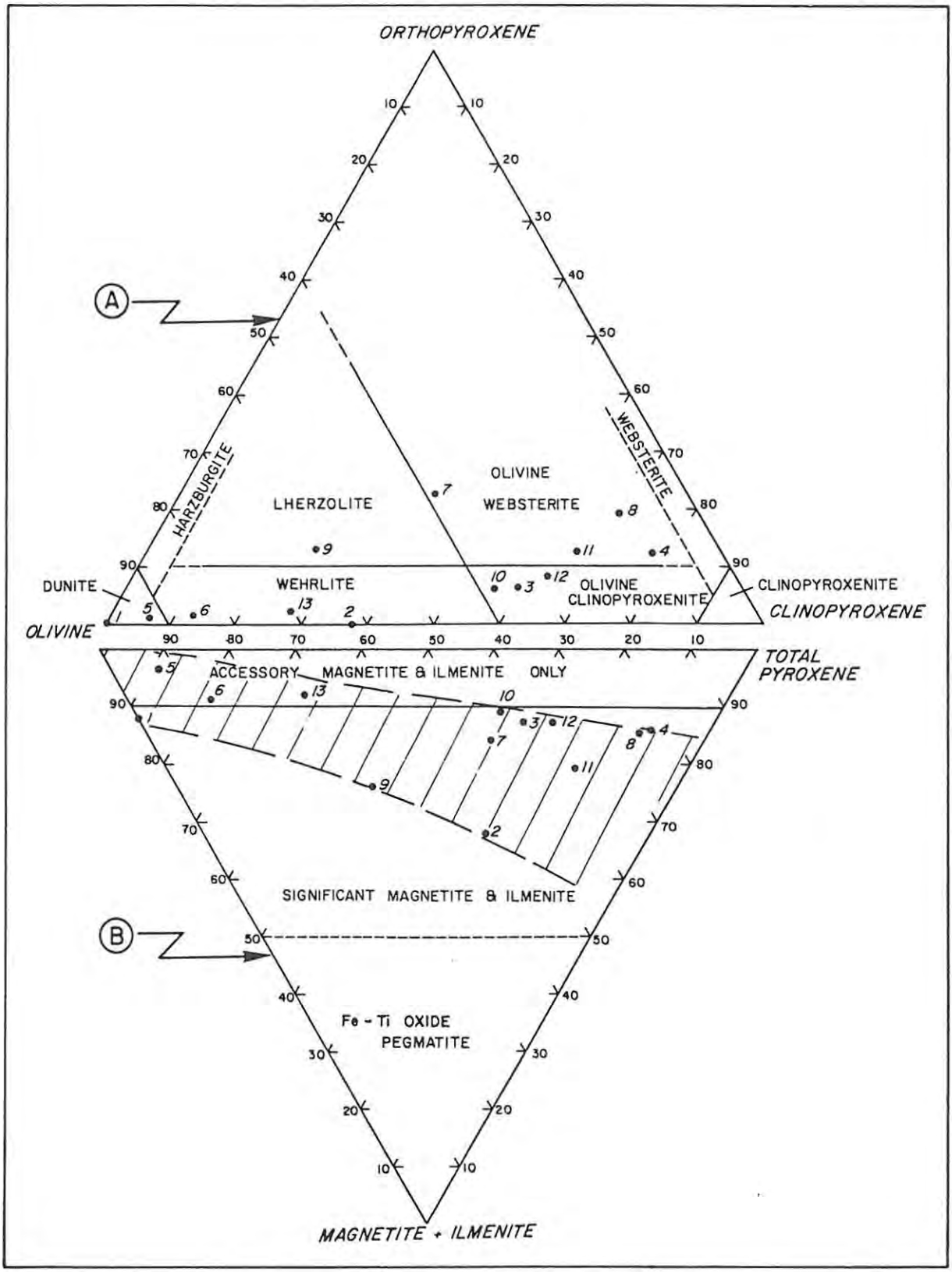

FIGURE 8.9 TERNARY DIAGRAMS OF THE CIPW NORM

(A) olivine - orthopyroxene - clinopyroxene;

(B) olivine - (magnetite + ilmenite) - (orthopyroxene + clinopyroxene).

For tabulation of complete CIPW norms see Appendix 6 - normative olivine = FO + FA; normative orthopyroxene = HYEN + HYFS; normative clinopyroxene = DIEN + DIFS + DIWO; normative magnetite = MT; and normative ilmenite = IL.

In this diagram each data point corresponds to the relevant analysis in Table 8.1 - they represent 13 selected samples of iron-rich ultramafic pegmatite from various localities in the Bushveld Complex. Fields defining a classification scheme, based essentially on plutonic rock nomenclature, are superimposed (see text).

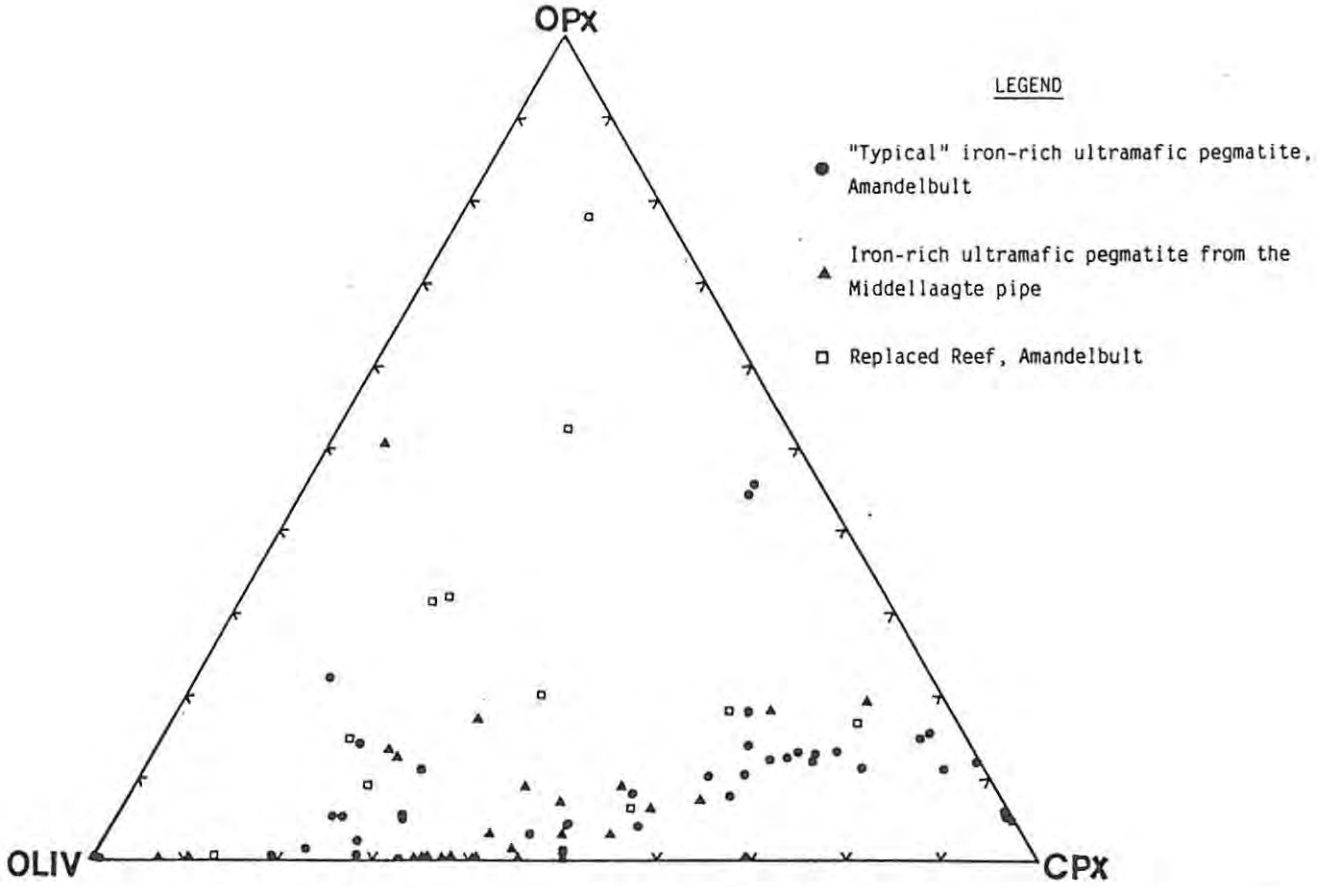

FIGURE 8.10 TERNARY DIAGRAM OF NORMATIVE OLIVINE - ORTHOPYROXENE - CLINOPYROXENE.
All samples of iron-rich ultramafic pegmatite from the upper critical - lower main zone at Amandelbult.

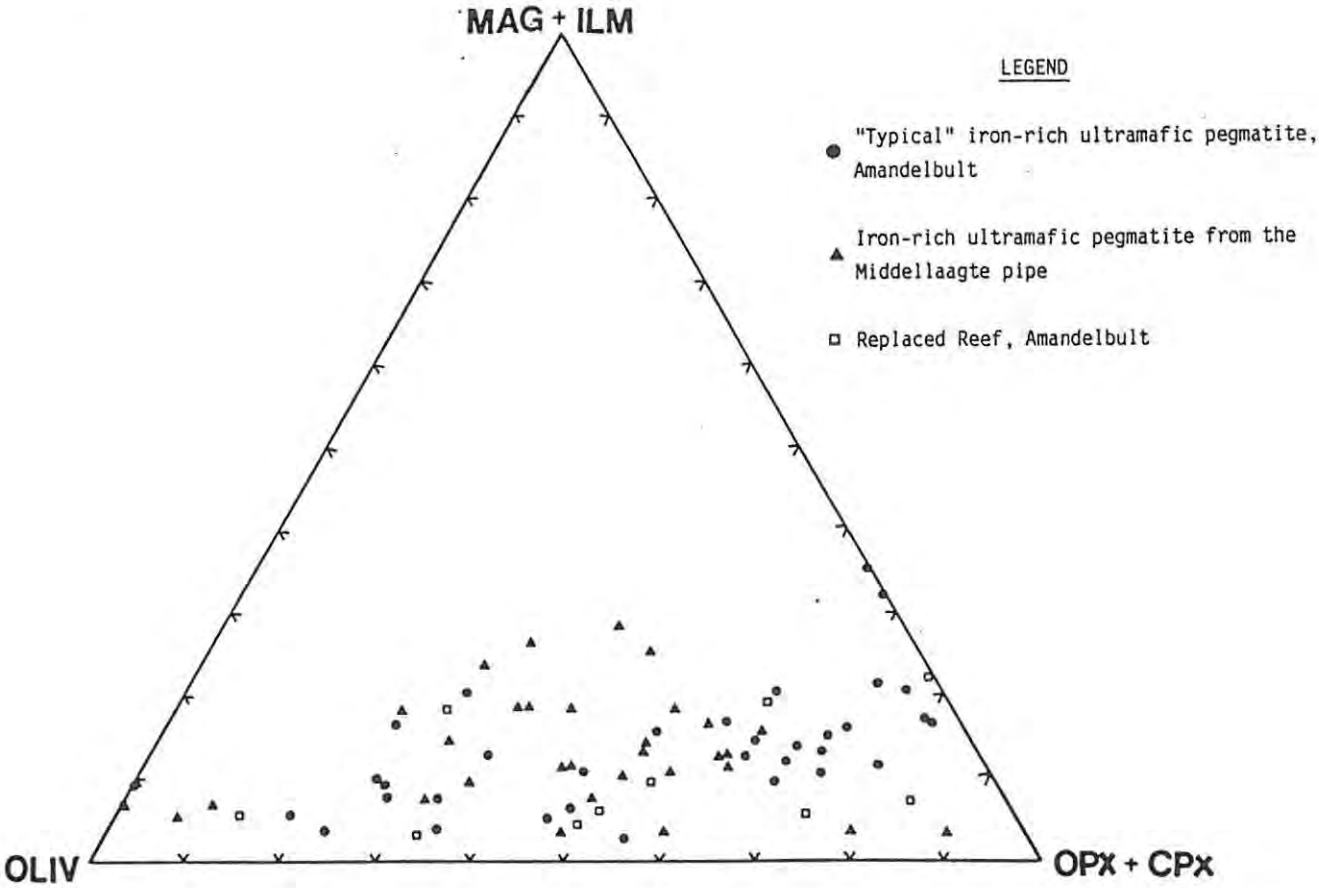

FIGURE 8.11 TERNARY DIAGRAM OF NORMATIVE OLIVINE - (MAGNETITE + ILMENITE) - (ORTHOPYROXENE + CLINOPYROXENE).
All samples of iron-rich ultramafic pegmatite from the upper critical - lower main zone at Amandelbult.

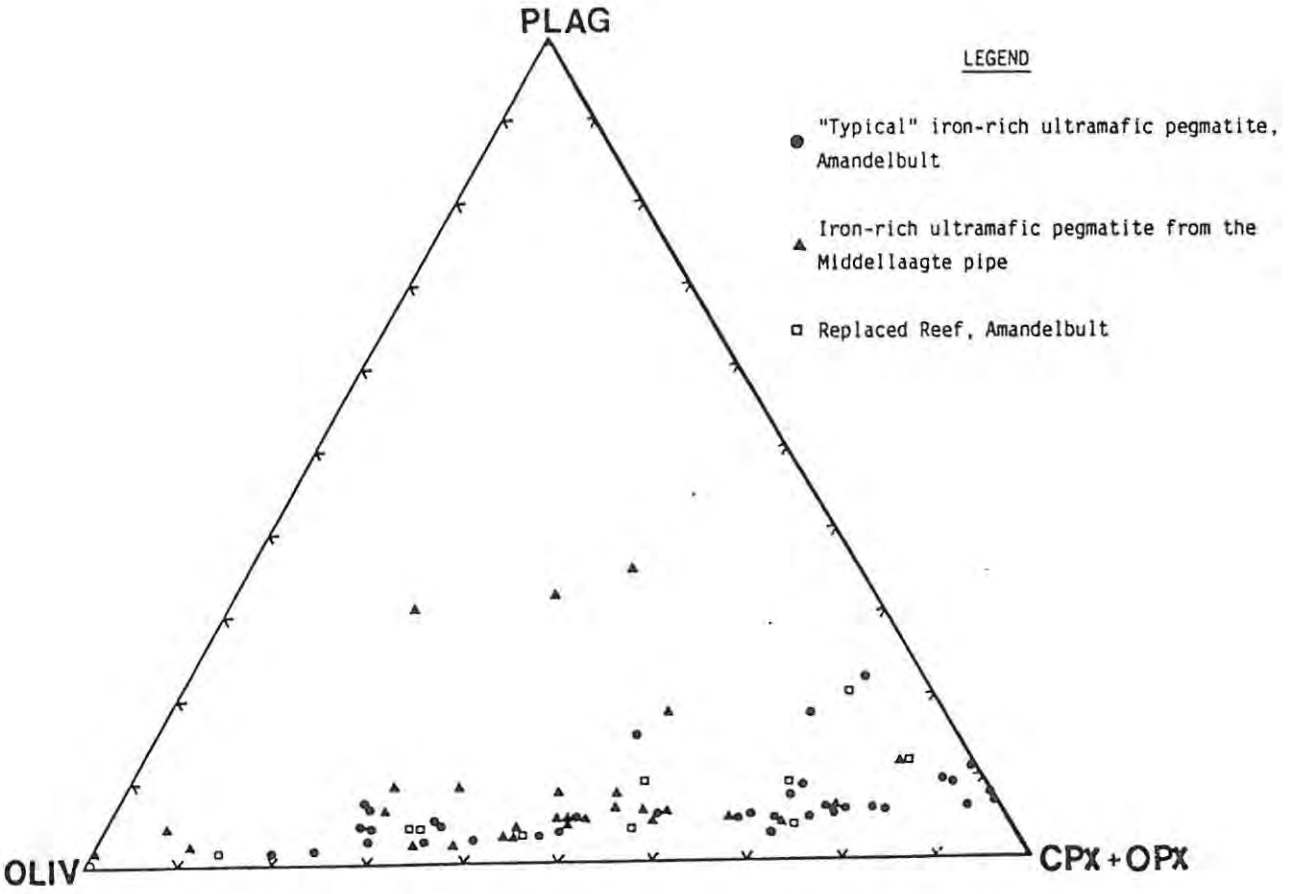

FIGURE 8.12 TERNARY DIAGRAM OF NORMATIVE OLIVINE - PLAGIOCLASE - (ORTHOPYROXENE + CLINOPYROXENE).
All samples of iron-rich ultramafic pegmatite from the upper critical - lower main zone at Amandelbult.

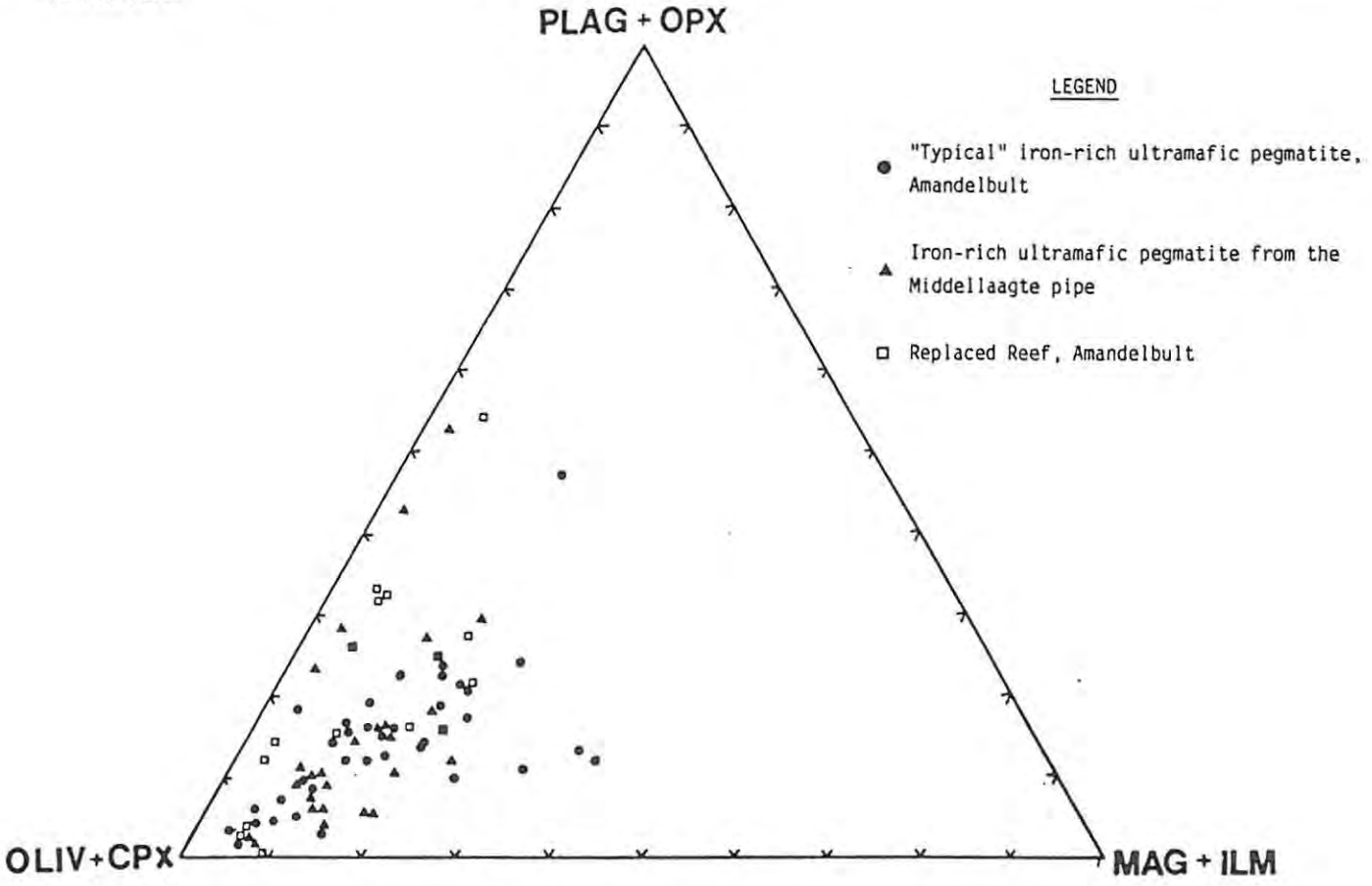

FIGURE 8.13 TERNARY DIAGRAM OF NORMATIVE (OLIVINE + CLINOPYROXENE) - (PLAGIOCLASE + ORTHOPYROXENE) - - (MAGNETITE + ILMENITE).
All samples of iron-rich ultramafic pegmatite from the upper critical - lower main zone at Amandelbult. Normative plagioclase = OR + AB + AN (see Appendix 6).

ical zones may be recognized (see figs. 12.1, 12.2):
(1) Olivine-rich pegmatite : this typically contains less than 10 normative percent Fe-Ti oxide and less than 3 normative percent plagioclase. It occurs at the top of this sheet-like body. This zone includes samples AE-8 to -12 (see Table 12.1). It may be described as an (olivine-rich) wehrlite pegmatite.
(2) Clinopyroxene-rich pegmatite : this typically contains over 10 normative percent Fe-Ti oxide and between 5 and 10 normative percent plagioclase. It occurs below the olivine-rich pegmatite and in the lower portion of this body. It includes samples AE-13 to -21 and AE-28 to -33A (Table 12.1). It may be described as an Fe-Ti oxide-olivine websterite pegmatite.
(3) "Mixed" zone : pegmatite in this zone contains varying proportions of olivine and clinopyroxene. It is characterised by between 10 and 20 normative percent Fe-Ti oxide, between 5 and 10 normative percent plagioclase and unusually high levels of incompatible elements (Nb, Zr and Y). It occurs as a poorly defined core enclosed by the clinopyroxene-rich pegmatite. It includes samples AE-23 to -27 (Table 12.1). It may be described as an Fe-Ti oxide-olivine websterite or clinopyroxenite pegmatite.

MINERALOGICAL ZONATION IN THE MIDDELLAAGTE PIPE

Samples of the Middellaagte pipe-like body all come from borehole core (see Appendix 1). These samples may be divided into several groups :
(1) Borehole ML27 : pegmatite from here is characterised by a relatively high content of Fe-Ti oxide (10-24 normative percent). The hole was drilled into the magnetic "core" of the pipe (see Chapter 7). The olivine:clinopyroxene ratio of this pegmatite is close to 1:1, and the samples lie in the fields covered by wehrlite, lherzolite and olivine clinopyroxenite. The plagioclase content is very low. Samples from this borehole are also characterised by an extremely low concentration of base-metal sulphide (see Chapter 11).
(2) Boreholes ML24, ML25 and ML26 : two pegmatite varieties are recognized in samples from these boreholes. Typical, plagioclase-poor pegmatite consists of variable proportions of olivine and clinopyroxene, and contains between 5 and 10 normative percent Fe-Ti oxide. Secondly, a plagioclase-orthopyroxene pegmatite is recognized which probably represents partially replaced cumulates (samples ML24-5,6,7 and ML26-8,12; all other samples are of the former variety). All of these samples contain fairly high concentrations of sulphide.
(3) Boreholes ML22 and ML29 : these intersect pegmatite from the margin of the main pipe-like body, and include small, irregular bodies from the lower part of the main zone (samples ML22-A3,A10,A18 and ML22-C9,C12) and pegmatite

from the upper critical zone (all other ML 22 samples and sample ML 29-1). The latter are comparable with pegmatite from small bodies in the upper critical zone at Amandelbult.

CHAPTER 9 CHEMISTRY OF THE SILICATE MINERALS

Iron-rich ultramafic pegmatite bodies exhibit convincing evidence of, at least in part, a metasomatic origin. In the ensuing discussion, however, it is assumed that the chemistry of the silicate phases is related to liquid crystallization trends, unless specific evidence can be presented to the contrary. This approach is enforced as most of the relevant literature relates to crystallization from liquids, and although metasomatism may simulate primary igneous features the processes are less well documented. The principal silicate minerals in iron-rich ultramafic pegmatite are olivine and clinopyroxene; accessory phases include plagioclase, orthopyroxene, amphibole and mica.

9.1 OLIVINE

9.1.1 PEGMATITE-HOSTED OLIVINE

ANALYTICAL AND SAMPLING DETAILS

Electron microprobe analyses of olivine from iron-rich ultramafic pegmatite at Amandelbult are presented in Table 9.1 (for analytical details see Appendix 7). These are all averages of samples that do not exhibit any major compositional variation (samples prefixed A-, 27-, and ML-; for sampling details see Appendix 1). Analyses of olivines from pegmatite bodies other than at Amandelbult have also been completed (Table 9.1). These include samples from pegmatite bodies in the upper critical zone at Townlands (TLP-), Boschkoppies (BK-), and Lavino (LA-), and from the main zone at Union Section (samples A-107, A-115, A-348; for sampling details see Appendix 2). Analyses of individual grains from metasomatic contact zones, adjacent to pegmatite bodies at Amandelbult are presented in Tables 9.3 and 9.4.

PARTITIONING OF Mg AND Fe BETWEEN OLIVINE AND SILICATE LIQUID

REVIEW

The distribution of Mg and Fe^{2+} between olivine (oliv) and silicate liquid (liq) may be expressed by the distribution coefficient K_D, thus :-

$$K_D = (X_{FeO} / X_{MgO})^{oliv} * (X_{MgO} / X_{FeO})^{liq} \quad \ldots (1)$$

where X_{MgO}, X_{FeO} are mole fractions. Roeder and Emslie (1970) investigated values of K_D for natural basaltic compositions and found that it was

TABLE 9.1 ELECTRON MICROPROBE ANALYSES OF OLIVINE IN IRON-RICH ULTRAMAFIC PEGMATITE

	AC-8			AD-5			AD-418			27-C2			27-F2			27-01			27-02			AE-8			AE-9			AE-12		
wt.%	x	d	n	x	d	n	x	d	n	x	d	n	x	d	n	x	d	n	x	d	n	x	d	n	x	d	n	x	d	n
SiO_2	35.16	.5364	5	34.66	.1697	2	34.82	.1697	2	35.17	.4581	4	34.84	.1414	2	35.13	.2635	6	34.66	.1626	2	34.26	.2416	6	34.56	.0819	3	34.31	.0566	2
FeO	42.67	.6981	5	45.05	.2404	2	45.45	.8202	2	42.93	.7557	4	45.03	.2546	2	43.65	.9226	6	41.46	.1555	2	46.18	.7146	6	46.10	.2117	3	46.04	.5020	2
MnO	.51	.0089	5	.51	.0071	2	.61	.0707	2	.52	.0171	4	.60	.0354	2	.58	.0358	6	.53	.0141	2	.58	.0207	6	.59	.0153	3	.61	.0212	2
MgO	22.03	.1234	5	20.53	.1980	2	19.95	.2475	2	22.10	.7315	4	20.60	.2121	2	21.59	.4489	6	21.97	.1768	2	18.93	.4724	6	19.80	.1836	3	19.56	.0141	2
CaO	.06	.0100	5	.08	.0424	2	.05	.0212	2	.04	.0173	3	.07	.0141	2	.05	.0207	6	.06	.0071	2	.04	.0121	6	.04	.0058	3	.06	-	2
NiO	.04	.0141	5	.04	.0071	2	.07	-	2	.06	.0157	3	.03	.0071	2	.07	.0129	6	.08	.0049	2	.03	.0084	6	.04	.0153	3	.03	.0071	2
TOTAL	100.47	-		100.87	-		100.95	-		101.02	-		101.17	-		101.27	-		98.76	-		100.02	-		101.12	-		101.61	-	
cations																														
Si	1.0091	-		1.0036	-		1.0092	-		1.0098	-		1.0061	-		1.0098	-		1.0097	-		1.0083	-		1.0034	-		1.0026	-	
Mn	.0124	-		.0125	-		.0150	-		.0126	-		.0147	-		.0140	-		.0131	-		.0145	-		.0145	-		.0151	-	
Mg	.9423	-		.8859	-		.8617	-		.9403	-		.8957	-		.9197	-		.9538	-		.8303	-		.8569	-		.8519	-	
Ca	.0018	-		.0025	-		.0016	-		.0012	-		.0216	-		.0015	-		.0019	-		.0013	-		.0012	-		.0019	-	
Ni	.0009	-		.0009	-		.0016	-		.0014	-		.0007	-		.0016	-		.0019	-		.0007	-		.0009	-		.0007	-	
TOTAL	2.9909	-		2.9964	-		2.9908	-		2.9902	-		2.9949	-		2.9902	-		2.9904	-		2.9917	-		2.9967	-		2.9974		
mol.% Fo	47.92	.4185	5	44.81	.3704	2	43.89	.1389	2	47.84	1.2573	4	44.91	.1150	2	46.85	.9564	6	48.57	.2948	2	42.21	.5223	6	43.35	.3037	3	43.09	.2497	2

	AE-20			AE-23			AE-25			AE-27			AE-28			AE-32			AG-13A			AH-3			AH-13			AH-17C		
wt.%	x	d	n	x	d	n		x	d	n	x	d	n	x	d	n	x	d	n	x	d	n	x	d	n	x	d	n	x	d	n
SiO_2	34.20	.1563	5	37.01	.5728	7	33.73	33.88	.1102	3	33.97	.1131	2	34.20	.1838	2	34.56	.3636	2	35.00	.1838	2	34.27	.2616	2	35.24	.2779	3			
FeO	46.63	.6829	5	27.67	.8037	7	46.01	46.31	.2747	3	46.11	.5798	2	46.08	.7407	3	45.86	.0212	2	42.32	.0636	2	45.26	.0283	2	42.37	.1415	3			
MnO	.58	.0303	5	.34	.0208	7	.57	.56	.0153	3	.60	-	2	.59	.0389	3	.61	-	2	.51	.0071	2	.57	.0071	2	.51	.0231	3			
MgO	18.89	.2657	5	33.39	.7346	7	18.79	18.61	.2815	3	19.30	.8910	2	18.96	.5484	3	20.10	.0990	2	23.32	.3323	2	19.96	.1273	2	23.88	.2743	3			
CaO	.06	.0055	5	.02	.0181	7	.03	.07	.0058	3	.05	.0071	2	.08	-	2	.03	.0212	2	.06	.0071	2	.09	.0071	2	.05	.0153	3			
NiO	.03	.0164	5	.51	.0462	7	.04	.02	.0100	3	.05	.0071	2	.04	.0252	3	.03			.05	.0283	2	.07	.0071	2	.11	.0320	3			
TOTAL	100.19	-		98.94	-		99.16	99.45	-		100.02	-		99.95	-		101.24	-		101.26	-		100.22	-		102.16	-			
cations																														
Si	1.0062	-		1.0027	-		1.0032	1.0054	-		1.0001	-		1.0073	-		1.0013	-		.9951	-		1.0022	-		.9921	-			
Fe^{2+}	1.1424	-		.6269	-		1.1444	1.1493	-		1.1353	-		1.1350	-		1.1113	-		1.0063	-		1.1070	-		.9976	-			
Mn	.0145	-		.0078	-		.0144	.0141	-		.0150	-		.0147	-		.0150	-		.0123	-		.0141	-		.0122	-			
Mg	.8282	-		1.3482	-		.8329	.8231	-		.8468	-		.8322	-		.8579	-		.9882	-		.8570	-		1.0020	-			
Ca	.0019	-		.0006	-		.0010	.0022	-		.0016	-		.0025	-		.0025	-		.0018	-		.0028	-		.0015	-			
Ni	.0007	-		.0112	-		.0010	.0006	-		.0012	-		.0010	-		.0007	-		.0011	-		.0017	-		.0025	-			
TOTAL	2.9938	-		2.9973	-		2.9968	2.9946	-		2.9999	-		2.9927	-		2.9987	-		3.0049	-		2.9978	-		3.0079	-			
mol.% Fo	42.02	.1157	5	68.25	1.0495	7	42.12	41.76	.4181	3	41.41	.9989	2	42.30	.3106	3	43.86	.1327	2	49.54	.3188	2	44.00	.1725	2	50.10	.3389	3			

	AH-21	AH-21B	AH-23			M.22-2A			M.22-5			M.22-11			M.24-1			M.24-7A			M.26-8A			M.27-38			M.27-5		
wt.%			x	d	n	x	d	n	x	d	n	x	d	n	x	d	n	x	d	n	x	d	n	x	d	n	x	d	
SiO_2	34.99	34.12	34.35	.1704	3	34.66	.2902	3	34.36	.0141	2	34.64	.1202	2	33.57	.1739	3	33.51	.1464	3	38.18	.3243	8	34.93	.2253	4	34.59	.3721	8
FeO	34.84	44.95	46.08	.2402	3	41.47	.2739	3	41.62	.0566	2	42.91	.1556	2	44.69	.2458	3	45.72	.2550	3	23.50	.2184	8	47.34	.1329	4	45.56	1.3084	8
MnO	.52	.57	.56	.0265	3	.55	-	3	.55	.0141	2	.60	.0283	2	.59	.0265	3	.61	.0265	3	.34	.0131	8	.67	.0287	4	.65	.0426	8
MgO	29.35	20.20	19.67	.0651	3	21.50	.3356	3	21.40	.0990	2	21.61	.0212	2	19.91	.2250	3	19.24	.2669	3	37.50	.3668	8	18.61	.1352	4	19.89	.6260	8
CaO	.04	.10	-	-		.07	.0493	3	.03	.0141	2	.05	.0071	2	.05	.0115	3	.09	.0436	3	.02	.0064	8	.07	-	1	.08	.0129	4
NiO	.10	.01	.03	.0153	3	.04	.0200	3	.04	.0212	2	.04	-	2	.04	.0115	3	.04	.0058	3	.24	.0247	8	.06	.0150	4	.06	.0125	8
TOTAL	99.84	99.96	100.69	-		98.29	-		98.00	-		99.85	-		98.85	-		99.21	-		99.78	-		101.68	-		100.83	-	
cations																														
Si	.9757	.9996	1.0026	-		1.0148	-		1.0110	-		1.0043	-		.9963	-		.9960	-		1.0021	-		1.0134	-		1.0065	-	
Fe^{2+}	.8126	1.1013	1.1248	-		1.0155	-		1.0241	-		1.0406	-		1.1093	-		1.1365	-		.5158	-		1.1486	-		1.1076	-	
Mn	.0124	.0141	.0138	-		.0136	-		.0137	-		.0147	-		.0148	-		.0154	-		.0076	-		.0165	-		.0160	-	
Mg	1.2201	.8820	.8656	-		.9382	-		.9384	-		.9337	-		.8807	-		.8523	-		1.1467	-		.8046	-		.8616	-	
Ca	.0023	.0031	-	-		.0022	-		.0009	-		.0016	-		.0016	-		.0029	-		.0006	-		.0022	-		.0025	-	
Ni	.0023	.0002	.0007	-		.0009	-		.0010	-		.0009	-		.0010	-		.0010	-		.0051	-		.0014	-		.0014	-	
TOTAL	3.0243	3.0004	2.9975	-		2.9852	-		2.9891	-		2.9957	-		3.0037	-		3.0040	-		2.9979	-		2.9966	-		2.9946	-	
mol.% Fo	60.02	44.47	43.20	.1680	3	48.03	.2739	3	47.81	.0815	2	47.29	.0658	2	44.25	.2913	3	42.86	.4146	3	74.00	.2660	8	41.19	.1984	4	43.76	1.4613	8

	M.29-K			M.29-J2			TLP-1A			TLP-2			BK-2			LA-1			LA-2	A-107			A-115			A-348		
wt.%	x	d	n		x	d	n	x	d	n	x	d	n	x	d	n	x	d	n		x	d	n	x	d	n	x	d	n
SiO_2	36.25	-	2	35.20	34.13	.0321	3	32.57	.0636	2	33.08	.0424	2	34.86	.0950	2	34.46			32.19	.3020	3	32.38	.0777	3	34.64	.1414	2
FeO	43.14	.0354	2	40.97	44.51	.1677	3	52.86	.1786	2	50.91	.8768	2	40.67	.2404	2	44.18			53.86	.1361	3	56.73	.3516	3	44.92	.1202	2
MnO	.58	-	2	.48	.56	.0153	3	.77	.0283	2	.73	.0212	2	.54	.0212	2	.57			.99	.0404	3	1.00	.0058	3	.62	-	2
MgO	23.89	.1626	2	22.96	21.33	.0777	3	13.98	.1485	2	14.73	.2899	2	23.15	.2687	2	20.33			11.71	.2196	3	10.73	.1115	3	20.15	.5728	2
CaO	.06	.0141	2	.08	.11	.0068	3	.10	.0071	2	.07	.0283	2	.10	.0071	2	.06			.09	.0306	3	.10	.0153	3	.09	.0071	2
NiO	.06	-	2	.06	.10	.0173	3	.015	.0707	2	.06	-	2	.06	.0071	2	.07			.01	.0153	3	.02	.0252	3	.025	.0071	2
TOTAL	103.97	-		99.73	100.74	-		100.30	-		99.58	-		99.37	-		99.67			98.85	-		99.96	-		100.45	-	
cations																													
Si	1.0015	-		1.0099	.9897	-		.9949	-		1.0068	-		1.0043	-		1.0078			1.0074	-		1.0093	-		1.0076	-	
Fe^{2+}	.9968	-		1.0794	1.1503	-		1.2958	-		1.2958	-		.9799	-		1.0806			1.4096	-		1.4528	-		1.0927	-	
Mn	.0136	-		.0117	.0138	-		.0199	-		.0188	-		.0132	-		.0141			.0262	-		.0264	-		.0153	-	
Mg	.9837	-		.9818	.9218	-		.6364	-		.6681	-		.9940	-		.8861			.5461	-		.4984	-		.8735	-	
Ca	.0018	-		.0025	.0034	-		.0033	-		.0228	-		.0031	-		.0019			.0030	-		.0033	-		.0028	-	
Ni	.0011	-		.0012	.0023	-		.0004	-		.0147	-		.0012	-		.0017			.0003	-		.0006	-		.0006	-	
TOTAL	2.9985	-		2.9901	3.0103	-		3.0052	-		2.9932	-		2.9957	-		2.9922			2.9926	-		2.9907	-		2.9924	-	
mol.% Fo	49.67	.1907	2	49.97	46.06	.0971	3	32.03	.3041	2	34.01	.8284	2	50.36	.4380	2	45.06			27.92	.3980	3	25.55	.0961	3	44.42	.7637	2

independent of temperature in the range 1150-1300°C. They quoted an average value for K_D of 0.3. If equilibrium conditions are assumed the MgO/FeO ratio of a silicate liquid may be calculated from knowledge of the olivine composition (see Appendix 13). The effects of changing T, P, fO_2 and melt composition have been investigated by more recent workers, but as these effects are small an average value for K_D of 0.3 ± 0.03 is generally accepted (Roeder, 1974; see also review by Deer et al., 1982, pp. 70-78). The dependence of olivine composition on that of the liquid, and the relative crystallization temperatures of different olivine compositions are discussed by Roeder (1974).

DISCUSSION

The composition of olivine from iron-rich ultramafic pegmatite at Amandelbult is invariably between Fo_{50} and Fo_{40} (Table 9.1). Olivine from small pegmatite bodies at Amandelbult, which all occur between the UG-2 and Bastard cyclic units, has an average composition of Fo_{44}, and olivine from the "core" of the large Middellaagte pipe has an average composition of Fo_{43} (Table 9.2). Compositional zonation in small pegmatite bodies at

TABLE 9.2 AVERAGE COMPOSITION OF OLIVINE AND CLINOPYROXENE

	1	2	3
OLIVINE			
MgO	20.24 (1.3212)	19.11 (.4089)	19.41 (.6189)
FeO	44.99 (1.5626)	46.18 (.2032)	45.83 (1.1052)
MnO	.56 (.0364)	.585 (.0160)	.63 (.0365)
NiO	.044 (.0174)	.035 (.0093)	.05 (.0115)
Fo	44.5 (2.47)	42.3 (.647)	43.0 (1.346)
No. of samples	20	8	4
No. of analyses	58	25	18
CLINOPYROXENE			
X_{Mg}	.64 (.0165)	.639 (.0162)	.657 (.0162)
Range	.61-.68	.61-.67	.64-.67
No. of samples	17	7	4
No. of analyses	54	26	18

1. All samples of iron-rich ultramafic pegmatite in upper critical zone, Amandelbult (excluding samples from Middellaagte pipe).
2. Individual, sheet-like pegmatite body, Amandelbult ("AE" samples, case-study (2), "replacing" Footwall cyclic unit).
3. Core of the Middellaagte pipe ("ML" samples, case-study (1)).

Amandelbult has not been detected. For example, olivine from a pegmatite body emplaced in the Footwall cyclic unit (case study (2), "AE" samples; see Appendix 1) has an average composition of $Fo_{42.3}$ (Table 9.2).

The composition of olivine from iron-rich ultramafic pegmatite bodies in the upper critical zone at other localities in the Bushveld Complex is probably similar. In the Townlands pipe, Rustenburg, however, two compositional ranges have been identified, namely Fo_{50} to Fo_{46} and Fo_{33} to Fo_{30} (samples TLP-1A and TLP-2, Table 9.1). These results are supported by whole-rock data (see TLP- samples in Table 12.3) and by the work of Phillips (in prep.). It is suggested that the magnesian olivine, which occurs in the core of the body, is the typical composition and the iron-rich (Fo_{33-30}) olivine, which occurs in the margin of the pipe, is atypical. This iron-rich olivine may have resulted from post-crystallization replacement of the magnesian olivine.

The composition of olivine in small, irregular bodies of iron-rich ultramafic pegmatite from the main zone at R.P.M. Union Section can be related to height in the cumulate pile. For example, using the Bastard Reef (B.R.) as a datum, compositions of $Fo_{44.4}$ (12.6 m above B.R.), $Fo_{27.9}$ (1399 m above B.R.) and $Fo_{25.6}$ (1350 m above B.R.) have been determined (samples A-107, A-115, A-348, Table 9.1; analyses from Mitchell, in prep.).

PARTITIONING OF NICKEL BETWEEN OLIVINE AND SILICATE LIQUID

REVIEW

Nickel is an ubiquitious trace element in magnesian olivine but may be absent, or present in only very low levels, in iron-rich olivine. The concentration of Ni in olivine may be used, in conjunction with the Fo content, as an indicator of fractionation. Typically, the NiO and MgO contents of olivine decrease with fractionation. The distribution of Ni between olivine and silicate liquid has been the subject of a number of investigations, many of which have been reviewed by Deer et al. (1982, pp. 78-88). The partitioning of Ni into Mg-rich olivine is attributed by Burns (1970) to its high octahedral site preference energy. More basic magmas have a higher proportion of octahedrally co-ordinated sites such that the partitioning of Ni may be dependent on bulk liquid composition, as well as on T, P and fO_2. Although this is a controversial subject, such that there is no generally accepted value for the partitioning of Ni between olivine and liquid the relationship determined by Hart and Davis (1978) has received acceptance amongst many workers. They synthesised olivine from a wide range of basaltic liquid compositions (T = 1250-1450^{o}C, P = 1 atm) in the system

Fo-Ab-An. The partition coefficient (D_{Ni}) is defined thus :-

$$D_{Ni} = (\text{Ni in olivine}) / (\text{Ni in liquid}) \quad \ldots (2)$$

Hart and Davis found that D_{Ni} was dependent on melt composition, thus :-

$$D_{Ni} = (124.13 / \text{MgO in liq}) - 0.897 \quad \ldots (3)$$

MgO being expressed in wt. percent. Hart and Davis found that D_{Ni} was independent of the Ni content of the liquid, and that the intrinsic temperature dependence is small and may be related to variations in melt composition with temperature. This relationship may be used in conjunction with formula (1) above to calculate the MgO, FeO and NiO contents of olivine and liquid in successive residual magmas which are undergoing olivine fractionation (see Appendix 13).

In the example presented in Appendix 13 it is shown that after 2 wt. percent olivine has crystallized the composition of the olivine (initially Fo_{79} with 0.42 wt. percent NiO) should be Fo_{77} with 0.30 wt. percent NiO. In this particular example, which starts with a relatively Ni-rich olivine, Ni is depleted from the liquid when the olivine reaches a composition of approximately Fo_{56}. It may be concluded that the Ni content of magnesian olivine is a much more sensitive indicator of fractionation than the Mg/Fe ratio.

Mysen and Kushiro (1976) investigated the relationship between D_{Ni} and fO_2 in a sample of carbonaceous chondrite. They found that the Ni content of silicates, including olivine, increased with increasing fO_2. However, the Ni/Mg ratio of olivine may not itself be dependent on fO_2. Mysen and Kushiro (1979) report that D_{Ni} is pressure-dependent and decreases with increasing pressure, a function of depolymerization in high pressure melts (10-20 kilobar range). Mysen (1979) investigated the compositional effect of bulk Ni in a silicate melt. He found that D_{Ni} is independent of Ni content until 1000 ppm is dissolved in forsterite ($T = 1300^{o}C$, $P = 1$ atm to 20 kilobars). The relationship between D_{Ni} and bulk melt composition has been investigated by Mysen and Virgo (1980). They found that the ratio of non-bridging oxygens to tetrahedral cations is important, such that as this ratio increases D_{Ni} decreases linearly. Thus, the atomic ratio Si/O has an important effect on D_{Ni}. Mysen and Virgo (1980) also investigated the influence of tetrahedral cations such as Fe^{3+}, P^{3+}etc., but because these are only minor components in most silicate melts they have little influence on the value of D_{Ni}. However, the Al^{3+} content may be very significant. Thus the distribution of Ni

between olivine and silicate liquid is a complex, and often controversial issue, consequently the selection of any one method for calculating values of D_{Ni} is open to debate.

DISCUSSION

The Ni content of olivine from iron-rich ultramafic pegmatite at Amandelbult varies between 0.08 and 0.01 wt. percent, with an average of 0.044 wt. percent NiO (Tables 9.1, 9.2). Olivine from the "core" of the Middellaagte pipe has an average content of 0.05 wt. percent NiO and olivine from the "AE" pegmatite body at Amandelbult contains an average of 0.035 wt. percent NiO. Olivine from the Townlands pipe appears to be slightly richer in Ni compared to that from Amandelbult (sample TLP-1). Extremely iron-rich olivine from the Townlands pipe and that from pegmatite bodies in the main zone contain less than 0.02 wt. percent NiO. From Figure 9.1 it is evident that some Ni depletion occurs as the composition becomes poorer in MgO, but in general the accuracy of these data are not sufficient to warrant detailed modelling.

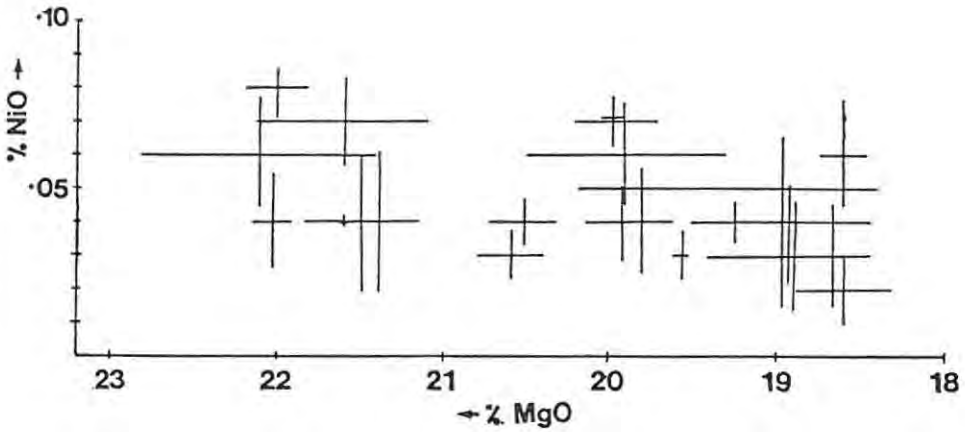

FIGURE 9.1 Plot of wt. % NiO vs. wt. % MgO in olivine.
Data points (error bars = plus-minus one standard deviation (d) from the mean (x)) based on averages of electron microprobe analyses in Table 9.1. All samples are from iron-rich ultramafic pegmatite bodies at Amandelbult.

DISTRIBUTION OF Mn IN OLIVINE

REVIEW

Manganese is an important minor constituent of most ferromagnesian minerals. Its distribution may be related to that of Fe^{2+}, such that in olivine Mn behaves in the reverse manner to Ni. The partitioning of Mn between olivine and silicate liquid (D_{Mn}) is not as sensitive as D_{Ni}, consequently it has not recieved such widespread attention. Watson (1977) determined values of D_{Mn} at various temperatures for a number of melt compositions. In the compositional range 48.9 to 60.4 wt. percent SiO_2, D_{Mn}

varies between 0.62 and 0.90 and 0.51 and 0.67 at temperatures of 1350 and 1450°C, respectively. At lower temperatures the partitioning is more composition dependent. The data of Duke (1976) and Watson (1977) indicate that the effect of iron on the partitioning of Mn is small, at typical basaltic liquidus temperatures.

DISCUSSION

The distribution of MnO in olivine from iron-rich ultramafic pegmatite at Amandelbult is illustrated in Figure 9.2. In this compositional range the MnO content increases approximately linearly as the olivine becomes more fayalitic. The MnO content is between 0.43 and 0.52 for olivine with a composition of Fo_{50}, and between 0.57 and 0.66 for olivine with a composition of Fo_{41} (see also Table 9.2). In even more iron-rich olivines, from other pegmatite samples, the MnO content increases rapidly, such that the FeO/MnO ratio becomes non-linear (fig. 9.6). For example, olivine with a composition of $Fo_{25.6}$ from a pegmatite body in the main zone contains 1.00 wt. percent MnO.

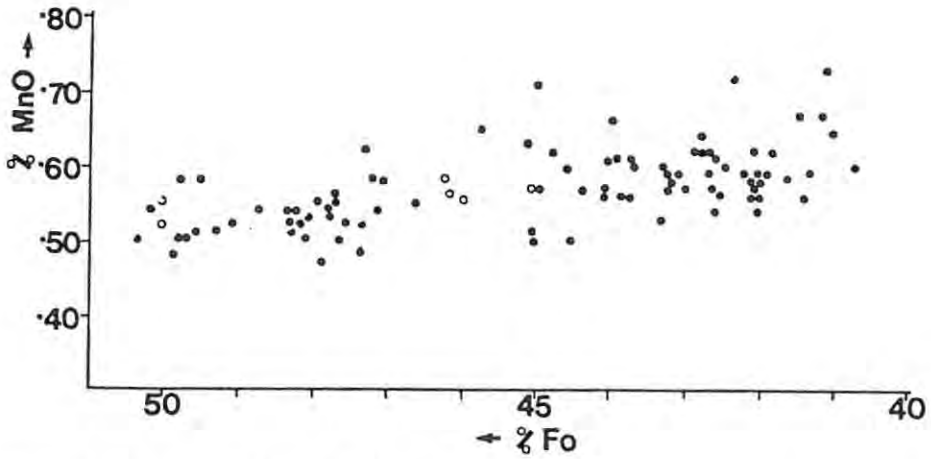

FIGURE 9.2 Plot of wt. % MnO vs. mol. % Fo in olivine.
Data points are individual electron microprobe analyses. Solid circles are samples from iron-rich ultramafic pegmatite bodies at Amandelbult, open circles are samples from the Townlands pipe (samples TLP-1A, TLP-1B).

DISTRIBUTION OF Ca IN OLIVINE

Binary graphs of wt. percent CaO versus molecular percent Fo and weight percent MgO (not shown here) exhibit a scattered range of data points. It may be concluded that the distribution of Ca in olivines in this study is of little petrogenetic significance. This may partly be a function of limited analytical accuracy, as the average CaO content of these olivines is very low (see Table 9.1).

OLIVINE IN METASOMATIC CONTACT ZONES

The preferential development of iron-rich ultramafic pegmatite in felsic cumulates may result in apparently sharp contacts between olivine-bearing ultramafic cumulates and postcumulus pegmatite bodies (see pp. 118, 143). Electron microprobe analyses of olivines across two such contacts are presented in Tables 9.3 (sample AD-37A) and 9.4 (sample AC-A). Individual analyses are labelled alphabetically so that precise sample positions may be located in Figures 9.3 and 9.4 - these diagrams represent vertical profiles across a thin section. In both cases the average composition of pegmatite-hosted olivine is based on a range of analyses from within that particular pegmatite body. The average composition of cumulus olivine is based on sample A-7/8 (Table 6.1).

Textural evidence suggests that olivine in these contact zones is related to metasomatism of pre-existing cumulus, magnesian olivine (see p. 144). This is supported by analytical data, as the composition of these metasomatic olivines is part-way between two end-members, the primary cumulus composition ($Fo_{81.3}$, in these examples) and average pegmatite compositions (Fo_{50-41}). Compositional variation is exhibited by the major elements, particularly MgO and FeO (as expressed by the Fo content) and the minor elements NiO and MnO. If the NiO and MnO contents are plotted against the MgO and FeO contents, respectively, they plot on straight lines (figs. 9.5, 9.6). This may be expressed by the following linear regressions (oxide values in wt. percent; n = number of analyses; cc = correlation coefficient) :-

MgO = (51.78 * NiO) + 21.57 (Sample AD-37A; n = 13; cc = .980) ... (4)

MgO = (48.12 * NiO) + 20.15 (Samples AC-A,B; n = 7; cc = .996) ... (5)

Data for these two samples result in slightly different linear regressions for NiO (fig. 9.5). The second data set includes an average pegmatite composition (sample AC-B), as it is part of the vertical profile (fig. 9.4). These linear regressions, however, do <u>not</u> include a value for the average cumulus composition, for reasons apparent in Figure 9.5 (see below).

FeO = (85.89 * MnO) - 1.63 (n = 22; cc = .972) ... (6)

This equation includes analyses of the metasomatic olivines (samples AD-37A and AC-A, n = 19), an average composition of the pegmatite-hosted olivines (samples AD-24 and AC-B, averages based on 2 and 5 analyses, respectively;

TABLE 9.3 ELECTRON MICROPROBE ANALYSES OF OLIVINES FROM A METASOMATIC CONTACT ZONE - SAMPLE AD-37A

	A	O	N	M	K	J	I	C	H	G	D	F	E
wt.%													
SiO_2	35.39	35.51	35.33	37.28	36.53	36.37	36.58	36.77	37.55	37.21	37.74	37.61	38.49
FeO	37.98	38.43	37.39	37.00	37.25	32.39	31.19	29.78	29.51	28.41	22.73	21.93	19.84
MnO	.47	.44	.46	.45	.45	.37	.37	.36	.37	.37	.33	.26	.25
MgO	25.75	25.41	26.75	26.44	26.68	30.90	31.84	33.09	33.43	33.43	38.82	39.20	39.14
CaO	.05	.05	.04	.01	.03	.03	.02	.03	.03	.14	.01	.04	.05
NiO	.08	.07	.10	.10	.12	.14	.21	.26	.22	.24	.32	.35	.31
TOTAL	99.72	99.91	100.07	101.28	101.06	100.20	100.21	100.28	101.11	99.61	99.95	99.39	98.08
cations													
Si	1.0009	1.0037	.9930	1.0257	1.0113	.9941	.9940	.9917	1.0005	1.0031	.9874	.9863	1.0101
Fe^{2+}	.8983	.9847	.8789	.8514	.8625	.7404	.7088	.6717	.6576	.6405	.4973	.4810	.4354
Mn	.0113	.0105	.0110	.0105	.0106	.0086	.0085	.0082	.0084	.0084	.0073	.0058	.0056
Mg	1.0853	1.0704	1.1206	1.0842	1.1008	1.2588	1.2894	1.3301	1.3275	1.3355	1.5136	1.5321	1.5308
Ca	.0015	.0015	.0012	.0003	.0009	.0009	.0006	.0009	.0009	.0040	.0003	.0011	.0014
Ni	.0018	.0016	.0023	.0022	.0027	.0031	.0046	.0057	.0047	.0052	.0068	.0074	.0066
TOTAL	2.9991	2.9963	3.0070	2.9743	2.9887	3.0059	3.0052	3.0083	2.9995	2.9969	3.0126	3.0137	2.9899
mol. %													
Fo	54.71	54.09	56.04	56.01	56.07	62.96	64.53	66.44	66.87	67.58	75.27	76.11	77.85

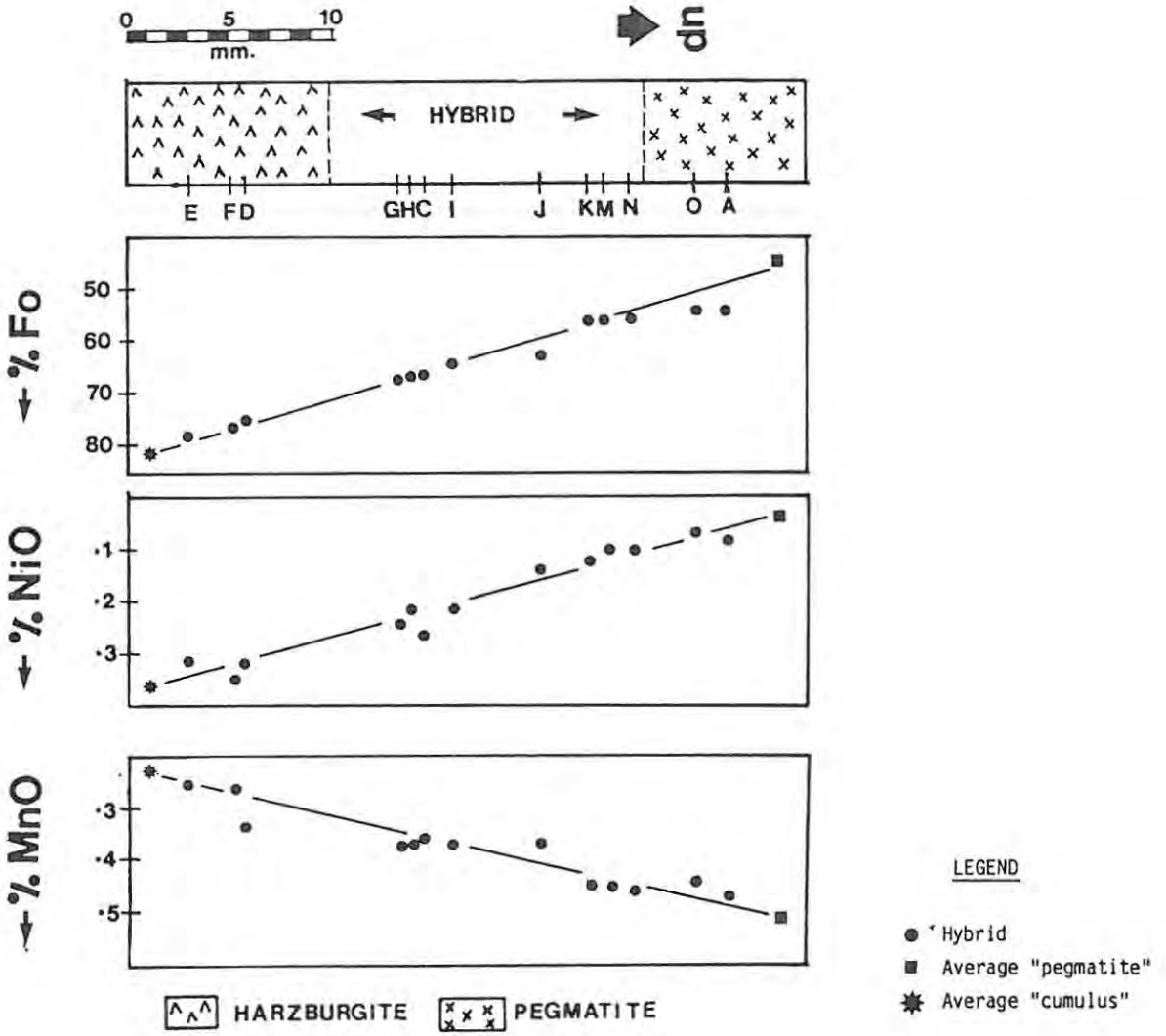

FIGURE 9.3 Compositional variation in olivine across a metasomatic contact zone - (1) Sample AD-37A.

Based on one probe slide cut normal to a transitional contact between the top of the upper pseudoreef B and a pegmatite body; the primary layering is preserved (see case-study (3), Appendix 1). Data for hybrid olivines from the contact zone are individual electron microprobe analyses (Table 9.3, labelled "A" - "O"), the average "pegmatite" composition is from sample AD-5 (Table 9.1), and the average "cumulus" composition is from sample A-7/8 (Table 6.1). NiO and MnO are in wt. % and Fo is in mol. %.

TABLE 9.4 ELECTRON MICROPROBE ANALYSES OF OLIVINES FROM A METASOMATIC CONTACT ZONE (SAMPLE AC-A)

	G	F	E	D	C	B	A
wt.%							
SiO_2	35.49	35.68	36.59	36.83	37.04	37.44	37.52
FeO	37.32	36.27	31.53	31.29	30.91	26.37	27.04
MnO	.47	.45	.37	.35	.38	.35	.33
MgO	26.10	26.49	31.07	31.30	31.84	34.17	34.92
CaO	.04	.02	.02	.01	.01	.03	.01
NiO	.17	.13	.22	.23	.26	.29	.30
TOTAL	99.59	99.04	99.80	100.01	100.44	98.65	100.12
cations							
Si	1.0021	1.0073	1.0000	1.0024	1.0016	1.0090	.9990
Fe^{2+}	.8813	.8564	.7206	.7122	.6990	.5944	.6021
Mn	.0112	.0108	.0086	.0081	.0087	.0080	.0074
Mg	1.0983	1.1146	1.2654	1.2700	1.2831	1.3724	1.3857
Ca	.0012	.0006	.0006	.0003	.0003	.0009	.0002
Ni	.0039	.0030	.0049	.0050	.0060	.0063	.0065
TOTAL	2.9979	2.9979	3.0000	2.9976	2.9984	2.9910	3.0011
mol. %							
Fo	55.48	56.55	63.72	64.06	64.73	69.78	69.71

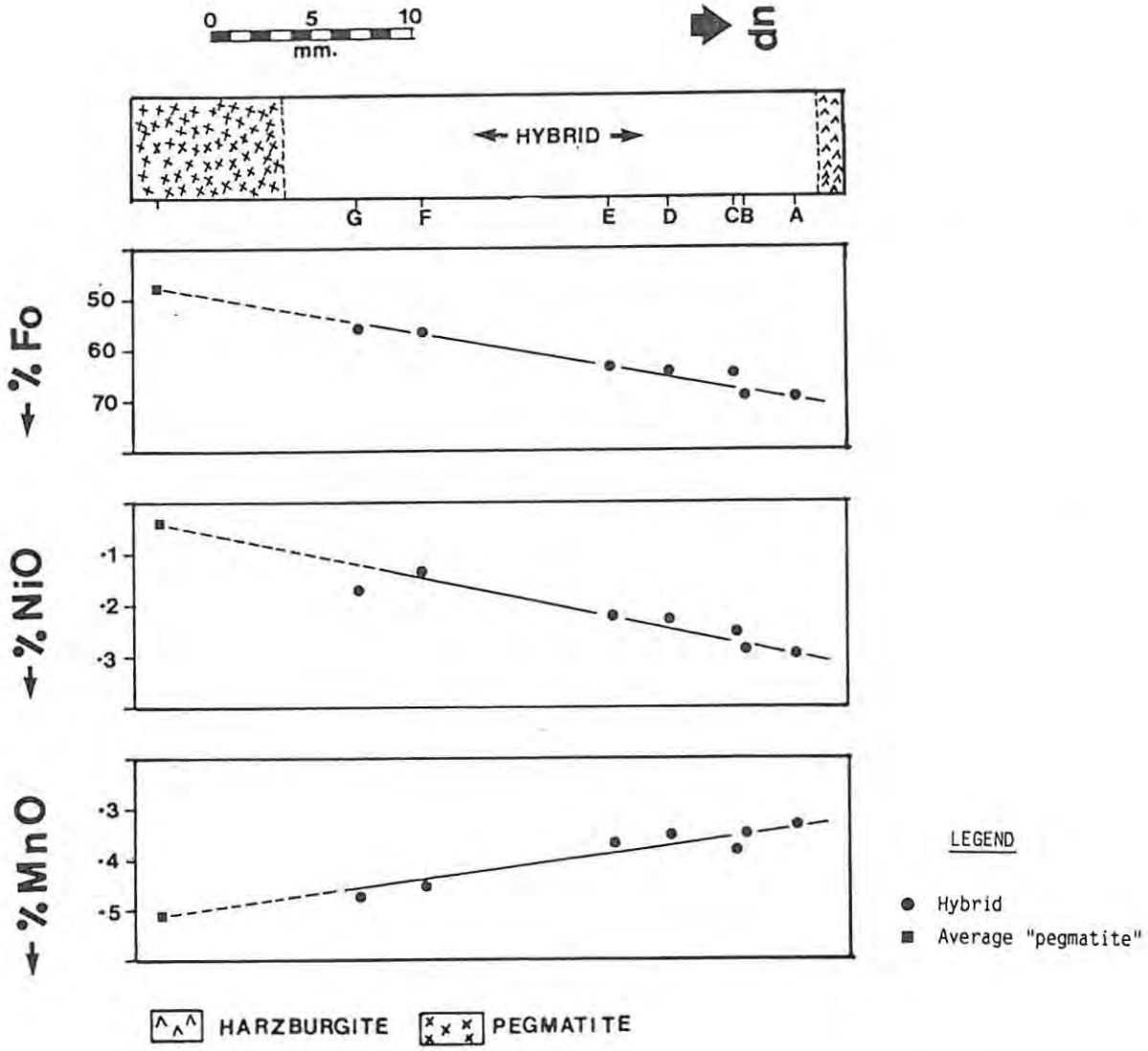

FIGURE 9.4 Compositional variation in olivine across a metasomatic contact zone - (2) Sample AC-A.

Based on two probe slides cut normal to a transitional contact between the base of the upper pseudoreef B and a pegmatite body; the primary layering is preserved (see case-study (4), Appendix 1). Data for hybrid olivines from the contact zone are individual electron microprobe analyses (Table 9.4, labelled "A" - "G"), the average "pegmatite" composition is from sample AC-B (Table 9.1). NiO and MnO are in wt. % and Fo is in mol. %.

see Table 9.1) and an average of the cumulus olivines (sample A-7/8, average based on 11 analyses; see Table 6.1). The validity of including the average pegmatite and average cumulus compositions is evident from examining Figure 9.6, and the above correlation coefficient.

9.1.2 COMPARISON WITH CUMULUS OLIVINES IN THE BUSHVELD COMPLEX

SAMPLING DETAILS

Electron microprobe analyses of cumulus, iron-rich olivines from the upper zone of the Bushveld Complex (samples WT-128, TSM, P-5, and IR-64 to IR-330) are presented in Table 9.5. All samples prefixed IR- are from Reynolds (in press). Analyses of cumulus, magnesian olivines from the upper critical zone are presented in Table 6.1.

Mg/Fe RELATIONSHIPS

In the layered sequence of the Bushveld Complex cumulus, magnesian olivine is restricted to the lower and critical zones; the highest occurrence of magnesium-rich olivine is probably in the Merensky Reef (see Chapter 6). Magnesium-rich olivine from the lower and lower critical zones is usually in the compositional range Fo_{87} to Fo_{83} (Cameron, 1978, 1980; see also Botha, in prep.), that from the upper critical zone is in the compositional range Fo_{82} to Fo_{76} (see Chapter 6). Cumulus olivine appears to be absent in the main zone, but iron-rich olivine is an important cumulus phase in the upper zone. Wager and Brown (1968) document some of the compositional trends exhibited by cumulus olivines in the Bushveld Complex, but as far as the author is aware the only published electron microprobe analyses of iron-rich olivine in the upper zone are those of Reynolds (in press); optically determined data are, however, also presented by Von Gruenewaldt (1973) and Molyneux (1972).

Sample WT-128 is of particular importance - it possibly represents the lowest occurrence of cumulus, iron-rich olivine in the layered sequence and is thus the first cumulus olivine to crystallize after the "olivine gap" in the main zone. This sample, which is from 8 m below the main magnetite layer (sample in borehole core, Amandelbult), has a composition of Fo_{56} (Table 9.5). Olivine is then a cumulus phase from this position until close to the roof of the complex, and thus defines a compositional range from Fo_{56} to approximately Fo_{0} (Wager & Brown, 1968; Reynolds, in press). These data imply that the compositional gap in the layered sequence of the Bushveld Complex is restricted to the compositional range Fo_{76} to Fo_{56}.

Olivine in iron-rich ultramafic pegmatite also defines an upward iron

TABLE 9.5 ELECTRON MICROPROBE ANALYSES OF CUMULUS OLIVINES FROM THE UPPER ZONE

	WT-128			TSM			P-5	IR-330	IR-266	IR-226	IR-138	IR-113	IR-64
wt.%	x	d	n	x	d	n							
SiO_2	35.24	.1768	3	34.76	.1725	4	34.93	33.15	32.48	31.78	31.31	31.12	30.10
FeO	37.20	.2616	3	44.08	.1967	4	43.95	51.26	54.07	56.23	58.71	60.65	65.36
MnO	.48	-	3	.60	-	4	.60	.76	.81	.90	1.04	1.03	1.48
MgO	26.73	.5233	3	22.26	.1519	4	21.76	15.29	12.75	10.54	8.77	7.53	2.72
CaO	.05	-	3	.07	.0219	4	.07	-	-	-	-	-	-
NiO	n.d.	-		n.d.	-	4	n.d.	-	-	-	-	-	-
TOTAL	99.70			101.77	-		101.29	100.46	100.11	99.45	99.83	100.33	99.66
cations													
Si	.9935	-		.9921	-		1.0005	1.0000	1.0004	1.0005	.9966	.9954	1.0019
Fe^{2+}	.8771	-		1.0522	-		1.0528	1.2932	1.3928	1.4805	1.5628	1.6224	1.8195
Mn	.0115	-		.0145	-		.0146	.0194	.0211	.0240	.0280	.0279	.0417
Mg	1.1230	-		.9469	-		.9289	.6874	.5853	.4945	.4160	.3589	.1349
Ca	.0015	-		.0021	-		.0021	-	-	-	-	-	-
Ni	-	-		-	-		-	-	-	-	-	-	-
TOTAL	3.0065			3.0079	-		2.9988	3.0000	2.9996	2.9995	3.0034	3.0046	2.9981
mol.%													
Fo	56.15	-		47.37	-		46.87	34.71	29.59	25.04	21.02	18.12	6.90

Samples prefixed "IR-" from Reynolds (in press).

enrichment trend and they are always more fayalitic than cumulus olivine for a given height. It may be predicted that postcumulus olivine in pegmatite bodies in the upper zone would lie in the compositional range ferrohortonolite to fayalite.

NiO-MgO RELATIONSHIPS

Cumulus olivines (in the compositional range Fo_{87} to Fo_{84}) in the lower and lower critical zones usually contain between 0.20 and 0.35 wt. percent NiO (Cameron, 1978, 1980; Botha, in prep.). The NiO content of cumulus olivine in the upper critical zone is highly variable (Chapter 6). In cumulus, iron-rich olivine from the upper zone, NiO is below the lower limit of determination on the electron microprobe used in this study. In Figure 9.5 a "cumulus" trend, related to a postulated fractionation path (ignoring cyclic units and new magma influxes) may be extrapolated between the Ni-rich magnesian olivines and the most magnesian of the Ni-poor, iron-rich olivines (e.g., sample WT-128).

This measured fractionation path may be duplicated using theoretically derived data, as discussed above (see Appendix 13). In Figure 9.5 a theoretical fractionation path is plotted based on initial liquid composition of 15 wt. percent MgO, assuming that it is in equilibrium with olivine with a composition of $Fo_{81.3}$ and 0.36 wt. percent NiO (sample A7/8, Table 6.1). Theoretical fractionation paths over-estimate the NiO content of fayalitic olivines as the Hart and Davis equation yields improbably large values for D_{Ni} as the liquid becomes MgO-poor. Thus, the actual fractionation path

probably plots closer to the MgO axis. The paths plotted in Figure 9.5 (labelled "A") are thus based on the most Ni-rich path possible for measured and theoretical compositions of cumulus olivine in the Bushveld Complex. Postcumulus olivines from the iron-rich ultramafic pegmatite suite are clearly unusually rich in Ni relative to these fractionation paths. A "pegmatite trend" (curve "B", fig. 9.5) may be inferred from these data.

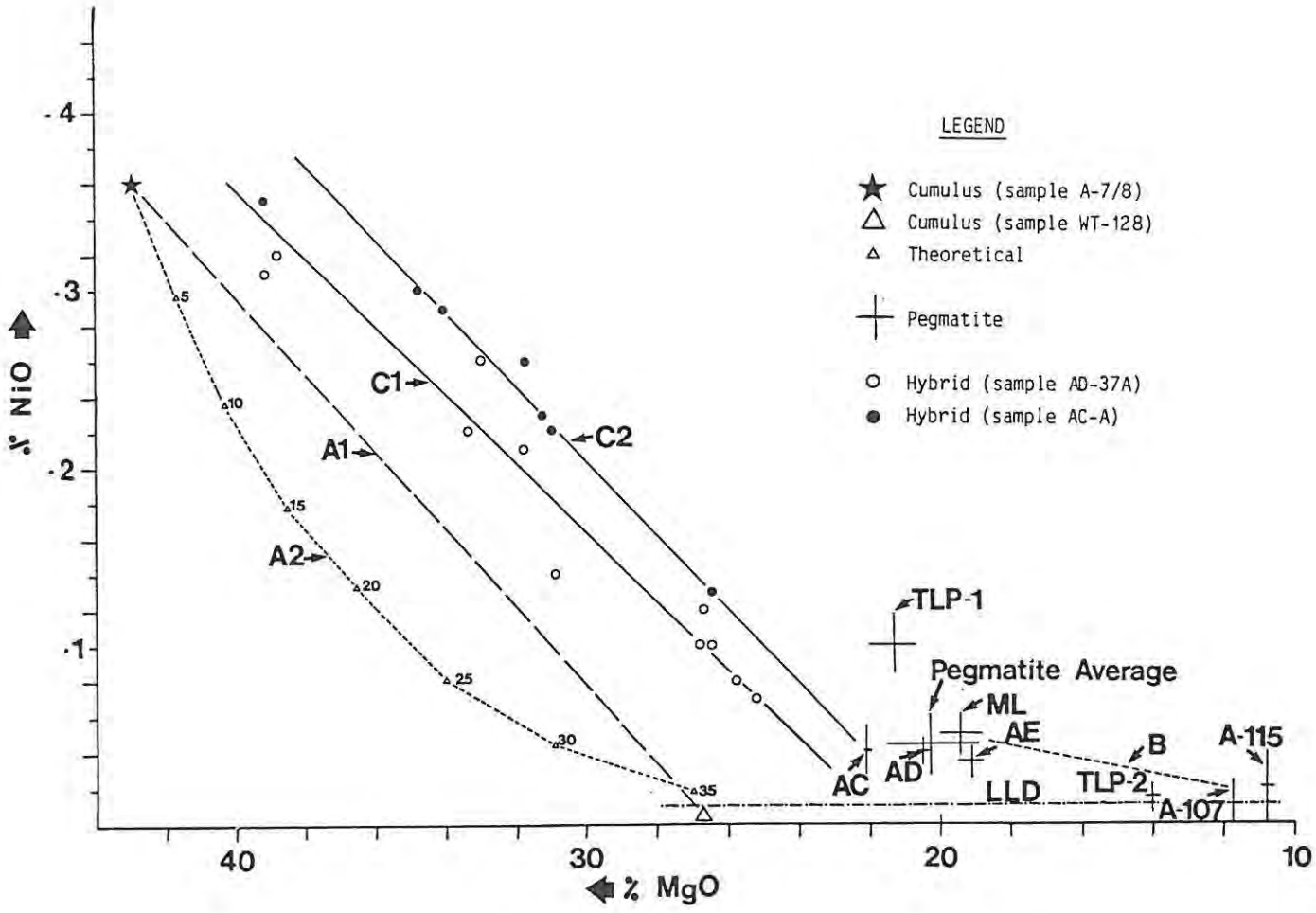

FIGURE 9.5 Plot of wt. % NiO vs. wt. % MgO in olivine.

This plot includes electron microprobe data for cumulus, pegmatite-hosted and hybrid olivines. LLD = lower limit of determination (= 0.01 wt. % NiO). CUMULUS SAMPLES - A-7/8 is from the upper pseudoreef B (Table 6.1) and WT-128 is from the base of the upper zone (Table 9.5). PEGMATITE SAMPLES - these data are based on averages (error bars = plus-minus one standard deviation (d) from the mean (x)); "pegmatite average" and the "AE" and "ML" samples are from the upper critical zone at Amandelbult (Table 9.2), samples TLP-1 (typical) and TLP-2 (unusually iron-rich) are from the Townlands pipe (Table 9.1), and samples A-107, A-115 are from pegmatite bodies in the main zone (see Table 9.1). HYBRID SAMPLES - from the metasomatic contact zones presented in Figures 9.3, 9.4). Pegmatite averages AD and AC are the end-members of these hyhrid samples. TREND "A1" represents the most Ni-rich measured fractionation path for cumulus olivine. TREND "A2" is a theoretical fractionation path, using sample A-7/8 as the initial composition (assuming initial liquid contains 15 wt. % MgO; data points on this trend are at intervals of 5 % crystallized - the liquid is depleted in Ni after 35 % crystallized). TREND "B" is the pegmatite fractionation path. The hybrid samples plot on separate straight lines, TRENDS "C1" and "C2" (see text); note that these trends do not regress back to the primary cumulus composition (sample A-7/8).

Olivines from the metasomatic contact zones described above plot on straight lines ("C1" and "C2", fig. 9.5). These data suggest that during metasomatism of magnesian olivine by iron-rich liquids or fluids (which have a much lower MgO/FeO ratio than the initial liquid in equilibrium with the primary olivine) NiO is "replaced" in the lattice less effectively than MgO by FeO. This results in olivine with an unusually high NiO/MgO ratio. If this metasomatic process is arrested after only a short interval it may result in olivine in which the Fo component is decreased by, say, 5 or 10 mol. percent, but the NiO content is unaffected; thus primary and metasomatic olivine may have similar NiO contents. This explains why "metasomatic" trends do not regress back to primary compositions.

In the Muskox Intrusion, Irvine (1980, pp.341, 353) reports olivines, which are an essential part of the cumulate sequence, with unusually high NiO/MgO ratios. Irvine explains this by his model of infiltration metasomatism, in which the cumulus olivines are exposed to upward-migrating, iron-rich (nickel-poor), intercumulus liquid. Metasomatism results in olivine with a lower Mg/Fe ratio whereas the Ni content is only slightly affected (see also Chapter 13).

Iron-rich olivines from the platiniferous ultramafic pipes also define a straight line relationship, and consequently it is inferred that they too are of a metasomatic origin (see pp. 50-54). It is, however, important to note that all metasomatic olivines distinguished in this study have resulted from replacement of pre-existing magnesian olivine in response to iron-rich liquids or fluids. These data do not imply that all of the pipe-hosted olivines are of a metasomatic origin, and in fact do not provide any direct pointer to the formation of the bulk of the olivine in these rocks.

Olivine in iron-rich ultramafic pegmatite is richer in Ni than might be expected if it is compared with similarly iron-rich, cumulus olivines in the Bushveld Complex. Field relationships and petrographic studies indicate that they only rarely result from metasomatic replacement of pre-existing cumulus olivines. Therefore, whether they are of a metasomatic origin or have crystallized directly from a liquid, their composition must be directly related to that of the putative pegmatitic liquid. This pegmatitic liquid may be Ni-rich in comparison with the primary Bushveld magma with a similar MgO/FeO ratio. Alternatively, it may be postulated that T, P and fO_2 in the pegmatitic liquid result in a much higher D_{Ni} than in the main magma chamber.

MnO-FeO RELATIONSHIPS

The Mn content of cumulus and pegmatite-hosted olivines in the Bushveld Complex is illustrated in Figure 9.6. The cumulus trend is based on analyses by the author and by Reynolds (in press, analyses prefixed IR; see Table 9.5). No data are available for cumulus compositions from Fo_{76} to Fo_{56}. Olivine more magnesian than Fo_{81} has not been plotted. For compositions between 17 and 54 wt. percent FeO (approximately Fo_{81} to Fo_{30}) the relationship between FeO and MnO is linear and may be described thus :-

FeO = (63.88 * MnO) - 4.1 (n = average of 9 samples; cc = .995) .. (7)

With compositions more fayalitic than Fo_{30} the MnO content increases much more rapidly than the FeO content, consequently the MnO/FeO relationship becomes asymptotic.

Pegmatite-hosted olivine in the compositional range Fo_{50} to Fo_{40} is slightly depleted in MnO as compared with the "cumulus" trend. However, the metasomatic olivines discussed above plot on a straight line which approximates the cumulus trend. Pegmatite-hosted olivine which is more fayalitic than Fo_{40} is richer in MnO than equivalent cumulus samples, consequently a "pegmatite" trend can be constructed which cuts across the cumulus trend, becoming asymptotic at a lower FeO content (fig. 9.6). The asymptotic nature of the MnO/FeO relationship in olivine may possibly be explained by a rapid increase in bulk MnO in the liquid or an increase in D_{Mn} in iron-rich liquids.

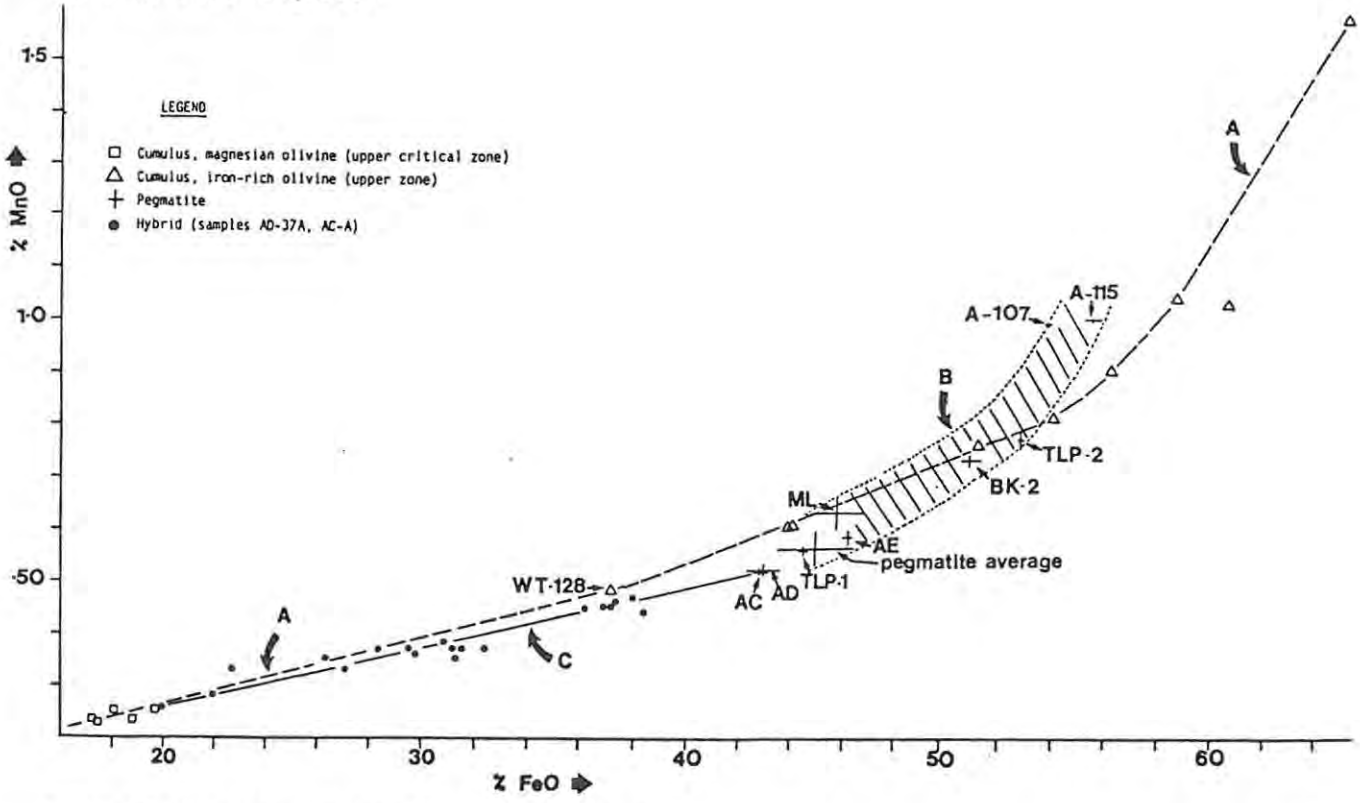

FIGURE 9.6 Plot of wt. % MnO vs. wt. % FeO in olivine.

This plot includes electron microprobe data for cumulus (averages from the upper critical zone (Table 6.1) and upper zone (Table 9.5)), pegmatite-hosted and hybrid olivines (same data as in Figure 9.5). Note differences between the cumulus fractionation path ("A") and the pegmatite fractionation path ("B"). The hybrid olivines define a single straight line "C".

9.2 CLINOPYROXENE

DISTRIBUTION OF Mg, Fe AND Ca

ANALYTICAL AND SAMPLING DETAILS

Electron microprobe analyses of clinopyroxene in iron-rich ultramafic pegmatite from Amandelbult are presented in Appendix 8. These are individual analyses as, for reasons which will become apparent, averages are not representative. These have been recalculated on the basis of six oxygens, assuming total iron is Fe^{2+}. These analyses include the minor elements Al, Ti, Mn, Na and Cr. Nickel was determined on a few samples, but it is very close to the lower limit of determination. A major problem with electron microprobe analysis of coarse-grained pyroxenes is the presence of exsolution lamellae. One method of overcoming this is by using a defocused beam with a large spot diameter (Buchanan, 1979). However, exsolution lamellae in the pegmatitic pyroxenes may be coarse enough to permit the use of a small, focused beam positioned between the lamellae. This results in an analysis of the host pyroxene, separately from the guest lamallae. In other samples exsolution lamellae are very narrow, requiring the use of a large spot size of approximately 30 to 40 microns.

DISTRIBUTION OF Mg AND Fe

Ca-rich clinopyroxene in iron-rich ultramafic pegmatite at Amandelbult is an iron-rich variety of augite with an average X_{Mg} ($Mg/(Mg+Fe^{2+})$) of 0.64 (Table 9.2). Similar averages are calculated for samples from one particular pegmatite body at Amandelbult ("AE" sample group) and from the Middellaagte pipe. All of these averages have low standard deviations, indicating that X_{Mg} is constrained within very limited ranges. Zonation, with respect to X_{Mg}, has not been detected in individual grains. No compositional differences were detected between any of the different textural habits of clinopyroxene. This may be used as further evidence to support the conclusions reached in Chapter 8 (cf. p. 139). Clinopyroxene from pegmatite bodies in the main zone exhibits an upward fractionation trend, as defined by a gradual decrease in the X_{Mg} ratio (fig. 9.7; see Mitchell, in prep.). The narrow compositional range of clinopyroxenes in iron-rich ultramafic pegmatite from the upper critical zone, and the upward iron-enrichment trend match the trends shown by olivine.

DISTRIBUTION OF Ca

Compared with the Bushveld trend of Atkins (1969), the pegmatite-hosted clinopyroxenes are relatively rich in Ca. Moreover, they exhibit a

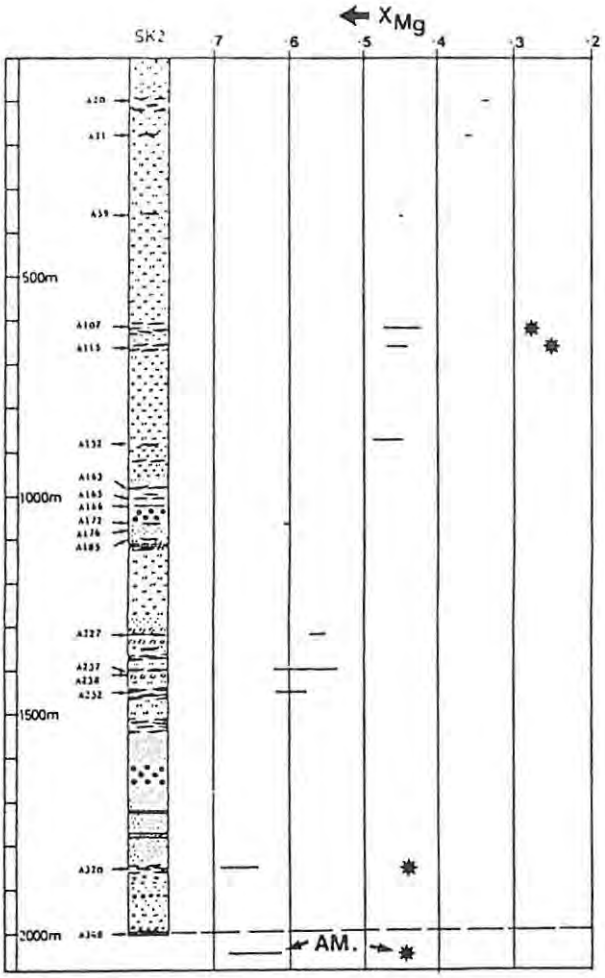

FIGURE 9.7 Variation in X_{Mg} of pegmatite-hosted clinopyroxene and olivine with height in the main zone. Based on data of Mitchell (in prep., see Table 9.1 and Appendix 8). Samples A-348, A-320 etc. refer to iron-rich ultramafic/mafic pegmatite bodies in borehole SK-2, Union Section (for explanation of other symbols and variation in X_{Mg} of cumulus pyroxenes with height see Mitchell, in prep.). Bars indicate the range in X_{Mg} of clinopyroxene, stars refer to the composition of olivine. Samples labelled "AM" are average data from the upper critical zone, Amandelbult (see Table 9.2).

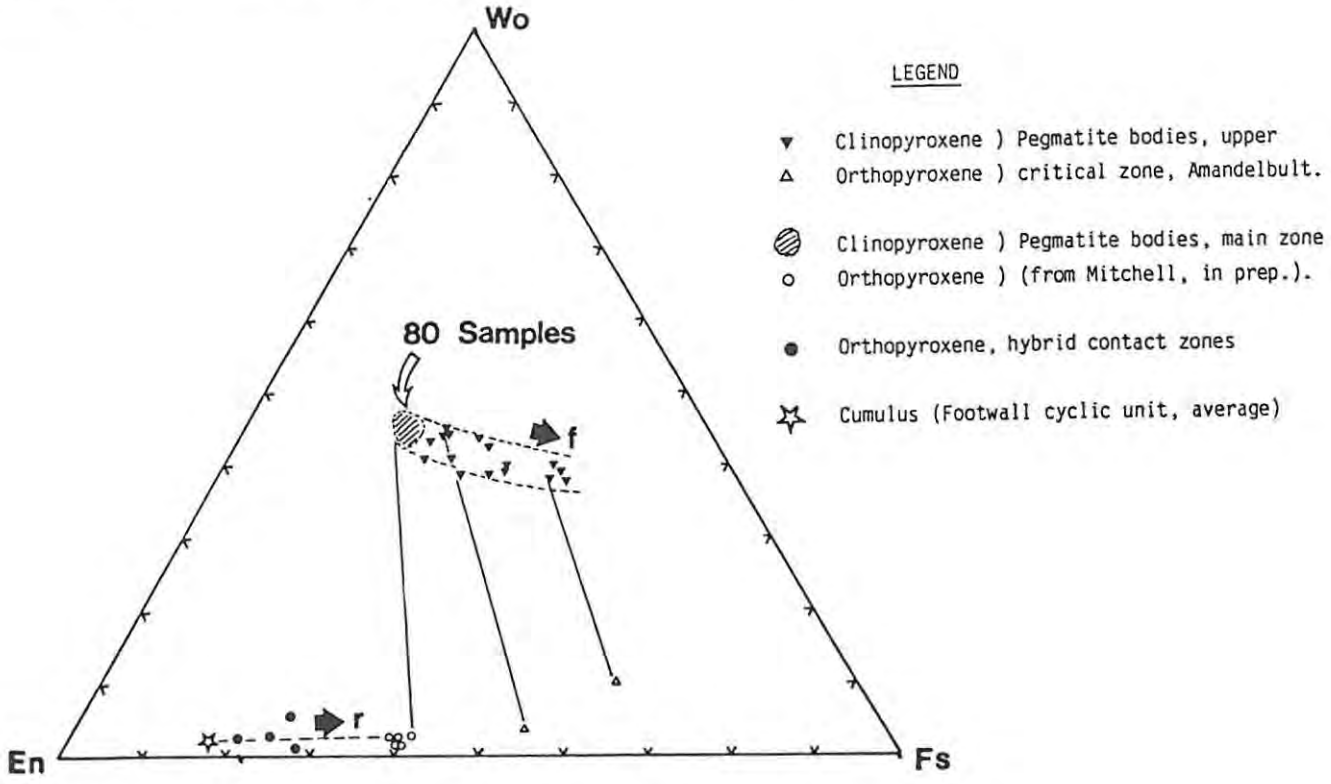

FIGURE 9.8 The pyroxene ternary diagram, En-Wo-Fs.
Note the pegmatite fractionation path ("f") and the replacement sequence ("r").

considerable range in Ca content (fig. 9.8). This may be a feature of the analytical technique used. For example, Buchanan (1979) found that electron microprobe analyses with a defocused beam, in comparison with a focused beam, were poorer in Ca and richer in Fe and Mg. This is to be anticipated in clinopyroxenes which contain exsolved laths of Ca-poor (Mg,Fe) orthopyroxene, but many of the pegmatite-hosted clinopyroxenes do not contain exsolution lamellae. It may be concluded that they are richer in Ca than cumulus samples with an equivalent X_{Mg} ratio. This may be related to primary liquidus compositions, as in the absence of Ca-poor pyroxene the composition of augite is not constrained by the solvus, but simply follows a path dictated by the liquid (see Morse, 1980, p. 341).

9.2.2 DISTRIBUTION OF THE MINOR ELEMENTS

TITANIUM

Duke (1976) and Pearce and Norry (1979) quote average values for the distribution of Ti between Ca-rich clinopyroxene and liquid, D_{Ti}, of 0.34 and 0.3, respectively. However, data from Karroo basalts has led Marsh (pers. comm.) to suggest that D_{Ti} for clinopyroxene may be close to unity. If fractional crystallization results in enrichment of Ti in the residual liquid it might be expected that the concentration of Ti in pyroxene would increase as X_{Mg} decreases. The composition of clinopyroxenes in the layered sequence of the Bushveld Complex has been investigated by Atkins (1969). He analysed 15 samples, comprising cumulus and intercumulus grains, based on a vertical traverse through the cumulate pile (from the critical zone to near the roof). These data do not exhibit a smooth increase of Ti as X_{Mg} decreases (with height), although samples from close to the roof are substantially richer in Ti than less fractionated samples ("cumulus trend", fig. 9.9A). Clinopyroxenes from the upper critical zone do not exhibit any clear relationship between Ti content and X_{Mg}, possibly because the range in X_{Mg} (0.84-0.66) is small (data of de Klerk, 1982 and Kruger, 1984). On a plot of wt. percent TiO_2 versus X_{Mg} these data are widely scattered, such that for clarity they have not been shown on Figure 9.9A.

Clinopyroxenes from iron-rich ultramafic pegmatite at Amandelbult plot in a narrow, near-vertical field in Figure 9.9A. These data cluster into two groups: (1) unaltered clinopyroxene (containing from 0.50 to 0.70 wt. percent TiO_2) and (2) clinopyroxenes which are amphibolised (containing from 0.10 to 0.30 wt. percent TiO_2). These samples define a very limited range in X_{Mg} (essentially from .68 to .61), although it is possible that amphibolisation results in a slight increase in X_{Mg}. Scatter between these two groups is

attributable to incomplete amphibolisation. This "amphibolisation trend" is not a primary feature, and two explanations may be offered. Firstly, Ti may be removed from the clinopyroxene during amphibolisation (note that the amphibole is Ti-rich), or, secondly, it may be attributed to subsolidus re-equilibration between clinopyroxene and Fe-Ti oxides. This would result in exchange of Ti and Fe for Mg, and thus also explains the slight increase in the X_{Mg} ratio. It is concluded that the primary clinopyroxene, prior to exposure to subsolidus effects, has the maximum TiO_2 contents and the lowest X_{Mg}.

ALUMINIUM

In clinopyroxene Al may occur in tetrahedral co-ordination with Si, or in octahedral co-ordination with Fe^{2+}, Mg etc. Le Bas (1962) found that the distribution of Al in pyroxene reflects the degree of silica saturation, rather than the bulk concentration of Al in the magma. The data of Atkins (1969) do not exhibit a smooth decrease in Al with decreasing X_{Mg}, but iron-rich samples from near the roof are relatively poor in Al as compared to the more primitive clinopyroxenes from the critical zone ("cumulus trend", fig. 9.9B). Cumulus and intercumulus clinopyroxenes from the upper critical zone do not exhibit any clear-cut relationships between Al and X_{Mg} (data of de Klerk, 1982 and Kruger, 1984).

Pegmatite-hosted clinopyroxenes from Amandelbult are slightly depleted in Al compared to cumulus samples with similar X_{Mg}. This may reflect the bulk Al content and silica activity of the residual magma, after crystallization of large quantities of cumulus plagioclase. A plot of weight percent Al_2O_3 versus X_{Mg} exhibits a similar trend to that discussed for Ti (fig. 9.9B). All of the samples from Amandelbult plot in a near-vertical field, which is, again, interpreted as a subsolidus trend.

The relationship between Ti and Al in clinopyroxenes is illustrated in Figure 9.9C. In this diagram samples of pegmatite-hosted clinopyroxenes from Amandelbult only are plotted. They define a a very narrow range in X_{Mg}. Ti and Al exhibit a poorly defined, positive, linear relationship.

MANGANESE

The distribution of Mn in ferromagnesian silicates is usually related to the bulk FeO content, such that a plot of wt. percent MnO versus X_{Mg} exhibits an increase in Mn with fractionation (fig. 9.10). No differences can be established between the cumulus and pegmatite trends. This may be compared with a similar plot for olivine (fig. 9.6). Duke (1976) quotes an average value for the distribution of Mn between clinopyroxene and silicate liquid,

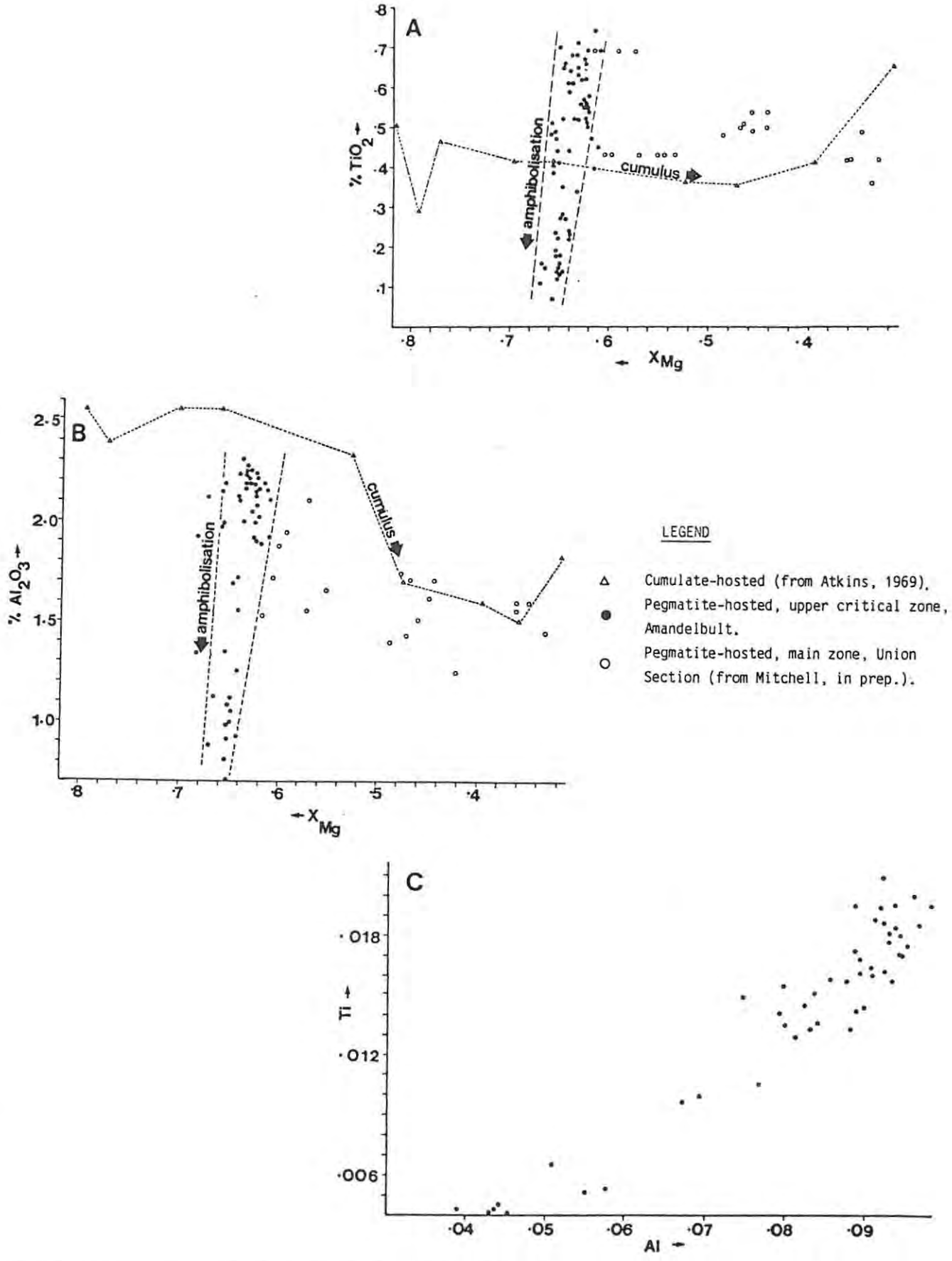

FIGURE 9.9 Distribution of the minor elements Ti and Al in clinopyroxene.
(A) Plot of wt. % TiO_2 vs. X_{Mg}
(B) Plot of wt. % Al_2O_3 vs. X_{Mg}
(C) cations Ti vs. cations Al

Samples in this study based on electron microprobe analyses. Note cumulus fractionation trend (X_{Mg} decreases with increasing height). Pegmatite fractionation trend is poorly-defined (not labelled). Pegmatite samples from Amandelbult define a non-liquidus trend, which may be ascribed to sub-solidus amphibolisation.

D_{Mn}, of 0.63.

SODIUM

Augite and ferroaugite commonly contain low levels of Na, but analytical precision at levels less than 1 wt. percent on the electron microprobe do not allow for any reliable assessment of these data.

CHROMIUM

Chromium occurs in substantial amounts in primitive clinopyroxenes but, as Cr is rapidly depleted from a basaltic magma undergoing fractional crystallization, iron-rich clinopyroxenes rarely contain significant amounts of this trace element. The distribution of Cr between clinopyroxene and liquid, D_{Cr}, may be highly variable; for example, Campbell and Borley (1974) quote a value for D_{Cr} of 40 and Cox et al. (1979) suggest a more realistic value of 10. The data of Atkins (1969) illustrate depletion in the Cr content of clinopyroxenes with fractionation. These data suggest that when X_{Mg} drops below 0.7, Cr is probably below the lower limit of determination or present in only very small quantities. In the Merensky and Bastard cyclic units the most iron-rich (intercumulus) clinopyroxenes typically contain between 0.05 and 0.10 wt. percent Cr_2O_3 (X_{Mg} = 0.7-0.66; data of de Klerk, 1982; Kruger, 1984; and this study). Similar Cr contents were found in clinopyroxenes in iron-rich ultramafic pegmatite at Amandelbult.

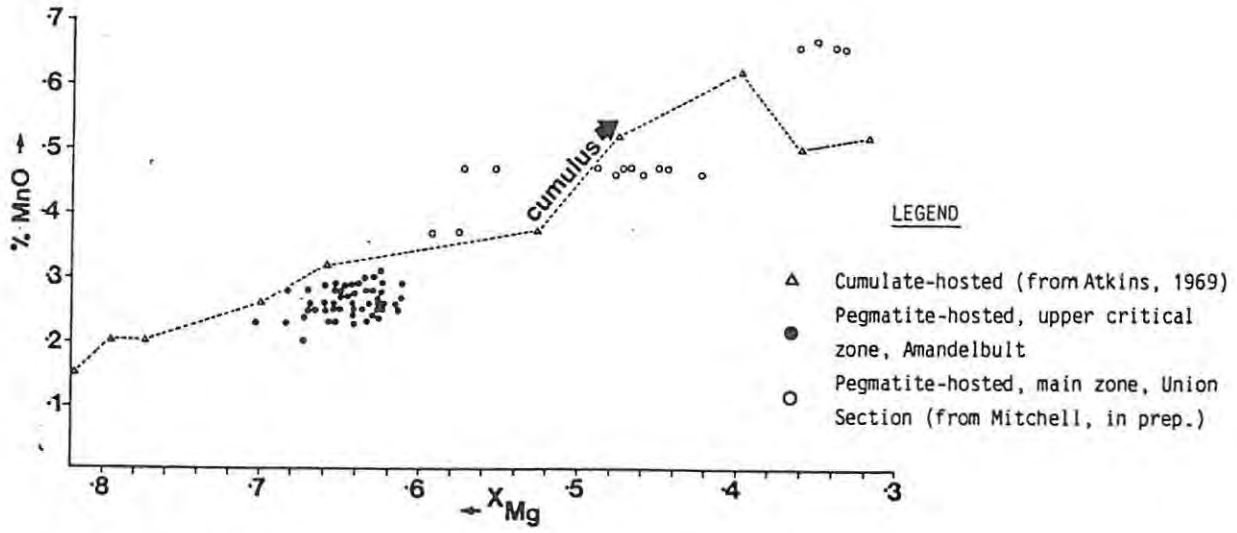

FIGURE 9.10 Plot of wt. % MnO vs. X_{Mg} in clinopyroxene.
Samples in this study based on electron microprobe analyses. Note cumulus trend related to fractionation (X_{Mg} decreases with increasing height). Pegmatite fractionation trend is poorly-defined (not labelled). Pegmatite samples from Amandelbult cluster below the cumulus trend; the MnO content does not appear to be influenced by sub-solidus processes.

Campbell (1977) found that when Cr^{3+} substitutes for Fe^{2+} and Mg^{2+}, simultaneous substitution of Si^{4+} by Al^{3+} is required to maintain charge balance. This may result in a positive relationship between the Cr and Al contents of pyroxenes (see p. 56). As the Cr content of the pegmatite-hosted clinopyroxenes is very low, the Al/Cr ratio is of little consequence in these samples (values between 20 and 100 are common).

9.3 ORTHOPYROXENE

Ca-poor orthopyroxene is only a minor constituent of iron-rich ultramafic pegmatite at Amandelbult. It may occur in two main forms, as exsolution lamellae in Ca-rich clinopyroxene and as relict cumulus grains (see Chapter 8). Primary grains which are directly related to the pegmatite are only rarely observed. Relict, cumulus orthopyroxene is most abundant in contact zones, and X_{Mg} of these grains is part-way between that of the primary cumulus composition and that which would indicate equilibrium with pegmatite-hosted olivine and clinopyroxene. Both textural and chemical evidence imply that they are in disequilibrium with the putative pegmatitic liquid. This is also applicable to partially replaced relict orthopyroxenes which occur in the centre of some pegmatite bodies (e.g., sample AE-23, Table 9.3).

9.4 PARTITIONING OF Mg AND Fe BETWEEN OLIVINE AND PYROXENE

Liquidus and subsolidus relationships between the Mg and Fe^{2+} content of co-existing olivines, orthopyroxenes and clinopyroxenes have been the subject of a number of investigations. Much of this literature has been reviewed by Deer et al., (1978, pp. 63-108 and pp. 326-342) and Deer et al., (1982, pp. 50-58). The following section presents some of the generally accepted partitioning relationships which are applicable to this study. Note that K_D may be used as a distribution coefficient to describe the distribution of Mg and Fe between a mineral and liquid (e.g., between olivine and liquid - see equation 1) or it may be used as a partition coefficient to describe the distribution of Mg and Fe between two minerals (e.g., olivine and orthopyroxene - see equation 8)

OLIVINE-ORTHOPYROXENE

The partitioning of Mg and Fe^{2+} between olivine and orthopyroxene in the temperature range 1300-1100°C is independent of temperature, but compositionally dependent (Larimer, 1968). The data of Medaris (1969), based

on a run temperature of 900°C, fit the equation:-

$$\log(X_{Fe}/X_{Mg})^{oliv} = 0.1630 + 1.1128 * \text{Log } (X_{Fe}/X_{Mg})^{opx} \quad \ldots (8)$$

Medaris found that K_D is not appreciably temperature-dependent over the temperature interval 1300-900°C. More recently, Morse (1979) relates X_{Mg} of olivine and orthopyroxene thus :-

$$(X_{Mg})^{opx} = 0.85 * (X_{Mg})^{oliv} + 0.15 \quad \ldots (9)$$

This is a generalised relationship that seems to be applicable to many natural and experimental assemblages, but may best be applicable to magnesian compositions, e.g., for olivines more magnesian than Fo_{60} small variations from the Morse equation have little effect on theoretical/measured compositions. Compositions of cumulus olivine and orthopyroxene from the upper critical zone are presented by de Klerk (1982). These data, together with those of the author are plotted in Figure 9.11A. These suggest minor variations from the Morse equation, but more data are required before a "Bushveld" trend can be established.

OLIVINE-CLINOPYROXENE

The thermodynamic data relevant to the distribution of Mg and Fe^{2+} between olivine and Ca-rich clinopyroxene have been reviewed by Obata et al. (1974). They found that $(K_D)^{oliv/cpx}$ is strongly temperature-dependent. Duke (1976) investigated the distribution of Mg and Fe^{2+} between olivine, Ca-rich clinopyroxene, and mafic liquid and declared that it was not affected by temperature, thus :-

$$\text{Log } (X_{Fe}/X_{Mg})^{oliv} = 0.198 + 1.30 * \text{Log } (X_{Fe}/X_{Mg})^{cpx} \quad \ldots (10)$$

Duke concluded that $(K_D)^{oliv/cpx}$ is not constant and varies with composition. This equation may be rearranged, to enable direct comparison with equation (9), thus :

$$\text{Log } ((1/X_{Mg}) - 1)^{oliv} = 0.198 + 1.30 * ((1/X_{Mg}) - 1)^{cpx} \quad \ldots (11)$$

A plot of X_{Mg} for olivine-clinopyroxene pairs from iron-rich ultramafic pegmatite does not define a straight line (fig. 9.11B). This may support petrographic data that these minerals are not in equilibrium (e.g., magmatic replacement of clinopyroxene by olivine).

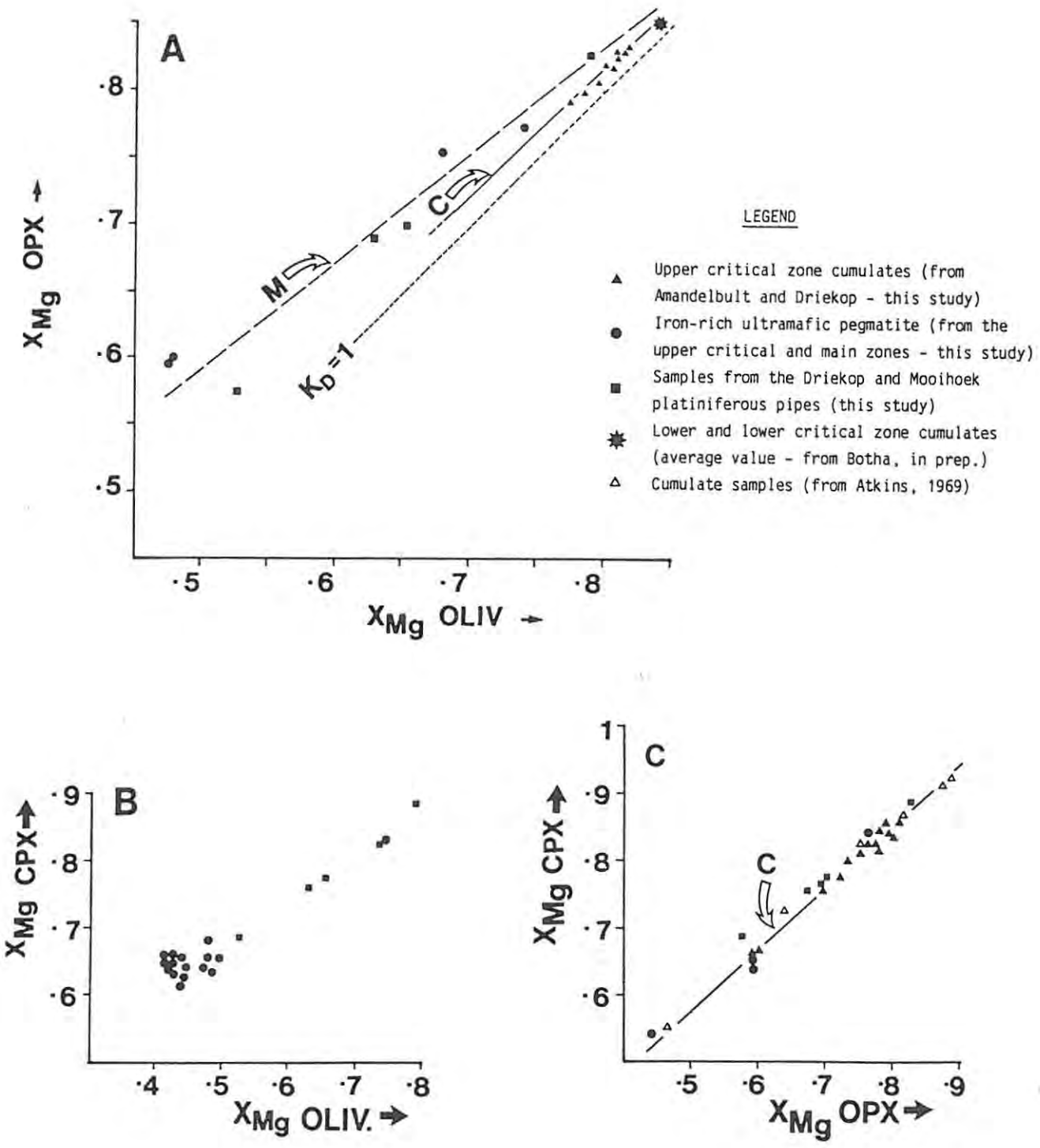

FIGURE 9.11 Plots of X_{Mg} of co-existing pairs of olivine, clinopyroxene and orthopyroxene.

(A) X_{Mg} orthopyroxene (OPX) vs. X_{Mg} olivine (OLIV). $K_D = (X_{Mg})^{oliv} / (X_{Mg})^{opx}$, and "M" is the relationship determined by Morse (1979) - see text. "C" is the cumulus trend determined in this study, thus :

$(X_{Mg})^{opx} = ((X_{Mg})^{oliv} * 0.96) + 0.05$; correlation coefficient = 0.98.

(B) X_{Mg} clinopyroxene (CPX) vs. X_{Mg} olivine (OLIV). These data do not fit a straight line.

(C) X_{Mg} clinopyroxene (CPX) vs. X_{Mg} orthopyroxene (OPX). For the cumulus samples in this plot the following relationship has been determined (labelled "C") :

$(X_{Mg})^{cpx} = ((X_{Mg})^{opx} * 0.93) + 0.11$; correlation coefficient = 0.99.

ORTHOPYROXENE-CLINOPYROXENE

Hess (1941) observed that tie-lines joining the compositions of coexisting Ca-poor and Ca-rich pyroxenes, expressed on a triangular diagram of En-Wo-Fs, intersect the En-Wo axis between Wo_{70} and Wo_{80}. This may be used to estimate X_{Mg} of coexisting pyroxenes. It also indicates that $(X_{Mg})^{cpx}$ is greater than $(X_{Mg})^{opx}$ assuming equilibrium conditions. This tie-line convergence apparently holds for most natural igneous and metamorphic systems. However, partitioning of Mg and Fe^{2+} is dependent on T, P and composition and is best expressed in terms of the distribution coefficient K_D. This distribution coefficient has been investigated by many workers. It usually plots as a curve where K_D typically lies between 0.50 and 0.90. Values of K_D increase with increasing temperature and decrease for more iron-rich compositions. Fleet (1974) has investigated the chemistry of pyroxene pairs from the Skaergaard and Bushveld intrusions. He suggests that the distribution of X_{MgSiO_3} and X_{FeSiO_3} should be considered separately as solutions of Mg and Fe in the two pyroxenes are non-ideal. This may partly be a feature of different values of a_{MgSiO_3} and a_{FeSiO_3}, rather than changes in K_D with temperature. It may be concluded that there is no simple relationship for the distribution of Mg and Fe between coexisting pyroxene pairs.

Orthopyroxene is only rarely a primary constituent of the iron-rich ultramafic pegmatite assemblage, such that this relationship is not of direct relevance to this study. However, a plot of X_{Mg} of coexisting pairs of, cumulus and intercumulus, Ca-poor and Ca-rich pyroxenes from the Bushveld Complex is presented in Figure 9.11C. A linear relationship appears to be applicable for compositions of clinopyroxene between X_{Mg} of 0.9 and 0.5.

9.5 PLAGIOCLASE

In this study the composition of plagioclase in iron-rich ultramafic pegmatite has not been investigated in detail. The chemistry of cumulus and intercumulus plagioclase from the Footwall, Merensky and Bastard cyclic units at Rustenburg has been investigated by Kruger (1984) and Kruger and Marsh (in press). A problem with electron microprobe analysis of plagioclase in the Bushveld Complex is the extreme chemical zonation exhibited by the majority of crystals. In the Merensky and Footwall cyclic units the anorthite (An) content of cumulus plagioclase lies roughly between An_{80} and An_{70}; intercumulus plagioclase may have more albitic compositions, An_{60} or lower. Analyses by the author of cumulus plagioclase from the Merensky and Footwall cyclic units at Amandelbult are comparable with the data of Kruger (see Table

TABLE 9.6 ELECTRON MICROPROBE ANALYSES OF PLAGIOCLASE AND ITS ALTERATION PRODUCTS

	AT-13	AT-13	27-E2	27-E2	AE-27	AE-27	AE-27	ML26-8A	ML26-8A	ML26-8A	ML26-8A	27-A1	27-A1	AM-5	AM-5
wt.%															
SiO_2	49.83	47.86	49.97	49.74	48.17	46.47	46.10	44.86	45.38	45.53	45.52	49.94	47.81	48.76	45.20
Al_2O_3	31.38	32.02	31.09	31.90	32.80	33.71	33.52	34.37	34.32	34.18	33.96	32.42	32.76	31.52	35.38
FeO	.48	.41	.15	.13	.24	.23	.88	.08	.14	.12	.40	.08	.08	.17	.13
CaO	15.29	16.05	16.87	17.74	17.05	17.15	16.31	17.43	17.18	17.05	17.25	15.55	15.54	14.83	18.47
Na_2O	2.83	2.50	2.02	1.77	1.78	1.85	1.99	1.74	2.42	1.76	1.51	2.73	2.53	2.82	.97
K_2O	.23	.14	.02	.04	.03	.02	.12	n.d.	.02	.02	.04	.05	.04	.09	.02
TOTAL	100.04	98.98	100.12	100.71	100.06	99.43	98.92	98.48	99.46	98.66	98.68	100.76	98.76	98.19	100.18
cations															
Si	2.280	2.221	2.283	2.260	2.208	2.150	2.148	2.100	2.107	2.123	2.125	2.262	2.214	2.267	2.081
Al	1.693	1.751	1.674	1.708	1.772	1.838	1.841	1.896	1.878	1.878	1.868	1.731	1.788	1.727	1.919
Fe^2	.018	.016	.006	.005	.009	.009	.034	.003	.005	.005	.016	.003	.003	.007	.005
Ca	.750	.798	.826	.834	.837	.850	.814	.874	.055	.852	.863	.755	.771	.739	.911
Na	.251	.225	.179	.156	.158	.166	.180	.158	.218	.159	.137	.240	.227	.254	.086
K	.013	.008	.001	.002	.002	.001	.007	-	.001	.001	.002	.003	.002	.005	.001
TOTAL	5.006	5.020	4.969	4.965	4.986	5.014	5.025	5.031	5.064	5.018	5.011	4.994	5.006	4.999	5.004
An	73.9	77.4	82.1	84.1	84.0	83.6	81.3	84.7	79.6	84.2	86.1	75.7	77.1	74.0	91.2
Ab	24.8	21.8	17.8	15.7	15.8	16.3	18.0	15.3	20.3	15.7	13.6	24.0	22.7	25.5	8.7
Or	1.3	.8	.1	.2	.2	.1	.7					.3	.2	.5	.1
DESCRIPTION**		---cumulus-----		partially --- replaced ---		------- pegmatitic ------			---------- pegmatitic ----------			--- cumulus ---		cumulus pegmatitic	

	27-D1	27-E1	27-E1	27-E1	27-E2	27-E2	AH-13	AH-12	AE-27*	AE-27*	AE-27*	ML26-8A*	AE-26*	AE-26*	AH-13*
wt.%															
SiO_2	48.97	49.65	50.26	49.05	50.39	48.85	44.26	43.46	39.40	39.33	40.05	42.42	39.30	37.38	36.11
Al_2O_3	33.86	33.44	32.99	32.02	32.76	32.23	33.73	34.00	32.18	32.97	31.62	34.60	29.22	31.15	30.12
FeO	.84	.25	.21	.17	.15	.12	.51	.32	2.39	.38	2.77	.25	9.37	5.94	4.23
CaO	17.21	16.99	17.60	17.49	17.09	16.92	17.63	17.88	23.74	24.76	24.13	18.46	22.55	19.51	23.52
Na_2O	1.05	1.88	.22	1.81	1.99	2.04	1.52	1.65	n.d.	.08	.06	.76	n.d.	.23	.07
K_2O	n.d.	.05	.01	.04	.04	.03	.04	n.d.	n.d.	n.d.	n.d.	.03	n.d.	.38	.01
TOTAL	101.92	102.25	101.29	100.58	102.42	100.19	97.69	97.31	97.71	97.51	98.62	96.52	100.49	94.59	94.06
cations															
Si	2.201	2.223	2.258	2.238	2.251	2.234	2.096	2.069	1.932	1.920	-	2.035	-	-	-
Al	1.794	1.765	1.747	1.722	1.725	1.737	1.882	1.908	1.860	1.897	-	1.956	-	-	-
Fe^2	.032	.009	.008	.006	.006	.005	.020	.013	.098	.016	-	.010	-	-	-
Ca	.829	.815	.847	.855	.818	.829	.894	.912	1.247	1.295	-	.949	-	-	-
Na	.092	.163	.019	.160	.172	.181	.140	.152	-	.008	-	.071	-	-	-
K	-	.003	.001	.002	.002	.002	.002	-	-	-	-	.002	-	-	-
TOTAL	4.947	4.978	4.879	4.983	4.974	4.988	5.034	5.053	5.138	5.135	-	5.023	-	-	-
An	90.1	83.1	97.7	84.0	82.4	81.9	86.3	85.7	100.0	99.4	-	92.9	-	-	-
Ab	9.9	16.6	2.2	15.8	17.4	17.9	13.5	14.3	-	.6	-	6.9	-	-	-
Or	-	.3	.1	.2	.2	.2	.2	-	-	-	-	.2	-	-	-
DESCRIPTION**														pegmatitic	
	pegmatitic	---------- partially replaced ----------						---------- pegmatitic clinozoisite ----------					------- epidote --------		

* Analysis excludes H_2O and L.O.I.

** See text for details.

9.6). It may be deduced that at this height in the sequence cumulus and intercumulus plagioclase is more albitic than An_{80}.

Partially replaced plagioclase grains in iron-rich ultramafic pegmatite at Amandelbult have compositions which vary between An_{80} and An_{98} (Table 9.6). Note that due to zonation these analyses are not necessarily representative of complete grains. However, grains which may be partially replaced by pegmatitic minerals or almost completely saussuritised do not appear to show any marked chemical zonation. Electron microprobe analyses of clinozoisite and epidote from saussuritised plagioclase grains are also presented in Table 9.6.

9.6 AMPHIBOLES

According to Deer et al. (1963) and Ernst (1968) amphiboles may be divided into three groups, based on the identity of the X cations, assuming the structure is described by the following formula: $W_{0-1}X_2Y_5Z_8O_{22}(OH,O,F)_2$ which represents one half the atoms in the unit cell. W represents 10-12 fold co-ordinated cations (large cations, Ca, K etc.), X represents 6 or 8 fold co-ordinated cations (Ca, Na, K,etc), Y represents 6 fold co-ordinated cations (Fe, Mg, Al, etc.), and Z refers to tetrahedrally co-ordinated cations in Si_3 and Si_2 sites (Si, Al). In many amphiboles the W structural site is unoccupied. Minor elements, which have been analysed in this study, include Mn (which may occur in both X and Y sites) and Fe^{3+}, Ti, Cr and Ni (in Y sites). This classification is as follows :

(1) X position occupied by (Mg,Fe^{2+}): anthophyllite-cummingtonite subgroup
(2) X position occupied by (Ca) : Ca-amphibole or hornblende subgroup
(3) X position occupied by (Na) : alkali amphibole subgroup.

In this study, the majority of amphiboles recognized in iron-rich ultramafic pegmatite at Amandelbult can be classified within the Ca-amphibole, or hornblende subgroup. These occur in two textural habits, as a result of incipient (deuteric) alteration of Ca-rich clinopyroxene, and as a primary pegmatite phase. Anthophyllite-cummingtonite may occur associated with serpentinised olivine and orthopyroxene (usually in metasomatic contact zones) and occasionally at the margins of pegmatite bodies. It is not a primary pegmatite mineral and has only been observed as an alteration product

The chemical classification of amphiboles has recently been revised by Leake (1978), who presents a scheme based on recalculated analyses. However, analyses in this study have been recalculated using the procedure

TABLE 9.7 ELECTRON MICROPROBE ANALYSES OF AMPHIBOLE AND MICA FROM IRON-RICH ULTRAMAFIC PEGMATITE

	AE-20	AE-20	AE-28	AE-28	AE-28	AE-28	AE-32	AE-32	AE-32	AE-32	AE samples			ML29-0	ML29-0	ML29-0	ML29-0		
wt.%											x	d	n				x	d	n
SiO_2	42.87	42.43	46.74	43.39	41.85	46.60	41.84	42.77	42.46	43.21	43.42	1.7878	10	36.30	36.69	36.65	36.55	.2146	3
TiO_2	2.12	2.80	2.79	1.82	3.29	.99	2.69	2.31	2.55	2.65	2.56	.4290	9	4.05	4.45	4.26	4.26	.1950	3
Al_2O_3	11.78	11.25	6.43	11.24	10.65	9.29	10.92	10.85	10.01	10.50	10.72	.7360	9	13.40	14.17	13.70	13.76	.3881	3
Fe_2O_3	4.34	4.98	4.44	4.42	4.99	4.46	4.85	4.65	4.82	4.82	4.68	.2459	10	6.32	5.64	6.25	6.07	.3740	3
FeO	10.85	12.45	11.10	11.06	12.47	11.14	12.12	11.63	12.05	12.06	11.70	.6132	10	15.81	14.10	15.63	15.18	.9396	3
MnO	.14	.14	.19	.12	.17	.23	.15	.14	.15	.01	.16	.0333	9	.11	.14	.11	.12	.0173	3
MgO	11.38	9.99	12.16	11.63	9.98	12.55	10.68	11.20	10.40	10.15	11.01	.9173	10	10.94	11.70	10.69	11.11	.5260	3
CaO	12.14	11.87	13.05	11.68	11.83	11.71	11.65	11.70	11.56	11.61	11.88	.4433	10	.04	.04	.02	.03	.0115	3
Na_2O	1.96	1.76	1.08	2.01	1.69	1.26	1.75	1.93	1.75	1.82	1.69	.3166	10	.26	.29	.36	.30	.0513	3
K_2O	.22	.13	.33	.21	1.21	.02	1.07	.99	.89	1.13	.61	.4195	8	8.96	9.30	9.41	9.22	.2346	3
Cr_2O_3	.89	1.43	.11	.27	.25	.23	.16	.30	.27	.12	.21	.0735	8	.26	.25	.23	.25	.0252	3
TOTAL	98.70	99.23	98.42	97.85	98.38	98.48	97.88	98.47	96.91	98.08	98.64	-		96.48	96.77	97.31	96.85	-	
cations/23 oxygens																			
Si	6.2970	6.2761	6.8477	6.3978	6.2528	6.7658	6.5296	6.3312	6.4007	6.4240	6.3913	-		5.7382	5.7521	5.9936	5.7362	-	
Ti	.2342	.3115	.3074	.2018	.3697	.1081	.3027	.2572	.2891	.2963	.2834	-		.4827	.5222	.5028	.5028	-	
Al	2.0395	1.9614	1.1104	1.9535	1.8756	1.5898	1.9256	1.8931	1.7786	1.8400	1.8599	-		2.4967	2.6062	2.6408	2.5454	-	
Fe^{3+}	.4802	.5543	.4894	.4909	.5609	.4869	.5457	.5180	.5469	.5397	.5181	-		.7523	.6625	.7696	.7174	-	
Fe^{2+}	1.3343	1.5402	1.3597	1.3639	1.5585	1.3528	1.5164	1.4394	1.5196	1.4996	1.4394	-		2.0803	1.8407	2.1383	1.9932	-	
Mn	.0174	.0175	.0236	.0150	.0215	.0283	.0190	.0175	.0192	.0012	.0199	-		.0147	.0185	.0153	.0160	-	
Mg	2.4912	2.2022	2.6550	2.5557	2.2222	2.7156	2.3812	2.4708	2.3365	2.2489	2.4153	-		2.5773	2.7208	2.6054	2.5986	-	
Ca	1.9107	1.8813	2.0486	1.8454	1.8939	1.8217	1.8676	1.8558	1.8673	1.8495	1.8738	-		.0068	.0067	.0035	.0050	-	
Na	.5581	.5047	.3068	.5746	.4894	.3547	.5076	.5539	.5114	.5246	.4823	-		.0797	.0877	.1141	.0091	-	
K	.0255	.0152	.0617	.0395	.2306	.0037	.2042	.1869	.1711	.2143	.1145	-		1.8068	1.8512	1.9631	1.8459	-	
Cr	.1668	.2698	.0127	.0315	.0295	.0264	.0189	.0051	.0322	.0141	.0244	-		.0350	.0308	.0297	.0310	-	
TOTAL	15.4716	15.3993	15.9121	15.4497	15.3893	15.2519	15.4464	15.4655	15.3870	15.3451	15.3652	-		15.1770	15.1468	15.1923	15.1849	-	
$Mg/Mg+Fe^T$	.579	.513	.589	.579	.512	.596	.536	.558	.531	.524	.552	-		.476	.521	.473	.489	-	
$Mg/Mg+Fe^{2+}$	.651	.588	.661	.652	.588	.667	.611	.632	.606	.600	.627	-		.552	.596	.549	.566	-	

	ML27-3A	ML27-3A	ML27-3A	ML27-3B	ML27-3B	ML27-3B	ML27-3B	ML27-3			ML29-0	ML29-0	ML29-0	ML29-0	ML29-0	ML29-0		
wt.%								x	d	n							x	d	n
SiO_2	41.94	42.49	41.66	41.81	44.29	42.40	43.09	43.53	.9177	7	47.37	44.54	48.86	43.83	49.10	46.74	2.4377	5
TiO_2	3.02	2.52	2.69	3.43	2.29	2.65	2.18	2.68	.4295	7	1.53	1.80	1.11	2.83	.79	1.61	.7831	5
Al_2O_3	10.14	9.85	10.90	10.37	8.90	10.28	10.34	10.11	.6200	7	8.70	9.52	6.15	10.09	5.96	7.58	1.7970	4
Fe_2O_3	5.06	5.12	4.60	5.04	5.08	4.69	4.60	4.88	.2398	7	4.75	5.08	4.82	4.92	4.70	4.85	.1509	5
FeO	12.62	12.80	11.50	12.59	12.71	11.72	11.51	12.21	.5979	7	11.83	12.58	12.05	12.31	11.76	12.11	.3411	5
MnO	.18	.14	.17	.20	.20	.15	.14	.17	.0261	7	.18	.27	.27	.21	.24	.23	.0391	5
MgO	10.11	9.92	11.04	9.86	10.75	11.07	11.65	10.63	.6812	7	11.38	10.19	12.58	10.25	13.09	11.50	1.3217	5
CaO	11.35	11.31	11.40	11.29	11.31	11.49	11.50	11.38	.0873	7	11.83	11.48	11.71	11.31	11.40	11.55	.2173	5
Na_2O	2.45	2.57	2.48	2.77	2.09	2.66	2.53	2.51	.2141	7	1.44	1.78	.93	1.92	1.01	1.42	.4439	5
K_2O	.69	.62	.41	.57	.64	.37	.34	.52	.1431	7	.70	.87	.43	.90	.43	.67	.2285	5
Cr_2O_3	.08	.05	.06	.07	.03	.08	.09	.07	.0207	7	.16	.24	.22	.30	.08	.20	.0837	5
TOTAL	97.63	97.39	97.05	98.00	98.29	97.08	97.97	98.69	-		99.87	98.35	99.12	98.87	98.56	98.46	-	
cations/23 oxygens																		
Si	6.3091	6.4028	6.2627	6.2679	6.5761	6.3364	6.3882	6.4296	-		6.8287	6.5874	7.0791	6.4632	7.1319	6.8588	-	
Ti	.3417	.2856	.3041	.3867	.2557	.2978	.2431	.2977	-		.1659	.2002	.1209	.3138	.0863	.1777	-	
Al	1.7980	1.7495	1.9314	1.8324	1.5576	1.8108	1.8069	1.7602	-		1.4783	1.6596	1.0503	1.7538	1.0204	1.3111	-	
Fe^{3+}	.5714	.5804	.5204	.5681	.5679	.5273	.5136	.5427	-		.5157	.5742	.5256	.5464	.5141	.5379	-	
Fe^{2+}	1.5876	1.6126	1.4460	1.5785	1.5780	1.4651	1.4270	1.5080	-		1.4328	1.5955	1.4605	1.5182	1.4285	1.4946	-	
Mn	.0229	.0179	.0216	.0254	.0254	.0190	.0176	.0213	-		.0220	.0338	.0331	.0262	.0295	.0286	-	
Mg	2.2666	2.2278	2.4734	2.2094	2.3788	2.4655	2.5740	2.3400	-		2.4449	2.2461	2.7164	2.2526	2.8337	2.5150	-	
Ca	1.8295	1.8262	1.8363	1.8136	1.7994	1.8399	1.8268	1.8011	-		1.8273	1.8193	1.8179	1.7870	1.7743	1.8161	-	
Na	.7145	.7508	.7228	.8051	.6016	.7707	.7272	.7188	-		.4024	.5104	.2612	.5489	.2844	.4040	-	
K	.1324	.1192	.0786	.1090	.1212	.0705	.0543	.0980	-		.1287	.1641	.0795	.1693	.0797	.1254	-	
Cr	.0095	.0060	.0071	.0083	.0035	.0095	.0105	.0082	-		.0182	.0280	.0252	.0350	.0092	.0232	-	
TOTAL	15.5170	15.5191	15.5651	15.5436	15.4044	15.5773	15.5669	15.4765	-		15.2005	15.3366	15.1300	15.3298	15.1521	15.2295	-	
$Mg/Mg+Fe^T$	.512	.504	.557	.506	.526	.5531	.570	.533	-		.557	.509	.578	.522	.593	.563	-	
$Mg/Mg+Fe2+$	.588	.580	.631	.583	.601	.6273	.643	.608	-		.631	.585	.650	.597	.665	.627	-	

of Allen and Boettcher (1983) which is based on a "dry" analysis, assuming 23 oxygens (see Appendix 9). Comparison with the classification scheme of Leake is, however, still valid. Recalculated electron microprobe analyses of amphiboles analysed in this study are presented in Table 9.7. All of these samples are of "hornblendes" from iron-rich ultramafic pegmatite at Amandelbult. In these analyses Mg/Fe ratios are presented as atomic $Mg/(Mg+Fe^{2+})$ and $Mg/(Mg+Fe^{T})$ where $Fe^{T} = Fe^{2+} + Fe^{3+}$.

They may be classified as calcic amphiboles, according to the scheme of Leake (1978) as the cations (Ca + Na) are greater than 1.34 and cations Na is less than 0.67. In calcic amphiboles cations Ca is typically greater than 1.34 (usually greater than 1.8 in this study). Furthermore, atomic Fe^{3+} is less than 0.75 such that the prefixes ferri or ferrian are not applicable, and other minor constituents (such as Ti, Mn, K) are too low to warrant prefixes. Using this classification scheme the following amphiboles are recognized - magnesian hastingsitic hornblende and edenite (in both of which (Na+K) is greater than 0.5, Ti is less than 0.5 and Fe^{3+} is greater than Al^{VI} (see Table 9.8).

Edenite is restricted to one occurrence, at the margin of the large Middellaagte pipe. Samples here (from borehole ML29) are unusually rich in hydrous ferromagnesian silicates.

Table 9.8 CLASSIFICATION OF AMPHIBOLES IN THIS STUDY

cations	1	2	3
Na + K	.5968	.8168	.5294
Ti	.2834	.2977	.1777
Fe^{3+}	.5181	.5427	.5379
Al^{VI}*	.2512	.1898	.1698
Si	6.3913	6.4296	6.8588
$(X_{Mg})^1$	.627	.608	.627
$(X_{Mg})^2$	.552	.533	.553
$(X_{Mg})^{cpx}$	.645	.658	-
K_D (1)	1.47	1.69	-
K_D (2)	1.08	1.24	-

1. "AE" samples (n = 10) : Magnesian hastingsitic hornblende
2. ML27-3 (n = 7) : Magnesian hastingsitic hornblende
3. ML29-0 (n = S) : Edenite

Note that Al^{VI} = Total Al - (8-Si)

$(X_{Mg})^1 = (Mg/(Mg+Fe^{2+}))$ and $(X_{Mg})^2 = (Mg/(Mg+Fe^{T}))$

K_D = ratio of $(X_{Mg})^{amp}$ to $(X_{Mg})^{cpx}$

In contrast, magnesian hastingsitic hornblende is the ubiquitous amphibole found in typical iron-rich ultramafic pegmatite, both at Amandelbult and in the core of the Middellaagte pipe. No major compositional differences have been recognised between discrete grains and those resulting from alteration of clinopyroxene. It is a relatively iron-rich hornblende, as might be expected. In comparison with the host clinopyroxene, this amphibole is enriched in Ti, Al, Na, K and possibly Cr, at the expense, essentially, of Si and Ca. The ratio of $(X_{Mg})^{amp}/(X_{Mg})^{cpx}$ is estimated at between 1.08 and 1.24 (1.47-1.69, if Fe^T is used instead of Fe^{2+} to calculate $(X_{Mg})^{amp}$).

9.7 MICAS

Phlogopite and annite form a solid solution series in which X_{Mg} (cations $Mg/(Mg+Fe^T)$ of phlogopite is greater than 0.66 . Biotite is a member of this series with X_{Mg} less than 0.66. In addition, in biotites further substitution of Al in both tetrahedral and octahedral sites occurs (Deer et al., 1962). Phlogopite is typical of ultrabasic and basic igneous rocks whereas biotite is widely distributed in many igneous rocks. This may be illustrated on a ternary diagram of $(Fe_2O_3+TiO_2)$-(FeO+MnO)-MgO (see Engel & Engel, 1960). Mica from this study, which is biotite (X_{Mg} = .566, 5 analyses on one sample only - see Table 9.7) plots within the field designated "diorites" on Engel and Engel's diagram.

The relationship between $X_{Fe^{2+}}$ and X_{Fe^T} of coexisting pairs of pyroxene, mica and hornblende has been investigated by De Vore (1957). According to De Vore biotite has a lower X_{Fe^T} value than coexisting hornblende, although the differences are small. In this study values for $(K_D)^{mica/amph}$ (calculated as X_{Mg}) are 1.29 (using Fe^{2+}) and 1.52 (using Fe^T).

9.8 SUMMARY OF X_{Mg} RELATIONSHIPS

Average values of X_{Mg} for silicates from iron-rich ultramafic pegmatite at Amandelbult are presented in Table 9.9

TABLE 9.9 AVERAGE X_{Mg} VALUES

	1	2	3
Clinopyroxene	.645	.658	-
Amphibole	.627	.608	.627
Biotite	-	-	.566
Olivine	.423	.430	-
Orthopyroxene*	.50	.52	-

1. "AE" samples (small pegmatite body, Amandelbult)
2. ML27-3 ("core" of the Middellaagte pipe)
3. ML29-0 (margin of the Middellaagte pipe)

* Theoretical composition calculated from olivine-orthopyroxene relationship of Morse (1979).

These may be summarised thus :-

$$(X_{Mg})^{cpx} > (X_{Mg})^{amp} > (X_{Mg})^{mica} > (X_{Mg})^{opx} > (X_{Mg})^{oliv}$$

CHAPTER 10 Fe-Ti-Cr OXIDE MINERALOGY AND CHEMISTRY

Disseminated Fe-Ti-Cr oxides are ubiquitous accessory constituents of typical, silicate-rich, ultramafic pegmatite (see Chapter 8). However, these phases may predominate over silicates such that they form rocks which are best described as Fe-Ti oxide pegmatite. A distinction between normal Fe-Ti oxide pegmatite and Cr-rich Fe-Ti oxide pegmatite was made in Chapter 2. Within these two groups, disseminated Cr-rich and Cr-poor Fe-Ti oxides are also recognized. This chapter discusses the mineralogy and chemistry of both massive and disseminated Cr-rich, and Cr-poor, Fe-Ti oxides. Much of our knowledge of Cr-rich spinels in these rocks is based on a comprehensive study by Cameron and Glover (1973).

10.1 INTRODUCTION

REVIEW

The term "spinel" refers to a group of oxide minerals that crystallize with a face-centered cubic crystal structure. The unit cell of this structure, which may accommodate up to 30 different cations, consists of 32 oxygens. Within this framework the cations occupy 8 tetrahedrally and 16 octahedrally co-ordinated sites. The generalised formula may be written as : XY_2O_4 (or $X_8Y_{16}O_{32}$ per unit cell) where X and Y represent cations of different valence states. Two types of spinel are recognized, "normal" and "inverse" types. In normal spinels the 8 X cations occupy 8 tetrahedral sites and the 16 Y octahedral sites, so that the formula can be written $X(Y_2)O_4$ where the brackets denote the octahedral sites. In inverse spinels 8 of the 16 Y cations occupy the tetrahedral sites, yielding a structure of the type $Y(YX)O_4$ (Deer et al., 1962; Lindsley, 1976; Reynolds, 1982).

The composition of naturally occurring chromites, or Cr-rich spinels, may be depicted on a prism (see Stevens, 1944). The following important end-members are recognized : chromite ($FeCr_2O_4$), picrochromite ($MgCr_2O_4$), spinel sensu stricto ($MgAl_2O_4$), hercynite ($FeAl_2O_4$), magnetite (Fe_3O_4), and magnesioferrite ($MgFe_2O_4$). Either partial or complete solid solution occurs between these end-members such that naturally occurring chromite grains contain variable proportions of Al and Mg, in addition to Cr, Fe^{3+} and Fe^{2+}. In addition, variable amounts of ulvöspinel (Fe_2TiO_4) are often present in naturally occurring chromite. The presence or absence of miscibility gaps in this solution series has been the subject of many investigations.

In magmatic ores or rocks Fe-Ti spinels are usually intermediate members

of the magnetite - ulvospinel solid solution series. Unexsolved members of this series are referred to as titanomagnetite. However, in slowly cooled magmatic rocks members of the magnetite-ulvöspinel series become unstable with decreasing temperature and decompose to form "composite" Fe-Ti oxide, usually referred to as Ti-magnetite. This normally shows a much more restricted compositional range than Cr-rich spinels, and only contains minor amounts of Cr, Al and Mg. However, these composite Ti-magnetite grains may contain a wide range of intergrown phases, often including ilmenite, ulvöspinel and pleonaste.

The end member composition of ilmenite is essentially $FeTiO_3$. It exhibits trigonal symmetry and may thus be distinguished optically from Fe-Ti spinels. Minor amounts of Mg and Mn may substitute for Fe^{2+} (Deer et al., 1962). Because ilmenite forms a solid solution series with hematite at high temperatures minor proportions of Fe^{3+} may be present in the ilmenite structure. According to Lindsley (1976), the composition may be expressed as $Fe^{3+}(Fe^{2+},Ti)_XO_3$, where X is the mole fraction of ilmenite. The value of X is usually calculated from the atomic proportions of chemical analyses.

RECALCULATION TECHNIQUES

In this study electron microprobe analyses of Fe-Ti-Cr oxides have been recalculated in terms of cations on an oxygen-free basis using the following techniques. Cr-rich spinels, in which Cr_2O_3 comprises over 2 wt. percent have been recalculated on the basis of 24 cations using an in-house computer program developed by H.V. Eales. Using this technique the proportion of Fe^{3+} is calculated from total iron, assuming stoichometry. Cr-poor spinels (with less than 2 wt. percent Cr_2O_3) and ilmenites have been recalculated using the technique of Stormer (1983). For specific comparison purposes Cr-poor spinels have also been recalculated using the former method. Full details of these procedures are given in Appendix 10.

10.2 Cr-RICH Fe-Ti OXIDE PEGMATITE

FIELD EXPOSURES AT AMANDELBULT

In the critical zone of the layered sequence at Amandelbult bodies of magnetic spinel were first reported by Wasserstein (1936). In two of these occurrences massive Fe-Ti-Cr oxides form cores within much larger, probably pipe-like bodies of silicate-rich pegmatite. They also form irregular veins and sheet-like bodies which cut both the silicate-rich pegmatite and the cumulate wallrocks. Outcrop is very poor, but two of these bodies are postulated to occur at the extrapolated position of the LG and MG chromitite

layers. A third body of massive Cr-rich Fe-Ti oxide pegmatite occurs at Amandelbult as a thin (1-2 m thick), sheet-like feature which crops out over a strike length of several hundred metres. It occurs at the extrapolated suboutcrop of the UG-1 chromite layer. Silicate-rich ultramafic pegmatite float, defining an ellipsoidal feature, is found in the hangingwall of this body. In general the poor outcrop at Amandelbult is such that surface exposures of these rocks cannot be examined in detail.

In mine exposures at Amandelbult thin Fe-Ti-Cr oxide stringers and layers may readily be observed. They invariably occur at the contacts between either unreplaced, or partially replaced cumulates and sheet-like bodies of iron-rich ultramafic pegmatite. They can be related to the presence of primary, cumulus chromitite layers. At Union Section, de Klerk (pers. comm.) observed similar Cr-rich Fe-Ti oxide pegmatite adjacent to the UG-1 chromitite layer. Unfortunately, exposures at Amandelbult are restricted to thin chromitite layers. In comparison, Cameron and Desborough (1964) and Cameron and Glover (1973) examined relatively thick chromitite layers.

Cameron and Glover (1973) observed that Cr-rich Fe-Ti oxide pegmatite is present in two main modes of occurrence. In the simpler, magnetic spinel forms a layer along either the upper or lower surface of a pre-existing chromitite layer which is in contact with a pegmatite body. This layer (which is usually 0.5 - 20 cm thick) may be even and regular or may project into the chromitite in an irregular manner. In the second mode of occurrence chromitite layers are brecciated and patchily replaced by magnetic spinel. Within the same layer sheet-like replacement may have occurred resulting in alternating layers of granular (unreplaced?) chromitite and hybrid magnetic spinel. This latter process is clearly fracture controlled (Cameron & Glover, 1973).

Large-scale fracture-controlled replacement of chromitite layers has not been observed at Amandelbult. However, where very thin chromitite layers (1 - 5 mm thick) are "replaced" fracture control may play an important role. The primary cumulate layering is usually preserved and Cr-rich Fe-Ti oxide pegmatite is laterally transitional into unreplaced chromitite. Replacement of the Merensky chromitite layers is illustrated schematically in Figure 7.9 (see pp. 121-122). The Merensky lower chromitite layer is often unrecognizable, but the upper chromitite layer, where it overlies replaced Reef, is usually intact. In this situation the partially replaced upper chromitite layer (or hybrid Fe-Ti-Cr oxide layer) may be traced laterally, with no disturbance, into areas where "normal" chromitite overlies "normal" Reef. The "normal" Merensky upper chromitite layer is approximately 15-20 mm

thick and contains an appreciabe proportion of intercumulus silicate material (highly variable, but estimated at 30-50 modal percent; fig. 10.1A). The replaced oxide layer is often in excess of 50 mm thick and contains only trace amounts of interstitial material (fig. 10.1C). The replaced oxide layer is thus characterised by a thicker and more massive nature. Bulk increases in oxide components of four to five times are typical. Locally the replaced Merensky upper chromitite layer may be cut and veined by pegmatitic material.

The chromitite layer above the upper pseudoreef A at Amandelbult is usually only a few millimetres thick and consists of very loosely packed grains. This layer typically consists of clusters of half a dozen grains which are separated by 1 to 2 mm of silicates and is overlain by a mottled anorthosite (fig. 10.2A). A pegmatite body may conformably overlie this chromitite layer, such that the harzburgite below the chromitite is not replaced (fig. 10.4). The contact between the pegmatite and unreplaced harzburgite is roughly conformable to the primary layering. It is marked by the development of a thin Cr-rich Fe-Ti oxide layer, which varies between 5 and 10 mm in thickness, but may locally exceed 30 mm in thickness. This oxide layer may be massive or may contain between 5 and 10 modal percent interstitial silicate material (fig. 10.2). This represents a bulk increase in oxide components approaching 20 times, as compared with the primary chromitite. The thicker parts of this oxide layer are very irregular and may project down into the overlying harzburgite. When this layer is traced along strike, past the discordant lateral margin of the pegmatite body (i.e. to the west of position "X" in Figure 10.4) it becomes thinner and less massive. Eventually, at a lateral distance of 1.2 m from position "X" it shows a step-like form and thins out rapidly (sample AH-19; fig. 10.2B). At a lateral distance of 1.5 m from position "X" this oxide layer is indistinguishable from the normal cumulus chromitite layer.

From a study of the field relationships it may be concluded that :-

(1) Hybrid oxide layers result from addition of material to the primary chromitite layers.
(2) Removal or replacement of intercumulus silicate material has occurred.
(3) The pegmatitic liquids were channelled along chromitite layers, resulting in replacement of the same for some lateral distance away from pegmatite bodies, as well as vertically above or below them.

TEXTURAL FEATURES

The hybrid Fe-Ti-Cr spinel is readily distinguished from primary chromite by its purple-grey colour, coarser grain size, metallic lustre and

magnetic properties. Ilmenite may be observed in this assemblage as silvery-grey grains that exhibit a high metallic lustre. The main textural features apparent in hand-specimen are the high degree of compaction and lack of interstitial silicate material.

Some of the progressive textural changes associated with the formation of hybrid Fe-Ti-Cr oxide layers are observed in the "AH" range of samples (fig. 10.4) and are illustrated in Figure 10.2. Sample AH-20B is the typical chromitite cumulate; sample AH-14 is the most Cr-rich composition found in the hybrid oxide layers; it is less well annealed and contains a considerably higher proportion of interstitial material than the other samples.

In reflected light Fe-Ti-Cr spinel may be distinguished from cumulus chromite by its higher reflectivity (Cameron & Desborough, 1964; Cameron & Glover, 1973). Grains which are compositionally closest to the primary cumulus composition are usually optically homogeneous and contain no silicate inclusions (compare to samples from Driekop - pp. 59-60). These features are similar to the optical properties exhibited by cumulus chromite. However, an Fe-Ti-Cr spinel containing less than 10 wt. percent Cr_2O_3 more closely resembles Ti-magnetite. These are usually coarser-grained than the Cr-rich spinels and typically host a complicated range of microintergrowths (see below). Ilmenite, which is not observed as discrete grains in chromitite cumulates, is an ubiquitous constituent of these hybrid oxide layers. Locally it may constitute in excess of 30 modal percent. It occurs both as discrete grains and as intergrowths in spinel.

CAPTION FOR FIGURE 10.1 "REPLACEMENT" OF THE MERENSKY CHROMITITE LAYERS

a. Section through the normal Merensky upper chromitite layer (sample AA-4).
b. Section through the normal Merensky lower chromitite layer; underlain by mottled anorthosite, overlain by the Merensky Reef (compare proportion of intercumulus material with that in "a" (sample AT-14).
c. Section through the basal contact of the replaced Merensky upper chromitite layer (or Fe-Ti-Cr oxide pegmatite), overlying replaced (olivine-rich) Reef. Compare massive nature of this layer (which in this sample is 50 mm thick) with that in the primary layer in "a" (sample 27-C1).
d. Microtexture of the normal upper chromitite, consisting of cumulus chromite (light grey) and intercumulus silicate (black) (as sample "a").
e. Microtexture of the replaced upper chromitite, consisting of granular Fe-Ti-Cr oxides. This sample, which is from the middle of the replaced layer, consists of Cr-rich spinel; the paucity of ilmenite and the poorly developed foam texture distinguish it from the well-annealed Cr-poor spinels in fig. 10.6a,b (as sample "c").
f. Duplex aggregate of Cr-poor Fe-Ti-Cr spinel ("s ") and ilmenite ("il") with minor interstitial silicate (black) in a "xenolith" of replaced lower chromitite. The abundance of ilmenite in this sample may reflect the greater proportion of intercumulus sites in the lower chromitite layer, as compared to the more massive nature of the upper chromitite layer (sample 27-F1).
G. Irregular upper contact of the replaced upper chromitite layer (grey). The overlying hangingwall pyroxenite (black) is partially replaced. Note minor sulphides (white) (sample AG-1).

("a", "b", "c" in plane polarised transmitted light, and "d" - ""g" in plane polarised reflected light; arrow indicates way up)

FIGURE 10.1 "REPLACEMENT" OF THE MERENSKY CHROMITITE LAYERS

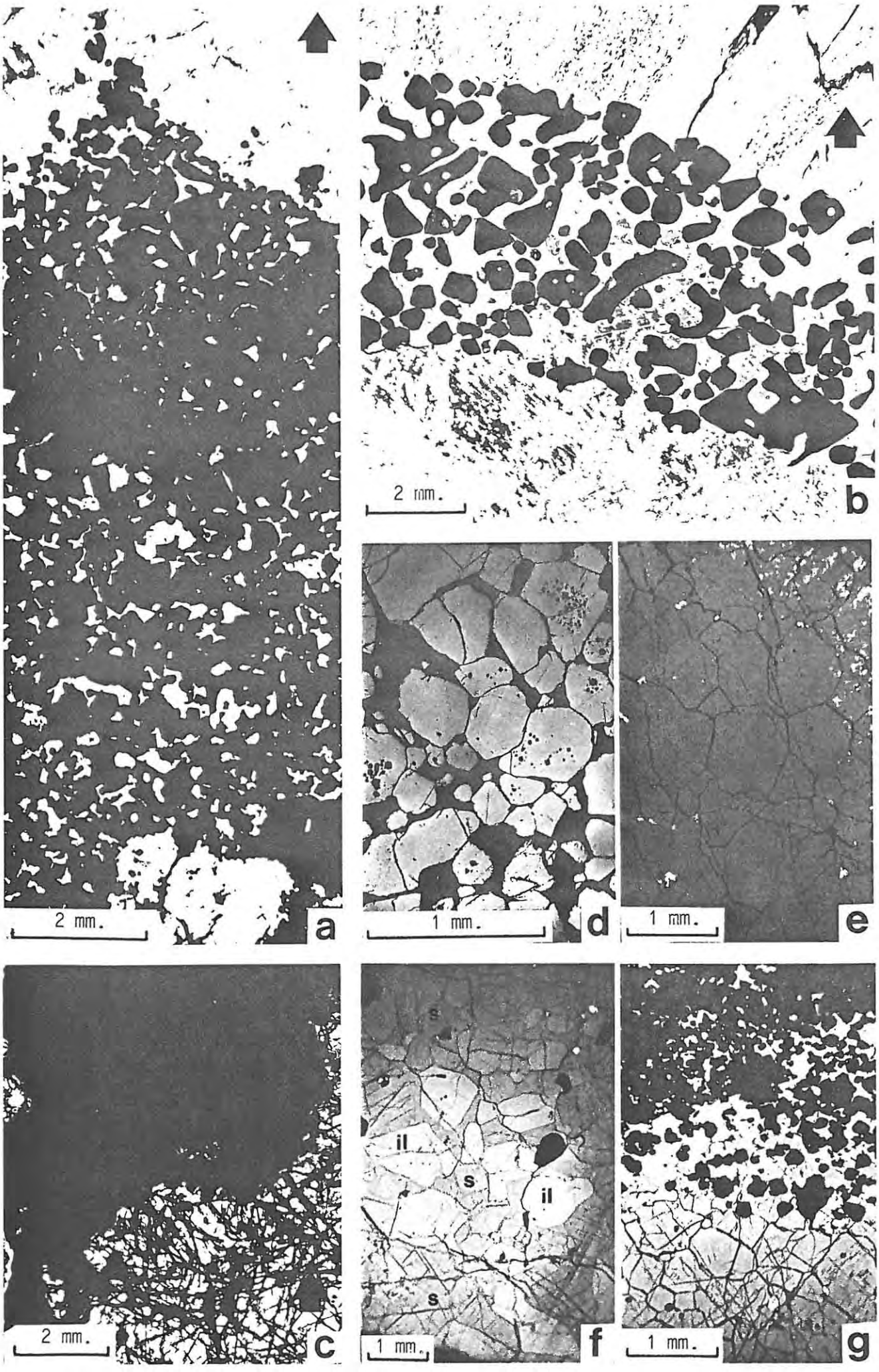

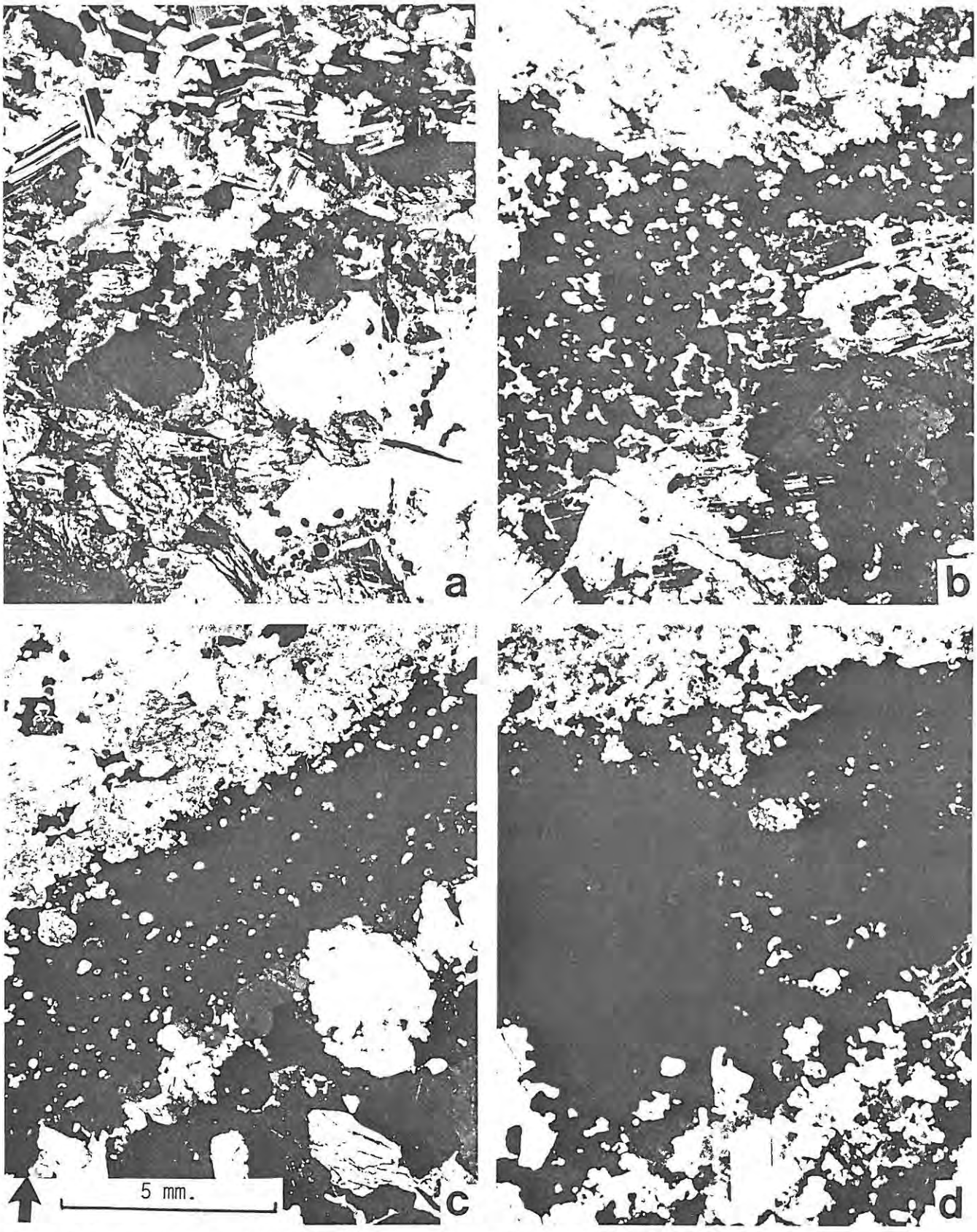

FIGURE 10.2 STAGES IN THE PROGRESSIVE FORMATION OF A Cr-RICH Fe-Ti OXIDE LAYER

a. Thin chromitite stringer at contact between a harzburgite (the upper pseudoreef A - below) and an anorthosite (above). Normal sequence (sample AH-20B). B. Step-like feature in early development of Cr-rich Fe-Ti oxide layer, which has formed, essentially at the expense of the harzburgite. Compare grain size of oxide here with primary chromite in "a" and note saussuritisation of plagioclase in the anorthosite (sample AH-19). c. Well-formed Cr-rich Fe-Ti oxide layer (which pseudomorphs the primary layering) at contact between relict body of anorthosite (saussuritised) and partially replaced harzburgite. Note scalloped edges of both upper and lower contacts and compare proportion of interstitial silicate material with that in "b" (sample AH-21). d. Massive Cr-rich Fe-Ti oxide layer with pegmatite (which has replaced anorthosite) above and partially replaced harzburgite below. Note replacement of silicates by the oxide (sample AH-14).

(All samples here are vertical sections from the same stratigraphic position - see fig. 10.4; All in transmitted light with crossed polarisers; arrow indicates way up)

These hybrid oxide layers usually exhibit a characteristic foam-like texture with well developed 120^{o} dihedral angle triple junctions. This texture is attributed to annealing (see pp. 137-140). The development of perfect foam-like textures is arrested by the presence of interstitial silicate and granular ilmenite (see fig. 10.6A-D). Ilmenite is less readily polygonised than Ti-magnetite and duplex aggregates of these two minerals do not show well developed foam-like textures (fig. 10.6F). Many of these textural changes may be observed in Figure 10.1 (D-G). These Fe-Ti-Cr spinels exhibit similar microstructures to those described by Cameron and Glover (see below).

The presence of granular ilmenite in Cr-rich Fe-Ti oxide pegmatite is of particular interest. It may have crystallized directly from the putative pegmatitic liquid (the most likely explanantion) or it may be of a metasomatic origin. It is also considered likely that some Fe-Ti spinel also crystallized directly from the putative liquid, probably due to preferential nucleation on pre-existing chromite grains. The formation of these hybrid oxide layers must also imply dissolution of the intercumulus silicate material.

SAMPLING AND ANALYTICAL DETAILS

1. AZ-1, AZ-2 : Cr-rich Fe-Ti oxide pegmatite associated with the LG and MG chromitite layers, respectively, Amandelbult (surface).
2. AS-A1, AS-A2 : Cr-rich Fe-Ti oxide pegmatite associated the with UG-1 chromitite layer, Amandelbult (surface).
3. LA-3, LA-3A : Cr-rich Fe-Ti oxide pegmatite from the pegmatite body on Grootboom-Annex Grootboom, Levino chromitite mine, eastern Bushveld Complex. (surface - see fig. 2.5)
4. 27-F1,F2 : Cr-rich Fe-Ti oxide pegmatite associated with the replaced Merensky lower chromitite layer, Amandelbult (underground).
5. 27-C1,C2 : Cr-rich Fe-Ti oxide pegmatite associated with the replaced Merensky upper chromitite layer, Amandelbult (underground).
6. "AH-samples" : Cr-rich Fe-Ti oxide pegmatite associated with the chromitite layer above the upper pseudoreef A, Amandelbult (underground).

Large, silicate-free samples of Cr-rich Fe-Ti oxide pegmatite were analysed using standard X-ray fluorescence techniques (see Appendix 5). These samples were hand sorted for purity, although in general this was hardly necessary. To ensure that suitable standards were available, and to overcome possible mass absorption problems, samples were diluted with roughly two thirds "specpure" SiO_2. The exact proportions of sample and SiO_2 were

then used to recalculate the analysis to the original total. The results are presented in Table 10.1. Because of the Cr-rich nature of these samples, even after dilution with SiO_2, suitable standards for XRF analysis of Cr were not available. For this reason Cr_2O_3 was determined by electron microprobe; it is presented in Table 10.1A on a normalised, loss-on-ignition free basis. Electron microprobe analyses of Cr-rich Fe-Ti spinels and ilmenite from these samples are presented in Tables 10.1 , 10.2 and 10.3. For analytical details see Appendix 10.

WHOLE-ROCK CHEMISTRY

Some of these samples exhibit fairly consistent TiO_2 contents (note that this includes granular ilmenite, ilmenite and ulvospinel exsolution bodies and TiO_2 in solid solution in the spinel), that may be only marginally higher than those determined by spot analyses of discrete spinel grains (compare samples AZ-1 and AZ-2; Table 10.1). Other whole-rock samples are relatively rich in TiO_2, an indication that granular ilmenite is a major constitutent (samples AS-A1, AS-A2, LA-3; Table 10.1). The Al_2O_3 and Cr_2O_3 contents of these rocks may be attributed almost entirely to spinel, whereas a significant proportion of MgO is present in both spinel and ilmenite. Variability in the Al_2O_3 and Cr_2O_3 contents may be attributed to primary cumulus compositions and to the proportion of new (pegmatitic) material, as compared to the primary chromitite layer. These data reflect the high V_2O_3 content of these oxides (see Chapter 12). The Cr-rich oxides are richer in V_2O_3 than are Cr-poor, Fe-Ti oxide pegmatites.

COMPOSITIONAL VARIATION - ELECTRON MICROPROBE DATA

Compositional variation in the chemistry of Fe-Ti-Cr spinels in these hybrid oxide layers has been clearly demonstrated by Cameron and Glover (1973). In this study this feature has been documented using electron microprobe analyses. The compositional variations found by Cameron and Glover (1973) are substantiated here. Two main sections have been studied : vertical profiles through the replaced Merensky upper chromitite (samples 27-C1/2; sample positions in fig. 10.3; analyses in Table 10.2) and a strike section along part of the replaced chromitite above the upper pseudoreef A (all "AH" samples; sample positions in fig. 10.4; analyses in Table 10.2).

Compositional variation in the replaced Merensky upper chromitite layer is illustrated in Figure 10.3. In this section pegmatite occurs both above and below the hybrid oxide layer, such that, not unexpectedly, the most Cr-rich compositions occur in the middle of the layer (e.g., sample 27-C1, analysis 3). Evidently, the chromitite layer has been exposed to pegmatitic

liquids from above and below. In a section in which the replaced chromitite layer is overlain by the normal hangingwall pyroxenite the the most Cr-rich compositions are furthest away from the pegmatite (results of an electron microprobe contour map - not presented here).

Compositional variation along a strike section of the replaced chromitite above the upper pseudoreef A is illustrated in Figure 10.4. These data are also plotted against the $Mg/(Mg+Fe^{2+})$ ratio (fig. 10.5). Most of these samples have re-equilibrated and do not show any variation relative to their position in the layer (unlike in the sequence illustrated in fig.10.3). The exception to this are samples AH-14 and AH-19. This is a function of the thickness of the oxide layer at these particular positions (see fig. 10.2). In the thick oxide layers re-equilibration has not resulted in complete homogenization, whereas in the thin layers it has modified primary compositions to produce an average composition. In Table 10.2 additional data for disseminated cumulus chromite grains from the harzburgite below the hybrid oxide layer are presented (sample AH-21B, nos. 1-4; compare with sample AH-21A which is of the actual layer).

Electron microprobe analyses of ilmenite from Cr-rich Fe-Ti oxide pegmatites are presented in Table 10.3. All of these samples are of discrete grains. Compared with disseminated ilmenite from pegmatite at Amandelbult (see below) they generally contain a higher percentage of the ulvöspinel molecule. Secondly, they are consistently richer in Mg which is possibly a function of subsolidus re-equilibration with adjacent spinel.

DISCUSSION

The composition of Cr-rich Fe-Ti oxide pegmatite may be explained by metasomatic exchange between cumulus chromite and pegmatitic liquid or subsolidus re-equilibration between cumulus chromite and Fe-Ti oxides (which are Cr-poor) that have crystallized directly from the pegmatitic liquid. Field relationships indicate that considerable addition of material has occurred. Evidence from disseminated spinels (their microstructures and chemistry) indicate that Ti-magnetite and ilmenite have crystallized from a liquid probably at magmatic temperatures. Evidently, pre-existing cumulus chromitite layers or disseminated cumulus chromite grains have acted as highly efficient nuclei.

Although some metasomatic exchange may have occurred the compositional variation within these hybrid oxide layers is best explained by subsolidus re-equilibration. This presumably occurs at relatively high temperatues during the early stages of cooling and is concomitant with exsolution and contemporaneous oxidation-exsolution processes. These processes are all

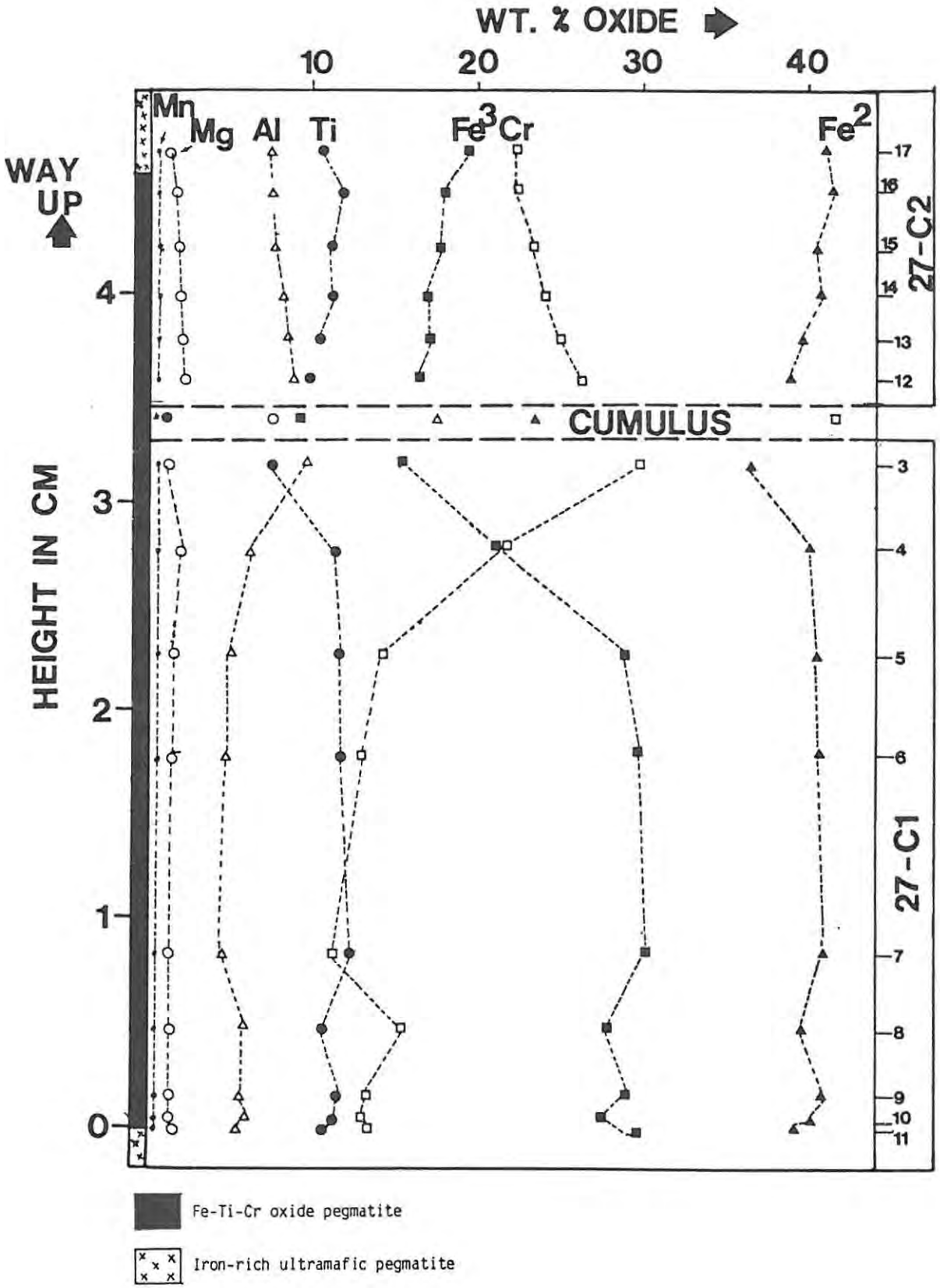

FIGURE 10.3 Compositional variation exhibited by Fe-Ti-Cr spinels through a vertical section of the replaced Merensky upper chromitite layer - plot of vertical height (in centimetres) against wt. % oxide. Based on electron microprobe analysis of spinel grains in two probe sections, 27-C1 and 27-C2; individual analyses are presented in Table 10-2 (27-C1, nos. 1-11; 27-C2, nos. 11-17). The composition of cumulus chromite from the normal (unreplaced) Merensky upper chromitite layer is presented in the break between the two probe sections (average data, sample AA-4, Appendix 10). Iron-rich ultramafic pegmatite occurs both above and below the oxide layer, consequently the most Cr-rich spinel (i.e. with a composition closest to that of the primary cumulus chromite) is found in the centre. For sample location see case-study (7), Appendix 1.

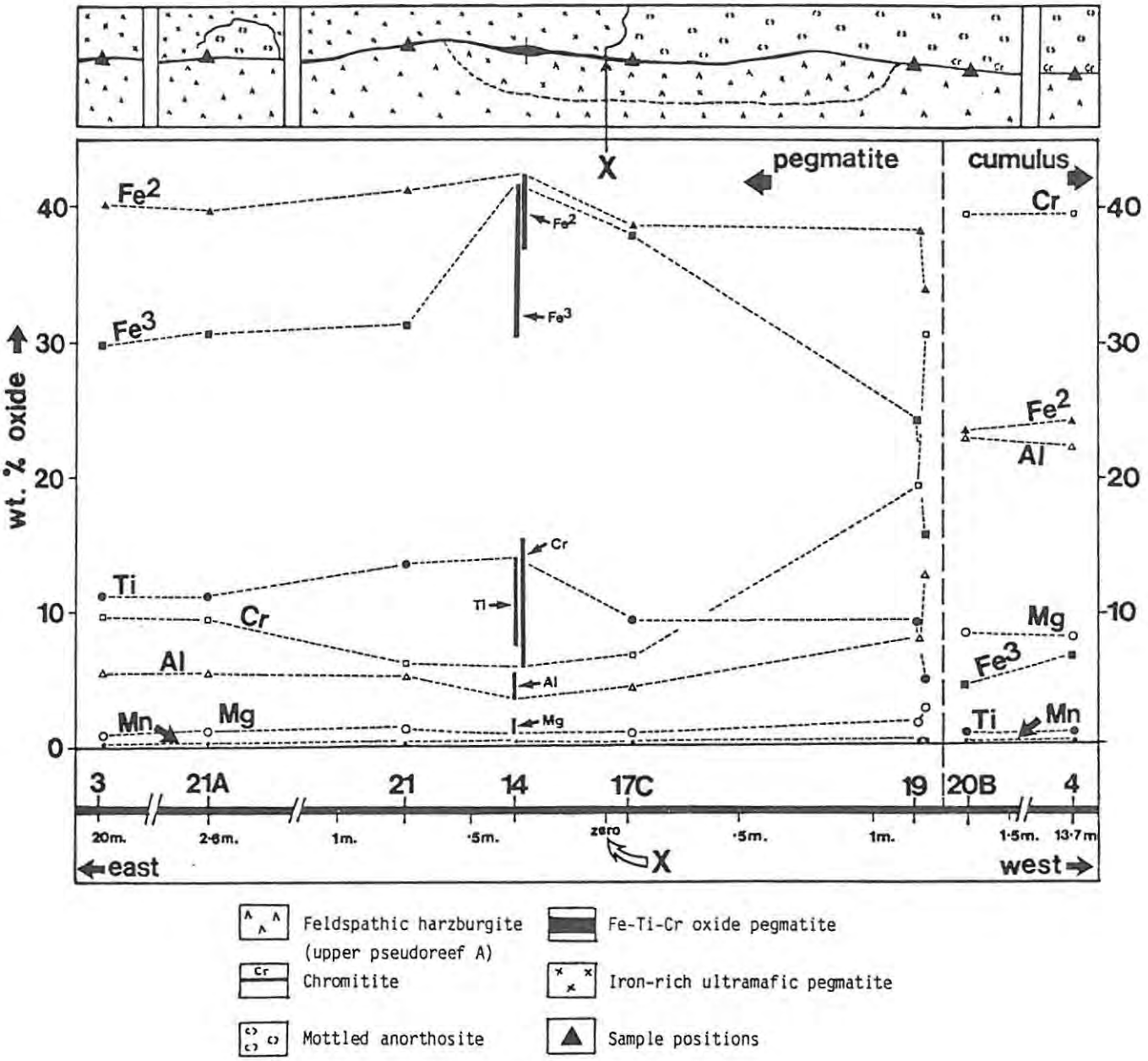

FIGURE 10.4 Compositional variation exhibited by Fe-Ti-Cr spinels along a strike section of the replaced chromitite layer above the upper pseudoreef A - plot of lateral distance (in metres) against wt. % oxide. Based on electron microprobe analysis of spinel grains in the "AH" sample group presented in Table 10.2 (samples AH-4, -20B, -19, -14, -21, -21A, -3; all samples cut normal to the layering, across the chromitite or Fe-Ti-Cr oxide layer - see case-study (5), Appendix 1). Samples AH-4 and AH-20B are of the normal (unreplaced), cumulus chromitite layer (fig. 10.2A); samples AH-17C, AH-21, AH-21A and AH-3 are of the typical Fe-Ti-Cr oxide layer (fig. 10.2C); sample AH-19 is of a step-like feature in the early development of the Fe-Ti-Cr oxide layer (fig. 10.2B); and sample AH-14 is of an unusually thick section of the Fe-Ti-Cr oxide layer (fig. 10.2D). All these data, with the exception of sample AH-14, are averages of a number of analyses across the chromitite or Fe-Ti-Cr oxide layer; note that sample AH-19 consists of two sets of data, that for the thick (analyses 2,3,4) and thin (analyses 5,6,7) parts of the oxide layer. In sample AH-19, however, the oxides have not re-equilibrated; these data are thus presented as a compositional range : the typical pegmatitic spinel is probably represented by the most Fe-Ti-rich and Cr-Al-Mg-poor analysis. Note that the hybrid oxide layer continues past the contact with the pegmatite body (e.g., to the west of position "X").

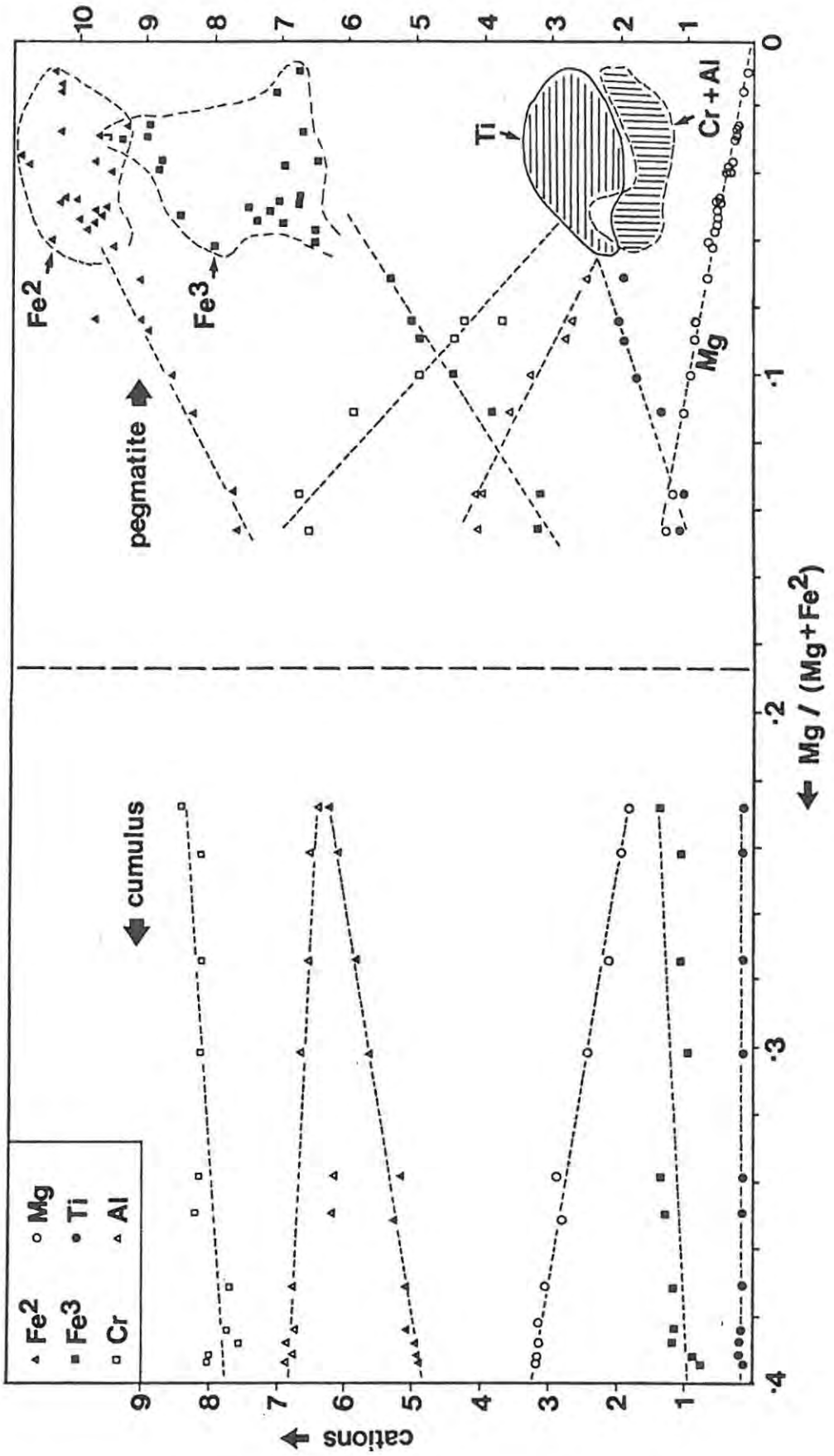

FIGURE 10.5 Plot of cations (Fe^{2+}, Fe^{3+}, Cr, Mg, Al, Ti) against the Mg / (Mg + Fe^{2+}) ratio.

Based on electron microprobe analysis of Fe-Ti-Cr spinel grains from the "AH" sample group (see Table 10.2). These data include analyses of normal, cumulus chromite (from the chromitite layer above the upper pseudoreef A) and pegmatitic Fe-Ti-Cr spinel from this replaced oxide layer (same samples as in fig. 10.4). Note that the Ti, Cr and Al content of the typical Fe-Ti-Cr oxide plot in small fields in this diagram, in which it is not possible to distinguish individual analyses. Variation in the composition of the cumulus chromite may be attributed to whether the samples occur in the layer or as disseminated grains in the harzburgite; the latter are relatively Cr-poor. Variation in the composition of the Fe-Ti-Cr spinels (which are all in the oxide layer) is evident from examining Figure 10.4 - it is related to their proximity to the main pegmatite body.

accompanied by annealing. If subsolidus re-equilibration is responsible for these compositional variations then these data (which might suggest that Al and Mg are more readily replaced than Cr) suggest that Cr and Fe^{3+} are more readily re-distributed during subsolidus reequilibration, whereas (Al and Mg) and (Ti and Fe^{2+}) are less mobile (see also Cameron & Glover, 1973).

SUMMARY

All the above data reflect the compositional variation. This may be summarised as follows :

(1) The pegmatitic, hybrid spinels are enriched in Fe^{3+}, Fe^{2+}, Ti and V and depleted in Cr, Al and Mg compared to the primary cumulus chromite. The Mn content shows little variation.

(2) The compositional break between cumulus chromite and the most Cr-rich pegmatitic composition is sharp, but an overall gradational transition from Cr-rich to Cr-poor spinel does occur.

(3) These compositional variations show that Cr and Fe^{3+} and (Mg and Al) and (Ti and Fe^{2+}) act as mirror-image pairs.

(4) Compositional variation in thick layers (e.g., 40 mm, or greater) is preserved, even though subsolidus re-equilibration has modified end-member compositions.

(5) Subsolidus re-equilibration in thin layers (e.g., 5 to 20 mm) modifies primary compositions, resulting in average compositions.

(6) When a thin chromitite layer in contact with pegmatite is examined along strike, a similiar compositional variation to that found in a thick layer is preserved reflecting lateral distance from the pegmatite body.

(7) Strike sections illustrate that pegmatitic liquids are channelled along chromitite layers, resulting in the formation of hybrid spinels over a lateral distance of several metres beyond the margins of a pegmatite body. In contrast, cumulus chromite grains only a few millimetres below the oxide layer may be unaltered.

(8) Chromitite layers act as impervious barriers to the pegmatitic liquids, but reaction with these liquids (metasomatism) or reaction with oxides which have crystallized from these liquids (subsolidus re-equilibration) results in the formation of hybrid layers. They consist of spinels intermediate in composition between chromite and Ti-magnetite.

10.3 DISSEMINATED Fe-Ti-Cr OXIDES

Cameron and Glover (1973) report that the Fe-Ti-Cr oxide content of iron-rich ultramafic pegmatite may vary from less than 1 to nearly 100 modal percent. Disseminated oxides are an ubiquitous constituent of silicate-rich pegmatite at Amandelbult. The Fe-Ti-Cr oxide mineralogy of pegmatite at Amandelbult is essentially comparable to that documented by Cameron and Glover (1973). However, as the previous authors observe, "it is very unlikely that all oxide mineral relationships in these (pegmatite) bodies have been discovered".

DISTRIBUTION

The oxide mineral content of pegmatite at Amandelbult is usually less than 25 modal percent, and average contents of 5-15 modal percent are characteristic; this is reflected by the CIPW norm (see Chapter 8). The proportion of ilmenite may be assessed from whole rock TiO_2 data, but the proportion of spinel is less readily determined. Ilmenite may be of greater abundance than spinel, and in specific samples may be the only oxide component, but in pegmatite from the upper critical zone ilmenite and spinel are usually of equal abundance. However, in pegmatite in the main zone Ti-magnetite is much more abundant than ilmenite; the oxide assemblages of large, pipe-like bodies are comparable to cumulate Ti-magnetite layers in which the relative abundance of granular ilmenite is usually less than 10 modal percent (Reynolds pers. comm.).

In pegmatite from the Middellaagte pipe, the modal proportion of disseminated oxide shows wide variation and tends to form specific (magnetic) cores. A similar pattern is found in small pegmatite bodies in the upper critical zone at Amandelbult. Here, the proportion of oxide may locally attain 25 modal percent. However, in the lower main zone, small pegmatite bodies containing a "core zone" of massive oxide and massive Fe-Ti oxide pegmatite, with only minor amounts of silicate are found.

10.3.1 GRANULAR ILMENITE

Ilmenite in iron-rich ultramafic pegmatite at Amandelbult is observed in two main forms : as discrete grains, or clusters of grains, and as oxidation-exsolution bodies in spinels (see below) and clinopyroxene (see Chapter 8). Granular ilmenite typically represents between 1 and 6 modal percent (whole-rock TiO_2 contents range from 0.5 to 3 wt. percent). It occurs as subhedral to anhedral grains (diameters of 1 - 5 mm are common). These form as

TABLE 10.1A XRF ANALYSES OF MASSIVE Cr-RICH AND Cr-POOR Ti-MAGNETITES

	MAG-1	MAG-4	LEU-1	LEU-2	LEU-3	LEU-4	AZ-1		AZ-2		AS-A1		AS-A2		LA-3	
wt.%																
TiO_2	13.24	14.69	19.96	24.07	20.82	20.40	23.08	20.61	20.99	20.42	20.71	18.56	21.69	19.41	23.26	20.56
Al_2O_3	3.22	3.65	2.39	2.30	3.04	2.92	4.19	3.74	3.52	3.43	5.29	4.74	4.05	3.62	3.56	3.15
Fe_2O_3	82.43	81.37	71.70	69.68	71.47	72.32	68.57	61.22	70.62	68.72	69.58	62.36	68.16	60.98	70.31	62.16
MnO	.45	.38	.46	.47	.30	.47	.54	.48	.45	.44	.51	.46	.74	.66	.45	.40
MgO	1.31	1.67	.91	.69	.47	.83	2.44	2.18	1.99	1.94	2.73	2.45	4.08	3.65	2.47	2.18
CaO	n.d.	n.d.	n.d.	n.d.	n.d.	n.d.	n.d.	-	n.d.	-	n.d.	-	.30	.27	n.d.	-
P_2O_5	n.d.	n.d.	.63	.66	.02	.05	n.d.	-	n.d.	-	n.d.	-	.02	.02	n.d.	-
Cr_2O_3	.18	.01	.04	.11	.02	.05	-	10.42**	-	3.48**	-	11.39**	-	11.39**	-	10.70**
V_2O_3	-	-	.12	.01	.64	.61	1.47	1.31	1.57	1.55	-	-	-	-	.85	.75
NiO	.08	.09	.01	.01	.01	.01	.05	.04	.05	.05	.05	.04	-	-	.11	.10
L.O.I.	(-1.78)	(-4.00)	.18	.46	1.18	1.07	(-3.96)	-	(-1.56)	-	(-5.26)	-	(-5.40)	-	(-3.43)	-
TOTAL	99.13	98.11	96.41	98.61	97.97	98.73	97.05	100.00	97.63	100.00	93.61	100.00	93.64	100.00	97.85	100.00
ppm																
Cr	1253	483	252	757	139	328	94300*		62800*		138300*		138000*		213000*	
V	21300*	23200*	788	1054	4307	4163	9985		10600		32000*		32800*		5760	
Co	363	264	148	118	181	164	290		298		321		339		287	
Ni	603	732	50	56	80	60	417		446		358		346		880	
Cu	116	132	47	34	68	73	34		37		52		46		32	
Zn	320	321	430	439	521	484	579		533		658		654		617	
Sc	57	59	104	104	74	73	88		79		93		87		35	
Nb	n.d.	-	4.0	-	3.6	5.0	n.d.		n.d.		n.d.		-		-	
Zr	24.4	-	13.2	-	47.5	56.9	17.4		19.2		22.3		-		-	
Y	6.9	-	9.6	-	21.3	6.8	4.5		9.5		5.9		-		-	
Sr	n.d.	-	26	-	3	3	n.d.		n.d.		n.d.		n.d.		-	

n.d.: not detected; Tr: Trace; - not determined; Total Fe as Fe_2O_3 * Suspect results (see text for details).
** : Samples of Cr- rich magnetite normalised loss on ignition free, with Cr_2O_3 determined by electron microprobe.

TABLE 10.1B ELECTRON MICROPROBE ANALYSES OF Cr-RICH Ti-MAGNETITES FROM TABLE 10.1A

	AZ-1	AZ-1	AZ-1	AZ-2	AZ-2	AS-A1	AS-A1	AS-A1	LA-3	LA-3	LA-3	LA-3A	LA-3A
wt.%													
TiO_2	19.30	20.86	18.53	18.79	17.90	14.91	15.25	15.30	7.93	8.50	9.16	10.41	11.14
Cr_2O_3	9.90	10.17	11.00	3.42	3.52	11.27	11.44	11.40	8.75	12.69	10.48	12.62	15.64
Al_2O_3	4.25	4.72	4.61	3.60	3.87	5.56	5.74	5.64	3.47	5.25	4.53	5.19	5.46
Fe_2O_3	17.31	13.98	17.24	25.62	27.15	22.88	22.52	22.67	41.32	33.57	36.32	32.17	27.76
FeO	45.68	47.33	45.39	45.81	45.26	41.91	42.41	42.48	36.52	36.43	37.24	38.60	39.09
MgO	2.26	2.32	2.07	1.85	1.79	2.25	2.34	2.35	1.46	1.84	1.89	2.13	2.35
MnO	.46	.45	.44	.36	.35	.42	.41	.40	.31	.37	.34	.41	.48
TOTAL	99.16	99.83	99.28	99.45	99.84	99.20	100.11	100.24	99.77	98.66	99.96	101.54	101.93
cations													
Ti	4.2305	4.5220	4.0557	4.1497	3.9374	3.2558	3.2947	3.3026	1.7658	1.8845	2.0137	2.2382	2.3744
Fe^{2+}	4.2305	4.5220	4.0557	4.1497	3.9374	3.2558	3.2947	3.3026	1.7658	1.8845	2.0137	2.2382	2.3744
Cr	2.2814	2.3168	2.5311	.7930	.8145	2.5866	2.5990	2.5877	2.0484	2.9578	2.4221	2.8526	3.5047
Al	1.4597	1.6045	1.5811	1.2466	1.3350	1.9013	1.9421	1.9093	1.2108	1.8239	1.5605	1.7485	1.8236
Fe^{3+}	3.7976	3.0345	3.7761	.6607	5.9755	5.0002	4.8694	4.8976	9.2090	7.4490	7.9898	6.9222	5.9226
Fe^{2+}	6.9045	6.8901	6.9935	7.1007	7.1339	6.9249	6.8950	6.8950	7.2278	7.0990	7.0922	6.9929	6.8920
Mg	.9819	.9989	.8980	.8089	.7791	.9744	1.0040	1.0074	.6444	.8086	.8235	.9077	.9928
Mn	.1135	.1109	.1084	.0903	.0870	.1006	.1009	.0974	.0777	.0923	.0841	.0992	.1152
R1	.354	.305	.350	.443	.455	.419	.413	.415	.558	.512	.529	.497	.462
R2	.254	.210	.254	.334	.350	.329	.323	.324	.504	.453	.467	.428	.389
R3	.503	.436	.478	.735	.735	.526	.517	.521	.738	.609	.667	.600	.526
R4	.124	.126	.113	.102	.098	.123	.127	.127	.081	.102	.104	.114	.125
R5	.081	.080	.075	.067	.065	.087	.089	.089	.066	.082	.082	.089	.096

For description of ratios see Table 10.2

TABLE 10.1C ELECTRON MICROPROBE ANALYSES OF ILMENITES FROM TABLE 10.1A

	AZ-1	AZ-1	AZ-2	AZ-2	AS-A1	AS-A1	LA-3	LA-3	LA-3A	LA-3A
wt.%										
TiO_2	51.98	52.30	50.84	51.79	51.62	51.77	51.88	49.18	53.03	53.38
Al_2O_3	.25	.15	.19	.24	.21	.26	.16	.91	.23	.29
FeO	40.28	39.39	39.42	40.23	39.29	39.71	38.86	36.00	39.57	39.38
Fe_2O_3	2.44	.69	4.47	3.54	3.07	2.55	3.00	5.66	2.75	2.96
MnO	.43	.41	.50	.47	.44	.41	.50	.56	.48	.47
MgO	3.38	3.36	3.25	3.29	3.75	3.61	4.09	4.30	4.28	4.57
Cr_2O_3	.11	.14	.04	.07	.13	.13	.14	1.10	.22	.50
TOTAL	98.87	96.44	98.71	99.63	98.51	98.44	98.63	97.71	100.57	101.56
cations (sum = 2.0000)										
Ti	.9724	1.0029	.9548	.9629	.9669	.9710	.9683	.9226	.9694	.9643
Al	.0073	.0045	.0056	.0070	.0062	.0076	.0047	.0268	.0066	.0082
Fe^{2+}	.8381	.8400	.8233	.8318	.8184	.8281	.8065	.7509	.8045	.7912
Fe^{3+}	.0457	.0132	.0840	.0659	.0575	.0478	.0561	.1063	.0503	.0536
Mn	.0091	.0089	.0106	.0098	.0093	.0087	.0105	.0012	.0099	.0096
Mg	.1253	.1277	.1210	.1212	.1392	.1342	.1513	.1599	.1550	.1636
Cr	.0022	.0028	.0008	.0014	.0026	.0026	.0027	.0217	.0042	.0095
mol.% ilmenite										
	97.53	99.29	95.48	96.45	96.87	97.40	96.93	94.00	97.23	97.02

TABLE 10-2 ELECTRON MICROPROBE ANALYSES OF SPINELS FROM Cr-RICH Fe-Ti-OXIDE LAYERS

	AH-3						AH-3 AVERAGE			AH-21A		AH-21A AVERAGE			AH-21				AH-21 AVERAGE		
	1	2	3	4	5	6	x	d	n	1	2	x	d	n	1	2	3	4	x	d	n
wt.%																					
TiO_2	11.29	11.21	11.60	10.16	11.33	11.50	11.18	.5205	6	11.56	10.67	11.12	.6293	2	14.20	13.07	14.84	12.53	13.66	1.0502	4
Cr_2O_3	8.93	9.50	9.51	9.97	9.46	10.77	9.69	.6235	6	9.53	9.30	9.42	.1626	2	6.19	6.52	5.65	6.78	6.29	.4830	4
Al_2O_3	5.21	5.45	5.27	5.12	5.23	5.40	5.28	.1236	6	5.39	5.87	5.63	.3394	2	5.20	5.69	4.43	5.16	5.12	.5193	4
Fe_2O_3	31.25	29.64	28.65	31.18	28.99	29.24	29.83	1.1244	6	29.89	30.93	30.40	.7354	2	29.32	30.37	28.60	31.34	29.91	1.2001	4
FeO	41.16	41.06	39.36	38.23	40.09	39.95	39.98	1.0971	6	40.14	39.02	39.58	.7920	2	42.30	41.77	43.32	41.04	42.11	.9593	4
MgO	.38	.24	1.26	1.12	.64	1.36	.83	.4768	6	1.13	1.27	1.20	.0990	2	1.49	1.21	.94	1.17	1.20	.2256	4
MnO	.41	.34	.35	.39	.34	.36	.37	.0288	6	.38	.35	.37	.0212	2	.36	.33	.35	.34	.35	.0129	4
TOTAL	98.63	97.43	96.00	96.16	96.08	98.57	97.16	-		98.02	97.40	97.72	-		99.05	98.96	98.12	98.36	98.64	-	
cations (sum = 24.000)																					
Ti	2.5300	2.5402	2.6468	2.3216	2.5967	2.5539	2.5311	-		2.5870	2.3956	2.4923	-		3.1384	2.8923	3.3359	2.7989	3.0406	-	
Fe^{2+}	2.5300	2.5402	2.6468	2.3216	2.5967	2.5539	2.5311	-		2.5870	2.3956	2.4923	-		3.1384	2.8923	3.3359	2.7989	3.0406	-	
Cr	2.1035	2.2628	2.2809	2.3948	2.2791	2.5142	2.3061	-		2.2419	2.1949	2.2194	-		1.4381	1.5167	1.3351	1.5920	1.4718	-	
Al	1.8298	1.9355	1.8646	1.8337	1.8786	1.8795	1.8735	-		1.8905	2.0655	1.9777	-		1.8013	1.9735	1.5607	1.8065	1.7862	-	
Fe^{3+}	7.0367	6.7213	6.5410	7.1283	6.6489	6.4984	6.7583	-		6.6937	6.9484	6.8183	-		6.4838	6.7252	6.4324	7.0038	6.6609	-	
Fe^{2+}	7.7278	7.8055	7.3404	7.3935	7.6216	7.3114	7.5333	-		7.4031	7.3465	7.3736	-		7.2578	7.3871	7.4923	7.3966	7.3829	-	
Mg	.1687	.1078	.5697	.5072	.2907	.5985	.3724	-		.5011	.5650	.5330	-		.6526	.5306	.4187	.5179	.5293	-	
Mn	.1035	.0868	.0899	.1004	.0878	.0900	.0943	-		.0958	.0885	.0934	-		.0896	.0823	.0886	.0855	.0877	-	
R1	.475	.463	.471	.491	.466	.471	.473	-		.475	.486	.480	-		.472	.477	.462	.486	.474	-	
R2	.406	.394	.396	.423	.394	.397	.402	-		.401	.416	.409	-		.384	.396	.373	.407	.390	-	
R3	.640	.616	.611	.628	.615	.597	.618	-		.618	.620	.619	-		.667	.658	.690	.673	.672	-	
R4	.021	.014	.072	.064	.037	.076	.047	-		.063	.071	.067	-		.032	.057	.053	.065	.057	-	
R5	.016	.010	.054	.050	.028	.057	.036	-		.048	.055	.051	-		.050	.049	.037	.048	.048	-	

	AH-17C					AH-17C AVERAGE			AH-14		AH-208			AH-208 AVERAGE		
	1	2	3	4	5	x	d	n	1	2	1	2	3	x	d	n
wt.%																
TiO_2	9.79	9.75	10.09	8.56	9.02	9.44	.6308	5	14.03	7.47	.91	1.02	.99	.97	.0569	3
Cr_2O_3	6.28	8.32	6.21	7.44	6.29	6.91	.9408	5	5.70	6.48	40.03	39.50	39.18	39.57	.4293	3
Al_2O_3	3.73	5.01	4.46	4.48	4.04	4.34	.4860	5	3.67	4.02	22.93	22.46	23.78	23.06	.6691	3
Fe_2O_3	38.29	35.83	37.66	38.84	39.67	38.07	1.4480	5	30.34	41.68	4.02	4.62	5.14	4.60	.5605	3
FeO	38.62	38.24	38.64	37.70	38.39	38.31	.3834	5	42.22	36.70	23.05	23.05	23.23	23.10	.1012	3
MgO	.84	1.42	1.22	.85	.65	1.00	.3144	5	.94	.63	8.40	8.33	8.79	8.51	.2479	3
MnO	.31	.34	.35	.32	.34	.33	.0164	5	.27	.26	.50	.50	.47	.49	.0173	3
TOTAL	97.85	98.90	98.63	98.19	98.39	98.40	-		97.17	97.23	99.84	99.49	101.58	100.30	-	
cations																
Ti	2.2269	2.1683	2.2616	1.9338	2.0420	2.1261	-		3.1993	1.7134	.1736	.1957	.1851	.1842	-	
Fe^{2+}	2.2269	2.1683	2.2616	1.9338	2.0420	2.1261	-		3.1993	1.7134	.1736	.1957	.1851	.1842	-	
Cr	1.5016	1.9449	1.4631	1.7668	1.4968	1.6360	-		1.3663	1.5624	8.0280	7.9669	7.6997	7.8969	-	
Al	1.3298	1.7462	1.5668	1.5862	1.4334	1.5320	-		1.3116	1.4451	6.8565	6.7542	6.9677	6.8515	-	
Fe^{3+}	8.7147	7.9724	8.4470	8.7794	8.9860	8.5798	-		6.9236	9.5658	.7681	.8876	.9524	.8732	-	
Fe^{2+}	7.5419	7.2891	7.3698	7.5381	7.6217	7.4700	-		7.5059	7.6465	4.7167	4.7247	4.4645	4.6936	-	
Mg	.3786	.6258	.5419	.3805	.2916	.4463	-		.4248	.2863	3.1758	3.1673	3.2565	3.2016	-	
Mn	.0794	.0852	.0884	.0814	.0867	.0837	-		.0693	.0572	.1074	.1081	.0990	.1048	-	
R1	.536	.522	.534	.538	.541	.535	-		.480	.556	.140	.158	.172	.157	-	
R2	.471	.457	.467	.481	.482	.472	-		.393	.505	.136	.153	.166	.152	-	
R3	.755	.684	.736	.724	.754	.730	-		.721	.761	.049	.057	.062	.056	-	
R4	.048	.079	.068	.048	.037	.056	-		.054	.036	.402	.401	.412	.406	-	
R5	.037	.052	.053	.039	.029	.044	-		.038	.030	.394	.392	.403	.396	-	

	AH-19							AH-4						AH-4 AVERAGE			AH-21B			
	1	2	3	4	5	6	7	1	2	3	4	5	6	x	d	n	1	2	3	4
wt.%																				
TiO_2	8.15	6.60	5.37	5.00	9.44	9.17	9.16	1.07	.97	1.02	.97	.94	.93	.99	.0540	6	.67	.73	.78	.81
Cr_2O_3	22.86	27.48	30.83	31.22	19.18	19.88	19.36	38.63	37.80	39.37	39.40	41.07	40.54	39.47	1.2012	6	39.94	39.69	39.59	40.27
Al_2O_3	10.11	11.15	12.77	12.73	8.08	8.38	7.43	23.35	23.43	22.90	23.27	20.78	20.35	22.35	1.3986	6	21.92	21.55	21.29	18.85
Fe_2O_3	21.66	18.73	15.79	15.36	23.61	23.36	25.38	6.36	7.07	6.22	6.31	6.63	7.10	6.61	.3890	6	4.94	5.26	5.40	6.96
FeO	37.57	36.11	33.98	33.81	38.39	38.10	38.60	23.86	22.72	23.94	24.55	24.86	24.30	24.06	.7441	6	26.02	26.89	28.06	28.10
MgO	2.33	2.54	3.26	2.95	1.97	2.09	1.66	8.49	9.02	8.39	8.16	7.49	7.61	8.19	.5738	6	6.31	5.72	5.03	4.65
MnO	.60	.50	.53	.56	.45	.47	.71	.50	.49	.47	.50	.52	.50	.50	.0163	6	.48	.53	.51	.51
TOTAL	103.27	103.10	102.53	101.62	101.11	101.45	102.30	102.26	101.50	102.32	103.17	102.27	101.32	102.16	-		100.27	100.37	100.66	100.14
cations (sum = 24.000)																				
Ti	1.6751	1.3486	1.0882	1.0238	2.0052	1.9371	1.9358	.1997	.1815	.1907	.1801	.1785	.1782	.1861	-		.1297	.1420	.1522	.1610
Fe^{2+}	1.6751	1.3486	1.0882	1.0238	2.0052	1.9371	1.9358	.1997	.1815	.1907	.1801	.1785	.1782	.1861	-		.1297	.1420	.1522	.1610
Cr	4.9389	5.9026	6.5670	6.7197	4.2826	4.4143	4.3007	7.5811	7.4393	7.7416	7.6932	8.2000	8.1698	7.7999	-		8.1317	8.1197	8.1268	8.4192
Al	3.2567	3.5708	4.0556	4.0852	2.6899	2.7744	2.4609	6.8301	6.8729	6.7117	6.7723	6.1839	6.1125	6.5852	-		6.6518	6.5711	6.5139	5.8739
Fe^{3+}	4.4643	3.8292	3.2010	3.1476	5.0171	4.9372	5.3670	1.1892	1.3245	1.1650	1.1741	1.2590	1.3610	1.2426	-		.9569	1.0250	1.0546	1.3946
Fe^{2+}	6.9121	6.8564	6.5700	6.6739	7.0631	7.0133	7.1358	4.7535	4.5498	4.7905	4.8914	5.0592	5.0006	4.8430	-		5.4731	5.6776	5.9412	6.0529
Mg	.9490	1.0285	1.3091	1.1970	.8292	.8749	.6952	3.1413	3.3469	3.1105	3.0040	2.8195	2.8914	3.0511	-		2.4221	2.2062	1.9467	1.8329
Mn	.1389	.1151	.1210	.1291	.1077	.1118	.1690	.1051	.1033	.0990	.1045	.1112	.1079	.1059	-		.1046	.1161	.1121	.1142
R1	.382	.358	.328	.320	.415	.413	.429	.200	.225	.195	.193	.198	.213	.204	-		.148	.152	.150	-
R2	.342	.318	.295	.290	.366	.366	.372	.193	.218	.189	.187	.193	.208	.198	-		.145	.149	.147	-
R3	.352	.288	.232	.226	.418	.407	.443	.076	.084	.074	.075	.080	.087	.080	-		.060	.065	.067	-
R4	.121	.130	.166	.152	.105	.111	.088	.397	.423	.393	.380	.357	.366	.387	-		.306	.279	.246	-
R5	.100	.111	.146	.135	.084	.099	.071	.388	.414	.384	.371	.349	.358	.378	-		.301	.274	.242	-

RATIOS : R1 =(Fe^{3+} / Fe^{3+} + octahedral Fe^{2+}) ; R2 =(Fe^{3+} / Fe^{3+} + total Fe^{2+}); R3 =(Fe^{3+} / Fe^{3+} + Al + Cr);

R4 =(Mg / Mg + octahedral Fe^{2+}); R5 =(Mg / Mg + total Fe^{2+}).

TABLE 10-2 (CONTINUED)

	27-C1											27-C2					
	1	2	3	4	5	6	7	8	9	10	11	12	13	14	15	16	17
wt.%																	
TiO_2	11.47	10.30	7.33	11.18	11.28	11.53	11.92	10.40	11.27	11.02	10.57	9.57	10.22	11.00	10.85	11.60	10.57
Cr_2O_3	12.96	15.67	29.50	21.28	14.02	12.64	11.19	15.13	13.14	13.52	13.08	26.17	24.71	23.84	23.20	22.07	22.03
Al_2O_3	5.17	5.64	9.60	6.19	4.99	4.73	4.48	5.81	5.45	5.87	5.40	8.78	8.38	8.00	7.56	7.25	7.30
Fe_2O_3	27.61	25.55	15.17	20.72	28.76	29.46	29.95	27.61	28.75	27.56	29.22	16.39	16.90	16.72	17.79	17.90	19.25
FeO	41.04	39.14	36.31	39.95	40.23	40.38	40.87	39.50	40.52	40.09	39.24	38.87	39.51	40.31	40.10	41.08	40.74
MgO	.77	1.28	2.19	1.89	1.51	1.40	1.20	1.37	1.27	1.26	1.41	2.10	1.98	1.88	1.81	1.60	1.16
MnO	.40	.42	.50	.52	.44	.42	.34	.43	.46	.41	.39	.52	.52	.54	.50	.52	.42
TOTAL	99.41	98.99	100.60	101.73	101.23	100.55	99.95	100.24	100.85	99.73	99.30	102.40	102.22	102.29	101.82	102.02	101.46
cations (sum = 24.0000)																	
Ti	2.3587	2.2739	1.5452	2.3798	2.4424	2.5191	2.6724	2.2658	2.4481	2.4142	2.3297	1.9935	2.1387	2.3058	2.2935	2.4525	2.2548
Fe^{2+}	2.3587	2.2739	1.5452	2.3798	2.4424	2.5191	2.6724	2.2658	2.4481	2.4142	2.3297	1.9935	2.1387	2.3058	2.2935	2.4525	2.2548
Cr	3.0153	3.6364	6.5372	4.7616	3.1910	2.9029	2.5927	3.4651	3.0334	3.1135	3.0305	5.7304	5.4355	5.2530	5.1503	4.9049	4.9400
Al	1.7934	1.9515	3.1718	2.0651	1.6934	1.6196	1.5477	1.9839	1.8554	2.0155	1.8654	2.8665	2.7484	2.6282	2.5023	2.4024	2.4407
Fe^{3+}	6.1139	5.8644	3.2005	4.4136	6.2309	6.4394	6.6048	6.0194	6.2481	6.0426	6.4446	3.4162	3.5388	3.5072	3.7604	3.7877	4.1097
Fe^{2+}	7.5626	7.3056	6.9664	7.0781	7.2448	7.2905	7.3914	7.3030	7.3408	7.3518	7.2873	7.0111	7.0564	7.0916	7.1236	7.2058	7.4087
Mg	.3377	.5600	.9149	.7973	.6479	.6062	.5242	.5915	.5467	.5471	.6159	.8569	.8211	.7809	.7575	.6703	.4904
Mn	.0997	.1044	.1187	.1247	.1073	.1034	.0844	.1055	.1125	.1012	.0968	.1220	.1226	.1275	.1189	.1238	.1009
R1	.447	.442	.315	.384	.462	.469	.472	.452	.460	.451	.469	.328	.334	.331	.345	.345	.357
R2	.377	.379	.273	.318	.391	.396	.397	.386	.390	.382	.401	.275	.278	.272	.285	.282	.298
R3	.560	.512	.248	.393	.561	.587	.615	.525	.563	.541	.568	.284	.302	.308	.329	.341	.358
R4	.043	.071	.116	.101	.082	.077	.066	.075	.069	.069	.078	.110	.104	.099	.096	.085	.062
R5	.032	.055	.097	.078	.063	.058	.050	.058	.053	.053	.060	.088	.082	.077	.074	.065	.048

TABLE 10-3 ELECTRON MICROPROBE ANALYSES OF ILMENITES FROM Cr-RICH Fe-Ti OXIDE LAYERS

	AH-3	AH-21A	AH-21A	AH-17C	AH-17C	AH-19	AH-19	AH			27-C1	27-C1	27-C1	27-C1	27-C1			27-F1	27-F1
								$\bar{x}$	d	n					$\bar{x}$	d	n		
wt.%																			
TiO_2	50.93	51.21	52.48	51.73	51.30	51.13	50.01	51.26	.7529	7	51.82	51.82	51.62	52.05	51.69	.3263	4	51.99	51.55
Al_2O_3	.22	.22	.22	.22	.21	.25	.24	.23	.0151	7	.20	.18	.23	.20	.20	.0206	4	.33	.25
FeO	40.62	41.60	41.40	41.09	41.28	40.41	39.81	40.89	.6359	7	42.69	42.42	42.35	42.21	42.29	.2016	4	43.38	43.10
Fe_2O_3	4.43	3.74	4.58	4.08	4.28	4.48	3.81	4.20	.3317	7	3.77	3.87	3.24	3.93	3.85	.3153	4	4.05	4.79
MnO	.49	.45	.46	.54	.48	.50	.45	.48	.0324	7	.68	.68	.53	.46	.59	.1106	4	.53	.49
MgO	2.63	2.24	2.99	2.74	2.45	2.84	2.64	2.65	.2478	7	1.81	1.96	1.98	2.32	2.02	.2155	4	1.59	1.55
Cr_2O_3	.18	.16	.14	.18	.18	.17	.13	.16	.0206	7	.15	.17	.18	.20	.18	.0208	4	.12	.14
TOTAL	99.49	99.62	102.27	100.58	100.18	99.78	97.09	99.87	-		101.12	101.10	100.14	101.36	100.80	-		101.99	101.87
cations (sum = 2.0000)																			
Ti	.9535	.9601	.9539	.9573	.9553	.9529	.9585	.9558	-		.9606	.9599	.9655	.9590	.9596	-		.9568	.9508
Al	.0065	.0065	.0063	.0064	.0061	.0073	.0072	.0067	-		.0058	.0052	.0067	.0058	.0058	-		.0095	.0072
Fe^{2+}	.8456	.8674	.8367	.8455	.8548	.8376	.8486	.8478	-		.8799	.8737	.8801	.8647	.8729	-		.8878	.8840
Fe^{3+}	.0830	.0702	.0833	.0756	.0798	.0835	.0731	.0784	-		.0700	.0717	.0606	.0724	.0715	-		.0747	.0884
Mn	.0103	.0095	.0094	.0113	.0101	.0106	.0097	.0101	-		.0142	.0142	.0112	.0095	.0123	-		.0110	.0102
Mg	.0976	.0832	.1077	.1005	.0904	.1049	.1003	.0979	-		.0665	.0719	.0733	.0847	.0743	-		.0580	.0567
Cr	.0035	.0031	.0027	.0035	.0035	.0033	.0026	.0031	-		.0030	.0033	.0035	.0039	.0035	-		.0023	.0027
mol.% ilmenite	95.59	96.30	95.54	95.97	95.77	95.54	96.11	95.83	-		96.33	96.23	96.82	96.18	96.24	-		96.11	95.40

TABLE 10-4 ELECTRON MICROPROBE ANALYSES OF DISSEMINATED ILMENITES FROM IRON-RICH ULTRAMAFIC PEGMATITE

	AG-13A	AE-25	AE-12	AE-28	AE-28	AE-28	AE-28	AE-28	AE-28			M.24-7A	M.24-7A	M.24-7A	M.24-7A	M.24-7A	M.24-7A		
									$\bar{x}$	d	n						$\bar{x}$	d	n
wt.%																			
TiO_2	50.62	50.39	50.80	51.09	51.04	50.83	50.55	50.71	50.75	.2380	8	49.87	51.33	51.74	50.76	50.27	50.79	.7602	5
Al_2O_3	.36	.12	.19	.15	.15	.19	.20	.13	.19	.0761	8	.23	.12	.27	.23	.19	.21	.0567	5
FeO	41.33	42.03	42.81	44.22	43.25	42.43	42.75	42.21	42.52	.8640	8	42.03	43.84	43.26	43.02	42.43	42.92	.7078	5
Fe_2O_3	4.15	5.95	4.73	4.74	4.78	5.51	5.41	5.96	5.27	.6519	8	6.90	4.77	4.69	5.69	6.34	5.68	.9660	5
MnO	.62	.48	.48	1.17	.66	.51	.49	.50	.53	.0739	7	.50	.25	.48	.50	.52	.45	.1127	5
MgO	2.00	1.57	1.34	.30	1.11	1.55	1.24	1.62	1.45	.2942	8	1.30	1.16	1.56	1.19	1.26	1.29	.1587	5
Cr_2O_3	.86	.15	.12	.08	.21	.14	.10	.15	.14	.0420	7	.05	.09	.08	.06	.05	.07	.0164	5
TOTAL	99.94	100.69	100.46	101.76	101.20	101.16	100.74	101.28	100.84	-		100.87	101.56	102.08	101.46	101.08	101.41	-	
cations (sum = 2.0000)																			
Ti	.9474	.9412	.9517	.9528	.9512	.9446	.9455	.9413	.9467	-		.9317	.9531	.9522	.9432	.9375	.9435	-	
Al	.0106	.0035	.0056	.0044	.0044	.0055	.0059	.0038	.0056	-		.0673	.0035	.0078	.0067	.0056	.0061	-	
Fe^{2+}	.8602	.8730	.8919	.9171	.8964	.8769	.8892	.8713	.8819	-		.8730	.9052	.8853	.8889	.8800	.8866	-	
Fe^{3+}	.0777	.1111	.0886	.0885	.0891	.1025	.1013	.1107	.0984	-		.1290	.0886	.0863	.1058	.1183	.1066	-	
Mn	.0131	.0101	.0101	.0246	.0139	.0107	.0103	.0105	.0111	-		.0105	.0062	.0100	.0105	.0109	.0094	-	
Mg	.0742	.0581	.0498	.0111	.0410	.0571	.0460	.0596	.0536	-		.0481	.0427	.0569	.0438	.0466	.0475	-	
Cr	.0169	.0029	.0024	.0016	.0041	.0027	.0020	.0030	.0027	-		.0010	.0018	.0015	.0012	.0012	.0014	-	
mol.% ilmenite	95.88	94.22	95.41	95.48	95.40	94.67	94.77	94.24	94.89	-		93.33	95.45	95.51	94.54	93.88	94.54	-	

	M.27-5	M.27-5	M.27-5	M.27-5	M.27-5	GM-4	GM-4	M.27-3A	M.27-3A	M.27-3A	M.22-11	M.22-11	AD-5	AD-5	AD-5	5322	5322
wt.%																	
TiO_2	51.05	50.43	50.45	50.45	50.04	49.18	49.43	50.94	51.57	50.99	49.66	50.19	49.67	50.56	50.39	50.62	50.04
Al_2O_3	.26	.16	.26	.15	.18	.29	.21	.21	.22	.36	.25	.19	.22	.23	.19	.19	.18
FeO	43.05	42.79	42.14	42.33	42.81	40.67	41.27	42.09	42.79	41.89	42.36	41.33	41.41	42.11	42.45	42.29	42.81
Fe_2O_3	4.51	4.53	5.63	5.05	4.81	5.70	6.39	4.45	3.66	4.20	4.95	5.80	5.47	4.07	3.41	5.19	4.81
MnO	.46	.12	.49	.52	.28	1.29	.86	.59	.58	.59	.53	.54	.52	.51	.52	.55	.28
MgO	1.34	1.37	1.53	1.41	1.07	1.26	1.30	1.75	1.68	1.89	.99	1.83	1.53	1.59	1.31	1.50	1.07
Cr_2O_3	.07	.05	.05	.05	.11	.07	.50	.05	.05	.07	.05	.04	.07	.10	.10	.02	.11
TOTAL	100.74	99.44	100.55	99.98	99.30	98.46	99.96	100.09	100.56	99.98	98.80	99.91	98.90	98.16	98.37	100.36	99.30
cations (sum = 2.0000)																	
Ti	.9534	.9543	.9431	.9496	.9505	.9404	.9317	.9547	.9521	.9548	.9484	.9424	.9440	.9570	.9635	.9484	.9505
Al	.0076	.0047	.0076	.0044	.0054	.0087	.0062	.0062	.0064	.0103	.0075	.0056	.0066	.0068	.0057	.0056	.0054
Fe^{2+}	.8941	.9003	.8761	.8859	.9042	.8649	.8651	.8772	.8878	.8722	.8995	.8629	.8752	.8865	.9027	.8811	.9042
Fe^{3+}	.0843	.0858	.1053	.0953	.0915	.1090	.1205	.0835	.0684	.0788	.0948	.1089	.1041	.0771	.0652	.0973	.0915
Mn	.0097	.0026	.0103	.0110	.0060	.0278	.0180	.0125	.0122	.0124	.0114	.0114	.0111	.0109	.0112	.0116	.0060
Mg	.0496	.0514	.0567	.0526	.0403	.0478	.0486	.0650	.0621	.0701	.0375	.0068	.0576	.0597	.0496	.0567	.0403
Cr	.0014	.0010	.0010	.0012	.0022	.0014	.0099	.0010	.0010	.0014	.0010	.0008	.0014	.0020	.0020	.0039	.0022
mol.% ilmenite	95.64	95.58	94.52	95.05	95.30	94.30	93.71	95.64	96.43	95.85	95.12	94.31	94.58	95.98	96.62	94.95	95.30

TABLE 10-5 ELECTRON MICROPROBE ANALYSES OF DISSEMINATED Cr-RICH Ti-MAGNETITES FROM IRON-RICH ULTRAMAFIC PEGMATITE

	AE-12	AE-12	AE-12	AE-20	AE-28	AE-28	AE-28	AE-28	AE-28	AE-28	AE-28			ML24-7A	ML24-7A	ML24-7A	ML24-7A	ML24-7A	ML24-7A		
wt.%											x	d	n						x	d	n
TiO_2	6.72	5.52	7.52	10.98	7.24	7.50	16.48	9.08	6.94	7.15	7.58	.8612	5	8.39	5.46	5.33	5.50	6.03	5.68	.1100	4
Cr_2O_3	2.79	2.97	2.79	3.81	4.65	4.90	4.18	4.86	5.97	5.28	4.97	.8069	6	3.15	2.78	2.70	2.77	3.65	2.98	.4614	4
Al_2O_3	2.28	1.64	2.55	4.17	3.13	3.58	4.79	4.00	5.79	3.89	4.20	.9531	6	3.54	1.25	1.25	1.23	1.18	1.23	.0330	4
Fe_2O_3	50.24	52.73	47.99	38.17	46.39	45.45	27.91	42.21	45.28	44.76	44.63	1.5723	5	44.43	54.14	54.05	53.83	52.44	53.61	.7941	4
FeO	36.47	35.19	37.02	40.52	37.56	37.67	45.91	38.59	36.88	36.76	37.66	.7333	5	37.98	35.70	35.27	35.28	36.02	35.58	.3622	4
MgO	.49	.43	.51	.44	.18	.43	.59	.80	.67	.68	.55	.2219	6	.44	.30	.36	.44	.39	.37	.0585	4
MnO	.27	.25	.30	.36	.41	.33	.58	.41	.28	.27	.38	.1152	6	.29	.12	.15	.22	.28	.19	.0718	4
TOTAL	99.26	98.73	98.67	98.44	99.55	99.86	100.43	99.94	99.81	98.79	99.97	-		98.22	99.73	99.10	99.27	99.98	99.54	-	
cations (sum = 24.000)																					
Ti	1.5312	1.2709	1.7191	2.4850	1.6385	1.6838	3.6226	2.0240	1.5560	1.6180	1.6932	-		1.9151	1.2466	1.2264	1.2624	1.3740	1.2779	-	
Fe^{2+}	1.5312	1.2709	1.7191	2.4850	1.6385	1.6838	3.6226	2.0240	1.5560	1.6180	1.6932	-		1.9151	1.2466	1.2264	1.2624	1.3740	1.2779	-	
Cr	.6682	.7188	.6706	.9064	1.1056	1.1574	.9587	1.1378	1.4065	1.2555	1.1670	-		.7558	.6684	.6530	.6684	.8743	.7174	-	
Al	.8142	.5918	.9136	1.4791	1.1100	1.2600	1.6502	1.3962	1.3302	1.3786	1.4704	-		1.2664	.4481	.4608	.4425	.4214	.4415	-	
Fe^{3+}	11.4553	12.1478	10.9776	8.6445	10.5075	10.2150	6.1387	9.4182	10.1513	10.1300	9.9763	-		10.1475	12.3904	12.4435	12.3643	11.9563	12.2854	-	
Fe^{2+}	7.7095	7.7390	7.6917	7.7135	7.8160	7.7253	7.5994	7.5439	7.6308	7.6295	7.6609	-		7.7264	7.8331	7.7970	7.7430	7.7520	7.7831	-	
Mg	.2212	.1962	.2310	.1973	.0787	.1917	.2570	.3521	.2987	.3028	.2435	-		.1990	.1360	.1641	.2001	.1761	.1679	-	
Mn	.0693	.0648	.0772	.0892	.1053	.0830	.1436	.1040	.0705	.0678	.0956	-		.0746	.0309	.0389	.0569	.0719	.0490	-	
R1	.598	.611	.588	.528	.573	.569	.447	.555	.571	.570	.566	-		.568	.613	.615	.615	.607	.612	-	
R2	.554	.574	.538	.459	.526	.521	.354	.496	.525	.523	.516	-		.513	.577	.580	.579	.567	.576	-	
R3	.885	.903	.874	.784	.826	.809	.701	.788	.788	.794	.791	-		.834	.917	.919	.918	.902	.914	-	
R4	.028	.025	.029	.025	.010	.024	.033	.045	.038	.038	.031	-		.025	.017	.021	.025	.022	.021	-	
R5	.023	.021	.024	.019	.008	.020	.022	.035	.031	.032	.025	-		.020	.015	.018	.022	.019	.018	-	

	27-F2	27-F2	27-F2	27-F1	27-F1	AO-5	AO-5	AG-13A	AG-13A	AG-13A	AG-13A	AG-13A	AG-13A	AE-20	AE-20	AE-20	AE-20	AE-25
wt.%																		
TiO_2	9.94	9.03	9.06	8.92	7.70	12.37	7.97	10.91	11.87	10.45	9.56	10.30	9.23	11.12	12.18	12.06	8.83	7.76
Cr_2O_3	4.95	5.01	5.37	3.93	3.95	4.26	4.27	10.50	9.93	9.75	9.72	10.43	8.64	4.01	3.24	3.14	3.07	3.22
Al_2O_3	3.64	3.73	4.02	3.20	2.82	6.32	4.70	4.72	4.93	5.00	4.27	5.12	4.70	10.97	4.16	4.25	3.00	3.81
Fe_2O_3	38.77	40.28	39.32	42.05	45.38	31.79	40.37	31.63	29.42	32.97	35.13	32.65	36.39	32.23	37.07	37.52	44.59	46.40
FeO	38.95	38.00	37.77	37.87	35.70	40.31	37.51	39.28	40.80	40.26	38.88	39.81	38.53	40.77	42.12	41.75	38.58	38.14
MgO	.51	.60	.71	.50	.58	1.34	n.d.	1.38	.89	.61	.72	.84	.78	1.89	.32	.51	.37	.36
MnO	.36	.29	.32	.31	.25	.31	.31	.40	.36	.41	.43	.44	.44	.34	.35	.38	.27	.25
TOTAL	97.12	96.93	96.56	96.77	95.74	96.70	95.31	98.81	98.20	99.45	98.70	99.59	98.71	101.53	99.44	99.60	98.70	99.94
cations (sum = 24.000)																		
Ti	2.2856	2.0795	2.0884	2.0667	1.6607	2.7902	1.8700	2.4276	2.6619	2.3229	2.1490	2.2806	2.0706	2.3737	2.7302	2.6942	2.0123	1.7412
Fe^{2+}	2.2856	2.0795	2.0884	2.0667	1.6607	2.7902	1.8700	2.4276	2.6619	2.3229	2.1490	2.2806	2.0706	2.3737	2.7302	2.6942	2.0123	1.7412
Cr	1.1964	1.2128	1.3012	.9571	.9753	1.0102	1.0533	2.4559	2.3408	2.2782	2.2967	2.4276	2.0374	.8839	.7634	.7374	.7354	.7594
Al	1.3118	1.3463	1.4523	1.1620	1.0381	2.2338	1.7280	1.6460	1.7327	1.7419	1.5043	1.7768	1.6525	3.6052	1.4614	1.4881	1.0715	1.3391
Fe^{3+}	8.9201	9.2819	9.0597	9.7476	10.6653	7.1754	9.4785	7.0428	6.6027	7.3342	7.9010	7.2343	8.1690	6.7635	8.3148	8.3861	10.1685	10.4191
Fe^{2+}	7.6744	7.6510	7.5926	7.6895	7.6639	7.3221	7.9181	7.2913	7.5136	7.6287	7.5704	7.5217	7.5421	7.1344	7.7695	7.6786	7.7636	7.7768
Mg	.2324	.2738	.3243	.2296	.2700	.5991	-	.6085	.3955	.2687	.3207	.3686	.3467	.7854	.1421	.2258	.1671	.1606
Mn	.0932	.0750	.0831	.0809	.0661	.0787	.0819	.1002	.0909	.1026	.1089	.1097	.1111	.0803	.0884	.0956	.0693	.0526
R1	.538	.548	.544	.559	.582	.494	.544	.491	.468	.490	.511	.490	.520	.487	.517	.522	.567	.573
R2	.472	.488	.484	.500	.534	.415	.491	.420	.394	.424	.448	.425	.459	.416	.442	.447	.510	.523
R3	.781	.784	.767	.821	.841	.688	.773	.632	.618	.646	.675	.632	.689	.601	.789	.790	.849	.832
R4	.029	.034	.041	.029	.034	.075	-	.077	.050	.034	.041	.047	.044	.099	.018	.029	.021	.020
R5	.023	.027	.032	.023	.028	.055	-	.059	.037	.026	.032	.036	.035	.076	.013	.021	.017	.017

RATIOS : R1 =(Fe^{3+} / Fe^{3+} + octahedral Fe^{2+}) ; R2 =(Fe^{3+} / Fe^{3+} + total Fe^{2+}); R3 =(Fe^{3+} / Fe^{3+} + Al + Cr);

R4 =(Mg / Mg + octahedral Fe^{2+}); R5 =(Mg / Mg + total Fe^{2+}).

TABLE 10-6 ELECTRON MICROPROBE ANALYSES OF DISSEMINATED Ti-MAGNETITES FROM IRON-RICH ULTRAMAFIC PEGMATITE

	ML27-5	ML27-5	ML27-5	ML27-5	ML27-5	ML27-5	ML27-5	ML27-5	ML27-5				GM-4	GM-4	ML22-2A	ML22-2A	ML22-2A	ML22-11	ML22-11	ML22-11
wt.%									x	d	n									
TiO_2	5.75	4.75	5.60	7.53	8.86	6.64	7.56	7.91	6.83	1.3811	8		8.17	8.09	8.79	5.59	10.08	10.55	5.53	7.12
Al_2O_3	1.76	3.09	1.67	1.91	1.92	1.86	1.49	2.05	1.97	.4849	8		2.44	2.27	3.60	2.63	3.12	3.16	2.31	3.41
FeO	35.66	35.06	35.53	37.14	38.53	36.33	37.12	37.36	36.60	1.1549	8		37.60	5.60	38.53	34.62	39.01	39.73	35.27	36.81
Fe_2O_3	54.43	55.28	54.77	51.95	48.52	52.65	51.07	49.57	52.27	2.4791	8		48.27	80.84	46.09	50.78	44.27	43.91	54.56	50.09
MnO	.17	.17	.17	.26	.26	.28	.23	.25	.22	.0466	8		.32	.23	.27	.22	.29	.29	.15	.26
MgO	.36	.46	.33	.66	.36	.39	.34	.43	.42	.1081	8		.45	.81	.46	.43	.65	.66	.51	.51
Cr_2O_3	.85	.97	.84	.67	.68	.80	.70	.86	.80	.1054	8		1.25	1.17	1.14	1.81	.46	.51	.46	.51
TOTAL	98.97	99.78	98.91	100.12	99.13	98.96	98.51	98.43	99.11	-			98.50	99.01	98.88	96.08	97.88	98.81	98.78	98.71
cations (sum = 3.0000)																				
Ti	.1652	.1344	.1611	.2129	.2532	.1905	.2182	.2275	.1954	-			.2342	.1588	.2492	.1644	.2887	.2992	.1586	.2027
Al	.0793	.1370	.0753	.0847	.0860	.0832	.0674	.0924	.1954	-			.1097	.0699	.1600	.1212	.1401	.1404	.1038	.1522
Fe^{2+}	1.1392	1.1032	1.1368	1.1675	1.2244	1.1593	1.1913	1.1949	1.1645	-			1.1983	.1222	1.2148	1.1320	1.2425	1.2528	1.2476	1.1656
Fe^{3+}	1.5647	1.5653	1.5770	1.4696	1.3873	1.5116	1.4750	1.4266	1.4967	-			1.3844	1.5883	1.3076	1.4941	1.2687	1.2460	1.5655	1.4271
Mn	.0055	.0054	.0055	.0081	.0084	.0090	.0075	.0081	.0071	-			.0103	.0051	.0086	.0073	.0094	.0093	.0048	.0083
Mg	.0205	.0258	.0188	.0372	.0204	.0222	.0194	.0245	.0238	-			.0256	.0315	.0258	.0251	.0369	.0371	.0290	.0288
Cr	.0257	.0289	.0254	.0220	.0204	.0242	.0212	.0260	.0241	-			.0378	.0241	.0340	.0559	.0138	.0152	.0136	.0153
mol.% ulvospinel																				
	22.03	18.47	21.29	29.88	38.40	26.29	30.67	33.63	27.35	-			36.34	14.93	42.57	23.93	49.20	52.09	21.14	30.77

primocrysts or grains that are interstitial to the silicates, as clusters of large polygonal grains (often with diameters in excess of 2 cm) and as composite aggregates associated with spinels. The latter are the most common; these usually occur as elongate forms that are interstitial to silicates, or as large masses (often with dimensions of over 10 cm) that may replace silicates. The granular aggregates typically show polygonal grain boundary relationships. Ilmenite in the pegmatites commonly shows rhombohedral or polysynthetic twinning. This may be either a deformation or annealing feature (figs. 10.6F, 10.7A).

Fe-Ti oxides are usually later than silicates in the pegmatites (see Chapter 8), but the paragenetic relationship between ilmenite and spinel is difficult to assess. The occurrence of small, subhedral primocryst ilmenite grains suggest that at least some of the ilmenite crystallized at the same time as the silicates. Spinel may be moulded around subhedral ilmenite in small aggregates (which have not annealed to polygonal bodies), suggesting that some ilmenite predates the spinel. Cameron and Glover (1973) report similar relationships (see also fig. 10.7C,D).

The granular ilmenite is optically and compositionally homogeneous. The results of electron microprobe analyses are presented in Table 10.4. These include samples from small pegmatite bodies at Amandelbult (samples AD-5, AE-12,25,28; AG-13A) and from the oxide-poor part of the Middellaagte pipe (samples ML22-11; ML24-7A) and the oxide-rich part of the Middellaagte pipe (samples ML27-3A,5; GM-4). Magnesium is a significant component (typically within the range 1 to 2 wt. percent). Compositionally they are comparable to granular ilmenites analysed by Cameron and Glover (1973).

10.3.2 SPINELS

REVIEW

Cameron and Glover (1973) recognized three varieties of disseminated spinel in iron-rich ultramafic pegmatite :

(1) Optically homogeneous Cr-rich Fe-Ti spinel, which occurs as euhedral-subhedral grains in pegmatite and in partially replaced cumulates adjacent to pegmatite bodies. These latter are pseudomorphous after cumulus chromite and represent various stages of partial metasomatism in response to Fe-Ti-rich fluids. They have variable compositions, but are Cr-rich in comparison with other spinels in these rocks. Compared with primary (cumulus) chromite they are enriched in Fe, Ti and V, and depleted in Cr and Mg (i.e. similar compositional trends to those recorded in replaced oxide layers). They are described as titanian aluminian chromites (Cameron & Glover). The composition

of these optically homogeneous, Cr-rich spinels exhibits a progressive increase in Ti and Fe and decrease in Cr, Al and Mg with increasing distance from the contact of a pegmatite body (Cameron & Glover). This, to the present author, represents convincing evidence that these spinels are pseudomorphous after cumulus chromite.

A feature unique to one specimen described by Cameron and Glover is the presence of optically heterogeneous spinels, consisting of 3 separate phases, which include Al-poor and Al-rich varieties. Needles of rutile may be present and these samples all exhibit selvages of amphibole (hornblende). Chromium does not exhibit a sympathetic relationship (as it does in the hybrid oxide layers). Cameron and Glover suggest that the breakdown of Ti-rich chromite into Al-rich and Al-poor spinels is related to the presence of amphibole. These heterogeneous spinels have not been observed at Amandelbult, but a parallel may be drawn with the heterogeneous "complex" spinels found at Driekop (see Chapter 4). Amphibole is often common as a selvage around discrete oxide grains, and replaced layers, but does not appear to influence oxide compositions at Amandelbult.

(2) The second type of spinel reported by Cameron and Glover (1973) occurs as anhedral grains that are intergrowths of magnetite and ulvöspinel (Ti-magnetite). Compositionally they may be compared with cumulus magnetite in the Bushveld Complex, with moderate to high TiO_2 contents and low contents of Al and Mg. The Cr content is, however, rather high. They may contain, other than ulvöspinel exsolution, intergrowths of ilmenite, possibly resulting from oxidation (Cameron & Glover).

(3) The third variety of spinel recognized by Cameron and Glover (1973) is referred to as "complex spinels". The basic spinel "components" are magnetite and ulvöspinel, but intergrowths (possibly exsolution) of hercynite and ilmenite are also common. Cameron and Glover supply detailed descriptions of the intergrowths exhibited by these complex spinels. Their analytical data, however, do not suggest significant differences between these spinels and those in group (2). The presence of hercynite (which may be Mg- and Cr-rich) may suggest that the original spinel was more Al-rich.

DISSEMINATED SPINELS AT AMANDELBULT

In pegmatite studied by the author, disseminated Fe-Ti-Cr spinels may be subdivided into two groups :

(1) Cr-rich Ti-magnetite which contains over 2 wt. percent Cr_2O_3; and

(2) Normal, Cr-poor Ti-magnetite, which contains less than 2 wt. percent Cr_2O_3 and usually less than 1 wt. percent Cr_2O_3.

(1) Cr-RICH Ti-MAGNETITE

This is the characteristic spinel of the oxide assemblage in pegmatite at Amandelbult. It occurs both as discrete grains and as large aggregates. The former are usually small (diameters of less than 2 mm are typical) and form extremely anhedral, often sinuous grains, that are interstitial to, and partially enclose early-formed olivine and clinopyroxene. Large, poikilitic aggregates of spinel and ilmenite (often with minor sulphide) also enclose, and replace, early formed silicates (see Chapter 8). Large, composite oxide aggregates, with dimensions in excess of 15 cm are common. The larger aggregates consist of polygonal, well annealed grains and are texturally similar to the hybrid oxide layers (fig. 7.6).

Microstructures exhibited by disseminated and layered Fe-Ti-Cr spinels are similiar. They are most readily observed in coarse-grained polygonal aggregates, where individual grains are commonly 1-2 mm in diameter. The most common intergrowths are as follows : trellis-like exsolution lamellae of ilmenite (fig. 10.7A) and coarse, bladed lamellae of ilmenite (which themselves are usually associated with granules of ilmenite along grain boundaries; fig. 10.7D). A very fine-grained set of trellis-like ilmenite lamellae may also occur. Ulvöspinel lamellae may occur between the trellis-like ilmenite lamellae, but this is at the limit of optical resolution. Relatively coarse-grained lamellae of pleonaste occur parallel to (100) in some grains. These may be replaced by diaspore (Reynolds, pers. comm; fig. 10.7E). Exsolved bodies of a transparent spinel (pleonaste ?) are commonly observed as quite large granules and vermicular bodies along the margins of grains or along the boundaries with coarse bladed ilmenite lamellae (fig. 10.8). These often form complex intergrowths with ilmenite. Many of these textures are described by Reynolds (1982) for typical magmatic Ti-magnetite, but the pleonaste-ilmenite intergrowths are evidently unusually well developed (these are described in the caption to fig. 10.8).

Disseminated Cr-rich Ti-magnetite grains from the following samples were analysed on the electron microprobe (Table 10.5) : AE-12,20,25,28; AD-5;AG-13A (small pegmatite bodies at Amandelbult) and ML24-7A (from the Middellaagte pipe). Significant compositional differences occur between each sample. For example, the Cr content varies between 2.7 and 10.5 wt. percent Cr_2O_3. The Al and Mg contents are unusually low - compared to the Cr contents, they vary between 1.23 and 6.32 wt. percent Al_2O_3 and between 0.18 and 1.39 wt. percent MgO (excluding one sample). The Ti content varies between 5.33 and 12.37 wt. percent TiO_2 (excluding one sample). Compositional variation is similar to that documented for Fe-Ti-Cr spinels from Cr-rich Fe-Ti oxide pegmatite. Usually Fe^{2+}, Fe^{3+} and Ti behave sympathetically, and

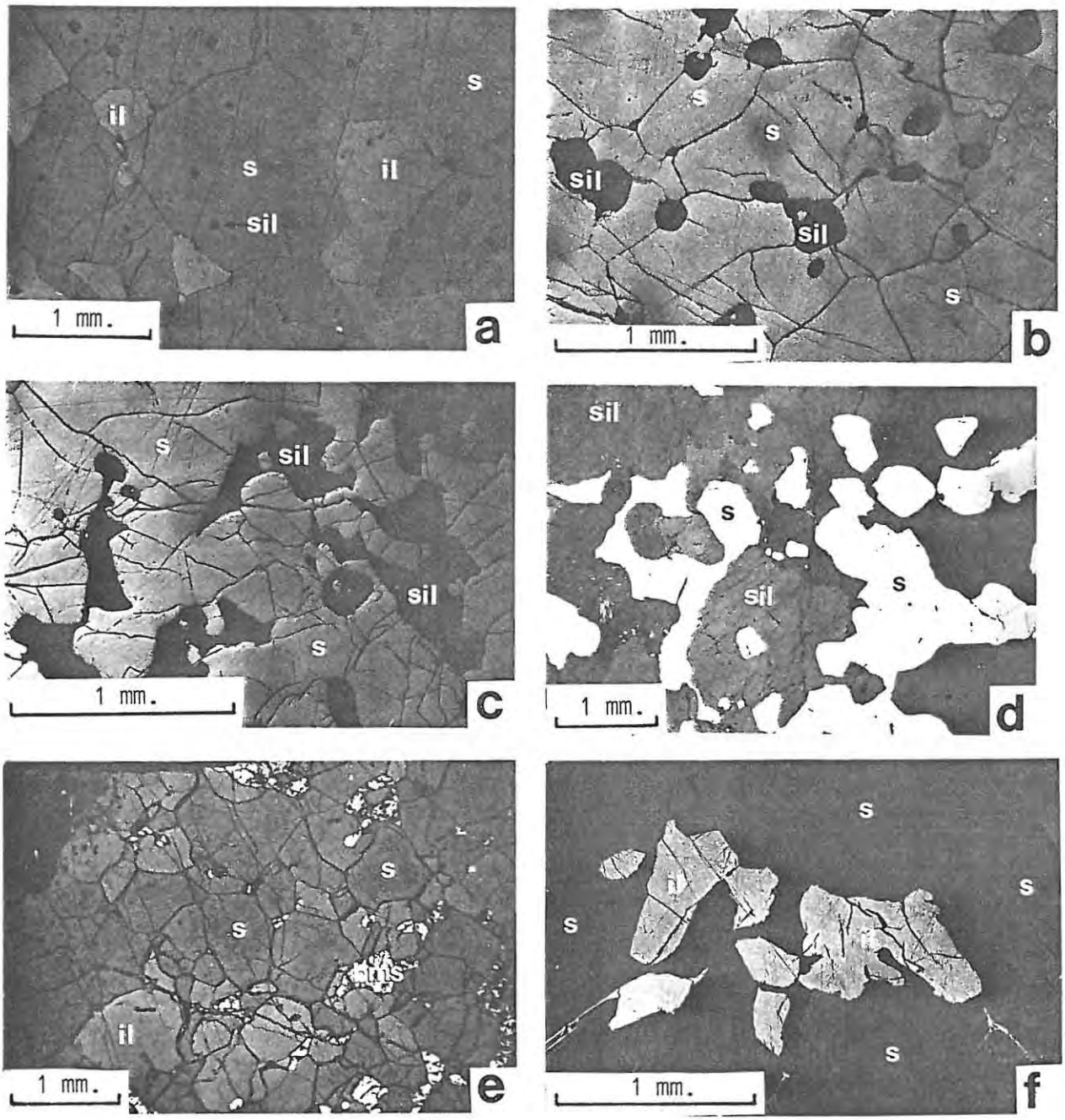

FIGURE 10.6 MICROSTRUCTURES IN Fe-Ti-Cr SPINEL - ILMENITE AGGREGATES

a. Granular aggregate of Fe-Ti-Cr spinel and ilmenite with only scattered inclusions of silicate (sample AS-A1). b. Granular Fe-Ti-Cr spinel with 5-10 modal % silicate inclusions, mostly as tricuspate bodies in interstitial sites (sample AH-21). c. Granular aggregate of Fe-Ti-Cr spinel with 20-30 modal % silicate inclusions, exhibiting a distinctive anhedral form (sample AH-19). d. Disseminated Ti-magnetite exhibiting anhedral form and interstitial to silicate in typical, silicate-rich, pegmatite (sample ML27-3A) . "a" through to "d" illustrate progressive stages in the formation of an annealed, granular aggregate of spinel with a gradual decrease in the proportion of silicate material. e. Granular aggregate of Fe-Ti-Cr spinel, ilmenite and sulphide (sample AH-14). f. Granular, coarse-grained ilmenite (anisotropic) and Fe-Ti-Cr spinel (isotropic), typical of disseminated aggregates in silicate-rich pegmatite. The presence of ilmenite also inhibits annealing and the subsequent development of a foam-like texture (sample AD-4).

(All in plane polarised reflected light with partially crossed polarisers; s - Fe-Ti-Cr spinel; mag - Ti-magnetite; il - ilmenite; sil - silicate; bms - base-metal sulphide)

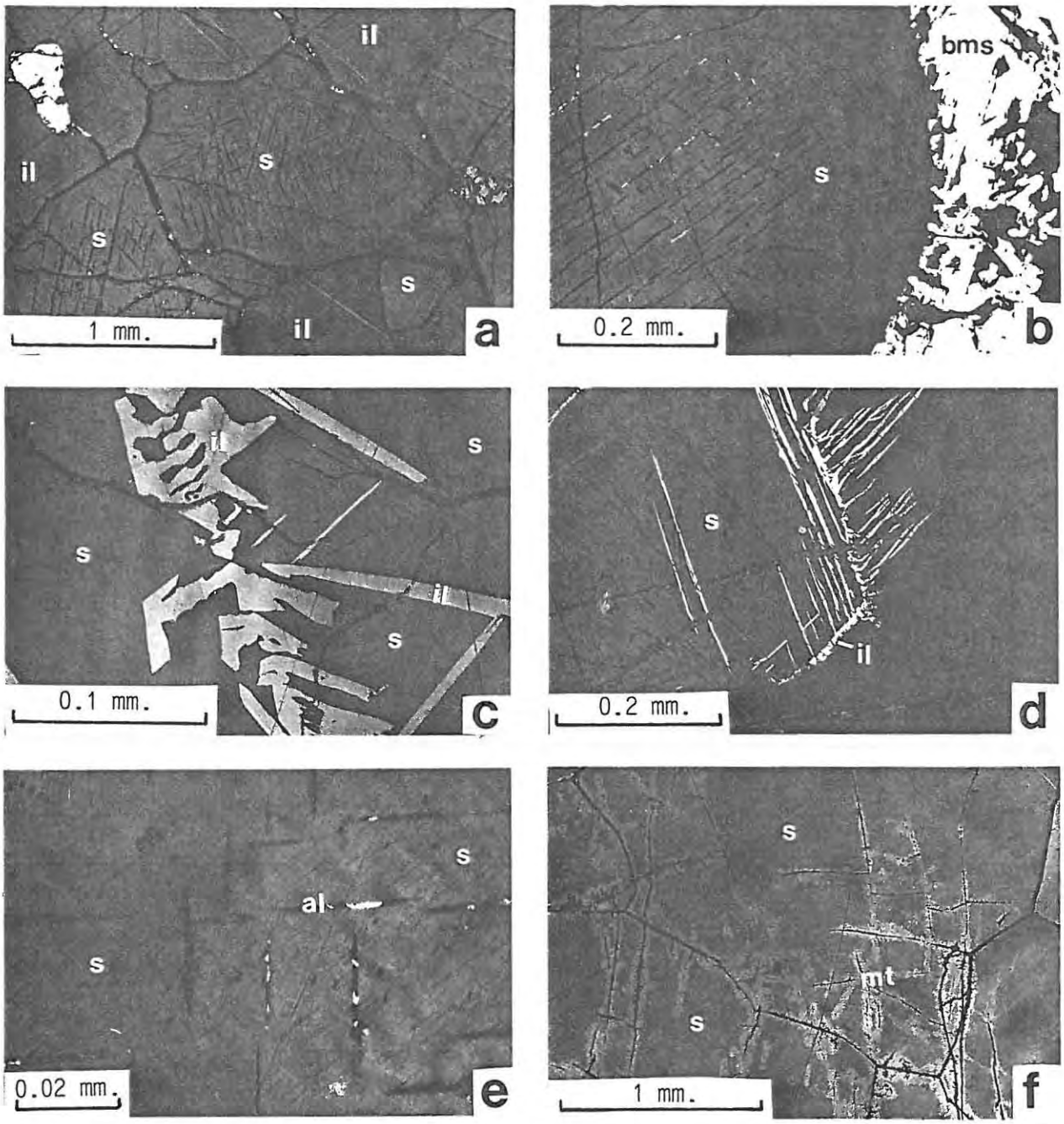

FIGURE 10.7 MICROTEXTURES IN Fe-Ti-Cr RICH SPINEL

a. Granular aggregate of spinel and ilmenite. Spinel exhibits 3 sets of well-formed, coarse, trellis-like ilmenite lamellae parallel to (111). Note also twinning of ilmenite and the well-developed foam-like texture (sample AH-14). b. Depletion zone (paucity of exsolution bodies) at margin of spinel grain, adjacent to a pyrrhotite grain (sample AH-14). c. Anhedral bodies and coarse lamellae of ilmenite in spinel, possibly resulting from replacement of granular ilmenite (sample AW-1). d. Bladed ilmenite lamellae in spinel - these represent an earlier (higher temperature) exsolution event than that resulting in the trellis-like lamellae in "a" (sample 27-C1). e. Two sets of pleonaste lamellae, partially altered to diaspore (which has plucked during polishing), exsolved parallel to (100) in spinel. Third generation ilmenite (?) exsolution lamellae are just visible cutting the pleonaste lamellae at 45^{o} (sample AH-14). f. Feathery intergrowth of martite along grain boundaries of Fe-Ti-Cr oxide, a typical feature of surface samples (sample AZ-1).

(All in reflected light with partially crossed polarisers; s - Fe-Ti-Cr spinel; il - ilmenite; al - Al-spinel (pleonaste); mt - martite; bms - base-metal sulphide)

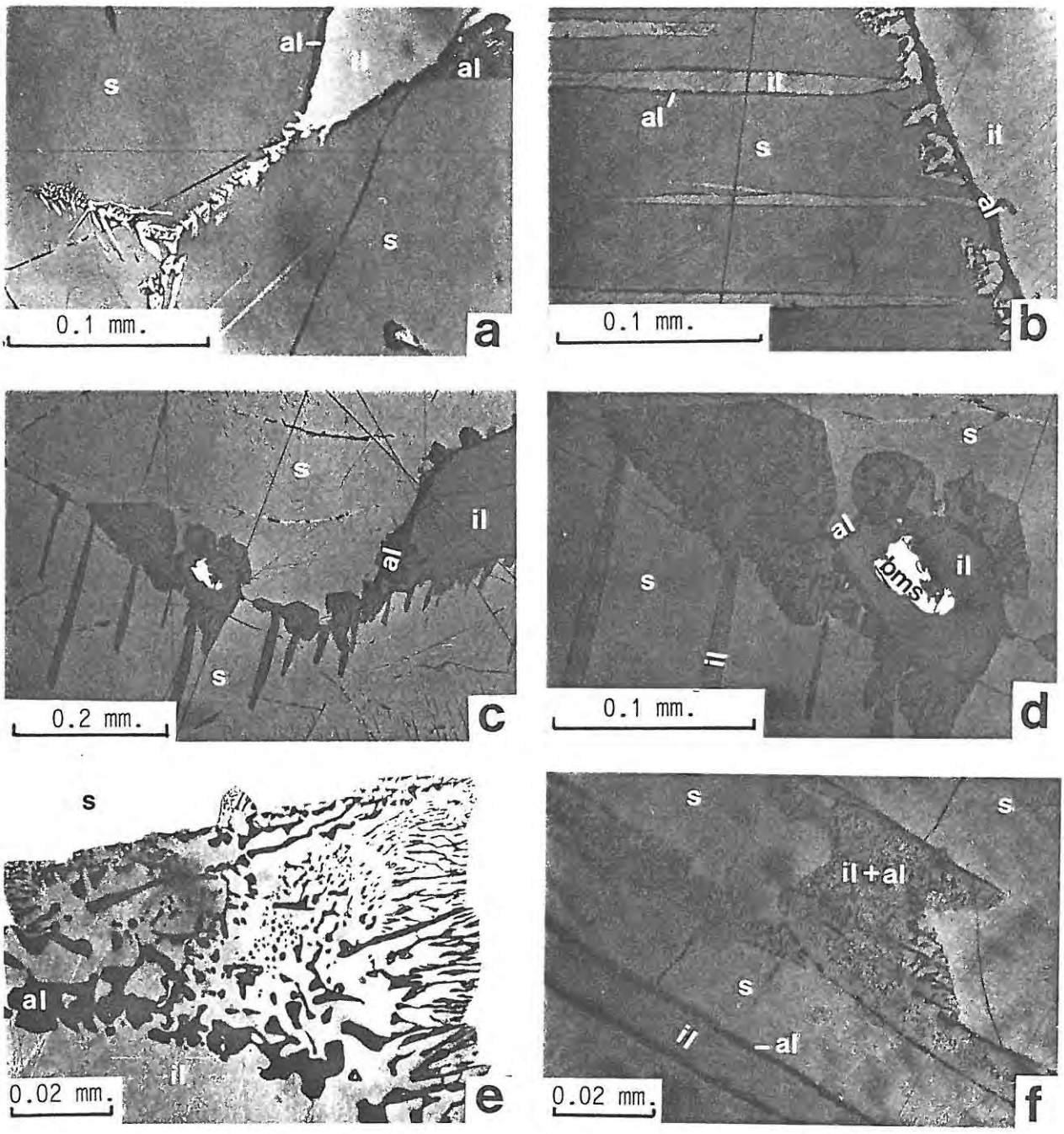

FIGURE 10.8 EXSOLVED INTERGROWTHS OF ILMENITE AND AL-SPINEL IN Fe-Ti-Cr SPINEL

a. Exsolved intergrowths of transparent Al-spinel, possibly pleonaste, and ilmenite along margins of spinel grains; note 120^{o} dihedral angles and granular ilmenite in upper right which has a well developed rim of Al-spinel; ilmenite exsolved from the spinel has migrated into the granular ilmenite. b. Intergrowth of Al-spinel and ilmenite along spinel-ilmenite grain boundary. First generation ilmenite lamellae (coarse blades) have a rim of Al-spinel; ilmenite here has migrated into the lamellae. c,d. Ilmenite exsolved from the spinel has migrated into external granules and coarse lamellae of ilmenite (these have well developed rims of Al-spinel), whereas complex Al-spinel - ilmenite intergrowths occur at spinel-spinel grain boundaries. Note also pure ilmenite and Al-spinel rim around sulphide grain. e. Symplectite-like intergrowth of ilmenite and Al-spinel adjacent to spinel host. f. Al-spinel rim around coarse ilmenite lamellae and intergrowth of Al-spinel and ilmenite in an adjacent lamella - addition of material to this lamella is evident.

(Sample 27-F1; all in reflected light with partially crossed polarisers; s - Fe-Ti-Cr spinel; il - ilmenite; al - Al-spinel (pleonaste); bms - base-metal sulphide)

anti-pathetically to Cr, Al and Mg. The Mn content shows little variation.

Individual grains do not usually show any compositional heterogenerity. Small differences may occur but this is related to exsolution features, not primary zonation. Samples with high Cr (and accordingly higher Al and Mg, and lower Fe^{2+}, Fe^{3+} and Ti) contents are almost always from very small grains. Larger grains show lower Cr contents and the much larger, often massive aggregates of annealed grains are usually Cr-poor; they consist of Ti-magnetite and ilmenite.

(2) NORMAL, Cr-POOR Ti-MAGNETITE

Texturally, normal (Cr-poor) Ti-magnetite is similar to Cr-rich Ti-magnetite, except that the complex pleonaste-ilmenite intergrowths are not usually observed, and pleonaste lamellae (exsolved on (100)) are much finer-grained.

Cr-poor Ti-magnetite usually contains between 0.45 and 1.25 wt. percent Cr_2O_3. Compared with Cr-rich spinels they are poor in Cr, Al and Mg and rich in Fe^{2+} and Fe^{3+} (Table 10.6). The proportion of Ti may not be any higher than in Cr-rich spinels because of the exsolution of large quantities of ilmenite and their association with granular ilmenite.

10.4 NORMAL Fe-Ti OXIDE-PEGMATITE

Normal Fe-Ti oxide pegmatite does not occur in the critical zone and is thus absent from the main field area at Amandelbult (for literature review see Chapter 2). However, Fe-Ti oxide pegmatite occurs as core-like features within small pegmatite bodies from the lower main zone at Amandelbult and has also been sampled from typical, pipe-like bodies in the upper zone of the northern sector of the Bushveld Complex.

In comparison with pegmatite in the upper critical zone at Amandelbult, small pegmatite bodies from the lower main zone (samples ML22-A, B and C; see Appendix 1) are unusually rich in Fe-Ti oxides. This results in the formation of practically monomineralic oxide cores, which are composed of granular ilmenite and Ti-magnetite. They exhibit a similar range of microstructures similar to those found in normal (Cr-poor) Ti-magnetite from pegmatite in the upper critical zone.

Microtextures of Fe-Ti oxides in large, pipe-like bodies of massive Fe-Ti oxide pegmatite have been described by Reynolds and Scoon (1983). They may show considerable differences compared with Fe-Ti oxides in cumulate layers in the Bushveld Complex. The main conclusions reached here are that exsolution and contemporaneous oxidation-exsolution processes have proceeded

to a much greater extent than in cumulus Ti-magnetite grains of the upper zone of the Bushveld Complex. This is reflected by the abundance of granular ilmenite, the paucity and modified nature of larger ilmenite intergrowths in the magnetite, the absence or paucity of fine-grained ilmenite or ulvöspinel intergrowths and the low residual Ti-contents of the magnetite hosts.

Massive Fe-Ti oxide pegmatite from a pipe-like body on the farm Leeukoppie, near Northam, was sampled (samples LEU-3, 4). This pipe-like feature, which has a poorly exposed outer shell of silicate-rich pegmatite, cuts magnetite layer number 6. This layer was sampled roughly 1 km from the pipe (samples LEU-1, 2). The main magnetite layer was also sampled for comparative purposes. (samples MAG-1, 4, Magnet Heights, eastern Bushveld Complex). The results of these analyses are presented in Table 10.1.

Cumulus Fe-Ti oxide layers in the Bushveld Complex show upward fractionation trends (becoming poorer in V and richer in Ti; see Molyneaux, 1970, 1972; Reynolds, in press), such that Fe-Ti oxide pegmatite should be compared with Fe-Ti oxide cumulates at the same height in the cumulate pile. The major element chemistry of the pipe-hosted Fe-Ti oxide from Leeukoppie is almost identical to that from the adjacent cumulate magnetite layer (note, however, the low Cr, Al and Mg contents in comparison to samples of massive Cr-rich Fe-Ti oxide pegmatite from the critical zone). Minor differences may, however, occur in the trace element chemistry, but more data are required before any definitive conclusions can be drawn. The pegmatite, or pipe-hosted, oxide is clearly enriched in V (compared to an Fe-Ti oxide cumulate at the same height) and may be slightly richer in Zr, Y, Cu, Co and Zn, but poorer in Sc and Cr. Note that the Kennedy's Vale body, which occurs relatively low in the main zone is considerably enriched in V, compared to the lowermost cumulate magnetite layers (see p. 21).

10.5 SPINEL CHEMISTRY - DISCUSSION

Considerable variation in the chemistry of spinels from iron-rich ultramafic pegmatite was documented in the preceding sections of this chapter. Chemical variation is apparent in diagrams in which the major cations are plotted against the ratio of cations $Mg/(Mg+Fe^{2+})$ (fig. 10.9A-D).

In these diagrams the following sample populations are recognized : (1) disseminated normal (Cr-poor) Ti-magnetite; (2) disseminated Cr-rich Ti-magnetite (or Fe-Ti-Cr spinel); (3) Cr-rich Fe-Ti oxide layers from surface samples; and (4) Cr-rich Fe-Ti oxide layers from underground samples. All samples plotted in these diagrams are from Amandelbult. In each diagram a "mixing line" can be drawn which relates the two end members, cumulus

chromite and pegmatite, Cr-rich Ti-magnetite. These mixing lines are only linear over that part of the compositional range closest to the Ti-magnetite end-member. Furthermore, it is apparent that the various cations show different trends (as discussed above).

From Figure 10.9A it can be seen that the Al content of these spinels falls within four, poorly defined, fields. The disseminated Ti-magnetite grains are depleted in Al, compared to the Fe-Ti-Cr oxides. Differences between Cr-rich Fe-Ti oxides from surface and underground layers at Amandelbult may be explained by primary differences between cumulus chromite compositions and the nature of the cumulate layers. These well-defined fields are not duplicated by the distribution of Cr (fig. 10.9B). The disseminated Ti-magnetites exhibit a low Cr-content (ranging from 0.1 - 0.5 cations), but show a slight spread in the $Mg/(Mg+Fe^{2+})$ ratio (0.015 - .038). As expected, the disseminated Fe-Ti-Cr spinels show considerable variation in Cr content, as do spinels from the hybrid oxide layers. The distribution of Cr in these spinels is best portrayed in terms of individual oxide layers (see fig. 10.5). From Figure 10.9C it is evident that if Fe^{3+} is plotted against the $Mg/(Mg+Fe^{2+})$ ratio a similar trend, but mirror-image to that for Cr, is obtained.

The distribution of Ti and Fe^{2+} with respect to the $Mg/(Mg+Fe^{2+})$ ratio is illustrated in Figure 10.9D. These two cations show a positive linear relationship. This can be illustrated further by plotting $(Fe^{2+} + Ti)$ against trivalent cations, such as Cr and Al (fig. 10.10). Some analyses of cumulus chromite are also included in this diagram. Cumulus chromite shows a negative relationship between Cr and Al, and both define opposing trends with respect to $(Fe^{2+} + Ti)$. In the case of Al this trend may be extrapolated to connect with that found in Fe-Ti-Cr spinels in the pegmatites. Chromium, however, shows a positive relationship with $(Fe^{2+}+Ti)$ in cumulus chromite, whereas in the pegmatite spinel Cr is depleted at the expense of Fe^{2+} and Ti. This may partly explain differences in the behaviour of Cr and Al during subsolidus re-equilibration.

In summary, the overall effect of interaction between cumulus chromite and the pegmatitic liquids or the pegmatitic oxides is to produce hybrid spinels which are relatively rich in Fe^{2+}, Fe^{3+} and Ti and poor in Cr, Al and Mg, as compared to the original cumulus compositions. Al and Mg show negative linear relationships with Fe^{2+} and Ti, whereas Cr shows a negative linear relationship to Fe^{3+}. Al and Mg are less readily redistributed than Cr.

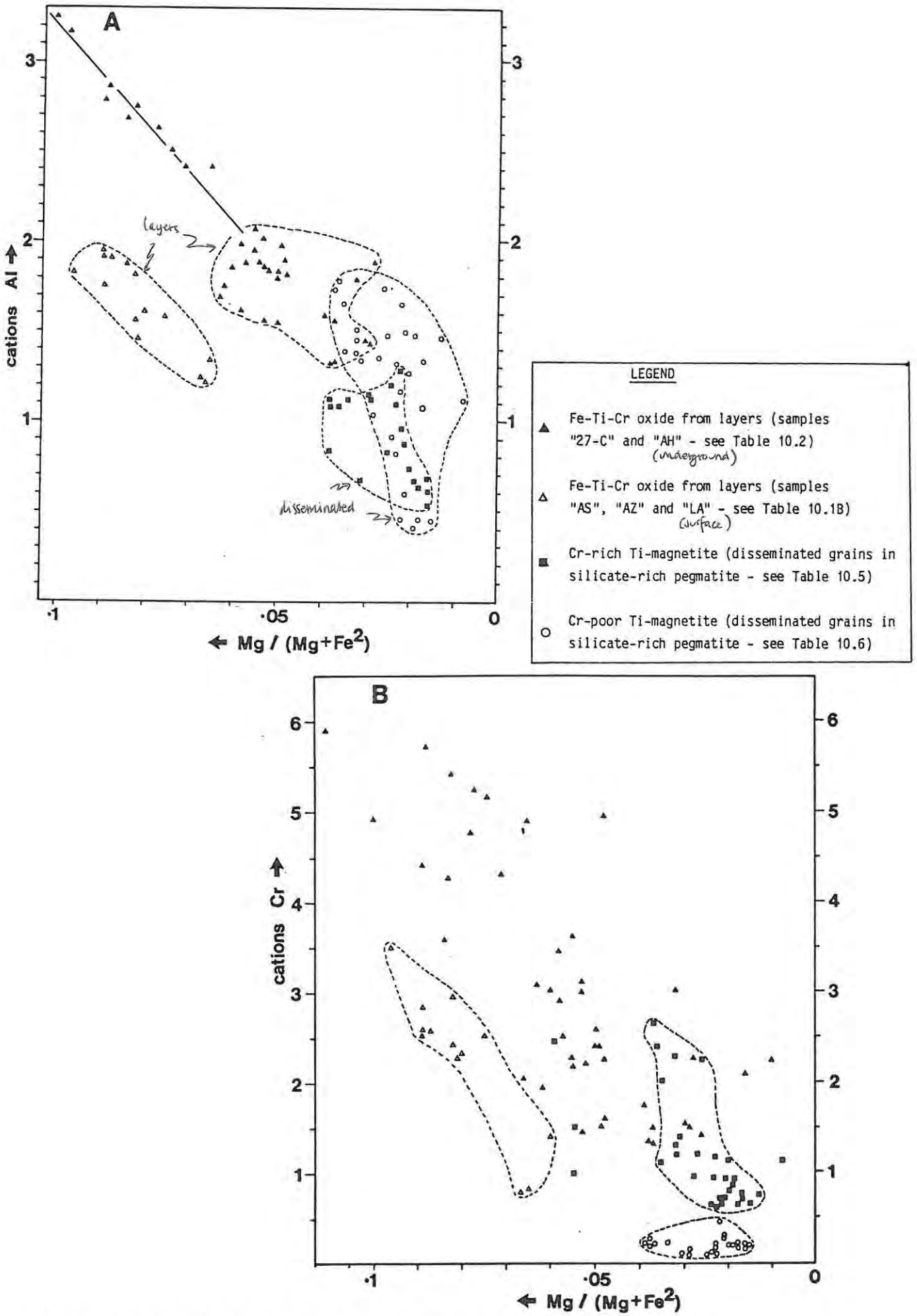

FIGURE 10.9 Plots of cations against the Mg / (Mg + Fe^{2+}) ratio for pegmatitic Fe-Ti-Cr spinels. (A) cations Al vs. Mg / (Mg + Fe^{2+}); (B) cations Cr vs. Mg / (Mg + Fe^{2+})
Based on electron micrprobe analysis of Fe-Ti-Cr spinels presented in Tables 10.1B, 10.2, 10.5 and 10.6.

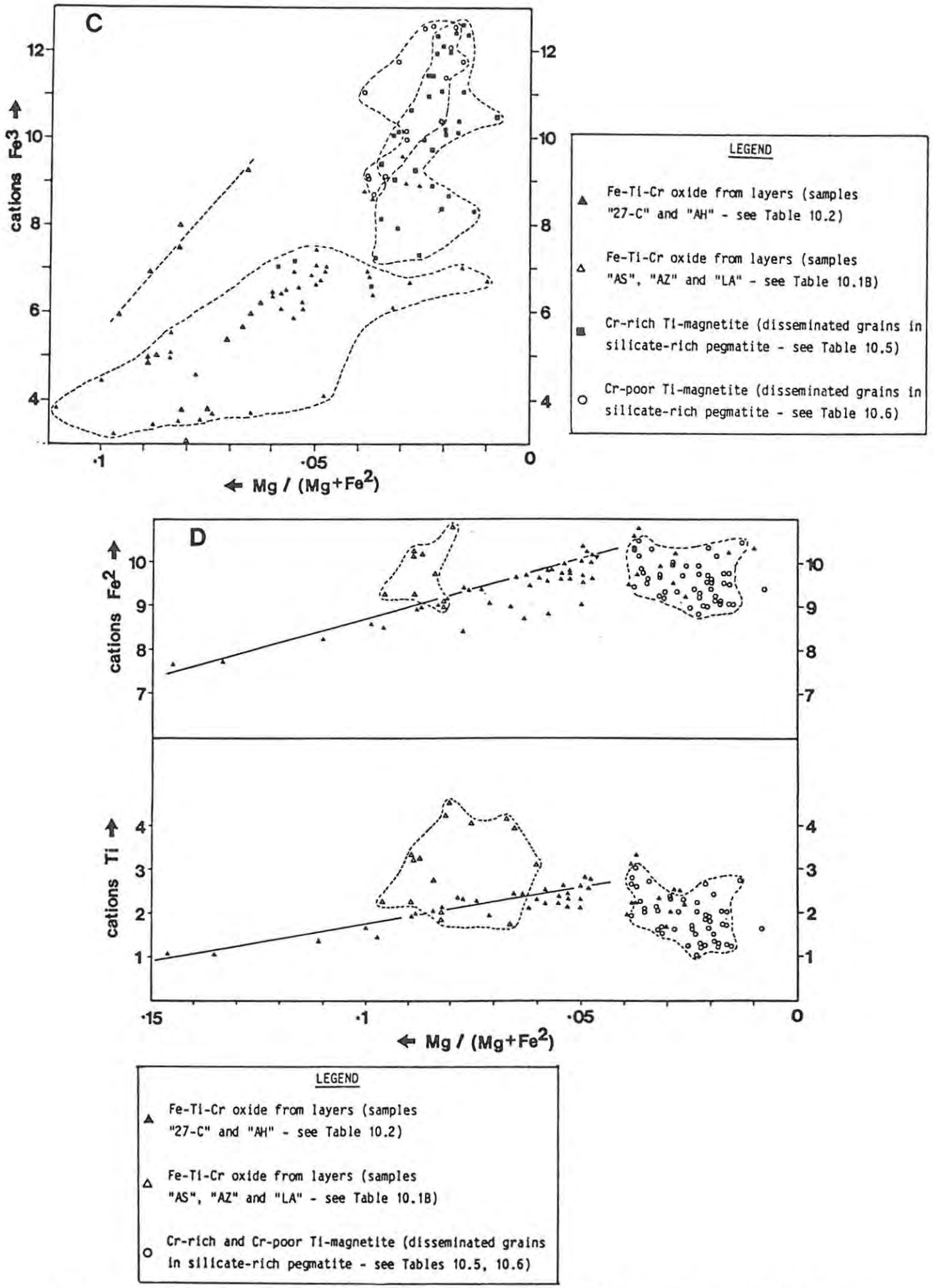

FIGURE 10.9 (continued) Plots of cations against the Mg / (Mg + Fe^{2+}) ratio for pegmatite-hosted Fe-Ti-Cr spinels. (C) cations Fe^{3+} vs. Mg / (Mg + Fe^{2+}); (D) cations Fe^{2+} and Ti vs. Mg / (Mg + Fe^{2+})

Based on electron micrprobe analysis of Fe-Ti-Cr spinels presented in Tables 10.1B, 10.2, 10.5 and 10.6.

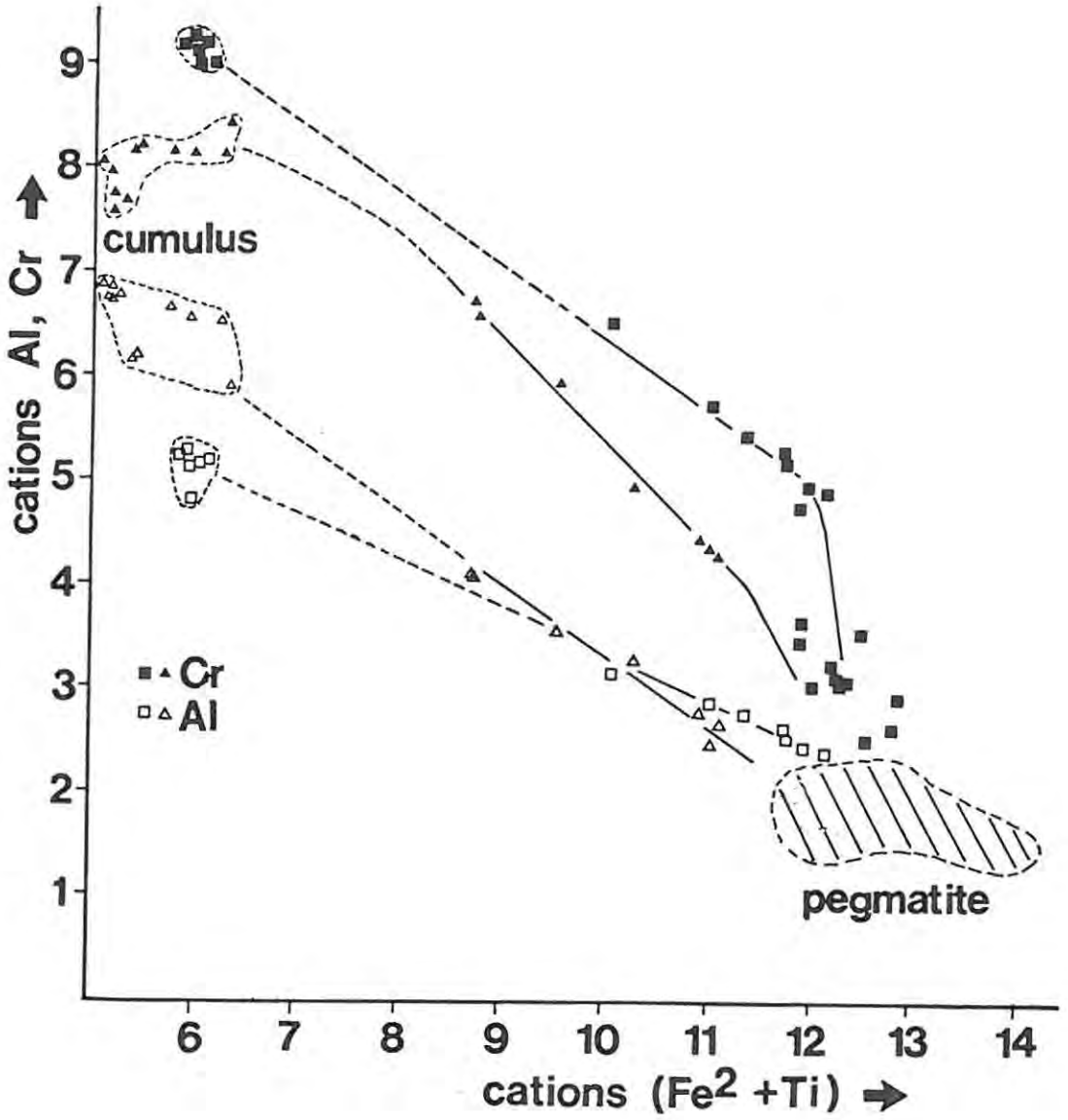

FIGURE 10.10 Plot of cations Al and Cr against cations (Fe^{2+} + Ti).

Based on electron microprobe data for two sample groups : (A) 27-C1, 27-C2, AA-4 (squares) - from the normal and replaced Merensky upper chromitite layer (see fig. 10.3); and (B) the "AH" samples (triangles) - from the normal and replaced chromitite layer above the upper pseudoreef A (see fig. 10.4). Cumulus (primary chromite) and pegmatitic compositions may be recognized for both Al and Cr in each sample group. Mixing lines between these two end-member compositions may be constructed for hybrid samples from partially "replaced" Fe-Ti-Cr oxide layers.

10.6 MICROSTRUCTURES - DISCUSSION

The development of microstructures in magmatic Ti-magnetite has been discussed by numerous workers; in this study the reviews of Haggerty (1976) and Reynolds (1982) have been used extensively. The nature and development of these microstructures may be related to primary features such as temperature of crystallization, fO_2, initial composition, cooling rate and changes in fO_2 during cooling. The nature of adjacent grains may also influence the microstructures, due to subsolidus re-equilibration processes. Initial composition and subsolidus re-equilibration with primary chromite are probably largely responsible for the differences in microstructures that are observed between disseminated Cr-rich and Cr-poor Ti-magnetites in the pegmatites. Cooling rate and changes in fO_2 during cooling are probably responsible for the development of the different microstructures in Ti-magnetites in Fe-Ti oxide pegmatite and those in cumulates in the upper zone of the layered sequence.

Reynolds (1978, 1982) has modelled the development of microstructures in magmatic Ti-magnetites in terms of cooling rate and fO_2. According to this modelling, the presence of coarse ilmenite lamellae and external ilmenite granules is a feature attributable to high fO_2 during subsolidus cooling. The formation of this exsolved ilmenite presumably occurred prior to exsolution of the fine trellis networks of ilmenite. The later may be attributable to moderate fO_2 at a later stage in the cooling history. In spinels studied here ulvöspinel is only observed as very fine-grained intergrowths. Exsolution of these probably occurred at a very late stage in the cooling history. According to Haggerty (1976) this results from intersecting the magnetite-ulvöspinel solvus and probably reflects a drop in fO_2. Buddington and Lindsley (1964) accounted for the coarse ilmenite exsolution by a contemporaneous oxidation-exsolution mechanism, in which ulvöspinel is exsolved and then oxidised to ilmenite and magnetite. The paucity of exsolved ulvöspinel and the abundance of ilmenite in these spinels may suggest that relatively high fO_2 conditions prevailed in their early cooling history. At a later-stage, fO_2 decreased enabling exsolution of ulvöspinel without oxidation to ilmenite to occur.

The crystallization of a magnetite-ulvöspinel solid solution probably occurs at temperatures above 1000°C, but at any rate must occur above 800°C, during typical magmatic conditions. Exsolution-oxidation of ilmenite probably occurs at temperatures of $\pm$ 600°C, whereas exsolution of the typical cloth-like ulvöspinel may occur at temperatures between 450 and 550°C (Reynolds, 1978).

Exsolution of other phases is probably dependent on composition. For example, excess Al in magnetite may be exsolved as pleonaste, usually along the margins of ilmenite grains or lamellae or as tiny lamellae orientated parallel to (100) (Haggerty, 1976; Reynolds, 1978). In Cr-poor Ti-magnetite in pegmatite at Amandelbult, disc-shaped lamellae of pleonaste are often present parallel to (100). These lamellae are relatively fine-grained and probably exsolved after the coarse-grained ilmenite lamellae and granules, but before the ulvöspinel. Similar features are exhibited by cumulus magnetite in the layered sequence (Reynolds, pers. comm.).

The complex pleonaste-ilmenite intergrowths found in Fe-Ti-Cr spinels in pegmatite at Amandelbult probably developed as a result of the Al-rich nature of these spinels. During exsolution of ilmenite an Al-rich spinel may be exsolved contemporaneously. This results in the formation of bodies of pleonaste and ilmenite at the margins of spinel and ilmenite grains and at the margins of ilmenite lamellae. Arrested stages in this process are represented by vermicular or emulsoid intergrowths of ilmenite and pleonaste. When this process goes to completion a rim of pleonaste (ilmenite-free) is found around granular or lamellar ilmenite; the ilmenite exsolved contemporaneously with the pleonaste has been incorporated into the primary, or early-exsolved ilmenite. The temperature range at which this process occurs is probably between that at which exsolution-oxidation of coarse-grained ilmenite and exsolution of ulvöspinel occurs. In the Fe-Ti-Cr oxides pleonaste is also observed as lamellae parallel to (100). They are distinctly coarser-grained than those in Ti-magnetite, a feature which may also be attributable to composition, rather than cooling rate.

10.7 CRYSTALLIZATION TEMPERATURES

Buddington and Lindsley (1964) investigated experimentally the system FeO-Fe_2O_3-TiO_2 and concluded that the composition of co-existing pairs of ilmenite and Ti-magnetite are determined by temperature and fO_2 at the time of crystallization. Spencer and Lindsley (1981) have produced a revised ilmenite - Ti-magnetite geothermometer which relates the composition of these co-existing phases to both temperature and fO_2. Two main problems are encountered in applying this calculation. Firstly it only produces minimum (blocking) temperatures in slowly-cooled samples and does not give any indication of liquidus temperatures and, secondly, the primary composition of Ti-magnetite cannot be obtained accurately using the electron microprobe due to exsolution features.

This calculation has been applied to a number of ilmenite-Ti-magnetite

pairs in which the latter is the Cr-poor variety (i.e. analyses in Table 10.6; for ilmenite analyses see Table 10.4). These give temperatures and fO_2 pairs in the range 700-550°C at Log_{10} 10^{-21} - 10^{-23}. These values lie very close to the QFM (quartz-fayalite-magnetite) buffer, as might be expected for magmatic oxide minerals. It must be stressed that these are minimum re-equilibration temperatures and are not representative of liquidus conditions.

10.8 SUMMARY

Cr-rich Ti-magnetite appears to be restricted to pegmatite in the critical zone, where cumulus chromite may be an important constituent of the pre-existing cumulates (note that the pegmatite bodies examined by Cameron and Glover occur adjacent to the MG-chromitite layers where disseminated chromite is a major accessory constituent). These spatial relationships may suggest that this spinel in the pegmatite results from replacement of the pre-existing chromite. A parallel with the hybrid oxide layers is applicable. However, whole-rock data does not support this conclusion as often pegmatite contains higher Cr_2O_3 than the felsic cumulates they are purported to replace (see Chapter 12). It must therefore be concluded that Cr is an intimate component of the pegmatite liquids. Moreover, the Cr content of the majority (if not all) of the pegmatitic spinels is related to that of the putative liquid. From the data and arguments presented in this chapter the following conclusions may be drawn :

(1) Some of the Fe-Ti-Cr oxides in iron-rich ultramafic pegmatite have originated by crystallization from pegmatitic liquids, such that an entirely metasomatic origin for these rocks is untenable.
(2) Cumulus chromite from replaced layered cumulates may be incorporated into pegmatite as xenocrysts, but there is no direct evidence for this.
(3) Fe-Ti-(Cr) oxides preferentially nucleated on, and around, cumulate chromitite layers.
(4) Subsolidus re-equilibration between cumulus chromite and pegmatitic Fe-Ti-(Cr) oxide overgrowths resulted in the formation of hybrid Fe-Ti-Cr oxide pegmatite. This process would only operate in the critical zone, where cumulus chromite is found.
(5) Granular ilmenite and Cr-poor Ti-magnetite in pegmatite bodies in the main zone, which are texturally and compositionally comparable with cumulus oxides in the layered sequence implies that the pegmatitic liquids were at magmatic temperatures, probably comparable to temperatures found in the cumulate pile during crystallization of

cumulus Ti-magnetite layers of the upper zone.

(6) Microstructures in the spinels indicate that they cooled slowly, under "pegmatitic" conditions, with associated changes of fO_2.

(7) Disseminated spinel in pegmatites in the upper critical zone is a Cr-rich Ti-magnetite; with progressive decrease in the Cr content this is replaced by normal (Cr-poor) Ti-magnetite in pegmatites in the main zone.

(8) In pegmatites in the upper critical zone Fe-Ti-oxides rarely represent more than 25 modal percent and ilmenite may be more abundant than disseminated Ti-magnetite. In the main zone, however, cores of Fe-Ti-oxide pegmatite and pipe-like bodies of massive Fe-Ti oxide pegmatite are common. An upward increase in the Fe-Ti oxide content of the pegmatites is inferred.

CHAPTER 11 BASE-METAL SULPHIDE AND PLATINUM-GROUP ELEMENT MINERALOGY

Notable concentrations of PGE in the Bushveld Complex are found in layered cumulates (e.g., the Merensky, UG-2 and Plat Reefs) and to a lesser extent in transgressive ultramafic bodies (e.g., the platiniferous ultramafic pipes). Because economic concentrations of PGE are usually associated with disseminated base-metal sulphides, there is significant production of Ni and Cu as by-products of platinum mining. Although the relationship between concentrations of PGE and base-metal sulphides may be over-stressed (see Chapter 6), it is useful to discuss the mineralogy of these phases together. All electron microprobe analyses of base-metal sulphides and PGM in this study have been performed at J.C.I. laboratories (see Appendix 12).

11.1 INTRODUCTION

Magmatic sulphide ores usually have a simple mineralogy and composition (Naldrett, 1981). Pyrrhotite, pentlandite, chalcopyrite and lesser amounts of pyrite are the main sulphide minerals with Fe, Ni, Cu, S, and very small amounts of PGE and Au being the most important constituents. Magnetite occurs in variable amounts and its presence is attributed to either the original oxygen content of the immiscible sulphide liquid or to oxidation of the ore after crystallization (Naldrett, 1981). The partitioning of Ni, Cu, Co, Fe and Zn between an immiscible sulphide liquid and the host silicate melt in the system FeS-FeO-SiO_2 at 1150^{o}C has been investigated by Maclean and Shimazaki (1976). Their results showed the following preference for the sulphide liquid : Ni > Cu > Co > Fe > Zn. In magmatic platinum ores PGE are often associated with unusual concentrations of base-metal sulphides (inter alia Naldrett & Cabri,1976; Crocket et al., 1976; Crocket, 1979; Cabri, 1981; Campbell et al., 1983). PGE also show an affinity for concentrations of chromite in peridotite-hosted ores (Wagner, 1929; Razin, 1976) and for chromitite cumulates in layered complexes (inter alia Wagner, 1929; Kinloch, 1982; see also Chapter 6).

The stratigraphic distribution of base-metal sulphide mineralization in the layered sequence of the Bushveld Complex may be governed by the relative chalcophile nature of base-metals, as determined by Maclean and Shimazaki (1976). Thus, Ni sulphides are essentially restricted to the lower and critical zones, Cu sulphides to the critical, main and lower upper zones and Co - Fe sulphides occur towards the roof of the layered sequence (see detailed review by Von Gruenewaldt, 1979). Sulphide mineralization in the

layered cumulates of the Bushveld Complex is restricted to minor disseminations; concentrations of Ni or Cu sulphides to warrant exploitation without the presence of PGE are not known. The abnormally high ratio of PGE to (Ni+Cu+Fe+S) of platinum ores in the Bushveld Complex is a characteristic feature, which cannot be accounted for by present theories of magmatic sulphide liquids (Naldrett et al., 1979; Campbell et al., 1983; Lee, 1983; see also Chapter 6).

The mineralogy of cumulate-hosted base-metal sulphides in the Bushveld Complex has been studied by Schneiderhöhn (in Wagner, 1929), Cousins (1964, 1969), Liebenberg (1970), Vermaak and Hendriks (1976), Brynard et al. (1976) and Von Gruenewaldt (1973, 1979). The mineralogy of PGE in these rocks has been studied by a number of authors, including Kingston (1966), Cousins (op. cit.), Vermaak and Hendriks (op. cit.), Brynard et al. (op. cit.), Cabri (1981) and Kinloch (1982).

11.2 SULPHIDES AND PGE IN TRANSGRESSIVE ULTRAMAFIC BODIES

Many of the different types of discordant bodies of ultramafic rock that transgress the layered sequence of the Bushveld Complex contain subeconomic concentrations of base-metal sulphides and PGE (see Wagner, 1929). These include the platiniferous ultramafic pipes, the Vlakfontein nickel bodies and the main class of iron-rich ultramafic pegmatite. The sulphide mineralogy of many of these discordant bodies, including the iron-rich ultramafic pegmatite suite, have been studied in detail by Liebenberg (1970). This, and other studies will be referred to where relevant in the ensuing discussion.

11.2.1 IRON-RICH ULTRAMAFIC PEGMATITE - SMALL BODIES AT AMANDELBULT

DISTRIBUTION

Base-metal sulphides typically represent between 1 and 2 modal percent (although locally this may increase to over 10 modal percent) of iron-rich ultramafic pegmatite assemblages at Amandelbult. Sulphides occur as fine disseminations, coarse blebs (with diameters of 0.5 - 5 mm) and massive segregations (with dimensions of over 30 cm). These consist of both discrete and composite grains that usually occur interstitially to, and moulded around, early-formed silicates. They are often attached to Fe-Ti-(Cr) oxide grains (this is a common feature of mafic sulphide ores and may possibly be explained by the positive relationship between the solubility of S in a mafic magma and the Fe^{2+} content, as determined by Haughton et al., 1974). Emulsoid intergrowths of Ti-magnetite and chalcopyrite are also commonly observed in

pegmatite samples at Amandelbult (fig. 11.1D; Naldrett, 1969, reports that in an O-rich system the pyrrhotite-magnetite cotectic results in co-precipitation of magnetite and monosulphide solid solution.

BASE-METAL SULPHIDE MINERALOGY

The dominant phase is pyrrhotite, which typically constitutes over 95 modal percent of the sulphide assemblage. Other major phases, which thus usually constitute less than 5 modal percent are cubanite, pentlandite and chalcopyrite. Cubanite is slightly more abundant than pentlandite, but the relative abundance of chalcopyrite is difficult to assess. This is because cubanite and pentlandite are almost invariably associated with pyrrhotite in the form of composite grains. A rough modal estimate suggests that composite sulphide grains in these rocks consist of 95 modal percent pyrrhotite, 3 modal percent cubanite and 2 modal percent pentlandite. Pyrrhotite in these grains is always an intergrowth of troilite and hexagonal pyrrhotite (fig. 11.1A). Pentlandite may occur in well formed, often cubic grains (fig. 11.1B; a characteristic feature which is not duplicated by the cumulate-hosted sulphides), but cubanite typically forms very irregular grains. These two phases usually occur in composite intergrowths within the host pyrrhotite (fig. 11.1A). Mackinawite is commonly observed in these composite sulphides, usually as tiny, vermicular bodies in cubanite or pentlandite (fig. 11.1B). Other minor phases include sphalerite, pyrite and very rare PGM. The latter are usually observed only in composite sulphide - Fe-Ti oxide grains or in Cr-rich Fe-Ti- oxide pegmatite (fig. 11.2).

In contrast, chalcopyrite usually occurs in discrete grains, and is only occasionally observed in composite intergrowths. Locally, chalcopyrite may be quite common. although it is usually found only in small grains (typically less than 1 mm in diameter). The proportion of chalcopyrite may increase in proximity to coarse segregations of composite sulphide grains.

Microstructures and microtextures of these sulphides are comparable to those described from other occurrences of iron-rich ultramafic pegmatite by Liebenberg (1970). The presence of only 4 main phases - pyrrhotite, cubanite, chalcopyrite and pentlandite is characteristic.

The composite sulphide grains probably resulted from the breakdown, during cooling, of a monosulphide solid solution (Mss) that crystallized at magmatic temperatures, as described by Kullerud et al. (1969) and Craig and Kullerud (1969). Discrete grains of chalcopyrite may represent material which has been leached from the cumulates or it may have resulted from the segregation of a Cu-rich solid solution early in the crystallization history of the Mss (see Yund & Kullerud, 1966).

The exceptionally high FeS/NiS ratio (the pyrrhotite : pentlandite ratio is probably over 50), the high FeS/CuS ratio, and the predominance of cubanite over both pentlandite and chalcopyrite are the most significant features. This is probably typical of magmatic sulphides derived from an highly fractionated, iron-rich silicate liquid.

11.2.2 REPLACED MERENSKY REEF AT AMANDELBULT

DISTRIBUTION

Small, transgressive bodies of iron-rich ultramafic pegmatite which cut or replace part of the Merensky cyclic unit have long been known. Wagner (1929) described several hortonolite dunite-wehrlite bodies form Doornspruit and Kookfontein in the Rustenburg area (fig. 2.7). The pegmatite at these occurrences is enriched in PGE, whereas at other localities it contains only trace amounts of PGE. Furthermore, the adjacent unreplaced or partially replaced Merensky Reef is depleted of PGE. Wagner concluded that the PGE content of the combined pegmatite body and partially replaced Merensky Reef at Kookfontein was equivalent to that of the normal unreplaced Merensky Reef. Wagner attributed these localised concentrations of PGE in pegmatite to leaching of pre-existing, platiniferous cumulates. Transgressive bodies of iron-rich ultramafic pegmatite which replace the Merensky Reef (the replaced Reef) are particularly abundant at Amandelbult (cf. pp. 121-122).

PGE MINERALOGY

The PGE mineralogy of normal Merensky Reef at R.P.M. Amandelbult has been investigated by Kinloch (1982). In samples from the western section of the mine Kinloch reports the following PGM (in modal percent) : Pt-Fe alloys (31.3), Pt-Pd tellurides (19.6), Pt-Pd sulphides (19), laurite (17.5), sperrylite (9.2) and Pd alloys (3.2). Pt-Fe alloy usually occurs as intergrowths with other phases and only a small proportion is found as Pt_3Fe crystals. It is important to realise that the PGE mineralogy of the Merensky Reef is not consistent throughout the Bushveld Complex (Kinloch, 1982); the proportions above are thus peculiar to the western section of Amandelbult.

In replaced Reef at Amandelbult the dominant PGM (in modal percent) are Pt-Fe alloy (82) and laurite (17), with less than 1 modal percent platinoid bismuthotellurides (Peyerl, 1978). Kinloch (1982) considers Pt-Fe alloys and laurite, as well as Pd alloys (all of which occur in the platiniferous ultramafic pipes) to be indicative of formation during volatile-enriched conditions with high fO_2 and low fS_2.

BASE-METAL SULPHIDE MINERALOGY

Base-metal sulphides in normal Merensky Reef at Amandelbult are typical of the Merensky Reef in the western Bushveld Complex (see pp. 98-99). In partially replaced Reef (see pp. 142-143) the total sulphide content is much higher than usual, as both pegmatite-related sulphides and relict cumulate-derived sulphides can be recognised. Composite grains of pegmatite-related sulphide consist essentially of pyrrhotite (an intergrowth of troilite and hexagonal pyrrhotite), with only minor cubanite, pentlandite and chalcopyrite (i.e. as described in section 11.2.1). Relict, cumulate-derived sulphides consist of hexagonal pyrrhotite with abundant pentlandite and chalcopyrite (i.e. as described in section 6.7). The presence of troilite and cubanite (also mackinawite) is a useful indication of pegmatite-related sulphides in a hybrid sulphide assemblage.

In completely replaced Reef the sulphide mineralogy is comparable to that of typical iron-rich ultramafic pegmatite.

DISCUSSION

At Amandelbult it is almost the norm to find that the Merensky upper chromitite and the hangingwall pyroxenite remain intact above replaced Reef. This presumably implies that they formed an, essentially, impervious barrier to the upward-streaming pegmatitic liquids (fig. 7.9). Coarse segregations of sulphide (often over 10 cm in diameter) are typically found above the Merensky upper chromitite layer, in the lower part of the Merensky pyroxenite above replaced Reef. Again, these sulphides are a hybrid mix of cumulate and pegmatite minerals.

The replaced Reef at Amandelbult is normally platiniferous. Typically, the PGE appear to be concentrated in a layer 10-20 cm thick above, and including, the Merensky upper chromitite layer. Although the Reef at Amandelbult is normally top-loaded (Kinloch, 1982) this suggests that, as iron-rich ultramafic pegmatite is normally non-platiniferous, the cumulate-hosted PGE and sulphides have been leached from the Merensky Reef and redistributed during the replacement process (see also Wagner, 1929).

11.2.3 IRON-RICH ULTRAMAFIC PEGMATITE : LARGE, PIPE-LIKE BODIES

THE MIDDELLAAGTE PIPE

In a detailed study of the ore mineralogy of the Middellaagte pipe, De Bruyn (1944) observed that base-metal sulphides are restricted to the olivine-rich parts of the pipe (see also pp. 112-116 and 149-150). The sulphide mineralogy is simple and, in order of decreasing abundance, the major phases

are pyrrhotite, pentlandite, cubanite and chalcopyrite. Valleriite (probably mackinawite) and sphalerite also occur. De Bruyn quoted an average "ore-grade" analysis of 0.46 wt. percent Ni and 0.47 wt. percent Cu. Recent investigations do not support these high values and the average sulphide Ni and Cu contents are extremely low. The base-metal sulphide mineralogy of this pipe is consistent with that of small bodies of pegmatite at Amandelbult. The distribution of the sulphide is extremely irregular; in borehole core pyrrhotite may locally comprise over 20 modal percent, whereas in other samples it may be less than 0.1 modal percent (see Table 11.5). The proportion of pentlandite, cubanite and chalcopyrite is extremely low and this body is of little economic interest. PGM have not been observed.

THE TOWNLANDS PIPE

A wide range of precious and base-metal minerals occurs in this body (Peyerl, 1981; Viljoen et al., 1983). This is atypical of the iron-rich ultramafic pegmatite suite in general, and it is evident that this pipe is unusual (see also pp. 19-20, 123-124 and 153).

The dominant base-metal sulphide is pyrrhotite, usually troilite (Phillips, pers. comm.). The intergrowth of troilite and hexagonal pyrrhotite which is characteristic of pegmatite at Amandelbult is not present here. The following discussion is summarised from the work of Peyerl (1981). Common sulphides, other than troilite, are pentlandite, cubanite, chalcopyrite and mackinawite. Valleriite co-exists with mackinawite (as at Mooihoek). An extensive range of Cu-Fe sulphides is recognized, incuding the rare minerals haycockite and mooihoekite. Secondary, probably low-temperature deuteric or possibly hydrothermal, minerals include chalcocite, cuprite, digenite, bornite and native copper. Native copper is commonly observed as fine stringers in serpentinite veinlets. Ilvaite is often associated with these sulphides; it has not been observed in other pegmatite bodies. Native silver, galena, niccolite, altaite and a number of unidentified Cu-Fe-Ni (?) sulphides also occur. In the peripheral parts of the pipe the mineralogy is similar, except that native copper and other secondary copper minerals are rare or absent. Additional minerals observed here are galena, clausthalite, native bismuth, froodite, graphite and nickel arsenides. PGM only occur in sparse amounts, except in the vicinity of the partially replaced UG-2 chromitite layer, where over 534 individual PGM grains were recognized in samples from borehole core (see also pp. 123-124).

Although this body is characterised by an exotic base-metal mineralogy the total sulphide-contained Cu and Ni is still low (see Table 11.5). A detailed investigation of the ore mineralogy of the Townlands pipe is being

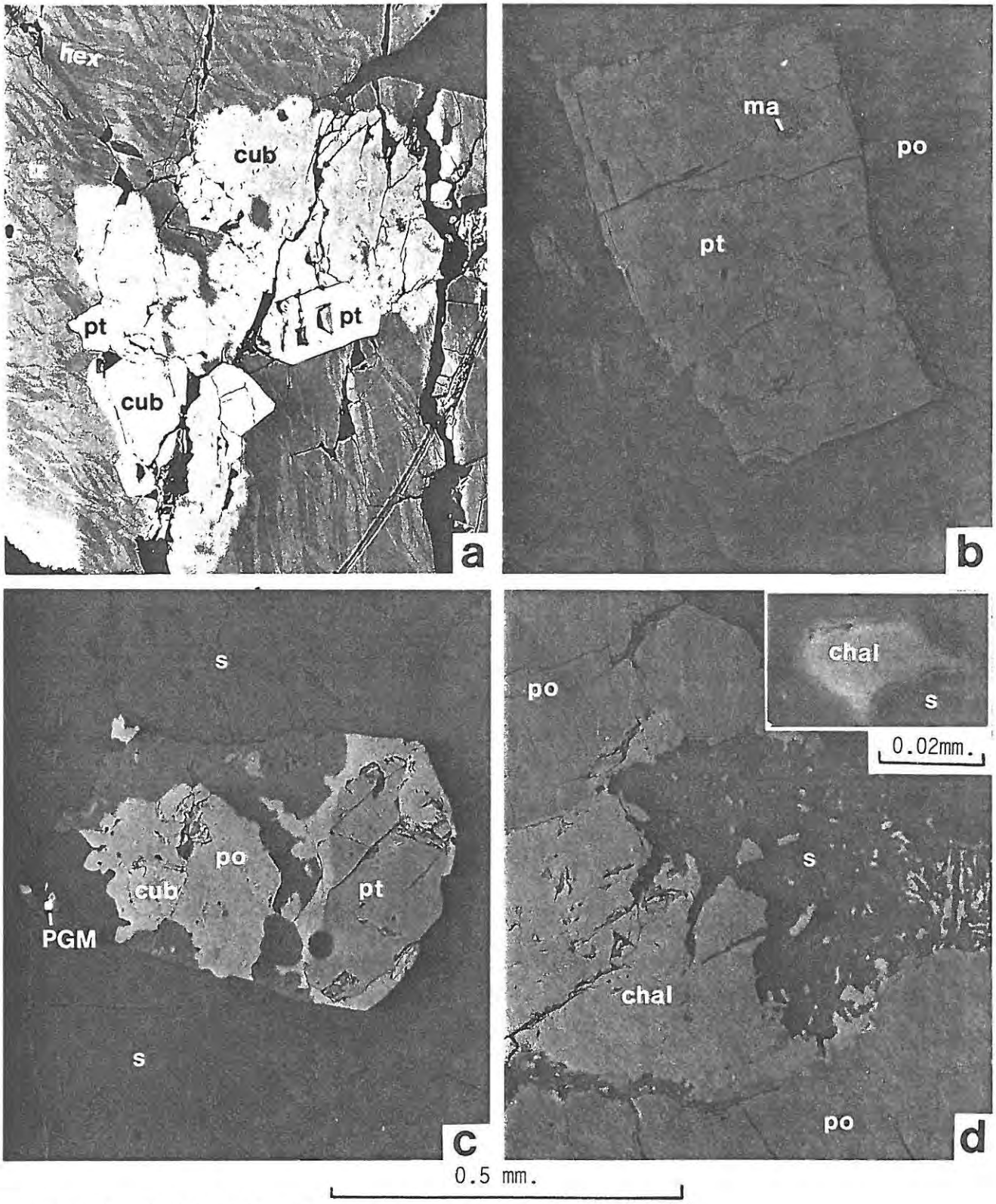

FIGURE 11.1 PHOTOMICROGRAPHS OF BASE-METAL SULPHIDES

a. Typical, flame-like intergrowth of hexagonal pyrrhotite (dark) and troilite (light). Pyrrhotite encloses a composite grain, consisting dominantly of cubanite with minor pentlandite and chalcopyrite. Part of a typical, composite sulphide grain (sample AG-6). b. Euhedral grain of pentlandite within a large pyrrhotite grain (euhedral form of pentlandite is a characteristic feature of this sulphide assemblage - see also "a"). Note also small, vermicular bodies of mackinawite (anisotropic) (sample AG-8). c. Composite sulphide grain, consisting of pyrrhotite, cubanite and pentlandite, within a coarse aggregate of spinel-ilmenite. Note also PGM (sample AG-1). d. Fine-grained intergrowth of Fe-Ti-Cr spinel and chalcopyrite. Inset shows a single chacopyrite inclusion in the spinel - note reaction rim. Composite sulphide grain in main photograph consists of pyrrhotite (exhibiting typical flame-texture) and chalcopyrite (sample AG-6).

(all in reflected light with partially crossed polarisers; hex - hexagonal pyrrhotite; tr - troilite; pt - pentlandite; cub - cubanite; chal - chalcopyrite; ma - mackinawite; s - Fe-Ti-Cr spinel)

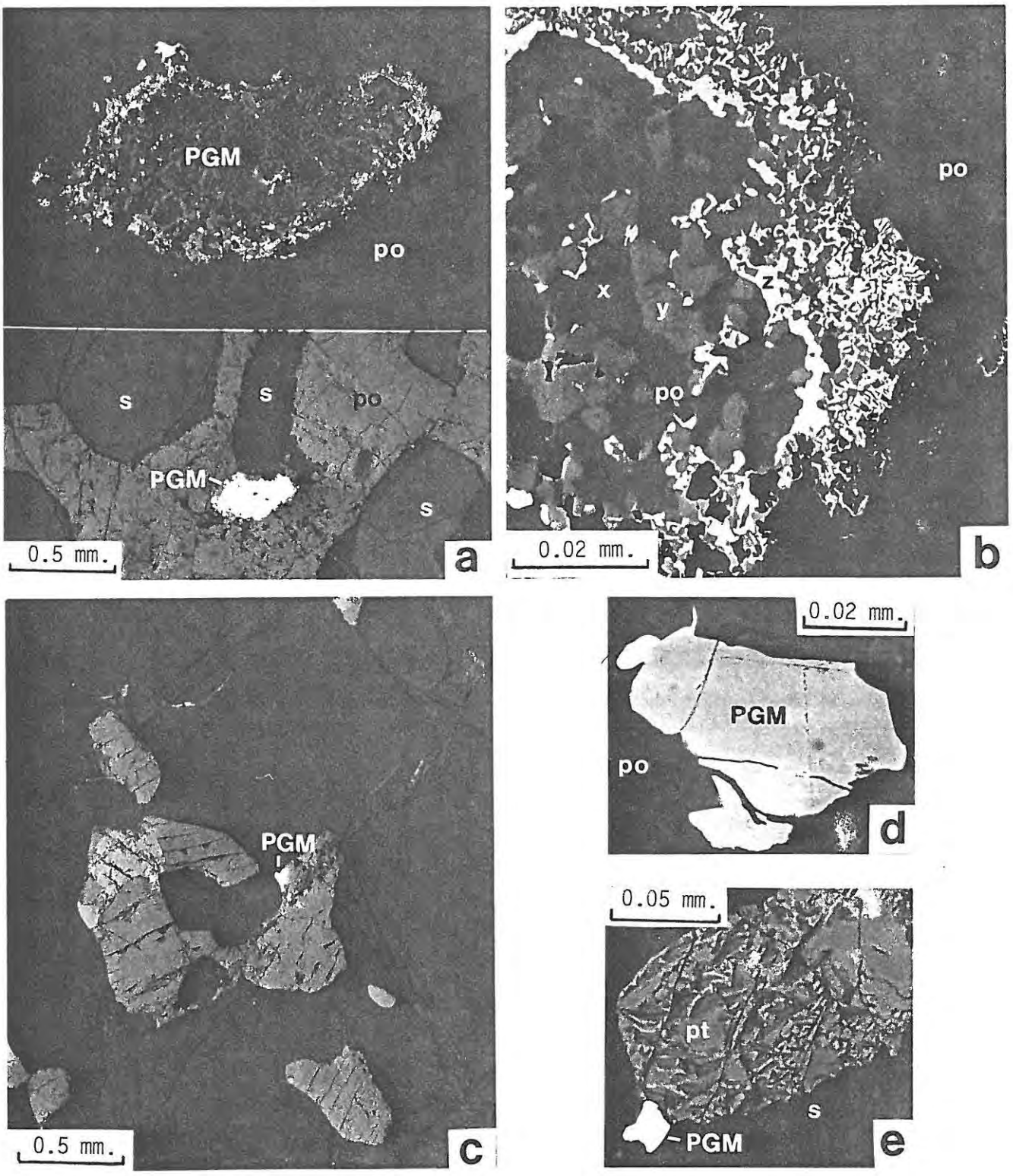

FIGURE 11.2 PHOTOMICROGRAPHS OF PGM

a. Composite, and unusually coarse PGM grain within large pyrrhotite grain. Whole is interstitial to spinel (note exsolution lamellae and well developed rims). Upper frame is a close-up of the PGM grain; here pyrrhotite is black (note relative reflectivities) (sample AH-14). b. Part of the composite PGM grain in "a". Consists of 3 main phases - $Pd(As,Hg)_2$ (dark grey - "x"), $PtAs_2$ (light grey - "y"), and $PdHg_2$ (white - "z"). Latter occurs dominantly as a rim to the composite grain (see "a"). Note also inclusions of pyrrhotite (black) and irregular replacement contact between PGM and pyrrhotite (as sample "a"). c. Composite sulphide grain with tiny PGM grain (consists of 2 phases, PdPb telluride and a Pt,Fe(Cu,Pd,Te) alloy (sample AH-21). d. Composite PGM grain consisting of (Ru,Ir)S and $(Pd,Fe)Hg_2$ (dark phases) and Pt,Fe alloy (white). Latter also occurs in microfractures in the host pyrrhotite (sample AG-1). e. Pt sulphide grain (white) attached to pentlandite. Dark grey is spinel (sample AK-1D).

(all in reflected light with partially crossed polarisers; po - pyrrhotite; pt - pentlandite; s - Fe-Ti-Cr spinel)

undertaken by Phillips (in prep.).

11.3 MINERAL CHEMISTRY

11.3.1 PYRRHOTITE-GROUP

REVIEW

Naturally occurring pyrrhotite-group minerals can be represented by the formulae $M_{1-x}S$, where x = 0 in the pure stoichiometric form and M = Fe, with minor Ni, Co, Mn, Cu, etc. Three common low temperature phases are recognized : troilite (atomic ratio of M/S close to 1) with a hexagonal structure; hexagonal pyrrhotite (M/S = 0.91-0.99) and monoclinic pyrrhotite (M/S < 0.90). Hexagonal and monoclinic pyrrhotite are the common varieties, but troilite is relatively rare in terrestrial occurrences. Stoichiometric troilite was long considered to be rare in terrestrial occurrences, but recent publications report a number of findings in which pyrrhotite consists of an intergrowth of troilite and hexagonal pyrrhotite. These phases may be distinguished optically, by etching, or by allowing the specimen to tarnish (troilite tarnishes most readily). They can also be identified by X-ray diffraction or electron microprobe analysis; the latter technique was used in this study. Typically only very minor substitution of Fe by Ni, Co, Zn etc. occurs, consequently the atomic Fe/S ratio accurately reflects the pyrrhotite polymorph (see also Power & Fine, 1976).

CHEMISTRY AND DISCUSSION

Averages of electron microprobe analyses of pyrrhotite are presented in Table 11.1 (for complete analyses see Appendix 12). In normal Merensky Reef, pyrrhotite is the hexagonal variety or an intergrowth of hexagonal and monoclinic pyrrhotite (Liebenberg, 1970; Vermaak & Hendriks, 1976; analysis 7, Table 11.1). Troilite, although reported from the Merensky Reef, is only rarely observed. However, as discussed above, in iron-rich ultramafic pegmatite and replaced Reef at Amandelbult pyrrhotite-group minerals usually comprise a fine-grained intergrowth of troilite and hexagonal pyrrhotite (analyses 3-6, Table 11.1). Troilite in these samples has a M/S ratio (M = Fe+Ni+Co) of greater than 0.98 (it is usually between 0.99 and unity). Cobalt and Ni are noticeably poorer in troilite compared to hexagonal pyrrhotite (compare analyses 3-6, Table 11.1). Hexagonal pyrrhotite from iron-rich ultramafic pegmatite exhibits few chemical differences to that in normal Merensky Reef (analyses 4,6 and 7, Table 11.1).

In comparison, pyrrhotite from the Vlakfontein nickel pipes is normally

TABLE 11.1 ELECTRON MICROPROBE ANALYSES OF PYRRHOTITES

	1		2		3		4		5		6		7	
wt. %	x	d	x	d	x	d	x	d	x	d	x	d	x	d
S	38.04	.181	38.37	1.266	36.40	.450	38.41	.325	36.97	.240	39.11	.071	37.9	.69
Fe	62.33	.177	61.37	1.118	62.80	.404	60.51	.509	63.33	.085	61.10	.099	59.9	.54
Co	-	-	-	-	.06	.063	.07	.057	n.d.	-	.09	-	.1	-
Ni	-	-	-	-	n.d.	-	.12	.075	n.d.	-	.16	.035	.2	-
TOTAL	100.37		99.75		99.26		99.11		100.30		100.46		98.1	
at. %														
S	51.53		52.13		50.22		52.44		50.42		52.61		52.37	
Fe	48.47		47.87		49.74		47.42		49.58		47.20		47.45	
Co	-		-		.04		.05		-		.07		.06	
Ni	-		-		-		.09		-		.12		.12	
M:S	.941		.918		.991		.907		.983		.901		.909	
Phase	?		Hexagonal		Troilite		Hexagonal		Troilite		Hexagonal		Hexagonal	
n	4		12		6		6		2		2		3	

- not analysed; n.d. not detected; x- mean; d- standard deviation; n- number of samples;
M:S - ratio of (Fe + Co + Ni) / S.

1. Core of the Mooihoek pipe
2. Vlakfontein nickel pipes
3,4 Replaced Merensky Reef, Amandelbult.
5,6. Typical iron-rich ultramafic pegmatite, Amandebult.
7. Normal Merensky Reef, Rustenburg (qouted in Vermaak & Hendriks, 1976)

an intergrowth of the hexagonal and monoclinic varieties (Liebenberg, 1970); this was confirmed by analyses on samples collected by the author (analysis 2, Table 11.1). Similarly it was confirmed that pyrrhotite from the platiniferous core of the Mooihoek pipe is the hexagonal variety (analysis 1, Table 11.1).

11.3.2 PENTLANDITE

REVIEW

Knop et al. (1965) showed that pentlandite, which had previously been considered to be $(Fe,Ni)_9S_8$, is a natural (Fe,Co,Ni,S) phase in which the the relative proportion of Fe, Ni and Co may vary within wide limits. The crystal structure does not require a fixed ideal value for the M/S ratio, although it is conventionally taken as 9:8. In typical, low-Co pentlandite the Ni/Fe ratio usually varies between 1.00 and 1.15, although a much wider range can be accommodated into the structural field (see fig. 11.3A). Iron and Ni can be completely substituted by Co such that Co-rich pentlandite, in which the composition may approach synthetic Co_9S_8 is known. Here the Ni/Fe ratio varies between much wider limits, from 0.70 to 1.29, although it is usually close to unity.

Knop et al. (1965) observed that the M/S ratio cannot be fixed

accurately because of analytical problems in determining S . Rajamani and Prewitt (1973) investigated this further and concluded that the structural formulae for Ni-rich pentlandite is $M_{9-x}S_8$, and for Fe-rich pentlandite is $M_{9+x}S_8$; as the M/S ratio decreases the Ni content increases. Kouvo et al. (1959) first described Co-rich pentlandite in the literature (from the Outokumpu mine, Finland), in which up to 49.33 wt. percent Co may occur. They reported that the optical properties were unchanged. Petruk et al. (1969) report cobaltian pentlandite (54.1 wt. percent Co) from the Cobalt district, Ontario, which is associated with an assemblage of low-temperature Co-Ag sulphides and arsenides. The physical properties of Co-rich and cobaltian pentlandites have been investigated by Rajamani and Prewitt (1973). Harris and Nickel (1972) found that the composition of pentlandite is dependent on the sulphide assemblage in which it occurs. They recognized a number of assemblages, including the following :

(1) Pentlandite - troilite, in which pentlandite has the lowest Ni/Fe ratio and contains greater than 3.0 atomic percent Co (in this group they include a sample from Mooihoek);

(2) Pentlandite - pyrrhotite, in which pentlandite commonly has less than 3.0 atomic percent Co and has higher Ni/Fe ratios than those in group -(1). The composition varies with that of pyrrhotite (hexagonal or monoclinic);

(3) Pentlandite - monoclinic pyrrhotite - pyrite/smythite;

(4) Pentlandite - pyrite/millerite;

(5) Pentlandite - heazlewoodite, in which the highest Ni/Fe ratios occur;

(6) Cobaltian pentlandite (10 - 20 atomic percent Co) and cobalt pentlandite (over 21 atomic percent Co) - heazlewoodite/awaruite.

Misra and Fleet (1974) investigated the phase relations of synthetic pentlandites and concluded that the composition of natural pentlandite varies sympathetically with the mineralogy of the host assemblage. Their findings support those of Harris and Nickel (1972).

CHEMISTRY

Averages of electron microprobe analyses of pentlandite are presented in Table 11.2 (for complete analyses see Appendix 12). Pentlandite from normal Merensky Reef at Amandelbult is a Co-poor variety (it usually contains less than 0.5 wt. percent Co) with low Ni/Fe ratios (analyses 6 and 8, Table 11.2). It is comparable to pentlandite in group (2) of Harris and Nickel's classification (it is associated with hexagonal or monoclinic pyrrhotite), athough the Ni/Fe ratio may be unusually low (fig. 11.3).

Pentlandite from iron-rich ultramafic pegmatite and replaced Reef at Amandelbult is invariably a Co-rich variety (usually containing 7-9 wt.

TABLE 11.2 ELECTRON MICROPROBE ANALYSES OF PENTLANDITES

	1		2		3		4		5		6		7	8	9
wt. %	x	d	x	d	x	d	x	d	x	d	x	d			
S	34.14	.338	33.93	.790	33.79	.433	33.33	.607	33.33	.445	33.59	.314	32.0	31.85	36.73
Fe	39.38	1.019	34.26	1.807	33.55	.806	30.81	1.087	31.91	.064	34.48	.847	38.4	32.95	54.99
Co	4.79	.337	1.75	.591	2.82	.247	8.25	.712	7.16	.106	.28	.180	4.3	.90	5.13
Ni	22.71	.717	31.09	2.018	30.27	.899	28.12	.444	28.07	-	30.78	1.162	23.7	33.55	3.98
TOTAL	101.02		101.03		100.43		100.18		100.46		99.13		98.4	99.25	100.83
at. %															
S	47.58		47.44		47.52		46.79		47.03		47.75		46.2	45.81	50.14
Fe	31.51		27.50		27.08		25.08		25.84		28.14		31.8	27.16	43.09
Co	3.63		1.33		2.16		6.36		5.50		.22		3.4	.69	3.81
Ni	17.28		23.74		23.24		21.77		21.63		23.89		18.6	26.34	2.97
Ni/Fe*	.55		.86		.86		.87		.84		.85		.59	.97	-
Ni/Ni+Co	.83		.95		.92		.77		.80		.99		.85	.97	-
M:S	8.81		8.87		8.84		9.10		9.01		8.75		9.32	9.40	.995
n	5		5		9		13		2		9		-	2	-

x- mean; d - standard deviation; n - number of samples; * - atomic ratios;
M : S - ratio of (Fe + Ni + Co) / S, assuming S = 8.

1. Core of the Mooihoek pipe.
2. Magnesian dunite, Driekop.
3. Vlakfontein nickel pipes.
4. Replaced Reef, Amandelbult.
5. Iron-rich ultramafic pegmatite, Amandelbult.
6. Normal Merensky Reef, Amandelbult.
7. Cobalt penatlandite, Mooihoek (Harris & Nickel, 1972).
8. Normal Merensky Reef, Rustenburg (Vermaak & Hendriks, 1976)
9. Mackinawite, iron-rich ultramafic pegmatite, Amandelbult.

percent Co; analyses 4 and 5, Table 11.2). This is typical of pentlandite in group (1) of Harris and Nickel's classification (it is normally associated with an intergrowth of troilite and hexagonal pyrrhotite). Cobaltian and cobalt pentlandites and rare Ni-Co sulphosalts have not been observed in the pegmatite suite at Amandelbult.

Mackinawite, a characteristic exsolution phase in pentlandite, cubanite and chalcopyrite in iron-rich ultramafic pegmatite at Amandelbult, is also a Co-rich variety (analysis 9 , Table 11.2). These samples occur as exsolution laths in Co-rich pentlandite.

Pentlandite from the the magnesian dunite unit at Driekop is a Co-poor variety, but that from the core of the Mooihoek pipe, where it is associated with pyrrhotite (usually an intergrowth of troilite and hexagonal pyrrhotite), is a Co-rich variety similar to that found in iron-rich ultramafic pegmatite at Amandelbult (analyses 1 and 2, Table 11.2) The Ni/Fe ratio is, however, quite different. Pentlandite from the Vlakfontein pipes is a Co-poor variety, which may be typical of an assemblage in which the pyrrhotite : pentlandite ratio is much lower than that for the more highly fractionated iron-rich ultramafic pegmatite suite (analysis 3, Table 11.2). It is similar to cumulus pentlandite in the upper critical zone.

DISCUSSION

These different sample groups are readily distinguished on a triangular diagram of Fe_9S_8 - Co_9S_8 - Ni_9S_8 (fig. 11.3A). Analyses from Harris and Nickel (1972) are incorporated in Figure 11.3B. Cobaltian and cobalt pentlandite have Ni/Fe ratios approaching unity, indicating that Co partitions equally between the Ni and Fe sites at high concentrations of Co. At lower concentrations, Co partitions preferentially into Ni sites, such that pentlandite with 5 to 10 wt. percent Co has low Ni/Fe ratios.

Samples from this study and from Harris and Nickel's groups 1 and 6 are plotted on graphs of Co vs. (Ni + Fe) and Co vs. Ni/Fe (fig. 11.4). A plot of Co vs. (Ni + Fe) gives a straight line, within analytical error, indicating that with increasing Co content the M/S ratio remains unchanged. Pentlandites from iron-rich ultramafic pegmatite scatter along this line depending on the percentage of Co.

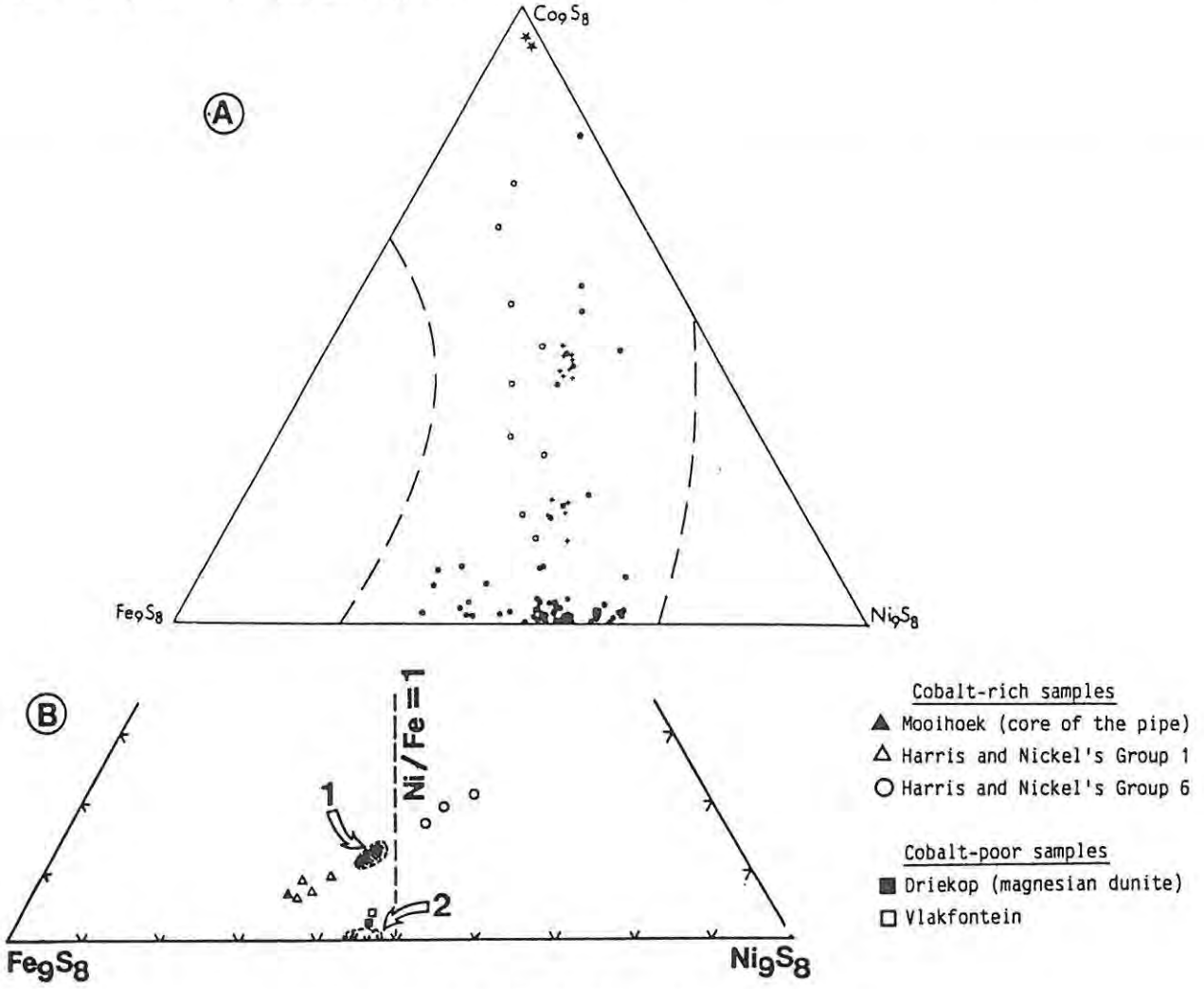

Figure 11.3 Pentlandite compositions plotted as at. % Fe_9S_8 - Co_9S_8 - Ni_9S_8.

A : from Harris and Nickel (1972); dashed lines represent the solid solution limits defined by Knop and Ibrahim (1961). Open circles and crosses represent cobalt pentlandites from Outokumpu, stars represent cobalt pentlandites from Cobalt, Ontario and solid circles are pentlandites with less than 12 at. % Co.

B : data in the present study; cobalt-rich pentlandites from the iron-rich ultramafic pegmatite suite plot in field "1" and cobalt-poor pentlandites from the Merensky Reef plot in field "2". Also includes samples from Harris and Nickel's Group 1 (samples from Mooihoek, Pefkos, Muskox and Del Norte Co.) and Group 6 (samples from Dumont and Univex).

If Co substitutes equally for both Fe and Ni a plot of Co vs. Ni/Fe should give a straight line, parallel with the Co-axis. From Figure 11.4B it can be seen that Co-poor pentlandite from the cumulates define an entirely separate field to that of Co-rich pentlandite from the pegmatites. The latter samples scatter along a straight line which indicates that for every 1 atomic percent increase in Co the Ni/Fe ratio increases by 0.11 atomic percent. Samples from Harris and Nickel's group 1 and of cobaltian pentlandites from Dumont (group 6) also define this trend. At moderate concentrations (3 to 11 atomic percent), Co preferentially occupies Fe sites in place of Ni sites at a rate of roughly 3 to 2. This does not hold true for low and high concentrations of Co.

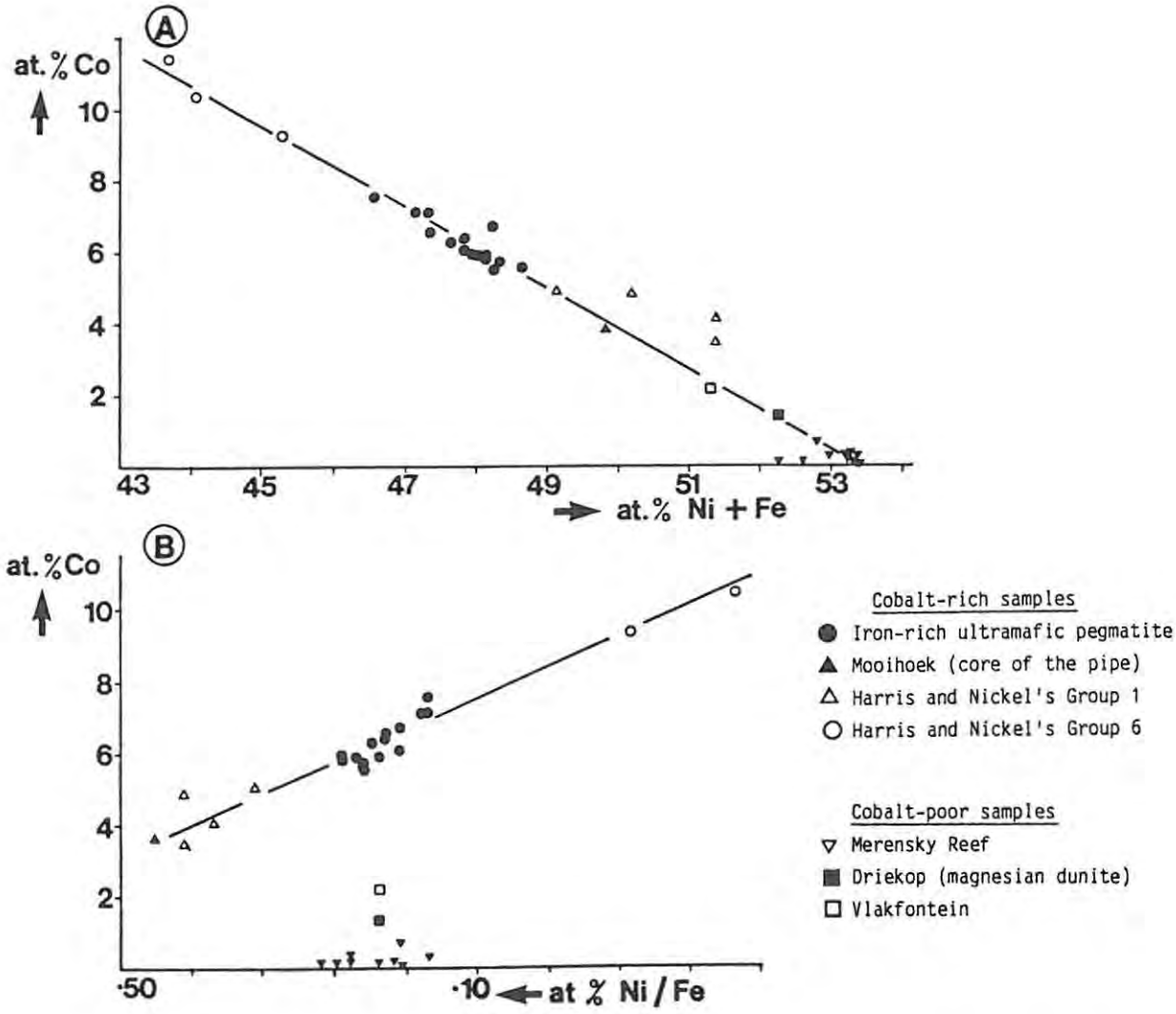

Figure 11.4 Pentlandite compositions plotted as : (A) at. % Co vs. at. % (Ni+Fe); and (B) at. % Co vs. at. % Ni/Fe. In (A) all samples plot on a straight line which reflects a constant M:S ratio (M = Fe+Ni+Co), but in (B) the cobalt-rich samples lie on a straight line (indicating that in this compositional range Co preferentially occupies Fe sites at the expense of Ni sites) and the cobalt-poor samples define a separate field.

TABLE 11.3 ELECTRON MICROPROBE ANALYSES OF CHALCOPYRITES AND CUBANITES

	1	2	3	4	5	6	7
wt. %							
S	34.36	34.95	35.17	35.68	35.35	35.21	35.71
Fe	30.53	40.69	30.47	40.96	41.10	31.08	41.90
Cu	33.77	22.85	33.65	22.67	22.34	33.34	22.50
TOTAL	98.66	98.49	99.29	99.31	98.79	99.75	100.11
at. %							
S	49.85	50.05	50.50	50.52	50.35	50.35	50.21
Fe	25.43	33.45	25.12	33.29	33.60	25.51	33.82
Cu	24.72	16.51	24.38	16.19	16.05	24.14	15.96
M:S	1.006	.998	.980	.986	.986	.986	.991
Cu/Cu+Fe	.49	.33	.49	.33	.32	.49	.32

M:S Ratio of (Fe+Cu)/S
1,2. Chalcopyrite, Replaced Merensky Reef, Amandelbult.
3,4. Chalcopyrite, typical iron-rich ultramafic pegmatite, Amandelbult.
5. Cubanite, Middellaagte pipe, Amandelbult.
6,7. Chalcopyrite, normal Merensky Reef, Amandelbult.

11.3.3 CUBANITE AND CHALCOPYRITE

Selected microprobe analyses of chalcopyrites and cubanites from iron-rich ultramafic pegmatite and the cumulates at Amandelbult are presented in Table 11.3. The M/S and Cu/(Cu + Fe) ratios indicate that they lie very close to ideal compositions and no chemical trends have been recognized.

11.3.4 PLATINUM-GROUP MINERALS

Iron-rich ultramafic pegmatite at Amandelbult is normally depleted in PGM, with the exception of the replaced Reef sequence discussed above. However, during analysis of sulphide phases by J.C.I. a number of PGM were located in pegmatite samples (see Table 11.4).

TABLE 11.4 ELECTRON MICROPROBE ANALYSES OF PGM IN IRON-RICH ULTRAMAFIC PEGMATITE AT AMANDELBULT

	1	2	3	4	5		6	7	8
wt.%									
Fe	.18	n.d.	.20	2.48	2.48	S	32.19	29.70	36.62
Ni	.43	n.d.	n.d.	n.d.	n.d.	Fe	.80	1.44	63.68
As	13.84	40.63	n.d.	n.d.	n.d.	Pd	n.d.	n.d.	.19
Pd	63.95	n.d.	36.11	37.72	37.78	Pt	n.d.	n.d.	.66
Pt	n.d.	54.64	n.d.	n.d.	n.d.	Ru	59.08	53.37	n.d.
Hg	14.67	n.d.	64.30	63.86	61.05	Ir	8.87	11.62	n.d.
TOTAL	93.08	95.32	100.61	103.11	101.31	TOTAL	100.94	96.14	101.16

1,2,3. Composite grain (350 *150 microns) (2-sperrylite,Pt,As; 3-Pd,Hg alloy; 1-(Pd,Hg)As.
4,5. Discrete grains of Pd,Hg alloy .
6,7. Laurite. 8. Pyrrhotite

TABLE 11.5 WHOLE-ROCK ANALYSES OF SULPHIDE-RICH SAMPLES OF IRON-RICH ULTRAMAFIC PEGMATITE

	27-H1	AE-14	AE-16	ML24-9	TLP-1A	ML27-5
wt.%						
SiO_2	53.47	24.74	32.99	35.30	35.85	32.42
TiO_2	2.57	1.14	3.36	3.35	.24	6.21
Al_2O_3	.48	.35	1.28	1.65	.17	.52
Fe_2O_3	3.97	2.72	4.84	4.88	1.80	7.71
FeO	33.73	55.23	36.42	32.24	38.50	32.17
MnO	.18	.32	.38	.44	.55	.60
MgO	4.20	12.61	15.06	13.70	20.05	15.39
CaO	.36	2.85	5.59	7.88	2.70	4.83
Na_2O	.03	.04	.07	.28	.03	.10
K_2O	n.d.	n.d.	n.d.	.07	n.d.	n.d.
P_2O_5	n.d.	.01	.02	.22	.12	.04
TOTAL	100.00	100.00	100.00	100.00	100.00	100.00
ppm						
Cr	4075	124	530	838	101	324
V	3170	250	910	1146	315	1330
Co	1178	893	403	319	323	255
Ni	5574	3815	1247	972	1263	322
Cu	6600	11367	2277	1521	2174	21
Zn	160	118	148	216	355	209

n.d.: not detected; - not determined; % Fe_2O_3 = % TiO_2 + 1.5
27-H1, AE-14 & AE-16 Typical, small body, Amandelbult;
ML24-9 Middellaagte Pipe; TLP-1A Townlands Pipe;
ML27-5 Sulphide-poor pegmatite, Middellaagte Pipe.

11.4 WHOLE-ROCK CHEMISTRY

The distribution of Ni, Cu and Co in iron-rich ultramafic pegmatite is obviously influenced by sulphides. Although sulphur has not been analysed for, whole rock data in conjunction with mineralogy enables the distribution of Ni, Cu and Co between co-existing silicate and sulphide phases to be described qualitatively (see also Chapter 12). Three analyses of sulphide-rich pegmatite (with greater than 10 modal percent sulphide) are presented in Table 11.5. The proportion of sulphide Ni, Cu and Co can be estimated by comparison with a sulphide-poor sample of similar bulk silicate composition. Typical analyses of sulphide-rich (disseminated ore) and sulphide-poor pegmatite from the Middellaagte pipe are also presented in Table 11.5. The Cu-poor nature of the sulphide in the Middellaagte pegmatite is evident in comparison with samples of sulphide-rich pegmatite from the Townlands pipe.

11.5 CO-EXISTING OLIVINE AND SULPHIDE

The distribution of Fe^{2+} and Ni between olivine and sulphide has major impications in determining the genesis of magmatic Ni-sulphide ores (see Chapter 6, cf. pp. 101-103).

COMPOSITION OF PEGMATITE-HOSTED OLIVINES AND SULPHIDES

Olivine from iron-rich ultramafic pegmatite is characterised by a slightly high NiO/MgO ratio, as compared to both theoretical compositions and to cumulus olivine from the layered sequence (see pp. 153-155 and 159-161). This is also true of iron-rich olivines from the platiniferous ultramafic pipes (see pp. 50-54). There does not appear to be any relationship beteween the Ni content of olivine in any of these samples and the presence or absence of sulphide (subsolidus reequilibration between sulphide and silicate was referred to in Chapter 6, pp. 101-102).

The distribution of Ni/Fe between sulphide and olivine is related by the distribution coefficient K_D (Thompson et al., 1984, quote an average value for K_D of 9.8, which is in agreement with that calculated for the Merensky Reef; see p. 101). The average Ni/Fe ratio of olivine in iron-rich ultramafic pegmatite at Amandelbult is 0.0008 (Table 9.2). Using a value of 10 for K_D the Ni/Fe ratio of the pegmatite-hosted sulphides may be estimated at 0.008. The modal proportions of sulphide assemblages are difficult to assess, but this value fits a composite sulphide assemblage consisting of 95 wt. percent pyrrhotite, 3 wt. percent combined cubanite and chalcopyrite and 2 wt. percent pentlandite (using the microprobe data in Tables 11.1 to 11.3). This seems reasonable, judging by petrographic studies.

CONCLUSIONS

It is suggested that S-saturation was only reached in the pegmatitic liquid after crystallization of olivine, at which stage only minor residual quantities of Ni could be scavenged by the immiscible monosulphide liquid solution. If S-saturation occurred early then it would be unrealistic to expect olivine to be Ni-rich, even though the Ni-poor nature of the sulphides could be accounted for by the Fe-rich nature of the pegmatitic liquid. This may be examined in relationship to knowledge of the sulphur solubility of ultramafic-mafic magmas.

SOLUBILITY OF SULPHUR IN ULTRAMAFIC-MAFIC MAGMAS

Increases in temperature, sulphur fugacity, (fS_2), FeO content and, to a lesser extent MgO and CaO content (as they affect aFeO), result in an

increase in the capacity of a mafic magma to dissolve sulphur. Conversely, increases in oxygen fugacity (fO_2) and, to a lesser extent, SiO_2 and Al_2O_3 (as they effect a_{FeO}) have a reverse effect (Fincham & Richardson, 1954; Maclean, 1969; Haughton et al., 1974; Shima & Naldrett, 1975). All common mafic magmas are within a range of fO_2 and fS_2 such that sulphide sulphur is the most important phase in the melt. The strongest positive correlation with the sulphur carrying capacity of a mafic magma is with the FeO content (Haughton et al., 1974). Haughton et al. showed that the amount of S dissolved in basaltic magma at 1200°C varied from 0.2 to 0.5 wt. percent S as the FeO content increased from 5 to 20 wt. percent, at fixed levels of fO_2 and fS_2. Shima and Naldrett (1975) found that an immiscible sulphide liquid will segregate from an ultramafic magma (23 wt. percent MgO, 12 wt. percent FeO) with an fO_2 of $10^{-10.4}$ atm. at an fS_2 between $10^{-2.4}$ and 10^{-2} atm., at which stage the melt contained 0.16 to 0.27 wt. percent S. At a higher fO_2 of $10^{-9.2}$ atm. it was not possible to saturate the melt, even with an fS_2 of $10^{-1,4}$atm. Theoretically, however, they predicted that at this higher oxygen fugacity segregation will occur at an fS_2 between 10^{-1} and $10^{-0.7}$, with 0.33 to 0.47 wt. percent S.

The presence of the trace elements Ni, Cu, Co, Zn etc. have very little effect on the solubility of sulphur in silicate magmas. When the sulphide liquid first segregates from the silicate magma it is widely distributed as small droplets, the composition of which will be buffered by the magma. Thus, the fO_2, fS_2 and a_{FeO}, a_{Ni} and a_{Cu} etc. must be the same in both the co-existing sulphide and silicate liquids (Naldrett, 1981). In a large magma chamber fO_2, fS_2 and a_{FeO} are buffered, such that the controlling factor is the total FeO content. This results in the formation of sulphide bodies in which the relative proportions of Fe, S, and O vary within small limits as this is dictated by the composition of the primary magma.

11.6 CRYSTALLIZATION TEMPERATURE

The melting relationships of the system Ni-Fe-S in the presence of 15 and 20 wt. percent synthetic magnetite have been examined by Craig and Naldrett (1963). They found that between 10 and 20 wt. percent Ni does not appreciably affect the melting point, whereas the presence of only 2 wt. percent Cu lowers the melting point of nickeliferous pyrrhotite by 15 to 20°C. The melting temperature also varies over a range of 50 to 60°C as the S content of the monosulphide liquid solution changes from about 36 to 39 wt. percent. Typical melting temperature of Mss is 1010°C plus or minus 30°C. Naldrett (1967) found that crystallization commenced at between 1010

and 1050°C for typical Mss compositions in the Fe-S-O system. Craig and Naldrett (1963) concluded that the minimum temperature at which Ni-pyrrhotite-magnetite ores might be emplaced as liquids or crystal mushes is between 1040 and 980°C. Naldrett and Richardson (1967) found that H_2O has no appreciable fluxing effects and Ni-sulphide ores have no connection with hydrothermal activity. In nature Skinner and Peck (1969) observed immiscible Ni-sulphide droplets in a melt collected at the Alae lava lake at a temperature of 1065°C, well below the melting point of pure pyrrhotite (1188°C).

11.7 SUMMARY

(1) The sulphide assemblage in iron-rich ultramafic pegmatite from the upper critical zone is characterised by an exceptionally high FeS/NiS ratio (the pyrrhotite : pentlandite ratio is probably over 50), a high FeS/CuS ratio, and the predominance of cubanite over both pentlandite and chalcopyrite.

(2) Pyrrhotite is usually an intergrowth of troilite and the hexagonal variety.

(3) Pentlandite is a Co-rich variety.

(4) Iron-rich ultramafic pegmatite is normally non-platiniferous.

(5) The sulphide assemblage of iron-rich ultramafic pegmatite is characteristic of fractionated, iron-rich ultramafic-mafic rocks and probably crystallized at magmatic temperatures.

(6) Sulphur saturation probably occurred after crystallization of olivine, consequently these sulphides are Ni-poor.

(7) Iron-rich ultramafic pegmatite that replaces the Merensky Reef is usually platiniferous and may contain a total PGE content equivalent to the normal, unreplaced Reef. However, it is characterised by different inter-element PGE ratios (e.g., high Pt and Ru).

(8) Replaced Reef is characterised by a unique PGE mineralogy (in which Pt-Fe alloys and laurite are predominant, with an absence of complex bismuthotellurides).

(9) Partially replaced Reef may contain a mixture of cumulate-related and pegmatite-related sulphides.

(10) It is concluded that the majority of the PGE and a proportion of the base-metal sulphides in replaced Reef have been leached from the pre-existing Merensky Reef.

CHAPTER 12 WHOLE-ROCK CHEMISTRY

Whole-rock analyses of iron-rich ultramafic pegmatite are presented herein and modelled in conjunction with mineralogical data discussed in the preceding chapters. Analyses include a selected range of trace elements which were not determined during electron microprobe analysis of discrete phases. Most of the whole-rock analyses presented here are of pegmatites from bodies in the upper critical zone (above the UG-2 chromitite layer) or the lower part of the main zone at Amandelbult. Mineralogical data indicate that these rocks become increasingly fractionated with height in the cumulate pile, but compositional variation in pegmatite from a constant position in the layered sequence is almost entirely dependent on modal variation. The composition of iron-rich ultramafic pegmatite may also be compared with that of their cumulate host rocks.

12.1 SAMPLING AND ANALYTICAL DETAILS

Samples of iron-rich ultramafic pegmatite analysed in this study may be subdivided into four groups. The results of these analyses are presented in Table 12.1 (samples from small bodies at Amandelbult, all from the upper critical zone), Table 12.2 (samples from the Middellaagte pipe, all from the upper critical - lower main zone), Table 12.3 (samples from the south-western sector of the Bushveld Complex) and Table 12.4 (samples from the eastern Bushveld Complex). Further sampling details (precise geographic and stratigraphic locations, explanation of acronyms etc.) are provided in Appendices 1 and 2.

Because of the pegmatitic character of these rocks individual samples are often not representative of their parent bodies. A second problem is encountered with these data because of the presence of relict cumulus minerals, consequently petrographic studies are required to distinguish between pegmatite sensu stricto and hybrid, pegmatite-cumulate rocks (cf. pp. 125-126).

All whole-rock analyses in this study were performed by X-ray fluorescence spectrometry (see Appendix 5). All major elements, including "loss on ignition", were analysed for, as were a range of selected trace elements, namely Cr, V, Co, Ni, Cu, Zn, Sc, Nb, Zr, Y, Sr and Rb.

TABLE 12.1 XRF ANALYSES OF WHOLE-ROCK SAMPLES OF IRON-RICH ULTRAMAFIC PEGMATITE FROM AMANDELBULT

	AE-8	AE-9	AE-10	AE-11	AE-12	AE-13	AE-15	AE-17	AE-18	AE-19	AE-20	AE-21
wt.%												
SiO_2	37.17	38.16	36.34	35.97	37.30	43.88	42.60	42.15	42.61	42.81	42.39	40.07
TiO_2	1.67	1.58	2.19	.99	.49	2.13	4.45	2.88	3.62	3.85	4.99	4.12
Al_2O_3	.74	.81	1.43	.54	.55	1.62	6.09	1.72	1.85	1.76	2.65	1.57
Fe_2O_3	3.12	3.01	3.62	2.44	1.94	3.56	5.88	4.39	5.06	5.29	6.43	5.55
FeO	33.13	31.82	33.25	37.16	36.14	20.49	14.29	21.30	19.01	18.42	15.76	22.40
MnO	.45	.46	.48	.42	.41	.26	.22	.28	.27	.26	.26	.32
MgO	17.39	17.09	17.07	17.86	17.78	13.81	10.63	13.46	12.71	12.46	11.40	13.40
CaO	6.20	6.96	5.45	4.57	5.32	14.05	15.42	13.68	14.72	15.00	15.93	12.48
Na_2O	.12	.09	.11	.04	.05	.16	.34	.14	.14	.13	.18	.10
K_2O	n.d.	n.d.	.01	n.d.	n.d.	.02	.04	n.d.	.01	.01	n.d.	n.d.
P_2O_5	.02	.03	.04	.01	.04	.04	.04	.02	.01	.02	.02	.01
ppm												
Cr	382	352	306	515	235	600	1047	1280	1279	1042	1496	1332
V	664	652	595	673	395	1020	1812	1871	1364	1728	2382	2153
Co	233	238	242	260	261	167	128	166	194	156	133	178
Ni	372	364	356	438	478	299	204	251	439	235	172	248
Cu	436	447	471	515	585	496	236	316	695	347	223	261
Zn	170	164	168	182	179	107	89	112	92	105	100	133
Sc	59.1	61.9	48.6	41.4	45.3	104	98.9	108	115	111	128	101
Nb	n.d.	n.d.	n.d.	n.d.	n.d.	n.d.	3.5	n.d.	n.d.	3.0	n.d.	58(?)
Zr	10.6	9.7	11.2	6.2	7.3	21.2	24.9	21.4	23.4	22.9	25.4	60(?)
Y	8.5	9.5	7.2	7.5	6.9	16.6	19.2	16.1	18.3	17.8	16.8	81(?)
Sr	5.3	6.3	18	5.3	5.1	15	88	13	14	13	31	-
Rb	n.d.	n.d.	n.d.	n.d.	n.d.	n.d.	n.d.	n.d.	n.d.	n.d.	n.d.	-

	AE-23	AE-24	AE-25	AE-26	AE-27	AE-28	AE-29	AE-31	AE-32	AE-33A	AU-1	AU-2
wt.%												
SiO_2	37.18	36.71	39.73	33.49	39.31	42.85	40.17	43.46	43.74	41.69	41.52	44.61
TiO_2	10.32	1.98	5.16	5.32	3.71	3.11	2.40	3.09	2.65	3.32	4.31	2.23
Al_2O_3	1.57	1.41	1.52	1.33	1.69	2.60	1.42	1.84	2.23	2.62	4.99	1.78
Fe_2O_3	11.74	3.42	6.69	6.71	5.25	4.58	3.84	4.50	4.09	4.76	5.74	3.66
FeO	14.56	33.43	20.37	32.87	24.33	19.92	26.00	18.77	19.30	19.44	16.94	19.26
MnO	.29	.45	.37	.45	.39	.30	.36	.31	.28	.28	.30	.29
MgO	11.31	16.82	13.08	16.41	14.05	13.32	15.04	13.22	13.80	12.17	11.37	13.15
CaO	12.88	5.64	12.96	3.31	11.10	13.06	10.48	14.67	13.57	14.37	14.37	14.80
Na_2O	.11	.10	.12	.06	.12	.12	.25	.12	.22	1.33	.34	.17
K_2O	.01	.03	n.d.	.03	.03	.09	.02	.01	.09	-	.01	.03
P_2O_5	.02	.01	.01	.02	.01	.05	.01	.02	.03	.01	.12	.03
ppm												
Cr	737	279	1181	489	1073	751	698	923	731	1566	953	1594
V	2034	658	1946	1116	1878	1375	1469	1596	1332	2366	1644	1921
Co	165	281	167	244	171	184	148	143	149	143	132	146
Ni	260	307	281	294	222	258	208	181	221	206	205	226
Cu	350	240	306	174	135	189	160	153	181	191	242	204
Zn	101	176	120	202	137	144	115	109	109	119	104	109
Sc	130	45.8	107	44.3	86.9	81.5	96.7	105	102	102	105	112
Nb	16.3	n.d.	5.1	6.7	3.6	n.d.	n.d.	n.d.	8.0	n.d.	5.4	n.d.
Zr	45.3	14.4	24.4	23.3	23.1	20.5	25.7	21.8	35.3	20.5	22.5	22.6
Y	14.4	10.4	13.6	9.2	14.7	14.0	19.0	17.0	15.5	17.7	16.6	20.7
Sr	10	20	10	4.4	16	12	27	15	20	31	71	15
Rb	n.d.	n.d.	n.d.	n.d.	n.d.	n.d.	n.d.	n.d.	9.8	n.d.	3.5	n.d.

Fe_2O_3 estimated by the method of Irvine and Baragar (1971).

All samples on this page from one, sheet-like pegmatite body (case-study (2)).

TABLE 12.1 (CONTINUED)

	AC-5		AO-32		AO-34		AO-37		AO-40		AO-41B		AV-5B		AV-6	
wt.%																
SiO_2	38.76	39.36	42.44	42.96	44.65	45.28	39.53	40.19	36.19	37.16	43.98	44.11	40.49	41.51	41.51	42.10
TiO_2	6.89	7.00	6.65	6.73	2.51	2.54	3.02	3.08	2.94	3.02	4.12	4.13	.08	.08	6.75	6.85
Al_2O_3	6.67	6.78	1.70	1.72	1.80	1.82	4.60	4.68	.81	.84	1.84	1.85	10.20	10.68	1.94	1.97
Fe_2O_3	8.39	8.52	8.07	8.16	3.93	3.99	4.42	4.53	4.36	4.47	5.56	5.57	1.58	1.65	8.25	8.37
FeO	12.63	12.83	11.95	12.09	16.53	16.77	21.01	21.36	29.87	30.68	15.24	15.28	11.88	12.44	11.99	12.16
MnO	.33	.34	.25	.25	.27	.27	.32	.32	.42	.44	.26	.27	.18	.19	.24	.24
MgO	8.89	9.03	11.33	11.47	12.50	12.67	12.95	13.16	16.36	16.80	11.99	12.03	23.76	24.87	11.29	11.45
CaO	15.50	15.74	16.23	16.42	16.24	16.47	12.25	12.46	6.32	6.49	16.57	16.62	6.93	7.26	16.46	16.69
Na_2O	.27	.27	.16	.16	.16	.16	.17	.17	.08	.08	.13	.13	.33	.34	.15	.16
K_2O	.12	.12	.01	.01	Tr	.01	.05	.05	.01	.01	n.d.	n.d.	.10	.11	n.d.	n.d.
P_2O_5	.02	.02	.02	.02	.02	.02	.01	.02	.01	.01	.02	.02	n.d.	n.d.	.02	.02
Cr_2O_3	.31	-	.19	-	.22	-	.26	-	.07	-	.15	-	.22	-	.20	-
NiO	.02	-	.02	-	.03	-	.05	-	.04	-	.03	-	.14	-	.03	-
L.O.I.	.97	-	.64	-	1.21	-	2.05	-	2.67	-	1.05	-	5.26	-	.53	-
TOTAL	99.79	100.00	99.66	100.00	100.07	100.00	100.69	100.00	100.14	100.00	100.94	100.00	101.13	100.00	99.36	100.00
ppm																
Cr	2137		1309		1521		1774		452		1042		1473		1363	
V	3088		2246		2057		1927		842		2208		101		1998	
Co	105		110		117		171		202		76		128		140	
Ni	153		187		225		378		315		229		1121		269	
Cu	125		121		121		375		120		178		9		367	
Zn	106		99		109		126		159		100		84		77	
Sc	115		135		114		79.5		60.1		119		12.4		162	
Nb	7.2		6.7		n.d.		n.d.		3.1		4.3		n.d.		5.9	
Zr	31.5		38.9		24.8		15.7		18.7		27.9		3.1		31.2	
Y	14.5		20.7		20.0		13.0		12.2		19.2		4.5		18.0	
Sr	104		16		17		161		14		17		132		17	
Rb	4.5		n.d.		n.d.		n.d.		2.0		n.d.		n.d.		n.d.	

	AV-12		AV-13		AH-32		AH-33A		AH-33B		AH-34		AH-35		AV-11	
wt.%																
SiO_2	39.87	40.49	46.19	47.92	43.39	44.11	36.03	37.46	44.54	45.12	39.17	39.45	33.78	34.36	33.72	35.28
TiO_2	5.77	5.86	.16	.17	3.92	3.99	1.87	1.95	.30	.30	9.09	9.15	3.91	3.98	11.63	12.17
Al_2O_3	3.59	3.65	1.86	1.93	2.65	2.69	2.10	2.18	27.27	27.62	2.56	2.57	2.41	2.45	1.59	1.66
Fe_2O_3	7.27	7.38	1.66	1.73	5.42	5.51	3.37	3.51	1.80	1.82	10.59	10.66	5.41	5.51	13.13	13.74
FeO	15.92	16.16	13.57	14.08	14.47	14.71	26.99	28.07	2.37	2.40	11.79	11.87	27.82	28.30	10.80	11.30
MnO	.28	.28	.18	.19	.24	.24	.35	.36	.05	.05	.26	.27	.37	.37	.35	.36
MgO	11.08	11.86	30.51	31.66	11.11	11.29	18.68	19.43	3.07	3.11	10.86	10.94	17.71	18.02	10.28	10.76
CaO	13.80	13.99	2.15	2.23	16.96	17.24	6.66	6.93	18.24	18.48	14.80	14.90	6.71	6.82	13.87	14.51
Na_2O	.23	.23	.09	.09	.19	.20	.11	.11	.96	.97	.12	.12	.17	.17	.13	.13
K_2O	.04	.04	.01	.01	.01	.01	n.d.	n.d.	.13	.13	n.d.	n.d.	Tr	Tr	.05	.05
P_2O_5	.05	.05	n.d.	n.d.	.02	.02	.01	.01	.01	.01	.07	.07	.01	.01	.03	.03
Cr_2O_3	.16	-	-	-	.17	-	1.00	-	.12	-	1.04	-	.09	-	1.56	-
NiO	.04	-	.34	-	.03	-	.15	-	.01	-	.15	-	.03	-	.03	-
L.O.I.	.74	-	4.26	-	.89	-	2.02	-	1.91	-	.30	-	1.35	-	2.90	-
TOTAL	99.40	100.00	100.80	100.00	99.46	100.00	98.33	100.00	100.75	100.00	100.78	100.00	99.76	100.00	100.08	100.00
ppm																
Cr	1122		-		1156		6821		793		7148		636		10667	
V	1636		-		2743		1258		156		3057		2038		2156	
Co	159		-		122		185		18		177		130		171	
Ni	314		2694		250		1175		58		1192		210		244	
Cu	389		677		287		108		20		137		222		653	
Zn	92		87		95		172		22		192		92		44	
Sc	124		20		110		35.7		19.1		40.0		128		172	
Nb	6.3		n.d.		n.d.		n.d.		n.d.		n.d.		14.0		n.d.	
Zr	30.6		5.3		26.1		11.7		4.4		14.0		43.0		7.7	
Y	16.5		5.6		18.1		10.1		5.0		11.6		21.3		8.0	
Sr	45.7		18		24		23		389		25.2		n.d.		29	
Rb	n.d.		n.d.		n.d.		n.d.		2.5		n.d.				n.d.	

Fe_2O_3 estimated by the method of Irvine and Baragar (1971).

Sample AH-33B of partially replaced anorthosite above the upper pseudoreef A.

Samples AH-32 and AH-33A of partially replaced upper pseudoreef A.

TABLE 12.1 (CONTINUED)

	27-B1		27-C1	27-D1		27-D2		27-D3		27-F1		27-G1		27-G2		27-G3	
wt.%																	
SiO_2	39.71	40.17	-	42.11	42.42	43.04	43.39	47.86	46.38	32.95	34.28	30.47	30.75	40.29	40.98	41.33	41.36
TiO_2	.24	.24	-	1.12	1.13	.68	.69	1.11	1.08	4.37	4.54	2.02	2.06	.92	.94	.36	.36
Al_2O_3	1.32	1.33	-	1.03	1.04	1.63	1.64	2.01	1.95	1.09	1.14	.15	.15	1.12	1.14	1.46	1.46
Fe_2O_3	1.74	1.76	-	2.62	2.64	2.18	2.20	2.61	2.53	5.87	6.10		3.58	2.42	2.46	1.86	1.86
FeO	29.38	29.72	-	26.41	26.60	23.55	23.75	18.57	17.99	30.70	31.94		43.78	27.46	27.92	25.93	25.96
MnO	.43	.44	-	.44	.44	.41	.42	.38	.37	.49	.51	.57	.58	.44	.44	.44	.44
MgO	19.75	19.98	-	20.14	20.28	22.27	22.46	14.53	14.09	16.23	16.89	18.11	18.39	15.30	15.56	22.80	22.82
CaO	6.16	6.23	-	5.32	5.36	5.27	5.31	15.97	15.48	4.32	4.49	.49	.50	10.25	10.42	5.47	5.47
Na_2O	.10	.10	-	.05	.05	.12	.12	.12	.11	.07	.07	.01	.01	.10	.10	.18	.18
K_2O	Tr	Tr	-	n.d.	n.d.	Tr	Tr	n.d.	n.d.	.01	.01	n.d.	n.d.	n.d.	n.d.	.04	.04
P_2O_5	.03	.03	-	.03	.03	.03	.03	.04	.04	.03	.04	.02	.02	.03	.03	.05	.05
Cr_2O_3	.47	-	(19.28) ?	.42	-	.41	-	.33	-	.51	-	.12	-	.07	-	.08	-
NiO	.35	-	-	.10	-	.16	-	.20	-	.08	-	.14	-	.07	-	.05	-
L.O.I.	1.30	-	-	1.28	-	.76	-	(-.02)	-	.82	-		-	1.30	-	1.85	-
TOTAL	100.96	100.00	-	101.00	100.00	100.51	100.00	103.72	100.00	97.54	100.00		100.00	99.77	100.00	101.91	100.00
ppm																	
Cr	3213		-	2893		2773		2235		3495		828		497		562	
V	144		(13242) ?	844		480		256		3341		978		840		1043	
Co	242		328	212		193		198		256		377		238		165	
Ni	2718		1321	764		1268		1562		601		951		522		325	
Cu	650		627	290		265		88		411		999		836		552	
Zn	142		669	149		146		167		217		190		135		94	
Sc	38		43.8	47.4		47.1		42.3		55.3		18.9		88.9		130	
Nb	n.d.		n.d.	n.d.		n.d.		n.d.		n.d.		n.d.		n.d.		n.d.	
Zr	46.1		14.1	7.9		7.3		8.7		17.0		4.5		13.2		15.7	
Y	12.1		8.3	8.7		8.5		9.2		7.4		n.d.		13.2		17.3	
Sr	12		6.1	4.1		14.8		14.0		7.7		n.d.		9.2		17.3	
Rb	n.d.		n.d.	n.d.		n.d.		n.d.		n.d.		8.8		n.d.		n.d.	

	AM-1		AM-2		AM-4A		AG-4		AG-5		AU-6		AK-1B		AK-2	
wt.%																
SiO_2	51.62	51.78	33.33	33.84	44.37	44.82	33.81	34.91	41.49	41.69	39.39	40.03	46.30	46.96	46.64	48.82
TiO_2	.29	.29	7.27	7.38	5.27	5.32	.93	.96	2.04	2.06	4.74	4.82	.80	.81	.96	1.00
Al_2O_3	3.98	3.99	1.11	1.13	2.32	2.34	.40	.42	3.11	3.12	1.30	1.32	3.07	3.11	5.73	6.00
Fe_2O_3	1.79	1.79	8.77	8.90	6.77	6.84	2.43	2.51	3.54	3.56	6.24	6.34	2.30	2.33	2.46	2.57
FeO	13.00	13.04	25.29	25.68	10.83	10.94	38.12	39.35	21.84	21.95	20.87	21.21	20.37	20.66	13.34	13.96
MnO	.26	.26	.38	.39	.23	.24	.48	.49	.33	.34	.32	.33	.34	.34	.27	.28
MgO	23.74	23.81	15.29	15.53	11.48	11.59	17.63	18.20	14.75	14.82	13.86	14.08	18.64	18.91	10.28	10.76
CaO	4.77	4.78	6.97	7.08	17.45	17.63	3.02	3.11	12.29	12.35	11.58	11.76	6.56	6.65	15.05	15.76
Na_2O	.24	.24	.06	.07	.18	.18	.04	.04	.09	.09	.09	.09	.20	.20	.43	.45
K_2O	.02	.02	n.d.	n.d.	.08	.08	Tr	Tr	.02	.02	n.d.	n.d.	.02	.02	.30	.31
P_2O_5	n.d.	n.d.	.01	.01	.02	.02	Tr	.01	.01	.01	.02	.02	.01	.01	.09	.10
Cr_2O_3	.43	-	.44	-	.08	-	.02	-	.41	-	-	-	.47	-	.06	-
NiO	.25	-	.10	-	.03	-	.05	-	.23	-	.08	-	.14	-	.02	-
L.O.I.	1.05	-	1.04	-	.82	-	2.18	-	.18	-	.93	-	1.33	-	1.39	-
TOTAL	101.43	100.00	100.06	100.00	99.93	100.00	99.11	100.00	100.33	100.00	99.41	100.00	100.54	100.00	97.00	100.00
ppm																
Cr	2922		2986		517		130		2792		-		3186		427	
V	167		2466		1526		286		347		-		377		321	
Co	109		223		119		263		193		-		155		89	
Ni	1959		812		252		429		1846		656		1135		163	
Cu	1228		379		274		590		282		327		376		77	
Zn	117		177		74		213		155		102		144		(4) ?	
Sc	35.5		67.9		149		33.7		45.6		107		48.8		98.0	
Nb	n.d.		8.5		8.7		n.d.		n.d.		6.4		n.d.		n.d.	
Zr	6.1		24.0		34.0		7.2		10.6		26.4		11.6		28.8	
Y	9.5		11.3		20.7		8.0		11.8		15.2		10.2		24.0	
Sr	51		6.7		23		4.1		7.6		11		34.5		88	
Rb	n.d.		n.d.		3.2		n.d.		n.d.		n.d.		n.d.		12.4	

Fe_2O_3 estimated by the method of Irvine and Baragar (1971).

Samples 27-D1, 27-D2, 27-D3, 27-F1, AM-2, AG-4, AG-5, AU-6, AK-1B, and AK-2 of partially replaced Merensky Reef. (they are not iron-rich ultramafic pegmatite sensu strictò).

Sample 27-C1 is the partially replaced Merensky upper chromitite layer.

Other hybrid pegmatite-cumulate samples on this page - 27-B1, AM-1

TABLE 12.2 XRF ANALYSES OF WHOLE-ROCK SAMPLES OF IRON-RICH ULTRAMAFIC PEGMATITE FROM THE MIDDELLAAGTE PIPE

	M.27-1		M.27-2		M.27-3		M.27-4		M.27-5		M.27-6		M.27-7		M.29-1	
wt.%																
SiO_2	35.01	35.31	37.17	36.75	32.47	32.63	42.86	42.50	32.30	32.42	35.70	35.79	42.80	41.97	40.52	40.46
TiO_2	4.61	4.65	4.65	4.60	6.76	6.79	2.70	2.68	6.18	6.21	4.59	4.60	3.80	3.72	2.94	2.94
Al_2O_3	.76	.77	.97	.96	1.22	1.22	1.26	1.25	.52	.52	1.07	1.07	1.08	1.06	1.98	1.98
Fe_2O_3	6.11	6.17	6.15	6.08	8.19	8.23	4.20	4.17	7.68	7.71	6.09	6.11	5.30	5.19	4.44	4.44
FeO	29.77	30.08	28.13	27.81	23.73	23.86	21.72	21.53	32.05	32.17	28.75	28.83	20.85	20.45	22.69	22.66
MnO	.52	.53	.52	.51	.37	.37	.41	.40	.60	.60	.48	.48	.45	.44	.39	.39
MgO	14.16	14.28	14.87	14.70	16.26	16.34	13.58	13.47	15.33	15.39	14.15	14.19	14.55	14.27	14.43	14.41
CaO	7.97	8.04	8.40	8.30	10.25	10.30	13.75	13.63	4.81	4.83	8.64	8.66	12.77	12.49	12.61	12.59
Na_2O	.18	.18	.25	.25	.21	.22	.31	.31	.10	.10	.23	.23	.31	.30	.09	.09
K_2O	n.d.	n.d.	.02	.02	.01	.01	.02	.02	Tr	Tr	.01	.01	.02	.02	n.d.	n.d.
P_2O_5	.05	.05	.05	.05	.03	.03	.05	.05	.04	.04	.03	.03	.05	.05	.05	.05
Cr_2O_3	.05	-	.04	-	.18	-	.05	-	.05	-	.07	-	.05	-	.17	-
NiO	.04	-	.04	-	.03	-	.03	-	.04	-	.03	-	.03	-	.04	-
L.O.I.	.37	-	.40	-	.44	-	.65	-	(-.09)	-	.30	-	.26	-	.90	-
TOTAL	99.62	100.00	101.64	100.00	100.15	100.00	101.58	100.00	99.62	100.00	100.14	100.00	102.32	100.00	101.26	100.00
ppm																
Cr	396		296		1231		332		324		509		417		1179	
V	1489		1117		3215		1359		1330		1744		1144		1092	
Co	137		214		184		164		255		224		158		203	
Ni	285		296		260		214		322		269		262		287	
Cu	43		36		38		31		21		23		29		227	
Zn	192		168		212		131		209		179		125		110	
Sc	84.5		86.6		110		107		65.2		87.8		101		112	
Nb	Tr		n.d.		n.d.		n.d.		n.d.		3.6		3.0		n.d.	
Zr	22.1		22.3		25.7		20.6		21.9		19.1		24.4		10.8	
Y	13.6		14.0		13.5		29.2		7.4		12.7		29.0		10.1	
Sr	14.4		16.5		10.2		19.2		6.2		13.8		19.7		9.4	
Rb	n.d.		n.d.		n.d.		n.d.		n.d.		n.d.		n.d.		n.d.	

	M.24-1		M.24-2		M.24-3		M.24-4		M.24-5		M.24-6		M.24-7		M.24-8	
wt.%																
SiO_2	33.35	33.98	40.40	41.38	38.78	39.14	40.71	41.44	48.85	49.06	50.48	50.89	44.68	45.45	34.14	34.79
TiO_2	1.22	1.24	1.50	1.54	1.74	1.76	2.01	2.05	.37	.38	.29	.29	.35	.36	.82	.83
Al_2O_3	.66	.67	1.35	1.39	2.37	2.39	2.03	2.07	1.94	1.95	3.64	3.67	1.60	1.63	1.14	1.17
Fe_2O_3	2.72	2.77	3.00	3.08	3.24	3.27	3.51	3.57	1.87	1.88	1.79	1.81	1.85	1.88	2.31	2.40
FeO	39.07	39.80	25.98	26.61	28.94	29.20	24.35	24.79	13.01	13.07	9.15	9.23	18.56	18.88	39.19	39.94
MnO	.52	.53	.39	.40	.40	.41	.38	.38	.31	.31	.23	.23	.31	.32	.54	.55
MgO	17.26	17.58	14.60	14.95	14.56	14.69	13.36	13.60	18.03	18.11	16.16	16.30	18.62	18.95	17.72	18.06
CaO	2.86	2.91	10.04	10.28	8.44	8.52	11.35	11.56	14.91	14.97	17.04	17.18	12.05	12.25	1.88	1.92
Na_2O	.15	.15	.26	.27	.44	.44	.38	.38	.23	.23	.34	.35	.24	.24	.28	.28
K_2O	.03	.03	.05	.05	.10	.10	.11	.11	.02	.02	.04	.04	.02	.02	.07	.07
P_2O_5	.34	.34	.06	.06	.07	.08	.05	.05	.03	.03	.03	.03	.03	.03	.03	.03
Cr_2O_3	.05	-	.04	-	.06	-	.07	-	.16	-	.18	-	.13	-	.03	-
NiO	.10	-	.05	-	.08	-	.07	-	.06	-	.05	-	.07	-	.09	-
L.O.I.	1.11	-	2.59	-	1.12	-	1.40	-	.71	-	.66	-	.78	-	.63	-
TOTAL	99.42	100.00	100.31	100.00	100.35	100.00	99.76	100.00	100.49	100.00	100.07	100.00	99.28	100.00	98.88	100.00
ppm																
Cr	335		291		379		482		1086		1242		895		210	
V	538		647		789		958		573		619		468		408	
Co	325		210		243		216		128		102		169		309	
Ni	751		402		619		512		471		354		514		622	
Cu	709		341		721		606		22		17		36		321	
Zn	206		150		164		133		83		53		112		220	
Sc	32.9		83.2		85.2		90.0		94.8		85.7		80.7		35.2	
Nb	n.d.		n.d.		n.d.		n.d.		n.d.		n.d.		n.d.		n.d.	
Zr	10.3		20.7		21.6		25.9		12.8		11.7		13.2		15.2	
Y	8.0		14.0		18.3		18.4		23.1		13.6		14.9		8.6	
Sr	9.5		18		26		26		24.7		52		20		18	
Rb	n.d.		n.d.		n.d.		n.d.		n.d.		n.d.		n.d.		n.d.	

TABLE 12.2 (CONTINUED)

	ML24-9		ML24-10		ML24-11		ML24-12		ML26-8		ML26-12		ML26-13		ML22-6	
wt.%																
SiO_2	34.82	35.30	41.69	42.48	41.14	42.13	41.46	41.63	44.53	45.52	45.93	47.19	30.01	32.16	38.53	39.59
TiO_2	3.31	3.35	2.68	2.74	2.75	2.82	2.32	2.33	.12	.12	.11	.11	1.14	1.22	2.47	2.54
Al_2O_3	1.62	1.65	2.22	2.26	1.59	1.63	1.58	1.59	10.57	10.81	2.31	2.38	.51	.55	2.21	2.27
Fe_2O_3	4.81	4.88	4.18	4.26	4.25	4.35	3.82	3.83	1.62	1.66	1.61	1.65	2.64	2.83	3.97	4.08
FeO	31.79	32.24	21.36	21.76	20.83	21.33	23.70	23.80	10.92	11.16	14.56	14.96	36.34	38.94	24.84	25.53
MnO	.43	.44	.35	.36	.41	.42	.44	.45	.20	.20	.27	.28	.48	.51	.32	.33
MgO	13.52	13.70	12.64	12.88	12.17	12.46	13.62	13.67	18.86	19.28	30.06	30.89	17.75	19.02	14.11	14.50
CaO	7.77	7.77	12.40	12.88	14.09	14.43	12.18	12.23	10.40	10.63	2.40	2.45	4.28	4.58	10.63	10.93
Na_2O	.28	.28	.48	.49	.35	.36	.29	.29	.59	.60	.10	.10	.13	.14	.22	.23
K_2O	.07	.07	.09	.09	.03	.03	.05	.05	.02	.02	Tr	Tr	.04	.04	.01	.01
P_2O_5	.22	.22	.05	.05	.04	.04	.15	.15	n.d.	n.d.	n.d.	n.d.	.02	.02	.01	.01
Cr_2O_3	.14	-	.11	-	.10	-	.11	-	.15	-	.19	-	.06	-	.09	-
NiO	.11	-	.04	-	.04	-	.04	-	.08	-	.13	-	.07	-	.04	-
L.O.I.	1.65	-	.76	-	1.03	-	1.03	-	1.64	-	2.94	-	7.15	-	1.77	-
TOTAL	100.53	100.00	99.05	100.00	98.82	100.00	100.77	100.00	99.68	100.00	100.59	100.00	100.61	100.00	99.20	100.00
ppm																
Cr	972		738		710		730		1003		1290		431		598	
V	1521		1313		1194		2000		187		167		728		2398	
Co	319		181		194		182		115		151		329		216	
Ni	838		346		348		309		647		1007		554		332	
Cu	1146		68		63		162		26		33		519		551	
Zn	216		171		175		158		83		121		268		160	
Sc	78.8		108		98.8		115		27.1		23.6		23.1		97.0	
Nb	n.d.		n.d.		n.d.		n.d.		n.d.		n.d.		n.d.		n.d.	
Zr	23.1		25.4		21.1		18.5		4.6		3.3		7.6		17.8	
Y	15.1		21.1		16.3		15.7		4.7		3.4		3.9		15.6	
Sr	19.7		37		28		24		130		26		5.3		14.7	
Rb	n.d.		n.d.		n.d.		n.d.		n.d.		n.d.		n.d.		n.d.	

	ML22-A3		ML22-A10		ML22-A18		ML22-C9		ML22-C12		ML22-7		ML22-10	
wt.%														
SiO_2	36.35	36.66	38.26	38.60	34.81	35.15	43.26	44.03	34.98	34.73	40.26	39.33	37.53	38.20
TiO_2	4.22	4.26	3.88	3.92	3.20	3.23	1.39	1.41	.33	.33	2.52	2.47	1.36	1.39
Al_2O_3	11.63	11.73	6.08	6.13	10.42	10.53	17.74	18.07	1.23	1.22	2.26	2.21	1.33	1.35
Fe_2O_3	5.72	5.77	5.38	5.43	4.70	4.74	2.88	2.94	1.83	1.82	4.02	3.93	2.86	2.92
FeO	19.17	19.33	21.63	21.82	25.96	26.22	10.14	10.33	39.37	39.10	24.05	23.49	29.65	30.18
MnO	.27	.27	.38	.38	.40	.41	.21	.22	.57	.57	.30	.30	.35	.36
MgO	6.10	6.15	9.54	9.62	9.71	9.80	6.39	6.41	19.75	19.62	16.53	16.14	17.02	17.33
CaO	14.57	14.70	13.47	13.59	9.16	9.25	14.68	14.96	2.45	2.44	12.14	11.86	7.93	8.07
Na_2O	.61	.62	.36	.37	.54	.55	1.10	1.12	.13	.13	.23	.23	.16	.17
K_2O	.42	.43	.04	.04	.08	.08	.42	.43	.02	.02	.02	.02	.01	.01
P_2O_5	.08	.08	.11	.11	.06	.06	.09	.09	.05	.05	.04	.04	.04	.04
Cr_2O_3	.03	-	.05	-	.03	-	.02	-	.01	-	.09	-	.04	-
NiO	.02	-	.04	-	.04	-	.01	-	.13	-	.09	-	.08	-
L.O.I.	3.35	-	1.71	-	1.35	-	1.95	-	1.79	-	1.88	-	1.84	-
TOTAL	102.54	100.00	100.93	100.00	100.46	100.00	100.15	100.00	102.63	100.00	104.44	100.00	100.19	100.00
ppm														
Cr	226		351		217		110		82		604		291	
V	1403		1270		1064		796		236		2196		1341	
Co	130		162		174		82		370		222		301	
Ni	182		340		307		97		903		741		546	
Cu	330		1038		654		69		1272		1465		944	
Zn	953		143		167		63		205		246		166	
Sc	72.3		108		40.9		55.1		24.7		107		75.8	
Nb	Tr		n.d.		n.d.		n.d.		4.4		n.d.		n.d.	
Zr	35.0		24.3		13.2		19.6		3.1		24.6		12.8	
Y	17.8		23.6		8.8		13.0		5.4		16.9		11.1	
Sr	150		89		168		330		18.3		16.7		7.8	
Rb	n.d.		n.d.		n.d.		6.1		n.d.		n.d.		n.d.	

Fe_2O_3 estimated by the method of Irvine and Baragar (1971).

Samples ML24-5, -6, -7, -8 of partially replaced orthopyroxene-rich cumulates.

Samples ML22-A3, -A10, -A18 from small pegmatite bodies in the lower main zone.

TABLE 12.3

XRF ANALYSES OF WHOLE-ROCK SAMPLES OF IRON-RICH ULTRAMAFIC PEGMATITE FROM THE SOUTH-WESTERN SECTOR OF THE BUSHVELD COMPLEX

	TLP-1A		TLP-1B		TLP-2		TLP-3		RB-5		BK-1		BK-2		BK-3	
wt.%																
SiO_2	34.43	34.84	34.48	35.85	32.35	32.95	32.01	32.60	35.07	35.61	42.36	43.02	43.71	47.80	29.63	31.14
TiO_2	.36	.36	.23	.24	1.80	1.83	2.91	2.96	6.09	6.18	3.43	3.48	.29	.31	1.84	1.94
Al_2O_3	.08	.08	.17	.17	.97	.99	.53	.54	2.22	2.26	1.40	1.42	3.97	4.34	.06	.07
Fe_2O_3	1.86	1.88	1.73	1.80	3.30	3.36	4.41	4.49	7.59	7.70	4.93	5.00	1.79	1.95	3.34	3.51
FeO	38.16	38.62	37.02	38.50	43.61	44.42	41.92	42.70	25.67	26.06	20.75	21.07	10.22	11.18	46.59	48.97
MnO	.53	.54	.53	.55	.67	.68	.65	.66	.45	.46	.43	.44	.25	.28	.70	.73
MgO	21.17	21.42	19.28	20.05	12.24	12.46	11.91	12.13	13.61	13.82	10.90	11.07	29.06	31.78	12.63	13.28
CaO	1.92	1.94	2.60	2.70	3.15	3.20	3.76	3.83	7.65	7.76	14.17	14.39	2.03	2.22	.30	.32
Na_2O	.03	.03	.02	.03	.08	.08	.05	.05	.11	.11	.08	.08	.05	.05	.01	.01
K_2O	n.d.	n.d.	n.d.	n.d.	n.d.	n.d.	.01	.01	.02	.02	.01	.01	.05	.05	n.d.	n.d.
P_2O_5	.30	.30	.11	.12	.03	.03	.03	.03	.03	.03	.03	.04	.01	.01	.03	.03
Cr_2O_3	.01	-	.01	-	.01	-	.01	-	.05	-	.09	-	1.80	-	.02	-
NiO	.12	-	.16	-	.05	-	.05	-	.02	-	.02	-	.17	-	.03	-
L.O.I.	.71	-	2.75	-	1.33	-	.76	-	.76	-	.77	-	9.11	-	1.79	-
TOTAL	99.67	100.00	99.10	100.00	99.56	100.00	99.01	100.00	99.32	100.00	99.36	100.00	102.52	100.00	96.96	100.00
ppm																
Cr	80		101		73		102		361		602		-		168	
V	260		315		176		262		1175		612		124		217	
Co	298		323		312		335		233		119		100		264	
Ni	970		1263		423		488		179		130		1305		239	
Cu	1459		2174		775		816		182		30		197		62	
Zn	188		355		193		176		157		117		136		223	
Sc	24.4		32.4		42.7		57.8		123		154		15.9		23.9	
Nb	n.d.		n.d.		n.d.		n.d.		n.d.		n.d.		n.d.		n.d.	
Zr	2.7		4.6		9.9		12.1		18.8		14.3		4.0		n.d.	
Y	8.6		8.0		5.7		8.6		8.7		10.0		n.d.		4.6	
Sr	4.2		n.d.		17		6.5		29		13		82		n.d.	
Rb	n.d.		n.d.		n.d.		n.d.		n.d.		n.d.		n.d.		n.d.	

TABLE 12.4 XRF ANALYSES OF WHOLE-ROCK SAMPLES OF IRON-RICH ULTRAMAFIC PEGMATITE FROM THE EASTERN SECTOR OF THE BUSHVELD COMPLEX

	LA-1		LA-2		EB-1		EB-2		EB-4		KLF-17		KLF-18	
wt.%														
SiO_2	30.50	30.61	31.25	31.69	40.65	41.05	42.77	43.15	51.55	52.57	40.56	45.86	46.25	
TiO_2	2.93	2.94	8.01	8.12	2.90	2.93	3.70	3.73	.26	.26	.82	1.45	1.46	
Al_2O_3	.58	.58	2.25	2.28	1.70	1.72	2.22	2.24	5.89	6.01	1.21	1.97	1.99	
Fe_2O_3	4.43	4.45	9.51	9.64	4.40	4.40	5.20	5.24	1.76	1.79	2.28	2.96	2.98	
FeO	39.83	39.97	25.77	26.13	23.02	23.25	17.86	18.02	10.54	10.75	31.25	18.52	18.67	
MnO	.54	.54	.40	.40	.42	.42	.35	.36	.24	.24	.54	.37	.37	
MgO	20.03	20.10	9.81	9.95	12.90	13.02	11.03	11.13	22.73	23.18	14.39	12.22	12.33	
CaO	.80	.80	11.51	11.67	12.90	13.02	15.84	15.98	4.70	4.79	8.41	15.59	15.73	
Na_2O	.01	.01	.09	.09	.12	.13	.12	.13	.37	.38	.11	.18	.18	
K_2O	n.d.	n.d.	n.d.	n.d.	n.d.	n.d.	Tr	Tr	.03	.04	.01	.01	.01	
P_2O_5	.01	.01	.03	.03	.04	.04	.04	.04	n.d.	n.d.	.42	.03	.03	
Cr_2O_3	.43	-	1.42	-	-	-	.16	-	.44	-	-		-	
NiO	.04	-	.03	-	.02	-	.02	-	.07	-	-		-	
L.O.I.	.44	-	.84	-	1.03	-	1.20	-	.73	-	-	.69	-	
TOTAL	100.58	100.00	100.90	100.00	100.07	100.00	100.50		99.31	100.00	100.00	98.84	100.00	
ppm														
Cr	2941		9732		-		1275		3482					
V	2750		2203		-		1698		160					
Co	314		182		-		116		97					
Ni	346		201		180		149		538					
Cu	54		34		29		61		13					
Zn	239		166		115		104		89					
Sc	24.0		153		136		154		37.7					
Nb	n.d.		n.d.		-		n.d.		n.d.					
Zr	6.1		12.6		-		16.0		4.7					
Y	3.2		10.2		-		12.2		7.2					
Sr	n.d.		12		-		16		94					
Rb	n.d.		n.d.		-		n.d.		n.d.					

Fe_2O_3 estimated by the method of Irvine and Baragar (1971).

12.2 COMPOSITIONAL VARIATION DUE TO MODAL EFFECTS

Compositional variation in these rocks may be discussed in conjunction with modal effects related to the principal mineral phases, namely clinopyroxene, olivine, Fe-Ti-(Cr) spinel, ilmenite and base-metal sulphides. Additional modal variation is caused by the presence of relict cumulus minerals, plagioclase, orthopyroxene and chromite. The mineralogy of the samples analysed in this study may be estimated by reference to the CIPW norm (see section 8.4 and Appenedix 6). Because the major ferromagnesian minerals in these samples exhibit only limited compositional range it is useful to summarise average, or typical, analyses of these minerals (Table 12.5). The following sections outline briefly the modal controls on the whole-rock chemistry of these rocks. Informative major and trace element variations are then discussed in detail later in this chapter. Because of the wide range of compositions the following trends are discussed initially only in very broad terms. Furthermore, because of sampling limitations this discussion is restricted to samples from the upper critical zone or lower main zone at Amandelbult.

12.2.1 MAJOR ELEMENTS

The SiO_2 content of iron-rich ultramafic pegmatite typically varies between 35 and 45 wt. percent. Clinopyroxene-rich pegmatite is the most siliceous, whereas the presence of olivine and, of course, Fe-Ti-(Cr) oxides and base-metal sulphides decreases the SiO_2 content. SiO_2 is not a useful parameter for evaluating modal variation.

The TiO_2 content of iron-rich ultramafic pegmatite usually varies between 1 and 5 wt. percent. Small quantities of TiO_2 occur in amphibole and clinopyroxene, but ilmenite and, to a lesser extent, Fe-Ti-(Cr) spinel are the dominant titanium minerals. The high TiO_2 content is a characteristic feature of these rocks and it is a useful indicator for evaluating compositional variations related to modal effects.

The Al_2O_3 content of iron-rich ultramafic pegmatite is usually less than 2 wt. percent, and is often less than 1 wt. percent. In iron-rich ultramafic pegmatite sensu stricto low levels of Al_2O_3 are attributed to amphibole, clinopyroxene and spinel (see Table 12.5), but relict cumulus plagioclase is the principal aluminous phase. Contents of Al_2O_3 in excess of 2 wt. percent are attributed to plagioclase. The low Al_2O_3 content of these rocks is a further characteristic feature, and is obviously related to their ultramafic nature.

TABLE 12.5 AVERAGE MINERAL AND WHOLE-ROCK CHEMISTRY OF "AE" SAMPLES

	OLIVINE	CLINOPYROXENE	ILMENITE	Fe-Ti-Cr SPINEL	AMPHIBOLE	PLAGIOCLASE	WHOLE-ROCK
SiO_2	34.11	51.00	-	-	44.02	47.91	38.97
TiO_2	-	.57	50.32	8.56	2.60	-	3.29
Al_2O_3	-	1.96	.19	3.30	10.87	33.34	1.72
Fe_2O_3	-	-	5.23	44.37	4.74	-	7.03
FeO	46.14	12.33	42.17	38.49	11.86	.45	23.85
MnO	.58	.26	.53	.35	.16	-	.34
MgO	19.09	12.17	1.44	.52	11.16	-	14.05
CaO	.05	21.43	-	-	12.04	16.84	10.58
Na_2O	-	.18	-	-	1.71	1.87	.13
K_2O	-	-	-	-	.62	.06	.02
P_2O_5	-	-	-	-	-	-	.03
Cr_2O_3	-	.07	.14	4.41	.21	-	Tr.*
NiO	.04	Tr.	-	-	-	-	Tr.*
X_{Mg}	.42	.64	-	-	.63	-	.51

Olivine : average of samples AE-8,9,12,20,25,27,28,32; n= 25 (see Tables 9.1, 9.2).
Clinopyroxene : average of samples Ae-9,12,25,28,32,34; n= 26 (see Table 9.2).
Ilmenite : average of samples AE-12,25,28; n = 7 (see Table 10.4).
Fe-Ti-Cr spinel : average of samples AE-12,20,28; n = 10 (see Table 10.5).
Amphibole : average of samples AE-20,28,32; n = 10 (see Table 9.7).
Plagioclase : sample AE-27; n = 3 (see Table 9.6).
Whole-rock : average of AE samples (excluding AE-33A); n = 21 (see Table 12.1).* Whole-rock sample includes trace elements (in ppm) : Cr (797), V (1367), Co (191), Ni (290), Cu (329), Sc (87), Zr (20), Y (14) and Sr (17).

As the name "iron-rich ultramafic pegmatite" suggests, these rocks are extremely rich in total iron, or FeO^T ($FeO^T = FeO + Fe_2O_3$). The FeO^T content may be in excess of 40 wt. percent, but is usually between 25 and 35 wt. percent. In Fe-Ti oxide pegmatite the FeO^T content is obviously much higher (see Chapter 10). FeO^T is present dominantly, in decreasing order of abundance, in Fe-Ti-(Cr) spinel, ilmenite / olivine, and clinopyroxene. Because all the principal minerals in these rocks contain iron, FeO and Fe_2O_3 are not useful parameters for evaluating modal variations. The Fe_2O_3 content of these rocks has been estimated by the method of Irvine and Baragar (1971; see Appendix 5). Fe_2O_3 is concentrated dominantly in Fe-Ti-(Cr) spinel with lesser amounts in ilmenite, amphibole and possibly clinopyroxene.

The MnO content of iron-rich ultramafic pegmatite usually varies between 0.25 and 0.50 wt. percent, with the lowest contents found in clinopyroxene-rich pegmatite and the highest contents in olivine-rich pegmatite. The presence of Fe-Ti-(Cr) oxides does not appreciably affect the MnO content.

Iron-rich ultramafic pegmatite, although extremely rich in FeO^T, also has a high content of MgO. These rocks exhibit a wide range in MgO contents, such that in olivine-rich pegmatite MgO varies between 15 and 20 wt. percent, whereas in clinopyroxene-rich pegmatite it decreases to a minimum of 12 wt. percent. The presence of Fe-Ti oxides also results in a decrease in the MgO

content. These rocks, although highly fractionated with respect to the Mg/Fe ratio are, however, fairly rich in MgO. MgO is a useful indicator for evaluating compositional variations related to modal affects.

In these rocks CaO is almost exclusively found in clinopyroxene. Other pegmatite minerals contain only trace amounts of CaO, although, of course, both amphibole and relict cumulus plagioclase are significant calcium minerals. In olivine-rich pegmatite the CaO content may be as low as 4 wt. percent, although in pure dunitic pegmatite (e.g.,from the Townlands pipe) it is less than 1 wt. percent. In clinopyroxene-rich pegmatite the CaO content is often between 12 and 15 wt. percent. CaO is also a useful indicator for evaluating compositional variations related to modal effects.

The extremely low contents of Na_2O and K_2O are characteristic features of iron-rich ultramafic pegmatite. Low levels of Na_2O are attributed to clinopyroxene and amphibole and K_2O is found exclusively in amphibole and mica. However, contents of Na_2O greater than 0.20 wt. percent, and of K_2O greater than 0.03 wt. percent, are attributed to relict plagioclase.

Iron-rich ultramafic pegmatite from the upper critical zone typically contains less than 0.05 wt. percent P_2O_5. Considering the fractionated nature of these rocks this is surprisingly low. However, apatite becomes a significant component of pegmatites in the main zone (Mitchell, in prep.).

From the foregoing discussion it will be apparent that the various pegmatite assemblages described in Chapter 8 are characterised by different whole-rock chemical signatures. Clinopyroxene-rich pegmatite, compared with other pegmatite assemblages in this study, is characterised by high SiO_2 and CaO contents, moderate MgO, Al_2O_3 and Na_2O contents and low FeO^T, TiO_2 and MnO contents. Olivine-rich pegmatite is characterised by a combination of high FeO^T and MgO contents and low SiO_2, Al_2O_3, TiO_2, and Na_2O contents. Addition of Fe-Ti-(Cr) oxides to these assemblages results in an increase in the bulk content of FeO^T and TiO_2. Contamination by relict plagioclase is evidenced by anomalously high contents of Al_2O_3 and Na_2O. The contents of K_2O and P_2O_5 do not exhibit any modally controlled variation in these samples.

12.2.2 TRACE ELEMENTS

Three approaches have been used in this study to determine the behaviour of the trace elements analysed here, namely electron microprobe data, whole-rock variation diagrams and information from the literature. Electron microprobe data are restricted to trace elements which are present in reasonably high levels in specific minerals. For example, in this study the

following trace element-mineral combinations have been investigated using the electron microprobe: Olivine (Ni); clinopyroxene (Cr); ilmenite (Cr); Fe-Ti--Cr spinel (Cr); orthopyroxene (Cr, Ni); and amphibole (Cr). Typical values for these data are summarised in Table 12.5. The following section documents the behaviour of the trace elements Cr, V, Co, Ni, Cu, Zn, Sc, Nb, Zr, Y, Sr and Rb in relationship to modal variation, using the three techniques outlined above. This section does not attempt to model or offer any explanation for these trends and relevant variation diagrams are not discussed until later in this chapter; the ensuing section is simply an introduction.

Iron-rich ultramafic pegmatites have rather low Cr contents considering their ultramafic character. In olivine-clinopyroxene pegmatite the Cr content typically varies between 300 and 500 ppm, with higher values in this range associated with clinopyroxene-rich assemblages (see Table 12.5). The presence of significant quantities of Fe-Ti-(Cr) oxides obviously has a marked influence on the Cr content, such that pegmatite in which oxides comprise between 10 and 15 modal (or normative) percent typically contain between 1000 and 1500 ppm Cr. This results in a wide range of Cr contents. The Cr content of these rocks is further complicated by the presence of relict cumulus chromite. For example, in hybrid samples of partially replaced Merensky Reef (Table 12.1) the Cr content may exceed 3000 ppm. It is a useful indicator of hybrid pegmatite, assuming that the replaced cumulates contain appreciable chromite. In summary, pegmatite sensu stricto usually contains between 300 and 1500 ppm Cr.

Iron-rich ultramafic pegmatite is characterised by extremely high V contents, which typically vary between 500 and 3000 ppm. Low V contents are associated with olivine-rich pegmatite (dunitic pegmatite may contain less than 200 ppm V), moderate values are associated with clinopyroxene-rich pegmatite and maximum V contents are related to Fe-Ti-(Cr) oxides. Vanadium is concentrated, in decreasing order of abundance, in spinel and clinopyroxene, with only very low concentrations in olivine and ilmenite.

The Co content of these rocks is usually between 150 and 250 ppm, and does not exhibit extensive variation. Cobalt is present, in decreasing order of abundance, in base-metal sulphides, olivine and clinopyroxene. Fe-Ti-(Cr) oxides may contain low levels of Co. Olivine-rich pegmatite is richer in Co than clinopyroxene-rich pegmatite and, if accessory sulphides are absent, Co may be a useful guide to modal variation.

Iron-rich ultramafic pegmatite is characterised by fairly low levels of Ni, which is preferentially present in sulphides and olivine, with only very low concentrations in clinopyroxene. Typical Ni contents are between 200 and

500 ppm Ni, with levels in excess of this attributed to unusual concentrations of base-metal sulphide.

Copper in these rocks may be attributed almost exclusively to base-metal sulphides, such that in sulphide-poor samples the Cu content is probably less than 30 ppm. In sulphide-rich samples it may increase to over 1000 ppm, although values of between 150 and 500 ppm are probably typical. Copper may be considered as an incompatible element with respect to the silicate and oxide constituents of these rocks.

The Zn content of iron-rich ultramafic pegmatite is usually between 100 and 200 ppm. Zinc is probably dominantly found in olivine with lesser amounts in clinopyroxene and only minor amounts in oxides and sulphides.

In these rocks Sc is preferentially concentrated in clinopyroxene and Fe-Ti-(Cr) oxides with only very small quantities present in olivine. The Sc content of olivine-rich pegmatite is usually between 40 and 50 ppm, although dunitic pegmatite may contain as little as 24 ppm. Clinopyroxene-rich pegmatite usually contains between 80 and 120 ppm Sc.

Iron-rich ultramafic pegmatite typically contains low Sr contents, a function of its ultramafic character. In iron-rich ultramafic pegmatite sensu stricto the Sr content is usually between 10 and 30 ppm, although in olivine-rich pegmatite it may be less than 10 ppm. Maximum values are associated with clinopyroxene-rich assemblages. The presence of even very small quantities of relict cumulus plagioclase, however, results in major increases in the Sr content.

In iron-rich ultramafic pegmatite Nb, which is usually described as an incompatible element during fractional crystallization of a tholeiitic magma, is usually present in amounts below the lower limit of determination (see Appendix 5). However, in specific samples it may be present in appreciable quantities (e.g., samples AE-21 to AE-32). Again, Zr is an incompatible element and consequently it is only found in very low levels in all but the most highly fractionated ultramafic-mafic rocks. In iron-rich ultramafic pegmatite the Zr content is usually between 10 and 25 ppm. Minimum concentrations are associated with olivine-rich pegmatite and higher values may be related to clinopyroxene- and Fe-Ti-(Cr) oxide-rich assemblages. Thus, Zr is not completely incompatible in these rocks and is subject to some modal control. Yttrium is also an incompatible element; in iron-rich ultramafic pegmatite the Y content is usually between 10 and 20 ppm and, again, high levels are associated with clinopyroxene-rich pegmatite. The Rb content of iron-rich ultramafic pegmatite is usually below the lower limit of determination (see Appendix 5). Occasionally it is found in small amounts, usually less than 10 ppm.

12.2.3 INTERNAL ZONATION WITHIN A SINGLE PEGMATITE BODY

Many of the compositional and modal variations discussed above are evident from studying internal zonation that is found within one particular pegmatite body at Amandelbult. This occurs as a small, sheet-like body that replaces the Footwall cyclic unit (case study (2), "AE" samples; Appendix 1). From petrographic studies it was concluded that this body could be subdivided into four units (or zones) : an upper unit of olivine-rich pegmatite (samples AE-8 to -12), upper central (samples AE-13 to -21) and lower (samples AE-28 to -33A) units of clinopyroxene-rich pegmatite and a core-like unit of "mixed" olivine-clinopyroxene pegmatite (samples AE-23 to -27). The latter are characterised by maximum concentrations of Fe-Ti-(Cr) oxides and may also contain anomalous concentrations of plagioclase (see Chapter 8). Mineralogical studies indicate that the composition of olivine and clinopyroxene is constant within this body, irrespective of modal zonation Whole-rock chemistry is thus controlled essentially by modal variation.

This is apparent from a diagram in which vertical height (representing sample positions that were based on a lateral traverse, assuming a dip of 20^{o}, which is that of the layered cumulates; see fig.7.7) is plotted against CIPW wt. percent norms, major element oxides and trace elements (figs. 12.1, 12.2).

Modal olivine exhibits a strong positive correlation with FeO, MgO, MnO, Ni, Co, and Zn, and tends to exhibit a negative correlation with most other elements. Modal clinopyroxene exhibits a strong positive correlation with CaO, SiO_2, Cr, V and Sc and has less clear correlations with TiO_2, Al_2O_3, Na_2O and Sr. Modal Fe-Ti-(Cr) oxides exhibit a positive correlation with TiO_2 (and thus Fe_2O_3), Cr and V. Clinopyroxene and Fe-Ti-(Cr) oxides tend to exhibit a positive correlation with each other, consequently it is difficult to establish which of these minerals exerts the main control on elements such as Cr and V. Relict cumulus plagioclase exhibits a strong positive correlation with Al_2O_3, Na_2O and Sr. K_2O, P_2O_5 and Cu apparently behave incompatibly with respect to these minerals. Nb, Zr and Y are all concentrated within clinopyroxene-rich pegmatite, relative to olivine-rich pegmatite and are also preferentially concentrated within the "core-like" assemblage of this body. This suggests that, although Y and Zr are found in low levels in clinopyroxene, these trace elements are still incompatible and concentrated within the pegmatitic liquid. Nb and Zr may show a slight preference for Fe-Ti-(Cr) oxides, but this is by no means a clear relationship.

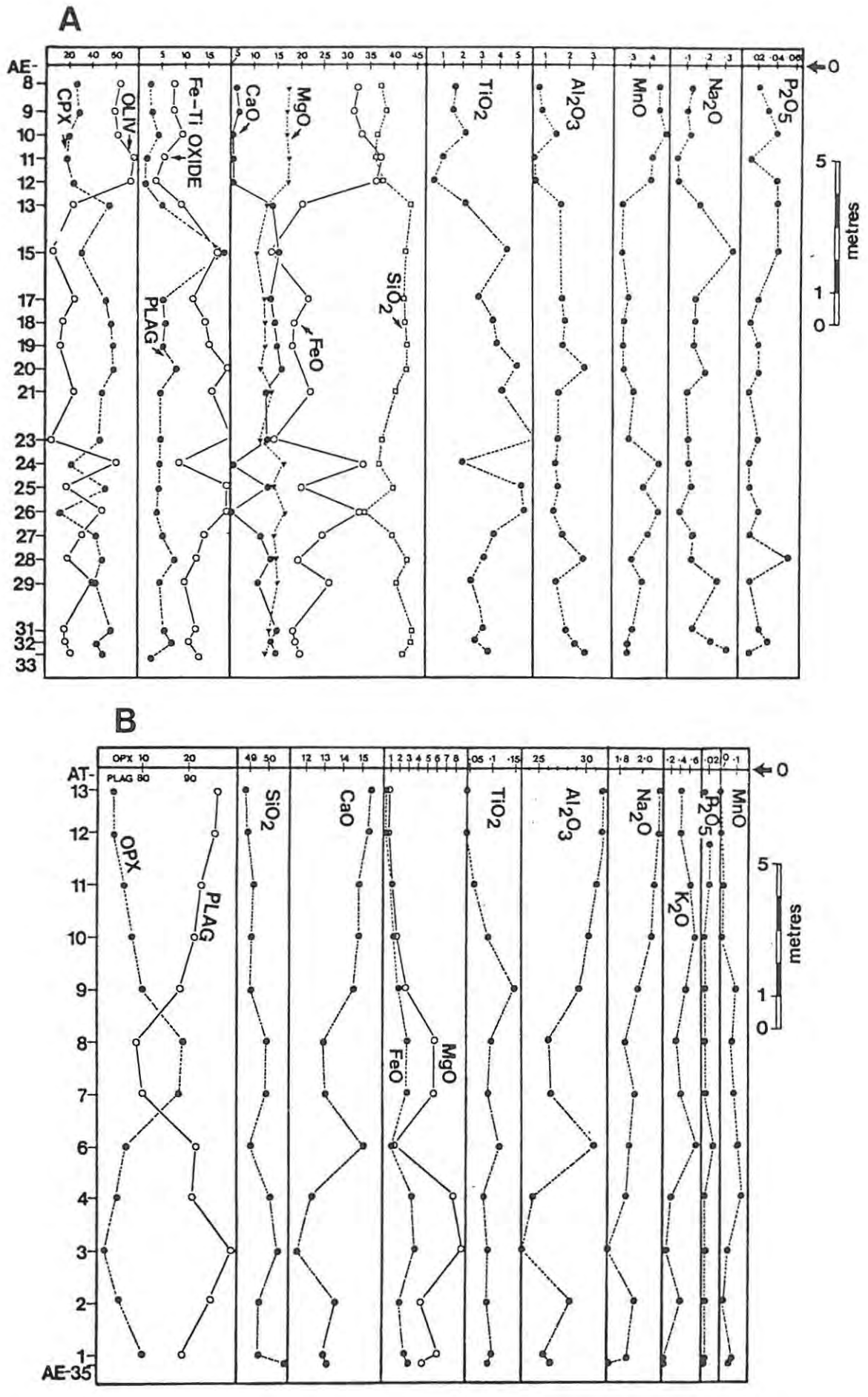

Figure 12.1 Vertical traverses through a pegmatite body (A) and the corresponding cumulate sequence (B). Plots include the wt. % CIPW norms (CPX - clinopyroxene; OLIV - olivine; PLAG - plagioclase; Fe-Ti OXIDE - magnetite + ilmenite; OPX - orthopyroxene) and major element oxides (in wt. %). Pegmatite samples are the "AE" samples (case-study (2)) and the cumulate samples include AT-1 through AT-13 and AE-35. For sample locations see Figure 5.5 and Map 6. The top of both traverses corresponds to the base of the Merensky Reef.

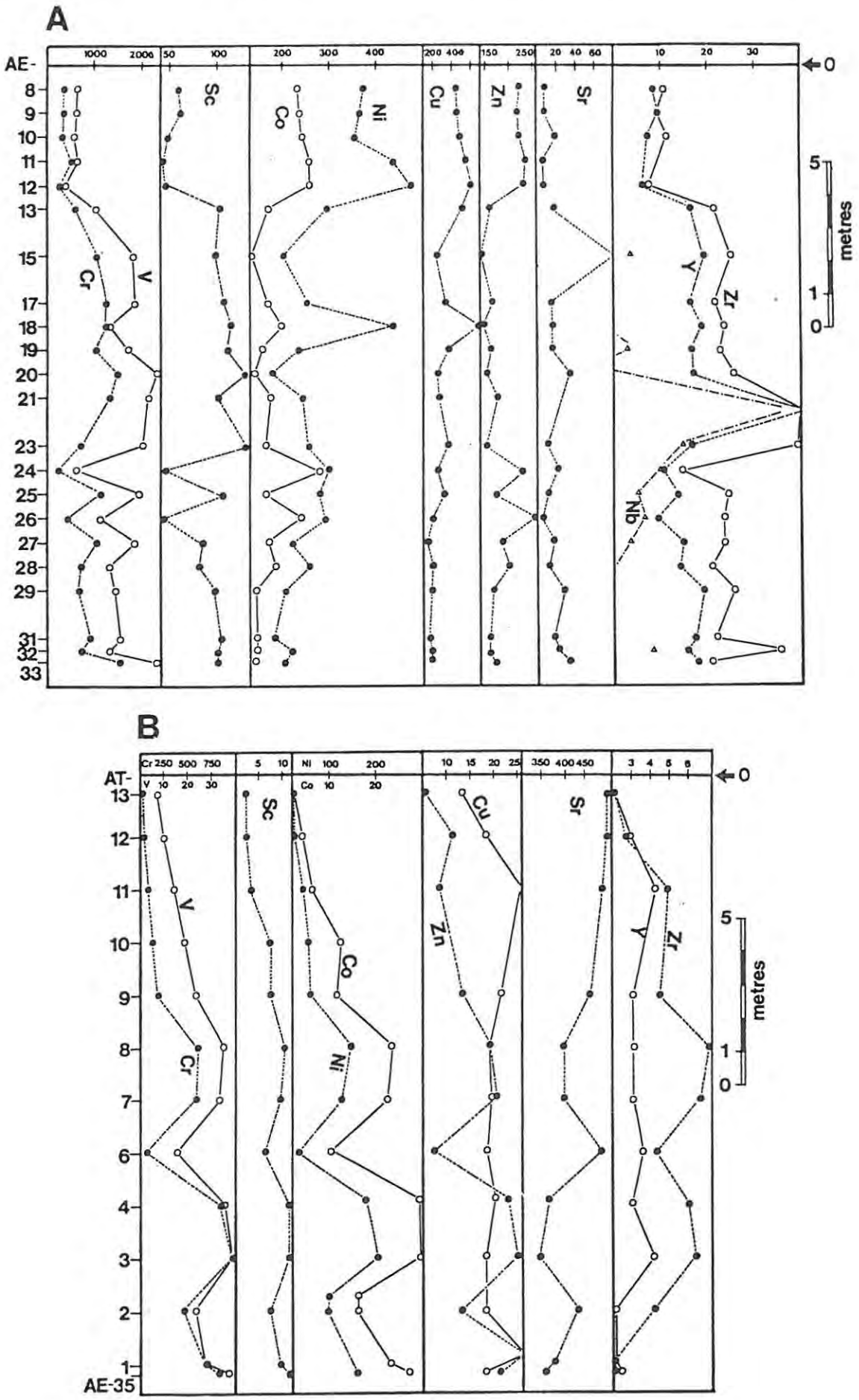

Figure 12.2 Vertical traverses through a pegmatite body (A) and the corresponding cumulate sequence (B). As Figure 12.1 but for selected trace elements (data in ppm).

12.2.4 INTERNAL ZONATION WITHIN LARGE, PIPE-LIKE BODIES

Lateral mineralogical zonation within the MIDDELLAAGTE PIPE has already been described (cf. p. 149). This zonation is also reflected in whole-rock chemistry as, again, mineralogical studies indicate that the composition of olivine and clinopyroxene are constant. Samples from borehole ML27 (drilled into one of the "magnetic cores") are characterised by high contents of TiO_2 and V, a function of the high modal Fe-Ti oxide content of this assemblage. They are further characterised by extremely low Cu values (and subsequently low Ni and Co contents), a feature which is attributed to the paucity of base-metal sulphides in this assemblage (see Chapter 11). In comparison, samples from bore-holes ML 24 and ML 26 are similar to those from small pegmatite bodies at Amandelbult. In these latter bore-holes a number of samples (ML24-5,-6,-8 and ML26-12) represent hybrid pegmatite-cumulate rocks in which relict orthopyroxene (note high whole rock MgO contents) and plagioclase occur.

The mineralogy of the TOWNLANDS PIPE has also been referred to previously (cf. p. 123). This pipe differs from others examined in that two compositional ranges of olivine (and clinopyroxene) are found (cf. p. 153). Samples from bore-hole TLP-1 are applicable to this study as the composition of olivine here is typical for pegmatite from a body in the upper critical zone. This assemblage may be described as an hortonolite dunite pegmatite; it is much more olivine-rich than pegmatite at Amandelbult and is consequently of considerable interest. However, pegmatite from boreholes TLP-2 and TLP-3 is much more fractionated with respect to the Mg/Fe ratio, and is not discussed here.

12.3 COMPARISON WITH THE CHEMISTRY OF THE HOST CUMULATES

Field relationships and detailed petrographic studies indicate that, at least in part, iron-rich ultramafic pegmatites were formed by replacement of their cumulate hosts. Metasomatic contact features are evident, but if a replacement origin is favoured for the main body of pegmatite, mineralogical studies indicate that this has occurred at magmatic temperatures. If this reasoning is correct it may be argued that the whole-rock chemistry of these rocks is influenced by the composition of the pre-existing cumulates. This line of thought played a major role in influencing selection of samples for analysis. For example, both pegmatites and cumulates from the same height in the layered sequence have been sampled, and a number of samples were selected from the marginal parts of small pegmatite bodies and adjacent cumulates

based on exact "stratigraphic" positions.

However, subsequent petrographic studies indicate that olivine, clinopyroxene and Fe-Ti-(Cr) oxides do not exhibit preferential replacement of any particular cumulus mineral. Not surprisingly, it is concluded from data discussed below that the chemistry of the postcumulus pegmatites is not influenced by that of the pre-existing cumulates (this, obviously, is not applicable to hybrid pegmatite-cumulate rocks). The chemistry of postcumulus pegmatites and neighbouring, pre-existing cumulates has been investigated from a number of data sets.

In the first of these, the "AE" sample group of pegmatites (as discussed above) may be compared with the "AT" sample group, which are based on a traverse through "normal" cumulates at the same height in the layered sequence (see fig. 5.5, Map 6). These data are plotted on diagrams of height versus CIPW norm, major element oxides and trace elements (figs. 12.1, 12.2). Compositional variation in the pegmatites was discussed above. In the cumulates (note that these samples are of the Footwall cyclic unit which does not exhibit any appreciable fractionation; see Chapters 5 and 6) compositional variation is also related to modal effects. Plagioclase exhibits a positive correlation with CaO, Al_2O_3, Na_2O, K_2O and Sr, and orthopyroxene exhibits a positive correlation with SiO_2, FeO, MgO, TiO_2, MnO, Cr, V, Sc, Ni, Co and Zn. Zr and Y show a slight positive correlation with orthopyroxene. Cu, and possibly P_2O_5 are incompatible in this assemblage.

These pegmatites do not therefore appear to exhibit any compositional variation that may be related to the adjacent pre-existing cumulates. In comparison, the pegmatite is enriched in bulk contents of FeO^T, MgO, TiO_2, MnO, P_2O_5, Cr, V, Sc, Co, Ni, Cu, Zn, Nb, Zr and Y; it is depleted in SiO_2, Al_2O_3, Na_2O, K_2O, Sr and possibly, Rb. The CaO content does not show any appreciable overall change.

Further evidence for this is found in large, pipe-like bodies such as Middellaagte and Townlands. Both of these bodies exhibit extensive lateral zonation (see above) but evidence from boreholes suggests that vertical zonation is absent. This statement is made with the proviso that partially replaced cumulates are found in both of these pipes, enclosed by typical pegmatite. This suggests that specific cumulates are preferentially replaced at the expense of others, as described in Chapters 7 and 8. Ignoring these features, it is concluded that large, pipe-like bodies do not exhibit any vertical zonation that may be related to the composition of pre-existing cumulates.

These conclusions have important applications as, if these data are rigorously tested to eliminate hybrid pegmatite-cumulate samples (which

exhibit compositional trends related to both relict cumulus minerals and pegmatite minerals), it may be assumed that the chemistry of iron-rich ultramafic pegmatite is representative of the putative pegmatitic liquid. This assumption is valid whether a magmatic replacement or liquid crystallization model is favoured. Note, however, that this does not necessarily imply that they directly reflect a liquid composition.

12.4 CONTACT FEATURES

Many pegmatite samples from the marginal parts of small bodies may be categorised as hybrid rocks (see discussion on contact relationships in Chapter 8). Secondly, alteration aureoles occur in the wallrocks adjacent to the contacts of many pegmatite bodies. These are characterised by extensive saussuritisation of cumulus plagioclase. A number of samples have been analysed to establish whether any cryptic chemical trends are present in these alteration aureoles. These include samples AC-7 (normal cumulate) and AC-6 (alteration aureole) and AD-27 (normal cumulate) and AD-41A (alteration aureole) From these, and other samples, it is concluded that no bulk chemical changes related to the putative pegmatic liquids are apparent in these contact aureoles (see Appendix 5 for analyses).

12.5 FRACTIONATION INDICES

The Mg-number (atomic percent $Mg/(Mg+Fe^{2+})$) may be a sensitive index of fractionation in tholeiitic rocks, the value of which varies between unity (primitive) and zero (fractionated). This index is modally sensitive as, obviously, all ferromagnesian minerals contribute and it is also affected by the calculation of Fe^{3+}, as Fe^{2+} (not Fe^{T}) is normally used. The Mg-number of iron-rich ultramafic pegmatite in the upper critical zone is typically between 0.55 and 0.46. Higher values are associated with clinopyroxene-rich pegmatite and lower values with olivine-rich assemblages. The presence of significant quantities of Fe-Ti-(Cr) oxides and base-metal sulphides results in anomalously low Mg-numbers. For these reasons it is preferable to use mineralogical data based on electron microprobe analyses (see Table 9.9). The Mg-number of the cumulates in the upper critical zone is typically between 0.81 and 0.78 (it is not as modally dependent as in the pegmatites). Iron-rich ultramafic pegmatite is thus more fractionated than its cumulate hosts for a given position in the cumulate pile.

The felsic index, as defined by Simpson (1954), is the ratio (wt.

percent ($Na_2O + K_2O$)/($Na_2O + K_2O + CaO$)). In rocks in which plagioclase is the major calcic phase (e.g., the upper critical zone cumulates) this index is a useful guide to fractionation. However, in rocks in which both clinopyroxene and plagioclase occur it is of limited value. Furthermore, in ultramafic rocks in which clinopyroxene is a major constituent (e.g., iron-rich ultramafic pegmatite) this ratio approaches zero and is of little use. This is simply a function of the paucity of sodic and potassic phases in these rocks.

These indices may be combined by use of an AFM triangular diagram, in which A represents ($CaO + Na_2O + K_2O$), F represents FeO and M represents MgO. Various other configurations of this diagram have been plotted, omitting CaO from "A", and adding Fe_2O_3 and TiO_2 to "F", for example, but that described above is the most informative. In this diagram the Mg-number may be obtained by extending a line that connects the relevant sample and the "A" apex with the M-F side. (Note that this gives the MgO/FeO ratio and it is necessary to convert this to the atomic ratio $Mg/(Mg + Fe^{2+})$).

In Figure 12.3 thirteen samples of iron-rich ultramafic pegmatite from various localities in the Bushveld Complex are plotted. These samples (labelled 1-13) correspond to analyses (with full sample numbers) presented in Table 8.1 and plotted on a CIPW norm diagram in Figure 8.9. Variation in

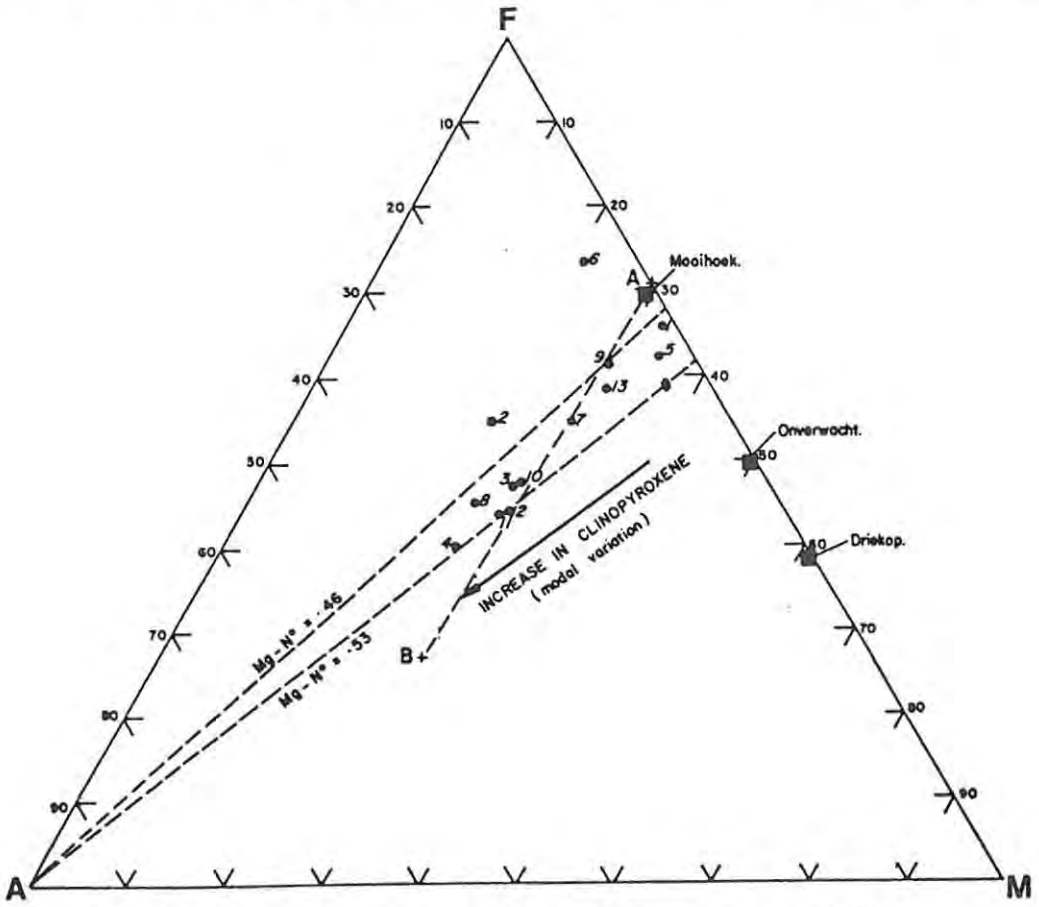

Figure 12.3 Selected samples of iron-rich ultramafic pegmatite plotted on an AFM diagram. A = ($CaO+Na_2O+K_2O$); F = FeO; M = MgO. Sample numbers (1 -13) correspond to those plotted in Figure 8.9 and presented in Table 8.1. Most of these samples plot between the indicated Mg-numbers. Points "A" and "B" represent averages of electron microprobe analyses of olivine and clinopyroxene, respectively.

the chemistry and modal mineralogy of these samples is apparent from reference to these two diagrams. For example, sample 13, a wehrlite pegmatite is richer in FeO and poorer in ($CaO + Na_2O + K_2O$) than, say, sample 8, an Fe-Ti oxide-olivine websterite. However, the Mg-number of these two samples is comparable (Table 8.1). Samples 2 and 6 are, however, atypical; they are characterised by unusually low Mg-numbers (and extremely iron-rich olivine). Scatter in samples which plot between the indicated Mg-numbers is attributable to modal variation. Scatter towards the FeO-MgO side is caused by an increase in olivine and towards the ($CaO + Na_2O + K_2O$) apex relates to an increase in clinopyroxene. Scatter towards the MgO apex may be caused by slight compositional variation from "typical" data. Scatter towards the FeO apex is related to major quantities of Fe-Ti oxide. Electron microprobe analyses (averages) of olivine (position "A") and clinopyroxene (position "B") corroborate that the scatter in this diagram is largely a function of modal variation.

In Figure 12.4 all samples of iron-rich ultramafic pegmatite from Amandelbult, including those from the Middellaagte pipe, are plotted on an AFM diagram. Three broad sample groups may be recognised: (1) "typical" pegmatite from the upper critical- lower main zone. These plot in a fairly

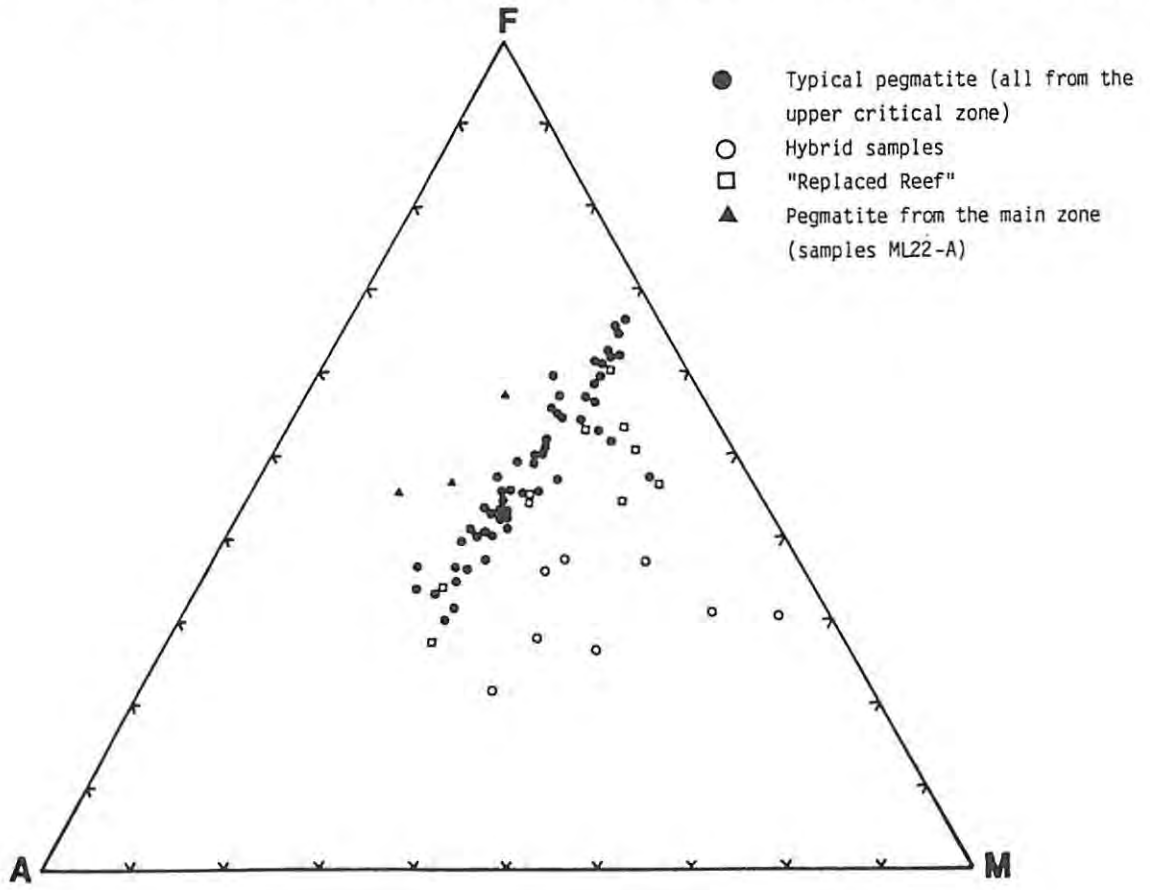

Figure 12.4 All samples of iron-rich ultramafic pegmatite from Amandelbult plotted on an AFM diagram. $A = (CaO+Na_2O+K_2O)$; F = FeO; M = MgO. Pegmatites from the upper critical zone plot in a linear field (as defined by the Mg-number - see Figure 12.3), hybrid samples plot towards the M-apex (the cumulates have a much higher Mg-number - see Figure 6.5) and pegmatite from the main zone plot towards the F-apex (they have a lower Mg-number.

tightly controlled linear field, within which the Mg-number varies, due to modal effects, between extremes equivalent to olivine (X_{Mg} = 0.49 - 0.42) and clinopyroxene (X_{Mg} = 0.65 - 0.62). Typically it is between 0.55 and 0.46. Again, scatter off this trend towards the FeO apex is caused by large quantities of Fe-Ti-(Cr) oxide; (2) hybrid pegmatite-cumulate rocks, in which relict cumulus minerals may be recognized. These all plot towards the MgO apex and are characterised by higher Mg-numbers. They produce a scattered distribution which is dependent on modal effects. It may be expected that they would plot in a wedge-shaped field, in which the base of the wedge corresponds to the cumulate trend (with a high Mg-number; see fig. 6.5) and the top of the wedge corresponds to the pegmatite trend above; (3) pegmatite from the main zone (samples ML 22-A3, A10, A18) is characterised by much lower Mg-numbers; consequently these samples plot closer to the FeO apex.

12.6 SELECTED TRACE ELEMENT MODELLING

In this section specific trace elements have been selected for more detailed modelling. These are divided into four groups, based on the modal controls discussed above : (1) Cr, V and Sc, whose distribution is predominantly related to clinopyroxene and Fe-Ti-(Cr) spinel; (2) Ni, Cu and Co, whose distribution is controlled by ferromagnesian silicates, specifically olivine, and base-metal sulphides; (3) Sr, whose distribution is controlled dominantly by plagioclase; and (4) Zr and Y, the so-called "incompatible elements".

Four major element oxides have been selected as indicators of modal variation, namely MgO (olivine), CaO (clinopyroxene), TiO_2 (Fe-Ti-(Cr) oxides) and Al_2O_3 (plagioclase). These parameters are then plotted against certain of the above trace elements on binary graphs. In each of these diagrams three data sets may be recognized : (1) typical pegmatite from the upper critical - lower main zone at Amandelbult, including samples from the Middellaagte pipe, and pegmatite from borehole TLP-1 from the Townlands Pipe (but excluding other samples); (2) cumulates from the upper critical zone at Amandelbult which host the pegmatites; and (3) hybrid, pegmatite-cumulate samples.

The trace element chemistry of iron-rich ultramafic pegmatite is rather complicated and only limited modelling can be attempted with these data. This is partly a function of the mineralogy of these rocks (e.g., due to the presence of oxides and sulphides), but is also constrained by a sample population that demonstrates only very limited fractionation trends.

12.6.1 Cr, V AND Sc

In iron-rich ultramafic pegmatite Cr, V and Sc (which all occur dominantly in the trivalent state) exhibit similar modal controls : their distribution is related to clinopyroxene, Fe-Ti-(Cr) spinel and to a lesser extent olivine. They do not exhibit any chalcophile characteristics and are almost totally rejected by plagioclase. In ultramafic-mafic rocks in which spinel and sulphide phases are absent the distribution of these elements may be closely related to that of Ni and Co. For example, in orthopyroxene-plagioclase and olivine-plagioclase cumulates V and Sc exhibit a positive correlation with Co (fig. 6.6). However, in the pegmatites Ni and Co are influenced by both ferromagnesian silicates and sulphides.

MODAL CONTROLS ON Cr

From a binary graph of wt. percent MgO versus ppm Cr two "cumulus" trends (i.e. related to samples of upper critical zone cumulates) are recognized (fig. 12.5A). Firstly, a straight line, representing a mixing line between plagioclase and orthopyroxene, may be constructed for plagioclase-orthopyroxene cumulates. Scatter from this line is related to accessory chromite. Secondly, samples of harzburgites plot in a small cluster. Samples of iron-rich ultramafic pegmatite plot in a broad field, in which the MgO content is between 19 and 11 wt. percent and the Cr content is between 100 and 1600 ppm. This is a negative trend, the inclined part of which represents a mixing line between olivine and clinopyroxene. Scatter from this line is caused by the presence of accessory Fe-Ti-(Cr) spinel. This trend flattens out at approximately 11 wt. percent MgO and 800 ppm Cr; samples which contain more than 800 ppm Cr contain significant Fe-Ti-(Cr) spinel. Similar features are also evident from a graph of wt. percent CaO versus ppm Cr (fig. 12.5B), although the "pegmatite" trend here has a positive correlation and is relatively poorly defined. The modal control exhibited by Fe-Ti-(Cr) spinel is evident from a plot of wt. percent TiO_2 versus ppm Cr (fig. 12.5C). In this diagram samples of the cumulates have been omitted as they all contain less than 0.20 wt. percent TiO_2. Two "pegmatite" trends are recognized : a positive correlation which is related to modal increase in Fe-Ti-(Cr) spinel and a trend, parallel to the TiO_2-axis, which may be related to modal increase in ilmenite. The Cr content of these oxides was investigated by mineralogical analysis (see Chapter 10). In Figure 12.5C hybrid pegmatite-cumulate samples define two trends which may be related to the presence of relict cumulus orthopyroxene and chromite.

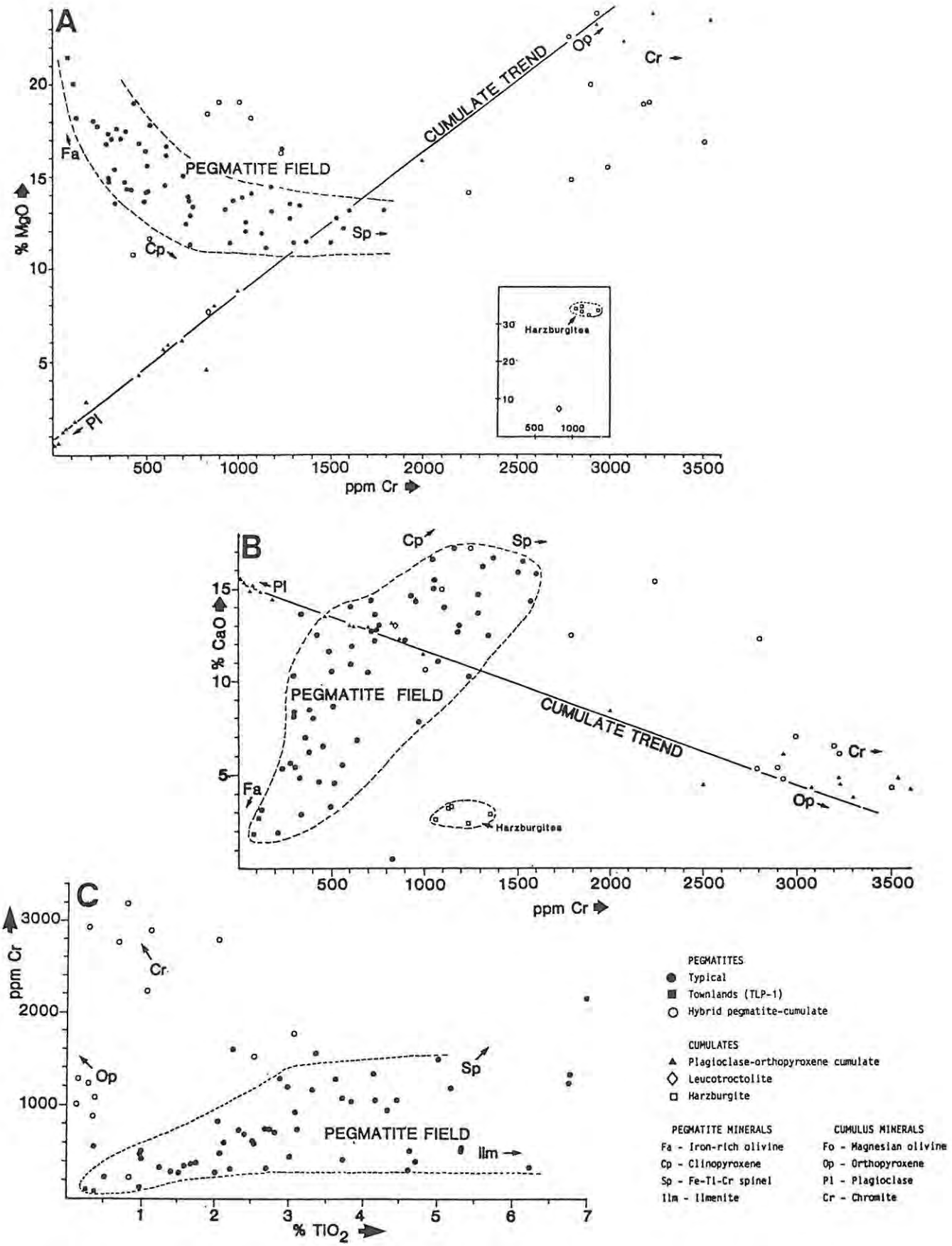

Figure 12.5 Binary plots of wt. % MgO, CaO and TiO_2 vs. ppm Cr.

"A" and "B" include samples of pegmatites and their cumulate hosts, all from the upper critical zone at Amandelbult (plus 2 samples from Townlands). Samples of the cumulates may be divided into two groups, plagioclase-orthopyroxene cumulates (these plot on a straight line) and olivine-bearing cumulates (the latter are plotted as an inset in "A"). Samples of the pegmatites may also be divided into two groups, pegmatite sensu stricto and pegmatite-cumulate hybrids; the former plot in a reasonably well constrained field, but the hybrid samples scatter between this field and the cumulate trend. Scatter from these fields or linear trends may be related to modal variation, as indicated e.g., "Cp" refers to modal control by clinopyroxene in direction indicated by the arrow. In "C" samples of the cumulates have not been plotted; scatter from the pegmatite field here may be related to the presence of relict cumulus orthopyroxene and chromite.

MODAL CONTROLS ON V

From a binary plot of wt. percent MgO versus ppm V it is evident that the pegmatites are much richer in V than the host cumulates (fig. 12.6A). Two "cumulus" trends may be recognized: plagioclase-orthopyroxene and plagioclase-olivine mixing lines. The V content of the cumulates does not seem to be affected by the presence of accessory chromite, as in these rocks V is dominantly found in orthopyroxene, with lesser amounts in olivine. Plagioclase almost totally rejects V. The pegmatite samples, in which the V content varies between 400 and 3000 ppm or greater, exhibit a negative trend in Figure 12.6A. Hybrid pegmatite-cumulate samples are usually depleted in V as compared with typical pegmatite. The "pegmatite" trend may be interpreted as representing a mixing line between olivine (low V) and clinopyroxene (high V). This trend flattens out at between 1000 and 1500 ppm V, and contents in excess of this, and scatter from the olivine-clinopyroxene mixing line is attributed to Fe-Ti-(Cr) spinel. A binary graph of wt. percent CaO versus ppm V exhibits similar features, but results in a broad positive correlation (fig. 12.6B). The modal control exhibited by Fe-Ti-(Cr) oxides is evident from a plot of wt. percent TiO_2 versus V (fig. 12.6C). This graph exhibits a broad scatter of data points, probably because Fe-Ti-(Cr) spinel has a much higher V/TiO_2 ratio than does ilmenite. The maximum slope on this graph may be attributed to ilmenite and the minimum slope to spinel.

MODAL CONTROLS ON Sc

From a binary plot of wt. percent MgO versus ppm Sc two "cumulus" trends may be recognized, which represent olivine-plagioclase and orthopyroxene-plagioclase mixing lines (fig. 12.7A). Olivine-orthopyroxene-plagioclase cumulates, such as the Merensky Reef, plot between these two trends. Samples of iron-rich ultramafic pegmatite define a broad negative distribution, which may be interpreted as a mixing line between olivine (low Sc) and spinel and clinopyroxene (both high Sc). These trends exhibit less scatter on a graph of wt. percent CaO versus ppm Sc (fig. 12.7B). On this graph, samples of iron-rich ultramafic pegmatite show a positive correlation, which represents a mixing line between olivine and clinopyroxene. Scatter from this line may be caused by Fe-Ti-(Cr) spinel. However, a plot of TiO_2 versus Sc does not exhibit any clear-cut correlation, and it is difficult to assess whether the spinel in these rocks is richer in Sc than is clinopyroxene (fig. 12.7C).

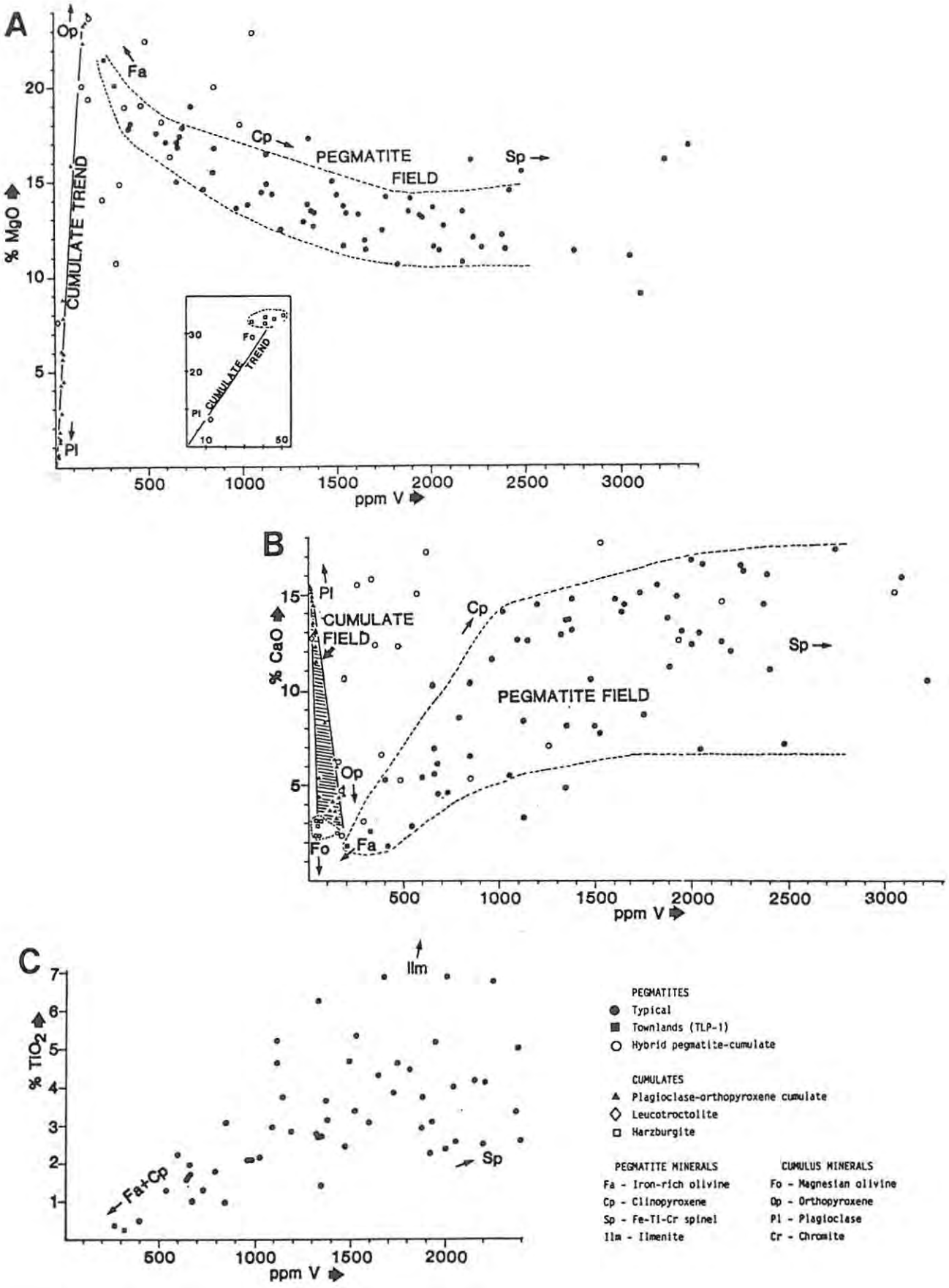

Figure 12.6 Binary plots of wt. % MgO, CaO and TiO_2 vs. ppm V.

"A" and "B" include samples of pegmatites and their cumulate hosts, all from the upper critical zone at Amandelbult (plus 2 samples from Townlands). Samples of the cumulates may be divided into two groups, plagioclase-orthopyroxene cumulates and olivine-bearing cumulates (the latter are plotted as an inset in "A"), both of which define straight lines. Samples of the pegmatites may also be divided into two groups, pegmatite sensu stricto and pegmatite-cumulate hybrids; the former plot in a reasonably well constrained field, whereas the hybrid samples scatter between this field and the cumulate trend(s). In "C" only samples of pegmatites sensu stricto have been plotted.

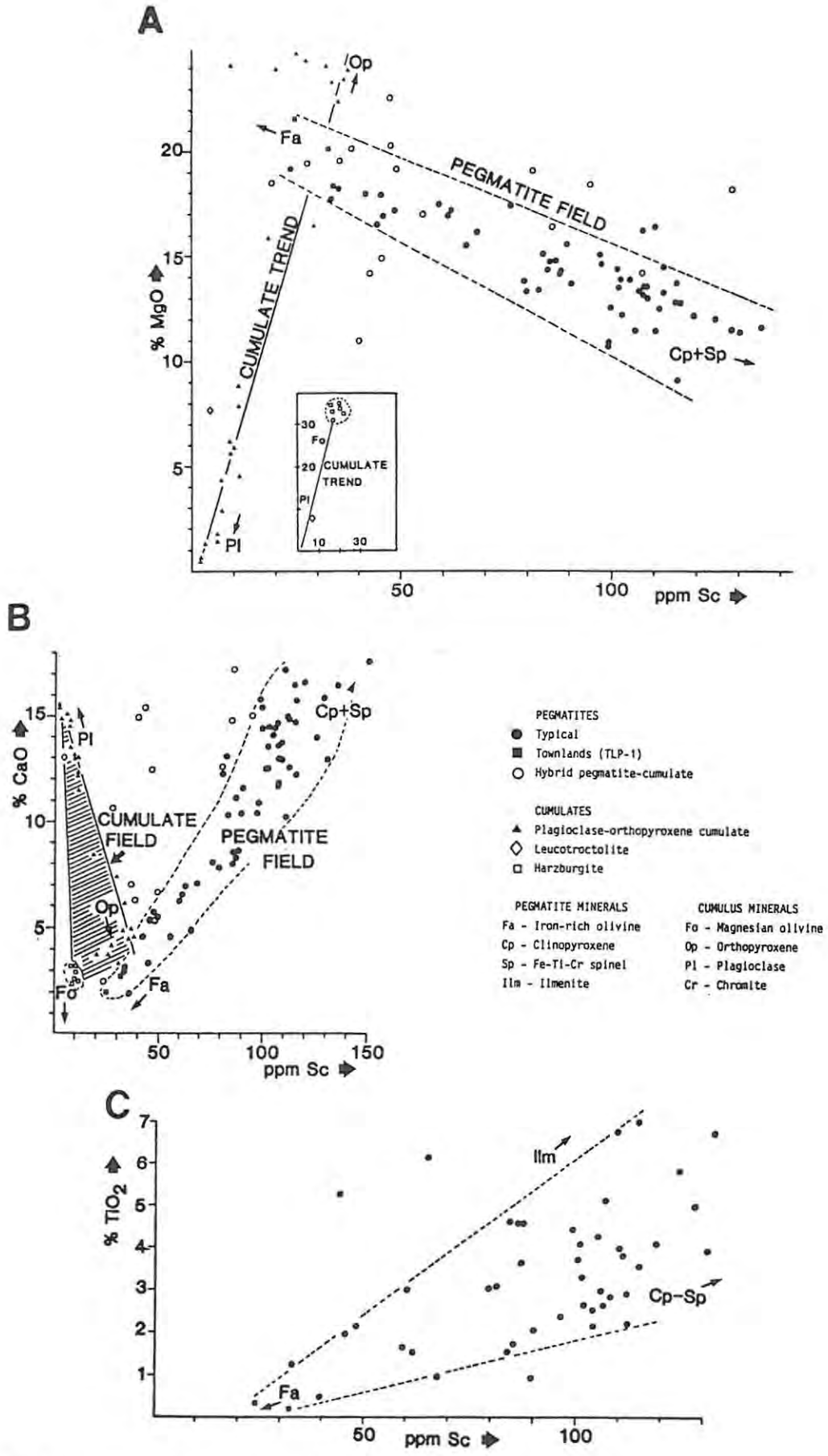

Figure 12.7 Binary plots of wt. % MgO, CaO and TiO_2 vs. ppm Sc.

"A" and "B" include samples of pegmatites and their cumulate hosts, all from the upper critical zone at Amandelbult (plus 2 samples from Townlands). Samples of the cumulates may be divided into two groups, plagioclase-orthopyroxene cumulates and olivine-bearing cumulates (the latter are plotted as an inset in "A"), both of which define straight lines. Samples of the pegmatites may also be divided into two groups, pegmatite sensu stricto and pegmatite-cumulate hybrids; the former plot in a reasonably well constrained field, whereas the hybrid samples scatter between this field and the cumulate trend. In "C" only samples of pegmatite sensu stricto have been plotted.

MINERAL CHEMISTRY AND DISTRIBUTION COEFFICIENTS

(1) Cr

The distribution of Cr between pyroxene and silicate liquid was discussed briefly in Chapter 9 : values of 10 for D^{cpx} and 2 for D^{opx} (after Cox et al., 1979) are suggested. Cox et al., quote a value of 0.2 for D^{oliv}, but other authors suggest values above unity (e.g., 2.7 - Duke, 1976; 3.1 - Paster et al., 1974). D^{plag} is probably very low, and Cox et al. suggest a value of 0.01.

The onset of crystallization of clinopyroxene, because of its high D_{Cr} may arrest the formation of Cr-spinel. Furthermore, Cr is rapidly depleted in a basaltic magma undergoing fractional crystallization such that it is unlikely that Ti-magnetite, which crystallizes late in the history of a cooling magma, would contain appreciable Cr (Eales et al., 1981). The Fe-Ti-(Cr) spinel found in iron-rich ultramafic pegmatite is unique and its formation may be related to the unusual composition of the pegmatitic liquid. Furthermore, it is unusual to find clinopyroxene and Cr-spinel coexisting.

During fractional crystallization clinopyroxene becomes increasingly iron-rich, a trend which is typically accompanied by decreasing levels of Cr. The pegmatitic clinopyroxene contains similar Cr contents to cumulus clinopyroxene with similar X_{Mg} ratios, namely between 0.05 and 0.07 wt. percent Cr_2O_3 (350 - 500 ppm Cr). The spinel is these rocks may contain over 3 wt. percent Cr_2O_3. From Figures 12.6A and 12.6B the Cr-content of the pegmatitic olivine may be estimated at less than 100 ppm. Note that hortonolite dunite (monomineralic olivine rock with no spinel) from Mooihoek contains 41 ppm Cr.

(2) V

Frey et al. (1978) quote values of 1.5 for D^{cpx} and 0.3 for D^{opx}. Duke (1976) quotes a value of 0.05 for D^{oliv} and Leeman et al., (1978) suggest an average value for D^{mag} of 27 (this latter value may be strongly dependent on composition and temperature).

The V content of dunites from the platiniferous ultramafic pipes does not change with composition, and it may be concluded from this, and the discussion above, that the V content of the pegmatitic olivines is probably less than 100 ppm. Data for clinopyroxenite pegmatites at Driekop (in which spinel is absent) indicate that the V content of this clinopyroxene is between 500 and 600 ppm. Data in this chapter do not permit the V content of the pegmatitic clinopyroxene to be calculated, although it may be estimated to be in the range 500-800 ppm. In summary then, in the pegmatites

V is concentrated in spinel, with lesser amounts in clinopyroxene and only very small amounts in olivine.

(3) Sc

The data in this study suggest that Sc is preferentially concentrated in spinel and clinopyroxene, with only minor amounts in olivine. The Sc content of dunites from the platiniferous ultramafic pipes appears to increase as the Fo content of the olivine decreases. Magnesian dunites probably contain less than 10 ppm Sc, whereas hortonolite dunite from Mooihoek contains 18 ppm Sc. A similar value is applicable to olivine-rich pegmatite at Amandelbult, and it may be concluded that the pegmatitic olivine contains a maximum (and possibly much less) of 20 ppm Sc. Clinopyroxene from Driekop may contain from 90 to 100 ppm Sc and, although it is difficult to calculate a definite value, the Sc content of pegmatitic clinopyroxene from Amandelbult may be estimated at between 100 and 120 ppm. If this estimate is correct then it must be inferred that Fe-Ti-(Cr) spinel in these rocks is richer in Sc than is the clinopyroxene.

Paster et al. (1974) quote a value of 0.33 for D^{oliv}, whereas values of 3.1 for D^{cpx} and 1.1 for D^{opx} are presented by Frey et al. (1978). The relative differences between these D's corroborate some of the conclusions reached above. However, published values for D^{mag} (magnetite is the closest "common" spinel to the Fe-Ti-(Cr) spinel in these rocks) vary between less than unity (e.g., Schock (1979) quotes a value of 0.5 and Paster et al. (1974) quote one of 0.73) to 12 (Leeman et al., 1978) or greater. It may be that D^{mag} is strongly dependent on composition and temperature and, of course, is almost certainly dependent on the composition of the spinel phase (e.g., competition with other trivalent cations may play an important role). Furthermore, during prolonged annealing subsolidus re-equilibration between spinels and silicates (such as clinopyroxene) may modify primary trends.

12.6.2 Ni, Cu AND Co

The distribution of these elements in cumulates from the upper critical zone was discussed in Chapter 6. It was concluded that Cu behaves as an almost perfect chalcophile element in these rocks, consequently its distribution is directly related to the presence of base-metal sulphides. In comparison, the distribution of Ni and Co is influenced by both ferromagnesian silicates and base-metal sulphides. From electron microprobe studies of ferromagnesian minerals in iron-rich ultramafic pegmatite it was found that olivine is richer in Ni than clinopyroxene. However, both these

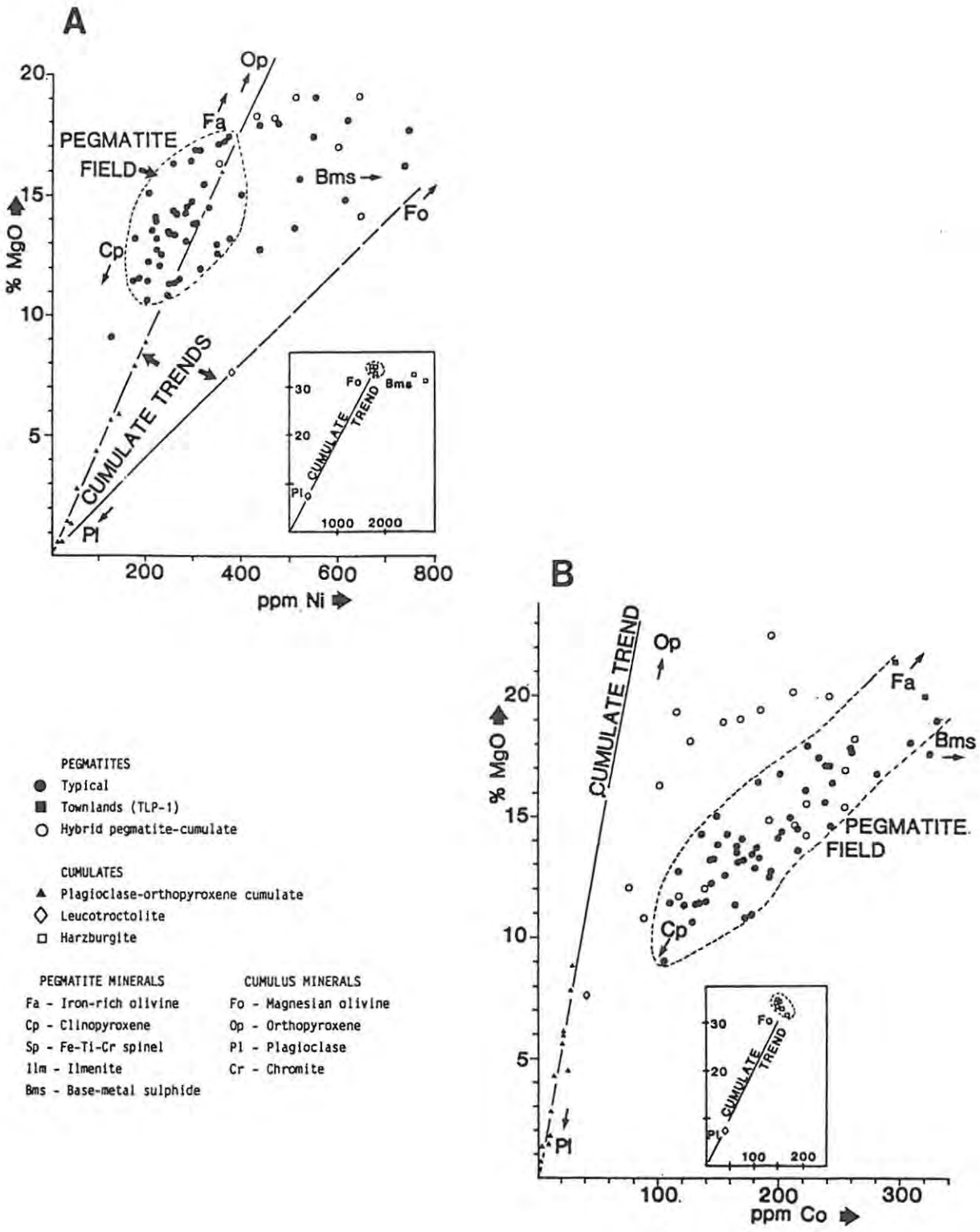

Figure 12.8 Binary plots of wt. % MgO vs. ppm Ni (A) and wt. % MgO vs. ppm Co (B).

These include samples of pegmatites and their cumulate hosts, all from the upper critical zone at Amandelbult (plus 2 samples from Townlands). Samples of the cumulates may be divided into two groups, plagioclase-orthopyroxene cumulates and olivine-bearing cumulates (the latter are plotted as an inset in "A"), both of which define straight lines (these plots exclude sulphide-rich cumulates - for justification of cumulate trends see Figure 6.8). Samples of the pegmatites may also be divided into two groups, pegmatite sensu stricto and pegmatite-cumulate hybrids; the former plot in a reasonably well constrained field, whereas the hybrid samples scatter between this field and the cumulate trends.

minerals contain only low levels of this element, as may be expected from their iron-rich composition (Chapter 9). Similarly, base-metal sulphides in these rocks are characterised by low bulk Ni and Cu contents, although, as compared with cumulus sulphides in the upper critical zone they are rather Co-rich (Chapter 11).

The ferromagnesian silicate control on the distribution of Ni and Co is evident from binary plots of these elements plotted against wt. percent MgO (fig. 12.8). However, compared with the "cumulus" trends the pegmatite trend is poorly developed. Scatter in these samples may be related to the presence of sulphides, which is evident from using Cu as a sulphide-indicator. A plot of MgO versus Cu has not been included here as it exhibits a broad scatter of data points. From Figure 12.8A it may be estimated that pegmatitic olivine contains roughly 450 ppm Ni and clinopyroxene contains roughly 200 ppm Ni (see also electron microprobe data). The Co content of these minerals may be estimated from Figure 12.8B at roughly 300 and 140 ppm, respectively.

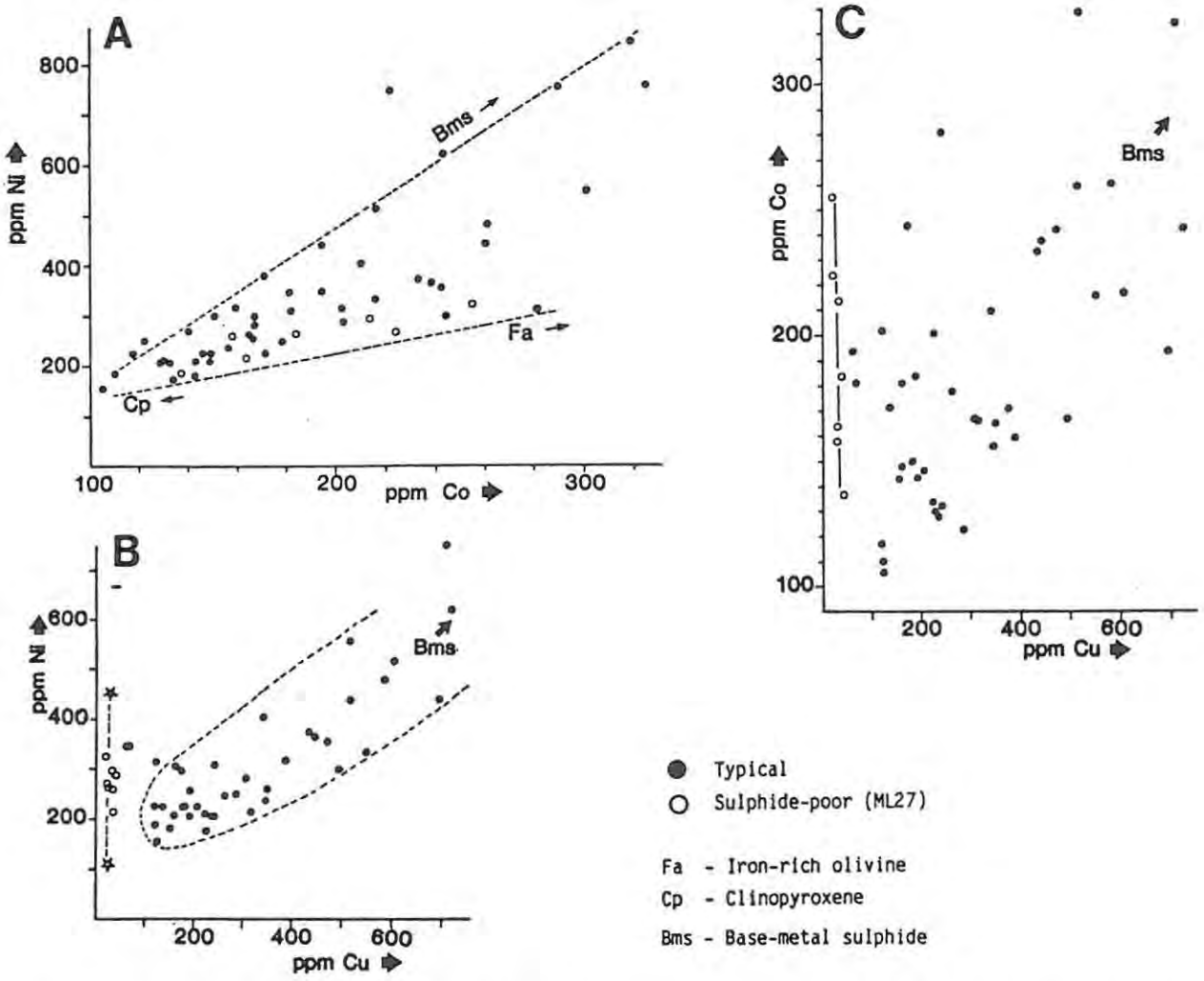

Figure 12.9 Binary plots of ppm Ni vs. ppm Co (A), ppm Ni vs. ppm Cu (B) and ppm Co vs. ppm Cu (C). These include only samples of pegmatite sensu stricto, all from the upper critical zone at Amandelbult. The open star indicates the composition of clinopyroxene, and the solid star the composition of olivine (see text for details).

One group of pegmatites is unusually depleted in sulphide - those from borehole ML 27 (see also Chapter 11). This is evident from petrographic studies and whole-rock Cu contents (Table 12.2). It is suggested that Ni in these samples, which varies from 214 to 322 ppm, and Co, which is between 137 and 255 ppm, may be concentrated almost entirely in olivine and clinopyroxene. Furthermore, the low levels of Cu in these samples, (average 32 ppm) may be attributed to microscopic specks of chalcopyrite in magnetite (see fig. 11.1D). In comparison, sulphide-rich pegmatite from the Middellaagte pipe is found in many samples from boreholes ML 24 and ML 26. Here, Cu is present in sulphides, but Ni and Co occur in both sulphides and silicates.

Plots of Ni versus Cu and Co were found to be of particular use for interpreting the distribution of these elements in the cumulates (fig. 6.8). Samples of iron-rich ultramafic pegmatite are plotted on similar graphs, together with one of Co versus Cu in Figure 12.9. For clarity, the cumulate rocks are not plotted here. Furthermore, samples of hybrid pegmatite-cumulate rocks are also omitted; these would define a scattered distribution (i.e. depleted in Cu and Co, but richer in Ni, than typical pegmatite) between the "cumulus" and "pegmatitic" trends. Unfortunately, similar trends cannot be established with any degree of confidence for the pegmatites. From the plot of Ni versus Cu, sulphide-poor ("ML27" samples) and sulphide-rich (all other samples) pegmatite trends may be established. The sulphide-poor trend represents a mixing line between olivine and clinopyroxene and it can be seen that the Cu content of these minerals is comparable (both very low). Sulphide-rich pegmatite is richer in both Ni and Cu, and a Ni/Cu sulphide ratio of between 0.7 and unity may be estimated (as compared to a ratio of between 1 and 2 for cumulate-hosted sulphides in the upper critical zone). A sulphide-poor mixing line between olivine and clinopyroxene is also evident in a plot of Co versus Cu, but sulphide-rich samples give a scattered distribution such that it is not possible to estimate the Co/Cu ratio of the sulphide. The plot of Ni versus Co also exhibits a scattered distribution of data points, but a sulphide-poor trend between clinopyroxene and olivine is apparent. The Ni/Co ratio of the pegmatitic sulphides, may very roughly be estimated at between 2 and 5 (as compared with a value of 40 for the cumulate-hosted sulphides in the upper critical zone).

12.6.3 Sr

In cumulates from the upper critical zone Sr is concentrated almost exclusively in plagioclase; very minor quantities may occur in orthopyroxene but it is almost totally rejected by olivine (see p. 96). It was also concluded that plagioclase from different cyclic units is characterised by different Sr contents. From Figure 12.10 it can be seen that most samples of iron-rich, ultramafic pegmatite contain less than 3 wt. percent Al_2O_3 and less than 30 ppm Sr. Samples outside of this range contain relict cumulus plagioclase. Although these latter data are restricted to a few samples they plot on a straight line which may be regressed to pure plagioclase containing 33 wt. percent Al_2O_3 (An_{100-80}; see Table 9.6). and roughly 600 ppm Sr. Plagioclase in these rocks is interpreted as partially metasomatised cumulus relicts, thus it may be deduced that progressive increases in the CaO/Na_2O ratio are accompanied by an increase in the Sr content.

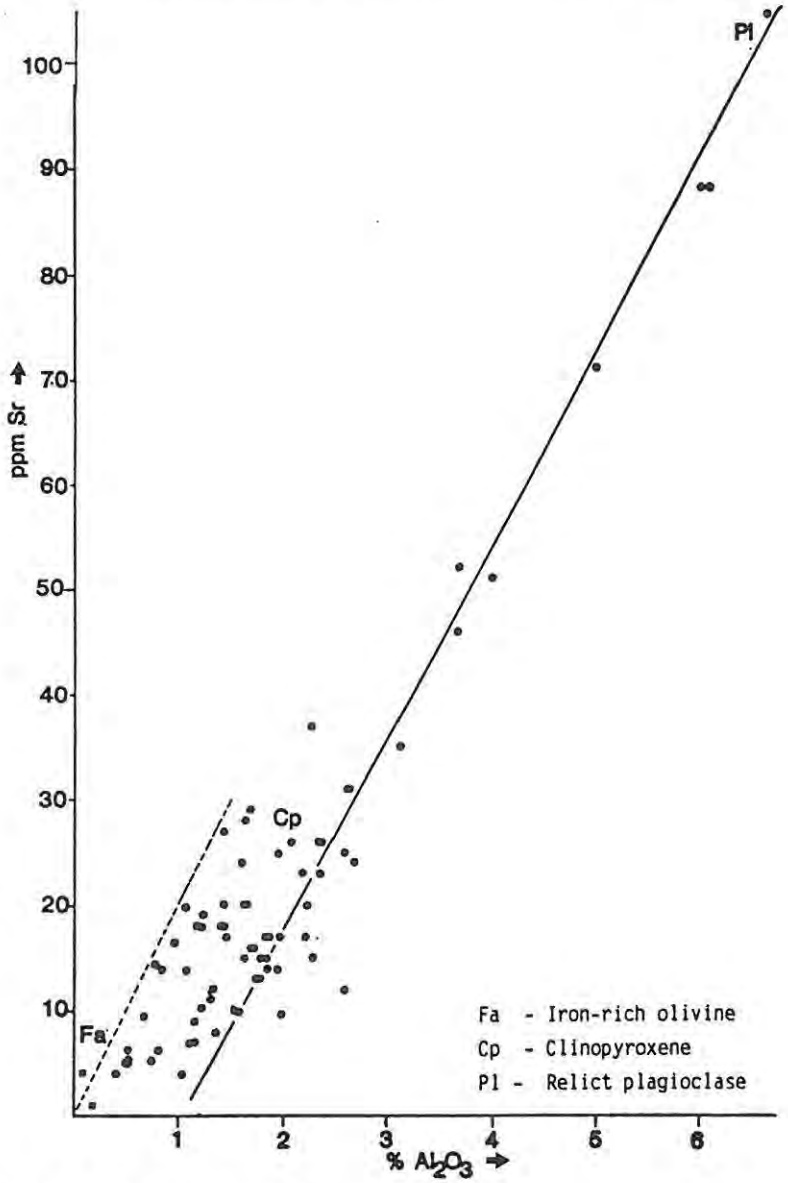

Figure 12.10 Binary plot of ppm Sr vs. wt. % Al_2O_3.

This plot includes samples of pegmatite sensu stricto and hybrid, plagioclase-rich pegmatite from the upper critical zone at Amandelbult (all shown as solid circles). Hybrid, plagioclase-rich samples contain more than 30 ppm Sr; they lie on a straight line as indicated.

The broad scatter of data points in Figure 12.10 suggests that olivine -plagioclase and clinopyroxene-plagioclase mixing lines may be constructed. The former may be extrapolated through zero, whereas the latter intersects the Al_2O_3 axis at approximately 1.0 wt. percent. Assuming an average Al_2O_3 component in the pegmatitic clinopyroxene of 2 wt. percent (see p. 165) it is deduced that this mineral contains roughly 15 ppm Sr. In comparison, cumulus orthopyroxene contains negligible Sr (see p. 165). These results are corroborated by distribution coefficients quoted by Frey et al. (1969; according to whom $D^{cpx} = 0.165$ and $D^{opx} = 0.016$).

12.6.4 Y AND Zr

The incompatible behaviour of Zr and Y in tholeiitic magma suggests that these elements should be concentrated in the residual liquid during a process of fractional crystallization. If both Zr and Y behave as perfectly incompatible elements it may be expected that the Zr/Y ratio will remain constant during fractionation. In cumulates from the upper critical zone this is in fact the situation and a Zr/Y ratio of between 1 and 2 was determined, although in the Merensky Reef this ratio is much higher (possibly due to the presence of zircon). Both Zr and Y are, however, concentrated preferentially in ultramafic cumulates at the base of cyclic units in this sequence (see p. 96). Samples of both the iron-rich ultramafic pegmatites and upper critical zone cumulates are plotted on binary diagrams of wt. percent CaO versus Zr and Y and wt. percent TiO_2 versus Zr (fig. 12.11).

Zr exhibits a positive correlation with both CaO (and hence clinopyroxene-rich pegmatite) and TiO_2 (and hence Fe-Ti-(Cr) oxide-rich pegmatite) for the pegmatite samples. Hybrid pegmatite-cumulate samples are depleted in Zr relative to typical pegmatite. Scatter from the olivine-rich pegmatite - clinopyroxene-rich pegmatite mixing line in Figure 12.11A is caused by Fe-Ti-(Cr) oxides; however, no pegmatites plot towards the CaO axis. In Figure 12.11C it is evident that Zr is preferentially concentrated in Fe-Ti-(Cr) oxide pegmatite. For example, olivine-rich pegmatite typically contains between 6 and 8 ppm Zr and clinopyroxene-rich pegmatite up to 25 ppm Zr, but the presence of Fe-Ti-(Cr) oxide results in much higher contents of Zr.

This may partly be explained by relative distribution coefficients for Zr, as $D^{mag} > D^{cpx} > D^{oliv}$. These data do not, however, permit the calculation of the Zr contents of these minerals. For example, from Figure 12.11A it could be implied (by extrapolation of the olivine-clinopyroxene mixing line) that clinopyroxene contains roughly 30 ppm Zr (i.e. from

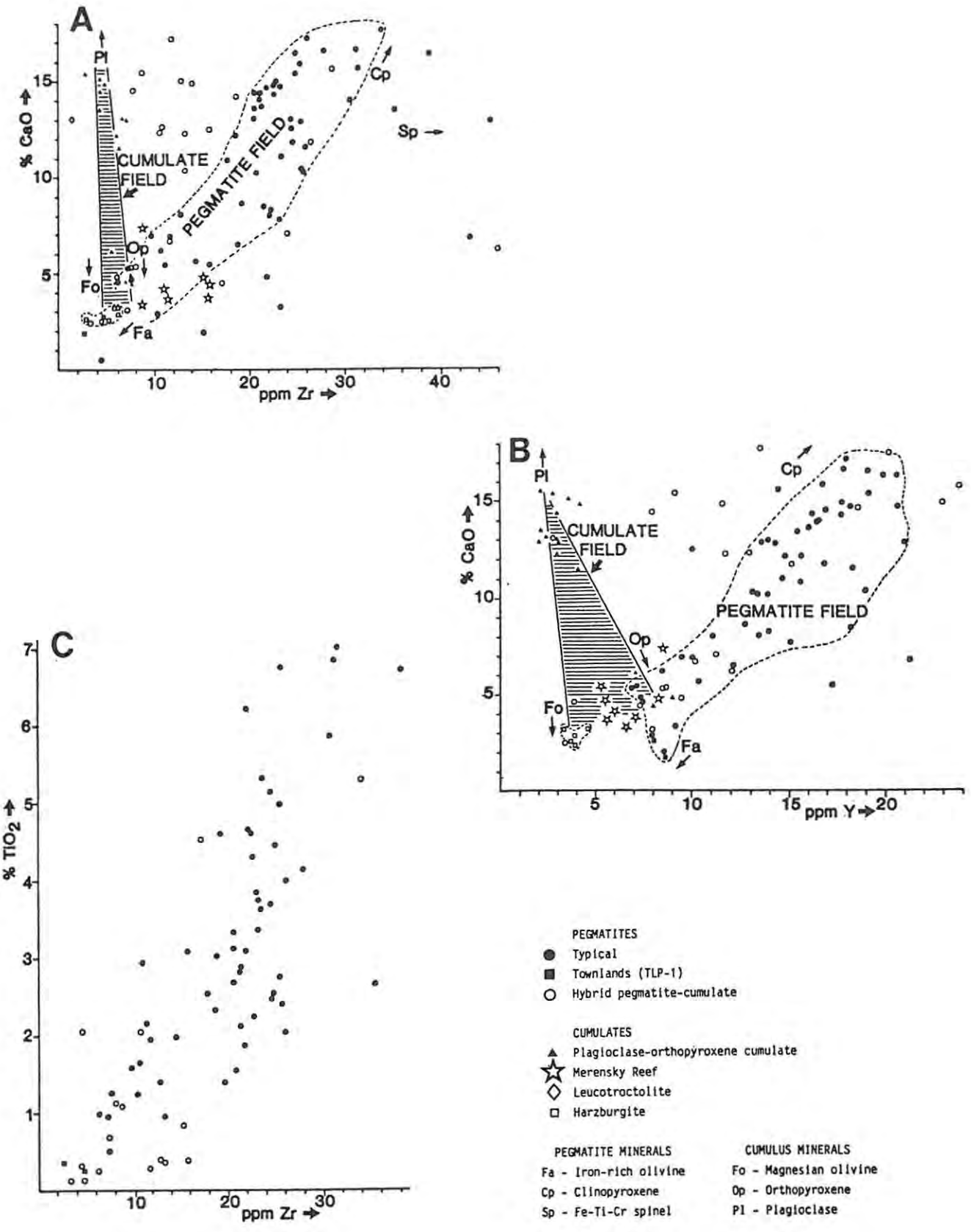

Figure 12.11 Binary plots of wt. % CaO vs. ppm Zr (A), wt. % CaO vs. ppm Y (B) and wt. % TiO_2 vs. ppm Zr (C).

"A" and "B" include samples of pegmatites and their cumulate hosts, all from the upper critical zone at Amandelbult (plus 2 samples from Townlands). Samples of the cumulates may be divided into two groups, plagioclase-orthopyroxene cumulates and olivine-bearing cumulates, both of which define straight lines. Samples of the pegmatites may also be divided into two groups, pegmatite sensu stricto and pegmatite-cumulate hybrids; the former plot in a reasonably well constrained field, whereas the hybrid samples scatter between this field and the cumulate trends. In "C" only samples of pegmatite have been plotted. Note that the Merensky Reef is unusually enriched in both Zr and Y as compared with the other cumulates.

knowledge of the CaO content). However, from Figure 12.11C it is evident that a sample with a TiO_2 content equivalent to clinopyroxene would only contain between 6 and 8 ppm Zr. This indicates that the Zr content is not modally dependent and it is deduced that interstitial amphibole, mica etc., as well as Fe-Ti-(Cr) oxides host much of the Zr.

In Figure 12.11B two "cumulus" trends may be recognized, which are related to plagioclase-olivine and plagioclase-orthopyroxene mixing lines. Samples of the Merensky Reef plot between these two trends. Evidently, the distribution of Y is also controlled by ferromagnesian minerals and it may be concluded that $D^{opx} > D^{oliv} > D^{plag}$. The pegmatites define a broad trend in which Y exhibits a positive correlation with CaO (and hence modal clinopyroxene). This trend is better defined than that for Zr, as Fe-Ti-(Cr) oxides evidently do not have high D's for Y. A plot of TiO_2 versus Y, not included here, exhibits a broad scatter of data points with no discernible trends. Olivine-rich pegmatite has a similar Y content (6 - 8 ppm) to orthopyroxene cumulates, but clinopyroxene-rich pegmatite is much richer and may contain over 20 ppm Y. These data indicate that D^{cpx} is much greater than D^{opx}, for pegmatitic and cumulate samples, respectively. It is suggested that Y is modally controlled by clinopyroxene and, in these rocks, is not as "incompatible" as Zr.

These data support distribution coefficients for Y quoted in the literature; for example: $D^{cpx} = 0.1$; $D^{opx} = 0.03$; D^{oliv} and $D^{Plag} = 0.01$ (Pearce & Norry, 1979) and $D^{cpx} = 0.5$ (Pearce & Norry), 0.2 (Frey et al., 1978); $D^{opx} = 0.2$ (Pearce & Norry), 0.009 (Frey et al.); $D^{oliv} = 0.01$ and $D^{Plag} = 0.01$ (Pearce & Norry).

If samples of iron-rich ultramafic pegmatite are plotted on a binary graph of Y versus Zr they give a scattered distribution of data points (not shown here). This is readily explained by the above discussion. Olivine-rich pegmatite usually has whole-rock Zr/Y ratios close to unity but in clinopyroxene-rich pegmatite these increase to over 1.5. Oxide-rich pegmatite may have Zr/Y ratios of over 2.

CHAPTER 13 FORMATION OF IRON-RICH ULTRAMAFIC PEGMATITE

The study of transgressive bodies of postcumulus rock in layered complexes, such as the iron-rich ultramafic pegmatite suite, is hampered by our lack of knowledge as to how the cumulate rocks themselves formed. It is generally accepted, however, that the formation of these postcumulus rocks is intimately related to processes that operated within the crystallizing cumulate pile. If this line of reasoning is accepted then two possible hypotheses may be established : (1) remobilisation of pre-existing cumulates and subsequent intrusion of these into other parts of the cumulate pile; and (2) segregation of a silicate liquid, hydrothermal fluid or aqueous vapour from the main column of magma and the crystallizing cumulate pile; subsequent migration of this liquid or fluid through the cumulate pile may then produce postcumulus rocks by replacement (or metasomatism) of pre-existing cumulates or by crystallization directly from the silicate liquid. Although no detailed modelling has been completed, most authors support a metasomatic origin for iron-rich ultramafic pegmatite in the Bushveld Complex. Furthermore, metasomatism is usually ascribed to migrating intercumulus liquids (see p. 24).

Before the formation of the iron-rich ultramafic pegmatite suite is modelled, it is useful to discuss the formation of postcumulus "replacement" bodies within other layered intrusions, and to compare these rocks with iron-rich cumulates.

13.1 POSTCUMULUS, "REPLACEMENT" BODIES WITHIN OTHER LAYERED INTRUSIONS

Transgressive bodies of postcumulus, ultramafic rock in the Bushveld Complex may be grouped into a number of different varieties (see p. 9). Two of these, namely non-platiniferous bodies of magnesian dunite and the iron-rich ultramafic pegmatite suite, are considered to be the most abundant types and may possibly be related to similar features in other layered intrusions.

13.1.1 DISCORDANT BODIES OF MAGNESIAN DUNITE

Discordant bodies of magnesian dunite, described as "secondary dunite" by Hess (1960), are prevalent in the Stillwater Complex. They consist

essentially of magnesian olivine with X_{Mg} similar to, or slightly lower than, that of cumulus orthopyroxene from the host cumulates (Hess, 1960; Raedeke & McCallum, 1984). These secondary dunites, unlike those in the Bushveld Complex, are restricted to ultramafic (orthopyroxene, olivine or orthopyroxene-olivine) cumulates. Field relationships usually imply an origin by volume-for-volume replacement. Hess (1960) interprets them as resulting from replacement of serpentinised cumulus orthopyroxene and olivine. However, Raedeke and McCallum (1984) question this hypothesis and quote the work of Evans and Trommsdorff (1974) who found that olivine replacing serpentine is expected to be more magnesian than normal igneous olivine. Raedeke and McCallum also suggest that the textures of these rocks are unlike those in regenerated ultramafic rocks (no details provided) and that the stratigraphic relationships are difficult to reconcile with the Hess hypothesis. They invoke a metasomatic origin related to aqueous fluids (see below). However, Page (1977, p.28), on the basis of field relationships, interprets these bodies as remobilised olivine cumulates.

Discordant bodies of magnesian dunite and olivine clinopyroxenite, that transgress pyroxene-rich cumulates, are abundant in the Duke Island layered complex (Irvine, 1967, 1974, 1980). Field relationships favour an origin by in situ volume-for-volume replacement, as relict primary cumulate layering is preserved in the dunite. Olivine in these replacement bodies is texturally similar to secondary olivine in recrystallized olivine cumulates, and is slightly less magnesian than the cumulus olivine (Irvine, 1974, p.43). Accessory chromite in the replacement dunites resembles that in the primary cumulates. Late-stage veins and coarse segregations of pegmatitic olivine clinopyroxenite and clinopyroxenite are widespread in the dunite-peridotite zones and are often associated with the replacement dunite bodies. Chromite is usually absent in these replacement bodies of olivine clinopyroxenite. These latter (which may possibly be compared with the iron-rich ultramafic pegmatite suite in the Bushveld Complex) may represent displaced material resulting from formation of the dunite that reprecipated a short distance away (Irvine, 1980, p.375).

Discordant, tabular bodies of magnesian dunite, that post-date their host peridotites, are described by Dungan and Ave Lallemant (1978) from Canyon Mountain, Oregon (an alpine-type peridotite). Field relationships favour an origin by in situ replacement. Chromian spinel is a ubiquitous accessory constituent of the dunite. It is often rimmed by alteration assemblages of ferrian chromite plus Cr-rich chlorite or, less commonly, magnetite and Fe-Ni alloy. These "complex" chromites are absent from the host peridotite, consequently their formation is related to the replacement

process. Dungan and Ave Lallemant conclude that these dunite bodies are a result of a metasomatic reaction produced by aqueous vapour percolating along a system of brittle fractures in the peridotite (essentially a harzburgite) at subsolidus temperatures (see below).

In many of the replacement bodies of dunite discussed in the literature, orthopyroxene is the main mineral replaced, consequently formation by metasomatism is based on Bowen and Tuttle's (1949) experimental study, which demonstrated that enstatite can be converted to forsterite by leaching and diffusion of SiO_2 through an aqueous vapour phase (Irvine, 1974, p.158; see also Cameron and Desboroughs'(1964) model for discordant bodies in the Bushveld Complex). In Duke Island this hypothesis is complicated by two problems (Irvine, 1974). If replacement occurred on a volume-for-volume basis than there must have been removal, as well as addition, of material and, secondly, clinopyroxene is the main mineral replaced at Duke Island, thus other constituents besides silica were involved. Irvine (1974, p.159) discusses several possible sources of water required for the metasomatising vapour. However, Irvine (1980, p.377) suggests that intercumulus silicate liquids would probably provide a much more effective metasomatising medium than H_2O vapour and relates the formation of these bodies to his model of infiltration metasomatism (see below). These bodies are also closely associated with pegmatite, thus some H_2O was also involved, but as a constituent of a silicate liquid rather than as a vapour (Irvine, 1980).

Dungan and Ave Lallemant (1978) suggest that olivine in the replacement bodies of dunite at Canyon Mountain resulted by incongruent breakdown of unstable pyroxene (essentially orthopyroxene) with subsequent removal of Si and Ca. Two possible temperature regimes were suggested. A low-temperature formation is based on the lower stablity limit of the assemblage Fo-En-H_2O (approximately 700°C at 2kb) during metamorphism of serpentinites, as determined by Greenwood (1963). The presence of CO_2 in the vapour results in even lower temperatures. Secondly, Dungan and Ave Lallemant (1978) refer to the work of Nakamura and Kushin (1974), who studied the system Mg_2SiO_4-SiO_2-H_2O, and concluded that enstatite becomes unstable in the presence of vapour at subsolidus temperatures much higher than 700°C. For example, vapour co-existing with enstatite and forsterite contains 18 wt. percent SiO_2 at 1280°C. Dungan and Ave Lallemant (1978) discuss a number of possible sources for this vapour, depending on which temperature regime is preferred.

13.1.2 DISCORDANT, PEGMATITIC ASSEMBLAGES

In the Skaergaard intrusion, layered gabbros (with or without olivine)

may be replaced by a quasi-anorthositic rock composed of labradorite (An_{65}) and poikilitic ilmenite and augite (Irvine, 1980, p.377). They often have a thin outer selvage of iron-rich olivine (Fo_{65}), and upper contacts are often irregular and scalloped. Irvine relates these features to infiltration metasomatism (see also discussion of Duke Island bodies above).

Raedeke and McCallum (1984) describe pyroxene-olivine "pegmatoids" that are associated with discordant bodies of magnesian dunite in the Stillwater Complex (see above). Both orthopyroxene and clinopyroxene (grain sizes of 10 to 30 cm) occur in these rocks, which may form layers with discordant lower contacts and concordant upper contacts. These pegmatite bodies (sic) may be completely discordant or broadly stratiform (comparable with locally concordant form of iron-rich ultramafic pegmatite bodies at Amandelbult). They commonly contain chromite as disseminations, pods, stringers, or stratiform layers. Field relationships indicate that both the discordant bodies of magnesian dunite and pyroxene-olivine pegmatites formed by pene-contemporaneous replacement of the cumulates. Raedake and McCallum (1984) discuss a metasomatic model for the dunites in conjunction with an aqueous vapour (see above), and suggest that the pyroxene-olivine pegmatites may have resulted from components released during formation of the dunites (Irvine, 1974, discusses a similar model for the Duke Island bodies; see above). Raedeke and McCallum (1984) do not present any data to indicate whether pyroxene and olivine in the pegmatites are compositionally different from the adjacent cumulus minerals.

Myers (1978) discusses "mafic pegmatites", composed of hornblende gabbro and ultramafite, that cut across cumulate layering in the Fiskenaesset Anorthosite Complex in southwest Greenland. The pipes form irregular networks in which all vertical portions are massive and pegmatitic, whereas some horizontal portions exhibit layering (both mineral graded layers and comb layers). From examination of field relationships Myers concludes that these pipes formed by a process of magmatic drilling, rather than metasomatic replacement, and the alternation of comb and mineral-graded layers indicates that changes in physico-chemical conditions occurred. The similarity between the ferromagnesian and alkali chemistry of the pipes and the host cumulates suggests that the pipes are derived from magma within the Complex. They probably represent a late stage in the evolution of these magmas, but are not fractionated enough to be interpreted as representing residual, intercumulus liquids (Myers, 1978).

13.1.3 SUMMARY

(1) Spatial relationships, particularly at Duke Island and Stillwater indicate that discordant bodies of magnesian dunite and clinopyroxene-olivine pegmatite are related, whereas this is not the case in the Bushveld Complex.
(2) Discordant bodies of magnesian dunite from a number of layered complexes are probably similar to those in the Bushveld Complex.
(3) Most authors favour a replacement origin for discordant bodies of magnesian dunite in layered complexes; two main hypotheses are presented, metasomatism in response to an aqueous vapour, and magmatic replacement of pre-existing cumulates by an intercumulus silicate liquid (specifically Irvine's (1980) infiltration metasomatism model). Data presented in this study do not support a replacement model for the magnesian dunite unit in the Driekop pipe (see Chapter 4).
(5) The iron-rich ultramafic pegmatite suite in the Bushveld Complex is not directly comparable with discordant, pegmatitic bodies in other layered complexes.

13.2 COMPARISON WITH IRON-RICH CUMULATES

13.2.1 THE UPPER ZONE OF THE SKAERGAARD INTRUSION

According to the subdivision of Wager and Brown (1968) the upper zone (UZ) of the layered series of the Skaergaard intrusion is characterised on the presence of iron-rich olivine as a cumulus phase. Other important cumulus minerals are plagioclase, iron-rich pyroxenes, and magnetite. These rocks may be described as ferrodiorites (plagioclase is less calcic than An_{50}). The upper zone is divided into three main subzones, UZa (iron-rich olivine becomes a major cumulus phase), UZb (apatite becomes a cumulus phase) and UZc (ferrohedenbergite is a cumulus phase). In UZa rhythmic layering reaches its maximum intensity, such that "gravity-stratified" layers alternate with layers of uniform rock; it may occur as normal, planar layering or "trough banding" (see Wager & Brown, p.81). The "normal" rock, equivalent to the average compositon of subzone UZa, is a ferrodiorite, which consists of cumulus plagioclase, iron-rich augite and olivine, and magnetite (pigeonite may occur towards the base). Minor intercumulus phases include apatite, quartz and micropegmatite (see Wager & Brown, fig. 49). However, rhythmic layering in UZa may involve alternating layers of leucocratic and melanocratic cumulates (e.g., samples 5321 and 5322, described below).

Three samples, numbers 5321, 5322 (both from UZa) and 5196 (from UZb),

from the original Wager collection were kindly provided by Prof. Vincent (Geology Department, Oxford University) for study by the author. Sample 5321 is essentially an anorthosite with minor cumulus (?) Fe-Ti oxides and intercumulus clinopyroxene and olivine. The intercumulus ferromagnesian silicates occur as tiny, often triangular, anhedral grains, unlike the "mottles" observed in anorthosites in the upper critical zone of the Bushveld Complex (see Wager & Brown, fig. 61). Sample 5322, which is immediately adjacent to sample 5321, is an ultramafic rock, consisting of approximately equal proportions of coarse-grained, cumulus olivine, clinopyroxene and Fe-Ti oxide (see Wager & Brown, fig. 62). Plagioclase may occur in variable amounts as either a cumulus or intercumulus phase. Minor amounts of apatite occur as an intercumulus phase. The Fe-Ti oxides comprise both Ti-magnetite (which exhibits a range of microstructures) and ilmenite. Sample 5196 consists of cumulus plagioclase, olivine, Fe-Ti oxides and apatite (see Wager & Brown, fig. 65).

Electron microprobe analysis of olivines from these samples are presented in Appendix 7. The composition of olivine from samples 5322 ($Fo_{37.3}$) and sample 5196 ($Fo_{32.1}$) lies within the compositional range for cumulus olivine in UZa and UZb, as determined by Wager and Brown (1968). However, intercumulus olivine from sample 5321 has a composition of $Fo_{15.5}$, which is much more iron-rich than cumulus olivine at the same position in the cumulate pile.

Samples 5322 and 5196, apart from the presence of minor plagioclase and apatite, are texturally similar to iron-rich ultramafic pegmatite. The alternation of anorthositic and ultramafic layers in UZa suggests a comparison with iron-rich ultramafic pegmatite that is associated with mottled anorthosite layers in the Bushveld Complex.

13.2.2 THE UPPER ZONE OF THE BUSHVELD COMPLEX

Iron-rich ultramafic pegmatite has a number of features in common with iron-rich cumulates in the upper zone of the Bushveld Complex. According to Wager and Brown (1968) the base of this zone is marked by the introduction of Ti-magnetite as a significant cumulus phase. This is normally associated with the introduction of iron-rich olivine, ilmenite and apatite as cumulus phases, together with minor amounts of quartz, alkali feldspar, hornblende and biotite. The extreme iron-enrichment, which is comparable with that found in the Upper Zone of the Skaergaard intrusion, is evinced not only by the Ti-magnetite layers but also by the low Mg/Fe ratios of the ferromagnesian silicates. The upper zone of the Bushveld Complex is

subdivided into three subzones, UZa (Ti-magnetite becomes a major cumulus phase), UZb (iron-rich olivine becomes a major cumulus phase) and UZc (apatite becomes a major cumulus phase; Wager & Brown, 1968). Plagioclase (in the compositional range andesine) is a ubiquitous cumulus phase throughout most of the upper zone. Consequently, these rocks are described as ferrodiorites (Wager & Brown,. p.376). Iron-rich clinopyroxene is present throughout most of the upper zone, but pigeonite is present in only minor amounts and disappears at approximately 120 m below the roof in the exposures examined by Wager and Brown (1968). Ultramafic layers which directly resemble iron-rich ultramafic pegmatites, such as those described from the Skaergaard intrusion, are not found.

The composition of cumulus olivine in the upper zone forms a more or less continuous series from Fo_{56} to, essentially, Fo_0 (see p. 158). According to Wager and Brown (p.378) olivine (with a composition of Fo_{49}) enters as a significant cumulus phase at approximately 300 m above the base of the upper zone in UZb. Apatite, which enters as a cumulus phase at approximately 750 m, is essentially absent from UZb. In UZb the principal cumulus phases are plagioclase (andesine), clinopyroxene (ferroaugite), iron-rich olivine (hortonolite), and Ti-magnetite. The compositions of olivine and clinopyroxene (in terms of the Mg/Fe ratio) in this subzone are comparable with that in iron-rich ultramafic pegmatite from the upper critical zone. The mineralogy of iron-rich ultramafic pegmatite from the upper critical and lower main zones may thus be compared with that of iron-rich cumulates in subzone UZb. The major mineralogical difference between these two groups of rocks is the absence of plagioclase in the pegmatites. Furthermore, relict plagioclase associated with the pegmatites is more calcic than cumulus plagioclase from both the upper critical and upper zones.

If the proportion and composition of plagioclase in the pegmatites was comparable to that in cumulates of UZb then it would be feasible to propose that these two suites of rocks formed from a similar magma. However, data in this study clearly imply that the putative pegmatitic liquid was unsaturated in plagioclase. Similarities in the composition of olivine, clinopyroxene, Ti-magnetite, and ilmenite from these rocks may, however, suggest that the pegmatites formed from magmatic liquids at temperatures comparable to those prevailing during cumulus mineral formation in UZb. Apatite is absent from iron-rich ultramafic pegmatite bodies in the upper critical and lower main zones, but is an important constituent of pegmatite bodies in the middle of the main zone. Here it is associated with olivine in the compositional range Fo_{28-26}. It is significant that apatite only becomes a cumulus phase in UZc, where it also is associated with ferrohortonolite (not hortonolite).

13.2.3 Fe-Ti OXIDE ORES

Possible genetic relationships between the formation of anorthosite cumulates and discordant bodies of iron-rich ultramafic pegmatite in the Bushveld Complex are discussed below (see also Viljoen & Scoon, in press). Because of this relationship the formation of Fe-Ti oxide deposits in anorthosite massifs may be of relevance. Many anorthosite massifs have been subjected to high-grade metamorphic events, but those in the Nain Province of Labrador are virtually unaffected by post-emplacement metamorphism and deformation (Sawkins, 1984). Disseminated Fe- and Fe-Ti oxides are a common feature of anorthosite bodies, but in some instances irregular bodies of ilmenite are found (Sawkins, 1984). Fe-Ti oxide bodies in anorthosite massifs occur in both discordant and layered bodies.

The formation of pipe-like bodies of Fe-Ti oxide pegmatite, which are an integral part of the iron-rich ultramafic pegmatite suite (Chapter 2), may be related to the development of almost pure Fe-Ti oxide liquids. A relationship with cumulus Ti-magnetite layers is implied. It has long been believed that the formation of cumulus Ti-magnetite layers in the Bushveld Complex has resulted from some form of magmatic segregation (Molengraaf, 1904, quoted in Hall, 1932), although no one detailed hypothesis has yet been widely accepted (see review by Reynolds, in press). A relationship between concordant Fe-Ti oxide ores in anorthositic massifs and Ti-magnetite cumulates in layered intrusions has also been postulated (Osborne, 1928; Lister, 1966). Osborne suggested that Fe-Ti oxide layers in anorthositic bodies result from accumulation of a late-stage residual Fe-Ti oxide liquid that was filter pressed from the surrounding, partially consolidated silicate rock. Hall (1932) and Bateman (1951) consider Ti-magnetite layers in the Bushveld Complex to represent late gravitative accumulation of oxide liquids onto the consolidated crystal pile. Philpotts (1976) established experimentally that phosphorus-rich Fe-Ti oxide liquids may be immiscible in certain basaltic systems. Osborne's hypthesis, which is discussed and extended by Lister (1966), may be applicable to the formation of Fe-Ti oxide pegmatite in the Bushveld Complex.

13.2.4 DISCUSSION

(1) Comparison of the mineralogy of iron-rich ultramafic pegmatite and cumulates from UZb in the Bushveld Complex suggests that the pegmatites may have formed by crystallization, under similar magmatic conditions, of a silicate liquid.

(2) There is probably a direct genetic relationship between cumulus Ti-magnetite layers and discordant bodies of Fe-Ti oxide pegmatite in the Bushveld Complex.
(3) An immiscibility hypothesis for both the cumulus Ti-magnetite layers and the Fe-Ti oxide pegmatite bodies is attractive, but there is no experimental evidence to substantiate immiscibility between phosphorous-poor Fe-Ti oxide liquids and basaltic magmas.
(4) The association of anorthosite cumulates and discordant bodies of iron-rich ultramafic pegmatite in the upper critical and main zones of the Bushveld Complex may be compared with alternating layers of plagioclase-rich and iron-rich ultramafic cumulates found in UZb in the Skaergaard intrusion, although this does not imply that they are genetically related (note also that the observations of Wager & Brown are referred to, but this does not imply that the cumulus theory is applicable to the formation of these rocks - see below).

13.3 DERIVATION OF AN IRON-RICH, PLAGIOCLASE-UNDERSATURATED, POSTCUMULUS LIQUID IN THE UPPER CRITICAL ZONE

In the introduction to this chapter it was observed that the formation of iron-rich ultramafic pegmatite is commonly ascribed to migrating intercumulus liquids. A number of criticisms may be levelled against this hypothesis, the most important of which are as follows :
(1) Ferromagnesian minerals in iron-rich ultramafic pegmatite are characterised by a much lower X_{Mg} than that of either cumulus or intercumulus phases at the same position in the layered sequence.
(2) Fe-Ti oxides are an important constituent of these rocks, whereas chromite is the stable spinel in the host cumulates in the upper critical zone.
(3) The putative pegmatitic liquid is clearly undersaturated in plagioclase.

The ensuing discussion, based on a combination of new data and theoretical speculation, explores how an iron-rich, plagioclase-undersaturated, intercumulus (or postcumulus) liquid may be derived during crystallization of the upper critical zone of the Bushveld Complex.

The distinction between an intercumulus and postcumulus liquid is important to this argument (see pp. 3-4). Thus, intercumulus liquid may be defined as a residual liquid that is trapped between the cumulus framework of crystals (where it crystallizes in situ), and postcumulus liquids are defined as late-stage liquids that have segregated from both the residual magma in

the main chamber and the specific crystallizing cumulate from which they were derived. Possibly the bulk of these postcumulus liquids comprise intercumulus liquids that have been expelled from their original position. However, the possibility that they may include other residual liquids cannot be completely ignored (see below).

13.3.1 CYCLIC UNITS

Derivation of iron-rich postcumulus liquids, it is postulated, is intimately related to the formation of cyclic units (see Chapter 6). The most complete cyclic units in the upper critical zone, it is believed, are probably capped by either spotted anorthosite or mottled anorthosite (see p. 91). It is not proposed to consider the contentious issue of anorthosite being a derivative of a separate liquid, as advocated by Todd et al. (1982) and Irvine et al. (1983), as many of the critical relationships that would support such a model appear to be missing in the upper critical zone. If it is assumed that the upper zone of the layered sequence does not represent an entirely separate intrusion, then it may be concluded that the bulk composition of cyclic units in the upper critical zone would not yield a liquid composition equivalent to an acceptable, putative magma. Crystallization of the cumulates in these cyclic units would presumably result in formation of a residual magma that is more fractionated than the putative magma. It may be assumed that, after formation of a considerable thickness of cumulates (e.g., represented by the main zone ?), this fractionated, residual magma would then crystallize iron-rich cumulates (in the upper zone ?). Obviously, this is a very simplistic hypothesis which ignores many issues, such as influxes of new magma. However, the crux of this argument is that, for whatever reason, cyclic units in the upper critical zone are capped by anorthosite, such that more fractionated cumulates (e.g., ferrodiorites) did not form until much higher in the cumulate pile.

The order in which successive rock types within a cyclic unit appear is the same as the generally accepted crystallization order of mafic melts (see also p. 90). In cyclic units in the upper critical zone the following sequence of cumulus mineral formation is evident : chromite - Mg-olivine, orthopyroxene - plagioclase (with the above proviso). From the study of cumulates in the main and upper zones this sequence of cumulus mineral formation may be continued, thus : clinopyroxene - Fe-Ti oxides - iron-rich olivine - apatite (inter alia Willemse, 1969a). Plagioclase remains a cumulus phase throughout this sequence.

In the upper critical zone the Merensky and Bastard cyclic units, both of which are capped by a layer of mottled anorthosite, exhibit considerable fractionation. The composition of orthopyroxene in the Merensky cyclic unit, expressed as X_{Mg}, varies between 0.82 - 0.79 (in the Merensky Reef at the base of the cyclic unit; see p. 96) and 0.697 (in mottled anorthosite towards the top of the cyclic unit; sample M-12, Kruger, 1984). The Bastard cyclic unit becomes even more iron-rich; the X_{Mg} of orthopyroxene in mottled anorthosite towards the top of this cyclic unit is 0.592 (sample B-30, Kruger, 1984; see Table 13.1). In comparison, orthopyroxene in cyclic units above the Bastard cyclic unit does not become as iron-rich until the middle of the main zone (Mitchell, in prep.). It may be concluded that the Merensky and Bastard cylcic units have undergone exceptional fractionation in a closed system, segregated from the main column of magma (see Kruger & Marsh, 1983).

13.3.2 RELATIONSHIP WITH MOTTLED ANORTHOSITES

Iron-rich ultramafic pegmatite bodies exhibit a close spatial relationship with thick layers of anorthosite cumulates. Furthermore, the distribution of iron-rich ultramafic pegmatite bodies appears, on a regional basis, to be controlled by the distribution of cumulus plagioclase in the layered sequence (see Chapters 2 and 7). These features led Viljoen and Scoon (in press) to speculate that the formation of iron-rich ultramafic pegmatite is intimately related to the development of mottled anorthosite cumulates. The results of two preliminary studies, which present some new data to support this hypothesis, are presented below.

IRON-RICH PYROXENES

In mottled anorthosites in the upper critical zone, the mottles usually consist of orthopyroxene and/or clinopyroxene (see p.87). Pyroxenes also occur in mottled anorthosites as tiny, sliver-like grains that are moulded around plagioclase grains. In mottled anorthosites examined by the author these latter are invariably clinopyroxene. The formation of the mottles is controversial, but textural evidence clearly implies that the sliver-like grains are intercumulus. In the Merensky footwall mottled anorthosite at Amandelbult, it is apparent that the proportion of mottles decreases with increasing height, eventually resulting in a relatively pure anorthosite (see analyses AT-9 to AT-13, Appendix 5). However, the sliver-like grains of clinopyroxene are still present.

In the Footwall cyclic unit at Rustenburg the average X_{Mg} of orthopyroxene is, approximately 0.80 to 0.78 (Kruger, 1984). For example, in

TABLE 13.1 X_{Mg} RATIO OF INTERCUMULUS PYROXENES IN MOTTLED ANORTHOSITES

UNIT	SAMPLE	REFERENCE	CLINOPYROXENE x	CLINOPYROXENE d	CLINOPYROXENE n	ORTHOPYROXENE x	ORTHOPYROXENE d	ORTHOPYROXENE n	HEIGHT RELATIVE TO MERENSKY REEF*
Bastard c.u.	B-30	Kruger (1984)	.660	.018	4	.592	.006	4	+ 66 m.
Merensky c.u.	M-12	Kruger (1984)	.759	.009	4	.697	.006	4	+ 9 m.
Footwall c.u.	AT-13	This study	.725	.009	10	-	-	-	- 0.1 m.
Footwall c.u.	F-27	Kruger (1984)	.821	.016	2	-	-	-	- 0.5 m.
Footwall c.u.	AT-11	This study	.865	.002	4	.795	.003	4	- 3 m.
Footwall c.u.	F-24	Kruger (1984)	.851	.007	4	.808	.006	4	- 6 m.
Pegmatite	"average"	This study	.640	.017	54	-	-	-	-

x - mean; d - standard deviation; n - number of analyses; c.u.- cyclic unit.
Pegmatite "average" from Table 9.2. For location of samples AT-11,13 see Figure 5.5.
For analyses in this study see Appendix 8. * approximation only.

sample F-24 (a leuconorite, approximately 6 m below the Merensky Reef) the X_{Mg} of orthopyroxene and clinopyroxene is 0.808 and 0.851, respectively (Kruger, 1984; Table 13.1). These data are comparable with whole-rock analyses of samples from Amandelbult (samples AT-1 to AT-13; see Appendix 5) and with electron microprobe analyses of mottles from the Merensky footwall anorthosite (sample AT-11, Table 13.1). The X_{Mg} of clinopyroxene from sample F-27 (a mottled anorthosite, approximately 0.5 m below the Merensky Reef at Rustenburg) is 0.821. However, the X_{Mg} of sliver-like grains of clinopyroxene from sample AT-13 (a mottled anorthosite, only a few centimetres below the Merensky Reef at Amandelbult) is 0.725 (Table 13.1).

MAGNETIC ANORTHOSITES

Linear magnetic anomalies in the upper critical and main zones, which are correlated with thick layers of anorthosite, are characterised by the absence of large bodies of iron-rich ultramafic pegmatite (see p. 18). The magnetic characteristics of these rocks are discussed by Viljoen and Burvenich (1983) and their mineralogy is being examined by I.M. Reynolds, who has kindly allowed the author to disclose some preliminary results. The magnetic properties of these rocks may be related to three possible sources : (1) the presence of tiny, opaque needles within plagioclase, that may represent exsolution of excess Fe^{3+} in the form of magnetite; (2) the presence of Fe-rich pyroxenes, that often contain exsolved platelets of a semi-translucent phase, possibly ilmenite; and (3) interstitial (or intercumulus) Fe-Ti oxides, essentially ilmenite, with insignificant Ti-magnetite. These latter represent the most obvious source of the magnetism but are usually present in

virtually insignificant amounts. The morphology and nature of the interstitial oxides clearly indicate that they are late-stage phases that crystallized from entrapped intercumulus liquid (Reynolds, pers. comm.).

CONCLUSIONS

(1) Sliver-like grains of intercumulus clinopyroxene in mottled anorthosites are even more iron-rich than the mottles; they have presumably crystallized from entrapped intercumulus liquid.

(2) Assuming equilibrium conditions, X_{Mg} of cpx > opx > oliv, thus crystallization of intercumulus clinopyroxene rapidly lowers the Mg/Fe ratio of the liquid.

(3) "Magnetic" anorthosites in the main zone represent a more advanced stage of intercumulus fractionation than was recorded in anorthosites in the upper critical zone (even though the composition of the cumulus plagioclase may not be markedly different).

(4) This "intercumulus fractionation trend" may be expressed, sequentially, thus : orthopyroxene-clinopyroxene (mottles), clinopyroxene (iron-rich, sliver-like grains), Fe-Ti oxides (interstitial grains).

(5) Intercumulus fractionation may result in an intercumulus liquid with a sufficiently low Mg/Fe ratio to crystallize clinopyroxene and olivine in iron-rich ultramafic pegmatite in the upper critical zone. For example, the average X_{Mg} of pegmatite-hosted clinopyroxene at Amandelbult is 0.64; this is similar to the composition of intercumulus clinopyroxenes from mottled anorthosites at the top of the Bastard cyclic unit.

(6) Intercumulus fractionation is probably not preserved in plagioclase grains due to zonation or subsolidus re-equilibration.

(7) Many of the upper contacts of cyclic units in the upper critical zone are unconformable and exhibit evidence of resorption. It is possible that complete intercumulus fractionation trends are not preserved for documentation.

13.3.3 IRON-RICH, RESIDUAL LIQUID

Examination of the Currywongaun-Doughruagh intrusion in Connemara, Eire, led Kanaris-Sotiriou (1974) to propose a model for adcumulus growth of very thin pyroxene bands (which conform to the primary layering) in anorthositic cumulates. This model relies on the adcumulus hypothesis of Wager et al. (1960), consequently it assumes that adcumulate crystallization proceeds near the top of the crystal pile. Kanaris-Sotiriou proposes that a thin zone of liquid, supersaturated in those components not required for adcumulus growth

(plagioclase in this example) is formed in the magma just above the crystal-liquid interface. Crystallization from this magma results in the formation of a layer with a radically different composition to that in the adcumulate (pyroxenite in this example). Kanaris-Sotiriou proposes that the exchange of components occurs by diffusion, but other mechanisms such as annealing may also be applicable.

Campbell et al. (1983, p.154) observe that "the accumulation of a dense, iron-rich liquid at the bottom of the chamber lowers the amount of supercooling at the crystal-liquid interface and thus slows the rate of crystal growth". This could conceivably limit the bottom growth of plagioclase, and, in the upper critical zone, mark the end of a cyclic unit. If this residual liquid is compositionally similar to the iron-rich intercumulus liquid (assuming both are derived from the same mottled anorthosite layer) then it may be expected that it also would not crystallize in situ, unless it remained there until the temperature dropped appreciably.

It is often assumed that this iron-rich, residual liqiud is returned to or remains within, the supernatant liquid column. It is proposed here that this is not necessarily the case, and that a residual liquid developing above a mottled anorthosite may result in the formation of an iron-rich, postcumulus liquid that is trapped within the crystallizing cumulate pile, which, if it is particularly dense, may migrate down through the anorthosite layer and mix with entrapped intercumulus liquid. This may be achieved by commencement of crystallization of the next cyclic unit or by a new influx of magma (that is less dense than this residual liquid). Both these mechanisms could effectively isolate the residual liquid from the supernatant liquid column.

Before the formation of iron-rich ultramafic pegmatites can be related to these iron-rich intercumulus and/or residual liquids derived during crystallization of mottled anorthosite cumulates, it is first necessary to examine the movement of intercumulus liquids within the cumulate pile. Furthermore, Irvine's model of infiltration metasomatism (Irvine, 1980) may be directly applicable to the formation of the pegmatites, with the proviso that suitable intercumulus liquids can only be derived from mottled anorthosites.

13.4 MOVEMENT OF INTERCUMULUS LIQUIDS AND INFILTRATION METASOMATISM

The formation of adcumulates is, in theory, intimately related to the removal of intercumulus liquids by postcumulus processes (which may include diffusion). Calculation of the initial porosity of a cumulus mush is a major

problem in studies of layered igneous rocks, although it is usually estimated at between 20 and 50 percent (Jackson, 1961; Wager & Brown, 1968). Adcumulates may contain less than 5 percent trapped intercumulus material, which illustrates the proportion of intercumulus liquid that has to be removed (and, of course, is available for pegmatite formation). The removal of small amounts of pore-liquid may be related to processes such as local diffusion, subsolidus reequilibration and leaching effects, but large-scale movements are probably related to mechanical compaction (filter pressing) and annealing. Many of these postcumulus processes are related to Irvine's model of infiltration metasomatism (Irvine, 1980).

Cyclic units in the Muskox intrusion may be related to replenishment of the chamber with new influxes of magma (Irvine, 1980). However, chemical breaks occur in the cumulate pile at varying levels above predicted positions related to modally determined cyclic units. Irvine explained this by metasomatic reaction between upward migrating intercumulus liquid and pre-existing cumulus crystals. Upward movement of intercumulus liquid is essentially related to compaction of the crystal pile as a result of addition of new material, according to Irvine (1980). Irvine calculated that the initial porosity of the cumulates is approximately 58 percent (although he concedes that this figure is probably to high), and that the final porosity varies between 5 and 10 volume percent. He concluded that the Muskox layered series was unconsolidated down to depths of up to 300 m, and that filter pressing occurred to depths of at least 100 m. Because up to 50 percent of the intercumulus liquid may be expelled from the crystallizing cumulate pile and returned to the main body of the magma, this process must also be a considerable factor in the primary differentiation of the magma (Irvine, 1980, p.360). The models of Hess (1972) and Irvine (1980) imply that adcumulus growth does not occur at the cumulate depositional surface, but operates at relatively deep levels in the cumulate pile.

Irvine (1980, p.375) also relates the process of infiltration metasomatism to the formation of igneous bodies by postcumulus replacement (or metasomatism), and describes some minor modal effects that may be related to infiltration metasomatism in the Muskox intrusion. However, Irvine observes that large, transgressive bodies within other layered complexes offer more convincing evidence of postcumulus replacement processes. These include examples from the Duke Island ultramafic complex, the Skaergaard intrusion and the Stillwater and Bushveld Complexes (Irvine refers to replacement bodies of "dunite" in the latter). Irvine suggests that these transgressive bodies result from a process of magmatic replacement in response to migrating intercumulus, silicate liquids (see also section 13.1).

13.5 FORMATION OF IRON-RICH ULTRAMAFIC PEGMATITE

13.5.1 THE PEGMATITIC LIQIUD

Formation of the iron-rich ultramafic pegmatite suite in the Bushveld Complex is ascribed to postcumulus liquids derived from within the crystallizing cumulate pile. Migration of these postcumulus liquids through the crystallizing cumulate pile is accommodated within Irvine's model of infiltration metasomatism (Irvine, 1980). However, the formation of iron-rich ultramafic pegmatite cannot be solely attributed to infiltration metasomatism as the mineralogy and chemistry of the pegmatites (specifically the absence of plagioclase) apply major contraints on the composition of the putative pegmatitic liquid. The putative pegmatitic liquids are therefore regarded as dominantly intercumulus liquids derived from thick layers of mottled anorthosite, but they may also comprise residual liquids that have become segregated from the supernatant liquid column (as described in section 13.3.3).

Derivation of pegmatitic liquids from specific layers within the crystallizing cumulate pile explains why the composition of pegmatite is related to its position in the layered sequence and why the separate bodies exhibit increasing degrees of fractionation with height. Compositional variations in the pegmatite suite are thus attributed to intercumulus fractionation trends. These trends will be more advanced than cumulus fractionation trends, consequently, compositional variation exhibited by pegmatite in the upper critical and main zones is simulated by cumulus trends in the upper zone.

A major problem with this hypothesis is that it is difficult to envisage a residual, or intercumulus tholeiitic liquid derived from crystallization of an anorthosite that is completely undersaturated in plagioclase. For example, by analogy with the cumulates in the upper zone of the Bushveld Complex it may be predicted that this liquid would crystallize, besides iron-rich clinopyroxene, olivine and Fe-Ti oxides, a relatively sodic plagioclase. Two suggestions may be offered. Firstly, sodic plagioclase could crystallize from the intercumulus liquid in situ (i.e. before expulsion of the remaining pore liquid) as overgrowths on cumulus plagioclase. Secondly, a proportion of the "plagioclase components" could be incorporated into pegmatitic minerals, including clinopyroxene, amphibole and mica. If the former suggestion is favoured then it will be evident that the stage at which the postcumulus liquids are removed from their host cumulate is critical. Possibly, the framework of cumulus plagioclase crystals through which the

postcumulus liquid migrates would promote rapid nucleation of plagioclase overgrowths. In summary, however, it is evident that the paucity of plagioclase in the pegmatites is very difficult to explain with this hypothesis.

An analogy with alternating layers of anorthosite and iron-rich ultramafic cumulates in UZa of the Skaergaard intrusion may be applicable, athough, of course, the pegmatites themselves are not cumulates. Although it is not proposed to consider the formation of the cumulates in UZa of the Skaergaard intrusion, it is necessary to point out that the author does not favour the cumulus theory of Wager et al. (1960) (even though the observational and mineralogical data of Wager and Brown (1968) are constantly referred to in section 13.2.1).

13.5.2 FORMATION OF PEGMATITE BODIES

Small, even microscopic, segregations of iron-rich material found in magnetic anorthosites are interpreted as representing an initial stage in the formation of discordant pegmatite bodies. This is followed by migration of intercumulus liquid, initially laterally, within the mottled anorthosite layer. Movement of intercumulus liquids may be explained by Irvine's models of adcumulate growth and infiltration (Irvine, 1980). These liquids may then coalesce and subsequently crystallize in situ to form small, probably highly irregular, often pod-like, pegmatite bodies. Coalescence may be related to irregular distribution of pore spaces or to migration in response to pressure differentials (an analogy with partial melts may be applicable). These small pegmatite bodies are considered not to replace the anorthosite, so much as displace it in response to volume re-adjustments within the layer. This may be assisted by annealing processes. These early-formed pegmatite bodies thus form pene-contemporaneously with their host cumulates (see also Raedeke & McCallum, 1984 and section 13.1.2).

Because of their high density, the pegmatitic liquids may migrate downwards within, and from an anorthosite layer. Downward movement over vertical heights of a few metres may be quite common, but this is unlikely to occur over any considerable distance. Formation of pegmatite bodies from downward-migrating liquids, or addition of material at the bottom of a pegmatite body, is supported by field relationships. In some examples it is evident that harzburgite or chromitite layers have acted as barriers to arrest downward migrating liquids. Pegmatite bodies may thus form by ponding of pegmatitic liquids above a cumulate layer that has restricted further movement. Alternatively, these pegmatite bodies may result from selective,

lateral replacement of felsic cumulates accompanied by local downward movement within the specific layer. The pegmatitic liquids would be in disequilibrium with cumulates other than the anorthosites from which they were derived, consequently they may replace them.

Continued lateral migration of pegmatitic liquid within mottled anorthosite layers, possibly with some migration in underlying cumulates, will only occur in response to a major increase in overpressure, or if a large pressure differential exists. Increases in overpressure may be related to new influxes of magma into the chamber. Pressure differentials may be related to non-homogeneity in cumulate layers or lateral changes along strike. However, field relationships indicate a correlation between large, pipe-like bodies of pegmatite and structurally disturbed zones. This may suggest that many faults were also zones of weakness or active during formation of the layered sequence, and in fact evidence does point to this for the Steelpoort fault in the eastern limb of the Complex. It is postulated that these faults or weak zones acted as areas to which the pegmatitic liquids migrated. These then provided vertical conduits through the crystallizing cumulate pile up which the pegmatitic liquids streamed, to form large, pipe-like bodies.

These zones of weakness could provide conduits for migrating pegmatitic liquids from more than one source-horizon, resulting in composite pegmatite bodies. If the pegmatitic liquids were derived from vastly different levels in the layered sequence this may result in disequilibrium and replacement of pre-existing pegmatite (e.g., in the Townlands pipe). The irregular lateral form of pipe-like bodies may be explained by either lateral migration of material along specific cumulate layers, or selective replacement outwards from the pipe, again in specific cumulate layers. Similarly, the concentration of small, satellite bodies around large pipes may be explained by either of these models.

13.5.3 CRYSTALLIZATION OR REPLACEMENT ?

The early-formed, pene-contemporaneous pegmatite bodies probably formed by crystallization from the pegmatitic liquid, rather than by a process of magmatic replacement or metasomatism. The latter alternative is not favoured because it necessitates disequilibrium between the pegmatitic liquids and the anorthosite from which they were derived. Thus the composition of pegmatite here is directly equivalent to the putative pegmatitic liquid. By analogy with intercumulus material that is trapped within cumulates and, possibly with iron-rich cumulates, it may be deduced that this silicate

liquid crystallized under magmatic conditions. This is supported by mineralogical data presented in this thesis.

Field relationships exhibited by large, pipe-like bodies and small, irregular, often sheet-like bodies, that cut cumulates other than mottled anorthosites do not indicate an intrusive origin. However, whether this means they support a replacement origin is open to debate. Specific field relationships and contact features imply that local replacement of pre-existing cumulates has occurred. However, other observations, discussed in the main text, argue against an origin entirely by replacement for complete pegmatite bodies. It is postulated that many of the larger pegmatite bodies also formed pene-contemporaneously with their cumulate hosts, again by crystallization from a liquid with subsequent volumetric re-adjustments of the still, unconsolidated cumulate pile.

13.5.4 SUMMARY

In reality it is very difficult to establish whether the pegmatites formed by magmatic replacement or by crystallization from a liquid. The most important conclusions reached from data collated in this study are that in many cases the composition of the pegmatites is equivalent to that of the putative pegmatitic liquids, and that these crystallized at magmatic temperatures. Iron-rich ultramafic pegmatite is thus interpreted as a magmatic rock, that formed either by crystallization from, or replacement related to, a silicate liquid. They are not the result of metasomatism related to aqueous fluid or vapour. The putative pegmatitic liquid is ascribed to postcumulus liquids (intercumulus and/or residual liquids) derived during crystallization of mottled anorthosite cumulates. It is implied that the putative pegmatitic liquid will only commence to form in the cumulate pile after mottled anorthosite cumulates occur, and they will cease to form after the residual liquid line of descent reaches the peak of the iron enrichement fractionation path. In summary, formation of iron-rich ultramafic pegmatite may be considered as an ongoing, dynamic series of events that are an integral part of the crystallization of a cumulate pile.

CHAPTER 14 SUMMARY AND CONCLUSIONS

The main characteristics of the iron-rich ultramafic pegmatite suite are summarised, under five headings, field relationships, mineralogy, chemistry, genesis, and a summary of economic considerations.

14.1 FIELD RELATIONSHIPS

(1) They clearly post-date the formation of the cumulate layering, consequently they are described as postcumulus rocks.
(2) Discordant bodies of iron-rich ultramafic pegmatite are considerably more abundant in the layered sequence of the Bushveld Complex than was previously recognized, particularly in the upper critical and main zones; they clearly form an integral and very significant component of the layered sequence.
(3) The distribution of these bodies is related to two major stratigraphic controls - they occur largely above the ultramafic cumulates in the lower and lower critical zones, but they rarely occur above the highest cumulus Ti-magnetite layer in the upper zone.
(4) Their distribution is also controlled by major structural features, thus they are abundant in structurally disturbed areas characterised by faulting and post-Bushveld dykes.
(5) They occur in both small, irregular bodies and large, pipe-like features which may have diameters in excess of 1 km.
(6) Iron-rich ultramafic pegmatite bodies are discordant to the cumulate layering, although small bodies may be concordant, and may form extensive sheet-like features.
(7) The cumulate layering adjacent to these bodies is usually undisturbed.
(8) The pipe-like bodies usually cut the cumulate layering approximately at right angles, but adjacent to the Townlands pipe the cumulate layering is structurally disturbed and downwarped (note similarity with Driekop pipe).
(9) Relict cumulate layers occur within certain pipe-like bodies, but whether these are undisturbed in relation to the primary layering has not been ascertained.
(10) Small, irregular bodies of iron-rich ultramafic pegmatite are preferentially concentrated in areas adjacent to large, pipe-like bodies, where they may form a complicated series of bodies that are possibly interlinked by minor feeder channels, dykes and veins.
(11) Pegmatite in the small bodies may exhibit striking evidence of selective

"replacement", as felsic cumulates (particularly anorthosites) act as traps for the pegmatitic liquids, whereas ultramafic cumulates (particularly harzburgites and chromitites) behave as fairly impervious barriers.
(12) Coarse-grained aggregates of recrystallized plagioclase are commonly observed in the marginal parts of pegmatite bodies; these are interpreted as contact features.

14.2 MINERALOGY

(1) Two main varieties are recognized, namely typical, silicate-rich pegmatite and Fe-Ti oxide pegmatite; the latter comprises normal and Cr-rich varieties.
(2) In the upper critical zone typical, silicate-rich pegmatite is dominantly composed of iron-rich clinopyroxene (augite) and olivine (hortonolite), usually with less than 20 modal percent Fe-Ti-(Cr) oxides and less than 5 modal percent base-metal sulphide and only very minor amphibole and mica.
(3) Cr-rich Fe-Ti oxide pegmatite, which is composed of an unusual Fe-Ti-Cr spinel and ilmenite, is restricted to the critical zone; its formation is related to interaction between primary chromitite layers and pegmatitic liquids.
(4) Normal Fe-Ti oxide pegmatite, which is essentially composed of Ti-magnetite and ilmenite, is rarely observed in the upper critical zone; it becomes common in the main zone, but is abundant in the upper zone where it may exhibit a close spatial relationship with cumulus Ti-magnetite layers.
(5) Minor quantities of plagioclase may occur in silicate-rich pegmatite. However, field relationships and textural and chemical studies imply that plagioclase is a relict cumulus mineral; it is not related to pegmatite sensu stricto.
(6) Iron-rich ultramafic pegmatite is always more fractionated, with respect to Mg/Fe ratios, than cumulates at the same position.
(7) The large, pipe-like bodies usually exhibit an internal mineralogic zonation. This may take two forms. In the first of these an irregular zonation occurs in which the lateral parts of a "pipe" are composed of clinopyroxene-rich pegmatite, with internal parts composed of Fe-Ti oxide-olivine-rich pegmatite, possibly with cores of Fe-Ti oxide pegmatite. Secondly, zonation may be related to mineral composition (evidenced by the Mg/Fe ratio of ferromagnesian silicates) resulting in at least two pegmatite-assemblages, possibly of different ages. The distribution of base-metal sulphides may be extremely irregular in these composite bodies.
(8) These rocks exhibit a mineralogical and chemical relationship with

respect to height in the cumulate pile. In the upper critical - lower main zone they are composed of augite and hortonolite, usually with less than 20 modal percent Fe-Ti-(Cr) oxides. In the middle of the main zone ferroaugite and ferrohortonolite are found, Fe-Ti oxides become abundant, the spinel is a Cr-poor variety, and apatite becomes an important accessory constituent. In the upper zone Fe-Ti oxide pegmatite is probably dominant over silicate-rich pegmatite. Thus, the silicates exhibit a decrease in X_{Mg} and the proportion of Fe-Ti oxides increases with height.

(9) They do not exhibit any mineralogical or chemical relationship with their cumulate hosts, although different contact features are apparent depending on whether the pegmatites replace felsic, mafic or ultramafic cumulates. In felsic cumulates ferromagnesian silicates are replaced first, whereas in ultramafic-mafic cumulates intercumulus plagioclase is replaced before cumulus orthopyroxene and olivine.

(10) In iron-rich ultramafic pegmatite sensu stricto the following paragenetic sequence is evident : clinopyroxene → olivine → ilmenite → Fe-Ti-(Cr) spinel → (base-metal sulphide – amphibole – mica). Each mineral in this sequence may replace earlier minerals.

(11) Mineralogical and textural studies are consistent with an origin for disseminated grains of Fe-Ti oxides in this assemblage by crystallization from an Fe-Ti-(V)-rich liquid at magmatic temperatures.

(12) The base-metal sulphide mineralogy of iron-rich ultramafic pegmatite in the upper critical zone is typical of a highly fractionated magmatic assemblage. It consists of approximately 95 modal percent pyrrhotite (intergrowth of troilite and hexagonal pyrrhotite), 3 modal percent cubanite and chalcopyrite and less than 2 modal percent pentlandite (a Co-rich variety).

(13) Iron-rich ultramafic pegmatite is normally non-platiniferous.

14.3 CHEMISTRY

(1) At a constant position in the layered sequence pegmatite-hosted olivine and clinopyroxene define a very limited compositional range, as evidenced by X_{Mg}.

(2) The minor element chemistry of clinopyroxene and olivine in these rocks is generally comparable to that of cumulus minerals with similar X_{Mg}, although olivine is slightly richer in Ni.

(3) In pegmatite in the upper critical zone the spinel is an unusual Fe-Ti-Cr variety; it possibly reflects the unusual composition of the pegmatitic liquids. The abundance of Fe-Ti oxides in these rocks may point to

relatively high fO_2.

(4) The base-metal sulphide assemblage of pegmatites in the upper critical zone is characterised by an exceptionally high Fe/(Ni+Cu) ratio, a high Cu/Ni ratio and a high Co content (in comparison with the mineralogy of cumulus sulphides in the upper critical zone).

(5) The relationship between the Fe/Ni ratio of co-existing olivines (Ni-rich) and sulphides (Ni-poor) suggests that olivine crystallized before the pegmatitic liquids reached sulphur saturation.

(6) The whole-rock chemistry of the pegmatites is characterised by high FeO, Fe_2O_3, TiO_2 and extreme paucity in Al_2O_3 and Na_2O.

(7) The trace element levels are essentially modally dependent.

(8) Iron-rich ultramafic pegmatite is enriched in incompatible elements as compared with cumulates from the same height in the layered sequence.

(9) Metasomatism of the cumulate wallrocks is evident at the contacts of pegmatite bodies. This may result in progressive alteration of cumulus minerals to pegmatitic olivine and clinopyroxene (accompanied by the relevant chemical changes) and saussuritisation of plagioclase.

14.4 GENESIS

(1) The putative pegmatitic liquid is ascribed to intercumulus, and possibly residual, liquids segregated from crystallizing (thick) layers of mottled anorthosite cumulates.

(2) The pegmatitic liquid is thus a silicate liquid that was at magmatic temperatures.

(3) Suitable pegmatitic liquids will only commence to form in the cumulate pile after mottled anorthosite cumulates occur, and they will cease to form after the residual liquid line of descent reaches an absolute enrich ment in total iron.

(4) In many cases the composition of iron-rich ultramafic pegmatite is probably equivalent to that of the pegmatitic liquid.

(5) Iron-rich ultramafic pegmatite is thus a magmatic rock which formed either by crystallization from, or replacement related to, a silicate liquid.

(6) Iron-rich ultramafic pegmatite has not resulted from metasomatism related to aqueous fluid or vapour.

(7) Formation of iron-rich ultramafic pegmatite may be considered as an ongoing, dynamic series of events that are an intergral part of the crystallizing cumulate pile.

14.5 ECONOMIC CONSIDERATIONS

The platiniferous ultramafic pipes in the eastern limb of the Bushveld Complex, which were once the major source of platinum in the Transvaal, are no longer of any direct commercial value. Other, pipe-like bodies in the Bushveld Complex that were once mined include the nickel-rich Vlakfontein bodies and the vanadiferous orebody at Kennedy's Vale. None of these pipe-like orebodies is presently being mined and, paradoxically, many of the discordant bodies of ultramafic rock in the Bushveld Complex have a detrimental effect on modern mining activities. Consequently, it is suggested that ore reserve calculations should take into account the disruptive effects of these rocks on cumulate orebodies. In areas of poor outcrop detailed magnetic surveys provide a useful guideline to the approximate distribution and relative abundance of these bodies. Adjacent to large, pipe-like bodies (such as Driekop and Townlands) the cumulate wallrocks may be structurally disturbed over considerable areas, resulting in much larger ore reserve losses than may at first be apparent.

Small, irregular bodies of iron-rich ultramafic pegmatite also have a detrimental effect on mining activities. Because of their irregular nature it is practically impossible to accurately predict the distribution of these bodies on a scale sufficient to assist day-to-day mining activities. Again, detailed magnetic surveys may assist with delineating general areas that are characterised by extensive pegmatite development, but specific bodies cannot be assessed. At the Amandelbult Section of RPM iron-rich ultramafic pegmatite has not presented as major a problem as was initially anticipated.

This may be explained by two observations. Firsly, magnetic surveys exaggerate the size of a pegmatite body and do no take into account their irregular nature. Secondly, many pegmatite bodies at Amandelbult that replace the Merensky Reef do not replace the Merensky upper chromitite layer or the hangingwall pyroxenite; consequently, the replaced Reef can be delineated and mined almost as usual . In other circumstances, if the upper chromitite layer and the hangingwall pyroxenite were also replaced, it is predicted that delineation of the replaced Reef would be extremely difficult, if not impossible, and the PGE mineralisation would probably have been leached (and reprecipated some distance from the original Reef).

Mining of replaced Reef may result in two problems. Firstly, if the Reef is completely replaced then it is evident that base-metal sulphides from the primary Reef are remobilised and precipated in an irregular zone above the upper chromitite layer. This results in a sulphide-poor Reef, with maximum concentrations of Ni-Cu-rich sulphides in the hangingwall. Sulphides

in the replaced Reef are dominantly Ni-Cu-poor, and are thus related to the iron-rich ultramafic pegmatite. If PGE are redistributed with the sulphides then the majority of the PGE will be in an irregular layer in, and above, the upper chromitite; the replaced Reef itself probably carries only very minor PGE. Ideally, mining of replaced Reef should include a thicker than normal slice of the hangingwall. Detailed studies of the distribution of PGE in, and above, replaced Reef are required. Secondly, extraction problems may result from mining replaced Reef, which has a very different whole-rock chemistry to normal Merensky Reef.

Iron-rich ultramafic pegmatite in the upper critical zone of the Bushveld Complex is normally non-platiniferous. The possibility that pegmatite in the upper zone may contain economic concentrations of PGE cannot be overruled, although it is considered unlikely. Also, iron-rich ultramafic pegmatite is unlikely to contain appreciable quantities of Ni-sulphide (except possibly for rare occurrences in the lower and lower critical zones), although they may contain economically insignificant concentrations of copper. In general, sulphides in these rocks are characterised by exceptionally high Fe/(Ni+Cu) ratios.

REFERENCES

ALLEN, J.C. & BOETTCHER, A.L. (1983) : The stability of amphibole in andesite and basalt at high pressure. Amer. Mineral. 68, 307-314.

ATKINS, F.B. (1969) : Pyroxenes of the Bushveld intrusion, South Africa. J. Petr. 10, 222-249.

BATEMAN, A.M. (1951) : The formation of late magmatic oxide ores. Econ. Geol. 46, 404-426.

BOCTOR, N.Z. (1982) : The effect of fO_2, fS_2 and temperature on Ni partitioning between olivine and iron sulfide melts. Carnegie Inst. Washington, Ann. Rept. Dir. Geophys. Lab. 1981-82, 366-369.

BOTHA, M.J. : Mineralogy and geochemistry of units B to E on Zandspruit 168JP, Western Bushveld Complex. M.Sc. thesis (in prep.), Rhodes Univ., Grahamstown.

BOWEN, N.L. & SCHAIRER, J.F. (1935) : The system, MgO-FeO-SiO_2. Amer. J. Sci. 37, 487-500.

--------- & TUTTLE, O.F. (1949) : The system MgO-SiO_2-H_2O. Geol. Soc. Amer. 60, 439-460.

BRIDGWATER, D. SUTTON, J. & WATTERSON, J. (1974) : Crustal downfolding associated with igneous activity. Tectonophysics 21, 57-77.

BRISTOW, D.M. & WILSON, A.H. (1983) : Some aspects of pegmatoid development in the Winterveld mine - Eastern Bushveld Complex. Sym. on the Bushveld Complex, Pretoria, Abstr.

BROWN, G.M. (1956) : The layered ultrabasic rocks of Rhum, Inner Hebrides. Phil. Trans. Roy. Soc. London B. 240, 1-53.

BRYNARD, H.J., DE VILLIERS, J.P.R. & VILJOEN, E.A. (1976) : A mineralogical investigation of the Merensky Reef at the Western Platinum mine, near Marikana, South Africa. Econ. Geol. 71, 1299-1307.

BUCHANAN, D.L. (1979) : A combined transmission electron microscope and electron microprobe study of the Bushveld pyroxenes from the Bethal area. J. Petr. 20, 327-354.

BUDDINGTON, A.F. & LINDSLEY, D.H. (1964) : Iron-titanium minerals and synthetic equivalents. J. Petr. 5, 310-357.

BURNS, R.G. (1970) : Crystal field spectra and evidence of cation disordering in olivine minerals. Amer. Mineral. 55, 1608-1632.

CABRI, L.J. (Ed.) (1981) : Platinum-group elements : Mineralogy, geology, recovery. Can. Inst. Mining & Metallurgy Spec. Vol. 23, 276p.

---------- & HALL, S.R. (1972) : Mooihoekite and haycockite, two new copper-iron sulphides, and their relationship to chalcopyrite and talnakhite. Amer. Mineral. 57, 689-708.

CAMERON, E.N. (1977) : Chromite in the central sector of the eastern Bushveld Complex, South Africa. Amer. Mineral. 62, 1082-1096.

---------- (1978) : The lower zone of the eastern Bushveld Complex in the Olifants River trough. J. Petr. 19, 437-462.

---------- (1980) : Evolution of the lower critical zone, eastern Bushveld Complex, and its chromitite deposits. Econ. Geol. 75, 845-871.

---------- (1982) : The upper critical zone of the eastern Bushveld Complex - precursor of the Merensky Reef. Econ. Geol. 77, 1307-1321.

---------- & DEŠBOROUGH, G.A. (1964) : Origin of certain magnetite-bearing pegmatites in the eastern part of the Bushveld Complex, South Africa. Econ. Geol. 59, 197-225.

---------- & GLOVER, E.D. (1973) : Unusual titanium-chromian spinels from the eastern Bushveld Complex. Amer. Mineral. 58, 172-188.

CAMPBELL, I.H. (1977) : A study of macro-rhythmic layering and cumulate processes in the Jimberlana Intrusion, Western Australia. J. Petr. 18, 183-215.

---------- & BARNES S.J. (1984) : A model for the geochemistry of the platinum-group elements in magmatic sulfide deposits. Can. Mineral. 22, 151-160.

---------- & BORLEY, G.D. (1974) : The geochemistry of pyroxenes from the Lower Layered Series of the Jimberlana Intrusion, Western Australia. Contr. Mineral. Petr. 47, 281-298.

---------- & NALDRETT, A.J. (1979) : The influence of silicate:sulfide ratios on the geochemistry of magmatic sulfides. Econ. Geol. 74, 1503-1506.

---------- & BARNES, S.J. (1983) : A model for the origin of platinum-rich sulfide horizons in the Bushveld and Stillwater Complexes J. Petr. 24, 133-165.

CLARK, T. & NALDRETT, A.J. (1972) : The distribution of Fe and Ni between synthetic olivine and sulfide at 900°C. Econ. Geol. 67, 939-952.

COERTZE, F.J. (1962) : The Rustenburg fault as a controlling factor of ore-deposition, S.W. Pilanesberg. Geol. Soc. South Africa, Trans. 65, 253-257.

---------- (1966) : The genesis and geological environment of the Bushveld magnetite in the area south-west of the Leolo Mountains. Geol. Surv. South Africa, Bull. 47, 57p.

---------- (1974) : The geology of the Basic Portion of the Western Bushveld Igneous Complex. Geol. Surv. South Africa, Mem. 66, 148p.

---------- & Schumann, F.W. (1962) : The basic portion and associated minerals of the Bushveld Igneous Complex north of Pilanesberg. Geol. Surv. South Africa, Bull. 38, 48p.

COUSINS, C.A. (1964) : The platinum deposits of the Merensky Reef. In Haughton, S.H. (ed.) The geology of some ore deposits of Southern Africa, 2, Geol. Soc. South Africa, 226-237.

---------- (1969) : The Merensky Reef of the Bushveld Igneous Complex. In Magmatic Ore Deposits, Econ. Geol. Mon. 4, 239-251.

COX, K.G., BELL, J.D. & PANKHURST, R.J. (1979) : The interpretation of igneous rocks. George Allen & Unwin, London, 450p.

CRAIG, G. & KULLERUD, G. (1969) : Phase relations in the Cu-Fe-Ni-S system and their application to magmatic ore deposits. In Magmatic Ore Deposits, Econ. Geol. Mon. 4, 344-358.

CROCKET, J.H. (1979) : Platinum-group elements in mafic and ultramafic rocks : a survey. Can. Mineral. 17, 391-402.

--------- TERUTA, Y. & GARTH, J. (1976) : The relative importance of sulfides, spinels, and platinoid minerals as carriers of Pt, Pd, Ir and Au in the Merensky Reef at Western Platinum Limited, near Marikana, South Africa. Econ. Geol. 71, 1308-1323.

DE BRUYN, P.L. (1944) : A new occurrence of nickeliferous ore in the Bushveld Complex. Ann. Univ. Stellenbosch, 22(a), 63-96.

DEER, W.A., HOWIE, P.A., & ZUSSMAN, J. (1962) : Rock forming minerals vol. 5, Non-silicates, Longmans, 371p.

---------- (1962) : Rock forming minerals vol. 3, Sheet silicates, Longmans, 270p.

---------- (1963) : Rock forming minerals vol. 2, Chain silicates, Longmans, 379p.

---------- (1978) : Rock forming minerals vol. 2A, Single chain silicates , Longmans, 668p.

---------- (1982) : Rock forming minerals vol. 1A, Orthosilicates, Longmans, 919p.

DE KLERK, W.J. (1982) : The geology, geochemistry and silicate mineralogy of the upper critical zone of the N.W. Bushveld Complex, at R.P.M. Union Section. M.Sc. thesis, (unpub.), Rhodes Univ., Grahamstown.

DE VORE, G.W. (1957) : The association of strongly polarising cations with weakly polarizing cations as a major influence in element distribution, mineral composition, and crystal growth. J. Geol. 65, 178-195

DE WAAL, A. (1975) : The mineralogy, chemistry and certain aspects of reactivity of chromitite from the Bushveld Igneous Complex. Johannesburg. Nat. Inst. Metallurgy (South Africa). Rept. 1709, 80p.

DUKE, J.M. (1976) : Distribution of the period four transition elements among olivine, calcic pyroxene and mafic silicate liquid. J. Petr. 17, 499-521.

--------- (1979) : Computer simulation of the fractionation of olivine and sulfide from mafic and ultramafic magmas. Can. Mineral. 17, 507-514.

--------- & NALDRETT, A.J. (1978) : A numerical model of the fractionation of olivine and molten sulfide from komatiite magma. Earth Planet. Sci. Lett. 39, 255-266.

DUNGAN, M.A. & AVE LALLEMENT, H.G. (1978) : Formation of small dunite bodies by metasomatic transformation of harzburgite in the Canyon Mountain Ophiolite, northeast Oregon. Bull. Oregon Dept. Mineral. Ind. 96, 109-128.

EALES, H.V. : The features and genetic significance of chromite layers in the upper critical zone at RPM Union Section mine, western Bushveld Complex. In Guidelines to the evolution of chromitite ore-fields (in press), Hutchinson & Ross.

---------- & REYNOLDS, I.M. (1983) : The nature of the chromitite layers within the UG-1 - Bastard Unit interval, RPM Union Section. Sym. on the Bushveld Complex, Pretoria, Abstr.

---------- & GOUWS, D.A. (1981) : The spinel-group minerals of the central Karoo tholeiitic province. Geol. Soc. South Africa, Trans. 83, 243-253.

---------- MITCHELL, A.A., & BOTHA, M.J. (1983) : Partioning of Cr, V, Ti, Co and Ni between silicate and oxide phases within sections of the western Bushveld Complex. Final report, National Geoscience Programme, C.S.I.R. South Africa.

ENGEL, A.E.J. & ENGEL, C.G. (1960) : Progressive metamorphism and granitization of the Major paragneiss, northwest Adirondack Mountains, New York. Part 2, Mineralogy. Geol. Soc. Amer. Bull. 71, 1-58.

ERNST, W.G. (1968) : Amphiboles. Springer-Verlag Berlin. 125p.

EVANS, B.W. & TROMMSDORFF, V. (1974) : Stability of enstatite and talc and CO_2-metasomatism of metaperidotite, Val d'Efra, Lepontine Alps. Amer. J. Sci. 274, 274-296.

FERGUSON, J. & MCCARTHY, T.S. (1970) : Origin of an ultramafic pegmatoid in the eastern part of the Bushveld Complex. Geol. Soc. South Africa, Spec. Pub. 1, 74-79.

FERRINGA, G. (1959) : The geological succession in a portion of the north-western Bushveld (Union Section) and its interpretation. Geol. Soc. South Africa, Trans. 62, 219-233.

FINCHAM, C.J.B. & RICHARDSON, F.D. (1954) : The behaviour of sulphide in silicate and aluminate melts. Roy. Soc. London Phil. Trans. 223, 40-62.

FLEET, M.E. (1974) : Partitioning of Mg and Fe^{2+} in coexisting pyroxenes. Contr. Mineral. Petr. 44, 251-257.

---------- (1979) : Partitioning of Fe, Co, Ni and Cu between sulfide liquid and basaltic melts and the composition of Ni-Cu sulfide deposits - a discussion. Econ. Geol. 74, 1517-1519.

--------- & MACRAE, N.D. (1983) : Partition of Ni between olivine and sulfide and its application to Ni-Cu sulfide deposits. Contr. Mineral. Petr. 83, 75-81.

---------- & HERZBERG, C.T. (1977) : Partition of nickel between olivine and sulfide : a test for immiscible sulfide liquids. Contr. Mineral. Petr. 65, 191-197.

---------- & OSBORNE, M.D. (1981) : The partition of nickel between olivine, magma and immiscible sulfide liquid. Chem. Geol. 32, 119-127.

FREY, F.A., GREEN, D.H. & ROY, S.D. (1978) : Integrated models of basalt petrogensis : A study of quartz tholeiites to olivine melilites from south eastern Australia utilizing geochemical and experimental petrological data. J. Petr. 19, 463-513.

GAIN, S.B. (1980) : The geology and PGE distribution in the upper chromitite layers at Maandagshoek 254KT, eastern Bushveld Complex. Inst. Geol. Res. Bushveld Complex, Univ. Pretoria Spec. Rep. 22, 24p.

GREENWOOD, H.J. (1963) : The synthesis and stability of anthophyllite. J. Petr. 4, 317-351.

GROUT, F.F. (1945) : Scale models of structures related to batholiths. Amer. J. Sci. 243-A (Daly Vol.), 260-284.

HAGGERTY, S.E. (1976) : Opaque minerals in terrestrial igneous rocks. In Rumble, D. (Ed.) Oxide minerals, Min. Soc. Amer. short course notes vol. 3, 101-300.

HALL, A.L. (1932) : The Bushveld Igneous Complex of the Central Transvaal. Geol. Surv. South Africa, Mem. 28, 560p.

HAMILTON, W. (1977) : Sr-isotope and trace element studies of the Great Dyke and Bushveld mafic phase and their relation to early Protozoic magma genesis in Southern Africa. J. Petr. 18, 24-52.

HARRIS, D.C. & NICKEL, E.H. (1972) : Pentlandite compositions and associations in some mineral deposits. Can. Mineral. 11, 861-878.

HART, S.R. & Davis, K.E. (1978) : Nickel partitioning between olivine and silicate melt. Earth Planet. Sci. Lett. 40, 203-219.

HATCH, F.H., WELLS, A.K. & WELLS, M.K. (1974) : Petrology of the igneous rocks. Thomas Murphy and Co. 13th. ed., 551p.

HATTON, C.J. & VON GRUENEWALDT, G (1983) : Magma intrusion and faulting in the development of the middle group of chromitite layers in the Eastern and Western Bushveld Complex. Sym. on the Bushveld Complex, Pretoria, Abstr.

HAUGHTON, D.R., ROEDER, P.L. & SKINNER, B.J. (1974) : Solubility of sulfur in mafic magmas. Econ. Geol. 69, 451-467.

HECKROODT, R.O. (1959) : The geology around the dunite pipe on Driekop, eastern Transvaal. Geol. Soc. South Africa, Trans. 62, 59-73.

HEIDSTRA, P.T. (1978) : Report on detailed ground magnetometer survey, Amandelbult Section, RPM, J.C.I. Geophysics Section Rep. 32/78 (unpub. internal rep.)

HESS, G.B. (1972) : Heat and mass transport during crystalllization of the Stillwater Igneous Complex. Geol. Soc. Amer. Mem. 132, 503-520.

HESS, H.H. (1941) : Pyroxenes of common mafic magmas, part 2. Amer. Mineral. 26 573-594.

---------- (1960) : Stillwater Igneous Complex, Montana. Geol. Soc. Amer. Mem. 80, 230p.

HULBERT, L.J. & VON GRUENEWALDT, G. (1982) : Nickel, copper and platinum mineralization in the lower zone of the Bushveld Complex, south of Potgietersrus. Econ. Geol. 77, 1296-1306.

HUNTER, D.R. & HAMILTON, P.J. (1978) : The Bushveld Complex. In Evolution of the Earth's Crust, Tarling (Ed.), 107-172.

HUPPERT, H.E. & SPARKS, R.S.J. (1980) : The fluid dynamics of a basaltic magma chamber replenished by influx of hot, dense ultrabasic magma. Contr. Mineral. Petr. 75, 279-289.

IANELLO,I. (1967) : Pipes of pyroxenite-shonkinite on Grootkuit 376 KQ Thabazimbi District. Geol. Surv. South Africa, Ann. 6, 91-97.

IRVINE, T.N. (1967) : Chromian spinel as a petrogenetic indicator : part 2. Petrologic applications. Can. J. Earth Sci. 4, 71-103.

---------- (1974) : Petrology of the Duke Island Ultramafic Complex, Southeastern Alaska. Geol. Soc. Amer. Mem. 138.

---------- (1980) : Magmatic infiltration metasomatism, double-diffusive fractional crystallization and adcumulus growth in the Muskox and other layered intrusions, In Physics of magmatic processes, Hargreaves, R.B. (Ed.), Princeton Univ. Press, 325-383.

---------- (1982) : Terminology for layered intrusions. J. Petr. 23, 127-162.

---------- & BARAGAR, W.R.A. (1971) : A guide to the chemical classification of the common volcanic rocks. Can. J. Earth Sci. 8, 523-548.

IRVINE, T.N., KEITH, T.N. & TODD, S.G. (1983) : The J-M Platinum-Palladium Reef of the Stillwater Complex : 2. Origin by double-diffusive convective magma mixing and implications for the Bushveld Complex. Econ. Geol. 78, 1287-1334.

---------- & SHARPE, M.J. (1983) : Bushveld chilled margin liquids 2 : Implications for the critical zone. Sym. on the Bushveld Complex, Pretoria, Abstr.

JACKSON, E.D. (1961) : Primary textures and mineral associations in the ultramafic zone of the Stillwater Complex, Montana. U.S. Geol. Surv. Prof. Paper 358, 106p.

---------- (1970) : The cyclic unit in layered intrusions : a comparison of repetitive stratigraphy in the ultramafic parts of the Stillwater, Muskox, Great Dyke and Bushveld Complexes. Geol. Soc. South Africa Spec. Pub. 1 391-424.

JAHNS, R.H. (1955) : The study of pegmatites. Econ. Geol. 50th Ann. vol., 1025-1130.

JONES, J.P. (1974) : Pegmatitic bodies in mafic rocks of the Bushveld Complex, Bafokeng leasehold area, Western Transvaal. M.Sc. thesis (unpub.), Univ. Witwatersrand, Johannesburg.

--------- (1976) : Pegmatoidal nodules in the layered rocks of the Bafokeng leasehold area. Geol. Soc. South Africa, Trans. 79, 312-320.

KANIRIS-SOTIROIU, R. (1974) : Fine-scale layering in igneous intrusions : a possible mechanism for a non-depostional origin. Geol. Mag. 111, 157-162.

KELSEY, C.H. (1961) : Calculation of the C.I.P.W. norm. Mineral. Mag. 34, 276-283.

KENNEDY, D & DE WET, P. (1983) : The occurrences and geological setting of graphite in the upper critical zone of the Bushveld Complex in the Rustenburg area. Sym. on the Bushveld Complex, Pretoria, Abstr.

KINGSTON, G.A. (1966) : The occurrence of platinoid bismuthotellurids in the Merensky Reef at Rustenburg platinum mine in the western Bushveld. Mineral. Mag. 35, 815-834.

KINLOCH, E.D. (1982) : Regional trends in the platinum-group mineralogy of the critical zone of the Bushveld Complex. Econ. Geol. 77, 1328-1347.

KNOP, O., IBRAHIM, M.A., & SUTARNO (1965) : Chalcogenides of the transition elements IV : pentlandite. Can. Mineral. 8, 291-316.

KORZHINSKII, D.S. (1965) : The theory of systems with perfect mobile components and processes of mineral formation. Amer. J. Sci. 263, 193-205.

KOUVO, O., HUHMA, M. & VUORELAINEN, Y. (1959) : A natural cobalt analogue of pentlandite. Amer. Mineral. 44, 897-900.

KRUGER, F.J. (1984) : The petrology of the Merensky cyclic unit and associated rocks and their significance in the evolution of the western Bushveld Complex. Ph.D thesis (unpub.), Rhodes Univ., Grahamstown.

---------- & MARSH, J.S. (1982) : The significance of 87Sr/86Sr ratios in the Merensky cyclic unit of the Bushveld Complex. Nature 298, 53-55.

---------- (1983) : The petrology of the Merensky cyclic unit in the western Bushveld Complex. Sym. on the Bushveld Complex, Pretoria, Abstr.

KULLERUD, G., YUND, R.A. & MOH, G.H. (1969) : Phase relations in Cu-Fe-S, Cu-Ni-S Fe-Ni-S systems. In Magmatic ore deposits, Econ. Geol. Mon. 4, 323-343

KUPFERBURGER, W. & LOMBAARD, B.V. (1937) : The chromite deposits of the Bushveld Igneous Complex. Geol. Surv. South Africa, Bull. 10.

KUSHIRO, I. (1969) : The system forsterite-diopside-silica with and without water. Amer. J. Sci. 267-A (Schairer vol.), 269-294.

LARIMER, J.W. (1968) : Experimental studies on the system Fe-MgO-SiO_2-O_2 and their bearing on the petrology of chondritic meteorites. Geochim. Cosmochim. Acta 32, 1187-1207.

LEAKE, B.E. (1978) : Nomenclature of amphiboles. Can. Mineral. 16, 501-520.

LE BAS, N.J. (1962) : The role of Al in igneous clinopyroxenes with relation to their parentage. Amer. J. Sci. 260, 267-288.

LEE, C.A. (1983) : Trace and platinum-group element geochemistry and the development of the Merensky Unit of the Western Bushveld Complex. Mineralium Deposita 18, 173-190.

--------- SHARPE, M.R. & VILJOEN, E.A. (1983) : The chemistry of chromitite layers in the Bushveld Complex, with special reference to chromitite-plagioclase reaction. Sym. on the Bushveld Complex, Pretoria, Abstr.

LEEMAN, W.P., MA, M-S., MURALI, A.V. & SCHMITT, R.A. (1978) : Empirical estimation of magnetite/liquid distribution coefficients for some transition elements. Contr. Mineral. Petr. 65, 269-272.

LESHER, C.M., LEE, R.F., GROVES, D.I., BICKEL, M.J. & DONALDSON, M.J. (1981) : Geochemistry of Komatiites from Kambalda, Western Australia. I. Chalcophile element depletion - a consequence of sulfide liquid separation from Komatiite Magma. Econ. Geol. 76, 1714-1728.

LIEBENBERG, L. (1970) : The sulfides in the layered sequence of the Bushveld Complex. Geol. Soc. South Africa, Spec. Pub. 1, 108-207.

LINDSLEY, D.H. (1976) : The crystal chemistry and structure of oxide minerals as exemplified by Fe-Ti oxides and experimental studies of oxide minerals In Oxide Minerals, Mineral. Soc. Amer. Short Course notes, L1-L88.

LISTER, G.F. (1966) : The composition and origin of selected iron-titanium deposits Econ. Geol. 61, 275-310.

LOMBAARD, B.V. (1956) : Chromite and dunite of the Bushveld Complex. Geol. Soc. South Africa, Trans. 59, 59-74. (see also discussions p. 75-76).

MACLEAN, W.H. (1969) : Liquidus phase relations in the FeS-FeO-SiO_2 system and their application in geology. Econ. Geol. 64, 865-884.

--------- & SHIMAZAKI, H. (1976) : The partition of Co, Ni, Cu and Zn between sulfide and silicate liquids. Econ. Geol. 71, 1049-1057.

MARSH, B.D. (1982) : On the mechanics of igneous diapirisim, stoping, and zone melting. Amer. J. Sci. 282, 808-855.

MCBIRNEY, A.R. & NOYES, R.M. (1979) : Crystallization and layering of the Skaergaard intrusion. J. Petr. 20, 487-554.

MCTAGGART, K.C. (1971) : On the origin of ultramafic rocks. Geol. Soc. Amer. Bull. 82, 23-42.

MEDARIS, L.G. (1969) : Partitioning of Fe^{2+} and Mg^{2+} between coexisting synthetic olivine and orthopyroxene. Amer. J. Sci. 267, 945-968.

MISRA, K.C. & FLEET, M.E. (1974) : Composition variations in a Ni-Co-As assemblage Can. Mineral. 12, 431 (Abstr.).

MITCHELL, A.A. : The geochemistry and origin of the main zone, western Bushveld Complex. Ph.D thesis (in prep.), Rhodes Univ., Grahamstown.

MOLYNEUX, T.G. (1970) : The geology of the area in the vicinity of Magnet Heights, Eastern Transvaal, with special reference to the magnetic iron ore. Geol. Soc. South Africa, Spec. Pub. 1, 228-241.

---------- (1974) : A geological investigation of the Bushveld Complex in Sekhukhuneland and part of the Steelpoort valley. Geol. Soc. South Africa, Trans. 77, 329-338.

MORSE, S.A. (1979) : Reaction constants for En-Fo-Sil equilibria : an adjustment and some applications. Amer. J. Sci. 279, 1060-1069.

---------- (1980) : Basalts and phase disgrams. Springer-Verlag, 493p.

MOSSOM, R. (1977) : Report on Driekop, Forest Hill, and Hackney : JCI (unpub. internal rep.).

MYERS, J.S. (1978) : Pipes of mafic pegmatite in the stratiform Fiskenaesset Anorthosite Complex, S.W. Greenland. Lithos 11, 277-282.

MYSEN, B.O. (1979) : Nickel partitioning between olivine and silicate melt : Henry's law revisited. Amer. Mineral. 64, 1107-1114.

---------- & KUSHIRO, I (1976) : Partitioning of iron, nickel, and magnesium between metal, oxide and silicates in Allende meteorite, as a function of fO_2. Carnegie Inst. Washington, Ann. Rept. Dir. Geophys. Lab. 1975-76, 678-684.

---------- (1979) : Pressure dependence of nickel partitioning between Fo and aluminous silicate melts. Earth Plan. Sci. Lett. 42, 383-388.

--------- & VIRGO, D. (1980) : Influence of melt structure on crystal-liquid trace-element partitioning. Carnegie Inst. Washington, Ann. Rept. Dir. Geophys. Lab. 1979-80, 326-327.

NAKAMURA, Y & KUSHIRO, I. (1974) : Compositions of the gas phase in the system Mg_2SiO_4-SiO_2-H_2O at 15 kbar. Carnegie Inst. Washington, Ann. Rept. Dir. Geophys. Lab. 1973-74, 255-258.

NALDRETT, A.J. (1967) : Melting relations over a portion of the Fe-S-O system and their bearing on the temperature of crystallization of natural sulphide-oxide liquids. Carnegie Inst. Washington, Ann. Rept. Dir. Geophys. Lab. 1966-67, 419-427.

---------- (1979) : Partitioning of Fe, Co, Ni and Cu between sulfide liquid and basaltic melts and the composition of Ni-Cu sulfide deposits - a reply and further discussion. Econ. Geol. 74, 1520-1528.

---------- (1981) : Nickel sulfide deposits; classification, composition and genesis. Econ. Geol., 75th Anniv. Vol., 628-685.

---------- & CABRI, L.J. (1976) : Ultramafic and related mafic rocks : their classification and genesis with special reference to the concentration of nickel sulfides and platinum-group elements. Econ. Geol. 71, 1131-1158.

---------- HOFFMAN, E.L., GREEN, A.H., CHOU, C.L., NALDRETT, S.R. & ALCOCK, R. (1979) : The composition of Ni-sulfide ores with particular reference to their content of PGE and Au. Can. Mineral. 17, 403-416.

--------- GASPARRINI, C., BARNES, S.J., SHARPE, M.R. & VON GRUENEWALDT, G. (1983) : Cyclic units at the top of the critical zone of the Bushveld Complex and the origin of the Merensky Reef. Sym. on the Bushveld Complex, Pretoria, Abstr.

NOBLE, J.A. & TAYLOR, H.P. (1960) : Correlation of the ultramafic complexes of S.E. Alaska with those of other parts of N. America and the world. Internal. Geol. Cong. 21st session Rept., Pt. 13, 188-197.

OSBORNE, F.F. (1928) : Certain magmatic titaniferous iron ores and their origin. Econ. Geol. 23, 724-761.

PAGE, N.J. (1977) : Stillwater Complex, Montana : Rock succession, metamorphism and structure of the Complex and adjacent rocks. U.S. Geol. Surv. Prof. Paper 999.

PASTER, T.P., SCHAUWECKER, D.S. & HASKIN, L.A. (1974) : The bahaviour of some trace elements during solidification of the Skaergaard layered series. Geochim. Cosmochim. Acta 34, 307-322.

PEARCE, J.A. & NORRY, M.J. (1979) : Petrographic implications of Ti, Zr, Y and Nb variations in volcanic rocks. Contr. Mineral. Petr. 69, 33-47.

PETRUK, W., HARRIS, D.C. & STEWART, J.M. (1969) : Langisite, a new mineral and the rare minerals cobalt pentlandite, siegenite, parkerite and bravoite from the Langis Mine Cobalt-Gowganda area, Ontario. Can. Mineral. 9, 597-616.

PEYERL, W. (1979) : The Pegmatoid Replaced Reef from the SW area of Amandelbult Section of RPM with special reference to its sulphide and platinoid mineralogy. JCI Minerals Lab. (unpub. internal rep.).

---------- (1981) : Mineralogical examination of selected borehole core samples from the Townlands dunite pipe, Rustenburg Section of RPM. JCI Minerals Lab. (unpub. internal rep.).

---------- (1982) : The influence of the Driekop pipe on the platinum-group mineralogy of the UG-2 chromitite in its vicinity. Econ. Geol 77, 1432-1438.

PHILLIPS, D. : Mineralogy and petrology of the Townlands iron-rich ultramafic pegmatite. M.Sc. thesis (in prep.), Rhodes Univ., Grahamstown.

PHILPOTTS, A.R. (1967) : Origin of certain iron-titanium oxide and apatite rocks. Econ. Geol. 62, 303-315.

POWER, C.F. & FINE, H.A. (1976) : The iron-sulphur system part 1. The structure and physical properties of the compounds of the low-temperature phase fields. Mineral. Sci. Eng. 8, 106-126.

PUTNIS, A. (1979) : Electron petrography of high-temperature oxidation in olivine from the Rhum layered intrusion. Mineral. Mag. 43, 293-296.

RAEDEKE, L.D. & MCCALLUM, I.S. (1984) : Investigations in the Stillwater Complex: part 2. Petrology and petrogenesis of the Ultramafic Series. J. Petr. 25, 395-420.

RAJAMANI, V. & NALDRETT, A.J. (1978) : Partitioning of Fe, Co, Ni and Cu between sulfide liquid and basaltic melts and the composition of Ni-Cu sulfide deposits. Econ. Geol. 73, 82-93.

---------- & PREWITT, C.T. (1973) : Crystal chemistry of natural pentlandites. Can. Mineral. 12, 178-187.

RAYLEIGH, C.B. (1968) : Experimental deformation of ultramafic rocks and minerals. In Ultramafic and related rocks, Wyllie, P.J. (Ed.), 191-199. John Wiley and Sons.

RAZIN, L.V. (1976) : Geologic and genetic features of forsterite dunites and their platinum-group mineralogy. Econ. Geol. 71, 1371-1376.

REYNOLDS, I.M. (1978) : A mineralogical investigation of co-existing iron-titanium oxides from various igneous rocks with special reference to some South African titaniferous iron ores. Ph.D thesis (unpub.), Rhodes Univ., Grahamstown, South Africa.

---------- (1982) : Magmatic ore deposits, a review. Sym. on the evolution of metalliferous ore deposits, Rhodes Univ., Grahamstown.

---------- : The nature and origin of titaniferous magnetite-rich layers in the upper zone of the Bushveld Complex : a review and synthesis. Econ. Geol. (in press).

---------- : Contrasted mineralogy and textural relationships in the uppermost titaniferous magnetite layers of the Bushveld Complex in the Bierkraal area, north of Rustenburg. Econ. Geol. (in press).

---------- & SCOON, R.N. (1983) : The iron-titanium oxide mineralogy of some ultramafic pegmatites from the critical and main zones of the Bushveld Complex. Sym. on the Bushveld Complex, Pretoria, Abstr.

ROBINSON, P., JAFFE, H.W., ROSS, M. & KLEIN, C. (1971) : Orientation of exsolution lamellae in clinopyroxenes and clinoamphiboles : consideration of optimal phase boundaries. Amer. Mineral. 56, 909-939.

ROEDER, P.L. (1974) : Activity of iron and olivine solubility in basaltic liquids. Earth Planet. Sci. Lett. 23, 397-410.

---------- & EMSLIE, R.F. (1970) : Olivine-liquid equilibrium. Contr. Mineral. Petr. 29, 275-289.

---------- CAMPBELL, I.A. & JAMIESON, H.E. (1979) : A re-evaluation of the olivine-spinel geothermometer. Contr. Mineral. Petr. 68, 325-354.

SAWKINS, F.J. (1984) : Metal deposits in relation to plate tectonics. Springer-Verlag, 325p.

SCHIFFRIES, C.M. (1982) : The petrogenesis of a platiniferous dunite pipe in the Bushveld Complex : chloride complexing and cation exchange metasomatism. Econ. Geol. 77, 1439-1453.

SCHOCK, H.H. (1977) : Trace element partitioning between phenocrysts of plagioclase, pyroxenes and magnetite and the host pyroclastic matrix. J. Radioanal. Chem. 38, 327-340.

SCHWELLNUS, C.M. (1935) : The nickel-copper occurrence in the Bushveld Igneous Complex, west of Pilanesberg. Geol. Surv. South Africa, Bull. 5, 36p.

SCHWELLNUS, J.S.I., ENGELBRECHT, L.N.J., COERTZE, F.J., RUSELL, M.D., MAHERBE, S.J., VAN ROOYEN, D.P. & COOKE, R. (1962) : The geology of the Olifants River area, Transvaal. Geol.Surv. South Africa Expl. Sheets 2429B, 2430A, 87p.

SCOON, R.N. & DE KLERK, W.J. : The relationship between olivine cumulates, mineralization and cyclic units in the upper critical zone of the northwestern Bushveld Complex. Can. Mineral. (in press).

SHARPE, M.R. (1981) : The chronology of magma influences to the eastern compartment of the Bushveld Complex as exemplified by its marginal border groups. Geol. Soc. London J. 138, 307-326.

SHIMA, H. & NALDRETT, A.J. (1975) : Solubility of sulfur in an ultramafic melt and the relevance of the system Fe-S-O. Econ. Geol. 70, 960-967.

SIMPSON, E.S.W. (1954) : On the graphical representation of differentiation trends in igneous rocks. Geol. Mag. 91, 238-244.

SKINNER, B.J. & PECK, D.L. (1969) : An immiscible sulfide melt from Hawaii. In Magmatic ore deposits, Econ. Geol. Mon. 4, 310-322.

SMEWING, J.D. (1981) : Mixing characteristics and compositional differences in mantle-derived melts beneath spreading axes : evidence from cyclically layered rocks in the ophiolite of North Oman. J. Geophys. Res. 86, 2645-2659.

SÖHNGE, P.G. (1963) : Genetic problems of pipe deposits in South Africa. Geol. Soc. South Africa, Proc. 66, xix-lxxii

SOUTH AFRICAN COMMITTEE FOR STRATIGRAPHY (SACS) (1980) : Stratigraphy of South Africa. Part 1. Geol. Surv. South Africa, Handbook 8, 223-241.

SPARKS, R.S.J. & HUPPERT, H.E. (1984) : Density changes during the fractional crystallization of basaltic magmas : fluid dynamic contributions. Contr. Mineral. Petr. 85, 300-309.

SPENCER, K.J. & LINDSLEY, D.H. (1981) : A solution model for co-existing iron-titanium oxides. Amer. Mineral. 66, 1189-1201.

SPRY, A. (1969) : Metamorphic textures. Pergammon Press. Lond. 350p.

STANTON, R.L. (1972) : Ore Petrology. McGraw-Hill, New York. 713p.

STEVENS, R.E. (1944) : Composition of some chromites of the western hemisphere. Amer. Mineral. 29, 1-34.

STORMER, J.C. (1983) : The effects of recalculation on estimates of temperature and oxygen fugacity from analyses of multicomponent iron-titanium oxides. Amer. Mineral. 68, 116-594.

STRECKEISEN, A. (1976) : To each plutonic rock its proper name. Earth Sci. Reviews 12, p.1-33.

STUMPFL, E.F.& RUCKLIDGE, J.C. (1982) : The platiniferous dunite pipes of the Eastern Bushveld. Econ. Geol. 77, 1419-1431.

TANKARD, A.J., JACKSON, M.P.A., ERIKSON, K.A., HOBDAY, D.K., HUNTER, D.R. & MINTER, W.E.L. (1982) : Crustal evolution of southern Africa. Springer-Verlag New York, 523p.

TARKIAN, M. & STUMPFL, E.F. (1975) : Platinum mineralogy of the Driekop mine, South Africa. Mineralium Deposita 10, 71-85.

THOMPSON, F.H., BARNES, S.J. & DUKE, J.M. (1984) : The distribution of nickel and iron between olivine and magmatic sulfides in some natural assemblages. Contr. Mineral. Petr. 22, 55-66.

TODD, S.G., KEITH, D.W., SCHISSEL, D.J., LEROY, L.L., MANN, E.L. & IRVINE, T.N. (1982) : The J-M Platinum-Palladium Reef of the Stillwater Complex : 1. Stratigraphy and petrology. Econ. Geol. 77, 1454-1480.

VAN RENSBURG, W.C.J. (1965) : The mineralogy of the titaniferous magnetite and associated sulfides on Kennedy's Vale 361KT, Lydenburg, District, Transvaal. Geol. Surv. South Africa, Ann. 4, 113-127.

VAN ZYL, J.P. (1970) : The petrology of the Merensky Reef and associated rocks on Swartklip 988, Rustenberg District. Geol. Soc. South Africa Spec. Publ. 1, 80-107.

VERMAAK, C.F. (1976a) : The nickel pipes of Vlakfontein and vicinity, Western Transvaal. Econ. Geol. 71, 261-286.

---------- (1976b) : The Merensky Reef - thoughts on its environment and genesis. Econ. Geol. 71, 1270-1298.

---------- & HENDRIKS, L.P. (1976) : A review of the mineralogy of the Merensky Reef, with special reference to new data on the precious metal mineralogy. Econ. Geol. 71, 1244-1269.

VILJOEN, M.J. & BURVENICH, T. (1983) : Some stratigraphic magnetic anomalies in the Bushveld Complex. Sym. on the Bushveld Complex, Pretoria, Abstr.

---------- & FEUCHTWANGER, T. (1977) : The northern gap area of the Bushveld Igneous Complex. JCI (unpub. internal rep.).

---------- HIEBER, R. & PEYERL, W. (1983) : The geology of the Townlands dunite/pegmatoid pipe, Rustenburg Section of R.P.M. Sym. on the Bushveld Complex, Pretoria, Abstr.

VILJOEN, M.J., THERON, J.C., UNDERWOOD, B., WALTERS, B.M., WEAVER, J., & PEYERL, W. : The geology of Amandelbult Section of R.P.M. with special reference to the Merensky Reef. In Mineral deposits of Southern Africa (a, in press).

---------- DE KLERK, W.J., COETZER, P.M., HATCH, N.P., KINLOCH, E. & PEYERL, W. : The geology of Union Section of R.P.M. with special reference to the Merensky Reef. In Mineral deposits of Southern Africa (b, in press).

---------- & SCOON, R.N. : The distribution and main geological features of discordant bodies of iron-rich ultramafic pegmatite in the Bushveld Complex. Econ. Geol. (in press).

VON BACKSTRÖM, J.W., FOURIE, G.P., MEYER, E.I., MORGAN, R.P.E., COERTZE, F.J., DURR, K.W. & SCHUMANN, F.W. (1960) : The geology of Rustenburg and surrounding area. Geol. Surv. South Africa, Expl. Sheet 4, 93p.

VON GRUENEWALDT, G. (1973) : The main and upper zones of the Bushveld Complex in Roossenekal area, E. Transvaal. Geol. Soc. South Africa, Trans. 76, 207-227.

---------- (1979) : A review of some recent concepts of the Bushveld Complex, with particular reference to sulfide mineralization. Can. Mineral. 17, 233-256.

WAGER, R.L. & BROWN, G.M. (1968) : Layered igneous rocks. Oliver and Boyd, London, 588p.

---------- & WADSWORTH, W.J. (1960) : Types of igneous cumulates. J. Petr. 1, 73-85.

WAGNER, P.A. (1925) : Notes on the platinum deposits of the Bushveld Igneous Complex. Geol. Soc. South Africa, Trans. 28, 83-133.

---------- (1929) : The platinum deposits and mines of South Africa. Oliver and Boyd, Edinburgh, 326p.

WASSERSTEIN, B. (1936) : Some notes on the critical zone of the Bushveld gabbro at the Swartkop chrome mine in the Rustenburg District. Geol. Soc. South Africa, Trans. 39, 215-222.

WATSON, E.B. (1977) : Partitioning of manganese between forsterite and silicate liquid. Geochim. Cosmochim. Acta 41, 1363-1374.

WELLS, R.A. (1977) : Pyroxene thermometry in simple and complex systems. Contr. Mineral. Petr. 62, 129-139.

WILLEMSE, J. (1969a) : The geology of the Bushveld Igneous Complex, the largest repository of magmatic ore deposits in the world. In Magmatic ore deposits, Econ. Geol. Mon. 4, 1-22.

---------- (1969b) : The vanadiferous magmatic iron ore of the Bushveld Igneous Complex. In Magmatic ore deposits, Econ. Geol. Mon. 4, 187-208.

WILSON, A.H. (1982) : The geology of the Great "Dyke", Zimbabwe. J. Petr. 23, 240-292.

WYLLIE, P.J. (Ed.) (1967) : Ultramafic and related rocks. John Wiley and Sons, Inc., New York, 464p.

YODER, H.S. (Ed.) (1979) : The evolution of the igneous rocks. Princeton Univ. Press, New Jersey, 588p.

YUND, R.A. & KULLERUD, G. (1966) : Thermal stability of assemblages in the Cu-Fe-S system. J. Petr. 7, 454--488.

ZECK, H.P, SHENOUDA, H.H., RONSBO, J.G. & POORTER, P.E. (1982) : Hypersthene-ilmenite(/magnetite) symplectites in coronitic olivine gabbronorites. Lithos 15, 173-182.

APPENDIX 1 IRON-RICH ULTRAMAFIC PEGMATITE BODIES AT AMANDELBULT

All samples listed here are of iron-rich ultramafic pegmatite bodies from the upper critical zone at Amandelbult. These have been divided into seven case-studies.

CASE-STUDY (1) : THE MIDDELLAAGTE PIPE (ML-SAMPLES)

Samples in this case-study are from six boreholes, ML 22, ML 24, ML 25, ML 26, ML 27 and ML 29 drilled by JCI on the farm Middellaagte (see figs. 7.2, 7.3 and Map 3). Schematic borehole logs are presented below. In addition, two samples, GM-3 and GM-4, are of borehole core presented by General Mining (exact positions not known).

SAMPLE	DEPTH	DESCRIPTION
All samples from borehole ML24 approximately 0.5 m in length; depth = depth from surface to base of sample; for pegmatite read "typical, iron-rich ultramafic pegmatite").		
ML24-1	29.9	Pegmatite
ML24-2	39.9	Pegmatite
ML24-3	44.9	Pegmatite
ML24-4	49.6	Pegmatite
ML24-5	50.7	Pegmatite (plagioclase-rich)
ML24-6	51.7	Pegmatite (plagioclase-rich)
ML24-7	56.7	Pegmatite
ML24-8	61.7	Pegmatite
ML24-9	66.7	Pegmatite
ML24-10	68.2	Pegmatite
ML24-11	71.6	Pegmatite (fine-grained)
ML24-12	75.0	Pegmatite (fine-grained)
ML26-8	57.0 - 59.9	Pegmatite (plagioclase-rich)
ML26-9	59.9 - 62.7	Pegmatite (plagioclase-rich)
ML26-12	66.2 - 68.8	Pegmatite (fine-grained)
ML26-13	68.8 - 72.1	Pegmatite
ML27-1	22.0 - 25.0	Pegmatite
ML27-2	25.0 - 30.0	Pegmatite
ML27-3	30.0 - 35.0	Pegmatite
ML27-4	35.0 - 40.0	Pegmatite
ML27-5	40.0 - 45.0	Pegmatite
ML27-6	45.0 - 50.0	Pegmatite
ML27-7	50.0 - 51.0	Pegmatite
ML29-1	89.3 - 90.3	Pegmatite
ML29-J	84.1	Contact : pyroxenite / pegmatite
ML29-0	57.2	Pegmatite (amphibole-rich)
ML22-A : continuous length of core from 154.5 - 158.1 m. of small pegmatite body in lower main zone.		
ML22-A1	154.5	Norite
ML22-A3	155.0	Pegmatite
ML22-A10	156.0	Pegmatite
ML22-A18	158.0	Pegmatite
ML22-B : continuous length of core from 238.0 - 239.0 m. of small pegmatite body in lower main zone - no analyses).		

ML22-C : continuous length of core from 454.0 - 462.8 m. of pegmatite body above Merensky Reef.

ML22-C1	454.0	Norite
ML22-C9	457.0	Pegmatite
ML22-C12	459.0	Pegmatite
ML22-2	400.0	Pegmatite
ML22-5	420.0	Pegmatite
M122-11	440.0	Pegmatite
GM-3	-	Pegmatite
GM-4	-	Pegmatite

CASE-STUDY (2) : A SHEET-LIKE BODY IN THE FOOTWALL CYCLIC UNIT

This occurrence, 5 level / 27W crosscut, forms part of the extensive stratabound body described from the 30W - 25W area of Amandelbult in Chapter 7 (fig. 7.7). Samples prefixed "AE-" were collected on a horizontal traverse at intervals of 2 m. Additional samples were collected adjacent to the lower contact of the normal cumulates (AE-33B,-34) and two samples were collected of the unusual plagiolase-rich assemblage in the centre of the body (AU-1,-2 - both weighing roughly 5 kg). This pegmatite body replaces norites and anorthosites of the Footwall cyclic unit.

SAMPLE	DESCRIPTION
AE-8	Pegmatite (olivine-rich)
AE-9	Pegmatite (olivine-rich)
AE-10	Pegmatite (olivine-rich)
AE-11	Pegmatite (olivine-rich)
AE-12	Pegmatite (olivine-rich)
AE-13	Pegmatite (clinopyroxene-rich)
AE-14	Pegmatite (sulphide-rich)
AE-15	Pegmatite (plagioclase-rich)
AE-16	Pegmatite (clinopyroxene-rich)
AE-17	Pegmatite (plagioclase-rich)
AE-18	Pegmatite (clinopyroxene-rich)
AE-19	Pegmatite (clinopyroxene-rich)
AE-20	Pegmatite (oxide-rich)
AE-21	Pegmatite (oxide-rich)
AE-23	Pegmatite (oxide-rich)
AE-24	Pegmatite (oxide-rich)
AE-25	Pegmatite (oxide-rich)
AE-26	Pegmatite (oxide-rich)
AE-27	Pegmatite (oxide-rich); hybrid ?
AE-28	Pegmatite (oxide-rich)
AE-29	Pegmatite (clinopyroxene-rich)
AE-31	Pegmatite (clinopyroxene-rich)
AE-32	Pegmatite (clinopyroxene-rich)
AE-33A	Pegmatite (clinopyroxene-rich)
AE-33B	Norite (at contact)
AE-34	Pegmatite (clinopyroxene-rich)
AE-35	Norite
AE-36	Melanorite
AU-1	Pegmatite (plagioclase-rich)
AU-2	Pegmatite (plagioclase-rich)

CASE-STUDY (3) : "REPLACEMENT" OF THE P2 MIDDLING ANORTHOSITE

This occurrence is also 5 level/ 27W crosscut. A suite of samples (prefixed "AD-") were collected from the eastern sidewall at this exposure, as illustrated below. These include samples of the pegmatite and of the normal cumulates.

SAMPLE	DESCRIPTION
AD-4*	Pegmatite
AD-5*	Pegmatite
AD-20	Upper Pseudoreef C
AD-24	Upper Pseudoreef B
AD-25A	Plagioclase layer
AD-25B	Leucotroctolite
AD-26	Leuconorite
AD-27	Leuconorite
AD-28	Spotted anorthosite
AD-29	Spotted anorthosite
AD-32	Pegmatite
AD-33	Contact : Leucotroctolite / Pegmatite
AD-34	Pegmatite
AD-36	Upper Pseudoreef B
AD-37	Contact : Pseudoreef / Pegmatite
AD-38	Upper Pseudoreef C
AD-40	Pegmatite
AD-41	Contact : Anorthosite (A) / Pegmatite (B)

* Samples from the east sidewall (not shown in diagram).

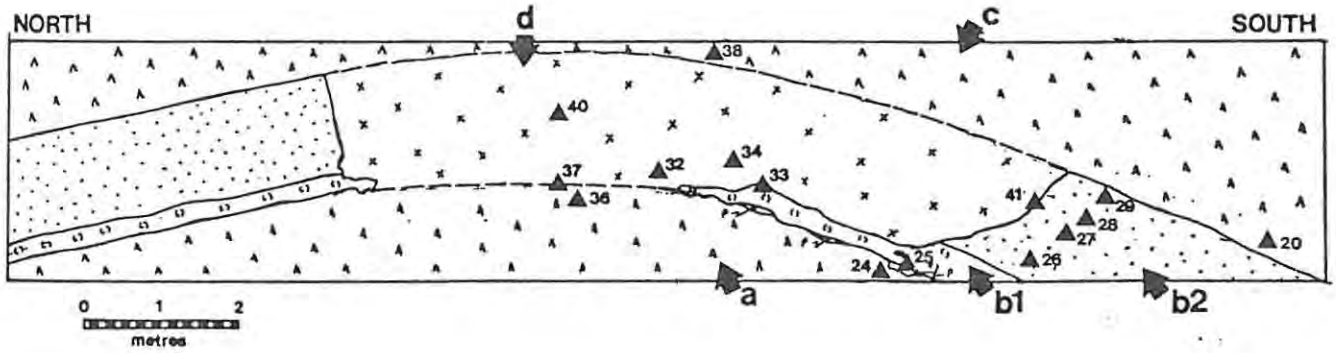

CASE-STUDY (3) - "AD" SAMPLES - 5L / 27W crosscut, east sidewall

a - upper pseudoreef B;
b - "P2 middling" (1 - leucotroctolite; b - leuconorite)
c - upper pseudoreef C
d - iron-rich ultramafic pegmatite

Note selective replacement, initially of the leuconorite layer in the P2 middling anorthosite and secondly of the leucotroctolite layer. The pegmatite body is constrained by the harzburgite layers.

CASE STUDY (4) : A PEGMATITE BODY IN THE FOOTWALL OF THE UPPER PSEUDOREEF UNIT B

The occurrence sampled is 5 level haulage between 27W and 25W crosscuts. A suite of samples (prefixed AC-) were collected from the southern sidewall at this exposure, as illustrated below.

SAMPLE	DESCRIPTION
AC-A	Contact : Upper pseudoreef B / Pegmatite
AC-B	Upper pseudoreef B
AC-C	Contact : Anorthosite / Pegmatite
AC-2	Upper pseudoreef B
AC-5	Pegmatite
AC-6	Spotted anorthosite
AC-7	Spotted anorthosite

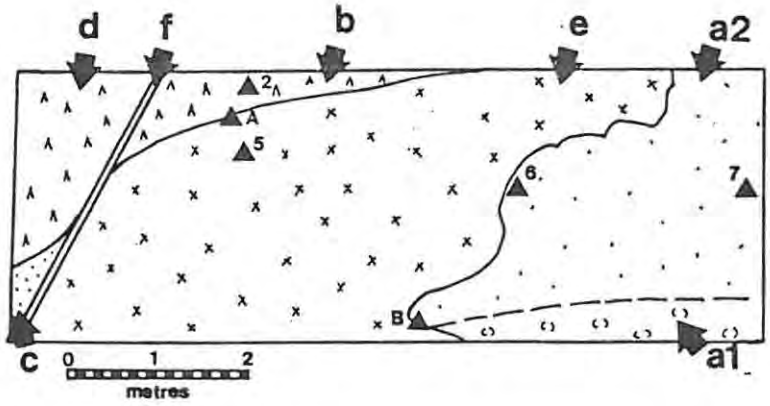

CASE-STUDY (4) - "AC" SAMPLES - 5L / 27W haulage, south sidewall

a - felsic cumulates in Pseudo cyclic unit A (1 - mottled anorthosite; 2 - leuconorite)
b - upper pseudoreef B
c - "P2 middling"
d - upper pseudoreef C
e - iron-rich ultramafic pegmatite
f - fault

The pegmatite body is constained by the pseudoreef and is cut by the fault.

CASE-STUDY (5) : A PEGMATITE BODY IN THE HANGINGWALL OF THE UPPER PSEUDOREEF UNIT-A

The occurrence sampled is 4 level haulage, just east of 30W crosscut. Samples (prefixed AH-) were collected along a traverse of the magnetite-chromitite layer marking the contact between the pegmatite and the Pseudoreef, as illustrated below.

SAMPLE	DESCRIPTION
AH-3	Contact : Upper pseudoreef A / Pegmatite
AH-4	Contact : Upper pseudoreef A / Anorthosite
AH-14	)
AH-17C	)
AH-19	) Contact :
AH-20B	) Upper pseudoreef A - Oxide layer -
AH-21	) Pegmatite.
AH-21A	)
AH-21B*	)
AH-30	Upper pseudoreef A
AH-31	Mottled anorthosite
AH-32	Partially replaced pseudoreef
AH-33A	Partially replaced pseudoreef
AH-33B	Partially replaced anorthosite
AH-34	Pegmatite
AH-35	Pegmatite

* same postion as sample AH-21A.

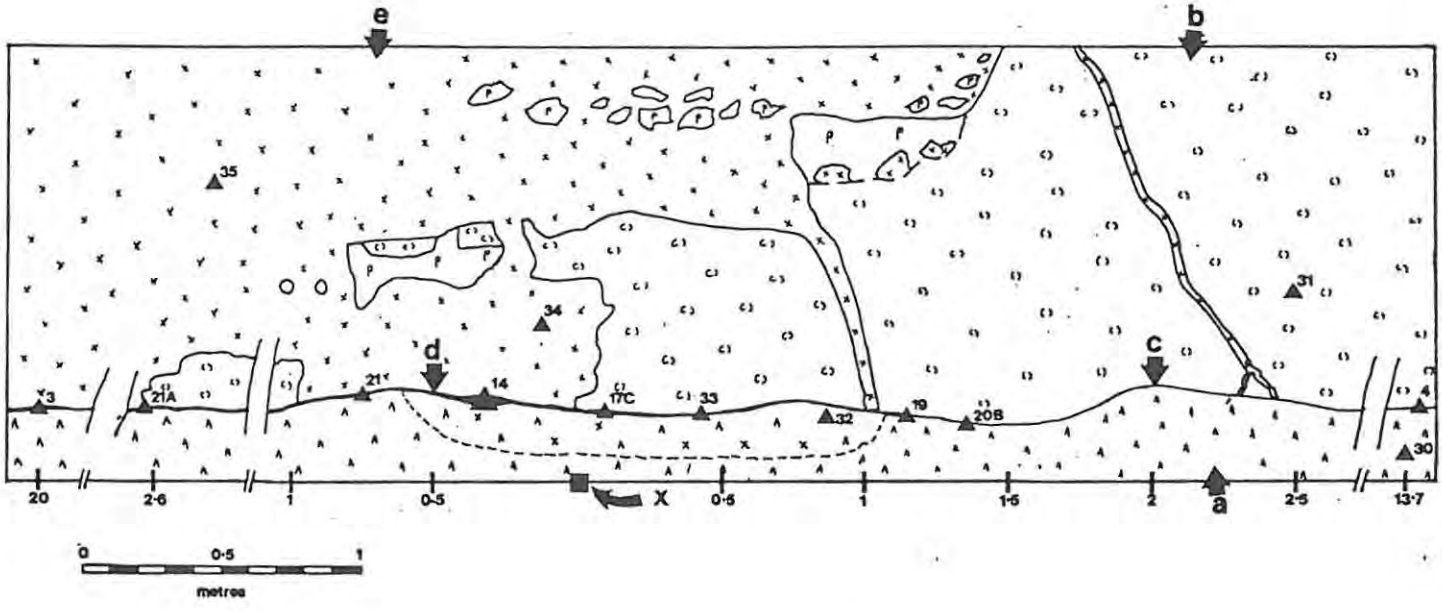

CASE-STUDY (5) - "AH" SAMPLES - 4L / 30W haulage, south sidewall

a - upper pseudoreef A (or top of P1 marker)
b - mottled anorthosite (felsic cumulates in Pseudo cyclic unit A)
c - chromitite stringer
d - Fe-Ti-Cr oxide pegmatite
e - iron-rich ultramafic pegmatite
p - massive segregations of recrystallized plagioclase

CASE-STUDY (6) : A PEGMATITE BODY IN THE HANGINGWALL OF THE UPPER PSEUDOREEF UNIT-A

This occurrence is at 3 level haulage 4 E section. Sample positions (samples "AV-") are illustrated below.

SAMPLE	DESCRIPTION
AV-3	Pegmatite
AV-4	Pegmatite
AV-5A	Spotted anorthosite
AV-5B	Pegmatite
AV-6	Pegmatite
AV-8A	Upper pseudoreef A
AV-8B	Plagioclase layer
AV-9	Mottled anorthosite
AV-10	Leuconorite
AV-11	Pegmatite
AV-12	Pegmatite
AV-13	Pegmatite

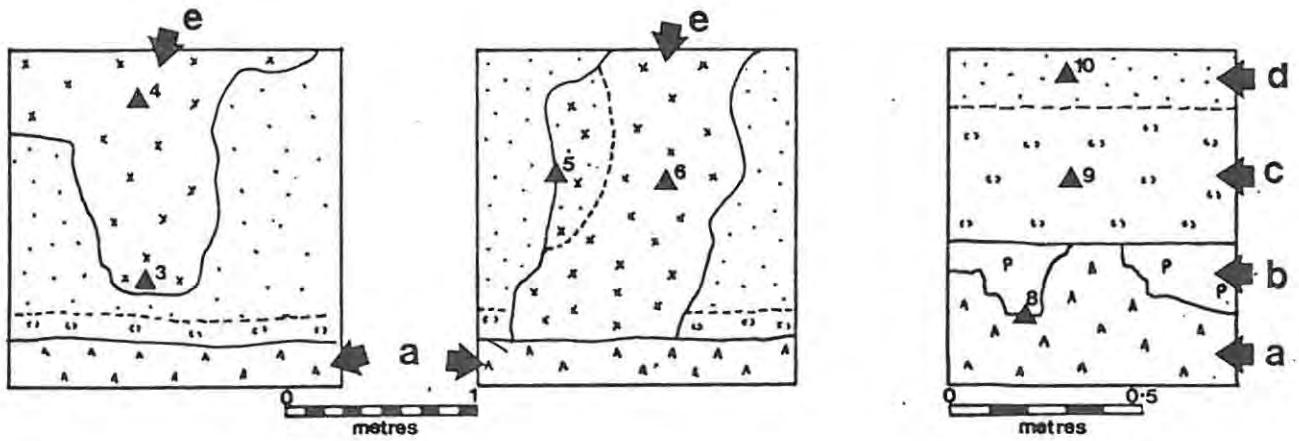

CASE-STUDY (6) - "AV" SAMPLES - 3L / 4E haulage, south sidewall

a - upper pseudoreef A (or top of P1 marker)
b - plagioclase layer
c - mottled anorthosite
d - leuconorite
e - iron-rich ultramafic pegmatite

Distribution of pegmatite bodies here imply that the pegmatitic liquids moved downwards, as they are constrained by the underlying harzburgite layer.

CASE-STUDY (7) : "REPLACEMENT OF THE MERENSKY REEF

This case study includes samples of the so-called replaced Reef and of pegmatite occurrences in the immediate footwall and hanging-wall of the Merensky Reef. Samples were collected from a number of localities :
(1) 5 level / 27W crosscut (prefixed 27/A-G, AG- and AU-samples)
(2) 3 level / 30W stope (prefixed AM-)
(3) 2 and 3 level / 44W stope (prefixed AK-)
Sample locations are illustrated schematically below. Samples designated with the prefix "27-" are from a horizontal borehole drilled from the 5 level / 27W crosscut. These samples are of quarter-sectioned BX core over continuous lenghts as indicated below.

SAMPLE	DESCRIPTION
AF-A1	Merensky hangingwall pyroxenite
AF-A2	Merensky hangingwall pyroxenite
AF-A3	Partially replaced upper chromitite
AF-A4	Partially replaced Reef
AF-A5	Partially replaced Reef
AF-A6	Partially replaced Reef
AF-A7	Partially replaced Reef
AF-A8	Partially replaced lower chromitite
AF-A9	Pegmatite
AF-2	Replaced Reef
AF-3	Pegmatite (replaced footwall)
AF-4	Upper chromitite and hangingwall pyroxenite
AF-5	Replaced Reef
AG-1	Replaced lower chromitite layer
AG-2	Replaced Reef
AG-3	Replaced footwall
AG-4	Replaced Reef
AG-5	Hangingwall pyroxenite
AG-6	Replaced upper chromitite
AG-7	Hangingwall pyroxenite
AG-8	Replaced upper chromitite
AG-9	Replaced Reef
AG-10	Replaced Reef
AG-13	Replaced upper chromitite layer
AM-1	Replaced hangingwall pyroxenite
AM-2	Pegmatite (Replaced Reef)
AM-4	Pegmatite (Replaced footwall)
AM-11	Merensky footwall anorthosite
AU-4	Merensky Reef
AU-6	Partially replaced Reef
AK-1B	Partially replaced Reef
AK-2	Partially replaced Reef

SAMPLE	DEPTH (m)	DESCRIPTION
27-A1	23.0	Hangingwall pyroxenite
27-A2	20.0	Hangingwall pyroxenite
27-A3	19.1 - 19.5	Hangingwall pyroxenite
27-A4	18.8 - 19.0	Hangingwall pyroxenite
27-B	18.55 - 18.8	Replaced hangingwall pyroxenite
27-C	18.5 - 18.55	Replaced upper chromitite
27-D1	17.9 - 18.5	Replaced Reef
27-D2	17.3 - 17.9	Replaced Reef
27-E1	16.8 - 17.3	Merensky Reef
27-D3	16.7 - 16.8	Replaced Reef
27-E2	16.3 - 16.7	Merensky Reef
27-F	16.1 - 16.3	Replaced lower chromitite
27-G1	15.6 - 16.1	Pegmatite (replaced footwall)
27-G2	15.0 - 15.6	Pegmatite (replaced footwall)
27-G3	12.5	Pegmatite (replaced footwall)
27-G4	8.0	Pegmatite (replaced footwall)
Ms	10.8 - 12.5	Massive sulphide in pegmatite

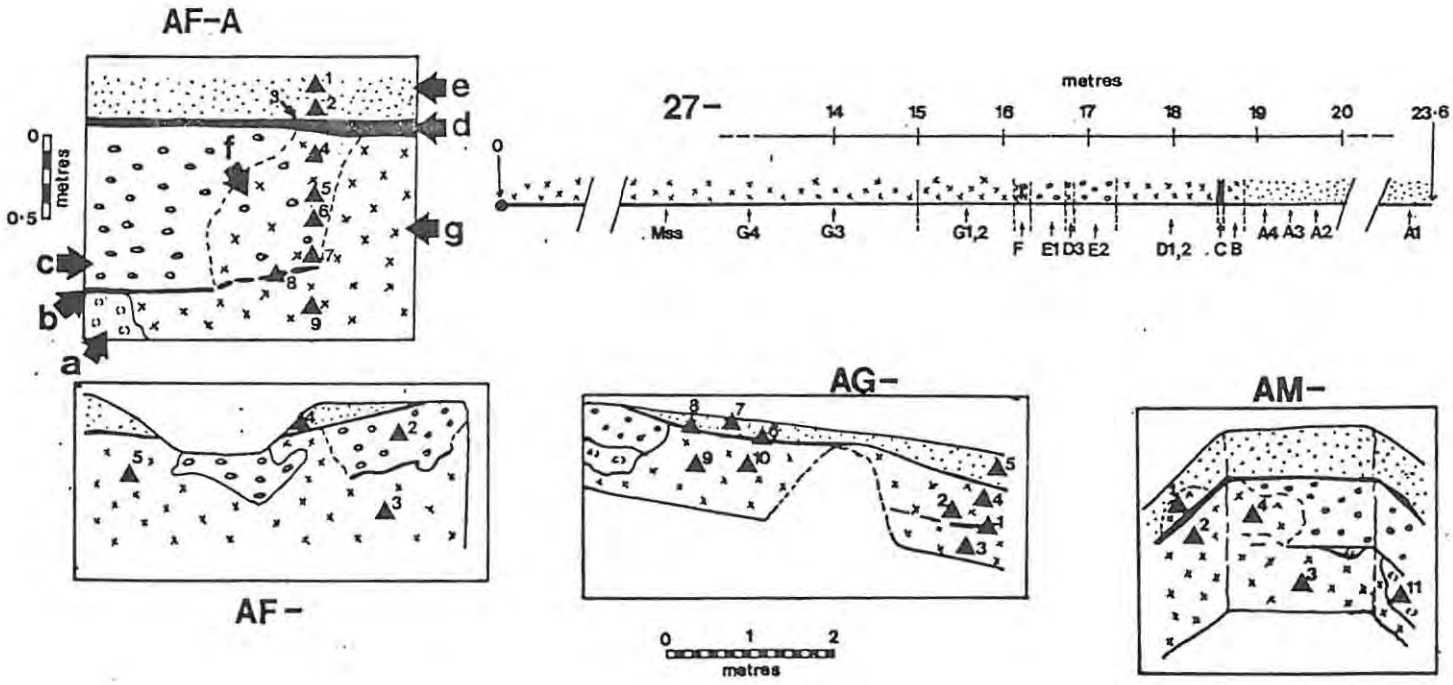

CASE-STUDY (7) - "AF", "AF-A", "AG", "AM", and "27" SAMPLES - various localities (see above).

a - Merensky footwall anorthosite
b - Merensky lower chromitite layer
c - Merensky Reef
d - Merensky upper chromitite layer
e - Merensky hangingwall pyroxenite
f - Partially replaced Reef
g - iron-rich ultramafic pegmatite (including replaced Reef)

BOREHOLE LOGS

(ML series, Middellaagte, Amandelbult; note for "pegmatite" read "iron-rich ultramafic pegmatite")

ML 24
POSITION : Collared in Ni-Cu geochemical soil anomaly, middle of pipe.
DIRECTION : Vertical
END OF HOLE : 75.02 m.
0.0 - 3.00 "Red" soil
3.00 - 26.67 Weathered zone
26.67 - 29.92 Partially weathered
29.92 - 49.62 Pegmatite
49.62 - 51.74 Zone of plagioclase-orthopyroxene-rich "pegmatite" (hybrid unit)
51.74 - 75.02 Pegmatite

ML 25
POSITION : Collared in Ni-Cu geochemical soil anomaly, middle of pipe.
DIRECTION : Vertical
END OF HOLE : 102.95 m.
0.0 - 2.80 "Red" soil
2.80 - 32.27 Weathered zone
32.27 - 102.95 Pegmatite
(minor plagioclase only in this hole).

ML 26
POSITION : Collared in Ni-Cu geochemical soil anomaly, middle of pipe
DIRECTION : Vertical
END OF HOLE : 72.05 m.
0.0 - 3.00 "Red" soil
3.00 - 24.80 Weathered zone
24.80 - 57.00 Pegmatite
57.00 - 62.65 Plagioclase - orthopyroxene-rich "pegmatite" (hybrid unit)
62.65 - 63.99 Pegmatite
63.99 - 66.20 Plagioclase - orthopyroxene-rich "pegmatite" (hybrid unit)
66.20 - 72.05 Pegmatite (miner plagioclase until 68.84m).

ML 27
POSITION : Collared in centre of magnetic anomaly, middle of pipe
DIRECTION : Vertical
END OF HOLE : 50.95 m
0.00 - 3.00 "Red" soil
3.00 - 22.00 Weathered zone
22.00 - 50.95 Pegmatite

AMANDELBULT

B.H. 5/27W/1
POSITION : 5 level 27W crosscut (27m south of peg A6439)
DIRECTION : Vertical (+90°)
END OF HOLE : 7.31 m
0.0 - 2.57 Iron-rich ultramafic pegmatite (typical)
2.57 Magnetic Cr-Fe-Ti oxide layer
2.57 - 3.30 Merensky Reef (partially replaced, olivine-rich; + sulphides)
3.30 - 3.77 "Replaced" Reef (+sulphides)
3.77 Magnetic Cr-Fe-Ti oxide layer
3.77 - 4.32 Iron-rich ultramafic pegmatite (unusually fine-grained, + sulphides)
4.32 - 7.31 Merensky hanging-wall pyroxenite (fine- to medium-grained, poikilitic feldspathic orthopyroxenite)

B.H. 5/27W/2
POSITION : 5 level 27W crosscut (27m south of peg A6439)
DIRECTION : Horizontal
END OF HOLE : 23.57 m.

0.0	- 16.00	Iron-rich ultramafic (typical; with massive sulphide at 3.0 m)
16.12	- 16.29	"Replaced" Reef (with "xenoliths" of magnetic Cr-Fe-Ti oxide)
16.29	- 17.32	Merensky Reef (partially replaced, with replaced Reef at 16.72 - 16.80m
17.32	- 18.50	"Replaced" Reef (+ sulphides)
18.50	- 18.55	"Replaced" Merensky upper chromitite layer (strongly magnetic)
18.55	- 18.79	Iron-rich ultramafic pegmatide
18.79	- 23.57	Merensky hangingwall pyroxenite (normal)

B.H. 5/27W/3
POSITION : 5 level naulayer (35m west of peg A.7127)
DIRECTION : + 40 north
END OF HOLE : 49.14 m

0.0	- 0.41	Leuconorite
0.41	- 0.71	Mottled anorthosite
0.71	- 2.85	Upper Pseudoreef (unit C, or top band of P2 marker)
2.85	- 3.05	Feldspathic harzburgite (1cm chromitite at 2.85)
3.05	- 6.65	Melanorite
6.65	- 17.33	Norite
17.33	- 17.80	Leuconorite
17.80	- 18.70	Footwall marker
18.70	- 22.75	Norite
22.75	- 29.57	Leuconorite
29.57	- 39.31	Mottled anorthosite (Merensky footwall anorthosite)
39.31	- 40.63	Merensky Reef (Chromitite layers at top and base)
40.63	- 47.00	Merensky hanging-wall pyroxenite
47.00	- 49.14	Melanorite - norite

B.H. 4E-WINZE/1
POSITION : Surface
DIRECTION : Vertical
END OF HOLE : 145.98 m

0.0	- 51.30	No core
51.30	- 55.74	Giant mottled anorthosite
55.74	- 56.68	Norite
56.68	- 56.91	Iron-rich ultramafic pegmatite
56.91	- 62.84	Norite
62.84	- 64.01	Iron-rich ultramafic pegmatite
64.01	- 68.60	Norite, grading into melanorite at 67.00
68.60	- 73.02	Feldspathic orthopyroxenite (fine grained)
73.02	- 76.98	Bastard Reef
76.94	- 85.44	Iron-rich ultramaficx pegmatite
85.44	- 86.77	Norite (altered)
86.77	- 87.50	Iron-rich ultramafic pegmatite
87.50	- 91.30	Merensky hanging-wall pyroxenite
91.30	- 93.12	Merensky Reef (some "Replaced" Reef)
93.12	- 106.53	Iron-rich ultramafic pegmatite
106.53	- 107.52	Melanorite
107.52	- 111.60	Upper Pseudoreef (unit B/C or P2 marker)
111.60	- 114.23	Iron-rich ultramafic pegmatite
114.23	- 114.32	Massive Cr-Fe-To oxide layer
114.32	- 122.29	Feldspathic orthopyroxenite
122.29	- 123.71	UG-2 chromitite layer
123.71	- 124.50	Feldspathic orthopyroxenite (+ Chromitite stringers)
124.50	- 138.28	Feldspathic orthopyroxenite
138.28	- 140.26	UG-1 chromitite layer
141.20	- 145.98	Iron-rich ultramafic pegmatite

B.H. 57E WINZE/3
POSITION : Surface
DIRECTION : Vertical
END OF HOLE : 141.20 m.

0.0	-	73.85	Iron-rich ultramafic pegmatite
73.85	-	80.74	Post-Bushveld dyke (carbonatite ?)
80.74	-	94.70	Iron-rich ultramafic pegmatite
94.70	-	95.85	Dyke (?)
95.85	-	126.35	Iron-rich ultramafic pegmatite
126.35	-	126.85	Norite
126.85	-	128.58	Iron-rich ultramafic pegmatite
128.58	-	128.69	Norite
128.69	-	137.20	Iron-rich ultramafic pegmetite
137.20	-	139.64	Olivine-bearing norite (serpentinized)
139.64	-	141.20	Iron-rich ultramafic pegmatite.

B.H. 57E WINZE/2
POSITION : Surface
DIRECTION : Vertical
END OF HOLE : 93.90 m.

0.0	-	19.60	Leuconorite
19.60	-	31.50	Mottled anorthosite
31.50	-	36.00	Spotted/mottled anorthosite
36.00	-	38.70	Leuconorite
38.70	-	39.20	Spotted/mottled anorthosite
39.20	-	47.10	Giant mottled anorthosite
47.10	-	50.15	Iron-rich ultramafic pegmatite
50.15	-	57.60	Norite, melanorite at base
57.60	-	65.98	Iron-rich ultramafic pegmatite (intruded by numerous post-Bushveld dyke material)
65.98	-	66.14	Leuconorite
66.14	-	67.33	Iron-rich ultramafic pegmatite
67.33	-	67.95	Norite grading up into leuconorite
67.95	-	68.97	Merensky hanging-wall pyroxenite
68.97	-	68.98	Magnetic Cr-Fe-Ti oxide layer
68.98	-	69.07	"Replaced" Reef (no lower chromitite)
69.07	-	69.46	Mottled anorthosite (Merensky footwall anorthosite)
69.46	-	70.76	Iron-rich ultramafic pegmatite
70.76	-	71.62	Mottled anorthosite
71.62	-	72.80	Leuconorite
72.80	-	73.42	Iron-rich ultramafic pegmatite
73.42	-	76.90	leuconorite grading into norite at 76.00
76.90	-	77.10	Footwall marker
77.10	-	79.55	Norite and leuconorite
79.55	-	81.56	Melanorite
81.56	-	83.51	Norite
83.51	-	93.90	Upper Pseudoreef (unit B/C or P2 marker)

APPENDIX 2 IRON-RICH ULTRAMAFIC PEGMATITE BODIES AT OTHER LOCALITIES

CASE STUDY-(8) PEGMATITE BODIES FROM THE MAIN ZONE

This includes samples from R.P.M. Amandelbult and Union Sections. Samples from Amandelbult are restricted to core from borehole ML22 (for sample positions see Case Study-(1), Appendix 1). Samples from R.P.M. Union Section were collected and analysed by A.A. Mitchell (in prep.) - for sample locations see stratigraphic column below :

SAMPLE	DESCRIPTION	LOCALITY
ML22-A1	Norite	Amandelbult
ML22-A3	Pegmatite	Amandelbult
ML22-A10	Pegmatite	Amandelbult
ML22-A18	Pegmatite	Amandelbult
A-107	Pegmatite	Union
A-115	Pegmatite	Union
A-348	Pegmatite	Union

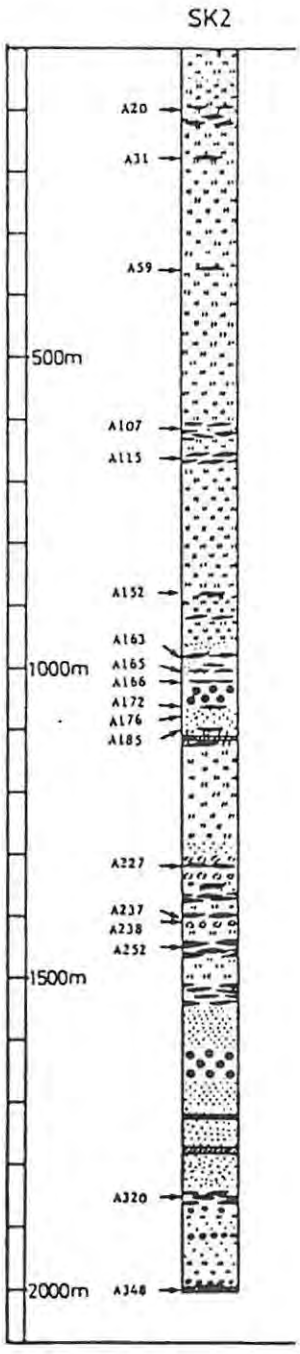

CASE STUDY-(9) : PEGMATITE BODIES FROM THE RUSTENBURG AREA

This includes samples from large pipe-like bodies, namely Townlands (samples prefixed TLP- ; from boreholes TLP-1, TLP-2, TLP-3 and TLP-4), Brakspruit (sample RB-5) and Boschkoppie (samples prefixed BK-), and from small, irregular bodies adjacent to the Brakspruit pipe (other samples prefixed RB-) For sample locations see Figure 2.7.

SAMPLE	DESCRIPTION
TLP-1A	Pegmatite (hortonolite dunite)
TLP-1B	Pegmatite (hortonolite dunite)
TLP-2	Pegmatite (wehrlite)
TLP-3	Pegmatite (wehrlite)
BK-1	Pegmatite
BK-2	Pegmatite
BK-3	Pegmatite (hybrid ?)
RB-5	Pegmatite

CASE STUDY-(10) : PEGMATITE BODIES FROM THE EASTERN BUSHVELD COMPLEX

This includes samples from the large sheet-like body on the farm Tweefontein, adjacent to the Lavino Chrome Mine (originally examined by Cameron and Desborough, 1964) (samples prefixed LA-), from a small body on the farm Spitskop (samples prefixed EB-) and from boreholes KLF-17 and KLF-18 on the farm Klipfontein. For sample locations see Figure 2.1.

SAMPLE	DESCRIPTION
LA-1	Pegmatite
LA-2	Pegmatite
LA-3	Pegmatite (massive Fe-Ti-Cr oxide)
LA-3A	Pegmatite (massive Fe-Ti-Cr oxide)
EB-1	Pegmatite
EB-2	Pegmatite
EB-3	Pegmatite (massive Fe-Ti-Cr oxide)
EB-4	Pegmatite
KLF-17	Pegmatite
KLF-18	Pegmatite

CASE STUDY-(11) : Fe-Ti-Cr OXIDE PEGMATITE

The following samples (other than those from underground at Amandelbult which are listed in Appendix 1) have been analysed :

AZ-1 : Small, zoned, pipe-like body which cuts the LG-chromitite layers, north of Amandelbult.
AZ-2 : Small, zoned, pipe-like body which cuts the MG-chromitite layers, north of Amandelbult.
AS-A1, A2 : Sheet-like body which is postulated to have replaced the UG-1 chromitite layer at 7E section, Amandelbult.
LA-3, 3A : Magnetite-chromitite layer adjacent to the pegmatite body on Tweefontein in the eastern Bushveld Complex.
EB-3 : Small, pipe-like body on Spitskop in the eastern Bushveld Complex.
LEU-1, 2 : Large, zoned, pipe-like body on the farm Leeukoppie, near Northam. In the upper zone, cuts Magnetite layer number 8.
LEU-3, 4 : Cumulus magnetite (layer number 8) adjacent to the pipe on Leeukoppie.
MAG-1, 4 : Cumulus magnetite (Main Seam), Magnet Heights.

APPENDIX 3 THE PLATINIFEROUS ULTRAMAFIC PIPES

These comprise samples from the four platiniferous ultramafic pipes, namely Driekop (DR-), Mooihoek (MO-), Onverwacht (ON-), and Twyfelaar (TW-). Sample locations are as follows (for samples from Driekop see Map 2, in folder).

Sample(s)	Description	Location
DR-0 - DR-20	Magnesian dunite	Main pipe
DR-22	Magnesian dunite (+ cpx)	Main pipe (contact between magnesian dunite unit and marginal envelope of olivine clinopyroxenite)
DR-24 - DR-27	Olivine clinopyroxenite	Main pipe (margin)
DR-A1 -A2, -2A	Platiniferous, iron-rich dunite	Main pipe (core)
DR-31B, -31C, -31D, -32C, -33D, -37, -38A :	Olivine clinopyroxenite/clinopyroxenite	Satellite bodies
DR-40B, -41, -42, -43, -43A, -434B, -43C, -45, -45A, -46, -46A, -46Y, -46Z, -49, -49A, -49B, -49C :	Lherzolite pegmatite	Mostly associated with partially replaced UG-3
DR-105, -111, -113, -131 :	Magnesian dunite	Satellite bodies
DR-35B	Contact : pegmatite / leuconorite	Wallrocks
DR-28, -29, -30, -32A, -32B, -32D, -36A :	Leuconorite (cumulate)	Wallrocks
DR-34	Mottled anorthosite	Wallrocks
DR-50A, -50C, -51B, -52	Bronzitite (above UG-2)	1 km from pipe
MO-1	Platiniferous, iron-rich dunite	Mine dumps
MO-2	Massive Fe-Ti-oxide	Mine dumps
MO-3	Platiniferous, iron-rich wehrlite	Mine dumps
MO-4	Platiniferous, hortonolite dunite	Mine dumps
MO-5	Massive Fe-Ti-oxide	Mine dumps
MO-6	Massive Fe-Ti-oxide	Mine dumps
MO-10	Massive Fe-Ti-oxide	Mine dumps
MO-11	Massive Fe-Ti-oxide	Mine dumps
MP-2	Massive Fe-Ti-oxide	Mine dumps
ON-1	Platiniferous, hyalosiderite dunite	Surface, in-situ, core of pipe
ON-2	Platiniferous, hyalosiderite dunite	Surface, in-situ, core of pipe
ON-12	Magnesian dunite	Surface, in situ, main body
ON-13	Magnesian dunite	Surface, in situ, main body
ON-16	Magnesian dunite	Surface, in situ, main body
TW-1	Magnesian dunite	Surface, in-situ, main body
TW-2	Magnesian dunite	Surface, in-situ, main body
TW-3B	Magnesian dunite	Surface, in-situ, main body

In addition samples of cumulus magnesian dunites from the lower-lower critical zone were analysed.

DUN-1 Cumulus dunite, Jagdlust ("Cameron section"), lower zone, eastern Bushveld Complex.
DUN-2 Cumulus dunite, lower zone, north-western, Bushveld Complex (provided by M.J. Botha).
DUN-3 Cumulus dunite, Jagdlust ("Cameron Section"), lower zone, eastern Bushveld Complex.

APPENDIX 4 CUMULATES

(1) CUMULATES FROM AMANDELBULT

Samples in this study may be divided into the following groups :

AE - series (see case study (2), Appendix 1) : 5L-27W crosscut
AD - series (see case study (3), Appendix 1) : 5L-27W crosscut
AC - series (see case study (4), Appendix 1) : 5L-27W haulage
AH - series (see case study (5), Appendix 1) : 4L-30W haulage
AV - series (see case study (6), Appendix 1) : 3L-4E haulage

AT - series : suite of samples from 5L-25W crosscut, a "normal" cumulate succession adjacent to the "replaced" succession sampled in SL-27W crosscut (for sample locations see fig. 5.4)

SAMPLE	DESCRIPTION	CYCLIC UNIT / MARKER
AT-1	Melanorite	Footwall
AT-2	Leuconorite	Footwall
AT-3	Leuconorite	Footwall
AT-4	Leuconorite	Footwall
AT-6	Mottled anorthosite	Footwall Marker
AT-7	Leuconorite	Footwall
AT-8	Leuconorite	Footwall
AT-9	Spotted anorthosite	Footwall
AT-10	Mottled anorthosite	Merensky Footwall
AT-11	Mottled anorthosite	Merensky Footwall
AT-12	Mottled anorthosite	Merensky Footwall
AT-13	Mottled anorthosite	Merensky Footwall
AT-14	Chromitite	Merensky lower chromitite layer
AT-15	)	Merensky Reef
AT-16	) Pegmatoidal, feldspathic	Merensky Reef
AT-17	) olivine orthopyroxenite	Merensky Reef
AT-18	)	Merensky Reef
AT-19	Chromitite	Merensky upper chromitite layer
AA-4	Chromitite	Merensky upper chromitite layer
27-A1	Feldspathic orthopyroxenite	Merensky Hangingwall
27-A2	Feldspathic orthopyroxenite	Merensky Hangingwall
27-A3	Feldspathic orthopyroxenite	Merensky Hangingwall
27-A4	Feldspathic orthopyroxenite	Merensky Hangingwall
AD-20	Feldspathic harzburgite	Upper Pseudoreef C
AD-24	Feldspathic harzburgite	Upper Pseudoreef B
AD-36	Feldspathic harzburgite	Upper Pseudoreef B
AD-38	Feldspathic harzburgite	Upper Pseudoreef C
AD-25A	Plagioclase	"P2 Middling"
AD-25A	Leucotroctolite	"P2 Middling"
AD-26	Leuconorite	"P2 Middling"
AD-27	Leuconorite	"P2 Middling"
AD-28	Spotted anorthosite	"P2 Middling"
AD-29	Spotted anorthosite	"P2 Middling"
AD-41A	Leuconorite	"P2 Middling"

SAMPLE	DESCRIPTION	CYCLIC UNIT / MARKER
AC-6	Spotted anorthosite	Upper Pseudo A
AC-7	Spotted anorthosite	Upper Pseudo A
AH-4	Chromitite stringer above Upper Pseudoreef A	
AH-30	Feldspathic harzburgite	Upper Pseudoreef A
AH-31	Mottled anorthosite	Upper Pseudo A
AV-5A	Leuconorite	Upper Pseudo A
AV-8	Feldspathic harzburgite	Upper Pseudoreef A
AV-9	Mottled anorthosite	Upper Pseudo A
AV-10	Leuconorite	Upper Pseudo A

In addition, samples 27-E1, 27-E2, AK-1D, AK-3 and AU-4 are of the Merensky Reef adjacent to pegmatite replaced Reef (they may possibly be partially replaced).

(2) OTHER SAMPLE LOCATIONS

Samples of olivine-rich cumulates from R.P.M. Union Section examined in this study were from the collection at Rhodes University of W.J. de Klerk (see de Klerk, 1982). Whole-rock analyses are from de Klerk (1982), electron microprobe analyses of olivines are partly after de Klerk (1982) and partly by the author (see Appendix 7).

Samples from the upper zone are from a borehole drilled on the farm Bierkraal in the western Bushveld Complex (see Reynolds, in press). Samples referred to here include : IR-64,-113,-138,-226,- 330 (analyses from Reynolds (in press), TSM (so-called "troctolite sisal marker") and P-5 (contains 5 cumulus phases, namely olivine, orthopyroxene, clinopyroxene, plagioclase and Ti-magnetite) were analysed by the author. Sample WT-128 was provided by A.A. Mitchell (from a borehole drilled near Northam).

APPENDIX 5 WHOLE-ROCK ANALYSES BY XRF

All whole-rock analyses presented in this study were completed by the author in the Geology Department at Rhodes University, unles otherwise stated. Analyses were performed on a Phillips PW 1410 semi-automatic X-ray fluorescence spectrometer (XRF) using standard techniques employed at Rhodes University (Marsh, 1979). International (IUGS) and in-house standards of suitable whole-rocks were used; spiked or artificial standards were not employed. Major elements, excluding sodium, were analysed on fusion discs after the method of Norrish and Hutton (1969). Sodium and selected trace elements (Cr, V, Co, Ni, Cu, Zn, Sc, Nb, Zr, Y, Sr, and Rb) were determined on powder briquettes. In-house computer programs were used for data reduction (see Marsh, 1979). Full corrections were made for instrumental drift, dead time, background, tube and spectral line interferences and matrix affects. Operating conditions are summarised below.

XRF ANALYTICAL CONDITIONS

ELEMENT	TUBE	CRYSTAL	TIME	COUNTER	COLLIMATOR	L.L.D.	C.E..
Si	Cr	PET	40	FLOW	COARSE	-	-
Ti	Cr	LIF(200)	10	FLOW	FINE	-	-
Al	Cr	PET	40	FLOW	COARSE	-	-
Fe	Cr	LIF(200)	20	FLOW	FINE	-	-
Mn	Cr	LIF(200)	20	FLOW	COARSE	-	-
Mg	Cr	TLAP	100	FLOW	FINE	-	-
Ca	Cr	LIF(200)	10	FLOW	FINE	-	-
Na	Cr	TLAP	100	FLOW	FINE	-	-
K	Cr	LIF(200)	10	FLOW	FINE	-	-
P	Cr	GE	40	FLOW	COARSE	-	-
Sr	W	LIF(220)	200	SCINT	FINE	3.0	1.0
Rb	W	LIF(220)	200	SCINT	FINE	3.0	1.0
Zr	W	LIF(220)	200	SCINT	FINE	3.0	0.8
Y	W	LIF(220)	200	SCINT	FINE	3.0	0.9
Nb	W	LIF(220)	200	SCINT	FINE	4.0	1.0
Co	W	LIF(220)	100	FLOW	FINE	4.4	1.5
Cr	W	LIF(220)	100	FLOW	FINE	5.0	2.0
V	W	LIF(220)	100	FLOW	FINE	6.0	2.0
Zn	Mo	LIF(220)	100	FLOW + SCINT	FINE	1.4	0.6
Cu	Mo	LIF(220)	100	FLOW + SCINT	FINE	1.5	0.7
Ni	Mo	LIF(220)	100	FLOW + SCINT	FINE	2.0	1.0
Sc	Cr	LIF(200)	200	FLOW	FINE	1.5	0.4

L.L.D. = lower limit of determination; C.E. = counting error (L.L.D and C.E. are base on counting statistics - see Marsh, 1979; values presented here are averages, rounded off to 1 or 2 significant figures).
By convention, major element oxides are rounded off to 0.01 percent.
Emission line for each element is Kα and tube is run at 55kV, 40mA.

Loss on ignition (L.O.I.) was determined by heating samples in a closed oven at 1000°C for a minimum of 8 hours. $(H_2O)^-$ was not measured. Total iron was determined as Fe_2O_3. The relative proportion of Fe^{2+} and Fe^{3+} have been calculated as follows :

(1) For all samples containing disseminated Ti-magnetite and ilmenite the percentage of Fe^{3+} has been calculated using the technique of Irvine and Baragar (1971), thus :

$$\text{wt. \% } Fe_2O_3 = \text{wt. \% } TiO_2 + 1.5.$$

This technique has been used for samples of iron-rich ultramafic pegmatite and iron-rich dunite and iron-rich wehrlite from the platiniferous ultramafic pipes.

(2) An Fe_2O_3 / FeO ratio of 0.005 has been used for samples of magnesian dunite.

(3) An Fe_2O_3/FeO ratio of 0.10 has been used for samples of cumulates from the critical and main zones of the layered sequence, in accordance with other Bushveld-workers at Rhodes University.

The results of analyses not discussed in the main text are presented in the following tables :

TABLE A.5-1 : Whole-rock analyses of the platiniferous ultramafic pipes.

TABLE A.5-2 : Whole-rock analyses of cumulates from the upper critical zone at Amandelbult

TABLE A.5-3 : Whole-rock analyses of pegmatites from the main zone in borehole SK-2 at Union Section (from Mitchell, in prep.).

REFERENCES

MARSH, J.S, (1979) : A manual for X-ray fluorescence determination of major and trace elements in natural silicate rock materials. Unpub. Manual (41p.), Rhodes Univ., Grahamstown.

MITCHELL, A.A. : The geochemistry and origin of the main zone, western Bushveld Complex. Ph.D thesis (in prep.), Rhodes Univ., Grahamstown.

NORRISH, K & HUTTON, J.T.(1969) : An accurate x-ray spectrographic method for analysis of a wide range of geological samples. Geochim. Cosmochim. Acta 33, 431-453.

TABLE A.5-1 WHOLE-ROCK ANALYSES OF THE PLATINIFEROUS ULTRAMAFIC PIPES

Fe_2O_3 / FeO = 0.005, except samples labelled * for which Fe_2O_3 has been calculated using the technique of Irvine and Baragar.

** denotes cumulus dunites from the lower and lower critical zones.

	DR-1		DR-2		DR-3		DR-6		DR-8		DR-10		DR-12		DR-16		DR-18		DR-20	
wt.%																				
SiO_2	38.17	38.71	37.80	38.62	37.97	39.02	38.24	38.77	38.53	39.19	38.41	38.80	38.92	38.66	38.18	38.45	37.57	38.59	37.85	38.34
TiO_2	.02	.02	.02	.02	.02	.02	.02	.02	.02	.02	.03	.03	.02	.02	.02	.02	.01	.01	.02	.02
Al_2O_3	.32	.32	.12	.13	.19	.20	.16	.16	.17	.17	.22	.22	.16	.16	.17	.17	.06	.06	.08	.08
Fe_2O_3	.08	.08	.09	.09	.08	.08	.08	.08	.08	.08	.08	.08	.08	.08	.08	.09	.08	.08	.08	.08
FeO	14.95	15.16	17.57	17.96	15.39	15.82	16.08	16.30	16.31	16.59	15.07	15.22	15.21	15.11	16.73	16.85	15.39	15.81	15.28	15.48
MnO	.22	.22	.23	.24	.25	.26	.24	.25	.24	.24	.24	.24	.23	.23	.21	.21	.20	.20	.18	.18
MgO	43.65	44.26	41.02	41.91	42.33	43.50	42.93	43.52	42.02	42.74	44.09	44.54	45.23	44.93	43.15	43.47	43.29	44.46	44.45	45.02
CaO	.19	.19	.54	.55	.41	.43	.36	.36	.48	.49	.20	.21	.07	.07	.15	.16	.19	.19	.11	.11
Na_2O	.02	.02	.02	.02	.01	.01	.01	.01	Tr	Tr	.01	.01	.01	.01	.01	.01	n.d.	-	.01	.01
K_2O	n.d.	-	n.d.	-	n.d.	-	n.d.	-	n.d.	-	n.d.	-	n.d.	-	n.d.	-	n.d.	-	n.d.	-
P_2O_5	n.d.	-	n.d.	-	n.d.	-	n.d.	-	n.d.	-	n.d.	-	n.d.	-	n.d.	-	n.d.	-	n.d.	-
Cr_2O_3	.72	.73	.27	.27	.43	.44	.39	.39	.31	.31	.43	.43	.52	.52	.31	.31	.34	.34	.44	.44
NiO	.28	.29	.21	.21	.23	.24	.14	.14	.16	.16	.23	.23	.23	.22	.26	.27	.25	.26	.24	.24
L.O.I.	1.82	-	2.01	-	2.95		1.32	-	2.25	-	1.59	-	1.46	-	1.53	-	1.64	-	1.28	-
TOTAL	100.43	100.00	99.88	100.00	100.26	100.00	99.96	100.00	100.56	100.00	100.59	100.00	102.13	100.00	100.80	100.00	99.00	100.00	100.01	100.00
ppm																				
Cr	4947		1818		2935		2650		2092		2907		3567		2130		2292		3001	
V	72		47		63		56		53		40		57		33		40		54	
Co	207		211		188		169		196		190		194		196		200		196	
Ni	2232		1621		1830		1061		1256		1754		1771		2074		1946		1858	
Cu	24		12		11		24		51		12		8		12		9		9	
Zn	95		98		85		87		86		81		87		76		89		90	
Sc	5		7		7		6		8		5		5		5		6		5	

	DR-A1		DR-A2		DR-2A		ON-2		ON-12		MO-4		MO-1*		MO-3*		DUN-1**		DUN-2**	
wt.%																				
SiO_2	35.19	37.57	36.74	37.88	36.67	37.88	36.27	36.73	35.63	38.24	33.22	34.02	45.44	45.89	45.87	46.18	38.79	40.27	32.14	37.41
TiO_2	.02	.02	.01	.01	.02	.02	.03	.03	.05	.05	.16	.17	.27	.27	.47	.47	.03	.03	.07	.08
Al_2O_3	n.d.	-	n.d.	-	.01	.01	n.d.	-	.67	.72	.12	.13	1.96	1.98	1.80	1.81	.74	.77	1.16	1.35
Fe_2O_3	.11	.12	.11	.11	.11	.12	.15	.15	.08	.09	.22	.23	1.77	1.79	1.97	1.98	.06	.06	.07	.08
FeO	22.18	23.68	22.05	22.73	22.54	23.28	30.27	30.65	16.57	17.79	43.91	44.97	13.92	14.06	17.29	17.41	11.82	12.27	13.29	15.47
MnO	.28	.32	.28	.30	.32	.33	.48	.48	.29	.31	.65	.67	.30	.30	.35	.35	.17	.17	.17	.20
MgO	35.33	37.73	37.24	38.39	35.98	37.17	30.73	31.12	37.82	40.60	18.60	19.04	24.00	24.24	18.19	18.31	43.13	44.77	35.74	41.60
CaO	.30	.32	.27	.29	.87	.90	.59	.60	.50	.53	.67	.69	10.75	10.86	12.83	12.92	.39	.40	.08	.09
Na_2O	n.d.	-	n.d.	-	.01	.01	.02	.02	n.d.	-	.03	.03	.12	.12	.17	.17	n.d.	-	n.d.	-
K_2O	n.d.	-	n.d.	-	n.d.	-	n.d.	-	n.d.	-	n.d.	-	n.d.	-	.02	.02	n.d.	-	n.d.	-
P_2O_5	n.d.	-	n.d.	-	n.d.	-	n.d.	-	.02	.02	Tr	Tr	.03	.03	.02	.02	n.d.	-	n.d.	-
Cr_2O_3	.03	.03	.08	.09	.02	.02	.02	.02	1.35	1.45	.01	.01	.35	.35	.29	.29	.97	1.01	3.03	3.53
NiO	.23	.25	.21	.22	.27	.28	.18	.18	.18	.20	.06	.06	.10	.10	.07	.07	.24	.25	.17	.20
L.O.I.	5.41	-	3.57	-	3.29	-	.78	-	7.65	-	.87	-	2.16	-	1.52	-	4.89	-	13.48	-
TOTAL	99.07	100.00	100.57	100.00	100.08	100.00	99.52	100.00	100.81	100.00	98.52	100.00	101.17	100.00	100.84	100.00	101.22	100.00	99.39	100.00
ppm																				
Cr	184		560		102		115		9251		41		2405		2004		6631		20747	
V	47		52		40		57		162		52		-		574		38		152	
Co	247		243		253		296		183		398		-		154		154		135	
Ni	1816		1655		2143		1424		1439		445		810		517		1876		1348	
Cu	44		13		106		23		14		51		23		54		12		109	
Zn	106		111		98		159		95		166		94		103		68		87	
Sc	7		7		10		12		9		18		57		69		7		6	
Zr	n.d.		n.d.		n.d.		n.d.		n.d.		2.8		10.0		15.8		n.d.		n.d.	
Y	2.9		n.d.		2.4		3.5		n.d.		2.9		11.2		16.6		n.d.		n.d.	
Sr	n.d.		n.d.		3		n.d.		3		n.d.		19		16		n.d.		n.d.	
Rb	n.d.		n.d.		n.d.		n.d.		n.d.		n.d.		n.d.		n.d.		3		n.d.	

TABLE A.5-1 (CONTINUED)

Fe_2O_3 has been calculated using the technique of Irvine and Baragar, except samples labelled * for which Fe_2O_3 / FeO = 0.1.

	DR-22		DR-24		DR-26		DR-27		DR-31B		DR-31C		DR-32C		DR-37A		DR-38B		DR-38C	
wt.%																				
SiO_2	39.02	39.39	47.34	47.67	47.77	48.09	49.95	49.80	51.06	52.41	51.06	51.96	51.79	52.28	51.56	52.07	50.06	50.72	50.92	51.76
TiO_2	.03	.03	.19	.19	.17	.17	.20	.20	.22	.23	.22	.22	.25	.25	.34	.34	.35	.35	.29	.29
Al_2O_3	.37	.37	2.07	2.08	5.25	5.29	3.85	3.87	3.27	3.36	3.22	3.28	3.27	3.30	2.15	2.17	3.25	3.29	4.19	4.26
Fe_2O_3	1.53	1.54	1.69	1.70	1.67	1.68	1.70	1.71	1.72	1.77	1.72	1.75	1.75	1.77	1.84	1.86	1.86	1.87	1.79	1.82
FeO	14.26	14.39	13.80	13.90	12.38	12.46	10.86	10.91	10.77	11.05	10.65	10.84	9.83	9.92	8.47	8.55	8.63	8.75	8.18	8.32
MnO	.20	.20	.26	.26	.21	.22	.25	.25	.26	.27	.33	.34	.31	.31	.28	.28	.29	.29	.24	.24
MgO	42.86	43.24	22.04	22.19	19.08	19.21	17.92	18.01	18.58	19.07	18.62	18.95	17.73	17.90	16.36	16.52	16.21	16.43	15.06	15.31
CaO	.38	.38	11.71	11.79	12.54	12.62	14.71	14.79	11.15	11.44	12.02	12.23	13.76	13.89	17.58	17.75	17.65	17.89	17.11	17.39
Na_2O	.02	.02	.04	.04	.09	.09	.27	.27	.26	.27	.23	.23	.25	.25	.20	.20	.24	.24	.36	.37
K_2O	.07	.07	.01	.01	.01	.01	.01	.01	.01	.01	.07	.07	.01	.01	.06	.06	n.d.	-	.05	.05
P_2O_5	n.d.	-	n.d.	-	n.d.	-	.01	.01	.01	.01	.01	.01	Tr	Tr	.03	.03	.01	.01	.01	.01
Cr_2O_3	.19	.19	.09	.09	.09	.09	.11	.11	.07	.07	.07	.07	.07	.07	.10	.10	.11	.11	.13	.13
NiO	.18	.18	.07	.07	.07	.07	.06	.06	.05	.05	.05	.05	.05	.05	.05	.05	.04	.04	.04	.04
L.O.I.	.70	-	1.12	-	.95	-	1.29	-	1.07	-	1.26	-	1.48	-	1.22	-	.92	-	1.05	-
TOTAL	99.81	100.00	100.43	100.00	100.28	100.00	100.78	100.00	98.50	100.00	99.53	100.00	100.55	100.00	100.24	100.00	99.60	100.00	99.42	100.00
ppm																				
Cr	1308		616		590		769		476		470		449		662		756		864	
V	143		315		323		112		383		393		425		550		497		487	
Co	196		125		130		415		104		103		95		89		92		76	
Ni	1402		572		536		440		418		413		498		388		340		283	
Cu	32		27		25		30		17		18		164		67		16		25	
Zn	100		86		75		78		84		73		68		51		49		59	
Sc	24		61		57		68		67		68		70		88		91		90	
Zr	3.4		5.7		4.9		6.0		5.0		6.4		9.4		15.0		9.2		14.0	
Y	4.1		7.4		6.7		8.8		8.9		8.4		11.4		14.8		13.1		12.6	
Sr	8		27		78		58		34		35		36		19.4		34		48	
Rb	n.d.		n.d.		n.d.		n.d.		n.d.		n.d.		n.d.		3.1		n.d.		n.d.	

	DR-39**		DR-42**		DR-49**		DR-28*		DR-29*		DR-31D*		DR-32A*		DR-32B*		DR-34B*	
wt.%																		
SiO_2	47.30	49.01	43.25	43.56	51.60	51.83	49.86	50.60	48.30	49.37	51.13	51.44	50.52	51.59	50.83	50.84	43.30	44.34
TiO_2	.75	.78	.06	.06	.26	.26	.09	.09	.06	.06	.09	.09	.09	.09	.10	.10	.03	.03
Al_2O_3	10.90	11.29	6.43	6.48	3.70	3.72	20.62	20.93	22.44	22.94	18.70	18.82	17.41	17.77	19.52	19.52	26.71	27.36
Fe_2O_3	2.25	2.33	1.56	1.57	1.76	1.77	.46	.46	.42	.43	.60	.61	.63	.65	.60	.60	.33	.33
FeO	6.31	6.54	11.18	11.26	9.90	9.94	4.57	4.65	4.20	4.30	6.01	6.05	6.32	6.45	5.99	6.00	3.25	3.33
MnO	.18	.19	.20	.20	.26	.26	.10	.10	.12	.12	.16	.16	.17	.189	.20	.20	.08	.08
MgO	8.79	9.11	28.98	29.19	18.09	18.17	9.74	9.89	7.89	8.07	10.30	10.37	11.03	11.26	9.99	9.99	9.54	9.77
CaO	13.94	14.44	7.43	7.48	13.29	13.35	11.25	11.41	12.78	13.06	10.67	10.73	10.05	10.26	11.05	11.05	13.56	13.88
Na_2O	.57	.59	n.d.	-	.30	.30	1.68	1.71	1.45	1.48	1.58	1.59	1.54	1.58	1.53	1.53	.68	.70
K_2O	1.05	1.09	n.d.	-	.01	.01	.06	.06	.08	.08	.07	.07	.07	.07	.07	.07	.05	.05
P_2O_5	4.39	4.55	n.d.	-	.01	.01	n.d.	-	.03	.03	n.d.	-	.01	.01	Tr	Tr	.01	.01
Cr_2O_3	.06	.06	.19	.19	.33	.33	.08	.08	.08	.08	.08	.08	.08	.09	.07	.07	.04	.04
NiO	.02	.02	-	-	.05	.05	.02	.02	.02	.02	.03	.03	.03	.03	.03	.03	.03	.03
L.O.I.	4.66	-	1.00	-	.92	-	.90	-	.67	-	1.25	-	1.01	-	.91	-	1.38	-
TOTAL	101.17	100.00	100.28	100.00	100.48	100.00	99.45	100.00	98.53	100.00	100.64	100.00	98.83	100.00	100.89	100.00	99.03	100.00
ppm																		
Cr	396		1316		2227		426		550		525		572		471		292	
V	182		89		391		74		100		116		123		114		11	
Co	45		149		97		39		43		51		53		52		49	
Ni	158		-		405		220		171		195		225		202		609	
Cu	21		8		42		60		27		19		29		19		11	
Zn	32		72		64		40		42		43		64		49		19	
Sc	34		18		65		13		16		20		21		20		3	
Nb	16.3		n.d.		n.d.		n.d.		n.d.		n.d.		n.d.		n.d.		n.d.	
Zr	26.1		2.4		7.6		n.d.		2.8		2.5		n.d.		n.d.		n.d.	
Y	27.5		2.2		10.8		n.d.		2.2		2.8		2.7		3.5		1.9	
Sr	216 5		84		37		317		281		244		243		261		301	
Rb	51.5		n.d.		n.d.		n.d.		n.d.		n.d.		n.d.		n.d.		n.d.	

TABLE A.5-2 WHOLE-ROCK ANALYSES OF CUMULATES FROM THE UPPER CRITICAL ZONE

AT AMANDELBULT

Fe_2O_3 / FeO = 0.1.

	AE-36		AE-35		AT-1		AT-2		AT-3		AT-4		AT-6		AT-7		AT-8		AT-9	
wt.%																				
SiO_2	51.39	51.81	51.38	50.90	49.22	49.53	49.22	49.46	50.28	50.54	50.07	50.08	48.63	49.05	49.81	49.82	51.37	49.88	48.79	49.01
TiO_2	.10	.10	.09	.09	.10	.10	.09	.09	.09	.09	.08	.08	.11	.11	.09	.09	.11	.10	.15	.15
Al_2O_3	16.04	16.18	26.48	26.23	26.33	25.50	28.22	28.35	23.13	23.26	24.13	24.13	30.55	30.81	26.34	26.34	26.83	26.05	29.09	29.22
Fe_2O_3	.58	.58	.31	.31	.26	.26	.20	.20	.37	.37	.32	.32	.13	.13	.28	.28	.30	.29	.20	.20
FeO	5.78	5.82	3.11	3.08	2.58	2.60	1.98	1.99	3.66	3.68	3.22	3.22	1.27	1.28	2.75	2.75	2.97	2.88	1.98	1.99
MnO	.11	.11	.02	.02	.03	.03	.01	.01	.02	.02	.05	.05	.04	.04	.03	.03	.03	.03	.04	.04
MgO	15.76	15.88	4.55	4.51	6.07	6.10	4.29	4.31	8.75	8.80	7.86	7.86	1.38	1.40	5.59	5.59	6.02	5.85	2.82	2.83
CaO	8.31	8.38	13.27	13.15	12.88	12.96	13.48	13.54	11.44	11.50	12.30	12.31	15.00	15.13	13.05	13.05	13.34	12.96	14.40	14.46
Na_2O	1.08	1.09	1.67	1.65	1.81	1.82	1.90	1.91	1.61	1.62	1.82	1.82	1.85	1.86	1.92	1.92	1.87	1.82	1.93	1.96
K_2O	.05	.05	.07	.07	.10	.10	.14	.14	.11	.11	.12	.12	.17	.17	.14	.14	.14	.13	.15	.15
P_2O_5	n.d.	n.d.	.01	.01	.01	.01	.01	.01	.01	.01	.01	.01	.03	.03	.01	.01	.01	.01	.01	.01
Cr_2O_3	.29	-	.12	-	.10	-	.07	-	.14	-	.13	-	.01	-	.09	-	.09	-	.03	-
NiO	.02	-	.02	-	.14	-	.01	-	.03	-	.02	-	Tr	-	.02	-	.02	-	.01	-
L.O.I.	1.10	-	.94	-	.75	-	.41	-	.83	-	.41	-	.48	-	.61	-	.63	-	.39	-
TOTAL	100.61	100.00	102.03	100.00	100.36	100.00	100.03	100.00	100.47	100.00	100.55	100.00	99.65	100.00	100.70	100.00	103.73	100.00	99.99	100.00
ppm																				
Cr	1992		823		689		456		992		869		69		589		611		175	
V	79		37		27		23		38		36		15		33		35		23	
Co	57		27		23		15		31		29		10		22		23		11	
Ni	362		155		1122		96		200		175		31		120		142		53	
Cu	35		18		161		18		18		20		18		19		19		21	
Zn	51		21		157		13		25		23		7		20		19		13	
Sc	18		11		9		7		11		11		6		9		10		7	
Nb	n.d.		n.d.		n.d.		n.d.		n.d.		n.d.		n.d.		n.d.		n.d.		n.d.	
Zr	n.d.		n.d.		n.d.		4.2		6.3		6.0		4.3		6.6		7.0		4.4	
Y	3.5		2.4		2.0		2.1		4.1		3.0		3.6		3.0		3.1		3.0	
Sr	213		358		375		421		345		362		474		394		393		449	
Rb	n.d.		n.d.		n.d.		3.1		n.d.		n.d.		n.d.		n.d.		n.d.		n.d.	

	AT-10		AT-11		AT-12		AT-13		27-A1		27-A2		27-A3		27-A4		AD-25A		AD-25B	
wt.%																				
SiO_2	49.98	49.09	49.27	49.19	49.28	48.83	48.86	48.77	53.00	53.58	53.63	53.55	51.55	52.24	50.44	50.62	46.88	45.22	46.72	
TiO_2	.09	.09	.06	.06	.04	.04	.04	.04	.24	.24	.27	.27	.23	.23	.22	.22	.09	.06	.06	
Al_2O_3	30.88	30.33	31.12	31.07	32.16	31.86	31.23	31.83	5.31	5.37	5.00	4.99	4.81	4.87	4.06	4.08	31.41	26.11	26.93	
Fe_2O_3	.14	.14	.11	.11	.09	.09	.08	.08	1.05	1.07	1.09	1.09	1.12	1.13	1.60	1.60	.07	.31	.32	
FeO	1.43	1.41	1.13	1.12	.89	.88	.83	.84	10.55	10.66	10.92	10.91	11.16	11.31	15.95	16.01	.70	3.10	3.20	
MnO	.01	.01	.01	.01	n.d.	n.d.	n.d.	n.d.	.29	.29	.27	.27	.27	.27	.32	.32	.04	.03	.03	
MgO	1.82	1.79	1.27	1.27	.60	.60	.55	.56	23.12	23.37	23.83	23.80	22.91	23.22	22.24	22.32	1.36	7.31	7.56	
CaO	15.14	14.87	14.88	14.86	15.51	15.36	15.23	15.53	4.89	4.94	4.54	4.54	6.07	6.15	4.41	4.43	16.67	12.63	13.06	
Na_2O	2.13	2.10	2.14	2.13	2.20	2.18	2.14	2.18	.43	.44	.51	.51	.52	.53	.36	.36	2.41	1.78	1.84	
K_2O	.17	.17	.16	.16	.14	.14	.14	.14	.03	.03	.04	.04	.02	.02	.02	.02	.34	.23	.24	
P_2O_5	.01	.01	.02	.02	.02	.02	.01	.01	.01	.01	.04	.04	.02	.02	.02	.02	.02	.01	.01	
Cr_2O_3	.02	-	.01	-	Tr	-	Tr	-	.52	-	.47	-	.43	-	.45	-	-	.12	-	
NiO	-	-	Tr	-	Tr	-	Tr	-	.11	-	.09	-	.27	-	.43	-	-	.06	-	
L.O.I	.33	-	.36	-	.26	-	.30	-	1.06	-	.56	-	.67	-	.99	-	-	3.31	-	
TOTAL	102.17	100.00	100.55	100.00	101.19	100.00	99.41	100.00	100.61	100.00	101.27	100.00	100.03	100.00	101.50	100.00	100.00	100.27	100.00	
ppm																				
Cr	112		59		27		4		3628		3223		2922		3070		573	837		
V	18		14		9		7		168		173		152		150		8	12		
Co	12		6		4		2		101		110		119		160		3	42		
Ni	-		39		19		15		894		680		2140		3388		20	378		
Cu	-		37		18		13		216		100		993		1339		13	15		
Zn	-		8		11		5		85		98		80		106		30	109		
Sc	7		3		2		2		36		37		33		35		3.2	4.3		
Nb	n.d.		n.d.		n.d.		n.d.		n.d.		n.d.		n.d.		n.d.		n.d.	n.d.		
Zr	-		4.8		2.7		n.d.		7.5		7.0		5.5		7.8		n.d.	n.d.		
Y	-		4.2		2.8		2.1		9.0		10.4		7.1		8.0		n.d.	2.8		
Sr	-		477		487		487		63		67		55		48		485	412		
Rb	-		3.1		2.2		n.d.		n.d.		3.0		n.d.		n.d.		5.2	4.3		

TABLE A.5-2 (CONTINUED)

Fe_2O_3 / FeO = 0.1.

	AT-15		AT-16		AT-17		AT-18		AK-1D		AK-3		AU-4		27-E1		27-E2	
wt.%																		
SiO_2	46.67	48.72	50.88	51.62	50.83	52.51	52.66	53.42	52.02	52.93	45.83	46.48	47.09	48.45	51.34	51.73	49.41	50.05
TiO_2	.15	.15	.17	.17	.17	.17	.36	.36	.19	.19	.95	.96	.50	.51	.18	.18	.43	.44
Al_2O_3	9.11	9.51	11.65	11.82	5.57	5.75	4.67	4.74	5.68	5.77	6.54	6.63	11.84	12.21	4.08	4.11	5.67	5.74
Fe_2O_3	1.02	1.07	.86	.87	1.07	1.11	1.11	1.12	1.05	1.07	1.72	1.74	1.25	1.29	1.22	1.23	1.27	1.29
FeO	10.23	10.68	8.59	8.72	10.70	11.05	11.05	11.21	10.05	10.70	17.20	17.44	12.51	12.89	12.19	12.28	12.69	12.85
MnO	.20	.21	.13	.13	.18	.18	.22	.22	.20	.21	.30	.30	.19	.19	.29	.29	.28	.28
MgO	22.90	23.91	19.21	19.49	24.02	24.82	24.23	24.58	23.73	24.15	10.97	11.12	15.70	16.18	26.29	26.49	23.65	23.95
CaO	4.28	4.47	5.38	5.46	3.61	3.73	3.65	3.70	4.11	4.19	14.55	14.76	7.18	7.40	3.30	3.32	4.77	4.83
Na_2O	.58	.60	.91	.92	.50	.52	.43	.43	.67	.68	.43	.43	.72	.75	.31	.31	.46	.46
K_2O	.64	.66	.78	.79	.15	.16	.19	.19	.10	.11	.10	.10	.12	.13	.03	.03	.07	.07
P_2O_5	.01	.01	.02	.02	.01	.01	.02	.02	.02	.02	.03	.03	.01	.01	.02	.02	.04	.04
Cr_2O_3	.36	-	.18	-	.57	-	.60	-	.53	-	.09	-	-	-	.65	-	.47	-
NiO	.20	-	.15	-	.36	-	.12	-	.16	-	.03	-	.26	-	.26	-	.17	-
L.O.I.	4.22	-	1.20	-	2.04	-	1.41	-	1.14	-	1.86	-	1.86	-	.99	-	1.13	-
TOTAL	100.56	100.00	100.10	100.00	99.78	100.00	100.72	100.00	100.12	100.00	100.60	100.00	99.14	100.00	101.16	100.00	100.50	100.00
ppm																		
Cr	2497		1241		3877		4137		3606		583		-		4422		3215	
V	53		44		108		133		121		368		-		140		166	
Co	125		100		130		105		105		108		-		136		131	
Ni	1538		1143		2860		958		1250		229		2069		2012		1308	
Cu	111		99		820		130		340		129		1041		651		175	
Zn	68		57		80		92		83		105		100		98		97	
Sc	9		4		20		25		27		85		29		30		32	
Nb	n.d.		n.d.		n.d.		n.d.		n.d.		n.d.		n.d.		n.d.		n.d.	
Zr	14.7		85.0		15.6		11.4		11.0		18.6		8.7		8.6		15.1	
Y	5.5		5.3		5.6		7.1		6.0		18.7		8.5		6.6		8.3	
Sr	109		145		65		49		76		112		201		45		77	
Rb	29		28		5		6		5		3		2		n.d.		3	

	AC-6		AC-7		AH-31		AV-5A		AV-9		AV-10		AD-26	AD-27	AD-29	AD-41A
wt.%																
SiO_2	45.04	46.05	48.80	48.77	49.07	48.84	48.63	47.92	46.61	45.71	48.57	48.93	49.82	49.87	48.39	49.97
TiO_2	.19	.19	.16	.16	.10	.10	.08	.08	.16	.16	.06	.06	.11	.09	.04	.07
Al_2O_3	31.16	31.85	31.16	31.14	29.36	29.22	30.27	29.83	30.46	29.87	28.83	29.04	24.03	25.17	32.29	24.71
Fe_2O_3	.18	.18	.11	.11	.18	.18	.21	.21	.41	.41	.21	.21	.34	.29	.08	.31
FeO	1.79	1.83	1.06	1.05	1.79	1.78	2.09	2.06	4.13	4.05	2.10	2.12	3.38	2.94	.75	3.13
MnO	Tr	Tr	n.d.	n.d.	.01	.01	.01	.01	.02	.02	Tr	Tr	.04	.03	n.d.	.03
MgO	1.18	1.21	1.06	1.05	3.66	3.65	3.47	3.42	3.02	2.96	3.99	4.02	8.73	7.57	.95	7.86
CaO	15.82	16.17	14.82	14.81	14.36	14.30	14.88	14.66	15.64	15.34	14.05	14.16	11.81	12.22	15.12	12.08
Na_2O	2.21	2.26	2.65	2.65	1.84	1.83	1.72	1.69	1.43	1.40	1.37	1.38	1.65	1.72	2.13	1.72
K_2O	.24	.24	.27	.27	.10	.09	.13	.13	.07	.07	.09	.09	.08	.08	.25	.10
P_2O_5	.02	.02	.01	.01	.01	.01	Tr	Tr	.02	.02	n.d.		Tr	.01	Tr	.03
Cr_2O_3	.08	-	.08	-	.09	-	.10	-	.07	-	.10	-	-	-	-	-
NiO	Tr	-	Tr	-	.01	-	.01	-	.12	-	.01	-		-		-
L.O.I.	2.88	-	1.56	-	.46	-	.66	-	.47	-	.57	-		-		-
TOTAL	100.78	100.00	101.70	100.00	101.02	100.00	102.26	100.00	102.54	100.00	99.94	100.00	100.00	100.00	100.00	100.00
ppm																
Cr	571		592		638		664		463		693		1150	972	410	1030
V	49		15		21		28		32		23		36	31	9	33
Co	9		5		14		14		24		14		31	26	4	28
Ni	34		26		84		72		931		85		198	173	32	140
Cu	18		17		19		12		210		13		24	24	9	53
Zn	30		7		13		15		144		13		24	21	5	70
Sc	8		6		6		9		10		10		10	9	4	10
Nb	n.d.		n.d.		n.d.		n.d.		n.d.		4.9		n.d.	n.d.	n.d.	n.d.
Zr	n.d.		5.6		n.d.		n.d.		n.d.		n.d.		2.1	n.d.	n.d.	n.d.
Y	3.7		4.1		3.7		3.4		2.2		4.7		2.7	2.9	n.d.	2.2
Sr	464		456		437		411		423		425		360	373	479	377
Rb	5.4		6.6		n.d.		n.d.		n.d.		3.0		n.d.	n.d.	3.0	n.d.

TABLE A.5-2 (CONTINUED)

Fe_2O_3 / FeO = 0.1. All samples here of the pseudoreefs.

	AH-30		AV-8		AD-20	AD-24		AD-36		AD-38
wt.%										
SiO_2	37.94	41.57	39.93	43.67	43.89	39.25	43.29	38.46	43.06	44.70
TiO_2	.16	.18	.10	.11	.13	.19	.21	.11	.13	.18
Al_2O_3	5.67	6.21	3.86	4.22	6.20	4.31	4.75	3.21	3.59	4.55
Fe_2O_3	1.22	1.33	1.31	1.43	1.15	1.16	1.28	1.18	1.32	1.19
FeO	12.18	13.35	13.12	14.35	11.48	11.59	12.79	11.77	13.17	11.93
MnO	.19	.21	.18	.20	.19	.15	.17	.15	.17	.15
MgO	28.91	31.69	30.01	32.82	33.07	31.05	34.25	31.03	34.74	33.73
CaO	2.35	2.57	2.24	2.45	3.20	2.39	2.64	2.87	3.22	2.94
Na_2O	.26	.28	.13	.15	.18	.13	.14	.11	.12	.12
K_2O	.03	.04	.03	.04	.06	.06	.07	.06	.06	.05
P_2O_5	n.d.	n.d.	n.d.	n.d.	.01	n.d.	n.d.	n.d.	n.d.	n.d.
Cr_2O_3	1.99	2.18	.18	.20	.19	.17	.17	.18	.18	.21
NiO	.36	.39	.33	.36	.26	.25	.25	.26	.26	.24
L.O.I.	8.36	-	8.57	-	-	10.45	-	10.91	-	-
TOTAL	99.69	100.00	100.01	100.00	100.00	101.15	100.00	100.30	100.00	100.00
ppm										
Cr	13609		1227		1139	1056		1126		1346
V	145		41		34	41		51		46
Co	169		166		139	152		146		145
Ni	2854		2590		1791	1827		1780		1746
Cu	688		386		11	10		8		21
Zn	97		63		79	83		80		67
Sc	9		11		8	8		10		10
Nb	n.d.		n.d.		n.d.	n.d.		n.d.		n.d.
Zr	2.9		4.4		5.8	5.2		5.9		6.2
Y	n.d.		3.8		3.3	3.7		4.6		3.9
Sr	61		53		75	60		54		59
Rb	n.d.		n.d.		2.4	2.5		n.d.		n.d.

TABLE A.5-3 WHOLE-ROCK ANALYSES OF PEGMATITES FROM THE MAIN ZONE

IN BOREHOLE SK2 AT UNION SECTION

Total Fe presented as Fe_2O_3. From Mitchell (in prep.).

	A20	A31	A59	A107	A115	A152	A163	A165	A166	A172	A176	A185	A227	A237	A238	A252	A320	A348
SiO_2	47.29	42.15	-	39.45	41.22	49.51	46.57	42.65	50.99	41.68	-	46.26	46.62	-	-	24.47	47.96	26.29
TiO_2	0.98	3.17	-	0.67	1.65	0.58	1.35	2.23	0.39	3.26	-	1.62	1.87	-	-	6.61	1.16	7.94
Al_2O_3	11.56	6.72	-	11.79	12.12	15.51	2.27	12.32	19.34	11.74	-	13.41	13.59	-	-	3.03	4.35	1.99
Fe_2O_3	21.92	28.47	-	30.31	27.08	15.01	23.84	24.29	7.64	23.83	-	15.58	16.18	-	-	51.45	18.12	47.56
MnO	0.26	0.39	-	0.38	0.33	0.23	0.28	0.22	0.11	0.25	-	0.20	0.18	-	-	0.33	0.20	0.37
MgO	4.72	5.25	-	5.75	4.99	4.02	12.54	6.14	4.63	7.23	-	6.48	6.24	-	-	6.37	12.98	10.91
CaO	12.52	13.03	-	8.29	10.96	13.14	15.13	12.08	13.35	11.93	-	13.53	13.61	-	-	8.36	15.55	6.29
Na_2O	2.24	1.46	-	2.07	2.09	2.98	0.21	1.87	2.82	1.66	-	2.26	1.41	-	-	0.23	0.39	0.08
K_2O	0.22	0.13	-	0.22	0.18	0.21	0.00	0.12	0.29	0.10	-	0.13	0.23	-	-	0.01	0.03	0.00
P_2O_5	0.31	0.17	-	2.28	2.16	1.19	0.01	0.01	0.00	0.01	-	0.01	0.05	-	-	0.00	0.01	0.00
LOI	+1.09	+1.14	-	+1.23	+1.15	+0.29	+1.53	+1.61	0.20	+0.68	-	+0.45	+0.53	-	-	+1.83	+0.62	+2.44
H_2O-	0.38	0.03	-	0.04	0.03	0.07	0.01	0.00	0.05	0.03	-	0.04	0.04	-	-	0.02	0.10	0.01
TOTAL	101.31	99.83	-	100.02	101.55	101.99	100.68	100.32	99.77	101.04	-	99.07	99.47	-	-	98.69	100.23	99.00
Co	53	59	60	128	83	38	174	247	41	132	5	91	90	124	83	482	117	285
Cr	77	29	36	26	10	6	155	78	11	61	5	242	67	291	351	502	703	1465
V	88	276	112	31	65	19	566	492	91	696	8	352	376	383	388	1285	1090	2076
Zn	113	183	168	156	127	252	96	124	56	10	20	89	97	83	71	314	496	294
Cu	58	156	140	104	145	82	730	2009	75	36	32	187	151	140	98	9583	2842	643
Ni	58	189	184	52	39	55	250	563	60	13	19	110	65	103	141	1111	1369	548
Zr	26.2	34.8	16.5	6.9	8.8	11.7	16.2	9.3	7.2	17.6	2.2	11.5	14.3	26.0	13.0	14.4	16.3	16.9
Y	20.1	25.5	35.1	24.0	29.7	30.0	17.0	10.2	8.1	12.6	1.2	9.3	14.3	18.6	12.2	9.9	15.6	8.2
Nb	nd	nd	nd	nd	nd	nd	nd	nd	nd	2.1	nd	nd	nd	nd	nd	nd	nd	nd
Rb	nd	nd	nd	nd	nd	nd	nd	nd	4.9	nd	nd	1.9	4.5	6.5	1.8	nd	nd	1.3
Sr	250	139	274	301	308	368	19	207	334	180	556	234	234	31	160	30	40	10
Ba	123	90	101	129	122	151	19	61	86	72	108	64	113	38	81	30	28	26
Sc	91	162	62	15	43	73	119	65	45	74	3.3	77	79	134	66	319	117	86

APPENDIX 6 THE CIPW NORM

CIPW norms have been calculated for most of the whole-rock samples analysed in this study, using an in-house computer program based on an algorithm developed by Kelsey (1965). In this study the weight percent norm has been used exclusively. Major element oxides (normalised, L.O.I. free, using the relevent Fe_2O_3/FeO ratio) are input into the program. Cr_2O_3 and NiO were only input where thay comprise significant components. CIPW norms calculated in this study are presented in Table A.6.

The following abbreviations are used :

AP (apatite); CM (chromite); IL (ilmenite); OR (orthoclase); AB (albite); AN (anorthosite); C (corundum); RU (rutile); MT (magnetite); DIEN (clinopyroxene - enstatite); DIFS (clinopyroxene - ferrosilite); DINO (climopyroxene - mollastonite); HYEN (arthopyroxene - enstatite); HYFS (orthopyroxene - ferrosilite); Q (quartz); FO (olivine - fosterite); FA (olivine-fayalite); NE (nepheline); LC (leucite); CS (sodium metasilicate) KP (kerrophyllite).

In addition, two ratios are also tabulated, namely, the differentiation index (D.I. = norm. A + Or + Ab + Ne + Ks + Lc) and the Mg-number (Mg # = atomic % $Mg/(Mg + Fe^{2+})$.

REFERENCES

KELSEY, C.H. (1965) : Calculation of the CIPW norm. Mineral. Mag. 34, 276-283.

TABLE A.6 C.I.P.W. NORMS OF WHOLE ROCK ANALYSES

SAMPLE	AE-8	AE-19	AE-20	AE-21	AU-1	AU-2	AE-23	AE-24	AE-25	AE-26	AE-27	AE-28
AP	.05	.05	.05	.02	.28	.07	.05	.02	.02	.05	.02	.12
IL	3.21	7.41	9.60	7.73	8.29	4.29	19.96	3.81	9.93	10.24	7.14	5.98
OR	.00	.06	.00	.00	.06	.18	.06	.18	.00	.18	.18	.53
AB	1.02	1.10	1.52	.85	2.89	1.44	.93	.85	1.02	.51	1.02	1.02
AN	1.48	4.19	6.42	3.84	12.06	4.01	3.76	3.31	3.61	3.27	3.98	6.29
MT	4.52	7.67	9.32	8.05	8.32	5.31	17.02	4.96	9.70	9.73	7.61	6.64
DIEN	5.29	16.03	18.35	12.38	13.77	14.89	21.45	4.49	14.01	2.51	10.46	12.75
DIFS	6.88	12.18	10.26	11.25	9.63	13.27	.27	5.89	10.34	2.88	10.44	10.84
DIWO	12.17	29.27	30.26	24.22	24.40	28.90	25.06	10.27	25.31	5.44	21.30	24.29
HYEN	1.00	6.01	6.98	4.22	5.18	5.77	6.73	2.14	5.58	8.01	3.45	7.89
HYFS	1.30	4.56	3.90	3.84	3.62	5.14	.08	2.86	4.12	9.18	3.44	6.71
Q	.00	.00	.00	.00	.00	.00	4.89	.00	.00	.00	.00	.00
FO	25.96	6.31	2.16	11.76	6.58	8.49	.00	24.79	9.11	21.28	14.78	8.80
FA	37.20	5.28	1.33	11.78	5.07	8.33	.00	36.59	7.41	26.88	16.26	8.24
TOTAL	100.07	100.12	100.14	100.13	100.13	100.06	100.16	100.06	100.15	100.15	100.10	100.09
D.I.	1.02	1.16	1.52	.85	2.94	1.62	5.88	1.02	1.02	.68	1.19	1.55
MG#	.48	.55	.56	.52	.54	.55	.58	.47	.53	.47	.51	.54

SAMPLE	AE-29	AE-31	AE-32	AE-33A	AE-9	AE-10	AE-11	AE-12	AE-13	AE-15	AE-17	AE-18
AP	.02	.05	.07	.02	.07	.09	.02	.09	.09	.09	.05	.02
IL	4.62	5.95	5.10	6.39	3.04	4.21	1.91	.94	4.10	8.56	5.54	6.97
OR	.12	.06	.53	.00	.00	.06	.00	.00	.12	.24	.00	.06
AB	2.12	1.02	1.86	1.60	.76	.93	.34	.42	1.35	2.88	1.18	1.18
AN	2.69	4.45	4.83	1.18	1.81	3.38	1.29	1.28	3.64	14.97	4.07	4.39
MT	5.57	6.52	5.93	6.90	4.36	5.25	3.54	2.81	5.16	8.53	6.37	7.34
DIEN	9.67	15.33	13.84	15.11	5.95	4.24	3.63	4.25	13.97	10.34	13.44	15.40
DIFS	10.65	12.20	11.35	13.36	7.58	5.52	5.34	6.21	12.85	4.20	12.53	12.28
DIWO	26.56	28.46	26.91	29.25	13.56	9.77	8.90	10.38	27.47	15.66	26.59	28.63
HYEN	1.66	5.99	6.45	.00	2.13	2.17	.12	.65	4.87	20.20	3.52	5.45
HYFS	1.83	4.77	5.29	.00	2.71	2.83	.17	.95	4.48	8.19	3.28	4.34
FO	18.32	8.14	9.87	10.66	24.18	25.31	28.56	27.61	10.91	3.55	11.61	7.58
FA	22.24	7.14	8.93	10.38	33.91	36.29	46.23	44.45	11.06	1.59	11.93	6.66
NE	.00	.00	.00	5.23	.00	.00	.00	.00	.00	.00	.00	.00
TOTAL	100.06	100.10	100.08	100.08	100.06	100.06	100.04	100.05	100.09	98.99	100.10	100.31
D.I.	2.23	1.07	2.39	6.83	.76	.99	.34	.42	1.47	3.11	1.18	1.24
MG#	.51	.56	.56	.53	.49	.48	.46	.47	.55	.64	.53	.54

SAMPLE	ML22-10	ML29-1	ML22-A3	ML22A10	ML22A18	AM-2	AG-4	AK-18	AK-2	AU-6	27W-D1	27W-D2
AP	.09	.12	.19	.26	.14	.02	.02	.02	.24	.05	.07	.07
IL	2.67	5.66	8.20	7.54	6.22	14.24	1.85	1.56	1.92	9.28	2.17	1.33
OR	.06	.00	.00	.24	.00	.00	.00	.12	1.83	.00	.00	.00
AB	.03	.76	.00	1.19	.00	.59	.34	1.69	3.81	.76	.51	1.02
AN	2.89	5.00	27.96	14.95	26.03	2.77	.97	7.53	13.44	3.20	2.57	3.94
MT	4.23	6.44	8.37	7.87	6.87	12.90	3.64	3.38	3.73	9.19	3.83	3.19
DIEN	6.99	12.01	6.45	9.59	3.14	7.49	2.40	5.84	14.14	12.63	5.10	5.13
DIFS	8.31	11.31	10.18	11.94	5.10	5.48	3.68	4.37	11.82	9.49	4.60	3.80
DIWO	15.40	23.86	14.29	21.61	8.11	13.48	6.01	10.60	26.76	22.97	9.95	9.27
HYEN	.00	1.60	.00	.00	.00	8.05	.31	25.76	6.79	8.08	15.32	16.28
HYFS	.00	1.51	.00	.00	.00	5.89	.47	19.30	5.67	6.07	13.83	12.95
FO	25.36	15.62	6.81	10.07	14.91	16.23	29.58	10.68	4.12	10.67	21.10	24.22
FA	33.26	16.21	11.65	13.81	26.70	13.08	50.48	8.98	3.79	8.34	20.99	19.76
NE	.76	.00	2.84	1.05	2.52	.00	.00	.00	.00	.00	.00	.00
LC	.00	.00	1.99	.00	.37	.00	.00	.00	.00	.00	.00	.00
CS	.00	.00	3.17	.00	.01	.00	.00	.00	.00	.00	.00	.00
TOTAL	100.07	100.10	102.29	100.12	100.12	100.23	100.04	100.03	98.06	100.13	100.05	100.05
D.I.	.85	.76	4.83	2.48	2.89	.59	.34	1.81	5.64	.76	.51	1.02
MG#	.51	.53	.36	.44	.40	.52	.45	.62	.58	.54	.58	.63

SAMPLE	27W-F1	27W-B1	AM-1	AG-5	AM-4A	27W-B1	27W-B2	27W-B3	27W-B4	27W-E2
AP	.09	.07	.00	.02	.05	.05	.07	.12	.02	.09
IL	8.74	.46	.56	3.94	10.24	3.96	1.81	.89	2.27	.85
OR	.06	.00	.12	.12	.47	.00	.00	.24	.00	.41
AB	.59	.85	2.03	.76	1.52	.00	.85	1.52	.85	3.89
AN	2.77	3.18	9.75	8.05	5.34	.36	2.66	3.06	2.83	13.39
MT	8.84	2.55	2.60	5.16	9.92	5.19	3.57	2.70	3.99	1.87
DIEN	3.75	5.46	3.91	11.20	25.49	.00	9.03	5.29	10.43	2.90
DIFS	4.20	5.88	1.48	10.50	5.38	.00	11.30	4.31	11.67	1.08
DIWO	8.04	11.50	5.83	22.19	34.24	.00	20.39	9.92	22.35	4.30
HYEN	5.59	4.06	48.52	2.85	3.38	.00	1.34	7.37	.51	39.11
HYFS	6.25	4.36	18.38	2.67	.71	.00	1.67	6.01	.57	14.63
Q	.00	.00	.00	.00	3.39	-.89	.00	.00	.00	.00
FO	22.95	28.21	4.83	16.93	.00	32.11	19.90	30.97	19.95	12.36
FA	28.28	33.44	2.02	16.56	.00	58.01	27.44	27.83	24.60	5.11
NE	.00	.00	.00	.00	.00	.05	.00	.00	.00	.00
CS	.00	.00	.00	.00	.00	.51	.00	.00	.00	.00
TOTAL	100.14	100.02	100.02	100.06	100.14	99.46	100.03	100.03	100.04	100.02
D.I.	.65	.85	2.15	.88	5.39	-.84	.85	1.76	.65	4.31
MG#	.49	.55	.77	.55	.65	.43	.50	.61	.52	.77

TABLE A.6 (continued)

SAMPLE	ML27-3	ML27-5	ML27-1	ML27-2	ML27-6	ML27-4	ML27-7	ML24-1	ML24-8	ML24-9	ML24-2	ML24-3
AP	.07	.09	.12	.12	.07	.12	.12	.81	.07	.52	.14	.19
IL	13.07	11.95	8.95	8.85	8.85	5.16	7.16	2.39	1.60	6.45	2.96	3.39
OR	.00	.00	.00	.12	.06	.12	.12	.18	.41	.41	.30	.59
AB	.00	.85	1.52	2.12	1.95	2.62	2.54	1.12	2.37	.56	2.28	3.72
AN	2.31	.97	1.29	1.44	1.86	1.96	1.49	1.07	1.73	3.04	2.43	4.25
MT	11.93	11.18	8.95	8.82	8.86	6.05	7.53	4.02	3.42	7.08	4.47	4.74
DIEN	10.18	4.40	7.17	7.82	7.83	13.59	13.63	1.92	1.25	5.88	9.10	6.72
DIFS	6.62	5.00	8.73	8.41	9.12	13.12	10.71	2.90	1.97	8.69	10.88	8.95
DIWO	14.93	9.49	15.98	16.46	17.08	27.28	25.20	4.66	3.17	14.45	20.12	15.66
HYEN	.00	4.77	1.38	3.49	.71	2.28	6.18	.00	.06	.00	2.93	.26
HYFS	.00	5.42	1.69	3.75	.82	2.20	4.85	.00	.10	.00	3.51	.34
FO	22.48	20.45	18.94	17.74	18.80	12.40	11.04	29.42	30.62	19.80	17.67	20.76
FA	16.11	25.60	25.44	21.03	24.13	13.19	9.56	51.62	53.27	32.26	23.27	30.49
NE	1.01	.00	.00	.00	.00	.00	.00	.08	.00	.98	.00	.00
LC	.05	.00	.00	.00	.00	.00	.00	.00	.00	.00	.00	.00
CS	3.97	.00	.00	.00	.00	.00	.00	.00	.00	.90	.00	.00
TOTAL	102.73	100.16	100.15	100.16	100.13	100.09	100.11	100.06	100.04	100.12	100.06	100.06
D.I.	1.05	.85	1.52	2.23	2.01	2.74	2.66	1.38	2.78	1.95	2.58	4.31
MG#	.55	.46	.46	.49	.47	.53	.55	.44	.45	.43	.50	.47

SAMPLE	ML24-4	ML24-10	ML24-11	ML24-12	ML24-5	ML24-6	ML26-8	ML24-7	ML26-12	ML26-13	ML22-6	ML22-7
AP	.12	.12	.09	.36	.07	.07	.00	.07	.00	.05	.02	.09
IL	3.94	5.27	5.43	4.48	.73	.56	.23	.67	.21	2.35	4.89	4.75
OR	.65	.53	.18	.30	.12	.24	.12	.12	.00	.00	.06	.00
AB	3.22	4.15	3.05	2.45	1.95	2.96	5.08	2.03	.85	.00	1.95	.00
AN	3.62	3.70	2.74	2.89	4.23	8.33	26.75	3.31	6.05	.75	5.13	4.94
MT	5.18	6.18	6.31	5.55	2.73	2.62	2.41	2.73	2.39	4.10	5.92	5.70
DIEN	10.17	11.95	13.93	11.15	18.30	21.48	7.20	13.47	1.75	.00	9.61	10.98
DIFS	11.97	12.13	14.22	12.29	9.08	8.15	2.87	9.45	.60	.00	10.62	9.92
DIWO	22.30	24.50	28.64	23.72	29.16	32.03	10.85	23.91	2.55	.00	20.47	20.49
HYEN	1.27	3.12	.02	2.48	11.13	11.91	8.32	5.06	34.35	.00	.38	.00
HYFS	1.49	3.17	.02	2.73	5.53	4.52	3.32	3.55	11.80	.00	.42	.00
Q	.00	.00	.00	.00	.00	.00	.00	.00	.00	-5.29	.00	.00
FO	15.73	11.93	11.98	14.32	11.00	5.06	22.79	20.10	28.64	33.21	18.31	20.83
FA	20.41	13.35	13.48	17.39	6.02	2.11	10.01	15.55	10.85	52.59	22.31	20.75
NE	.00	.00	.00	.00	.00	.00	.00	.00	.00	.64	.00	1.05
LC	.00	.00	.00	.00	.00	.00	.00	.00	.00	.00	.00	.09
CS	.00	.00	.00	.00	.00	.00	.00	.00	.00	6.76	.00	1.42
AP	.00	.00	.00	.00	.00	.00	.00	.00	.00	.13	.00	.00
TOTAL	100.07	100.09	100.08	100.10	100.03	100.04	99.93	100.02	100.03	95.30	100.10	101.02
D.I.	3.87	4.68	3.22	2.75	2.06	3.20	5.19	2.15	.85	-4.51	2.01	1.15
MG#	.49	.51	.51	.51	.71	.76	.75	.64	.79	.47	.50	.55

SAMPLE	AD-37	AD-40	AH-30	AD-20	AD-24	AD-36	AD-38	AV-8	AT-1	AT-2	AT-3	AT-4
AP	.05	.02	.00	.02	.00	.00	.00	.00	.02	.02	.02	.02
CM	.00	.00	.00	.28	.25	.27	.31	.27	.00	.00	.00	.00
IL	5.93	5.81	.35	.25	.42	.25	.35	.21	.19	.17	.17	.15
OR	.30	.06	.24	.35	.41	.35	.30	.24	.59	.83	.65	.71
AB	1.44	.68	2.45	1.52	1.18	1.02	1.02	1.27	15.40	16.16	13.71	15.40
AN	11.86	1.90	13.10	15.86	12.18	9.13	11.78	10.72	65.85	67.11	55.87	57.32
C	.00	.00	1.05	.06	.00	.00	.00	.00	.00	.46	.00	.00
MT	6.57	6.48	2.71	1.67	1.86	1.91	1.74	2.07	.38	.29	.54	.46
DIEN	10.46	5.80	.00	.00	.29	2.06	.88	.41	.11	.00	.33	1.09
DIFS	9.69	6.72	.00	.00	.08	.56	.22	.13	.03	.00	.10	.31
DIWO	20.80	12.62	.00	.00	.40	2.88	1.21	.60	.16	.00	.46	1.54
HYEN	1.70	4.40	15.71	18.23	16.63	13.07	22.12	20.23	14.48	10.74	21.60	16.31
HYFS	1.61	5.10	4.43	4.55	4.42	3.58	5.57	6.52	4.24	3.36	6.25	4.67
Q	.00	.00	.00	.00	.00	.00	.00	.00	.00	.87	.31	.00
FO	14.45	22.19	45.76	45.22	48.21	50.30	43.06	41.96	.43	.00	.00	1.53
FA	15.06	28.22	14.23	12.44	14.11	15.16	11.94	14.91	.14	.00	.00	.48
TOTAL	100.11	100.09	100.02	100.46	100.45	100.54	100.48	99.56	100.02	100.02	100.01	100.01
D.I.	1.73	.74	2.69	1.38	1.60	1.37	1.31	1.51	15.99	17.86	14.67	16.11
MG#	.52	.49	.81	.54	.83	.82	.83	.80	.81	.79	.81	.81

SAMPLE	AT-7	AT-8	AT-10	AT-11	AT-12	AT-13	AT-16	AT-17	AT-18	AE-35	AE-36	AT-9
AP	.02	.02	.02	.05	.05	.00	.05	.02	.05	.02	.00	.02
CM	.00	.00	.00	.00	.00	.00	.27	.84	.88	.00	.00	.00
IL	.17	.19	.17	.12	.08	.08	.33	.33	.69	.17	.19	.29
OR	.83	.77	1.00	.95	.83	.83	4.67	.95	1.12	.41	.30	.89
AB	16.24	15.40	17.77	18.02	18.44	18.44	7.78	4.40	3.64	13.96	9.22	16.41
AN	62.84	62.53	72.83	73.59	76.07	76.66	25.79	12.88	10.44	63.96	39.11	70.58
C	.00	.00	.00	.42	.24	.00	.00	.00	.00	.00	.00	.00
MT	.41	.42	.20	.16	.13	.12	1.26	1.61	1.62	.45	.84	.29
DIEN	.53	.49	.22	.00	.00	.08	.34	1.62	2.27	.32	.74	.29
DIFS	.18	.17	.12	.00	.00	.08	.11	.51	.71	.15	.19	.14
DIWO	.77	.71	.36	.00	.00	.16	.49	2.32	3.25	.51	1.03	.45
HYEN	13.40	14.09	4.24	3.16	1.49	1.32	36.90	49.96	55.22	10.92	37.45	6.76
HYFS	4.55	4.77	2.23	2.03	1.48	1.33	11.67	15.81	17.27	5.14	9.70	3.18
Q	.09	.45	.84	1.58	1.19	.88	.00	.00	.00	4.01	.00	.70
FO	.00	.00	.00	.00	.00	.00	7.94	7.20	2.67	.00	.96	.00
FA	.00	.00	.00	.00	.00	.00	2.77	2.51	.92	.00	.28	.00
TOTAL	100.03	100.01	100.01	100.08	100.00	99.97	100.35	100.95	100.75	100.03	100.01	100.01
D.I.	17.16	16.61	19.61	20.55	20.46	20.15	12.45	5.35	4.76	18.39	9.52	18.00
MG#	.78	.78	.69	.67	.55	.54	.80	.80	.80	.72	.83	.72

TABLE A.6 (continued)

SAMPLE	DUN-1	DUN-2	DR-A1	DR-A2	DR-2A	DR-Q	DR-1	DR-2	DR-4	DR-6	DR-8	DR-10
CM	1.49	5.20	.04	.13	.03	.80	1.08	.40	.65	.57	.46	.63
IL	.06	.15	.04	.02	.04	.04	.04	.04	.04	.04	.04	.06
AN	1.98	.45	.00	.00	.03	.57	.78	.26	.50	.50	.55	.56
C	.04	1.19	.00	.00	.00	.00	.00	.00	.00	.00	.00	.00
MT	.09	.12	.17	.16	.17	.13	.12	.13	.12	.12	.12	.12
HYEN	2.77	.88	.00	.00	.00	.00	.00	.00	.00	.00	.00	.00
HYFS	.55	.22	.00	.00	.00	.00	.00	.00	.00	.00	.00	.00
Q	.00	.60	-1.18	-.87	-1.23	-1.28	-1.10	-1.20	-.89	-1.21	-.54	-1.27
FO	76.23	72.02	65.88	67.03	64.90	73.25	77.28	73.18	75.95	75.99	74.63	77.77
FA	16.80	19.81	34.26	32.82	33.76	25.31	21.64	25.84	22.76	23.33	23.81	21.87
NE	.00	.00	.00	.00	.00	.00	.09	.09	.05	.05	.00	.05
CS	.00	.00	.49	.43	1.37	.70	.65	.76	.51	.40	.58	.15
TOTAL	100.02	100.03	99.71	99.72	99.06	99.52	99.98	99.50	99.68	99.78	99.63	99.92
D.I.	.00	.00	-1.18	-.87	-1.23	-1.28	-1.01	-1.10	-.84	-1.16	-.54	-1.22
MG#	.87	.83	.74	.75	.74	.81	.84	.81	.83	.83	.82	.84

SAMPLE	DR-12	DR-14	DR-16	DR-18	DR-20	DR-22	DR-24	DR-26	DR-27	DR-31B	DR-31C	DR-32C
AP	.00	.00	.00	.00	.00	.00	.00	.00	.02	.02	.02	.00
CM	.77	.97	.46	.50	.65	.28	.13	.13	.16	.10	.10	.10
IL	.04	.19	.04	.02	.04	.06	.37	.33	.38	.44	.44	.48
OR	.00	.00	.00	.00	.00	.00	.06	.06	.06	.06	.41	.06
AB	.00	.08	.00	.00	.00	.00	.34	.85	2.28	2.28	1.95	2.03
AN	.35	2.19	.42	.16	.17	.71	5.49	13.98	9.32	7.93	7.71	7.93
C	.02	.00	.00	.00	.00	.00	.00	.00	.00	.00	.00	.00
MT	.12	.13	.13	.12	.12	.12	.12	.10	.09	.09	.09	.09
DIEN	.00	6.53	.00	.00	.00	.00	13.78	12.49	16.67	12.86	13.97	16.20
DIFS	.00	2.81	.00	.00	.00	.00	7.07	6.69	8.49	6.28	6.78	7.70
DIWO	.00	10.02	.00	.00	.00	.00	22.17	20.34	26.76	20.40	22.13	25.53
HYEN	.00	2.65	.00	.00	.00	.00	11.69	13.15	11.64	29.50	25.75	23.34
HYFS	.00	1.14	.00	.00	.00	.00	5.99	7.05	5.93	14.40	12.51	11.09
Q	-1.39	.00	-1.44	-1.59	-1.98	-.42	.00	.00	.00	.00	.00	.00
FO	78.45	49.72	75.90	77.63	78.61	75.64	20.97	15.63	11.66	3.67	5.30	3.60
FA	21.63	23.57	24.26	22.77	22.17	22.62	11.85	9.23	6.54	1.97	2.84	1.88
NE	.05	.00	.05	.00	.05	.09	.00	.00	.00	.00	.00	.00
CS	.00	.00	.12	.24	.12	.36	.00	.00	.00	.00	.00	.00
KP	.00	.00	.00	.00	.00	.24	.00	.00	.00	.00	.00	.00
TOTAL	100.03	100.01	99.94	99.85	99.94	99.70	100.03	100.03	100.01	100.01	100.01	100.02
D.I.	-1.34	.08	-1.39	-1.59	-1.93	-.09	.40	.91	2.34	2.34	2.36	2.09
MG#	.84	.75	.82	.83	.84	.83	.72	.71	.72	.73	.73	.74

SAMPLE	DR-37A	DR-38B	DR-38C	DR-39	DR-42	DR-49	ON-2	ON-12	ON-16	MO-1	MO-3	MO-4
AP	.07	.02	.02	10.80	.00	.02	.00	.05	.07	.07	.05	.00
CM	.15	.16	.19	.09	.28	.49	.03	2.14	.97	.53	.44	.01
IL	.65	.69	.56	1.50	.12	.50	.06	.10	.83	.52	.90	.33
OR	.35	.00	.30	6.50	.00	.06	.00	.00	.18	.00	.12	.00
AB	1.69	2.03	3.05	4.99	.00	2.54	.00	.00	2.03	1.02	1.44	.00
AC	.00	.00	.00	.00	.00	.00	.15	.00	.00	.00	.00	.00
AN	4.85	7.93	9.86	24.99	17.71	8.80	.00	1.96	2.14	4.86	4.12	.22
MT	.07	.07	.07	.06	.09	.09	.14	.13	.06	.12	.14	.33
DIEN	22.35	21.59	29.31	4.10	5.66	15.35	.00	.00	29.34	13.05	13.69	.26
DIFS	10.10	10.00	9.62	2.68	1.81	7.09	.00	.00	10.07	6.17	10.44	.64
DIWO	34.75	33.78	31.96	7.10	8.14	23.99	.00	.00	42.32	20.53	25.03	.62
HYEN	12.81	7.88	12.21	18.65	6.92	23.20	.00	.00	6.73	6.17	5.08	.00
HYFS	5.79	3.65	5.78	12.17	2.21	10.71	.00	.00	2.31	2.92	3.87	.00
Q	.00	.00	.00	6.65	.00	.00	-.65	-.38	.00	.00	.00	.00
FO	4.26	8.09	4.00	.00	42.22	4.77	54.46	70.39	1.80	29.13	18.86	33.08
FA	2.12	4.13	2.09	.00	14.87	2.43	44.37	24.85	.68	15.17	15.84	64.14
NE	.00	.00	.00	.00	.00	.00	.00	.00	.00	.00	.00	.14
CS	.00	.00	.00	.00	.00	.00	.92	.17	.00	.00	.00	.53
TOTAL	100.01	100.03	100.01	100.27	100.02	100.03	99.49	99.90	100.03	100.25	100.03	100.40
D.I.	2.05	2.03	3.34	18.14	.00	2.60	-.65	-.38	2.21	1.02	1.56	.14
MG#	.74	.74	.73	.65	.80	.74	.64	.80	.78	.73	.63	.43

SAMPLE	DR-28	DR-29	DR-31D	DR-32A	DR-32B	DR-34B	TLP-1A	TLP-1B	TLP-2	TLP-3	BK-1	BK-2
AP	.00	.00	.00	.02	.00	.02	.28	.71	.07	.07	.09	.02
CM	.12	.12	.12	.13	.10	.06	.01	.01	.01	.01	.13	2.65
IL	.17	.10	.17	.17	.19	.06	.46	.69	3.52	5.70	6.70	.60
OR	.35	.47	.41	.41	.41	.30	.00	.00	.00	.06	.06	.35
AB	14.47	12.52	13.45	13.37	12.95	5.92	.25	.25	.68	.42	.68	.51
AN	49.26	55.72	44.01	41.19	46.19	68.80	.33	.08	2.34	1.22	3.49	10.95
C	.00	.00	.00	.00	.00	.94	.00	.00	.00	.00	.00	.16
MT	.67	.62	.88	.94	.87	.48	2.61	2.73	4.87	6.51	7.25	2.83
DIEN	2.12	2.54	2.53	2.65	2.35	.00	2.14	1.37	1.67	2.27	13.44	.00
DIFS	.70	.97	1.05	1.09	1.01	.00	3.01	1.80	4.14	5.35	14.42	.00
DIWO	3.07	3.79	3.85	4.03	3.60	.00	5.13	3.17	5.57	7.34	28.24	.00
HYEN	20.11	14.75	23.31	25.40	22.55	4.78	1.04	.45	.35	.96	7.55	42.21
HYFS	6.66	5.61	9.69	10.38	9.71	1.19	1.45	.59	.87	2.27	8.10	9.42
Q	.00	.00	.57	.54	.08	.00	.00	.00	.00	.00	.00	.00
FO	1.69	1.98	.00	.00	.00	13.71	32.78	36.13	20.34	18.91	4.62	25.91
FA	.62	.83	.00	.00	.00	3.75	50.70	52.20	55.69	49.06	5.46	6.37
TOTAL	100.01	100.01	100.05	100.34	100.01	100.00	100.20	100.18	100.12	100.16	100.23	101.98
D.I.	14.82	12.99	14.44	14.33	13.44	6.22	.25	.25	.68	.48	.74	.86
MG#	.79	.77	.75	.76	.75	.84	.48	.50	.33	.34	.48	.84

TABLE A.6 (continued)

SAMPLE	AC-6	AC-5	AH-32	AH-33A	AH-33B	AH-34	AH-35	AH-31	AH-30	AV-7	U/14	U/15
AP	.05	.05	.05	.02	.02	.17	.02	.02	.00	.00	.05	.00
CM	.00	.00	.00	.00	.00	.00	.00	.00	2.93	.00	.62	.85
IL	.37	13.47	7.68	3.75	.58	17.61	7.66	.19	.35	5.97	.46	.29
OR	1.42	.71	.06	.00	.77	.00	.00	.53	.24	.30	.53	.59
AB	10.93	2.28	1.69	.93	5.55	1.02	.00	15.48	2.37	6.80	6.77	5.41
AN	76.06	16.93	6.41	5.45	70.63	6.47	5.92	70.88	12.75	47.90	8.97	16.07
C	.00	.00	.00	.00	.00	.00	.00	.14	1.03	.00	.00	.00
MT	.26	12.35	7.99	5.09	2.64	12.62	7.99	.26	1.93	1.54	1.45	1.73
HM	.00	.00	.00	.00	.00	1.96	.00	.00	.00	.00	.00	.00
DIEN	.93	19.52	19.78	6.04	6.08	24.18	5.73	.00	.00	6.62	2.99	.96
DIFS	.32	4.60	11.47	5.75	1.96	.00	5.30	.00	.00	5.95	.86	.30
DIWO	1.68	25.46	32.98	12.05	8.76	27.97	10.97	.00	.00	12.90	4.22	1.37
HYEN	.00	3.98	5.60	.26	.00	3.08	.00	9.09	15.25	.00	48.83	26.81
HYFS	.00	.99	3.25	.24	.00	.00	.00	2.97	4.33	.00	14.01	8.39
Q	.00	.82	.00	.00	.00	5.17	.00	.44	.00	.00	.00	.00
FO	1.53	.00	1.93	29.51	1.17	.00	27.56	.00	44.64	6.08	6.46	27.75
FA	1.66	.00	1.23	30.97	.42	.00	28.10	.00	13.97	6.02	2.04	9.57
NE	4.44	.00	.00	.00	1.44	.00	.78	.00	.00	.03	.00	.00
CS	.00	.00	.00	.00	.00	.00	.49	.00	.00	.00	.00	.00
TOTAL	100.05	100.20	100.12	100.07	100.02	100.24	100.53	100.01	99.79	100.09	98.26	100.09
D.I.	16.79	3.82	1.75	.93	7.76	6.19	.78	16.45	2.61	7.12	7.30	6.01
MG#	.54	.56	.56	.55	.70	.62	.53	.79	.81	.51	.81	.80

SAMPLE	U/15A	U/16	U/31	U/27	U/25	U/24	U/26	AV-8	AV-5A	AD-41B	AD-32	AD-34
AP	.00	.00	.02	.05	.02	.00	.00	.05	.00	.05	.05	.05
CM	.75	.75	.78	.62	.24	.87	.40	.00	.00	.00	.00	.00
IL	.31	.31	.25	.29	.19	.35	.15	.31	.15	7.95	12.95	4.89
OR	.71	.59	.30	.65	.47	.24	.41	.41	.77	.00	.06	.06
AB	3.64	3.64	5.16	5.25	3.64	4.32	2.79	11.85	14.30	1.10	1.35	1.35
AN	11.09	9.78	10.76	15.28	9.65	12.03	11.14	75.02	72.73	4.46	3.95	4.22
C	.00	.00	.00	.00	.00	.00	.00	.00	.26	.00	.00	.00
MT	2.32	2.03	1.77	1.65	1.73	1.44	1.87	.59	.30	8.08	11.83	5.79
DIEN	.30	1.20	1.88	1.08	.68	1.99	.73	.20	.00	19.58	24.76	17.74
DIFS	.11	.40	.56	.30	.17	.53	.19	.19	.00	11.20	4.17	13.38
DIWO	.45	1.74	2.67	1.52	.94	2.77	1.00	.40	.00	32.51	32.31	32.30
HYEN	17.50	22.42	26.89	24.86	15.42	47.68	3.29	1.59	7.21	7.75	3.82	5.43
HYFS	6.74	7.51	7.92	7.01	3.81	12.62	.85	1.48	2.96	4.43	.64	4.10
Q	.00	.00	.00	.00	.00	.00	.00	.00	.00	.00	4.28	.00
FO	39.38	36.30	30.98	31.62	49.57	11.76	60.16	3.91	.92	1.85	.00	5.88
FA	16.72	13.41	10.06	9.83	13.50	3.43	17.02	4.02	.42	1.17	.00	4.89
TOTAL	100.02	100.08	99.99	100.01	100.01	100.00	100.00	100.02	100.01	100.12	100.17	100.07
D.I.	4.35	4.23	5.46	5.90	4.11	4.55	3.21	12.26	15.07	1.10	5.69	1.41
MG#	.77	.79	.81	.82	.84	.83	.83	.57	.75	.58	.63	.57

SAMPLE	AT-15	AT-6	27-A1	27-A2	27-A3	27-A4	27-E1	27-E2	AD-25A	AD-25B	AD-26	AD-27
AP	.02	.07	.02	.09	.05	.05	.05	.09	.05	.02	.00	.24
CM	.53	.00	.77	.69	.00	.00	.96	.69	.00	.18	.00	.00
IL	.29	.21	.46	.52	.44	.42	.35	.85	.17	.12	.21	.17
OR	3.90	1.00	.18	.24	.12	.12	.18	.41	2.01	1.42	.47	.47
AB	5.08	15.74	3.72	4.32	4.48	3.05	2.62	3.89	10.56	15.57	13.96	14.55
AN	21.31	74.87	12.67	11.21	10.85	9.46	9.74	13.39	73.89	64.65	57.93	59.97
C	.00	.13	.00	.00	.00	.00	.00	.00	.00	.00	.00	.28
MT	1.55	.19	1.55	1.58	1.64	2.32	1.78	1.87	.10	.46	.49	.42
DIEN	.23	.00	3.42	3.21	5.58	3.22	1.91	2.90	2.49	.01	.20	.00
DIFS	.07	.00	1.09	1.02	1.93	1.84	.63	1.08	.85	.00	.05	.00
DIWO	.34	.00	4.91	4.62	8.15	5.17	2.76	4.30	3.63	.01	.28	.00
HYEN	29.90	3.49	53.69	53.64	42.91	41.58	50.22	39.24	.00	.72	18.73	18.86
HYFS	9.49	2.14	17.13	17.13	14.30	21.17	16.49	14.61	.00	.21	5.01	5.07
Q	.00	2.18	.00	.00	.00	.00	.00	.00	.00	.00	.00	.06
FO	20.63	.00	.79	1.72	6.56	7.57	9.72	12.29	.63	12.69	1.98	.00
FA	7.22	.00	.28	.60	2.49	4.25	3.52	5.04	.24	4.12	.58	.00
NE	.00	.00	.00	.00	.00	.00	.00	.00	5.32	.00	.00	.00
TOTAL	100.56	100.02	100.68	100.59	100.01	100.02	100.91	100.66	99.93	100.18	99.90	100.09
D.I.	8.98	18.92	3.90	4.55	4.60	3.16	2.80	4.31	17.90	16.99	14.43	15.09
MG#	.80	.66	.80	.80	.79	.71	.79	.77	.78	.81	.82	.82

SAMPLE	BK-3	LAV-1	LAV-2	RB-5	EB-4	EB-1	EB-2	EB-3
AP	.07	.02	.07	.07	.00	.09	.09	.07
CM	.03	.63	2.09	.07	.65	.15	.24	1.03
IL	3.73	5.66	15.63	11.89	.50	5.64	7.18	35.98
OR	.00	.00	.00	.12	.24	.00	.00	.00
AB	.08	.00	.00	.93	3.22	1.10	1.10	.00
AN	.15	1.54	5.82	5.81	14.58	4.11	5.53	1.04
C	.00	.00	.00	.00	.00	.00	.00	1.80
MT	5.09	6.45	13.98	11.16	2.60	6.44	7.60	29.40
DIEN	.15	.00	9.85	6.90	2.68	11.94	16.21	.00
DIFS	.39	.00	10.38	6.44	.84	12.86	13.55	.00
DIWO	.52	.00	19.40	13.65	3.84	25.15	30.68	.00
HYEN	1.48	.00	.00	8.32	52.78	2.47	5.36	.00
HYFS	3.81	.00	.00	7.76	16.48	2.66	4.48	.00
Q	.00	-.74	.00	.00	.00	.00	.00	-1.46
FO	22.04	35.10	10.85	13.47	1.61	12.63	4.31	12.36
FA	62.57	50.58	12.60	13.85	.55	14.99	3.97	21.01
NE	.00	.05	.41	.00	.00	.00	.00	.00
CS	.00	.73	1.68	.00	.00	.00	.00	.00
TOTAL	100.11	100.02	102.75	100.25	100.55	100.24	100.30	101.24

APPENDIX 7 ELECTRON MICROPROBE ANALYSIS OF OLIVINE

All electron microprobe analyses presented in this study, unless otherwise stated, were completed by the author in the Geology Department at Rhodes University. These data were determined using a Cambridge Microscan Unit operating at an accelerating voltage of 20 KV, using wave length dispersive crystal spectrometers. Count rates were corrected using the Bence-Albee routine (Bence & Albee, 1968) on an in-house computer program developed by H.V. Eales.

The following analytical configuration was used for analysis of olivine :

Left Hand Spectrometer : (LiF crystal) FeO (St. John's Island olivine)
NiO (Nickel magnetite)
MnO (Rhodonite)
CaO (Pyroxene)

Right Hand Spectrometer : (RAP crystal) MgO (St. John's Island olivine)
SiO_2 (St. John's Island olivine)

Analyses of olivines not included in the main text are presented in the following Tables (for recalculation program see below) :

TABLE A.7-1 : Electron microprobe analysis of olivines from the platiniferous ultramafic pipes.

TABLE A.7-2 : Electron microprobe analysis of olivines from cumulates in the upper critical zone at Amandelbult.

TABLE A.7-3 : Electron microprobe analysis of olivines from the Skaergaard intrusion.

REFERENCES

BENCE, A.E. & ALBEE, A.L. (1968) : Empirical correction factors for the electron microanalysis of silicates and oxides. J. Geology 76, 382-403.

```
10  REM OLIVINE COMP. CALCULATIONS
20  PRINT "TYPE IN OLIVINE ANALYSIS (SIO2/FEO/MNO/MGO/CAO/NIO)"
30  INPUT A1,B1,C1,D1,E1,F1
40  LET A2=A1/60.09
50  LET B2=B1/71.85
60  LET C2=C1/70.94
70  LET D2=D1/40.32
80  LET E2=E1/56.08
90  LET F2=F1/74.41
100 LET A3=A2*2
110 LET G1=A3+B2+C2+D2+E2+F2
120 LET H1=4/G1
130 LET A4=H1*A2
140 LET B4=H1*B2
150 LET C4=H1*C2
160 LET D4=H1*D2
170 LET E4=H1*E2
180 LET F4=H1*F2
190 LET G4=B4+C4+D4+E4+F4
192 LET T=G4+A4
200 LET H4=100*D4/(D4+B4)
210 PRINT "     SIO2 = "A4
211 PRINT "      FEO = "B4
212 PRINT "      MNO = "C4
213 PRINT "      MGO = "D4
214 PRINT "      CAO = "E4
215 PRINT "      NIO = "F4
220 PRINT "     REST = "G4
222 PRINT "    TOTAL = "T
230 PRINT "     FO = "H4"%"
240 END
```

TABLE A.7-1 ELECTRON MICROPROBE ANALYSIS OF OLIVINES FROM THE PLATINIFEROUS ULTRAMAFIC PIPES

	DR-A1			DR-2A			DR-1			DR-6			DR-10			DR-12			DR-16			DR-22			DR-25			DR-27		
wt.%	x	d	n	x	d	n	x	d	n	x	d	n	x	d	n	x	d	n	x	d	n	x	d	n	x	d	n	x	d	n
SiO_2	38.55	.2861	4	37.67	.4441	4	39.26	.5246	7	39.81	.1411	3	39.85	.4636	4	40.02	.1131	2	39.35	.0283	2	38.11	.2316	4	38.03	.2473	4	38.28	.1998	4
FeO	24.22	.1352	4	25.26	.2431	4	15.65	.1858	7	15.19	.1153	3	15.66	.1573	4	15.15	.0283	2	16.60	.1131	2	24.31	.1682	4	30.32	.2532	4	30.73	.2317	4
MnO	.32	.0289	4	.35	.0221	4	.21	.0138	7	.21	.0058	3	.23	.0356	4	.23	.0212	2	.20	.0566	2	.30	.0171	4	.42	.0115	4	.43	.0330	4
MgO	36.89	.2576	4	37.21	.1996	4	44.59	.5456	7	44.69	.0971	3	44.38	.4135	4	44.27	.3182	2	43.30	.1273	2	38.00	.0963	4	32.31	.3607	4	31.67	.2117	4
CaO	.09	.0222	4	.07	.0250	4	.06	.0355	7	.06	-	3	.08	-	4	.09	.0566	2	.08	-	2	.03	.0141	4	.04	.0096	4	.04	.0408	4
NiO	.24	.0206	4	.27	.0200	4	.28	.0146	7	.21	.0100	3	.28	.0082	4	.26	-	2	.26	-	2	.27	.0171	4	.20	-	4	.21	.1189	4
TOTAL	100.01	-		100.83	-		100.05	-		100.17	-		100.48	-		100.02	-		99.79	-		101.02	-		101.32	-		101.36	-	
cations																														
Si	1.0046			.9880			.9906			.9994			.9997			1.0056			.9989			.9919			1.0133			1.0206		
Fe^{2+}	.5320			.5541			.3302			.3189			.3286			.3184			.3524			.5292			.6756			.6852		
Mn	.0071			.0078			.0045			.0045			.0049			.0049			.0043			.0066			.0095			.0097		
Mg	1.4440			1.4545			1.6767			1.6720			1.6593			1.6578			1.6381			1.4740			1.2830			1.2583		
Ca	.0025			.0020			.0016			.0016			.0022			.0024			.0022			.0008			.0011			.0011		
Ni	.0051			.0057			.0057			.0043			.0057			.0053			.0053			.0057			.0043			.0045		
TOTAL	2.9954			3.0120			3.0094			3.0006			3.0003			2.9944			3.0011			3.0081			2.9867			2.9794		
mol.%																														
Fo	73.08	.0688	4	72.41	.1893	4	83.54	.2927	7	83.98	.1041	3	83.47	.2588	4	83.89	.0707	2	82.30	.0566	2	73.58	.1258	4	65.50	.3699	4	64.75	.3014	4

	DR-32			DR-42			DR-46C			DR-46B			DR-111			ON-2			MO-4			MO-3			TW-1			DUN-1		
wt.%	x	d	n	x	d	n	x	d	n	x	d	n	x	d	n	x	d	n	x	d	n	x	d	n	x	d	n	x	d	n
SiO_2	36.87	.3960	2	39.37	.1778	4	38.96	.1380	3	39.56	.0566	2	39.96	.1253	4	37.68	.1344	5	35.23	.5026	5	36.13	.0493	3	41.02	1.4213	2	40.16	.6650	5
FeO	32.33	.2404	2	19.69	.1638	4	19.41	.1744	3	17.24	.2051	2	14.48	.1060	4	31.33	.2915	5	45.75	.1702	5	39.21	.1901	3	15.15	.0071	2	12.38	.1399	5
MnO	.47	.0141	2	.26	.0096	4	.27	-	3	.24	.0071	2	.20	.0058	4	.41	.0217	5	.66	.0476	5	.51	.0231	3	.21	.0141	2	.18	.0303	5
MgO	30.57	.6081	2	41.28	.3006	4	41.26	.1744	3	42.69	.1131	2	44.84	.2468	4	31.34	.2013	5	19.48	.3048	5	24.43	.2065	3	44.48	.6293	2	46.74	.3803	5
CaO	.03	.0283	2	.03	-	4	.03	-	3	.03	-	2	.01	.0153	4	.04	.0150	5	.04	.0305	5	.04	.0115	3	-	-		-	-	
NiO	.20	.0071	2	.32	.0171	4	.30	.0346	3	.34	.0200	2	.34	-	4	.21	.0164	5	.09	.0141	5	.13	.0153	3	.26	.0283	2	.30	.0164	5
TOTAL	100.47	-		100.95	-		100.23	-		100.10	-		99.83	-		101.01	-		101.25	-		100.45	-		101.12	-		99.76	-	
cations																														
Si	1.0038			1.0015			.9980			1.0036			1.0033			1.0127			1.0180			1.0175			1.0167			.9995		
Fe^{2+}	.7361			.4189			.4158			.3658			.3041			.7042			1.1056			.9235			.3140			.2577		
Mn	.0108			.0056			.0059			.0052			.0043			.0093			.0162			.0121			.0044			.0038		
Mg	1.2403			1.5650			1.5752			1.6141			1.6779			1.2553			.8389			1.0253			1.6430			1.7336		
Ca	.0009			.0008			.0008			.0008			.0003			.0012			.0012			.0012			-			-		
Ni	.0044			.0066			.0062			.0070			.0069			.0046			.0021			.0030			.0062			.0060		
TOTAL	2.9963			2.9985			3.0020			2.9964			2.9967			2.9873			2.9820			2.9826			2.9833			3.0005		
mol.%																														
Fo	62.76	.6435	4	78.88	.2547	4	79.11	.0819	3	81.52	.2192	2	84.66	.1680	4	64.06	.3358	5	43.14	.4383	5	52.61	.3259	3	83.95	.1838	2	87.06	.1346	5

TABLE A.7-2 ELECTRON MICROPROBE ANALYSIS OF OLIVINES FROM CUMULATES

IN THE UPPER CRITICAL ZONE AT AMANDELBULT

	1	2	3	4	5	6	7	8	9	10	11	12
wt.%												
SiO_2	39.44	39.39	39.45	38.79	38.75	38.65	38.60	38.23	37.73	38.11	37.56	38.55
FeO	17.49	17.44	17.29	17.06	18.14	18.01	18.03	19.53	18.90	18.88	19.02	19.93
MnO	.24	.29	.24	.22	.24	.25	.25	.28	.23	.24	.26	.24
MgO	41.54	42.62	41.88	42.49	41.96	41.79	41.81	41.64	42.16	41.89	41.02	41.30
CaO	.03	.01	.01	.03	.10	.07	.06	.02	.02	.01	.06	.04
NiO	.37	.36	.37	.38	.31	.30	.31	.42	.41	.44	.43	.42
TOTAL	99.11	100.12	99.24	98.97	99.50	99.07	99.06	100.10	99.45	99.57	98.35	100.48
cations												
Si	1.0116	1.0008	1.0100	.9966	.9951	.9963	.9954	.9837	.9759	.9834	.9833	.9891
Fe^{2+}	.3752	.3706	.3702	.3666	.3896	.3883	.3888	.4203	.4088	.4075	.4164	.4276
Mn	.0052	.0062	.0052	.0048	.0052	.0055	.0055	.0061	.0050	.0052	.0058	.0052
Mg	1.5879	1.6139	1.5980	1.6269	1.6059	1.6055	1.6068	1.5969	1.6252	1.6110	1.6004	1.5792
Ca	.0008	.0003	.0003	.0008	.0028	.0019	.0017	.0005	.0005	.0003	.0017	.0011
Ni	.0077	.0074	.0077	.0079	.0064	.0062	.0065	.0087	.0086	.0092	.0091	.0087
TOTAL	2.9884	2.9992	2.9904	3.0035	3.0049	3.0037	3.0046	3.0162	3.0241	3.0166	3.0167	3.0110
mol%												
Fo	80.69	81.33	81.19	81.61	80.48	80.53	80.52	79.16	79.90	79.81	79.35	78.69

	13	14	15	16	17	18	19	20	21	22	23
wt.%											
SiO_2	38.57	38.32	38.10	38.45	37.42	37.42	37.70	38.30	37.56	37.78	38.00
FeO	19.62	19.98	19.71	20.69	20.39	19.98	20.56	21.78	21.95	22.08	20.69
MnO	.26	.24	.26	.27	.22	.28	.26	.20	.28	.30	.26
MgO	41.38	41.19	41.58	40.58	40.56	40.67	40.46	39.76	39.62	39.54	40.61
CaO	.03	.16	.03	.04	.05	.05	.03	.03	.04	.01	.04
NiO	.42	.42	.46	.39	.38	.42	.42	.39	.39	.40	.42
TOTAL	100.28	100.31	100.13	100.41	99.02	98.82	99.43	100.46	99.84	100.11	100.02
cations											
Si	.9902	.9860	.9815	.9905	.9790	.9796	.9825	.9910	.9812	.9842	.9843
Fe^{2+}	.4212	.4300	.4246	.4458	.4462	.4375	.4481	.4713	.4796	.4811	.4482
Mn	.0057	.0052	.0057	.0059	.0049	.0062	.0057	.0044	.0062	.0066	.0057
Mg	1.5832	1.5796	1.5963	1.5580	1.5815	1.5868	1.5715	1.5533	1.5425	1.5352	1.5677
Ca	.0008	.0041	.0008	.0011	.0014	.0014	.0008	.0008	.0011	.0003	.0011
Ni	.0087	.0088	.0096	.0081	.0080	.0089	.0088	.0081	.0082	.0084	.0088
TOTAL	3.0098	3.0139	3.0185	3.0094	3.0210	3.0203	3.0175	3.0090	3.0188	3.0157	3.0158
mol%											
Fo	78.90	78.60	78.99	77.75	78.00	78.39	77.81	76.49	76.28	76.14	77.77

n.d.: not detected; - not determined.

1,2 : Lower pseudoreef (P1); 3,4 : Upper pseudoreef (P2); 5-7 : Troctolite, P2 middle marker;

8-19 : Normal Merenky Reef, Amandelbult; 20-23 : Remnant "unreplaced" Merensky Reef enclosed by pegmatite.

TABLE A.7-3 ELECTRON MICROPROBE ANALYSIS OF OLIVINES FROM THE SKAERGAARD

INTRUSION

	5196			5321			5322		
wt.%	x	d	n	x	d	n	x	d	n
SiO_2	32.37	.1286	3	30.76	.1286	3	33.88	.0778	2
FeO	51.20	.6158	3	60.41	.4215	3	49.04	.3253	2
MnO	.76	.0231	3	1.27	.0231	3	.71	.0141	2
MgO	13.59	.2466	3	6.20	.2261	3	16.35	.1909	2
CaO	.25	.0495	3	.07	.0208	3	.26	.0283	2
NiO	n.d.	-		n.d.	-		n.d.	-	
TOTAL	98.17	-		98.71	-		99.74	-	
cations									
Si	1.0059	-		1.0050	-		1.0112	-	
Fe^{2+}	1.3306	-		1.6506	-		1.2241	-	
Mn	.0200	-		.0351	-		.0179	-	
Mg	.6294	-		.3019	-		.7273	-	
Ca	.0083	-		.0025	-		.0083	-	
Ni	-	-		-	-		-	-	
TOTAL	2.9941	-		2.9950	-		2.9888	-	
mol.% Fo	32.12	.2463	3	15.46	.5214	3	37.26	.4282	2

APPENDIX 8 ELECTRON MICROPROBE ANALYSIS OF PYROXENE

Both orthopyroxene and clinopyroxene were analysed for using the following configuration :

Left Hand Spectrometer :	(LiF crystal)	CaO (Pyroxene)
		FeO (St. John's Island olivine)
		TiO_2 (ilmenite)
		Cr_2O_3 (Chromite)
		NiO (Nickel magnetite)
		MnO (Rhodonite)
Right Hand Spectrometer :	(RAP crystal)	SiO_2 (Jadeite)
		Na_2O (Jadeite)
		Al_2O_3 (Jadeite)
		MgO (St. John's Island olivine)

Relevant oxide pairs, FeO-MgO, Cr_2O_3 - Al_2O_3 etc. were analysed concomitantly to minimise errors.

Analyses were recalculated assuming a structural formulae bases on 6 oxygens (see below). In addition, the ratio of cations Al/cations Cr and the mmf, or X_{Mg} ratio (cations Mg/Mg + Fe^{2+}) have been calculated for each analysis. Total iron is presented as FeO.

The majority of analyses completed in this study are presented in the following Tables. "c" refers to analyses of the cores of grains and "m" denotes the margin. Averages of each sample group are presented where appropriate.

TABLE A.8-1 : Electron microprobe analysis of pyroxenes from iron-rich ultramafic pegmatite bodies at Amandelbult.

TABLE A.8-2 : Electron microprobe analysis of pyroxenes from the platiniferous ultramafic pipes.

TABLE A.8-3 : Electron microprobe analysis of pyroxenes from cumulates in the upper critical zone at Amandelbult.

TABLE A.8-4 : Electron microprobe analysis of pyroxenes from pegmatites bodies in the main zone in borehole SK2, Union Section (from Mitchell, in prep.).

REFERENCES

MITCHELL, A.A. : The geochemistry and origin of the main zone, western Bushveld Complex. Ph.D thesis (in prep.), Rhodes Univ., Grahamstown.

TABLE A.8-1 ELECTRON MICROPROBE ANALYSIS OF PYROXENES FROM IRON-RICH ULTRAMAFIC PEGMATITE BODIES AT AMANDELBULT

	AE-9	AE-9	AE-12	AE-12	AE-9,12			AE-20	AE-20	AE-20	AE-20	AE-20	AE-20	AE-20	AE-20		
wt.%	c	c	c	c	x̄	d	n	c	c	c	c	c	c	c	x̄	d	n
SiO_2	52.15	52.55	52.64	50.60	51.99	.9476	4	52.67	52.23	51.03	50.93	48.99	51.36	50.80	51.50	.7690	5
TiO_2	.67	.49	.51	.62	.57	.0866	4	.12	.15	.14	.16	.64	.18	.63	.15	.0224	5
Al_2O_3	2.08	2.08	2.04	2.08	2.07	.0200	4	.81	.88	.95	.98	2.13	1.24	2.11	.97	.1636	5
FeO	12.82	11.64	12.19	12.71	12.34	.5415	4	11.45	11.66	11.55	11.93	12.66	11,73	12.52	11.66	.1830	5
MnO	.30	.23	.32	.30	.29	.0395	4	.25	.25	.25	.25	.28	.23	.26	.25	.0089	5
MgO	12.19	12.45	13.23	12.38	12.56	.4584	4	12.10	12.26	12.00	12.50	12.70	12.48	12.06	12.27	.2230	5
CaO	21.27	22.01	20.49	21.13	21.23	.6238	4	23.24	22.85	21.99	21.99	21.52	22.60	21.21	22.53	.5465	5
Na_2O	.17	.15	.24	.24	.20	.0469	4	-	.03	.12	.14	.23	.01	.29	.08	.0645	5
Cr_2O_3	.06	.07	.07	.08	.07	.0082	4	.03	.06	.07	.04	.07	.04	.08	.05	.0172	5
NiO	-	-	-	-	-	-		-	-	-	-	-	-	-	-	-	
TOTAL	101.71	101.67	101.72	100.13	101.32	-		100.65	100.36	98.10	98.92	99.22	99.87	100.06	99.46	-	
cations/ 6 oxygens																	
Si	1.9416	1.6177	1.9483	1.9202	1.9399	-		1.9787	1.9702	1.9694	1.9539	1.8863	1.9496	1.9286	1.9523	-	
Ti	.0188	.0113	.0142	.0177	.0160	-		.0033	.0043	.0041	.0046	.0185	.0051	.0180	.0043	-	
Al	.0913	.7547	.0890	.0930	.0910	-		.0359	.0391	.0432	.0443	.0967	.0555	.0944	.0436	-	
Fe^{2+}	.3992	.2997	.3773	.4034	.3850	-		.3597	.3678	.3728	.3828	.4077	.3724	.3975	.3716	-	
Mn	.0095	.0060	.0100	.0096	.0092	-		.0080	.0080	.0082	.0081	.0091	.0074	.0084	.0081	-	
Mg	.6764	.5712	.7298	.7001	.6984	-		.6775	.6892	.6902	.7147	.7288	.7060	.6823	.6968	-	
Ca	.8485	.7260	.8126	.8592	.8488	-		.9355	.9236	.9094	.9039	.8879	.9192	.8628	.9198	-	
Na	.0123	.0090	.0172	.0177	.0145	-		-	.0022	.0090	.0104	.0172	.0007	.0213	.0059	-	
Cr	.0018	.0017	.0020	.0240	.0021	-		.0009	.0018	.0021	.0012	.0021	.0012	.0024	.0015	-	
Ni	-	-	-	-	-	-		-	-	-	-	-	-	-	-	-	
TOTAL	3.9992	3.9972	4.0006	4.0233	4.0048	-		3.9995	4.0062	4.0083	4.0240	4.0453	4.0173	4.0157	4.0138	-	
Wo	44.10	45.46	42.33	43.78	43.93	-		34.34	34.80	34.99	35.71	43.86	46.02	44.41	46.27	-	
En	35.15	35.77	38.01	35.68	36.15	-		18.24	18.57	18.90	19.13	36.00	35.34	35.12	35.05	-	
Fs	20.75	18.77	19.66	20.55	19.93	-		47.42	46.63	46.11	45.17	20.14	18.64	20.46	18.69	-	
mmf	.629	.656	.659	.634	.645	.0152	4	.653	.652	.649	.651	.641	.655	.632	.652	.0022	5
Al/Cr	51.69	44.30	43.45	38.77	44.09	-		40.26	21.87	20.23	36.53	45.37	46.22	39.32	28.93	-	

	AD-5	AD-5	AD-32	AD-32	AD-32	AD-41	AD-41	AD-41	AD-5,32,41			AC-5	AC-5	AC-5	AC-5	AC-5		
wt.%	c	c	c	c	c	c	c	c	x̄	d	n	c	c	c	c	x̄	d	n
SiO_2	51.45	51.09	52.18	51.47	51.72	51.18	51.73	51.09	51.49	.3788	8	51.38	50.43	50.78	50.57	50.79	.4188	4
TiO_2	.56	.47	.52	.55	.54	.57	.24	.69	.55	.0673	7	.57	.52	.59	.52	.55	.0356	4
Al_2O_3	1.94	1.78	1.89	1.81	1.91	2.02	1.61	2.12	1.92	.1176	7	2.08	2.39	2.00	1.89	2.09	.2146	4
FeO	12.76	12.68	13.06	13.12	12.91	12.85	12.01	12.86	12.78	.3434	8	12.03	12.43	12.04	12.32	12.21	.2014	4
MnO	.24	.26	.31	.26	.26	.27	.26	.25	.26	.0207	8	.25	.23	.23	.25	.24	.0115	4
MgO	12.13	11.59	12.23	12.31	11.94	12.00	12.07	11.92	12.02	.2218	8	11.34	12.03	12.04	12.10	11.88	.3597	4
CaO	22.03	21.58	22.02	22.18	22.86	22.15	23.06	22.41	22.18	.3925	7	22.43	22.13	22.31	22.12	22.22	.1417	4
Na_2O	.27	.14	.27	.12	.12	.12	-	.11	.12	.0110	5	.18	.27	.21	.18	.21	.0424	4
Cr_2O_3	.10	.09	.07	.08	.08	.04	.02	.04	.07	.0234	7	.05	.11	.07	.06	.07	.0263	4
NiO	.02	.01	.01	.01	.01	.02	.01	.05	.01	.0049	7	.02	.01	.03	-	.02	.0100	3
TOTAL	101.49	99.69	102.56	101.90	102.35	101.22	101.01	101.54	101.40	-		100.33	100.54	100.30	100.01	100.28	-	
cations/ 6 oxygens																		
Si	1.9280	1.9462	1.9345	1.9242	1.9258	1.9245	1.9440	1.9170	1.9309	-		1.9419	1.9090	1.9234	1.9233	1.9247	-	
Ti	.0158	.0135	.0145	.0155	.0151	.0161	.0068	.0195	.0155	-		.0162	.0148	.0168	.0149	.0157	-	
Al	.0857	.0799	.0826	.0798	.0838	.0895	.0713	.0938	.0849	-		.0927	.1066	.0893	.0847	.0934	-	
Fe^{2+}	.3999	.4040	.4049	.4102	.4020	.4041	.3775	.4036	.4008	-		.3803	.3935	.3814	.3919	.3870	-	
Mn	.0076	.0084	.0097	.0082	.0076	.0086	.0083	.0080	.0083	-		.0080	.0074	.0074	.0080	.0077	-	
Mg	.6774	.6580	.6757	.6859	.6626	.6725	.6760	.6666	.6718	-		.6387	.6787	.6794	.6858	.6709	-	
Ca	.8845	.8808	.8747	.8885	.9121	.8925	.9286	.9010	.8912	-		.9084	.8976	.9055	.9014	.9022	-	
Na	.0196	.0103	.0194	.0087	.0087	.0087	-	.0080	.0087	-		.0132	.0198	.0154	.0133	.0154	-	
Cr	.0030	.0027	.0021	.0024	.0024	.0012	.0006	.0012	.0021	-		.0015	.0033	.0021	.0018	.0021	-	
Ni	.0003	.0003	.0003	.0003	.0003	.0006	.0003	.0015	.0003	-		.0006	.0003	.0009	-	.0006	-	
TOTAL	4.0218	4.0042	4.0184	4.0236	4.0203	4.0184	4.0133	4.0200	4.0145	-		4.0014	4.0311	4.0218	4.0252	4.0197	-	
Wo	45.09	45.34	44.73	44.77	46.14	45.32	46.85	45.71	45.38	-		47.13	45.57	46.04	45.55	46.03	-	
En	34.53	33.87	34.56	34.56	33.52	34.15	34.11	33.82	34.21	-		33.14	34.45	34.56	34.65	34.23	-	
Fs	20.38	20.79	20.71	20.67	20.34	20.52	19.04	20.47	20.41	-		19.73	19.98	19.39	19.80	19.74	-	
mmf	.629	.620	.625	.626	.622	.625	.642	.623	.627	.0068	8	.627	.633	.641	.636	.634	.0059	4
Al/Cr	28.93	29.49	40.26	33.73	35.60	75.29	120.02	79.02	40.90	-		62.02	32.39	42.60	46.97	44.52	-	

TABLE A.3-1 (CONTINUED)

	AE-23	AE-23	AE-23	AE-23	AE-23	AE-23	AE-23	AE-23			AE-25	AE-25	AE-25	AE-25			AE-28	AE-28	AE-28	AE-28		
wt.%	c	c	c	m	c	c	m	x	d	n	c	c	c	x	d	n	c	c	c	x	d	n
SiO_2	54.56	54.68	54.56	52.24	53.87	54.70	54.89	54.21	.9278	7	51.04	49.40	51.09	50.51	.9616	3	50.97	51.53	50.91	51.14	.3420	3
TiO_2	.21	.12	.21	.28	.19	.16	.14	.19	.0535	7	.74	.62	.15	.68	.0849	2	.71	.40	.68	.60	.1710	3
Al_2O_3	1.03	1.71	1.03	1.20	1.38	1.59	1.34	1.33	.2618	7	2.08	2.04	1.02	2.05	.0283	2	2.17	2.01	2.20	2.13	.1021	3
FeO	15.69	13.84	15.69	16.34	15.60	15.34	15.78	15.47	.7789	7	13.40	12.80	11.24	12.48	1.1206	3	12.49	11.37	12.30	12.05	.5994	3
MnO	.33	.29	.33	.34	.31	.29	.29	.31	.0219	7	.26	.24	.25	.24	.0100	3	.28	.20	.29	.26	.0493	3
MgO	26.65	27.34	26.65	25.94	26.92	26.26	26.51	26.61	.4497	7	12.02	11.98	12.56	12.18	.3182	3	12.10	13.11	12.20	12.47	.5665	3
CaO	1.27	1.78	1.27	1.11	.69	1.88	1.11	1.30	.4109	7	21.49	21.13	23.23	21.95	1.1173	3	21.43	21.78	21.25	21.49	.2695	3
Na_2O	-	-	-	.12	-	-	-	-	-		.16	.09	.04	.13	.0495	2	.26	.22	.20	.23	.0006	3
Cr_2O_3	.25	.52	.25	.19	.29	.49	.33	.33	.1263	7	.11	.05	.09	.08	.0300	3	.07	.05	.06	.06	.0100	3
NiO	-	.09	-	.10	.11	-	.10	.10	.0082	4	-	-	-	-	-		-	-	-	-	-	
TOTAL	99.99	100.38	99.99	97.86	99.36	100.71	100.49	99.85			101.30	98.35	99.68	100.31	-		100.48	100.67	100.08	100.43		
cations/ 6 oxygens																						
Si	1.9717	1.9560	1.9717	1.9439	1.9581	1.9622	1.9724	1.9620	-		1.9197	1.9136	1.9464	1.9155	-		1.9256	1.9319	1.9274	1.9280	-	
Ti	.0057	.0032	.0057	.0078	.0052	.0043	.0057	.0052	-		.0209	.0181	.0040	.0194	-		.0199	.0113	.0194	.0170	-	
Al	.0439	.0721	.0439	.0526	.0591	.0672	.0568	.0567	-		.0922	.0931	.0453	.0921	-		.0962	.0888	.0982	.0947	-	
Fe^{2+}	.4742	.4141	.4742	.5085	.4742	.4602	.4742	.4683	-		.4215	.4147	.3578	.3958	-		.3945	.3565	.3895	.3799	-	
Mn	.0101	.0088	.0101	.0107	.0095	.0089	.0088	.0095	-		.0083	.0079	.0081	.0077	-		.0090	.0063	.0093	.0083	-	
Mg	1.4353	1.4576	1.4353	1.4358	1.4583	1.4039	1.4197	1.4353	-		.6738	.6916	.7126	.6884	-		.6815	.7325	.6884	.7006	-	
Ca	.0491	.0582	.0492	.0443	.0269	.0723	.0427	.0504	-		.8661	.8770	.9479	.8919	-		.8674	.8749	.8620	.8681	-	
Na	-	-	-	.0087	-	-	-	-	-		.0117	.0068	.0022	.0096	-		.0183	.0160	.0147	.0168	-	
Cr	.0071	.0147	.0071	.0056	.0083	.0139	.0094	.0094	-		.0033	.0015	.0024	.0024	-		.0021	.0015	.0018	.0018	-	
Ni	-	-	-	.0030	.0032	-	.0029	.0292	-		-	-	-	-	-		-	-	-	-	-	
TOTAL	3.9971	3.9973	3.9971	4.0235	4.0030	3.9929	3.9907	3.9998	-		4.0174	4.0244	4.0268	4.0227	-		4.0145	4.0197	4.0106	4.0152	-	
Wo	2.51	3.52	2.51	2.22	1.37	3.73	2.21	2.58	-		44.16	44.22	46.97	45.13	-		44.63	44.55	44.44	44.55	-	
En	73.28	75.14	73.28	72.24	74.43	72.50	73.31	73.46	-		34.35	34.87	35.31	34.84	-		35.07	37.30	35.49	35.95	-	
Fs	24.21	21.24	24.21	25.54	24.21	23.77	24.49	23.96	-		21.49	20.91	17.73	20.03	-		20.30	18.15	20.08	19.50	-	
mmf	.752	.779	.752	.739	.755	.753	.750	.754	.0121	7	.615	.625	.666	.635	.0268	3	.633	.673	.639	.648	.0216	3
Al/Cr	6.14	4.90	6.14	9.42	7.09	4.84	6.05	6.01	-		28.19	60.83	18.82	38.39	-		46.01	59.94	54.67	52.93	-	

	AE-32	AE-32	AE-32	AE-32			AE-34	AE-34	AE-34	AE-34	AE-34	AE-34	AE-34			27-C2	27-C2	27-C2	27-C2		
wt.%	c	c	c	x	d	n	c	c	c	c	c	c	x	d	n	c	c	m	x	d	n
SiO_2	51.44	52.22	52.51	52.06	.5534	3	51.19	51.13	51.26	51.38	50.64	50.86	51.08	.2753	6	51.56	52.05	51.51	51.82	.3253	2
TiO_2	.45	.35	.23	.34	.1102	3	.58	.55	.65	.62	.94	.62	.66	.1416	6	.51	.30	.48	.41	.0149	2
Al_2O_3	1.81	1.57	1.15	1.51	.3341	3	2.05	1.97	2.12	2.15	2.05	2.15	2.08	.0711	6	2.03	1.82	1.87	1.93	.1485	2
FeO	13.36	11.94	12.25	12.52	.7466	3	12.89	12.84	12.42	12.43	13.21	12.45	12.71	.3254	6	13.16	11.25	11.76	12.21	1.3606	2
MnO	.27	.28	.28	.28	.0058	3	.25	.25	.23	.23	.25	.28	.25	.0183	6	.28	.28	.26	.28	-	2
MgO	11.83	12.33	12.26	12.14	.2707	3	11.87	11.97	12.05	12.03	11.78	11.89	11.93	.1036	6	12.25	13.60	12.76	12.93	.9546	2
CaO	19.89	22.21	21.90	21.33	1.2595	3	21.99	21.45	22.11	22.06	21.79	22.09	21.92	.2558	6	20.69	20.57	21.06	20.63	.0849	2
Na_2O	.23	.09	-	.16	.0990	2	.18	.16	.17	.20	.17	.18	.18	.0137	6	.11	.15	.21	.13	.0283	2
Cr_2O_3	.07	.08	.05	.07	.0153	3	.08	.07	.06	.06	.05	.05	.06	.0084	6	.16	.45	.15	.31	.2051	2
NiO	-	-	-	-	-		.05	-	.03	.01	.02	-	.03	.0171	4	-	.04	-	.04	-	1
TOTAL	99.35	101.06	100.63	100.41	-		101.12	100.39	101.10	101.16	100.90	100.55	100.90	-		100.75	100.51	100.06	100.69	-	
cations/ 6 oxygens																					
Si	1.9608	1.9543	1.9693	1.9621	-		1.9265	1.9345	1.9254	1.9277	1.9413	1.9224	1.9250	-		1.9403	1.9466	1.9430	1.9430	-	
Ti	.0129	.0099	.0065	.0096	-		.0164	.0157	.0184	.0175	.0267	.0176	.0187	-		.0144	.0084	.0136	.0116	-	
Al	.0813	.0693	.0508	.0671	-		.0909	.0878	.0939	.0951	.0913	.0958	.0924	-		.0900	.0802	.0831	.0853	-	
Fe^{2+}	.4259	.3737	.3842	.3946	-		.4057	.4063	.3902	.3900	.4176	.3936	.4006	-		.4142	.3519	.3710	.3829	-	
Mn	.0087	.0089	.0089	.0089	-		.0080	.0080	.0073	.0073	.0080	.0090	.0080	-		.0089	.0089	.0083	.0089	-	
Mg	.6720	.6877	.6852	.6819	-		.6657	.6750	.6745	.6726	.6637	.6698	.6701	-		.6870	.7580	.7173	.7225	-	
Ca	.8124	.8906	.8800	.8614	-		.8867	.8696	.8899	.8868	.8826	.8947	.8852	-		.8343	.8243	.8512	.8288	-	
Na	.0170	.0065	-	.0117	-		.0131	.0117	.0124	.0145	.0125	.0132	.0132	-		.0008	.0109	.0154	.0095	-	
Cr	.0021	.0024	.0015	.0021	-		.0024	.0021	.0018	.0018	.0015	.0018	.0018	-		.0048	.0133	.0045	.0092	-	
Ni	-	-	-	-	-		.0015	-	.0009	.0003	.0006	-	.0009	-		-	.0012	-	.0012	-	
TOTAL	3.9931	4.0033	4.0097	3.9995	-		4.0170	4.0107	4.0146	4.0137	4.0189	4.0178	4.0158	-		4.0019	4.0037	4.0073	4.0029	-	
Wo	42.53	45.63	45.14	44.45	-		45.28	44.58	45.53	45.49	44.94	45.69	45.26	-		43.10	42.62	43.89	42.85	-	
En	35.18	35.23	35.15	35.19	-		34.00	34.60	34.52	34.50	33.79	34.21	34.26	-		35.50	39.19	36.98	37.35	-	
Fs	22.29	19.14	19.71	20.36	-		20.72	20.83	19.96	20.06	21.27	20.10	20.48	-		21.40	18.19	19.13	19.79	-	
mmf	.612	.648	.641	.634	.0156	3	.621	.624	.634	.633	.614	.630	.626	.0078	6	.624	.683	.659	.653	.0417	2
Al/Cr	38.55	29.26	34.29	32.16	-		38.21	41.96	52.68	53.43	61.13	53.43	51.69	-		18.92	6.03	18.59	9.28	-	

	27-C2	27-C2	27-01	27-01	27-01	27-01	27-01	27-01	27-02	27-02	27-F2	27-F2	27-F2	27-01,02,F2		
wt.%	c	c	c	c	m	c								x	d	n
SiO_2	53.13	53.36	52.69	51.56	52.51	48.60	51.60	51.68	50.23	51.02	51.26	51.60	51.76	51.26	.5763	6
TiO_2	.13	.06	.12	.11	.24	.22	.37	.47	.65	.66	.69	.61	.50	.60	.0907	6
Al_2O_3	.89	.82	1.56	1.77	1.23	1.07	1.73	1.88	2.37	2.48	2.00	2.01	1.79	2.13	.2859	6
FeO	24.53	24.90	15.75	24.37	24.12	24.82	10.03	12.21	11.81	11.81	13.72	12.11	12.90	12.28	.7249	6
MnO	.45	.48	.28	.40	.45	.46	.23	.29	.29	.27	.29	.24	.29	.28	.0204	6
MgO	20.74	20.71	24.88	18.99	20.91	20.59	13.30	13.16	12.14	12.09	12.07	12.21	12.00	12.28	.4376	6
CaO	.83	.76	2.73	1.40	1.41	1.36	22.15	20.39	21.19	21.43	20.81	22.19	21.16	21.20	.6071	6
Na_2O	-	-	-	-	.03	-	.18	.21	.24	.20	.12	.16	.05	.17	.0663	6
Cr_2O_3	.12	.12	.35	.46	.17	.13	.27	.30	.07	.09	.12	.09	.10	.13	.0857	6
NiO	.06	.04	.08	.01	.04	.06	.03	.03	.03	.03	.02	-	.03	.02	.0121	6
TOTAL	100.94	101.11	98.40	99.00	101.11	97.16	99.88	100.61	99.02	100.07	101.10	101.19	100.58	100.35	-	
cations/ 6 oxygens																
Si	1.9811	1.9839	1.9489	1.9643	1.9563	1.9070	1.9414	1.9393	1.9210	1.9274	1.9298	1.9321	1.9448	1.9344	-	
Ti	.0036	.0017	.0034	.0032	.0067	.0065	.0105	.0133	.0187	.0187	.0195	.0172	.0141	.0170	-	
Al	.0391	.0360	.0681	.0795	.0540	.4950	.0767	.0832	.1068	.1104	.0887	.0887	.0793	.0947	-	
Fe^{2+}	.7649	.7748	.4872	.7765	.7515	.8145	.3156	.3832	.3777	.3731	.4320	.3792	.4054	.3857	-	
Mn	.0142	.0151	.0088	.0129	.0142	.0152	.0073	.0092	.0094	.0086	.0092	.0076	.0092	.0090	-	
Mg	1.1525	1.1484	1.3715	1.0782	1.1610	1.2041	.7458	.7360	.6919	.6807	.6772	.6814	.6719	.6906	-	
Ca	.0332	.0303	.1082	.0572	.0563	.0672	.8830	.8199	.8683	.8574	.8395	.8903	.8686	.8572	-	
Na	-	-	-	-	.0022	-	.0131	.0153	.0178	.0146	.0088	.0116	.0036	.0124	-	
Cr	.0035	.0035	.0102	.0139	.0050	.0040	.0080	.0090	.0021	.0027	.0036	.0027	.0030	.0039	-	
Ni	.0018	.0009	.0024	.0003	.0012	.0016	.0009	.0009	.0009	.0009	.0006	-	.0009	.0006	-	
TOTAL	3.9940	3.9947	4.0086	3.9859	4.0085	4.0597	4.0123	4.0090	4.0147	4.0047	4.0089	4.0108	4.0018	4.0055	-	
Wo	1.70	1.55	5.50	2.99	2.86	2.75	45.69	42.82	44.81	45.15	43.08	45.64	44.67	44.33	-	
En	59.08	58.79	69.73	56.40	58.97	58.01	38.16	37.96	35.70	35.43	34.75	34.93	34.52	35.72	-	
Fs	39.22	39.66	24.77	40.61	38.17	39.24	16.15	19.76	19.49	19.42	22.17	19.44	20.82	19.95	-	
mmf	.601	.597	.738	.581	.607	.596	.703	.658	.647	.646	.611	.642	.624	.638	.0172	6
Al/Cr	11.06	10.19	6.65	5.74	10.79	12.27	9.55	9.34	50.48	41.08	24.86	33.30	26.69	24.43	-	

TABLE A.3-1 (CONTINUED)

	AH-3	AH-3	AH-3	AH-3	AH-3			AH-20B	AH-20B	AH-13	AH-17C	AH-17C	AH-21B	AH-21B	AH-21B	AH-21B	AH-21B	AH-21B		
wt.%	c	c	c	c	c	d	n	c	c	c	c	c	c	m	c	m	c	x	d	n
SiO_2	52.11	51.19	51.16	50.87	51.07	.1767	3	55.97	56.27	52.60	52.29	51.31	49.02	53.28	51.39	51.49	50.69	50.37	1.2176	3
TiO_2	.19	.38	.13	.44	.32	.1644	3	.21	.04	.40	.38	.70	.44	.23	.52	.23	.61	.52	.0850	3
Al_2O_3	1.31	2.30	2.47	2.45	2.41	.0929	3	1.31	.77	1.88	2.13	2.60	3.59	1.14	2.00	1.29	2.16	2.58	.8755	3
FeO	9.95	11.73	11.45	11.87	11.68	.2139	3	13.20	18.00	12.84	8.78	11.90	12.28	11.38	12.17	11.50	12.28	12.24	.0635	3
MnO	.25	.29	.24	.26	.26	.0252	3	.27	.40	.29	.22	.26	.22	.27	.25	.29	.25	.24	.0173	3
MgO	13.08	12.63	12.02	12.60	12.42	.3439	3	28.50	25.74	11.59	14.38	12.51	12.41	12.93	12.59	12.29	12.17	12.39	.2107	3
CaO	23.46	20.98	22.86	21.56	21.80	.9640	3	1.18	.54	21.33	22.16	21.91	20.85	22.81	21.37	22.27	21.57	21.26	.3717	3
Na_2O	.03	.28	.21	.21	.23	.0404	3	-	-	.12	.17	.16	.08	.03	.13	.10	.19	.13	.0551	3
Cr_2O_3	.23	.01	.10	.43	.18	.2211	3	.30	.05	.05	.60	.10	.07	.05	.03	.05	.04	.05	.0208	3
NiO	.01	.03	.02	.02	.02	.0058	3	.09	.10	.03	.07	.02	.03	.02	-	.01	.03	.03	-	2
TOTAL	100.61	99.82	100.66	100.70	100.39	-		101.03	100.92	101.13	101.18	101.47	98.99	102.13	100.44	99.52	99.99	99.81	-	
cations/ 6 oxygens																				
Si	1.9605	1.9355	1.9856	1.9139	1.9248	-		1.9753	1.9924	1.9671	1.9301	1.9139	1.8791	1.9675	1.9355	1.9576	1.9237	1.9130	-	
Ti	.0053	.0108	.0037	.0124	.0091	-		.0056	.0010	.0113	.0105	.0196	.0127	.0064	.0147	.0066	.0174	.0149	-	
Al	.0578	.1025	.1096	.1086	.1071	-		.0545	.0027	.0829	.0927	.1143	.1622	.0496	.0888	.0578	.0966	.1155	-	
Fe^{2+}	.3115	.3709	.3604	.3735	.3682	-		.3896	.5427	.4016	.2710	.3712	.3937	.3514	.3833	.3657	.3897	.3888	-	
Mn	.0079	.0093	.0077	.0083	.0083	-		.0081	.0122	.0092	.0069	.0082	.0071	.0084	.0080	.0093	.0080	.0077	-	
Mg	.7297	.7117	.6743	.7065	.6976	-		1.4990	1.3828	.6460	.7910	.6954	.7090	.7116	.7067	.6964	.6883	.7013	-	
Ca	.9409	.8600	.9220	.8687	.8804	-		.0446	.0209	.8547	.8764	.8757	.8564	.9025	.8524	.9072	.8771	.8652	-	
Na	.0022	.0206	.0153	.0153	.0168	-		-	-	.0087	.0122	.0116	.0060	.0021	.0095	.0074	.0140	.0096	-	
Cr	.0068	.0003	.0030	.0128	.0054	-		.0084	.0017	.0015	.0175	.0029	.0022	.0015	.0009	.0015	.0012	.0015	-	
Ni	.0003	.0009	.0006	.0006	.0006	-		.0026	.0029	.0009	.0021	.0006	.0009	.0006	-	.0003	.0009	.0009	-	
TOTAL	4.0129	4.0125	4.0221	4.0206	4.0183	-		3.9877	3.9893	3.9838	4.0104	4.0136	4.0291	4.0017	4.0097	4.0098	4.0170	4.0184	-	
Wo	47.47	43.98	47.12	44.58	45.24	-		2.31	1.07	44.93	45.21	45.08	43.71	45.92	44.17	46.07	44.86	44.25	-	
En	36.81	36.83	34.46	36.25	35.85	-		77.54	71.05	33.96	40.81	35.80	36.19	36.20	36.19	35.36	35.20	35.87	-	
Fs	15.72	19.19	18.42	19.17	18.92	-		20.15	27.88	21.11	13.98	19.11	20.10	17.88	19.64	18.57	19.93	19.88	-	
mmf	.701	.657	.652	.654	.655	.0025	3	.794	.718	.617	.745	.652	.643	.669	.648	.656	.638	.643	.0050	3
Al/Cr	8.49	-	36.83	8.50	19.96	-		6.51	19.13	56.06	5.29	38.77	76.47	33.99	99.40	38.47	80.51	76.93	-	

	M.27-3A	M.27-3A	M.27-3A	M127-3A	M.27-3A	M.27-3A	M.27-3A	M.27-3A	M.27-3A			M.27-3B	M.27-3B	M.27-3B	M.27-3B	M.27-3B	M.27-3B	M.27-3B	M.27-3B		
wt.%	c	c	c	c	c	c	c	c	x	d	n	c	c	c	c	c	c	c	x	d	n
SiO_2	51.47	52.05	52.18	52.84	51.49	52.18	52.09	52.26	52.07	.4392	8	52.16	52.34	51.88	51.73	52.33	50.14	53.41	52.00	.9819	7
TiO_2	.28	.11	.27	.27	.33	.13	.19	.18	.22	.0787	8	.07	.16	.23	.22	.22	.44	.16	.21	.1140	7
Al_2O_3	1.01	.56	.89	.59	1.24	.61	.71	.49	.76	.2609	8	.30	.40	.78	.53	.82	1.45	.46	.55	.2094	6
FeO	11.74	10.98	11.94	11.55	10.46	11.42	11.36	11.66	11.39	.4718	8	11.29	11.05	10.81	11.32	12.15	11.85	11.12	11.37	.4701	7
MnO	.27	.24	.28	.29	.23	.29	.27	.29	.27	.0233	8	.25	.28	.25	.28	.29	.25	.26	.27	.0172	7
MgO	12.19	12.58	12.44	11.84	12.65	12.05	12.12	12.21	12.26	.2763	8	12.23	12.61	12.24	11.94	12.23	11.92	12.63	12.26	.2827	7
CaO	23.15	22.67	22.59	23.16	23.19	22.43	22.83	22.91	22.87	.2878	8	22.70	22.79	23.19	22.90	21.77	21.80	22.83	22.57	.5566	7
Na_2O	.13	.06	.06	.13	.10	.06	.31	.12	.12	.0835	8	.13	.13	.20	.17	.34	.29	.11	.20	.0879	7
Cr_2O_3	.02	.01	.01	.01	.03	.02	.02	.01	.02	.0074	8	.01	.03	.03	.02	.02	.02	.01	.02	.0082	7
NiO	-	-	-	-	-	-	-	-	-	-		-	-	-	-	-	-	.01	-	-	
TOTAL	100.26	99.26	100.66	100.68	99.72	99.19	99.90	100.12	99.98	-		99.14	99.79	99.60	99.10	100.16	98.16	101.00	99.46	-	
cations/ 6 oxygens																					
Si	1.9222	1.9800	1.9644	1.9860	1.9498	1.9878	1.9744	1.9780	1.9713	-		1.9896	1.9816	1.9694	1.9775	1.9778	1.9402	1.9928	1.9785	-	
Ti	.0079	.0031	.0076	.0076	.0094	.0037	.0064	.0051	.0063	-		.0020	.0046	.0066	.0063	.0063	.0128	.0045	.0060	-	
Al	.0445	.0251	.0395	.0261	.0553	.0274	.0317	.0219	.0339	-		.0135	.0179	.0349	.0239	.0365	.0661	.0202	.0247	-	
Fe^{2+}	.3668	.3492	.3759	.3631	.3313	.3638	.3601	.3691	.3606	-		.3601	.3499	.3432	.3619	.3840	.3835	.3470	.3618	-	
Mn	.0085	.0078	.0089	.0092	.0071	.0094	.0087	.0093	.0087	-		.0081	.0090	.0080	.0091	.0093	.0082	.0082	.0087	-	
Mg	.6785	.7130	.6980	.6632	.7139	.6841	.6947	.6887	.6917	-		.6952	.7115	.6925	.6802	.6889	.6874	.7023	.6952	-	
Ca	.9264	.9238	.9112	.9327	.9410	.9155	.9272	.9291	.9277	-		.9278	.9245	.9433	.9380	.8816	.9039	.9127	.9201	-	
Na	.0094	.0037	.0044	.0095	.0073	.0044	.0228	.0088	.0088	-		.0096	.0095	.0147	.0126	.0249	.0218	.0080	.0147	-	
Cr	.0059	.0003	.0003	.0003	.0009	.0006	.0006	.0003	.0006	-		.0003	.0009	.0009	.0006	.0006	.0006	.0003	.0006	-	
Ni	-	-	-	-	-	-	-	-	-	-		-	-	-	-	-	-	.0003	-	-	
TOTAL	4.0229	4.0060	4.0103	3.9978	4.0163	3.9968	4.0155	4.0103	4.0096	-		4.0063	4.0093	4.0135	4.0109	4.0099	4.0245	3.9964	4.0120	-	
Wo	46.99	46.51	45.90	47.61	47.38	46.63	47.02	46.76	46.85	-		46.78	46.55	47.67	47.37	45.11	45.77	46.52	46.54	-	
En	34.41	35.90	35.16	33.85	35.94	34.84	34.72	34.66	34.93	-		35.05	35.23	34.99	34.35	35.24	34.81	35.79	35.16	-	
Fs	18.60	17.58	18.94	18.53	16.68	18.53	18.26	18.58	18.21	-		18.16	17.62	17.34	18.28	19.65	19.42	17.69	18.30	-	
mmf	.649	.671	.650	.646	.683	.653	.655	.651	.657	.0129	8	.659	.670	.669	.653	.642	.642	.669	.658	.0124	7
Al/Cr	75.29	83.49	-	89.97	61.63	45.47	52.93	73.06	56.66	-		44.73	19.88	38.77	39.51	61.13	-	68.58	41.00	-	

	M.22-2A	M.22-5	M.22-5	M.22-11	M.22-11	M.22-11	M.22-11	M.22-11	M.22-11			M.24-1	M.24-1	M.24-7A	M.26-8A	M.26-8A	M.26-8A	M.26-8A	M.26-8A		
wt.%	c	c	c	c	c	c	c	c	x	d	n	c	c	c	c	c	c	c	x	d	n
SiO_2	50.35	52.24	51.34	51.36	52.67	50.38	52.20	51.23	51.57	.8920	5	51.31	51.36	52.17	54.55	52.42	52.56	53.07	52.68	.3421	3
TiO_2	.49	.05	.36	.43	.15	.39	.36	.46	.36	.1224	5	.48	.47	.12	.22	.17	.30	.22	.23	.0656	3
Al_2O_3	2.11	.36	1.56	1.93	.97	1.93	1.69	1.95	1.69	.4187	5	1.76	1.69	.51	1.34	2.42	2.46	1.84	2.24	.3470	3
FeO	10.60	8.49	13.50	11.15	10.37	10.57	10.07	11.25	10.68	.5065	5	11.83	11.97	11.24	14.18	5.76	5.89	6.15	5.93	.1996	3
MnO	.26	.19	.31	.27	.30	.26	.26	.28	.27	.0167	5	.27	.29	.25	.32	.19	.19	.20	.19	.0058	3
MgO	12.75	13.05	13.51	12.98	12.58	13.07	12.83	12.21	12.73	.3467	5	12.92	12.30	12.17	27.16	16.56	16.09	16.46	16.37	.2476	3
CaO	22.02	23.63	17.89	21.26	23.00	21.79	22.50	22.07	22.12	.6652	5	20.80	21.14	22.20	1.45	21.54	21.12	21.25	21.30	.2150	3
Na_2O	.16	.08	.05	.11	.16	.17	.23	.14	.16	.0444	5	.16	.22	.06	.01	.29	.36	.13	.26	.1179	3
Cr_2O_3	.03	.01	.03	.03	.02	.01	.04	.01	.02	.0130	5	.02	.05	.01	.26	1.05	.50	.46	.67	.3297	3
NiO	.03	-	-	.01	-	-	.02	-	-	-		.02	.04	.02	.05	-	.05	.02	.04	.0212	3
TOTAL	98.80	98.10	98.55	99.53	100.22	98.57	100.20	99.60	99.60	-		99.57	99.53	98.75	99.54	100.37	99.52	99.80	99.91	-	
cations/ 6 oxygens																					
Si	1.9234	1.9925	1.9630	1.9429	1.9779	1.9275	1.9564	1.9425	1.9499	-		1.9446	1.9509	1.9932	1.9679	1.9220	1.9395	1.9532	1.9381	-	
Ti	.0141	.0014	.0104	.0122	.0042	.0112	.0101	.0131	.0102	-		.0137	.0134	.0034	.0060	.0047	.0083	.0061	.0064	-	
Al	.0950	.0162	.0703	.0861	.0429	.0870	.0747	.0872	.0753	-		.0786	.0757	.0230	.5700	.1046	.1070	.0798	.0971	-	
Fe^{2+}	.3389	.2708	.4317	.3528	.3257	.3382	.3156	.3568	.3377	-		.3750	.3803	.3591	.4278	.1766	.1818	.1893	.1825	-	
Mn	.0084	.0061	.0100	.0087	.0095	.0084	.0083	.0090	.0086	-		.0087	.0093	.0081	.0098	.0059	.0059	.0063	.0059	-	
Mg	.7259	.7418	.7699	.7318	.7040	.7452	.7166	.6900	.7174	-		.7298	.6963	.6929	1.4602	.9049	.8949	.9028	.8976	-	
Ca	.9013	.9657	.7330	.8618	.9255	.8933	.9036	.8967	.8962	-		.8447	.8604	.9088	.0560	.8483	.8351	.8380	.8397	-	
Na	.0118	.0059	.0037	.0081	.0117	.0126	.0167	.0103	.0117	-		.0118	.0162	.0044	.0007	.0206	.0258	.0093	.0186	-	
Cr	.0009	.0003	.0009	.0009	.0006	.0003	.0012	.0003	.0006	-		.0006	.0015	.0003	.0074	.0304	.0146	.0134	.0195	-	
Ni	.0009	-	-	.0003	-	-	.0006	-	-	-		.0006	.0012	.0006	.0015	-	.0015	.0006	.0012	-	
TOTAL	4.0205	4.0008	3.9929	4.0054	4.0020	4.0239	4.0039	4.0058	4.0077	-		4.0080	4.0052	3.9940	3.9943	4.0161	4.0043	3.9988	4.0065	-	
Wo	45.85	48.81	37.89	44.28	47.33	45.19	46.68	46.14	45.93	-		43.33	44.42	46.35	2.88	43.90	43.92	43.42	43.74	-	
En	36.92	37.50	39.80	37.60	36.01	37.70	37.02	35.50	36.76	-		37.43	35.95	35.34	75.11	46.94	46.53	46.78	46.76	-	
Fs	17.23	13.69	22.32	18.12	16.66	17.11	16.31	18.36	17.31	-		19.24	19.63	18.32	22.01	9.16	9.56	9.81	9.50	-	
mmf	.682	.733	.641	.675	.684	.688	.694	.659	.680	.0136	5	.661	.647	.659	.773	.837	.830	.827	.831	.0051	3
Al/Cr	-	53.67	77.53	96.92	72.31	-	62.99	-	-	-		-	50.40	76.04	7.68	3.44	7.34	5.96	4.98	-	

TABLE A.8-2 ELECTRON MICROPROBE ANALYSIS OF PYROXENES FROM THE PLATINIFEROUS ULTRAMAFIC PIPES

	DR-22			DR-25 & 27			DR-25 & 27			DR-32B			DR-32B			DR-38C			DR-38C			DR-40B			DR-40B*	DR-46B	DR-46B		
wt.%	x	d	n	x	d	n	x	d	n	x	d	n	x	d	n	x	d	n	x	d	n	x	d	n				x	d
SiO_2	53.13	.3547	3	53.18	.2377	7	54.08	.1982	6	52.38	.1229	3	53.72	.2798	4	52.82	.3800	4	53.31	.2687	2	52.83	.1982	4	52.95	53.39	55.68	.2475	2
TiO_2	.31	.0058	3	.28	.0168	7	.14	.0194	6	.31	.0577	3	.16	.0050	4	.28	.1190	4	.16	.0496	2	.27	.0216	4	.16	.26	.13	-	2
Al_2O_3	2.20	.2458	3	1.86	.0624	7	1.27	.1554	6	2.04	.0881	3	1.18	.0835	4	1.86	.0635	4	1.23	.0849	2	1.84	.0810	4	1.37	1.79	1.47	.1131	2
FeO	5.95	.1097	3	7.92	.7456	7	18.54	.4022	6	8.51	.5495	3	17.05	.4862	4	8.64	1.2636	4	20.28	1.5556	2	7.86	.2353	4	19.87	3.59	10.70	.1202	2
MnO	.25	-	3	.23	.0214	7	.36	.0841	5	.23	.0346	3	.35	.0299	4	.27	.0655	4	.36	.0707	2	.22	.0126	4	.46	.24	.31	.1061	2
MgO	16.07	.3931	3	15.36	.3259	7	24.33	.1776	6	15.23	.2954	3	25.00	.2956	4	14.93	.5883	4	23.18	.9051	2	14.95	.2488	4	23.70	15.78	29.19	.3111	2
CaO	21.52	.1153	3	21.17	.9970	7	1.06	.2396	6	20.71	.7441	3	1.74	.2434	4	21.01	1.7672	4	1.31	.6293	2	21.62	.4140	4	1.08	22.98	1.59	.4808	2
Na_2O	.25	.0462	3	.19	.0465	7	n.d.	-		.51	.3523	3	n.d.	-		.21	.0100	4	n.d.	-		.19	.0535	4	n.d.	.34	n.d.	-	
Cr_2O_3	.65	.2303	3	.14	.0267	7	.08	.0103	6	.35	-	3	.21	.0129	4	.15	.0096	4	.10	.0071	2	.15	.0150	4	.08	.75	.43	.0990	2
NiO	.04	-	1	.02	.0107	7	.03	.0207	6	.04	.0100	3	.06	.0206	4	.07	.0252	4	.08	.0100	2	.03	.0096	4	.05	-	.05	.0283	2
TOTAL	100.37	-		100.34	-		99.89	-		100.31	-		99.47	-		100.24	-		100.01	-		99.96	-		99.72	99.12	99.55	-	
cations/ 6 oxygens																													
Si	1.9455			1.9598			1.9793			1.9519			1.9685			1.9562			1.9692			1.9577			1.9589	1.9665	1.9754		
Ti	.0085			.0078			.0039			.0085			.0044			.0078			.0044			.0075			.0045	.0072	.0035		
Al	.0950			.0804			.0548			.0881			.0510			.0812			.0536			.0804			.0597	.0777	.0615		
Fe^{2+}	.1822			.2441			.5675			.2607			.5225			.2676			.6265			.2436			.6148	.1106	.3175		
Mn	.0078			.0072			.0112			.0071			.0109			.0085			.0113			.0069			.0144	.0075	.0093		
Mg	.8770			.8436			1.3271			.8315			1.3652			.8241			1.2761			.8256			1.3067	.8662	1.5434		
Ca	.8443			.8359			.0416			.8130			.0683			.8338			.0518			.8585			.0428	.9069	.0604		
Na	.0177			.0136			-			.0362			-			.0151			-			.0137			-	.0243	-		
Cr	.0188			.0041			.0023			.0101			.0061			.0044			.0029			.0044			.0023	.0218	.0121		
Ni	.0012			.0006			.0009			.0012			.0018			.0021			.0024			.0009			.0015	-	.0014		
TOTAL	3.9980			3.9970			3.9884			4.0086			3.9986			4.0007			3.9982			3.9992			4.0056	3.9887	3.9844		
Wo	44.36			43.46			2.15			42.67			3.49			43.30			2.65			44.53			2.17	48.15	3.15		
En	46.07			43.85			68.54			43.64			69.80			42.80			65.29			42.83			65.52	45.98	80.33		
Fs	9.57			12.69			29.31			13.69			26.71			13.90			32.06			12.64			31.30	5.87	16.52		
mmf	.828	.0062	3	.776	.0149	7	.700	.0053	6	.761	.0096	3	.723	.0081	4	.755	.0203	4	.671	.0255	2	.772	.0059	4	.680	.887	.829	.0007	2
Al/Cr	5.40	1.57	3	20.21	4.52	7	23.67	5.18	6	8.69	.378	3	8.38	.1650	4	18.49	.929	4	18.34	2.7754	2	18.29	2.0165	4	25.53	3.56	5.10	.803	2

	DR-49			DR-49			DR-111			MO-4			MO-4*		
wt.%	x	d	n	x	d	n	x	d	n	x	d	n	x	d	n
SiO_2	52.74	.0566	2	54.82	.9538	3	55.97	.4172	2	52.23	.8524	3	52.55	.2546	2
TiO_2	.31	.0212	2	.17	.0100	3	.17	-	2	.50	.0889	3	.16	.0071	2
Al_2O_3	2.19	.0778	2	1.26	.1563	3	1.45	.0283	2	2.34	.2201	3	1.16	.0141	2
FeO	8.56	.8061	2	17.67	.0862	3	11.55	.2263	2	10.56	.3798	3	25.09	.3253	2
MnO	.24	-	2	.45	.1061	2	.27	.0071	2	.27	.0321	3	.50	.0212	2
MgO	14.96	.6576	2	24.80	.3931	3	29.40	.1202	2	13.06	.2548	3	19.22	.2970	2
CaO	19.91	1.6193	2	1.50	.2730	3	1.67	.2333	2	20.70	.5205	3	.87	.0100	2
Na_2O	.30	.0849	2	n.d.	.0586	3	n.d.	-		.24	.1266	3	n.d.	-	
Cr_2O_3	.49	.0778	2	.23	.0154	3	.42	.0212	2	.18	.0115	3	.09	.0283	2
NiO	.03	-	1	.05	.0354	3	.10	.0071	2	.02	.0100	3	.03	.0071	2
TOTAL	99.73	-		100.95	-		101.00			100.10	-		99.67	-	
cations/ 6 oxygens															
Si	1.9569			1.9795			1.9658			1.9523			1.9892		
Ti	.0087			.0046			.0045			.0141			.0046		
Al	.0958			.0536			.0600			.1031			.0518		
Fe^{2+}	.2656			.5336			.3393			.3301			.7943		
Mn	.0075			.0138			.0080			.0085			.0160		
Mg	.8273			1.3346			1.5389			.7275			1.0843		
Ca	.7916			.0580			.0628			.8291			.0353		
Na	.0216			-			-			.0174			-		
Cr	.0144			.0067			.0117			.0053			.0027		
Ni	.0009			.0015			.0028			.0006			.0009		
TOTAL	3.9902			3.9858			3.9939			3.9881			3.9790		
Wo	42.00			3.01			3.24			43.94			1.84		
En	43.90			69.28			79.28			38.56			56.65		
Fs	14.10			27.70			17.48			17.50			41.50		
mmf	.757	.0092	2	.714	.0035	3	.820	.0035	2	.688	.0066	3	.577	.0071	2
Al/Cr	6.66	.8485	2	8.17	1.108	3	5.15	.1648	2	19.38	2.10	3	19.22	6.11	2

	DR-28,-29 & -30			DR-32B			DR-36B			DR-52			DR-28,-29 & -30*			DR-32B*	DR-36B*	DR-52**
wt.%	x	d	n	x	d	n	x	d	n	x	d	n	x	d	n			
SiO_2	55.61	.4440	7	54.77	.3290	5	55.92	.1746	4	55.43	.1909	2	54.50	.7839	5	52.85	55.03	53.22
TiO_2	.15	.0219	7	.17	.0217	5	.08	.0082	4	.13	.0071	2	.23	.0130	5	.33	.04	.30
Al_2O_3	.92	.1452	7	1.22	.0858	5	1.31	.0457	4	1.52	.0212	2	1.20	.3648	5	1.76	.80	2.49
FeO	14.63	.3223	7	14.60	1.5665	5	10.23	.2391	4	11.82	.6152	2	5.47	.4126	5	4.88	3.03	4.49
MnO	.31	.0215	7	.31	.0303	5	.25	.0115	4	.23	-	2	.16	.0277	5	.17	.12	.13
MgO	27.13	.5907	7	27.41	.8902	5	30.43	.1839	4	28.49	.1414	2	15.74	.2824	5	15.52	18.39	15.60
CaO	1.20	.2714	7	1.26	.1385	5	1.40	.4202	4	2.13	.9334	2	22.37	.5803	5	22.95	20.84	22.21
Na_2O	n.d.	-		n.d.	-		n.d.	-		n.d.	-		.17	.0251	5	.29	.16	.49
Cr_2O_3	.17	.0121	7	.43	.0733	5	.34	.0216	4	.49	.0212	2	.29	.0173	5	.83	.31	.93
NiO	.07	.0147	7	.09	.0055	5	.04	.0050	4	.10	-	2	.05	.0371	5	.02	.01	.04
TOTAL	100.19	-		100.26	-		100.00	-		100.34	-		100.18	-		99.60	98.73	99.90
cations/ 6 oxygens																		
Si	1.9914			1.9653			1.9698			1.9653			1.9920			1.9510	2.0079	1.9490
Ti	.0040			.0046			.0021			.0035			.0063			.0092	.0011	.0083
Al	.0388			.0516			.0544			.0635			.0517			.0766	.0344	.1075
Fe^{2+}	.4382			.4381			.3014			.3505			.1672			.1507	.0925	.1375
Mn	.0094			.0094			.0075			.0069			.0050			.0053	.0037	.0040
Mg	1.4479			1.4659			1.5975			1.5054			.8574			.8538	1.0000	.8614
Ca	.0460			.0484			.0528			.0809			.8761			.9078	.8148	.8715
Na	-			-			-			-			.0120			.0208	.0113	.0348
Cr	.0048			.0122			.0095			.0137			.0084			.0242	.0089	.0275
Ni	.0020			.0026			.0011			.0029			.0015			.0006	.0003	.0012
TOTAL	3.9827			3.9982			3.9961			3.9926			3.9776			3.9999	3.9750	3.9927
Wo	2.38			2.48			2.71			4.18			46.09			47.47	42.72	46.84
En	74.94			75.08			81.85			77.72			45.11			44.65	52.43	45.76
Fs	22.68			22.44			15.44			11.69			8.80			7.88	4.85	7.39
mmf	.768	.0050	7	.770	.0246	5	.841	.0024	4	.811	.0071	2	.837	.0113	5	.860	.915	.861
Al/Cr	8.07	1.07	7	4.23	.751	5	5.74	.073	4	4.63	.269	2	6.17	1.69	5	3.16	3.85	3.91

TABLE A.8-3 ELECTRON MICROPROBE ANALYSIS OF PYROXENES FROM CUMULATES

IN THE UPPER CRITICAL ZONE AT AMANDELBULT

	1	2	3	4	5	6	7	8	9	10	11	12	13	14
wt.%														
SiO_2	54.96	54.24	54.49	54.99	54.17	54.52	54.27	54.97	54.96	55.14	55.87	55.80	55.44	55.73
TiO_2	.12	.14	.15	.17	.13	.20	.27	.18	.17	.15	.17	.10	.17	.19
Al_2O_3	1.74	1.70	1.76	1.41	1.62	1.51	1.83	1.79	1.82	1.67	1.33	1.65	1.37	1.24
FeO	12.41	12.18	12.69	12.54	15.21	14.84	13.46	12.08	13.01	12.65	13.02	12.96	13.52	14.27
MnO	.28	.28	.22	.26	.29	.29	.28	.25	.29	.24	.29	.26	.26	.30
MgO	28.33	28.76	28.18	27.68	25.59	26.23	27.17	27.74	28.06	27.98	28.45	28.27	28.11	28.67
CaO	2.03	1.41	2.14	1.97	2.21	1.83	1.92	2.31	1.44	1.81	1.72	1.49	1.43	.84
Na_2O	n.d.	n.d.	n.d.	.18	.20	n.d.	.23	n.d.	.02	n.d.	n.d.	n.d.	n.d.	n.d.
Cr_2O_3	.58	.49	.44	.36	.49	.38	.44	.52	.51	.51	.52	.40	.45	.32
NiO	.11	.11	.12	.12	.13	.09	.09	.09	.10	.10	.10	-	.09	.08
TOTAL	100.56	99.31	100.19	99.68	100.03	99.89	99.95	99.93	100.38	100.25	101.46	100.93	100.84	101.64
cations/ 6 oxygens														
Si	1.9516	1.9469	1.9458	1.9698	1.9609	1.9677	1.9493	1.9609	1.9560	1.9624	1.9670	1.9716	1.9669	1.9647
Ti	.0032	.0038	.0040	.0046	.0035	.0054	.0073	.0048	.0046	.0040	.0045	.0027	.0045	.0050
Al	.0728	.0719	.0741	.0595	.0691	.0642	.0775	.0753	.0763	.0701	.0652	.0687	.0573	.0515
Fe^{2+}	.3686	.3656	.3790	.3757	.4605	.4480	.4043	.3604	.3872	.3766	.3834	.3830	.4012	.4207
Mn	.0084	.0085	.0067	.0079	.0089	.0089	.0085	.0076	.0087	.0072	.0086	.0078	.0078	.0090
Mg	1.4993	1.5385	1.4997	1.4777	1.3805	1.4109	1.4544	1.4748	1.4880	1.4843	1.4928	1.4890	1.4863	1.5063
Ca	.0772	.0542	.0819	.0756	.0857	.0708	.0739	.0883	.0549	.0690	.0649	.0564	.0544	.0317
Na	-	-	-	.0125	.0140	-	.0160	-	.0014	-	-	-	-	-
Cr	.0163	.0139	.0124	.0102	.0140	.0108	.0125	.0147	.0143	.0144	.0145	.0084	.0126	.0089
Ni	.0032	.0032	.0035	.0035	.0038	.0026	.0026	.0026	.0029	.0029	.0029	-	.0026	.0023
TOTAL	4.0006	4.0065	4.0070	3.9970	4.0010	3.9893	4.0064	3.9893	3.9948	3.9911	3.9937	3.9872	3.9936	4.0001
Wo	3.72	2.77	4.18	3.92	4.45	3.67	3.82	4.59	2.84	3.58	3.34	2.93	2.80	1.62
En	77.08	78.56	76.49	76.60	71.65	73.12	75.26	76.67	77.10	76.91	76.91	77.21	76.54	76.90
Fs	18.95	18.67	19.33	19.48	23.90	23.21	20.92	18.74	20.06	19.51	19.75	19.86	20.66	21.48
mmf	.803	.808	.798	.797	.750	.759	.782	.804	.794	.798	.796	.795	.787	.782
Al/Cr	4.47	5.17	5.96	5.84	4.93	5.92	6.20	5.13	5.32	4.88	3.81	3.20	4.54	5.78

n.d.: not detected; - not determined.

1-4 : Normal Merensky Reef (samples AT-15 & -17;cores of large cumulus grains)

5-8 : Merensky Reef enclosed by pegmatite (sample E2;5,7,8-cores of large cumulus grains,6-margin of grain 5)

9-14 : Merensky pyroxenite (samples AA-4 & A1;9-13-cores of large cumulus grains,14-margin of grain 13)

	1	2	3	4	5	6	7	8	9	10
wt.%										
SiO_2	54.71	55.54	55.89	55.40	55.17	55.79	52.40	54.89	55.56	55.24
TiO_2	.30	.17	.14	.11	.09	.12	.42	.20	.13	.12
Al_2O_3	1.39	1.29	1.71	1.64	1.72	1.32	2.06	1.33	1.29	1.50
FeO	14.12	13.79	11.09	10.83	11.25	10.76	5.85	12.35	13.44	13.00
MnO	.28	.32	.23	.22	.23	.21	.26	.22	.26	.24
MgO	27.22	28.14	29.18	29.63	30.05	30.56	14.50	27.36	28.48	28.44
CaO	1.05	.67	1.86	1.28	1.08	.89	23.23	3.36	.89	1.58
Na_2O	n.d.	n.d.	n.d.	n.d.	n.d.	n.d.	.31	n.d.	n.d.	n.d.
Cr_2O_3	.35	.31	.50	.50	.51	.34	.73	.49	.39	.57
NiO	.09	.12	.12	.07	.10	.07	.08	.12	.10	.08
TOTAL	99.51	100.34	100.71	99.74	100.19	100.06	99.84	100.32	100.54	100.77
cations/ 6 oxygens										
Si	1.9709	1.9772	1.9650	1.9655	1.9501	1.9664	1.9417	1.9604	1.9701	1.9588
Ti	.0081	.0046	.0037	.0029	.0024	.0032	.0117	.0054	.0035	.0032
Al	.0590	.0541	.0709	.0686	.0717	.0548	.0900	.0560	.0541	.0627
Fe^{2+}	.4254	.4106	.3261	.3154	.3326	.3172	.1813	.3689	.4001	.3855
Mn	.0085	.0096	.0068	.0066	.0069	.0063	.0082	.0067	.0078	.0072
Mg	1.4614	1.4930	1.5290	1.5667	1.5830	1.6053	.8008	1.4563	1.5105	1.5030
Ca	.0405	.0256	.0701	.0487	.0409	.0337	.9224	.1286	.0339	.0600
Na	-	-	-	-	-	-	.0223	-	-	-
Cr	.0100	.0087	.0139	.0140	.0143	.0095	.0214	.0138	.0100	.0160
Ni	.0026	.0034	.0034	.0021	.0029	.0020	.0024	.0035	.0029	.0029
TOTAL	3.9865	3.9868	3.9889	3.9903	4.0046	3.9983	4.0020	3.9994	3.9939	3.9987
Wo	2.10	1.32	3.64	2.52	2.09	1.72	48.43	6.58	1.75	3.08
En	75.82	77.39	79.42	81.14	80.91	82.07	42.05	74.54	77.68	77.13
Fs	22.07	22.07	21.28	16.34	17.00	16.22	9.52	18.88	20.57	19.79
mmf	.775	.784	.824	.832	.826	.835	.815	.798	.791	.796
Al/Cr	5.92	6.20	5.10	4.89	5.03	5.79	4.21	4.05	4.93	3.92

n.d.: not detected; - not determined.

1,2 : Mottled anorthosite, above P1 (sample AH-4;intercumulus orthopyroxenes in "mottles")

3-6 : Lower pseudoreef (P1) (samples AH-4 & AH-208;cumulus orthopyroxenes)

7 : Mottled anorthosite, above P1 (sample AH-208;cumulus clinopyroxene)

8-10 : Leuconorite in P2 middle marker (sample AD-41A;cumulus orthopyroxenes)

TABLE A.8-3 (CONTINUED)

	1	2	3	4	5	6	7	8	9	10
wt.%										
SiO_2	51.61	51.40	51.71	51.29	51.19	51.00	51.39	51.20	50.69	52.72
TiO_2	.34	.26	.34	.46	.50	.45	.34	.34	.34	.34
Al_2O_3	2.51	2.65	2.52	2.15	1.70	2.84	2.51	2.58	2.53	2.53
FeO	8.22	7.90	8.69	8.94	9.75	8.65	8.78	8.08	9.19	9.54
MnO	.22	.20	.22	.21	.24	.25	.22	.22	.22	.22
MgO	12.91	12.81	13.22	13.34	13.55	12.59	12.57	11.65	13.42	13.75
CaO	23.16	23.12	23.15	22.29	22.31	22.58	22.75	22.57	22.50	22.57
Na_2O	.32	.28	.32	.23	.28	.35	.32	.32	.32	.32
Cr_2O_3	.14	.12	.14	.13	.14	.13	.14	.14	.14	.14
TOTAL	99.43	98.74	100.31	99.44	99.66	98.84	99.02	97.10	99.35	100.13
cations/ 6 oxygens										
Si	1.9383	1.9405	1.9292	1.9371	1.9313	1.9294	1.9411	1.9655	1.9150	1.9356
Ti	.0096	.0074	.0095	.0131	.0142	.0128	.0097	.0098	.0097	.0094
Al	.1111	.1179	.1108	.0957	.0756	.1266	.1118	.1131	.1127	.1095
Fe^{2+}	.2582	.2494	.2711	.2824	.3076	.2737	.2774	.2594	.2904	.2929
Mn	.0070	.0064	.0070	.0067	.0077	.0080	.0070	.0072	.0070	.0068
Mg	.7226	.7207	.7350	.7508	.7619	.7099	.7076	.6666	.7556	.7524
Ca	.9320	.9352	.9254	.9021	.9019	.9153	.9208	.9284	.9108	.8761
Na	.0233	.0205	.0231	.0168	.0205	.0257	.0234	.0238	.0234	.0228
Cr	.0042	.0036	.0041	.0039	.0042	.0039	.0042	.0043	.0042	.0041
TOTAL	4.0062	4.0017	4.0129	4.0085	4.0249	4.0053	4.0030	3.9779	4.0287	4.0096
Wo	48.73	49.08	47.91	46.61	45.75	48.20	48.32	50.07	46.55	45.60
En	37.78	37.83	38.05	38.80	38.64	37.38	37.13	35.94	38.61	39.16
Fs	13.50	13.09	14.04	14.59	15.61	14.41	14.55	13.99	14.84	15.25
mmf	26.73	32.93	26.84	24.66	18.10	32.57	26.73	26.62	26.94	26.94
Al/Cr	.737	.743	.731	.727	.712	.722	.718	.720	.722	.720

Sample AT-13 - all sliver-like grains of intercumulus clinopyroxene in mottled anorthosite.

	1	2	3	4	5	6	7	8
wt.%								
SiO_2	55.19	54.89	55.56	55.24	53.37	53.06	52.94	53.33
TiO_2	.19	.20	.13	.12	.32	.35	.35	.32
Al_2O_3	1.40	1.33	1.29	1.50	3.35	2.95	2.94	2.45
FeO	13.19	12.35	13.44	13.00	4.17	4.29	4.06	4.81
MnO	.26	.22	.26	.24	.13	.15	.15	.14
MgO	28.60	27.36	28.48	28.44	15.31	15.39	14.55	15.49
CaO	1.01	3.36	.89	1.58	23.44	23.21	22.96	22.93
Na_2O	.01	-	-	-	.43	.42	.42	.32
Cr_2O_3	.41	.49	.39	.57	.68	.74	.74	.53
NiO	-	.12	.10	.08	-	-	-	-
TOTAL	100.26	100.32	100.54	100.77	101.10	100.56	99.11	100.32
cations/ 6 oxygens								
Si	1.9641	1.9604	1.9701	1.9588	1.9302	1.9334	1.9523	1.9486
Ti	.0051	.0054	.0035	.0032	.0087	.0096	.0097	.0088
Al	.0059	.0560	.0541	.0627	.1428	.1267	.1278	.1055
Fe^{2+}	.3926	.3689	.4001	.3855	.1261	.1307	.1252	.1470
Mn	.0079	.0067	.0078	.0072	.0040	.0046	.0047	.0043
Mg	1.5169	1.4563	1.5105	1.5030	.8252	.8357	.7997	.8435
Ca	.0385	.1286	.0339	.0600	.9084	.9062	.9073	.8978
Na	.0007	-	-	-	.0315	.0297	.0300	.0227
Cr	.0012	.0138	.0100	.0160	.0194	.0213	.0216	.0153
Ni	-	.0035	.0029	.0029	-	-	-	-
TOTAL	3.9960	3.9994	3.9939	3.9987	3.9950	3.9979	3.9783	3.9935
Wo	1.98	6.58	1.75	3.08	48.84	48.39	49.52	47.54
En	77.87	74.54	77.68	77.13	44.37	44.63	43.65	44.67
Fs	20.15	18.88	20.57	19.79	6.78	6.98	6.84	7.78
Al/Cr	5.09	4.05	4.93	3.92	7.35	5.94	5.92	6.89
mmf	.794	.798	.791	.796	.867	.865	.865	.852

Sample AT-11 - nos. 1-4 orthopyroxene mottles; 5-8 clinopyroxene mottles.

TABLE A.8-4 ELECTRON MICROPROBE ANALYSIS OF PYROXENES FROM PEGMATITE BODIES IN THE MAIN ZONE, FROM BOREHOLE SK2 AT UNION SECTION

(From Mitchell, in prep.).

	A20/1	A20/2	A20/3	A31/1	A31/2	A31/3	A59/1	A107/1	A107/2	A107/3	A115/1	A115/2	A152/1	A152/2	A152/3
SiO_2	49.23	49.68	49.29	49.37	49.35	49.77	50.34	50.58	49.98	50.59	50.40	50.45	50.70	50.61	50.68
TiO_2	0.42	0.36	0.49	0.41	0.42	0.42	0.16	0.54	0.54	0.54	0.50	0.51	0.48	0.50	0.49
Al_2O_3	1.34	1.29	1.49	0.67	1.49	1.35	0.54	1.40	1.14	1.63	1.60	1.60	1.29	1.34	1.51
FeO	24.26	23.79	23.04	35.84	23.46	23.69	31.59	21.38	24.52	19.24	19.95	18.61	17.42	18.56	20.11
MnO	0.66	0.66	0.67	0.65	0.66	0.66	0.88	0.46	0.46	0.47	0.47	0.47	0.47	0.47	0.47
MgO	6.77	6.82	6.93	9.44	7.39	7.52	14.43	10.16	10.01	9.81	8.89	9.14	9.28	9.22	9.16
CaO	17.46	17.93	18.44	4.57	17.45	17.31	2.62	16.22	13.77	18.27	18.60	20.33	21.11	20.25	18.20
Na_2O	0.17	0.11	0.19	0.18	0.16	0.16	0.00	0.15	0.15	0.14	0.13	0.13	0.12	0.13	0.13
Cr_2O_3	0.00	0.01	0.03	0.00	0.00	0.00	0.01	0.01	0.02	0.04	0.03	0.00	0.00	0.00	0.01
NiO	0.03	0.03	0.03	0.03	0.03	0.03	0.04	0.00	0.00	0.00	0.00	0.00	0.00	0.00	0.00
TOTAL	100.34	100.68	100.60	101.16	100.41	100.91	100.61	100.90	100.60	100.73	100.57	101.24	100.87	101.08	100.76
Recalculated as cations per 6 oxygens															
Si	1.952	1.959	1.944	1.972	1.948	1.954	1.969	1.953	1.953	1.949	1.953	1.941	1.950	1.949	1.958
Ti	0.013	0.011	0.015	0.012	0.012	0.012	0.005	0.016	0.016	0.016	0.015	0.014	0.014	0.014	0.015
Al	0.063	0.060	0.069	0.032	0.069	0.062	0.025	0.064	0.053	0.074	0.073	0.073	0.058	0.061	0.069
Fe	0.805	0.785	0.760	1.197	0.774	0.778	1.033	0.690	0.801	0.620	0.647	0.599	0.560	0.598	0.650
Mn	0.022	0.022	0.022	0.022	0.022	0.022	0.029	0.015	0.015	0.015	0.015	0.015	0.015	0.015	0.015
Mg	0.400	0.401	0.407	0.562	0.435	0.440	0.841	0.585	0.583	0.563	0.514	0.524	0.532	0.529	0.528
Ca	0.742	0.758	0.779	0.196	0.738	0.728	0.110	0.671	0.577	0.754	0.772	0.838	0.870	0.835	0.753
Na	0.013	0.008	0.015	0.014	0.012	0.012	0.000	0.011	0.011	0.010	0.010	0.010	0.009	0.010	0.010
Cr	0.000	0.000	0.001	0.000	0.000	0.000	0.000	0.000	0.001	0.001	0.001	0.000	0.000	0.000	0.000
Ni	0.001	0.001	0.001	0.001	0.001	0.001	0.001	0.000	0.000	0.000	0.000	0.000	0.000	0.000	0.000
At% En	20.56	20.63	20.93	28.75	22.33	22.61	42.39	30.05	29.73	29.08	26.57	26.73	27.11	26.97	27.32
Fs	41.33	40.38	39.04	61.24	39.77	39.97	52.07	35.47	40.87	32.00	33.46	30.54	28.56	30.46	33.66
Wo	38.11	38.99	40.03	10.01	37.90	37.42	5.53	34.48	29.40	38.92	39.97	42.74	44.38	42.57	39.02
MGF	0.332	0.338	0.349	0.319	0.360	0.361	0.449	0.459	0.421	0.476	0.443	0.467	0.487	0.470	0.448

	A172/1	A172/2	A227/1	A227/2	A237/1	A237/2	A237/3	A237/4	A237/5	A252/1	A252/2	A252/3	A320/1	A320/2	A320/3	A320/4
SiO_2	51.68	51.58	50.85	51.50	51.58	50.82	50.85	50.07	51.06	49.05	49.26	51.52	51.87	51.73	51.28	51.26
TiO_2	0.43	0.43	0.43	0.43	0.44	0.43	0.43	0.20	0.44	0.69	0.69	0.69	0.43	0.44	0.44	0.43
Al_2O_3	1.77	1.61	1.55	1.45	2.10	1.64	1.49	0.64	2.27	2.00	1.84	1.42	1.56	1.60	2.51	2.14
FeO	14.80	14.32	15.55	14.73	12.49	17.49	16.35	31.99	12.98	14.40	14.10	13.17	14.18	10.50	12.72	13.93
MnO	0.47	0.47	0.47	0.47	0.47	0.47	0.47	0.64	0.47	0.37	0.37	0.37	0.47	0.47	0.47	0.47
MgO	12.38	12.38	10.73	10.98	11.66	11.29	11.03	14.32	11.96	10.93	11.46	11.90	14.27	13.27	12.72	14.06
CaO	19.90	19.57	21.34	21.68	22.13	18.55	19.66	1.72	21.16	21.23	20.92	21.62	17.69	22.18	21.99	18.68
Na_2O	0.17	0.17	0.18	0.17	0.17	0.18	0.18	0.00	0.17	0.28	0.28	0.27	0.17	0.17	0.17	0.17
Cr_2O_3	0.02	0.03	0.04	0.03	0.10	0.02	0.03	0.02	0.08	0.02	0.01	0.02	0.06	0.02	0.11	0.06
NiO	0.00	0.00	0.00	0.00	0.02	0.02	0.02	0.03	0.02	0.00	0.00	0.00	0.02	0.02	0.02	0.02
TOTAL	101.62	100.56	101.14	101.44	101.16	100.91	100.51	99.63	100.61	98.97	98.92	100.98	100.72	100.40	100.43	101.22
Recalculated as cations per 6 oxygens																
Si	1.940	1.951	1.936	1.947	1.937	1.941	1.946	1.975	1.929	1.907	1.911	1.943	1.947	1.941	1.925	1.920
Ti	0.012	0.012	0.012	0.012	0.012	0.012	0.012	0.006	0.013	0.020	0.020	0.020	0.012	0.012	0.012	0.012
Al	0.078	0.072	0.070	0.065	0.093	0.074	0.067	0.030	0.101	0.092	0.084	0.063	0.069	0.071	0.111	0.094
Fe	0.465	0.453	0.495	0.466	0.392	0.559	0.523	1.055	0.410	0.468	0.457	0.415	0.445	0.330	0.336	0.436
Mn	0.015	0.015	0.015	0.015	0.015	0.015	0.015	0.021	0.015	0.012	0.012	0.012	0.015	0.015	0.015	0.015
Mg	0.693	0.698	0.609	0.619	0.653	0.643	0.629	0.842	0.673	0.633	0.663	0.669	0.798	0.742	0.712	0.785
Ca	0.800	0.793	0.871	0.878	0.890	0.759	0.806	0.073	0.856	0.884	0.869	0.874	0.711	0.892	0.884	0.749
Na	0.012	0.012	0.013	0.012	0.012	0.013	0.013	0.000	0.012	0.021	0.021	0.020	0.012	0.012	0.012	0.012
Cr	0.001	0.001	0.001	0.001	0.003	0.001	0.001	0.001	0.001	0.001	0.000	0.001	0.002	0.001	0.003	0.002
Ni	0.000	0.000	0.000	0.000	0.001	0.001	0.001	0.001	0.002	0.000	0.000	0.000	0.000	0.001	0.001	0.001
TOTAL	4.015	4.007	4.023	4.014	4.009	4.017	4.014	4.004	4.013	4.038	4.038	4.016	4.012	4.017	4.011	4.026
At% En	35.38	35.90	30.84	31.53	33.72	32.78	32.12	42.74	34.71	31.89	33.31	34.17	40.84	37.80	36.83	39.83
Fs	23.73	23.30	25.08	23.73	20.27	28.50	26.72	53.57	21.14	23.58	22.99	21.22	22.77	16.78	17.41	22.14
Wo	40.88	40.80	44.09	44.74	46.01	38.72	41.16	3.69	44.15	44.53	43.70	44.61	36.39	45.42	45.76	38.03
MGF	0.599	0.606	0.552	0.571	0.625	0.535	0.546	0.444	0.622	0.575	0.592	0.617	0.642	0.693	0.679	0.643

APPENDIX 9 ELECTRON MICROPROBE ANALYSIS OF AMPHIBOLE AND MICA

These analyses were performed using the same configuration on the electron microprobe as used for the analysis of pyroxenes, except that K_2O was determined on the left hand spectrometer using the quartz crystal with an orthoclase standard. Iron was analysed as total FeO. The percentage of Fe O was then calculated (see below) assuming Fe_2O_3/FeO equals 0.4, after the method of Allen and Boettcher, 1983). The structural formula was computed for 23 oxygens on a water-free basis, again, using the method of Allen and Boettcher (see below). All analyses are presented in the main text.

REFERENCES

ALLEN, J.C. & BOETTCHER, A.L. (1983) : The stability of amphibole in andesite and basalt at high pressures. Amer. Mineral. 68, 307-314.

```
10  REM CPX RECALCULATIONS
20  PRINT "TYPE IN CPX ANALYSIS (SI/TI/AL/FE/MN/MG/CA/NA/CR/NI)"
30  INPUT A1,B1,C1,D1,E1,F1,G1,H1,I1,J1
40  LET A2=A1/60.09
50  LET B2=B1/79.90
60  LET C2=C1/101.96
70  LET D2=D1/71.85
80  LET E2=E1/70.94
90  LET F2=F1/40.32
100 LET G2=G1/56.08
110 LET H2=H1/61.99
120 LET I2=I1/152.02
130 LET J2=J1/74.41
140 LET A3=2*A2
150 LET B3=2*B2
160 LET C3=3*C2
170 LET I3=3*I2
180 LET K1=A3+B3+C3+D2+E2+F2+G2+H2+I3+J2
190 LET L1=6/K1
200 LET A4=L1*A2
210 LET B4=L1*B2
220 LET C4=L1*C2
222 LET C5=C4*2
230 LET D4=L1*D2
240 LET E4=L1*E2
250 LET F4=L1*F2
260 LET G4=L1*G2
270 LET H4=L1*H2
272 LET H5=H4*2
280 LET I4=L1*I2
282 LET I5=I4*2
290 LET J4=L1*J2
300 LET M1=D4+F4+G4
310 LET N1=(D4/M1)*100
320 LET O1=(F4/M1)*100
330 LET P1=(G4/M1)*100
332  LET P4=A4+B4+C5+D4+E4+F4+G4+H5+I5+J4
334  LET P2=C5/I5
336  LET P3=F4/(F4+D4)
340 PRINT "     SIO2 = "A4
350 PRINT "     TIO2 = "B4
360 PRINT "    AL2O3 = "C5
370 PRINT "      FEO = "D4
380 PRINT "      MNO = "E4
390 PRINT "      MGO = "F4
400 PRINT "      CAO = "G4
410 PRINT "     NA2O = "H5
420 PRINT "    CR2O3 = "I5
430 PRINT "      NIO = "J4
432  PRINT "  TOTAL = "P4
440 PRINT "  WO = "P1"%"
450 PRINT "  EN = "O1"%"
460 PRINT "  FS = "N1"%"
462  PRINT "   AL/CR = "P2
464  PRINT "     MMF = "P3
470 END
```

```
10 REM AMPH RECALCULATIONS
20 PRINT "TYPE IN AMPH ANALYSIS (SI,TI,AL,TFE2,MN,MG,CA,NA,CR,NI,K)"
30 INPUT A1,B1,C1,D1,E1,F1,G1,H1,I1,J1,Y1
31 LET S1=D1*.7773
32 LET S2=S1/1.3599
33 LET S3=S2/.7773
34 LET S4=S1-S2
35 LET S5=S4/.6994
40  LET A2=A1/60.09
50  LET B2=B1/79.90
60  LET C2=C1/101.96
70 LET D2=S3/71.846
80  LET E2=E1/70.94
90  LET F2=F1/40.32
100 LET G2=G1/56.08
110 LET H2=H1/61.99
120 LET I2=I1/152.02
130 LET J2=J1/74.41
132 LET X2=S5/159.694
134 LET Y2=Y1/94.21
140 LET A3=2*A2
150 LET B3=2*B2
160 LET C3=3*C2
165 LET I3=3*I2
170 LET I3=3*I2
180 LET K1=A3+B3+C3+D2+E2+F2+G2+H2+I3+J2+Y2+X3
190 LET L1=23/K1
200 LET A4=L1*A2
210 LET B4=L1*B2
220 LET C4=L1*C2
222 LET C5=C4*2
230 LET D4=L1*D2
240 LET E4=L1*E2
250 LET F4=L1*F2
260 LET G4=L1*G2
270 LET H4=L1*H2
272 LET H5=H4*2
280 LET I4=L1*I2
282 LET I5=I4*2
290 LET J4=L1*J2
292 LET Y4=L1*Y2
293 LET Y5=Y4*2
294 LET X4=L1*X2
296 LET X5=X4*2
300 LET M1=D4+F4+G4
332 LET P4=A4+B4+C5+D4+E4+F4+G4+H5+I5+J4+Y4+X5
334 LET P2=F4/(F4+D4+X5)
336 LET P3=F4/(F4+D4)
340 PRINT "     SIO2 = "A4
350 PRINT "     TIO2 = "B4
360 PRINT "    AL2O3 = "C5
365 PRINT "    FE2O3 = "I5
370 PRINT "      FEO = "D4
380 PRINT "      MNO = "E4
390 PRINT "      MGO = "F4
400 PRINT "      CAO = "G4
410 PRINT "     NA2O = "H5
420 PRINT "    CR2O3 = "I5
430 PRINT "      NIO = "J4
431 PRINT "      K2O = "Y5
432  PRINT "  TOTAL = "P4
434 PRINT "   FEO = "S3
436 PRINT " FE2O3 = "S5
462 PRINT "MG/(MG+FE2+FE3) = "P2
464 PRINT "MG/(MG+FE2) = "P3
```

APPENDIX 10 ELECTRON MICROPROBE ANALYSIS OF Fe-Ti-Cr-OXIDES

Fe-Ti-Cr oxides, including chromium-spinel, iron-titanium-spinel and ilmenite were analysed on the electron microprobe using the following configuration :

Left Hand Spectrometer : (LiF crystal) Cr_2O_3 (Chromite)
NiO, FeO (Nickel magnetite)
TiO_2 (Ilmenite)
MnO (Rhodonite)

Right Hand Spectrometer : (RAP crystal) MgO (Synthetic spinel)
Al_2O_3 (Synthetic spinel)

Vanadium and zinc were not analysed for. Total iron was determined as FeO. The percentage of Fe_2O_3 was then calculated assuming structural stochiometry using one of two recalculation programs :

(1) An in-house computer program developed by H.V. Eales ("Spinel 3") which assumes a structural formulae (stoichometry is adjusted during the calculation of Fe_2O_3) based on 32 oxygens. This method was used for all Cr-rich spinels (chromites and chromium-magnetites). The recalculated cations sum to 24.000 (see below).

(2) For chromium-poor spinels (less than 2 wt. percent Cr_2O_3) and ilmenites the recalculation technique of Stormer (1983) was used. In this method the cations sum to 3.000 for magnetite and 2.000 for ilmenite. This technique also calculates the mole fractions of ilmenite and ulvospinel (see below).

The results of analyses not discussed in the main text are presented in the following Tables :

TABLE A.10-1 : Electron microprobe analysis of chromites from cumulates in the upper critical zone at Amandelbult.

TABLE A.10-2 : Electron microprobe analysis of Fe-Ti oxides from pegmatite bodies in the main zone in borehole SK2, Union Section (from Mitchell, in prep.).

REFERENCES

MITCHELL, A.A. : The geochemistry and origin of the main zone, western Bushveld Complex. Ph.D thesis (in prep.), Rhodes Univ., Grahamstown.

STORMER, J.C. (1983) : The effects of recalculation on estimates of temperature and oxygen fugacity from analyses of multicomponent iron-titanium oxides. Amer. Mineral. 68, 586-594.

```
10  PRINT "MODIFIED SPINELJ PROGRAM (RHODES GEOL DEPT)"
20  PRINT "  "
30  DIM A(8)
40  DIM B(8)
50  DIM C(8)
54  DIM D(8)
56  DIM E(8)
60  FOR I=1 TO 6
70  READ A(I)
80  NEXT I
85 PRINT "SAMPLE NUMBER"
86 INPUT Z$
90  PRINT "INPUT CHROMITE ANALYSIS IN ORDER (TI/AL/FE/MN/MG/CR)"
100 INPUT B(1),B(2),B(3),B(4),B(5),B(6)
110 FOR I=1 TO 6
120 LET C(I)=B(I)/A(I)
130 NEXT I
140 IF C(3)<(2*C(1)) THEN 300
150 LET C(3)=C(3)-(2*C(1))
160 LET M=C(5)+C(4)
170 LET M=M-C(6)-C(2)
180 IF M<0 THEN 200
190 IF M>C(3)/2 THEN 260
200 LET C(7)=(C(3)+M)/3
210 IF C(7)<0 THEN C(7)=0
220 LET B(7)=C(7)*159.70
230 LET C(3)=C(3)-(2*C(7))+(2*C(1))
240 LET B(3)=C(3)*A(3)
250 GO TO 300
260 LET C(7)=C(3)/3
270 LET B(7)=C(7)*159.70
280 LET C(3)=2*C(1)
290 LET B(3)=C(3)*A(3)
300 REM O = NO OXYGENS
310 LET O=(2*C(1))+(3*C(6))+(3*C(2))+(3*C(7))+C(3)+C(5)+C(4)
320 LET O=32/O
330 LET D(1)=(C(1)*O*10000)/10000
340 LET D(2)=(C(2)*O*20000)/10000
350 LET D(3)=(C(3)*O*10000)/10000
360 LET D(4)=(C(4)*O*10000)/10000
370 LET D(5)=(C(5)*O*10000)/10000
380 LET D(6)=(C(6)*O*20000)/10000
390 LET D(7)=(C(7)*O*20000)/10000
400 LET E(3)=D(3)-D(1)
410 LET T=B(1)+B(2)+B(3)+B(4)+B(5)+B(6)+B(7)
415 PRINT "SAMPLE NUMBER = "Z$
420 PRINT "ANALYSIS","WEIGHTI","CATIONS"
430 PRINT "TIO2",B(1),D(1)
440 PRINT "FEO"," -",D(1)
450 PRINT "CR2O3",B(6),D(6)
460 PRINT "AL2O3",B(2),D(2)
470 PRINT "FE2O3",B(7),D(7),"SUM: ";(D(1)*2)+D(6)+D(2)+D(7)
480 PRINT "FEO",B(3),E(3)
490 PRINT "MGO",B(5),D(5)
500 PRINT "MNO",B(4),D(4),"SUM: ";E(3)+D(5)+D(4)
510 PRINT "TOTAL",(INT(T*100))/100
520 PRINT "  "
530 PRINT "FE3/FE3+octFE2 = ";TAB(21);
540 PRINT (D(7)/(D(7)+E(3))*1000)/1000
550 PRINT "FE3/FE3+totFE2 = ";TAB(21);
560 PRINT (D(7)/(D(7)+D(3))*1000)/1000
570 PRINT "FE3/FE3+AL+CR = ";TAB(21);
580 PRINT (D(7)/(D(7)+D(2)+D(6))*1000)/1000
590 PRINT "MG/MG+octFE2 = ";TAB(21);
600 PRINT (D(5)/(D(5)+E(3))*1000)/1000
610 PRINT "MG/MG+totFE2 = ";TAB(21);
620 PRINT (D(5)/(D(5)+D(3))*1000)/1000
630 DATA 79.90,101.96,71.85,70.94,40.32,152.02
640 END
```

```
10 REM THIS PROGRAM COMPUTES ILMENITE AND MAGNETITE END-MEMBERS AND FE2O3 FOR EACH
14 PRINT "THIS PROGRAM CALCS IL OR MT END-MEMBERS & FE2O3 (STORMER,1983)"
16 PRINT "  "
17 PRINT "  ILMENITE? (Y OR N)"
18 INPUT A$
19 PRINT "SAMPLE NO"
20 INPUT B$
25 PRINT "TYPE IN ANALYSIS (TI,AL,FE2,MN,MG,CR)"
30 INPUT A1,B1,C1,D1,E1,F1
40 LET A2=A1/79.90
50 LET B2=(B1/101.96)*2
60 LET C2=C1/71.85
70 LET D2=D1/70.94
80 LET E2=E1/40.32
90 LET F2=(F1/152.02)*2
95 LET M1 = (A2+B2+C2+D2+E2+F2)
100 IF A$ = "N" THEN 108
105 LET G1=2/M1
106 GOTO110
108 LET G1=3/M1
110 LET A3=A2*G1
120 LET B3=B2*G1
130 LET C3=C2*G1
140 LET D3=D2*G1
150 LET E3=E2*G1
160 LET F3=F2*G1
170 LET H1=A3*4
180 LET I1=(C3+D3+E3)*2
190 LET J1=(B3+F3)*3
192 IF A$="Y" THEN 200
194 LET K1=ABS((H1+I1+J1)-8)
196 GOTO210
200 LET K1=ABS((H1+I1+J1)-6)
210 LET G3=((K1/G1)*159.70)/2
220 LET C4=((C3-K1)/G1)*71.85
230 LET G4=((G3/159.70)*2)*G1
240 LET C5=(C4/71.85)*G1
250 REM CALC OF END-MEMBER
252 IF A$="Y" THEN 260
254 LET I1=(A3*(C5/(C5+E3+D3)))/((0.5*G4)*(G4/(G4+B3+F3)))
256 GOTO270
260 LET X1=(SQR(C5*A3))/((0.5*G4)+(SQR(C5*A3)))
270 LET X2=I1*100
275 LET X3=A1+B1+C4+G3+D1+E1+F1
276 LET I1=A3+B3+C5+G4+D3+E3+F3
278 PRINT "SAMPLE NUMBER = "B$
280 PRINT "  OXIDE       WT%          CATIONS"
290 PRINT "   TIO2       "A1"           "A3
300 PRINT "  AL2O3          "B1"       "B3
310 PRINT "    FEO        "C4"          "C5
320 PRINT "  FE2O3        "G3"         "G4
330 PRINT "    MNO          "D1"       "D3
340 PRINT "    MGO        "E1"         "E3
350 PRINT "  CR2O3          "F1"       "F3
355 PRINT "  TOTAL      "X3"          "I1
360 PRINT "  "
362 IF A$="Y" THEN 370
364 PRINT "  I ULVOSPINEL = "I2
366 GOTO380
370 PRINT "  I ILMENITE = "I2
380 END
```

TABLE A.10-1 ELECTRON MICROPROBE ANALYSIS OF CHROMITES FROM CUMULATES

IN THE UPPER CRITICAL ZONE AT AMANDELBULT

	1	2	3	4	5	6	7	8	9	10	11	12	13	14	15	16	17	18
wt.%																		
TiO_2	1.80	1.89	1.82	1.59	1.59	1.87	.86	.96	.92	.82	.93	1.12	1.07	.97	1.02	.97	.94	.93
Cr_2O_3	43.29	44.24	44.11	44.58	44.31	46.50	40.87	40.79	41.28	41.12	41.10	41.73	38.63	37.80	39.37	39.40	41.07	40.54
Al_2O_3	16.79	16.44	16.72	17.03	16.53	18.17	17.41	17.47	16.75	17.84	17.27	14.96	23.35	23.43	22.90	23.27	20.78	20.35
Fe_2O_3	5.65	4.94	5.02	4.81	5.30	9.44	9.37	9.35	9.16	8.77	8.84	8.63	6.36	7.07	6.22	6.31	6.63	7.10
FeO	25.81	25.61	25.88	25.45	25.54	22.56	23.23	23.18	23.05	23.38	23.63	25.24	23.86	22.72	23.94	24.55	24.85	24.30
MgO	6.61	6.75	6.63	6.82	6.62	8.27	7.65	7.76	7.58	7.59	7.36	5.80	8.49	9.02	8.39	8.16	7.49	7.61
MnO	.47	.47	.46	.48	.49	.45	.48	.50	.52	.51	.49	.57	.50	.49	.47	.50	.52	.50
TOTAL	100.43	100.34	100.64	100.77	100.39	100.26	99.87	100.01	99.26	100.03	99.62	98.06	102.26	101.50	102.32	103.17	102.27	101.32
cations (sum = 24.000)																		
Ti	.3551	.3733	.3584	.3119	.3141	.1692	.1691	.1883	.1825	.1837	.1837	.2291	.1997	.1815	.1907	.1801	.1785	.1782
Fe^{2+}	.3551	.3733	.3584	.3119	.3141	.1692	.1691	.1883	.1825	.1837	.1837	.2291	.1997	.1815	.1907	.1801	.1785	.1782
Cr	8.9806	9.1873	9.1332	9.1950	9.2042	8.2837	8.4504	8.4151	8.6091	8.5372	8.5372	8.9765	7.5811	7.4393	7.7416	7.6932	8.2000	8.1698
Al	5.1915	5.0886	5.1600	5.2354	5.1178	5.5393	5.3654	5.3719	5.2067	5.3468	5.3468	4.7966	6.8301	6.8792	6.7117	6.7723	6.1839	6.1125
Fe^{3+}	1.1173	.9772	.9898	.9456	1.0495	1.8383	1.8458	1.8362	1.8190	1.7484	1.7484	1.7680	1.1892	1.3245	1.1650	1.1741	1.2590	1.3610
Fe^{2+}	5.4102	5.2525	5.3097	5.2418	5.2983	4.7122	4.9115	4.8712	4.9032	5.0086	5.0086	5.5163	4.7535	4.3498	4.7905	4.8914	5.0692	5.0006
Mg	2.5853	2.6428	2.5882	2.6521	2.5926	3.1891	2.9822	3.0183	2.9805	2.8823	2.8823	2.3523	3.1413	3.3469	3.1105	3.0040	2.8195	2.8914
Mn	.1044	.1045	.1020	.1060	.1090	.0986	.1063	.1105	.1161	.1090	.1090	.1313	.1051	.1033	.0990	.1045	.1112	.1079
R1	.173	.156	.157	.152	.165	.280	.273	.273	.270	.258	.258	.242	.200	.225	.195	.193	.198	.213
R2	.164	.147	.148	.145	.157	.273	.266	.266	.263	.252	.251	.235	.198	.218	.189	.187	.193	.208
R3	.073	.064	.064	.061	.068	.117	.117	.117	.116	.109	.111	.113	.075	.084	.074	.075	.080	.087
R4	.327	.334	.327	.335	.328	.403	.377	.382	.378	.373	.365	.298	.397	.423	.393	.380	.357	.366
R5	.313	.319	.313	.323	.315	.395	.369	.373	.369	.365	.356	.290	.388	.414	.384	.371	.349	.388

1-5 : Merensky Reef top chromitite seam (sample AA-4; 1-middle;5-top,in contact with orthopyroxene)

6-12 : Merensky Reef bottom chromitite seam (sample AT-14; 6,9,10,11-discrete grains comprising seam; 7-in f/w enclosed by plagioclase; 3,12-intragranular and intergranular grains respectively, associated with orthopyroxene in Merensky Reef).

13-18 : Thin chromitite seam above P1 (sample AH-4; 13,15,16-cores of discrete grains comprising seam ; 14-margin of grain 13; 17,18-intergranular grains enclosed in orthopyroxene in P1).

R1 = Fe^{3+} / Fe^{3+} + Fe^{2+} (octahedral); R2 = Fe^{3+} / Fe^{3+} + Fe^{2+} (total); R3 = Fe^{3+} / Fe^{3+} + Al + Cr; R4 = Mg / Mg + Fe^{2+} (octahedral); R5 = Mg / Mg + Fe^{2+}(total).

TABLE A.10-2 ELECTRON MICROPROBE ANALYSIS OF CHROMITES FROM PEGMATITE BODIES

IN THE MAIN ZONE, FROM BOREHOLE SK2 AT UNION SECTION

(From Mitchell, in prep.).

	A31/1	A31/2	A31/3	A31/4	A31/5	A56/1	A59/2	A59/3	A59/4	A107/1	A107/2	A107/3	A172/1	A172/2	A227/1
TiO_2	50.89	20.31	51.03	12.78	17.00	48.40	48.33	6.89	6.07	50.66	13.26	50.94	50.78	12.23	49.29
Al_2O_3	0.21	3.01	0.27	2.09	3.57	0.26	0.29	1.76	2.69	0.23	4.07	0.32	0.23	2.46	0.26
FeO	43.95	49.21	44.04	42.55	46.46	40.94	41.14	34.95	36.52	43.70	42.39	43.57	44.38	41.59	42.75
Fe_2O_3	5.00	25.14	4.63	42.03	31.58	10.06	9.35	52.29	53.88	4.57	37.34	4.57	5.53	41.31	8.28
MnO	0.63	0.51	0.66	0.35	0.41	1.20	1.34	0.40	0.32	0.71	0.44	0.66	0.86	0.33	0.90
MgO	0.66	0.14	0.66	0.28	0.25	0.77	0.54	1.02	0.14	0.64	0.39	0.68	0.23	0.27	0.37
Cr_2O_3	0.00	0.04	0.02	0.09	0.05	0.01	0.00	0.04	0.09	0.02	0.04	0.00	0.04	0.20	0.05
Total	101.34	98.36	101.31	100.17	99.32	101.64	100.99	97.35	99.71	100.53	97.93	100.84	102.05	98.39	101.90
Ti	0.95	0.58	0.95	0.36	0.48	0.90	0.91	0.20	0.17	0.95	0.38	0.95	0.94	0.35	0.92
Al	0.00	0.13	0.00	0.09	0.16	0.00	0.00	0.08	0.12	0.00	0.18	0.00	0.00	0.11	0.00
Fe^{2+}	0.91	1.55	0.91	1.33	1.45	0.85	0.86	1.13	1.15	0.91	1.34	0.91	0.92	1.32	0.89
Fe^{3+}	0.09	0.71	0.09	1.18	0.89	0.19	0.18	1.52	1.53	0.09	1.06	0.09	0.10	1.18	0.15
Mn	0.01	0.02	0.01	0.01	0.01	0.03	0.03	0.01	0.01	0.02	0.01	0.01	0.02	0.01	0.02
Mg	0.02	0.01	0.02	0.02	0.01	0.03	0.02	0.06	0.01	0.02	0.02	0.03	0.01	0.02	0.01
Cr	0.00	0.00	0.00	0.00	0.00	0.00	0.00	0.00	0.00	0.00	0.00	0.00	0.00	0.01	0.00

	A237/1	A237/2	A237/3	A237/4	A252/1	A252/2	A252/3	A252/4	A252/5	A252/6	A348/1	A348/2	A348/3	A348/4
TiO_2	6.42	49.22	50.73	6.89	4.09	51.33	14.07	2.23	4.90	50.66	50.91	13.60	51.37	12.96
Al_2O_3	2.31	0.30	0.31	3.25	1.61	0.23	11.79	1.43	1.99	0.23	0.28	4.49	0.24	4.11
FeO	36.89	42.80	43.87	38.31	34.34	42.78	43.58	33.53	33.27	43.28	42.04	43.28	42.33	42.49
Fe_2O_3	54.03	8.57	5.28	52.32	58.83	4.10	31.19	64.15	57.34	4.90	5.74	38.12	5.18	39.63
MnO	0.27	0.91	1.41	0.23	0.16	1.14	0.47	0.08	0.15	1.23	0.56	0.23	0.60	0.33
MgO	0.37	0.30	0.18	0.03	0.34	1.25	2.09	0.24	0.42	0.58	1.78	0.93	1.83	0.79
Cr_2O_3	0.73	0.03	0.08	0.88	0.29	0.04	0.28	0.33	0.34	0.03	0.03	0.87	0.03	0.92
Total	101.02	102.16	101.86	101.93	99.68	100.87	103.47	101.99	100.41	100.93	101.36	101.54	101.58	101.41
Ti	0.18	0.92	0.95	0.19	0.12	0.96	0.36	0.06	0.09	0.95	0.94	0.37	0.95	0.35
Al	0.10	0.01	0.01	0.14	0.07	0.01	0.47	0.06	0.09	0.01	0.01	0.19	0.01	0.18
Fe^{2+}	1.15	0.89	0.91	1.18	1.09	0.89	1.24	1.03	1.11	0.90	0.87	1.31	0.87	1.30
Fe^{3+}	1.52	0.16	0.10	1.45	1.69	0.08	0.80	1.80	1.62	0.09	0.11	1.04	0.10	1.09
Mn	0.01	0.02	0.03	0.01	0.01	0.02	0.01	0.00	0.00	0.03	0.01	0.01	0.01	0.01
Mg	0.02	0.01	0.01	0.00	0.02	0.05	0.11	0.01	0.02	0.02	0.07	0.05	0.07	0.04
Cr	0.02	0.00	0.00	0.03	0.01	0.00	0.01	0.01	0.01	0.00	0.00	0.02	0.00	0.03

APPENDIX 11 ELECTRON MICROPROBE ANALYSIS OF PLAGIOCLASE

The following configuration was used for the electron microprobe analysis of plagioclase and its alteration products clinozoisite-epidote :

Left Hand Spectrometer : (Quartz crystal)	CaO (Pyroxene)
	FeO (Ilmenite)
	K_2O (Orthoclase)
Right Hand Spectrometer : (KAP crystal)	SiO_2 (Pyroxene)
	Na_2O (Jadeite)
	Al_2O_3 (Synthetic spinel)

All plagioclase analyses completed by the author are presented in the main text. Total iron was analysed as FeO. The percentage of Fe_2O_3 has not been calculated. Plagioclase analyses were recalculated for cations using a computer program provided by A.A. Mitchell.

APPENDIX 12 ELECTRON MICROPROBE ANALYSIS OF SULPHIDES

Electron microprobe analyses of sulphide phases were determined on the authors samples at Johannesburg Consolidated Investment Minerals Processing and Research Laboratory (P.O. Box 13017, Knights, Johannesburg, 2000). The co-operation of Mr. E. Kinloch and his assistants is gratefully ack nowledged. These samples were analysed by either wave length dispersive (WDS) or energy dispersive (EDS) spectrometers. WDS gives maximum accuracy, whereas EDS techniques may be considered to be inaccurate for low levels of con centration. EDS analysis of cobalt is hampered due to interference effects of iron. Because of these features the analytical technique used is also recorded.

Samples from Amandelbult are divided into four groups :

A. Sulphides from iron-rich ultramafic pegmatite which replaces the Merensky Reef e.g., the Replaced Reef.
B. Sulphides from "typical" iron-rich ultramafic pegmatite.
C. Sulphides from the Middellaagte iron-rich ultramafic pegmatite body.
D. Cumulate-hosted sulphides from normal Merensky Reef.

Samples from Driekop and Mooihoek are divided into groups E, F, and G.

TABLE A.12-1 : Electron microprobe analysis of pyrrhotites

TABLE A.12-2 : Electron microprobe analysis of pentlandites

TABLE A.12-3 : Electron microprobe analysis of chalcopyrites and cubanites

TABLE A.12-4 : Electron microprobe analysis of sulphides from the platiniferous ultramafic pipes.

TABLE A.12-1 ELECTRON MICROPROBE ANALYSIS OF PYRRHOTITES

	A1		A2		A3		A4	A5	A6	A7	A8	A9	A10	A11	B1	B2	B3
wt %																	
S	38.17	35.97	38.05	36.10	38.14	35.36	37.05	38.62	38.80	36.64	38.63	36.65	37.63	37.08	39.16	39.06	37.14
Fe	59.96	62.28	59.91	62.42	60.45	62.91	62.47	61.06	61.07	63.29	60.63	63.12	63.60	62.34	61.03	61.17	63.27
Co	.09	.07	.10	n.d.	n.d.	n.d.	.14	.14	.08	.08	n.d.	n.d.	-	-	.09	.09	n.d.
Ni	.14	n.d.	.16	n.d.	.12	n.d.	.19	.22	.08	n.d.	n.d.	n.d.	-	-	.13	.18	n.d.
TOTAL	98.36	98.32	98.22	98.52	98.71	98.67	99.85	100.04	100.06	100.01	99.26	99.77	101.21	99.42	100.41	100.50	100.41
at %																	
S	52.30	50.12	52.42	50.19	52.31	49.89	50.69	52.28	52.49	50.18	52.60	50.28	50.75	50.89	52.69	52.55	50.56
Fe^{2+}	47.33	49.82	47.38	49.81	47.60	50.11	49.06	47.45	47.39	49.76	47.40	49.72	49.25	49.11	47.14	47.25	49.44
Co	.07	.05	.08	-	-	-	.10	.10	.06	.06	-	-	-	-	.07	.07	-
Ni	.10	-	.12	-	.09	-	.14	.16	.06	-	-	-	-	-	.10	.13	-
M:S	.905	.995	.908	.992	.912	1.004	.973	.913	.905	.993	.901	.989	.970	.965	.900	.903	.978
Phase	Hex.	Troil.	Hex.	Troil.	Hex.	Troil.	Troil.	Hex.	Hex.	Troil.	Hex.	Troil.	Troil.	Troil.	Hex.	Hex.	Troil.
Anal.	WDS	WDS	WDS	WDS	WDS	WDS	WDS	WDS	WDS	WDS	WDS	WDS	EDS	EDS	WDS	WDS	WDS

	B4	B5	B6	B7	B8	C1	C2	C3	C4	C5	D1	D2	D3	D4	D5	D6
wt %																
S	36.80	37.76	38.54	38.23	36.69	36.37	35.74	36.22	36.14	36.86	36.42	36.37	36.77	38.98	38.93	39.44
Fe	63.39	62.32	61.88	61.35	64.96	64.20	62.60	63.11	63.41	64.86	64.60	63.82	64.13	62.69	62.21	60.53
Co	n.d.	-	-	-	-	-	-	-	-	-	-	-	-	-	-	-
Ni	n.d.	-	-	-	-	-	-	-	-	-	-	-	-	-	-	-
TOTAL	100.19	100.88	101.42	99.58	101.65	100.57	98.33	99.33	99.55	101.33	101.02	100.18	100.91	101.67	101.14	99.97
at %																
S	50.28	51.35	52.03	52.05	49.59	49.67	49.86	50.00	49.82	49.90	49.55	49.82	49.97	52.00	52.16	53.15
Fe^{2+}	49.72	48.65	47.97	47.95	50.41	50.33	50.14	50.00	50.18	50.10	50.45	50.18	50.03	48.00	47.84	46.83
Co	-	-	-	-	-	-	-	-	-	-	-	-	-	-	-	-
Ni	-	-	-	-	-	-	-	-	-	-	-	-	-	-	-	-
M:S	.989	.942	.922	.921	1.017	1.013	1.006	1.000	1.007	1.004	1.018	1.007	1.001	.923	.917	.881
Phase	Troil.	?	Hex.	Hex.	Troil.	Troil.	Troil.	Troil.	Troil.	Troil.	Troil.	Troil.	Troil.	Hex.	Hex.	Hex(?)
Anal.	WDS	EDS	EDS	EDS	EDS	EDS	EDS	EDS	EDS	EDS	EDS	EDS	EDS	EDS	EDS	EDS

n.d. : not detected; - not analysed; Troil. : Troilite; Hex. : Hexagonal pyrrhotite; M:S - cations $(Fe^{2+} + Co + Ni)/S$;

GROUP A : Ultramafic pegmatite "replaced" Merensky Reef, Amandelbult.
1 - 3: Sample AG-6C (intergrowths of troilite and hexagonal pyrrhotite); 4 - 9: Sample AG-8; 10: Sample AG-13A; 11: Sample Z7 -F1.
GROUP B : Ultramafic pegmatite , Amandelbult.
1-4: Sample MS - 6; 5: Sample AH-21; 6 - 7: Sample AH-19; 8: Sample AE-32.
GROUP C : Ultramafic pegmatite , Middellaagte Pipe.
1 - 3: Sample GM-3; 4 - 5: Sample MLZ2-5.
GROUP D : Cumulates , Amandelbult.
1 - 3: Sample AK-1D (Merensky Reef adjacent to pegmatite body); 4 - 5: Sample Z7 -C1 (as AK-1D); 6: Sample AM-5 (F/W anorthosite).

TABLE A.12-4 ELECTRON MICROPROBE ANALYSIS OF SULPHIDES FROM THE

THE PLATINIFEROUS ULTRAMAFIC PIPES

	E1	E2	E3	E4	E5	F1	F2	F3	F4	F5
wt %										
S	33.71	34.12	34.54	33.93	34.40	33.64	34.28	34.66	34.40	32.69
Fe	40.11	37.62	39.40	39.90	39.88	34.89	36.55	31.94	32.99	34.91
Co	4.31	5.03	5.17	4.79	4.64	1.02	1.52	2.39	2.33	1.49
Ni	22.88	23.87	22.14	22.16	22.48	30.28	29.64	33.88	32.50	29.15
TOTAL	101.01	100.64	101.25	100.78	101.40	99.83	101.99	102.87	102.22	98.24

	G1	G2	G3	G4
wt %				
S	37.94	38.31	37.98	37.93
Fe	62.21	62.29	62.23	62.59
TOTAL	100.15	100.60	100.21	100.51

NOTE : All analyses here by EDS.

GROUP E : PENTLANDITES, CORE OF THE MOOIHOEK PIPE (Sample MO-2).
GROUP F : PENTLANDITES,) MAIN BODY OF THE DRIEKOP PIPE
GROUP G : PYRRHOTITES,) (Sample DR-10).
(For averages and cations see text)

TABLE A.12-2 ELECTRON MICROPROBE ANALYSIS OF PENTLANDITES

	A1	A2	A3	A4	A5	A6	A7	A8	A9	A10	A11	A12	A13	A14	A15	B1
wt %																
S	33.05	32.20	32.95	33.05	32.71	33.52	33.39	33.42	33.45	33.39	33.33	33.36	33.24	33.24	33.27	33.01
Fe	30.93	30.45	28.82	29.54	29.35	32.20	32.10	31.91	31.87	31.31	30.49	30.60	30.94	29.95	32.66	31.94
Co	8.31	8.57	9.64	9.17	9.14	7.71	7.53	7.63	7.49	7.64	8.47	7.82	8.07	6.97	5.84	7.23
Ni	28.17	28.45	28.28	28.63	28.77	27.29	27.52	27.84	28.22	28.24	27.99	28.53	27.68	28.30	27.63	28.07
Cu	n.d.	n.d.	.37	n.d.	n.d.	n.d.	n.d.	n.d.	n.d.	.59	.38	n.d.	n.d.	-	-	n.d.
TOTAL	100.46	99.67	100.06	100.39	99.67	100.72	100.54	100.80	101.03	101.17	100.66	100.31	99.93	98.46	99.40	100.25
at %																
S	46.74	46.06	46.96	46.79	46.57	47.16	47.04	46.99	46.99	47.06	47.13	47.14	47.15	-	-	46.75
Fe^{2+}	25.11	25.00	23.57	24.01	23.99	26.00	25.99	25.77	25.69	25.34	24.75	24.83	25.19	-	-	25.97
Co	6.39	6.65	7.47	7.06	7.07	5.90	5.78	5.82	5.72	5.86	6.51	6.01	6.23			5.57
Ni	21.75	22.23	22.00	22.14	22.37	20.96	21.18	21.38	21.64	21.74	21.61	22.02	21.44	-	-	21.71
Ni/Fe*	.87	.89	.93	.92	.93	.81	.81	.83	.84	.86	.87	.89	.86	-	-	.84
Ni/Ni+Co	.77	.77	.75	.76	.76	.78	.79	.79	.79	.79	.77	.79	.77	-	-	.80
M:S	9.12	9.36	9.04	9.10	9.18	8.97	9.01	9.02	9.03	9.00	8.99	8.97	8.97	-	-	9.11
Anal.	WDS	WDS	WDS	WDS	WDS	WDS	WDS	WDS	WDS	WDS	WDS	WDS	WDS	EDS	EDS	WDS

	B2	B3	B4	B5	C1	D1	D2	D3	D4	D5	D6	D7	D8	D9	D10	D11
wt %																
S	33.64	32.82	33.20	33.22	32.99	33.89	33.91	33.56	33.61	33.28	34.06	33.40	33.12	33.45	32.65	33.21
Fe	31.85	31.66	30.62	29.85	32.31	33.25	34.92	34.28	33.75	35.86	34.80	33.58	34.56	35.28	29.60	30.69
Co	7.08	6.01	4.70	6.10	5.30	.38	.20	.26	.66	.20	.19	n.d.	.26	.34	.33	.14
Ni	28.07	27.37	29.18	29.20	26.25	32.65	31.63	31.76	31.47	29.36	29.21	31.46	29.97	30.28	34.95	32.96
TOTAL	100.64	97.86	97.70	98.30	96.94	100.17	100.67	99.86	99.49	98.70	98.27	98.44	97.92	99.35	97.54	97.00
at %																
S	47.31	-	-	-	-	47.73	47.54	47.45	47.65	47.54	48.60	47.81	47.68	47.50	47.38	48.28
Fe^{2+}	25.71	-	-	-	-	26.87	28.10	27.82	27.47	29.40	28.50	27.60	28.56	28.76	24.66	25.45
Co	5.42	-	-	-	-	.29	.15	.20	.71	.16	.15	-	.20	.26	.26	.11
Ni	21.56	-	-	-	-	25.11	24.21	24.52	24.37	22.90	22.76	24.59	23.56	23.48	27.70	26.16
Ni/Fe*	.84	-	-	-	-	.93	.86	.88	.89	.78	.80	.89	.82	.82	1.12	1.03
Ni/Ni+Co	.80	-	-	-	-	.99	.99	.99	.97	.99	.99	-	.99	.99	.99	.99
M:S	8.91	-	-	-	-	8.80	8.83	8.86	8.82	8.83	8.46	8.73	8.78	8.78	8.88	8.57
Anal.	WDS	EDS	EDS	EDS	EDS	EDS	EDS	EDS	EDS	EDS	EDS	EDS	EDS	EDS	EDS	EDS

n.d.: not detected; - not analysed; * atomic ratios; M:S ratio = (Fe + Co + Ni) / S

GROUP A : Ultramafic pegmatite "replaced" Merensky Reef, Amandelbult.
1 - 5: Sample AG-6C; 6 - 13: Sample AG-13; 14: Sample AG-1A; 15: Sample 27 -F1.

GROUP B : Ultramafic pegmatite, Amandelbult.
1 -2: Sample MS-6; 3: Sample AE-32; 4: Sample AH-19; 5: Sample AH-21.

GROUP C : Ultramafic pegmatite, Middellaagte Pipe.
1: Sample ML22-5.

GROUP D : Cumulates, Amandelbult.
1 - 9: Samples of normal Merensky Reef (27 -E1;AG-1B;AK-1D) ;

TABLE A.12-3 ELECTRON MICROPROBE ANALYSIS OF CHALCOPYRITES AND CUBANITES

	A1	A2	A3	A4	A5	A6	A7	A8	A9	A10	A11	A12	A13	A14	A15	A16	A17
wt %																	
S	34.51	34.46	34.04	34.44	34.44	34.95	34.97	34.61	34.75	35.09	34.90	35.14	34.47	35.30	35.87	35.80	35.41
Fe	30.31	30.47	30.15	30.62	31.11	31.29	32.40	31.36	32.21	30.99	40.27	40.48	41.14	40.88	41.93	42.21	42.02
Cu	33.54	33.21	34.19	34.16	33.75	33.27	33.05	32.62	32.52	33.46	23.04	23.29	22.67	22.41	22.78	22.91	22.38
TOTAL	98.36	98.41	98.38	99.22	99.30	99.51	100.43	98.59	99.48	99.54	98.21	98.91	98.28	98.59	100.58	100.92	99.81
Phase	CP	CP	CP	CP	CP	CP	CP	CP	CP	CP	CUB	CUB	CUB	CUB	CUB	CUB	CUB
Anal.	WDS	WDS	WDS	WDS	WDS	EDS	EDS	EDS	EDS	EDS	WDS	WDS	WDS	WDS	EDS	EDS	EDS

	B1	B2	B3	B4	B5	B6	C1	C2	C3	D1	D2	D3	D4	D5	D6	D7	D8
wt %																	
S	35.12	35.22	35.37	35.57	35.78	35.64	35.37	35.18	35.49	35.71	35.49	35.60	35.35	34.61	35.27	35.31	34.87
Fe	30.28	30.66	31.23	40.69	41.22	42.13	41.24	41.08	40.97	41.90	31.70	31.65	31.42	31.16	30.50	30.54	30.56
Cu	33.68	33.61	33.52	22.60	22.74	22.46	22.68	22.51	21.83	22.50	33.46	34.02	33.67	33.08	33.11	33.23	33.66
TOTAL	99.09	99.49	100.12	98.86	99.74	100.24	99.29	98.77	98.29	100.11	100.64	101.26	100.43	98.35	98.88	99.07	99.08
Phase	CP	CP	CP	CUB	CUB	CUB	CUB	CUB	CUB	CUB	CP	CP	CP	CP	CP	CP	CP
Anal.	WDS	WDS	EDS	WDS	WDS	EDS	EDS	EDS	EDS	EDS	EDS	EDS	EDS	EDS	EDS	EDS	EDS

CP: Chalcopyrite; CUB: Cubanite.

GROUP A : Ultramafic pegmatite "replaced" Merensky Reef", Amandelbult (Samples AG-1A;AG-6C;AG-8;AG-13A;27 -D1;27 -D2).
GROUP B : Ultramafic pegmatite, Amandelbult (Samples MS-6;AH-19;AE-32).
GROUP C : Ultramafic pegmatite, Middellaagte (Samples ML22-5;GM-5).
GROUP D : Cumulates, Amandelbult (Samples of normal Merensky Reef, 27 -E1;AG-1B;AK-1D).

APPENDIX 13 CALCULATION OF THEORETICAL FRACTIONATION CURVES FOR THE DISTRIBUTION OF NiO AND MgO BETWEEN OLIVINE AND SILICATE LIQUID

1. PARTITIONING OF Mg AND Fe BETWEEN OLIVINE AND SILICATE LIQUID

The distribution of Mg and Fe^{2+} between olivine (oliv) and silicate liquid (liq) may be expressed by the distribution coefficient K_D, thus :-

$$K_D = (X_{FeO} / X_{MgO})^{oliv} * (X_{MgO} / X_{FeO})^{liq} \quad ....(1)$$

where X_{MgO} and X_{FeO} are mole fractions.

Roeder and Emslie (1970) obtained an average value of K_D of 0.3.

If equilibrium conditions are assumed the MgO / FeO ratio of a silicate liquid may be calculated from knowledge of the olivine composition. For example, consider olivine with a composition of Fo_{44}. Substituting in, and rearranging formulae (1) :-

$$(X_{MgO} / X_{FeO})^{oliv} = (\text{mol.\% Fo} / (1\text{-Fo})) * (\text{mol. wt. MgO / FeO})$$

$$= (.44/1-.44) * (40.33/71.846) = .4574$$

$$(X_{MgO} / X_{FeO})^{liq} = K_D * .4574 = 0.3 * .4574 = .1372$$

Therefore, assuming equilibrium conditions, a liquid with a wt. percent MgO/FeO ratio of 0.1372 will initially crystallize olivine with a composition of Fo_{44}.

2. DISTRIBUTION OF Ni BETWEEN OLIVINE AND SILICATE LIQUID

The partition coefficient (D_{Ni}) is defined thus :-

$$D_{Ni} = (\text{Ni in olivine}) / (\text{Ni in liquid})$$

Hart and Davis (1978) found that D_{Ni} was dependent on melt composition, thus :-

$$D_{Ni} = (124.13 / \text{MgO in liq}) - .897 \quad .....(2)$$

This relationship may be used in conjunction with the formula of Roeder and Emslie (1970) (formula (1) above) to calculate the MgO, FeO and NiO components of olivine and liquid in successive residual magmas which are undergoing olivine fractionation.

For example, consider olivine with a composition of Fo_{79} and containing 0.42 wt. percent NiO (approximately 3300 ppm Ni). This is typical of cumulus olivine from the Merensky Reef at Amandelbult (see Chapter 6). Assuming that this is the first product to crystallize from a magmatic melt under equilibrium conditions the MgO/FeO ratio of a liquid that is in equilibrium with this olivine is :-

$$(MgO / FeO)^{liq} = (.79/(1-.79) \times (40.33/71.846) \times 0.3 = .6335,$$

Assume the initial liquid contains 10 wt. percent FeO :-

MgO in liquid = 10 x .6335 = 6.335 wt. percent

Then from equation (2) above,

$$D_{Ni} = (124.13/6.335) - .897 = 18.7$$

and,

Ni in liquid = (Ni in olivine)/D_{Ni} = (3300/18.7) = 176 ppm

Thus an initial liquid containing 10 wt. percent FeO, 6.34 wt. percent MgO and 176 ppm Ni is in equilibrium with olivine with a composition of Fo_{79} (ideally with 41.385 wt. percent MgO and 9.727 wt. percent FeO) and 0.42 wt. percent NiO.

If 2 wt. percent of this olivine is removed from the initial liquid the residual liquid will have a composition thus :-

wt .percent MgO = 6.34 - (41.385 x 2)/100 = 5.512

wt. percent FeO = 10 - (9.727 x 2)/100 = 9.806

ppm Ni = 176 - (3300 x 2)/100 = 110

The composition of olivine that crystallizes from this liquid, which now has a wt. percent MgO/FeO ratio of .5621, is calculated, as before, thus :-

$$(X_{MgO} / X_{FeO})^{oliv} = 1/K_D \times .5621 = (1/0.3) \times .5621 = 1.8737$$

and

mol. percent Fo = 1/(1 + (1/(1.8737 x 71.846/40.33)) = .77

The Ni content of this olivine is calculated thus :-

$$D_{Ni} = (124.13/5.512) - .897 = 21.623$$

and,

Ni in olivine = 21.623 x 110 = 2379 ppm (.30 wt. percent NiO)

Therefore, after only 2 wt. percent has crystallized the composition of the olivine has changed from Fo_{79} with .42 wt. percent NiO to Fo_{77} with .30 wt. percent NiO. In this particular example, which starts with a relatively Ni-rich olivine, Ni is depleted when the olivine reaches a composition of approximately Fo_{56}. It may be concluded that Ni is rapidly depleted from a magma which is crystallizing magnesian olivine, and that the Ni content of magnesian olivine is a much more sensitive indicator of fractionation than the Fo component.

In this study this calculation has been applied to a number of different starting compositions using two computer programs, PE05 and PE06, provided by Dr. J.S. Marsh at Rhodes University (see below).

```
      PROGRAM PE05
C
C THIS PROGRAM COMPUTES MGO, FEO, AND NI CONCENTRATIONS IN
C SCCESIVE RESIDUAL MAGMAS UNDERGOING OLIVINE FRACTIONATION
C
      CHARACTER*80 TITLE
      REAL MGO,LFEO,LMGO,MGMOL
 1001 FORMAT(A80)
 2000 FORMAT(1H1,A80,///)
 2001 FORMAT(1H0,10HLIQ. FRAC.,2X,11HINITIAL FEO,2X,11HINITIAL MGO,2X,11
     $HOLIVINE FEO,2X,11HOLIVINE MGO,2X,12HRESIDUAL FEO,2X,
     $12HRESIDUAL MGO,2X,10HINITIAL NI,2X,11HRESIDUAL NI)
 2002 FORMAT(1H0,3X,F5.3,4X,4(F7.3,6X),1X,F7.3,7X,F7.3,5X,F7.1,5X,F7.1)
      READ(8,1001)TITLE
    5 N=0
      READ(8,*)FEO,MGO,CNI,STEPS,FEND,I
      WRITE(5,2000)TITLE
      WRITE(5,2001)
   10 N=N+1
      FEMOL=FEO/71.846
      MGMOL=MGO/40.311
      RATOL=(FEMOL/MGMOL)*0.3
      OLMGMOL=2.0/(1.0+RATOL)
      OLFEMOL=2.0-OLMGMOL
      OLMG=OLMGMOL*40.311
      OLFE=OLFEMOL*71.846
      OLSI=60.085
      TOT=OLMG+OLFE+OLSI
      OLMG=(OLMG/TOT)*100.
      OLFE=(OLFE/TOT)*100.
      FRACMG=OLMG*STEPS
      FRACFE=OLFE*STEPS
      LFEO=((FEO-FRACFE)/(100.-FRACFE-FRACMG))*100.
      LMGO=((MGO-FRACMG)/(100.-FRACMG-FRACFE))*100.
      DK=(124.13/MGO)-0.897
      CLIQ=CNI*(1.0-STEPS)**(DK-1)
      FRAC=1.0-STEPS**N
      WRITE(5,2002)FRAC,FEO,MGO,OLFE,OLMG,LFEO,LMGO,CNI,CLIQ
      CNI=CLIQ
       FEO=LFEO
      MGO=LMGO
      IF(FRAC.GE.FEND)GO TO 10
      IF(I.EQ.1)GO TO 5
      STOP
      END

      PROGRAM PE06
C
C THIS PROGRAM COMPUTES MGO, FEO, AND NI CONCENTRATIONS IN
C SUCCESSIVE OLIVINE CUMULATES
C
      CHARACTER*80 TITLE
      REAL MGO,LFEO,LMGO,MGMOL
 1001 FORMAT(A80)
 2000 FORMAT(1H1,A80,///)
 2001 FORMAT(1H0,10HOLV. FRAC.,2X,11HINITIAL FEO,2X,11HINITIAL MGO,2X,11
     $HOLIVINE FEO,2X,11HOLIVINE MGO,2X,12HTOTAL    FEO,2X,
     $12HTOTAL    MGO,2X,10HTOT. FE2O3,2X,11HTOTAL    NI)
 2002 FORMAT(1H0,3X,F5.3,4X,4(F7.3,6X),1X,F7.3,7X,F7.3,5X,F7.1,5X,F7.1)
      READ(8,1001)TITLE
    5 N=0
      READ(8,*)FEO,MGO,CNI,FE3,F,STEPS,FEND,I
      WRITE(5,2000)TITLE
      WRITE(5,2001)
      STEP=STEPS
   10 N=N+1
      FEMOL=FEO/71.846
      MGMOL=MGO/40.311
      RATOL=(FEMOL/MGMOL)*0.3
      OLMGMOL=2.0/(1.0+RATOL)
      OLFEMOL=2.0-OLMGMOL
      OLMG=OLMGMOL*40.311
      OLFE=OLFEMOL*71.846
      OLSI=60.085
      TOT=OLMG+OLFE+OLSI
      OLMG=(OLMG/TOT)*100.
      OLFE=(OLFE/TOT)*100.
      TOTMG=(OLMG*STEP)+MGO*(1.0-STEP)
      TOTFE=(OLFE*STEP)+FEO*(1.0-STEP)
      TOTFE3=FE3*(1.0-STEP)
      DK=(124.13/MGO)-0.897
      OLNI=CNI*((1.0-F**DK)/(1.0-F))
      TOTNI=(OLNI*STEP)+CNI*(1.0-STEP)
      WRITE(5,2002)STEP,FEO,MGO,OLFE,OLMG,TOTFE,TOTMG,TOTFE3,
     $TOTNI
      STEP=STEP+STEPS
      IF(STEP.LT.FEND)GO TO 10
      IF(I.EQ.1)GO TO 5
      STOP
      END
```